Interconnexion du métabolisme cellulaire et de la voie de glucuronidation

Thèse

Yannick Audet-Delage

Doctorat en sciences pharmaceutiques
Philosophiæ doctor (Ph. D.)

Québec, Canada

Interconnexion du métabolisme cellulaire et de la voie de glucuronidation

Thèse

Yannick Audet-Delage

Sous la direction de :

Chantal Guillemette, directrice de recherche

Résumé

La voie métabolique de glucuronidation, impliquant les enzymes uridine diphospho-glucuronosyltransférases (UGT), joue un rôle crucial dans le métabolisme des médicaments et contrôle l'exposition à divers composés exogènes via leur inactivation par la conjugaison à l'acide glucuronique. Cette voie métabolique a également comme rôle principal de maintenir l'homéostasie cellulaire et le contrôle de la biodisponibilité de nombreuses molécules endogènes. Nombre de ces composés sont impliqués dans des boucles de rétroaction régulant l'expression et l'activité de diverses voies métaboliques cellulaires, notamment via l'implication de récepteurs nucléaires et autres voies de signalisation. Une modification de l'expression et de l'activité de la voie de glucuronidation a donc le potentiel d'influencer le métabolisme cellulaire, au-delà du contrôle des substrats des enzymes UGT. Cette hypothèse est appuyée par des observations préliminaires démontrant la capacité des UGT à interagir avec des protéines d'autres voies métaboliques, affectant ainsi leur activité. De plus, les études récentes du laboratoire font état d'un transcriptome étendu de la grande famille de gènes *UGT*, permettant la production de protéines alternatives comprenant de nouveaux domaines peptidiques et dont les fonctions et les réseaux d'interaction demeurent inconnus.

Dans le cadre de cette thèse, nos premières investigations ont porté sur les changements métaboliques associés à une modification de l'expression cellulaire d'enzymes UGT, ainsi que de leurs protéines alternatives nouvellement identifiées. Une approche métabolomique non-ciblée a révélé des répercussions importantes au niveau métabolique, parfois communes, parfois divergentes, selon l'enzyme et l'isoforme alternative étudiée. À titre d'exemple, les niveaux cellulaires de lipides bioactifs comme l'acide arachidonique sont grandement affectés dans les lysats de cellules exprimant des enzymes UGT, alors qu'ils ne le sont pas dans les lysats de cellules exprimant des protéines alternatives. Dans une seconde série d'investigations, nous avons établi les réseaux d'interactions protéiques des UGT dans le tissu rénal et hépatique humain. À l'aide d'anticorps développés au laboratoire et dirigés contre les enzymes ou les protéines alternatives UGT, nous avons réalisé une purification d'affinité sur bille couplée à la spectrométrie de masse. Ceci a permis d'établir de façon non-biaisée les interactomes endogènes des enzymes UGT et de leurs protéines alternatives dans un environnement protéique physiologique, révélant l'existence de partenaires communs et de partenaires spécifiques. En plus d'identifier des protéines associées au métabolisme des médicaments, nos travaux ont révélé plusieurs partenaires

protéiques impliqués dans d'autres voies métaboliques, telles que les voies énergétiques (glycolyse, cycle des acides tricarboxyliques, oxydation des lipides, etc.). À l'aide de modèles cellulaires, nous avons démontré que certaines de ces interactions sont fonctionnelles et entrainent une modification significative de l'activité du partenaire des UGT, induisant des perturbations métaboliques et phénotypiques associées à la progression tumorale. Enfin, nos données ont révélé une induction différentielle de l'expression d'une enzyme UGT et de ses variants alternatifs suite à un traitement pharmacologique, influençant possiblement l'activité cellulaire en réponse à ces stimuli.

Nos travaux soutiennent une interconnexion entre le métabolisme de glucuronidation et le métabolisme cellulaire. Ils appuient également un rôle plus vaste et complexe des protéines UGT, impliquant notamment la production d'isoformes alternatives aux structures protéiques distinctes et possédant des fonctions régulatrices possiblement différentes de celles des enzymes. Ces travaux démontrent également des interactions protéiques avec diverses voies métaboliques, permettant sans doute de moduler la réponse cellulaire à divers stimuli tout en optimisant les ressources métaboliques de la cellule.

Abstract

The glucuronidation pathway, catalyzed by uridine diphospho-glucuronosyltransferases (UGTs), is crucial for drug metabolism and controls the body's exposure to several exogenous compounds by the conjugation of a glucuronic acid moiety leading to their inactivation. A main role for this pathway is also to controls cellular levels of several endogenous compounds in order to maintain homeostasis. Many of those compounds are involved in feedback loops and control the expression and activity of numerous metabolic pathways through the regulation of nuclear receptors and other signaling events. Altered expression or activity of the glucuronidation pathway thus has the potential to influence cellular metabolism, beyond UGT substrate regulation. This hypothesis is supported by preliminary observations showing that UGTs possess the capacity to interact with enzymes from other metabolic pathways, affecting their activity. Furthermore, recent studies from our laboratory exposed an extended transcriptome for *UGT* genes, producing new alternative proteins comprising new domains and for which the functions and interaction networks remain unknown.

In the context of this work, our first investigations explored the metabolic alterations induced by a modification in the cellular levels of UGT enzymes, as well as selected novel alternative proteins. A non-targeted metabolomics approach uncovered significant metabolic alterations, sometimes common or divergent, depending on the enzyme and the alternative isoform. As an example, bioactive lipids such as arachidonic acid were among the most modulated metabolites in lysates of cells expressing UGT enzymes but remained unchanged in cells expressing alternate proteins. In a second set of investigations, we established the interaction networks of UGT proteins in human liver and kidney tissues. We used in-house antibodies directed against UGT enzymes or their alternative proteins to conduct affinity purification coupled to mass spectrometry. These assays exposed an unbiased endogenous interactome in a physiologically relevant protein environment, revealing common and specific partners to UGT enzymes and alternative isoforms. In addition to proteins involved in drug metabolism, our work uncovered numerous partners implicated in other metabolic routes such as energetic pathways (glycolysis, tricarboxylic acids cycle, lipid oxidation, etc.). Using cellular models, we showed some of these interactions had a functional impact on cellular activity of the protein partners, triggering metabolic alterations associated with tumor progression. Lastly, our data further support a differential expression of UGT enzymes and their alternative isoforms following treatment

with pharmacological compounds that could lead to variable metabolic activity in response to stimuli.

Our results demonstrate functional crosstalk between UGT proteins and cell metabolism. This works also supports an extended and rather complex role for UGTs, notably through the production of numerous alternative isoforms presenting different peptide structures and likely diverse regulatory functions. Our findings indicate that one of the underlying mechanisms is related to protein-protein interactions between UGTs and proteins of other metabolic routes, likely permitting a fine regulation of cell response to stimuli while optimizing metabolic resources.

Table des matières

Résumé iii

Abstract v

Table des matières vii

Liste des tableaux xi

Liste des figures xii

Liste des abréviations xiii

Remerciements xvii

Avant-propos xix

Introduction 1

Chapitre 1 2

1. Métabolisme cellulaire 2

1.1. Glycolyse aérobie ou « effet Warburg » 3

1.2. Activité mitochondriale et glutaminolyse 5

1.3. Acides aminés 9

1.4. Synthèse des nucléotides 11

1.5. Lipides et lipogenèse 12

1.6. Voies métaboliques impliquées dans le contrôle de l'homéostasie de molécules endogènes et la défense de l'organisme envers les xénobiotiques 14

1.6.1. Les cytochromes P450 14

1.6.2. Les voies de conjugaison 14

2. La voie de glucuronidation médiée par les enzymes UDP-glucuronosyltransférases 16

2.1. Régulation de l'expression et de l'activité des UGT 19

2.1.1. Variabilité de la voie de glucuronidation et impact clinique 23

2.1.2. Nouveaux évènements d'épissage et interactions protéine-protéine 26

3. Hypothèses de recherche et objectifs 28

4. Méthodologie et importance des articles dans la démarche scientifique 30

Chapitre 2 : « Glucuronosyltransferase protein expression alters cellular metabolome » 38

Résumé 38
Abstract 41
Introduction 42
Materials and Methods 43
Results 46
Discussion 50
Acknowledgements 53
Declaration of interest 53
References 54
Figure Legends 61
Supplementary Material 70

Chapitre 3 : « Endogenous protein interactome of human UDP-glucuronosyltransferases exposed by untargeted proteomics » 72

Résumé 72
Abstract 75
Introduction 76
Materials and methods 77
Results 81
Discussion 85
References 89
Acknowledgements 94
Competing financial interests 94
Author contributions 94
Figure legends 98

Chapitre 4 : « Cross-talk between alternatively spliced UGT1A isoforms and colon cancer cell metabolism » 105

Résumé 105
Abstract 108
Introduction 109
Materials and Method 111
Results 116
Discussion 118

Conflict of interest 122
Acknowledgments 122
Authorship contributions 122
Footnotes 122
References 123
Figures legends 128
Supplemental Data 137
Chapitre 5 : « Posttranscriptional regulation of UGT2B10 hepatic expression and activity by alternative splicing » 142
Résumé 142
Abstract 145
Introduction 146
Materials and Methods 147
Results 152
Discussion 156
Acknowledgements 161
Authorship contribution 161
Financial disclosure 161
References 162
Footnotes 167
Figure legends 168
Supplementary Material 178
Chapitre 6 : « Divergent Expression and Metabolic Functions of Human Glucuronosyltransferases through Alternative Splicing » 185
Résumé 185
Summary 187
Introduction 188
Results 189
Discussion 193
Conclusions 196
Experimental Procedures 197
Competing Interests 200
Author contributions 200

Accession numbers 201
Acknowledgements 201
References 202
Figure Legends 205
Supplementary Material 213
Discussion 218
Des changements dans la voie des UGT entrainent des perturbations métaboliques étendues 218
Les protéines UGT font partie de réseaux d'interactions protéiques complexes et affectent l'activité de certains partenaires 224
Changements phénotypiques associés aux protéines UGT 229
Conclusion 233
Bibliographie 234
Annexe 1 : « Estradiol metabolites as biomarkers of endometrial cancer prognosis after surgery » 251
Annexe 2 : « Identification of metabolomic biomarkers for endometrial cancer and its recurrence after surgery in postmenopausal women ». 281

Liste des tableaux

Tableau 1. Exemples de substrats endogènes et exogènes d'enzymes UGT humaines. 18
Tableau 2. Récepteurs et facteurs de transcription impliqués dans la régulation transcriptionnelle des UGT, ainsi que leurs ligands. 22
Tableau 3. Sommaires des avantages et inconvénients des principales approches utilisées pour l'analyse de métabolites lors d'études métabolomiques. 31
Tableau 4. Description des différentes méthodes disponibles pour l'étude des interactomes protéiques. 35

Liste des figures

Figure 1. Schéma simplifié des principales voies métaboliques modifiées dans le cancer. 3
Figure 2. L'augmentation de l'activité glycolytique par les cellules cancéreuses permet de fournir des squelettes de carbone aux différentes voies métaboliques associées à la prolifération cellulaire. 5
Figure 3. Activité mitochondriale. 6
Figure 4. L'oncométabolite R-2-hydroxyglutarate (R2-HG) entraine un remodelage métabolique important des cellules cancéreuses 8
Figure 5. Voies métaboliques utilisant la sérine et la glycine. 9
Figure 6. Les acides aminés à chaîne latérale ramifiée (*branched-chain amino acids*; BCAA) semblent impliqués dans le métabolisme des cellules cancéreuses. 10
Figure 7. Métabolisme de l'acide arachidonique vers les différents eïcosanoïdes. 13
Figure 8. Schéma simplifié des différentes voies de conjugaison chez l'humain. 15
Figure 9. La réaction de glucuronidation par les UDP-glucuronosyltransférases (UGT). 17
Figure 10. Structure des gènes *UGT*. 21

Liste des abréviations

α-KG	alpha-cétoglutarate
αKDH	alpha-cétoglutarate déshydrogénase
12-HETE	acide 12-hydroxyeïcosatétraènoïque
15-HETE	acide 15-hydroxyeïcosatétraènoïque
20-HETE	20-hydroxyeïcosatétraènoïque
5-HETE	acide 5-hydroxyeïcosatétraènoïque
6GPDH	6-phosphogluconate déshydrogénase
AA	acide arachidonique
ACC	acétyl-CoA carboxylase
ACLY	ATP-citrate lyase
ACOT8	acyl-CoA thioestérase 8
ADP	adénosine diphosphate
Ahr	récepteur aux hydrocarbures aromatiques
AKT	protéine kinase B
ALAS	Acide aminolévulinique synthase
ALDO	aldolase
ANT	translocateur de nucléotide adénine
AR	récepteur aux androgènes
ARNm	ARN messager
ATP	adénosine triphosphate
BC-acyl-CoA	acyl-CoA à chaîne ramifiée
BCAA	acides aminés à chaîne latérale ramifiée
BCAT	*branched-chain aminoacid aminotransferase*
BCKA	alpha-céto acides à chaîne latérale ramifiée
CAR	récepteur constitutif aux androstanes
CB1	récepteur aux cannabinoïdes 1
CB2	récepteur aux cannabinoïdes 2
CoA	Coenzyme A
COMT	catéchol-O-méthyltransférase
CoQ	coenzyme Q
CS	citrate synthase
CYP	cytochrome P450
DHET	acide dihydroxyeïcosatriènoïque
dTMP	désoxythymidine monophosphate
dUMP	désoxyuridine monophosphate
EET	acide époxyeïcosatriènoïque
ENO	énolase
ER	récepteur aux estrogènes
FASN	acide gras synthase
FH	fumarate hydratase
FXR	récepteur au farnésoïde X
G-6-P	glucose-6-phosphate
G6PDH	glucose-6-phosphate déshydrogénase
GAPDH	glycéraldéhyde-phosphate déshydrogénase
GC	chromatographie gazeuse
Gln	glutamine
Glu	glutamate
GPR119	récepteur couplé aux protéines G 119
GPR55	récepteur couplé aux protéines G 55

GR	récepteur aux glucocorticoïdes
GSH	glutathion réduit
GSSG	glutathion oxydé
GST	glutathion S-transférase
HETE	acide hydroxyeïcosatétraènoïque
HIF-1	facteur induit par l'hypoxie 1
HK	hexokinase
HPETE	acide hydroxyépoxyeïcosatétraènoïque
IDH	isocitrate déshydrogénase
LC	chromatographie liquide
LDH	lactate déshydrogénase
LXR	récepteurs des oxystérols
MDH	malate déshydrogénase
MS	spectrométrie de masse
MS/MS	spectrométrie de masse en tandem
mTOR	*Mammalian Target of Rapamycin*
NAD+	nicotinamide adénine dinucléotide oxydé
NADH	nicotinamide adénine dinucléotide réduit
NADP+	nicotinamide adenine dinucleotide phosphate oxydé
NADPH	nicotinamide adenine dinucleotide phosphate réduit
NAPQI	N-acétyl-p-benzoquinone imine
Nrf2	facteur nucléaire 2
OAA	oxaloacétate
OGDC	complexe oxoglutarate déshydrogénase
OGDHL	*oxoglutarate dehydrogenase-like*
PDHK	pyruvate déshydrogénase kinase
PDHP	pyruvate déshydrogénase phosphatase
PEPCK-M	phosphoénolpyruvate carboxykinase – mitochondriale
PFK	phosphofructokinase
PGAM	phosphoglycérate mutase
PGB_1	prostaglandine B_1
PGE_2	prostaglandine E_2
PGI	phosphoglucose isomérase
PGK	phosphoglycérate kinase
PhIP	2-amino-1-méthyl-6-phénylimidazo[4,5-b]pyridine
PHKA2	*phosphorylase kinase regulatory subunit alpha 2*
PI3K	phosphoinositide 3-kinase
PK	pyruvate kinase
PLA2	phospholipase A2
PPAR	récepteurs activés par les proliférateurs de peroxysomes
PXR	récepteur au prégnane X
R2-HG	(R)-2-hydroxyglutarate
RE	réticulum endoplasmique
RMN ^1H	résonance magnétique nucléaire du proton
ROS	espèces oxygénées réactives
SCD	stéaryl-CoA désaturase
SCS	succinyl coenzyme A synthétase
SDH	succinate déshydrogénase
SH3KBP1	*SH3 domain containing kinase binding protein 1*
shRNA	court ARN en forme d'épingle à cheveux
siRNA	court ARN interférant
SN-38	7-éthyl-10-hydroxycamptothécine

SULT	sulfotransférase
TCDD	2,3,7,8-tétrachlorodibenzo-*p*-dioxin
TCGA	*The Cancer Genome Atlas*
TCPOBOP	1,4-bis[2-(3,5-dichloropyridyloxy)]benzène
TET	*ten-eleven translocation enzyme*
TRPV1	récepteur ionotrope sensible aux vanilloïdes
UDP	uridine diphosphate
UDP-Glc	UDP-glucose
UDP-GlcA	acide glucuronique
UGT	UDP-glucuronosyltransférase
VDR	Récepteur de la vitamine D

The most exciting phrase to hear in science,
the one that heralds new discoveries,
is not "Eureka!" (I found it!) but "That's funny…"

La phrase la plus excitante que l'on peut entendre en science,
celle qui annonce des nouvelles découvertes,
ce n'est pas « Eureka » (j'ai trouvé!) mais « c'est drôle… »

Isaac Asimov

Remerciements

Je voudrais tout d'abord remercier ma directrice de doctorat, Chantal Guillemette, qui a su me motiver et me pousser à aller toujours plus loin. Merci de m'avoir guidé lorsque mes idées manquaient de clarté, et merci de m'avoir encouragé à poursuivre celles auxquelles je croyais. Merci également de m'avoir fourni un environnement aussi stimulant, ainsi que les ressources nécessaires à l'accomplissement de mes objectifs. J'ai été très heureux dans votre laboratoire, et j'espère poursuivre ma collaboration avec vous dans le futur.

Merci aussi à toute l'équipe CG! Michèle, merci pour ton support quotidien, ton écoute et tes conseils. Tu es toujours là quand on a besoin de toi, et c'est très apprécié! Je vais m'ennuyer de ton œil de lynx, qui ne manque aucun détail (même ceux qu'on voudrait cacher!). Lyne, merci pour ta joie et ta bonne humeur contagieuses. En plus de mettre du bonheur dans notre quotidien avec tes histoires, tu es toujours d'une grande aide dans le laboratoire. Ton efficacité et ton dévouement sont des exemples à suivre! Merci également à Sylvie, Pat et Véro, pour votre soutien et vos conseils. Merci à Joanie, pour ton aide avec les essais enzymatiques. Je te souhaite le meilleur pour la suite! Je me dois également de remercier Adrien et Éric. J'ai beaucoup apprécié partager ces deux mètres carrés de cubicule avec vous. À nous trois, on aura créé un nouveau français international! Merci pour ces discussions quotidiennes au laboratoire, à brasser des idées pour nos manip et à essayer d'interpréter nos résultats. Merci également pour ces nombreux 5 à 7 et ces activités de fin de semaine; avec vous, je ne me suis pas seulement fait de nouveaux collègues, mais des amis hors pairs!

Merci à tous les anciens membres du labo. Merci Andréa, pour ton aide en culture, mais aussi pour tes nombreux lapsus et ton ouïe qui divague! Tu nous fais toujours rire, et je te souhaite le plus grand des bonheurs à la retraite! Merci aux « Trois Français » : Anaïs, Alan et Guillaume. J'ai beaucoup apprécié nos discussions sur les différences France-Québec, et avec un peu de pratique, on a fini par se comprendre! Merci à Anne-Marie, pour ton aide et pour ta bonne humeur quotidienne. J'espère avoir l'occasion de rejouer au badminton avec toi! Merci également à Camille, Sylvia, Mélanie, Isabelle. J'ai passé de très beaux moments avec vous toutes.

Merci aux membres des autres laboratoires. Mandy, notre démone rousse, je te remercie pour ton énergie et ton esprit grivois; tu mets de la vie dans nos journées! Merci également

pour ton implication dans le comité étudiant. Tu as été d'un grand support dans cette aventure! Merci aux membres présents et passés des labo OB et Durocher. Vous côtoyer est toujours un plaisir! Merci à Jean-Philippe et Étienne, pour vos conseils et votre implication dans les activités étudiantes. Je vous souhaite tous les *grants* que vous voulez, et j'espère avoir la chance de collaborer avec vous dans le futur.

Merci à mes amis les plus chers, Jeff et Anne. Les soirées, les soupers et les escapades avec vous m'ont permis de passer au travers ces années d'université. Merci pour votre présence et votre compréhension. Je veux aussi remercier Cédric. Tu es un frère spirituel pour moi. Même si on ne se voit pas aussi souvent qu'on le voudrait, sache que j'apprécie chaque discussion avec toi. Merci également à ma belle-famille. Sylvie, on aura terminé tous les deux l'aventure du doctorat! Merci pour le support moral, autant pour moi que pour Sarah! Je dédie également un énorme merci à ma famille. Merci à mon père et à ma mère : vous m'avez toujours poussé à aller au bout de mes ambitions, même si vous ne comprenez pas exactement ce que je fais! Merci aussi à mon frère Pascal. C'est toujours un plaisir de prendre un moment de pause et d'aller au cinéma avec toi!

Finalement, je voudrais remercier mon amour, ma muse, ma complice au quotidien, Sarah Elene. Merci d'avoir été là pendant les hauts et les bas de cette aventure qu'est le doctorat. Ta patience, ton amour et ton soutien ont été source de réconfort, et m'ont permis de garder le cap. Je souhaite de tout mon cœur partager d'innombrables nouvelles aventures avec toi dans les années à venir. Merci infiniment pour tout, je t'aime!

Avant-propos

La présente thèse, intitulée « Interconnexion du métabolisme cellulaire et de la voie de glucuronidation », est présentée à la Faculté des études supérieures et postdoctorales de l'Université Laval pour l'obtention du grade de *Philosophiae doctor*, et est rédigée sous la forme de thèse avec insertion d'articles.

Le premier article est intitulé « Glucuronosyltransferase protein expression alters cellular metabolome ». Cet article est en préparation et n'a pas encore été soumis pour publication. J'en suis le premier auteur, ayant contribué à 75% à la réalisation de cette étude. J'ai complété l'analyse des données métabolomiques, l'analyse de l'expression des gènes, les co-immunoprécipitations, la microscopie confocale et j'ai rédigé l'ensemble de l'ébauche de l'article. Michèle Rouleau, professionnelle de recherche, a participé à l'analyse des résultats, à l'écriture et à la révision du manuscrit. Lyne Villeneuve, également professionnelle de recherche, a procédé à la préparation des échantillons aux fins d'analyses métabolomiques. Chantal Guillemette, ma directrice de recherche, a conceptualisé et supervisé l'étude, effectué l'analyse et l'interprétation des résultats, rédigé et révisé le manuscrit. L'article inséré dans cette thèse sera bonifié pour fins de publication dans un journal revu par les pairs.

Le deuxième article est intitulé « Endogenous protein interactome of human UDP-glucuronosyltransferases exposed by untargeted proteomics » et a été publié dans la revue « Frontiers in Pharmacology » (Rouleau et coll., 2017). Je suis le deuxième auteur de cet article, et j'ai contribué à environ 50% à la réalisation de l'étude. J'ai effectué une partie des immunoprécipitations pour la protéomique, les analyses d'enrichissement de voies métaboliques, en plus de faire l'acquisition et l'analyse des images en microscopie confocale pour la co-localisation des partenaires et la quantification des gouttelettes lipidiques. J'ai également participé à la révision du manuscrit. Michèle Rouleau, première auteure, a élaboré les expériences de laboratoire, a compilé, analysé et interprété les résultats, et a rédigé l'ébauche de l'article. Sylvie Desjardins, professionnelle de recherche, a effectué certaines validations de partenaires par immunoprécipitation. Mélanie Rouleau, étudiante au doctorat ayant gradué au début de mon doctorat, a effectué une partie des immunoprécipitations pour la protéomique. Camille Girard-Bock, étudiante à la maitrise au moment de l'étude et ayant gradué depuis, a procédé à la compilation des peptides spécifiques aux isoenzymes UGT afin d'en évaluer l'abondance. Chantal Guillemette a

conceptualisé et supervisé l'étude, effectué l'analyse et l'interprétation des résultats, rédigé et révisé le manuscrit. L'article inséré dans cette thèse est identique à la version publiée.

Le troisième article est intitulé « Cross-talk between alternatively spliced UGT1A isoforms and colon cancer cell metabolism » et a été publié dans la revue « Molecular Pharmacology » (Audet-Delage et coll., 2017). Je suis le premier auteur de ce manuscrit et ma contribution à la réalisation de cette étude s'évalue à environ 75%. J'ai procédé à la réalisation des co-immunoprécipitations des UGT1A_i2 et de leurs partenaires pour les analyses protéomiques et pour la confirmation des partenariats. J'ai également fait l'analyse des enrichissements de voies métaboliques sur les données issues de ces analyses. J'ai fait l'acquisition et l'analyse des images issues de microscopie confocale. J'ai quantifié le lactate extracellulaire et fait l'analyse des flux métaboliques en temps réel. J'ai analysé et interprété les données métaboliques et les données de prolifération cellulaire. J'ai aussi complété les essais d'adhésion, et j'ai analysé et interprété les données du manuscrit. J'ai participé à la rédaction et à la révision du manuscrit. Michèle Rouleau a participé à la conception d'expériences de laboratoire et à l'analyse et l'interprétation des données, ainsi qu'à la rédaction et la révision du manuscrit. Mélanie Rouleau a effectué une partie des immunoprécipitations pour la protéomique, a participé à l'acquisition et l'analyse des images pour les essais de migration, en collaboration avec Joannie Roberge, professionnelle de recherche. Cette dernière a également généré les modèles cellulaires utilisés dans cette étude. Stéphanie Miard, professionnelle de recherche au laboratoire du Prof. Picard, a participé à la conception et la réalisation des essais de flux métaboliques en temps réel, et Frédéric Picard a supervisé ce travail et permis l'accès au matériel dans son laboratoire. Dr Bernard Têtu, pathologiste et professeur à la faculté de médecine, a rendu possible l'accès et la préparation de tissus tumoraux et non-tumoraux à partir de la biobanque du CHU de Québec et a contribué aux analyses immunohistochimiques. Chantal Guillemette a conceptualisé et supervisé l'étude, effectué l'analyse et l'interprétation des résultats, rédigé et révisé le manuscrit. L'article inséré dans cette thèse est identique à la version publiée.

Le quatrième article est intitulé « Posttranscriptional regulation of UGT2B10 hepatic expression and activity by alternative splicing » et a été publié dans la revue « Drug Metabolism and Disposition » (Labriet et coll., 2018). Je suis le quatrième auteur de ce manuscrit et j'ai contribué à environ 10% de sa réalisation. J'ai procédé à la prise d'images en microscopie confocale, ainsi qu'à leur interprétation pour démontrer la co-localisation des protéines à l'étude. Adrien Labriet, premier auteur et étudiant au doctorat, a réalisé les

analyses statistiques sur les données d'expression, fait les analyses d'immunobuvardage, les essais enzymatiques et les essais de glycosylation et de stabilité des protéines à l'étude. Il a aussi participé à l'obtention des modèles cellulaires et complété les essais de co-immunoprécipitation. Il a participé à la rédaction et la révision du manuscrit. Eric P Allain, étudiant au doctorat, a effectué les analyses de données de séquençage à haut débit. Michèle Rouleau a contribué à la conceptualisation et la supervision de l'étude, l'analyse et l'interprétation des données, et à la rédaction et la révision du manuscrit. Lyne Villeneuve a participé à la mise en place des modèles cellulaires et aux essais de stabilité protéique, en plus de faire les essais enzymatiques en cellules intactes. Chantal Guillemette a conceptualisé et supervisé l'étude, effectué l'analyse et l'interprétation des résultats, rédigé et révisé le manuscrit. L'article inséré dans cette thèse est identique à la version publiée.

Le cinquième article est intitulé « Divergent Expression and Metabolic Functions of Human Glucuronosyltransferases through Alternative Splicing » et a été publié dans la revue « Cell Reports » (Rouleau et coll., 2016). Je suis le septième auteur de cet article et ai contribué à environ 10% de sa réalisation. Ma participation a été d'acquérir les images de localisation subcellulaire par immunufluorescence et microscopie confocale. Michèle Rouleau, première auteure, a contribué à la conceptualisation et supervision de l'étude, l'analyse et l'interprétation des données, à la rédaction et la révision du manuscrit. Alan Tourancheau, étudiant au doctorat ayant gradué en 2017, a effectué l'analyse et l'interprétation des données de séquençage à haut débit, et a participé à la rédaction et la révision du manuscrit. Camille Girard-Bock a fait l'analyse et l'interprétation des données métabolomiques et les immunoprécipitations pour la protéomique. Lyne Villeneuve a contribué à l'élaboration des modèles cellulaires, aux essais de prolifération cellulaire en temps réel, ainsi qu'aux essais enzymatiques et de stabilité protéique. Dr Jonathan Vaucher, résident en pathologie au moment de l'étude, a fait l'analyse et l'annotation des marquages histologiques. Anne-Marie Duperré, étudiante à la maitrise au moment de l'étude, a réalisé l'amplification des transcrits alternatifs pleine longueur dans les tissus humains. Isabelle Gilbert, stagiaire postdoctorale, a contribué à la sélection et la préparation des échantillons pour le séquençage à haut débit. Dr Ion Popa, pathologiste et professeur à la faculté de médecine, a contribué aux analyses immunohistochimiques. Arnaud Droit, professeur de la faculté de médecine et co-directeur de M. Tourancheau, a supervisé l'analyse des données bio-informatiques, en plus de fournir les infrastructures nécessaires à leur analyse et leur stockage au CHU de Québec. Chantal Guillemette a conceptualisé et supervisé l'étude, effectué l'analyse et l'interprétation des

résultats, rédigé et révisé le manuscrit. L'article inséré dans cette thèse est identique à la version publiée.

Deux articles se trouvent également en annexe de cette thèse pour un projet mené en parallèle de mon projet principal et pour lequel ma contribution a été majeure. Celui-ci visait à identifier des biomarqueurs sanguins du cancer de l'endomètre et de sa récidive. Le premier article en annexe est intitulé « Estradiol metabolites as biomarkers of endometrial cancer prognosis after surgery » et a été publié dans la revue « The Journal of Steroid Biochemistry and Molecular Biology » (Audet-Delage et coll., 2018a). Je suis le premier auteur de ce manuscrit, et ma contribution se situe à environ 40%. J'ai fait une partie des analyses statistiques, leur compilation et leur interprétation, en plus de participer à la rédaction et la révision du manuscrit. Dr Jean Grégoire, gynécologue au CHU de Québec, a supervisé la partie clinique de l'étude, incluant le recrutement et le suivi des patientes ainsi que l'élaboration, la mise en place et le maintien de la base de données cliniques. Patrick Caron et Véronique Turcotte, tous deux professionnels de recherche, ont effectué les analyses de quantification des hormones dans les échantillons sanguins par spectrométrie de masse. Dr Marie Plante, également gynécologue au CHU de Québec, a contribué au recrutement des patientes. Pierre Ayotte, professeur à la faculté de médecine, a recruté la cohorte de femmes en santé. David Simonyan, statisticien à la plateforme de recherche clinique du CHU de Québec, a effectué les analyses statistiques. Lyne Villeneuve a été responsable de la gestion des échantillons et de la base de données. Chantal Guillemette a conceptualisé et supervisé l'étude, effectué l'analyse et l'interprétation des résultats, rédigé et révisé le manuscrit. L'article inséré dans cette thèse est identique à la version publiée.

Le deuxième article en annexe est intitulé « Identification of metabolomic biomarkers for endometrial cancer and its recurrence after surgery in postmenopausal women » et a été publié dans la revue « Frontiers in Endocrinology » (Audet-Delage et coll., 2018b). J'en suis le premier auteur et ma contribution se situe à environ 80%. J'ai fait les analyses statistiques, l'interprétation des résultats, la rédaction et la révision du manuscrit. Lyne Villeneuve a été responsable de la gestion des échantillons et de la base de données. Dr Jean Grégoire a supervisé la partie clinique de l'étude, incluant le recrutement et le suivi des patientes ainsi que l'élaboration, la mise en place et le maintien de la base de données cliniques. Dr Marie Plante a contribué au recrutement des patientes. Chantal Guillemette a conceptualisé et supervisé l'étude, effectué l'analyse et l'interprétation des résultats, rédigé et révisé le manuscrit. L'article inséré dans cette thèse est identique à la version publiée.

Introduction

L'homéostasie se définit par un ensemble de processus permettant le maintien à l'équilibre de plusieurs facteurs clés d'un système et ce, malgré de nombreuses contraintes internes et externes. Chez les êtres vivants, ces différents processus incluent notamment l'absorption de nutriments, la réponse à divers stimuli et la fabrication et l'inactivation de nombreux composés bioactifs et métabolites. La cellule, qui est la plus petite unité fonctionnelle de l'organisme, doit effectuer avec efficacité l'entièreté de ces processus afin de maintenir non seulement son intégrité et sa fonctionnalité, mais également celle de l'organisme tout entier. Or, cet équilibre peut être altéré, menant à des dysfonctions métaboliques potentiellement néfastes.

Les néoplasies sont un exemple de dysfonctions métaboliques : plusieurs voies métaboliques y sont modulées et altérées afin de soutenir la croissance rapide des cellules tumorales et d'échapper aux nombreux points de contrôles métaboliques (Hanahan et Weinberg, 2011). D'un point de vue pharmacologique, les différents effets secondaires et toxicités associés à la prise de médicament peuvent également être considérés comme des dérèglements de l'homéostasie : il est reconnu par exemple que certains médicaments causent des toxicités hépatiques ou rénales importantes lors d'un usage excessif, ou encore à dose normale chez des individus ayant un métabolisme de détoxication de moindre ou plus grande efficacité (Guillemette et coll., 2014; Dong et coll., 2018).

L'activité de la voie médiée par les enzymes UDP-glucuronosyltransférases (UGT) est cruciale pour mieux contrôler de telles perturbations métaboliques, étant responsable de l'inactivation de nombreux médicaments et molécules bioactives endogènes. Or, l'activité de la voie de glucuronidation est non seulement très variable entre les individus, mais peut également varier fortement chez un même individu en fonction des situations physiologiques et pathologiques (Court, 2010; Hardwick et coll., 2013; Margaillan et coll., 2015a). Les conséquences de cette hétérogénéité notamment causée par des variations génétiques communes et héréditaires, ont principalement été étudiées en lien avec l'activité de glucuronidation des médicaments et de composés endogènes associés au risque de développer certaines maladies (hyperbilirubinémie) et plusieurs types de cancer (Guillemette et coll., 2014; Stingl et coll., 2014). Cependant, très peu d'études se sont intéressées jusqu'à maintenant aux répercussions métaboliques cellulaires d'une modification de l'expression des UGT; l'un des objectifs de cette thèse.

Chapitre 1

1. Métabolisme cellulaire

Le métabolisme cellulaire regroupe la totalité des transformations biochimiques nécessaires au maintien de l'homéostasie via la biosynthèse, la conversion métabolique et la dégradation de divers composés. Le métabolisme inclut ainsi le catabolisme et l'anabolisme; le premier étant la dégradation des ressources énergétiques en ATP, tandis que le deuxième réfère non seulement à la transformation des biomolécules de base en produits plus complexes tels les lipides, les acides aminés et les nucléotides, mais également la modification et l'inactivation de molécules bioactives endogènes et exogènes. Ces nombreuses réactions biochimiques impliquent une vaste diversité de voies métaboliques, dont la glycolyse, le cycle des acides tricarboxyliques, la voie des pentoses phosphates, la lipogenèse, les voies de synthèse des acides aminés, et les voies d'oxydoréduction et de conjugaison. Il est entendu que ces voies sont interdépendantes et partagent divers intermédiaires chimiques, tels les squelettes de carbone provenant de la glycolyse et les groupements amines issus de la glutaminolyse, ainsi que diverses voies de signalisation (**Figure 1**).

Fort probablement en raison de l'apparition des techniques axées sur la génomique, le métabolisme cellulaire a été plutôt relégué au second plan durant la deuxième moitié du 20^{e} siècle en faveur de recherches intenses en génomique. Cependant, avec l'amélioration des techniques de spectrométrie de masse, l'étude des protéines et du métabolisme a été facilitée dans les dernières décennies, augmentant ainsi l'intérêt scientifique. Les découvertes issues de ces travaux ont notamment mené à l'ajout relativement récent du métabolisme cellulaire à la signature caractéristique du cancer (Hanahan et Weinberg, 2011).

Puisque le métabolisme cellulaire cancéreux diffère du métabolisme cellulaire normal, celui-ci représente une opportunité unique de mieux comprendre l'interconnexion entre les différentes voies métaboliques et les divers métabolites cellulaires. Ces modifications métaboliques impliquent un haut niveau de coopération et de régulation cellulaires via plusieurs mécanismes (transcription, traduction, stabilité des protéines, modification post-traductionnelles, etc.) (DeBerardinis et Chandel, 2016). Ce remodelage a pour conséquence d'affecter de nombreuses voies métaboliques, incluant le métabolisme des petites

molécules, leur signalisation cellulaire et leur inactivation, qui implique notamment la voie de glucuronidation (sujet de la thèse). Dans les prochaines sections, je présente une revue sommaire des principales voies métaboliques, ainsi que certaines de leurs modifications dans le cancer, impliquées dans la progression tumorale et le processus métastatique.

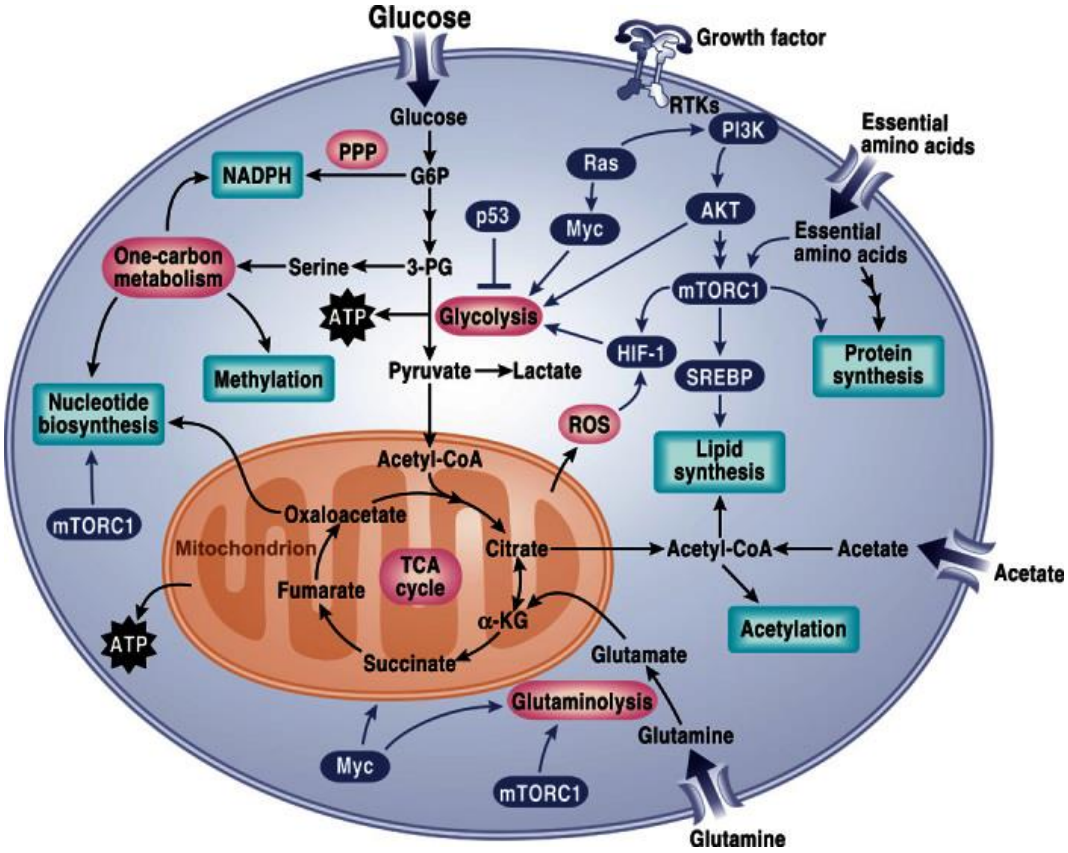

Figure 1. Schéma simplifié des principales voies métaboliques modifiées dans le cancer.
Tirée de DeBerardinis et Chandel (2016).

1.1. Glycolyse aérobie ou « effet Warburg »

Le flux énergétique des cellules cancéreuses a fait l'objet d'intenses recherches dans la première moitié du 20e siècle. Un des pionniers dans le domaine est le Prix Nobel Otto Warburg, qui a été le premier à caractériser l'augmentation de la synthèse d'énergie par la voie de la glycolyse dans les cellules tumorales (Warburg et coll., 1927; Warburg, 1956a; b; c). Malgré une mésinterprétation de ses résultats, le menant à l'hypothèse que cette voie était suractivée en raison d'une diminution de l'activité mitochondriale (Weinhouse, 1976; Fantin et coll., 2006; Moreno-Sanchez et coll., 2007), le fondement de ses recherches

demeure la pierre angulaire d'une meilleure compréhension du métabolisme des cellules cancéreuses.

Les cellules saines différenciées, en situation aérobie, utilisent normalement l'essentiel de leur fonction glycolytique pour soutenir l'activité mitochondriale via la formation de pyruvate. De cette façon, la mitochondrie génère la presque totalité de l'ATP cellulaire par le biais du cycle des acides tricarboxyliques et de la chaîne de phosphorylation oxydative. Toutefois, il se produit une consommation excessive de glucose dans les cellules cancéreuses, accompagnée d'une excrétion de lactate par la cellule. Ce phénomène a été qualifié de glycolyse aérobie, ou encore « d'effet Warburg » (Warburg et coll., 1927; Warburg, 1956a; b; c). Cependant, la fermentation lactique est moins efficace que la phosphorylation oxydative pour former de l'ATP, menant à seulement 2 ATP par molécule de glucose au lieu des 36 créés via la chaîne de phosphorylation oxydative (Koppenol et coll., 2011). Le recours à cette voie de moindre efficacité peut sembler illogique en regard des besoins énergétiques élevés de la cellule cancéreuse prolifération. Il importe donc de considérer la disponibilité des nutriments afin de mieux comprendre l'utilisation de cette voie par les cellules.

Plusieurs équipes ont observé que les nutriments ne semblaient pas être un facteur limitant pour de nombreux cancers (Kilburn et coll., 1969; Vander Heiden et coll., 2009). Même en stimulant au maximum la croissance de cellules en phase prolifération – menant à un métabolisme semblable à celui des cellules cancéreuses – plusieurs indicateurs soutiennent que les besoins en ATP sont remplis puisque ni le ratio ATP/ADP ni celui NADH/NAD+ ne sont modifiés (Christofk et coll., 2008; DeBerardinis et coll., 2008a). Par ailleurs, les phénomènes d'apoptose et d'autophagie ne sont pas augmentés dans de telles conditions, supportant la capacité des cellules à maintenir ce niveau d'activité (Vander Heiden et coll., 1999; Izyumov et coll., 2004; Shaw et coll., 2004; Lum et coll., 2005). L'hypothèse la plus plausible quant à l'utilisation de la glycolyse aérobie par les cellules cancéreuses stipule que celle-ci permettrait d'accumuler les biomolécules nécessaires à la prolifération cellulaire. Cette hypothèse est en accord avec le fait que l'activité mitochondriale demeure fonctionnelle dans les cellules cancéreuses, résultant donc en une consommation globalement plus élevée de glucose par la cellule (Zu et Guppy, 2004). L'imagerie médicale PetScan (*Positron Emission Tomography Scan*) utilise d'ailleurs cette altération du métabolisme des cellules cancéreuses pour en détecter la présence : l'injection d'un analogue radioactif du glucose est préférentiellement incorporé par les cellules tumorales

et les métastases, permettant leur visualisation (Phan et coll., 2014). Les squelettes de carbone issus du glucose serviraient donc à produire nucléotides (par la voie des pentoses phosphates), lipides (lipogenèse via le pyruvate et l'acétyl-CoA) et acides aminés non-essentiels (**Figure 2**). Ce phénomène serait par ailleurs concomitant avec une consommation excessive de glutamine par la cellule cancéreuse, un processus nommé glutaminolyse et qui permet l'incorporation du squelette de carbone et du groupement amine de cet acide aminé par les cellules cancéreuses.

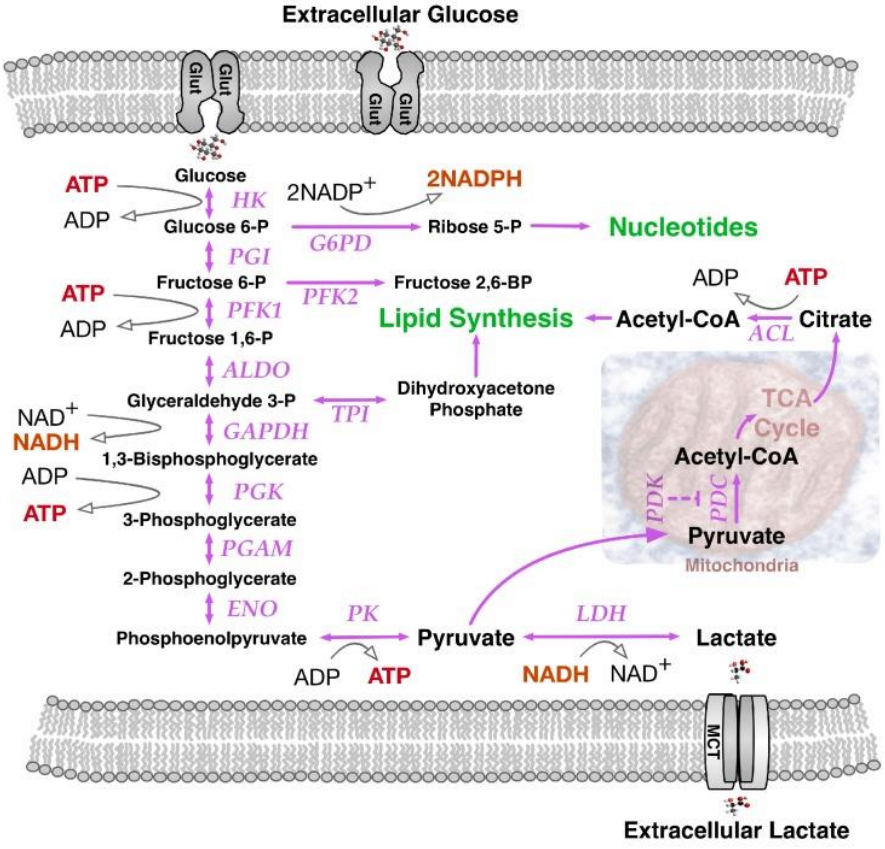

Figure 2. L'augmentation de l'activité glycolytique par les cellules cancéreuses permet de fournir des squelettes de carbone aux différentes voies métaboliques associées à la prolifération cellulaire.
HK, hexokinase; PGI, phosphoglucose isomérase; PFK, phosphofructokinase; ALDO, aldolase; GAPDH, glycéraldéhyde-phosphate déshydrogénase; PGK, phosphoglycérate kinase; PGAM, phosphoglycérate mutase; ENO, énolase; PK, pyruvate kinase; LDH, lactate déshydrogénase. Tirée de Burns et Manda (2017).

1.2. Activité mitochondriale et glutaminolyse

Tel que mentionné plus haut, les mitochondries sont responsables de générer une grande partie de l'énergie dans la cellule. Ainsi, le cycle des acides tricarboxyliques et la chaîne de phosphorylation oxydative permettent la formation d'une grande quantité d'ATP, puisant

l'acétyl-CoA à partir du pyruvate issu de la glycolyse, mais également à partir de la bêta-oxydation des acides gras (**Figure 3**).

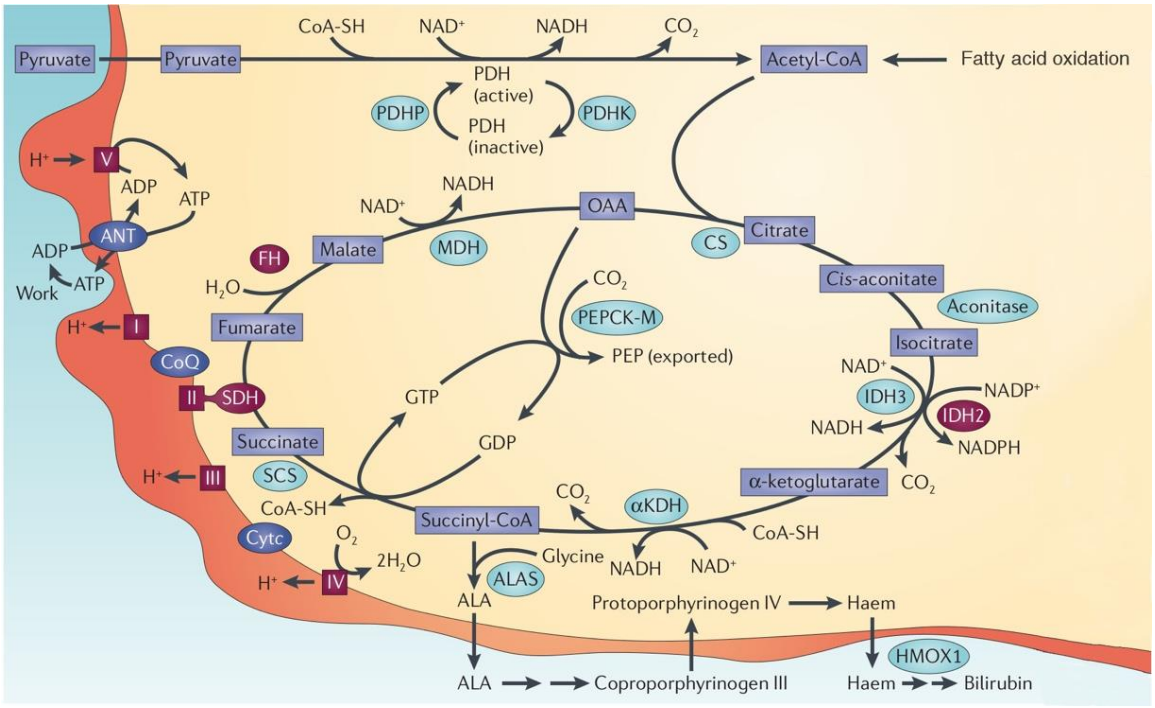

Figure 3. Activité mitochondriale.
Le cycle des acides tricarboxyliques et la chaîne de phosphorylation oxydative sont représentés. Noter que dans les cellules cancéreuses, l'α-cétoglutarate peut également être formé via la glutaminolyse (non représenté). OAA, oxaloacétate; PDHP, pyruvate déshydrogénase phosphatase; PDHK, pyruvate déshydrogénase kinase; CS, citrate synthase; IDH, isocitrate déshydrogénase; αKDH, alpha-cétoglutarate déshydrogénase; ALAS, acide aminolévulinique synthase; SCS, succinyl coenzyme A synthétase; SDH, succinate déshydrogénase; CoQ, coenzyme Q; ANT, translocateur de nucléotide adénine; FH, fumarate hydratase; MDH, malate déshydrogénase; PEPCK-M, phosphoénolpyruvate carboxykinase - mitochondriale. Adapté avec la permission du *Copyright Clearance Center, Inc.* pour *Macmillan Publishers Limited NATURE REVIEWS* © (Wallace, 2012).

Les mitochondries se transforment également en véritable usine à biomolécules dans les cellules cancéreuses (Boland et coll., 2013). Elles contribuent ainsi au métabolisme des lipides et des acides aminés, en plus de stimuler plusieurs voies de signalisation communes à maints cancers via la formation d'oncométabolites, c'est-à-dire des métabolites qui s'accumulent en présence de néoplasie (Collins et coll., 2017). Le (R)-2-hydroxyglutarate (R2-HG) est un exemple d'oncométabolite : celui-ci est formé à la suite d'une mutation somatique en condition néoplasique de l'enzyme mitochondriale isocitrate déshydrogénase, qui transforme alors l'oxoglutarate en R2-HG plutôt que de faire la conversion de l'isocitrate en oxoglutarate (Dang et coll., 2009). Au niveau cellulaire, le R2-HG entraîne différentes

cascades d'évènements, incluant la stimulation de la voie glycolytique via PI3K/AKT/mTOR et l'expression de l'oncogène HIF-1 (**Figure 4**) (M. Gagne et coll., 2017). L'accumulation du R2-HG s'accompagne également d'une diminution des concentrations d'oxoglutarate, ayant pour conséquence une réduction de l'activité déméthylase des enzymes TET, associée à des défauts de différentiation (Xu et coll., 2011). Des phénomènes semblables ont été observés pour d'autres enzymes et oncométabolites mitochondriaux, supportant l'importance de ces organelles dans le métabolisme tumoral (Astuti et coll., 2001; Tomlinson et coll., 2002).

Les mitochondries permettent également l'utilisation de la glutamine pour alimenter le métabolisme cellulaire, c'est-à-dire la glutaminolyse. Ce phénomène est amplifié dans le cancer, permettant aux dérivés marqués de la glutamine d'être utilisés dans l'imagerie diagnostique, tout comme ceux du glucose (Huang et McConathy, 2013). En plus d'être utilisée pour créer de l'ATP par le biais du cycle des acides tricarboxyliques, la glutamine permet aussi la formation de lipides via la production d'acétyl-CoA (**Figure 2**). En considérant la grande quantité de lipides nécessaires à la duplication cellulaire, notamment pour la formation des membranes cellulaires, la suractivation de cette voie représente donc un avantage métabolique pour les cellules cancéreuses. En ce sens, DeBerardinis et coll. (2007) ont observé 1) une forte synthèse de NADPH réducteurs issus de la glutaminolyse et nécessaires à la réduction de l'acétyl-CoA lors de la synthèse des lipides (lipogenèse; voir section plus bas) ; et 2) une augmentation de la synthèse d'alanine et d'ammoniaque par les cellules. Ces observations indiquent que la forte consommation de glutamine par les cellules cancéreuse servirait à intégrer les bases de carbone pour la formation de macromolécules essentielles à la duplication cellulaire, tout en diminuant l'acidité environnante de la cellule par l'action de l'ammoniaque (Medina, 2001). En addition aux rôles précédents, la consommation de glutamine servirait également au maintien de l'homéostasie oxydative via la réduction du glutathion oxydé, en plus d'être impliquée dans la signalisation cellulaire (Hensley et coll., 2013).

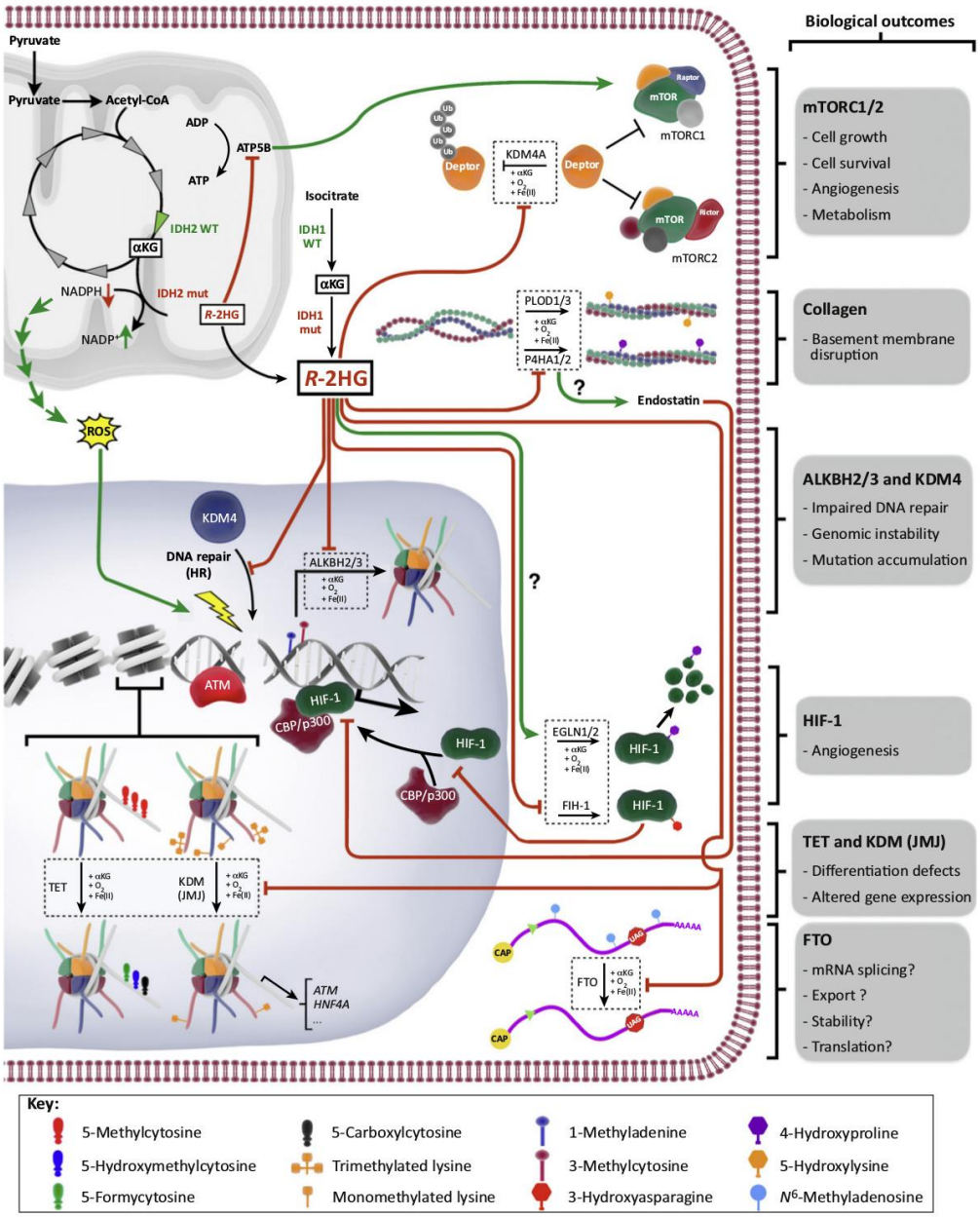

Figure 4. L'oncométabolite R-2-hydroxyglutarate (R2-HG) entraine un remodelage métabolique important des cellules cancéreuses.

L'enzyme IDH2 mutée transforme l'oxoglutarate en R2-HG. Cet oncométabolite modifie l'activité de la voie signalétique mTOR régulant la prolifération et le métabolisme cellulaire. Le R-2HG affecte également la méthylation de nombreux gènes via une modulation des protéines TET. Reproduit avec la permission du *Copyright Clearance Center, Inc.* pour *Elsevier Limited TRENDS IN CELL BIOLOGY* © (M. Gagne et coll., 2017).

1.3. Acides aminés

Les acides aminés sont classés en deux catégories, selon la capacité de l'organisme à les synthétiser ou non. On parle ainsi d'acides aminés non-essentiels et essentiels, respectivement. En plus de servir à la synthèse des protéines, les acides aminés représentent un réservoir de groupements réactifs (amine, méthyl, thiol, etc.) et de chaînes de carbone nécessaires aux différentes réactions enzymatiques de l'organisme. Les cellules néoplasiques tirent profit de plusieurs voies impliquées dans le métabolisme de ces molécules, notamment la voie de la sérine-glycine et celle des acides aminés à chaîne latérale ramifiée (*branched-chain amino acid* ; BCAA), en plus de la glutamine, tel que mentionné plus haut.

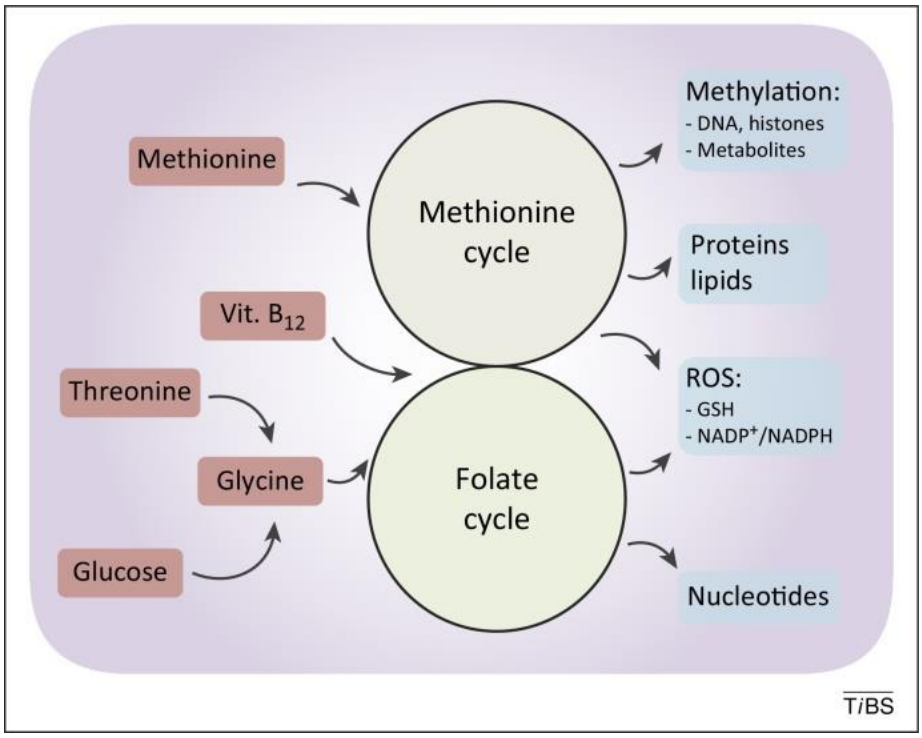

Figure 5. Voies métaboliques utilisant la sérine et la glycine.
La sérine et la glycine sont interconvertibles par le métabolisme cellulaire (non représenté). La glycine peut incorporer le cycle du folate pour soutenir la synthèse *de novo* des nucléotides et la synthèse d'antioxydants comme le glutathion, ou encore rejoindre le cycle de la méthionine pour soutenir la synthèse de protéines et la méthylation de l'ADN et de divers métabolites, incluant les lipides. Tirée de Amelio et coll. (2014)

De par leur structure simple, la sérine et la glycine sont impliquées dans de nombreuses voies métaboliques (**Figure 5**). Dans les cellules tumorales, la voie de conversion de la sérine en glycine est surexprimée, permettant une formation accrue du 5, 10-

méthylènetétrahydrofolate, un intermédiaire crucial à la synthèse des acides nucléiques. Ainsi, une inhibition de cette voie ou une privation en sérine et glycine permet de diminuer la prolifération tumorale dans plusieurs types de cancer (Labuschagne et coll., 2014; Maddocks et coll., 2017).

D'autres acides aminés sont nouvellement étudiés dans le contexte tumoral. C'est notamment le cas des BCAA, regroupant la valine, la leucine et l'isoleucine (Ananieva et Wilkinson, 2018). Ceux-ci peuvent servir à la synthèse des protéines, mais également être dégradés en intermédiaires du cycle des acides tricarboxyliques et servir à la synthèse de lipides, via l'acétyl-CoA, et de glutamate (**Figure 6**). Or, plusieurs études ont identifié une perturbation des niveaux de BCAA ou des enzymes leur étant associées dans différents types de cancer (Wang et coll., 2015; Zheng et coll., 2016; Zhang et Han, 2017). Cependant, les mécanismes en cause ne sont pas clairement définis, et d'autres études sont nécessaires afin de mieux comprendre leur implication dans ce contexte.

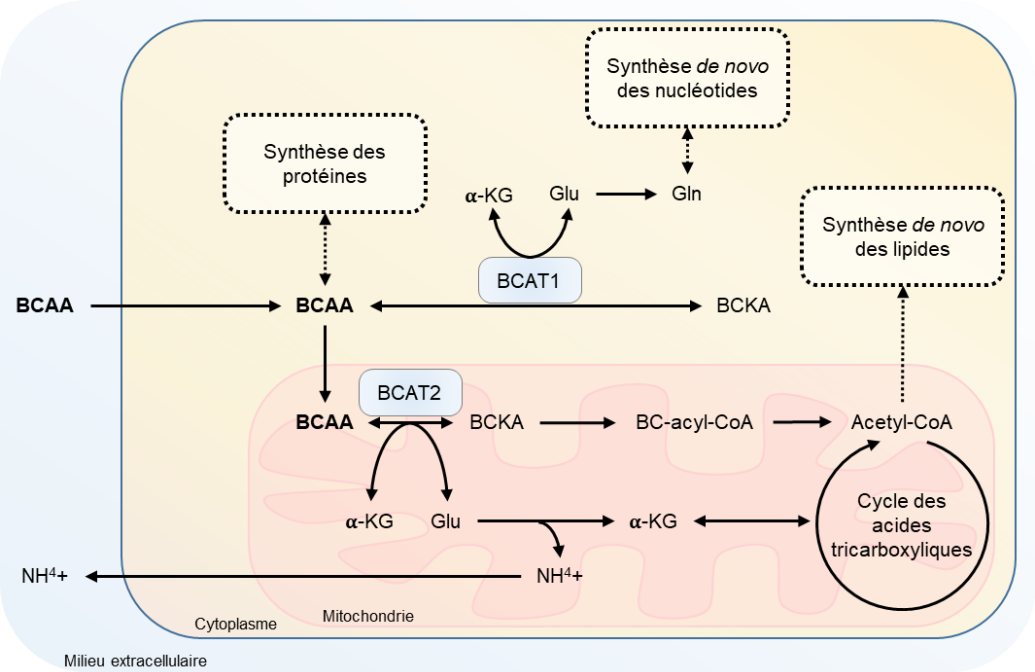

Figure 6. Les acides aminés à chaîne latérale ramifiée (*branched-chain amino acids*; BCAA) semblent impliqués dans le métabolisme des cellules cancéreuses.
Les BCAA peuvent participer à la synthèse des protéines, ou être dégradés pour incorporer la synthèse *de novo* des nucléotides, ou des lipides. BCAA, acides aminés à chaîne latérale ramifiée; BCKA, alpha-céto acides à chaîne latérale ramifiée; BCAT, *branched-chain aminoacid aminotransferase;* BC-acyl-CoA, acyl-CoA à chaine ramifiée; α-KG, alpha-cétoglutarate; Glu, glutamate; Gln, glutamine.

1.4. Synthèse des nucléotides

La voie des pentoses phosphates permet de fabriquer les acides ribonucléiques à partir du glucose-6-phosphate (G-6-P), un intermédiaire glycolytique. Le G-6-P est transformé en ribose-5-phosphate par l'action séquentielle de plusieurs enzymes, dont la glucose-6-phosphate déshydrogénase (G6PDH) et la 6-gluconate déshydrogénase (6GPDH). Cependant, ces enzymes génèrent aussi du NADPH via leur activité enzymatique (**Figure 2**) (Jonas et coll., 1992). De façon similaire à la glutaminolyse, la voie des pentoses phosphates permet donc de stimuler la lipogenèse et la réduction du glutathion oxydé (GSSG) via la production de NADPH, en plus de favoriser la synthèse des acides ribonucléiques (Cosentino et coll., 2011; Benito et coll., 2017; Hong et coll., 2018; Yang et coll., 2018).

En raison de son activité, cette voie est stimulée dans plusieurs types de cancer (Deberardinis et coll., 2008b; Riganti et coll., 2012). Par ailleurs, une inhibition de cette voie permettrait une diminution de la prolifération tumorale dans les cancers du sein et du poumon, notamment (Cho et coll., 2018; Hong et coll., 2018; Yang et coll., 2018).

Les voies de synthèse des bases puriques et pyrimidiques peuvent également être altérées dans le cancer. Puisque la synthèse des purines nécessite l'incorporation d'un atome de carbone via le N^{10}-formyltétrahydrofolate, une augmentation de la disponibilité de ce métabolite permet de stimuler la formation des bases puriques (Tedeschi et coll., 2013). Or, tel que mentionné précédemment, son précurseur le 5, 10-méthylènetétrahydrofolate est formé via la conversion de la sérine en glycine, couplant ainsi la synthèse des bases puriques au métabolisme des acides aminés. De plus, le cycle du tétrahydrofolate est également responsable de la régulation de l'activité de l'enzyme thymidylate synthase, nécessaire à la formation des pyrimidines. Cette voie est ciblée par différents médicaments antinéoplasiques, tel que le 5-fluorouracil et le méthotrexate, utilisés depuis de nombreuses années pour traiter le cancer (Wright et coll., 1951; Heidelberger et coll., 1957).

Hormis la glycine et la sérine, d'autres acides aminés sont également impliqués dans la synthèse des nucléotides. C'est le cas notamment de l'asparagine et de la glutamine, fournissant des squelettes de carbone et des groupements amines à la voie de synthèse des pyrimidines (Cory et Cory, 2006). Cette voie est également suractivée dans le cancer, et la conversion du désoxyuridine monophosphate (dUMP) en désoxythymidine

monophosphate (dTMP) est notamment ciblée afin de traiter le cancer des intestins et du côlon (Jackman et coll., 1991).

1.5. Lipides et lipogenèse

Les cellules en situation de prolifération ont de grands besoins en lipides, et les cellules cancéreuses n'échappent pas à cette réalité (Vander Heiden et coll., 2009; Vander Heiden et coll., 2011). Il existe une très grande diversité de molécules lipidiques, ayant toutes des fonctions précises. Par exemple, les glycérophospholipides sont les principaux composants des membranes des organelles et des cellules. Ceux-ci sont donc synthétisés en grande quantité pour soutenir la prolifération dans un contexte tumoral (Medes et coll., 1953; Kuhajda et coll., 1994; Santos et Schulze, 2012). Plusieurs enzymes sont impliquées dans ce processus, dont l'ATP-citrate lyase (ACLY), l'acétyl-CoA carboxylase (ACC), l'acide gras synthase (FASN) et la stéaryl-CoA désaturase (SCD). La formation des acides gras débute par une conversion de l'acétyl-CoA en malonyl-CoA par l'ACC, puis la FASN catalyse des réactions de condensation nécessitant du NADPH et menant ultimement à la formation de palmitate. Ensuite, la SCD peut désaturer ces acides gras, formant des acides gras mono-insaturés, qui arborent une conformation et des propriétés physicochimiques différentes de leurs homologues saturés (Fajardo et coll., 2011; Ajdzanovic et coll., 2013).

Cette voie peut être stimulée dans le cancer. Par exemple, une surexpression de l'enzyme FASN a été détectée dans le cancer du sein et de la prostate (Li et coll., 2000; Swinnen et coll., 2000; Menendez et Lupu, 2007; Yoon et coll., 2007; Santos et Schulze, 2012), alors que l'enzyme ACLY semble nécessaire à la formation de tumeurs prostatiques *in vitro* et *in vivo*, puisque son inactivation mène à la régression et à la l'apoptose de ces cellules tumorales (Bauer et coll., 2005; Hatzivassiliou et coll., 2005).

D'autres classes de lipides joueraient également un rôle dans la progression tumorale, dont les endocannabinoïdes (Sledzinski et coll., 2018). Ces lipides sont principalement issus de la conjugaison de groupements polaires (glycérol, acides aminés, éthanolamine) à des acides gras polyinsaturés tel l'acide arachidonique (C20:3n6), un acide gras oméga-6 obtenu principalement via l'alimentation. Étant des lipides bioactifs, les endocannabinoïdes influencent la réponse inflammatoire et le métabolisme des lipides via notamment des récepteurs couplés aux protéines G, comme les récepteurs aux cannabinoïdes CB1, CB2, GPR55 et GPR119; le récepteur ionotrope sensible aux vanilloïdes TRPV1; et les récepteurs activés par les proliférateurs de peroxysomes (PPAR) (Mackie, 2008; Patel et

coll., 2010; Pertwee et coll., 2010). Or, plusieurs études ont détecté des variations dans les concentrations de ces composés, des enzymes responsables de leur synthèse, et de leurs récepteurs dans plusieurs types de cancer (Sledzinski et coll., 2018). Cependant, les néoplasies ne répondent pas toutes de la même façon à une activation de cette voie (Stephen et coll., 2004; Brown et coll., 2013; Grabner et coll., 2017).

En plus de son activité intrinsèque, l'acide arachidonique peut aussi être enzymatiquement transformé en eicosanoïdes tels que les leucotriènes et les prostanoïdes. Ces lipides bioactifs sont des modulateurs de l'inflammation et de la contraction des muscles lisses, comme ceux retrouvés dans les vaisseaux sanguins (Pace et coll., 2017; Mitchell et Kirkby, 2018). Exploitant ces propriétés, plusieurs types cancéreux activent les voies métaboliques favorisant les eicosanoïdes possédant des propriétés anti-inflammatoires et pro-angiogéniques, comme l'acide 20-hydroxyeïcosatétraènoïque (20-HETE) (**Figure 7**) (Casos et coll., 2011; Feng et coll., 2017; Sano et coll., 2018). La formation de ces composés implique un nombre important d'enzymes, incluant lipoxygénases et cyclooxygénases, ainsi que les cytochromes P450 (CYP).

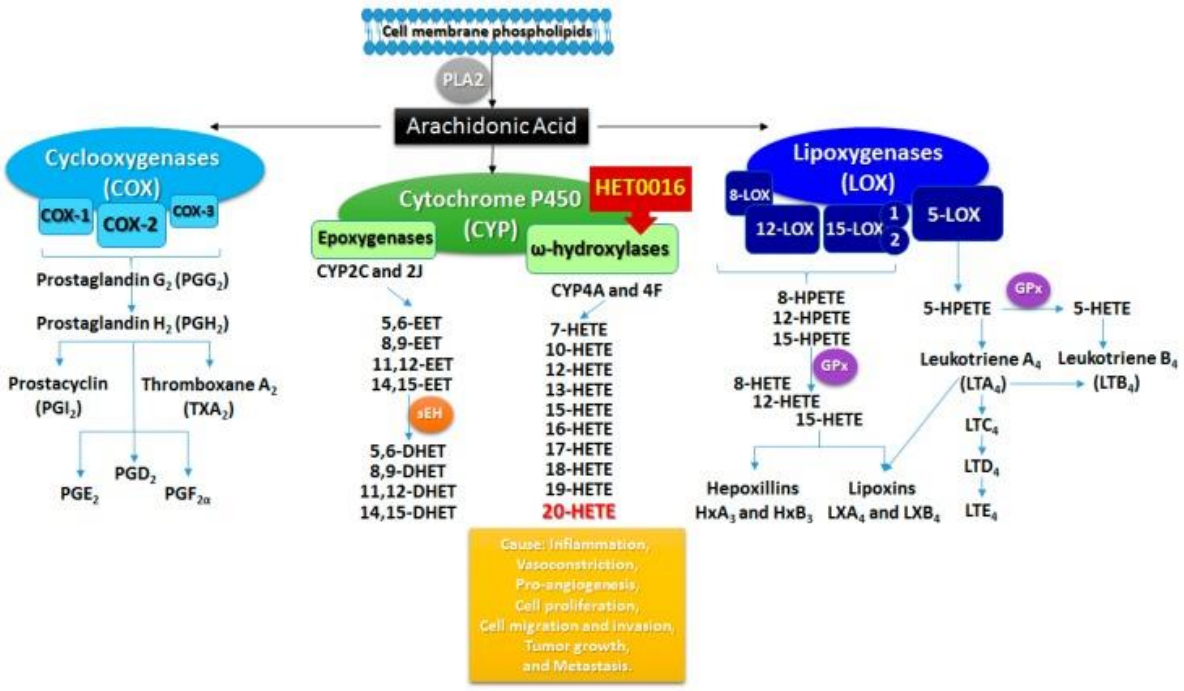

Figure 7. Métabolisme de l'acide arachidonique vers les différents eïcosanoïdes.
PLA2, phospholipase A2; EET, acide époxyeïcosatriènoïque; DHET, acide dihydroxyeïcosatriènoïque; HETE, acide hydroxyeïcosatétraènoïque; HPETE, acide hydroxyépoxyeïcosatétraènoïque. Tirée de Borin et coll. (2017).

1.6. Voies métaboliques impliquées dans le contrôle de l'homéostasie de molécules endogènes et la défense de l'organisme envers les xénobiotiques

1.6.1. Les cytochromes P450

Les CYP sont en mesure de biotransformer une très grande variété de molécules via leur activité monooxygénase, peroxydase et peroxygénase (Hrycay et Bandiera, 2015). Parmi leurs substrats, nous retrouvons diverses molécules exogènes et endogènes, dont certaines pouvant participer à la progression tumorale (Go et coll., 2015; He et Feng, 2015). En effet, plusieurs produits métaboliques de ces enzymes sont impliqués dans la régulation des voies métaboliques mentionnées plus haut. Par exemple, l'activité des CYP contrôle le métabolisme de la vitamine D, impliquée notamment dans la régulation de l'oxydation des lipides et du métabolisme énergétique (Jacobs et coll., 2013; Marcotorchino et coll., 2014; Ji et coll., 2016; Abu El Maaty et coll., 2017). De façon similaire, les androgènes, dont la régulation implique plusieurs enzymes de la famille des CYP, sont en mesure d'activer les voies de la glycolyse et du cycle des acides tricarboxyliques des cellules prostatiques tumorales (Niwa et coll., 2015; Audet-Walsh et coll., 2017). Grâce à leur très grande diversité de substrats, les CYP se retrouvent donc au croisement de nombreuses voies métaboliques. Or, les réactions catalysées par les CYP ont aussi pour effet d'augmenter l'affinité des molécules biotransformées pour le métabolisme de phase II des médicaments, c'est-à-dire les réactions de conjugaison.

1.6.2. Les voies de conjugaison

De façon générale, les réactions de conjugaison catalysent l'ajout d'une molécule aux groupements fonctionnels d'un substrat et ce, dans le but de l'inactiver et de faciliter son excrétion. Plusieurs types de molécules peuvent ainsi être transférées aux substrats, qui eux peuvent être de nature endogène ou exogène (**Figure 8**). De nombreux facteurs déterminent des voies empruntées par les substrats, tels que la nature de ceux-ci, les groupements fonctionnels qu'ils présentent, ainsi que l'affinité des enzymes et la capacité des voies. Par exemple, l'acétaminophène est connu pour emprunter plusieurs de ces voies, pouvant être excrété sous forme d'acétaminophène-glucuronide (métabolite majeur) et d'acétaminophène-sulfate (métabolite secondaire) (Court et coll., 2017). Parmi les métabolites mineurs de l'acétaminophène, on trouve également le *N*-acétyl-*p*-benzoquinone imine (NAPQI), formé par les CYP et possédant des propriétés hépatotoxiques (Dahlin et Nelson, 1982). Cependant, ce métabolite est produit préférentiellement lorsque les concentrations d'acétaminophène sont élevées et que les voies de glucuronidation et de

sulfatation sont saturées (Court et coll., 2017). Bien que la glutathionation puisse inactiver le métabolite NAPQI, de sérieux dommages hépatiques peuvent résulter d'une exposition à celui-ci (Ramachandran et Jaeschke, 2017).

Groupe transféré	Enzymes impliquées	Réaction
Méthyl	Méthyltransférases	Méthylation
Sulfate	Sulfotransférases	Sulfatation
Acide aminé (glycine, taurine)	Glycine N-acyltransférases	Aminoacylation
Acide glucuronique	UDP-glucuronosyltransférases	Glucuronidation
Glucide (glucose, xylose, etc.)	Glycosyltransférases	Glycosylation
Acétyl	N-acétyltransférases	Acétylation
Glutathion	Glutathion S-transférases	Glutathionation

Figure 8. Schéma simplifié des différentes voies de conjugaison chez l'humain.

Au niveau endogène, une situation similaire est observée pour les estrogènes. En effet, ces molécules sont métabolisées via plusieurs enzymes du métabolisme de conjugaison (SULT, COMT, GST, UGT), dont la coopérativité permet de contrôler l'activité biologique de ces hormones et de favoriser l'élimination de leurs dérivés quinones, ayant des propriétés génotoxiques (Rogan et coll., 2003; Lepine et coll., 2004; Gerstner et coll., 2008; Hui et coll., 2008; Cavalieri et Rogan, 2016). La prise en charge de ces différents métabolites illustre bien la synergie qui existe entre les voies de conjugaison, nécessaire au maintien de l'homéostasie cellulaire et métabolique, et en réponse à des stimuli.

Parmi les voies de conjugaison, la voie de glucuronidation prédomine, étant responsable de l'élimination de plus de 55% des médicaments les plus prescrits dans le monde (Guillemette et coll., 2014). Puisque cette voie a été le point focal des travaux rapportés dans cette thèse, la prochaine section présente l'état des connaissances sur celle-ci.

2. La voie de glucuronidation médiée par les enzymes UDP-glucuronosyltransférases

Il existe quatre sous-familles d'enzymes UDP-glucuronosyltransférases (UGT), basées sur la localisation chromosomique et l'homologie de séquence des gènes, soit les UGT1A, UGT2, UGT3 et UGT8. Relativement peu d'informations sont connues à propos des sous-familles UGT3 et UGT8, identifiées plus récemment et qui participeraient plutôt à la glycosylation en utilisant d'autres sucres que l'acide glucuronique (Bosio et coll., 1996; Mackenzie et coll., 2008; Meech et coll., 2015). Les enzymes issues des sous-familles UGT1A et UGT2B catalysent quant à elles la majeure partie de l'activité de glucuronidation intracellulaire en utilisant l'acide glucuronique (UDP-GlcA) comme co-substrat.

Les enzymes UGT sont des protéines transmembranaires du réticulum endoplasmique (RE) dont la majeure partie de la protéine est située dans la lumière du RE (**Figure 9**) (Radominska-Pandya et coll., 1999; Rowland et coll., 2013). Celles-ci conjuguent plusieurs médicaments de toutes classes, des composés exogènes toxiques et de nombreuses molécules endogènes (**Tableau 1**). Ainsi, ces enzymes hautement versatiles jouent un rôle déterminant dans l'inactivation et dans l'élimination de nombreux métabolites par la bile et l'urine (Guillemette et coll., 2014; Bock, 2015).

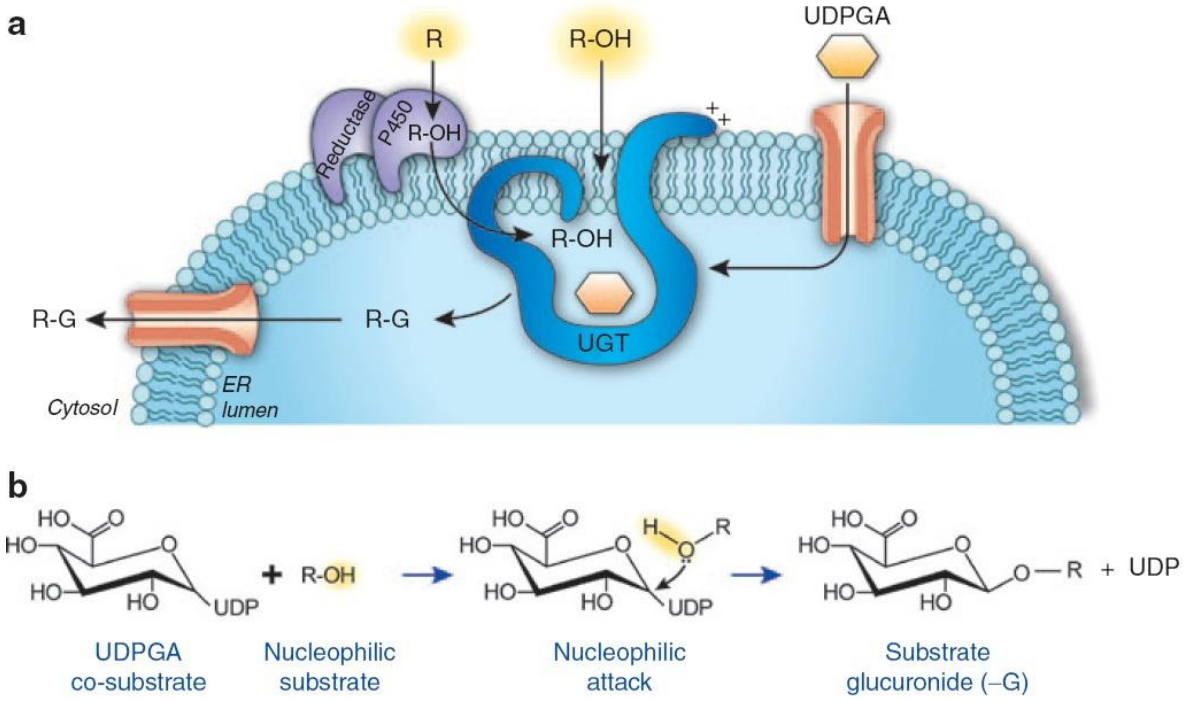

c

	Hydroxyl/carboxyl	Amines	Sulfhydryl	Enolic acids
Functional groups	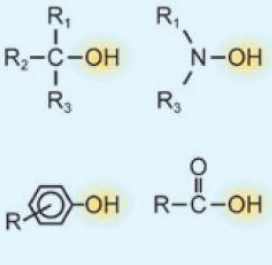	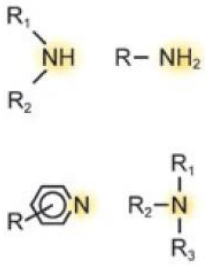		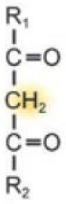
Glucuronides	*O*-linked	*N*-linked	*S*-linked	*C*-linked
UGTs	1A, 2A, 2B	1A, 2B7, 2B10	1A, 2A, 2B	1A9

Figure 9. La réaction de glucuronidation par les UDP-glucuronosyltransférases (UGT).
A) Les UGT sont des protéines transmembranaires localisées au réticulum endoplasmique. **B)** La réaction de glucuronidation requiert une attaque nucléophile initiée par le substrat, permettant au groupement sucre de se lier à ce dernier, tandis que l'UDP est expulsé. **C)** Groupements chimiques pouvant initier la réaction de glucuronidation par les UGT. Reproduit avec la permission du *Copyright Clearance Center, Inc.* pour *John Wiley and Sons CLINICAL PHARMACOLOGY & THERAPEUTICS* © (Guillemette et coll., 2014).

Tableau 1. Exemples de substrats endogènes et exogènes d'enzymes UGT humaines.

UGTs	Substrats exogènes	Substrats endogènes
1A1	SN-38, simvastatine, étoposide, ézétimibe, éthinylestradiol, atorvastatine, codéine	bilirubine, estrogènes, catéchols estrogènes, thyroxine, acide arachidonique, PGB_1
1A3	atorvastatine, simvastatine, ézétimibe, telmisartan, vorinostat	estrogènes, catéchols estrogènes, acide chénodésoxycholique, thyroxine
1A4	tamoxifène, lamotrigine, olanzapine, amitriptyline, midazolam, tacrolimus, trifluoperazine	androgènes
1A5†	1-hydroxypyrène	inconnu
1A6	Déférirprone, acétaminophène	sérotonine, 5-hydroxytryptophol
1A7†	SN-38, coumarine, thymol, vorinostat	inconnu
1A8†	acide mycophénolique, vorinostat	estrogènes, catéchols estrogènes
1A9	SN-38, acétaminophène, flavopiridol, propofol, entacapone, *R*-oxazepam, acide mycophénolique, édaravone, sorafénib, tolcapone, vorinostat	catéchols estrogènes, thyroxine, acide arachidonique, 20-HETE, 15-HETE
1A10†	SN-38, apigenin, vorinostat	estrogènes, catéchols estrogènes, dopamine
2B4	acétaminophène, déférirprone, fénofibrate, carvedilol	catéchols estrogènes, acides biliaires
2B7	zidovudine, épirubicin, fénofibrate, morphine, codéine, AINS, acide mycophénolique, chloramphénicol, éfavirenz, naproxène, naloxone	androgènes, estrogènes, catéchols estrogènes, acide tout-trans-rétinoïque, acide arachidonique, 20-HETE, 15-HETE, PGB_1, PGE_2
2B10	diphénhydramine, olanzapine, lévomédétomidine	12-HETE, 15-HETE
2B11	Inconnu	12-HETE, 15-HETE
2B15	tamoxifène, *S*-oxazépam, lorazépam, dabigatran, *R*-méthadone, tolcapone	androgènes
2B17	vorinostat	androgènes
2B28	inconnu	androgènes / estrogènes

†Isoenzymes exprimées exclusivement à l'extérieur du foie. La liste des substrats est non exhaustive. Les termes « acides biliaires », « androgènes », « estrogènes » et « catéchols estrogènes » ont été utilisés pour alléger le tableau, bien qu'il existe une spécificité et une régiosélectivité pour chacun de ces substrats. PGB_1, prostaglandine B_1; PGE_2, prostaglandine E_2; 5-HETE, acide 5-hydroxyeïcosatétraènoïque; 12-HETE, acide 12-hydroxyeïcosatétraènoïque. Adapté de Guillemette et coll. (2014) et de Bock (2015).

Les UGT nécessitent la présence d'un substrat et d'un co-substrat. Le co-substrat est l'UDP-GlcA, qui est ubiquitaire dans les tissus humains. Le mécanisme réactionnel postulé est de type SN2 et fait appel à une base catalytique capable d'activer l'accepteur par déprotonation. Il s'ensuit une attaque nucléophile sur le carbone 1 de l'acide glucuronique, conduisant à la

formation d'un β-D-glucuronide hydrosoluble avec inversion de configuration et libération d'UDP, facilitée par la présence d'un cation magnésium (**Figure 9**). L'UDP relargué peut être recyclé pour former une nouvelle molécule d'UDP-GlcA, alors que l'acide glucuronique est couplé au groupement réactif de la molécule non-polaire, formant ainsi un métabolite glucuronide. Cette réaction mène principalement à la formation de O-glucuronides (O-G), par le biais d'un lien éther ou ester, selon le groupement d'attache de type phényle ou carbonyle, respectivement. Malgré la prépondérance des O-G, l'attaque nucléophile peut également se produire à partir d'autres groupements actifs, menant à la glucuronidation d'un groupement de souffre (S-G), d'azote (N-G) ou de carbone (C-G) (**Figure 9**) (Burchell et Coughtrie, 1989). La conjugaison du groupement sucre permet d'augmenter la solubilité du composé lipophile en phase aqueuse et crée également un encombrement stérique qui rend généralement la molécule moins toxique et moins active, empêchant ainsi sa liaison aux récepteurs et autres effecteurs.

Il existe cependant quelques rares exceptions pour lesquelles le substrat des UGT n'est pas inactivé. Par exemple, la morphine peut être conjuguée à l'acide glucuronique sur deux positions, menant à la formation de morphine-6-G ou de morphine-3-G. Or, la morphine-6-G a un potentiel pharmacologique supérieur à celui du composé mère, affichant une activité analgésique près de 20 fois supérieure dans des essais *in vitro*, et un potentiel nociceptif prolongé dans des essais *in vivo* chez la souris et l'humain (Frances et coll., 1992; van Dorp et coll., 2008). De façon similaire, le glucuronide de l'acide tout-trans rétinoïque, un métabolite endogène de la vitamine A, demeure actif malgré la glucuronidation (Sidell et coll., 2000; Barua et Sidell, 2004). Bien que ce phénomène soit plutôt rare, il existe ainsi une possibilité que le substrat métabolisé possède un potentiel d'activité biologique ou pharmacologique.

2.1. Régulation de l'expression et de l'activité des UGT

Les membres de la sous-famille UGT1A comptent pour près de la moitié des 19 enzymes UGT humaines et sont tous issus du gène *UGT1* localisé au chromosome 2q37.1 (**Figure 10**) (Guillemette et coll., 2010). Celui-ci code pour neuf enzymes, soit les UGT1A1, 1A3, 1A4, 1A5, 1A6, 1A7, 1A8, 1A9 et 1A10 (Gong et coll., 2001). Ainsi, il existe une grande diversité d'enzymes UGT1A, rendue possible par la complexité des évènements d'épissage se produisant dans ce gène. Celui-ci présente neuf exons 1 alternatifs partageant une homologie de séquence entre 54 et 94%, et possédant chacun un promoteur unique

responsable de l'expression différentielle des isoenzymes UGT1A. Une fois transcrit, l'épissage du pré-ARN messager permet à l'un des exons 1 d'être couplé aux 4 exons communs (2-5a) (Ritter et coll., 1992; Gong et coll., 2001). Le premier exon code pour la région N-terminale de la protéine, impliquée dans la reconnaissance du substrat et qui est très variable entre les isoenzymes. C'est donc à cette diversité des exons 1 qu'est due la vaste gamme de substrats et des diverses structures chimiques prises en charge par les enzymes UGT1A. Quant à eux, les exons 2 à 5, communs à toutes les enzymes UGT1A, codent pour le domaine de liaison au co-substrat et le domaine transmembranaire, ainsi que le motif dilysine (KKXX ou KXKXX), impliqué dans la localisation cellulaire des enzymes vers le RE après modification post-traductionnelle dans l'appareil de Golgi (Teasdale et Jackson, 1996; Meech et Mackenzie, 1998). Les exons communs codent également pour un domaine appelé microrégion d'ancrage à la membrane, qui interviendrait aussi dans la localisation de la protéine au RE, de même que pour une séquence signature commune à toutes les protéines glycosyltransférases (**Figure 10**) (Ciotti et coll., 1998).

Les membres de la sous-famille UGT2B comprennent les enzymes UGT2B4, 2B7, 2B10, 2B11, 2B15, 2B17 et 2B28. La structure de leurs gènes est différente de celles des *UGT1* : les gènes, regroupés sur le chromosome 4q13, sont regroupés sous forme de *clusters* de gènes et sont issus de la duplication génique. Chaque gène code ainsi pour une isoenzyme différente, bien que démontrant une forte homologie de séquence, affichant jusqu'à 97% d'homologie entre certaines enzymes UGT2B (Nair et coll., 2015; Tourancheau et coll., 2016). Les gènes codant pour les UGT2B sont formés de 6 exons, dont la répartition des domaines protéiques reste similaire à celle des UGT1A (**Figure 10**).

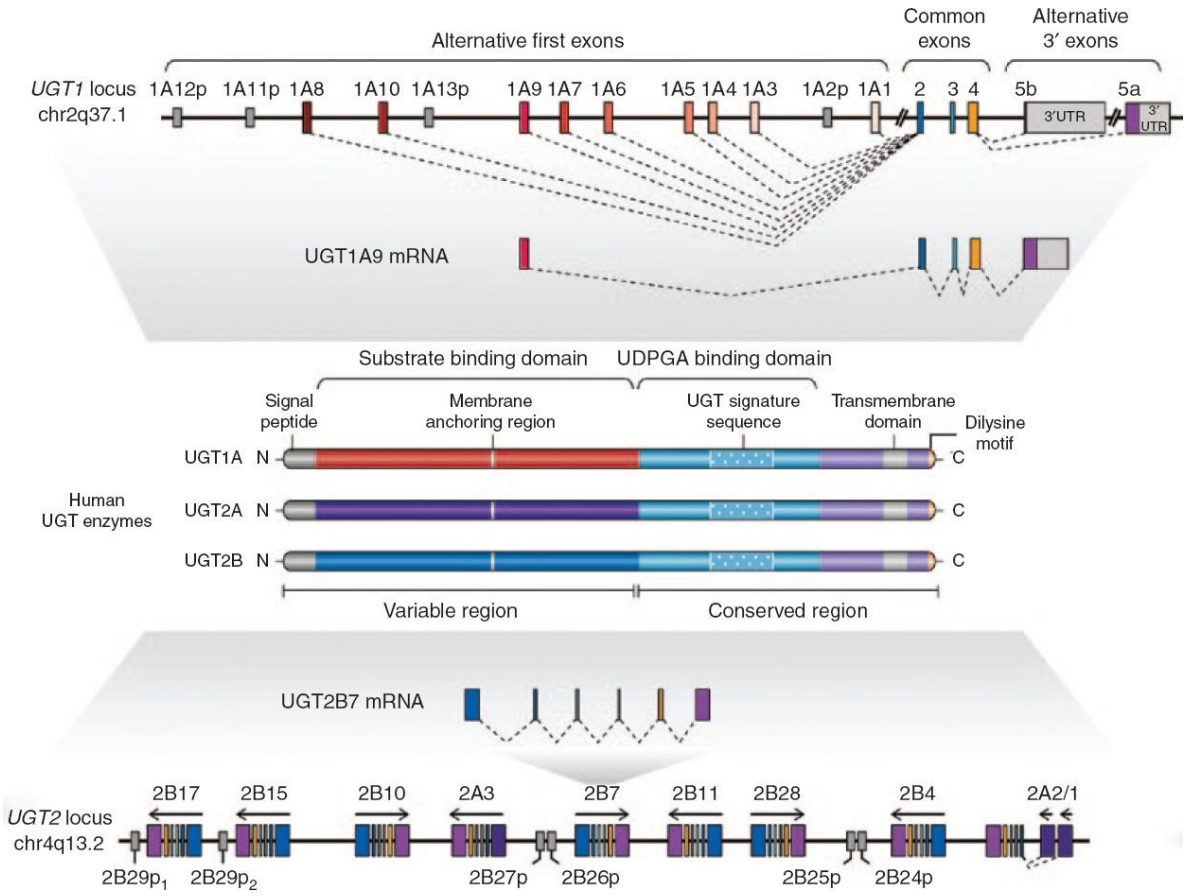

Figure 10. Structure des gènes *UGT*.
Les UGT1A sont toutes issues du même gène, codant pour neuf exons 1 mutuellement exclusifs et les exons 2-5 communs. Un événement d'épissage commun a aussi été identifié dans la partie 3' du gène, menant à la formation d'isoformes tronquées, utilisant l'exon 5b et nommées isoformes 2 ou i2. Les UGT2B sont issues de gènes distincts, issus de la duplication génique. Reproduit avec la permission du *Copyright Clearance Center, Inc. pour John Wiley and Sons CLINICAL PHARMACOLOGY & THERAPEUTICS* © (Guillemette et coll., 2014).

Bien qu'il existe un chevauchement de substrats, les enzymes UGT présentent une certaine spécificité et parfois même une régio-sélectivité (Burchell et coll., 1995; Tripathi et coll., 2013). Par exemple, la bilirubine est exclusivement métabolisée par l'enzyme UGT1A1, tandis que l'acétaminophène est glucuronidée au foie par les enzymes UGT1A1, 1A6, 1A9 et 2B4, quoique de façon prédominante par UGT1A6, ayant une affinité supérieure (Nagar et Remmel, 2006; Tripathi et coll., 2013). Par ailleurs, l'UGT2B7 catalyse préférentiellement la glucuronidation de l'estradiol en position 17 (estradiol-17-G), tandis que les autres isoenzymes, particulièrement celles de la famille UGT1A, catalysent plutôt l'ajout du sucre en position 3 (estradiol-3-G) (Lepine et coll., 2004). Le profil d'expression de ces enzymes diffère selon les tissus, et leur localisation est parfois spécifique aux types cellulaires,

comme c'est le cas dans les cellules luminales et basales de la prostate, qui n'offrent pas le même patron d'expression des enzymes UGT2B15 et 2B17 (Chouinard et coll., 2004).

Les enzymes UGT sont fortement exprimées au foie et au tractus gastro-intestinal, qui constituent la première ligne de défense contre les molécules exogènes potentiellement toxiques, alors que certaines isoenzymes affichent une expression exclusivement extrahépatique, comme c'est le cas d'UGT1A7, 1A8 et 1A10 (Nakamura et coll., 2008; Izukawa et coll., 2009). Les UGT sont aussi exprimées dans de nombreux autres organes, dont le rein, le cerveau, les voies aérodigestives, le tissu adipeux, et la peau, ainsi que dans plusieurs tissus hormono-dépendants, tels que prostate, testicule, ovaire, utérus et sein (Tchernof et coll., 1999; Luu-The et coll., 2007; Nakamura et coll., 2008; Ohno et Nakajin, 2009; Lepine et coll., 2010; Menard et coll., 2013b).

Tableau 2. Récepteurs et facteurs de transcription impliqués dans la régulation transcriptionnelle des UGT, ainsi que leurs ligands.

Récepteurs	Ligands	UGT ciblés
ERα	17β-estradiol, tamoxifène	1A4, 2B15, 2B17
AR	testostérone, dihydrotestostérone, R1881, flutamide	1A1, 1A3, 2B10, 2B11, 2B15, 2B17, 2B28
GR	cortisone, dexaméthasone	1A1
AhR	3-méthylcholanthrène, benzo[α]pyrène, bilirubine, TCCD, 12-HETE	1A1, 1A3, 1A4, 1A6, 1A7, 1A8, 1A10, 2B4
CAR	TCPOBOP, 3α,5α-androsténol, 3α,5α-androstanol, artémisinine	1A1, 2B7
FXR	acide chénodésoxycholique, acide cholique, acide désoxycholique, Z-guggulstérone	1A3, 2B4, 2B7
LXR	24(S)-hydroxycholestérol, 24(S),25-époxycholestérol	1A3
Nrf2	bilirubine, α-naphthoflavone, tert-butylhydroquinone, oltipraz	1A1, 1A6, 1A7, 1A8, 1A10, 2B7
PPARα	clofibrate, gemfibrozil, bézafibrate, GW7647, 20-HETE, 11,12-EET	1A3, 1A6, 1A9, 2B4
PPARγ	ciglitazone, troglitazone, 15-désoxy-D12,14-prostaglandine J2, GW9662	1A9
PXR	rifampicine, acide litocholique, hyperforine	1A1
VDR	25-hydroxyvitamine D3, 1,25-dihydroxyvitamine D3	2B15, 2B17

ER, récepteur aux estrogènes; AR, récepteur aux androgènes; GR, récepteur aux glucocorticoïdes; AhR, récepteur aux hydrocarbures aromatiques; CAR, récepteur constitutif aux androstanes; FXR, récepteur au farnésoïde X; LXR, récepteurs des oxystérols, Nrf2, facteur nucléaire 2; PPAR, récepteur activé par les proliférateurs du peroxysome; PXR, récepteur au prégnane X; VDR, récepteur de la vitamine D; EET, acide époxyeïcosatriènoïque; HETE, acide hydroxyeïcosatétraènoïque; TCDD, 2,3,7,8-tétrachlorodibenzo-*p*-dioxine; TCPOBOP, 1,4-bis[2-(3,5-dichloropyridyloxy)]benzène. Tiré de Hu et coll. (2014).

Plusieurs éléments de régulation génique ont été identifiés pour les UGT1A et UGT2B et impliquent notamment des récepteurs nucléaires ou biosenseurs métaboliques, tels que le récepteur aux estrogènes ER, le récepteur aux androgènes AR, le récepteur constitutif aux androstanes CAR, le récepteur au prégnane X PXR, le facteur nucléaire Nrf2, le récepteur aux hydrocarbures aromatiques AhR et les récepteurs activés par les prolifélateurs de peroxysomes PPAR (**Tableau 2**) (Hu et coll., 2014; Riches et Collier, 2015). Ainsi, la stimulation de ces récepteurs nucléaires mène à une modification de l'expression des UGT. Par exemple, il a été démontré que la stimulation des récepteurs PXR, AhR et CAR tend à faire augmenter l'expression d'UGT1A1 (Sugatani et coll., 2005; Liu et coll., 2014a; Moscovitz et coll., 2018). De plus, cette enzyme est également responsable de l'inactivation des ligands endogènes de ces récepteurs, tel que la bilirubine. On assiste donc à une boucle de rétroaction entre les niveaux des composés modifiant l'expression, et donc l'activité des UGT, puisque l'activité UGT est déterminante pour la concentration des substrats. Ce phénomène est important dans le cas d'autres substrats endogènes, puisqu'il permet de maintenir l'homéostasie cellulaire et systémique (Bock, 2012; 2015).

2.1.1. Variabilité de la voie de glucuronidation et impact clinique

Il existe une très grande variabilité interindividuelle dans l'expression et l'activité des UGT dans la population saine et en présence de néoplasie par exemple (Guillemette et coll., 2014; Stingl et coll., 2014). Puisque les enzymes UGT sont d'une importance cruciale dans le métabolisme de nombreux composés, ces variations peuvent modifier la réponse à certains médicaments (Iyer et coll., 1998; Court et coll., 2001; Ando et coll., 2002; Iyer et coll., 2002), la susceptibilité à certaines maladies, ainsi que leur évolution. Puisque les UGT sont impliquées dans l'élimination d'une vaste gamme de composés endogènes et exogènes, plusieurs groupes se sont intéressés au rôle fonctionnel de la voie UGT dans un contexte néoplasique. En effet, l'étiologie de certains cancers est associée à l'exposition à certaines molécules étant des substrats des UGT, telles que les hormones sexuelles stéroïdiennes, des contaminants environnementaux et des toxines issues de l'exposition professionnelle. Ainsi, parmi les maladies associées à une altération de la voie UGT, nous retrouvons des cancers hormono-dépendants : prostate, sein et utérus; ainsi que des cancers reliés à l'exposition à des composés toxiques, tels ceux du côlon, des voies aérodigestives, de la vessie et des poumons (Evans et Relling, 1999; Liston et coll., 2001; Guillemette, 2003; Nagar et Remmel, 2006; McGrath et coll., 2009; Pacheco et coll., 2009; Wang et coll., 2013a). Par exemple, dans le cas des cancers du côlon et du foie, il est connu

que divers composés ingérés par le biais de l'alimentation peuvent être la source de mutations génétiques carcinogènes, dont le PhIP (2-amino-1-méthyl-6-phénylimidazo[4,5-f]pyridine), une amine hétérocyclique formant des adduits à l'ADN et inactivée par les enzymes UGT1A (Nagao et coll., 1996; Ferrucci et coll., 2012; Miller et coll., 2013). Ainsi, une plus faible activité de glucuronidation causée par la présence de variations génétiques délétères, ou autres causes modifiant leur expression, pourrait entraîner une exposition accue à ces composés sur une longue période, résultant potentiellement à l'accumulation de dommages à l'ADN dus à la présence d'adduits (Reeves et coll., 2011; Jamin et coll., 2013).

En lien avec la variabilité interindividuelle de l'activité de glucuronidation, plusieurs polymorphismes génétiques ont été identifiés et expliquent une fraction de cette variabilité. Certains ont un impact sur l'expression ou l'activité de glucuronidation, tel le polymorphisme du promoteur d'UGT1A1, l'allèle *UGT1A1*28* (caractérisé par 7 répétitions TA au lieu de 6 pour l'allèle *1). Celui-ci, situé dans la boîte TATA de la région promotrice d'*UGT1A1*, entraîne une transcription moins efficace, une réduction de la quantité d'enzyme UGT1A1 au foie d'environ 50 % et une diminution de l'activité UGT1A1 hépatique de 30 à 50% (Bosma et coll., 1995; Guillemette et coll., 2000; Girard et coll., 2005). La présence de ce polymorphisme est ainsi associée à une augmentation du risque de développer un cancer colorectal, en interaction avec la consommation de viandes rouges, ainsi que du risque de développer un cancer du sein et de l'endomètre (Guillemette et coll., 2000; McGrath et coll., 2009; Jiraskova et coll., 2012). Ce variant génétique est également associé à une hyperbilirubinémie asymptomatique ou syndrome de Gilbert, causée par une diminution de la conjugaison de la bilirubine exclusivement pris en charge par l'enzyme UGT1A1 (Skierka et coll., 2013; Sticova et Jirsa, 2013; Travan et coll., 2014). Aussi, des individus porteurs de polymorphismes délétères à l'expression des UGT sont plus à risque de développer des toxicités reliées à l'utilisation de certains médicaments. Cela a notamment été observé pour l'agent anticancéreux irinotécan, utilisé dans les cas de cancers colorectaux métastatiques et autres tumeurs solides ou hématologiques, et dont une diminution de la capacité de conjugaison au foie par l'enzyme UGT1A1 cause une exposition accrue à ce métabolite toxique, entrainant une myélosuppression (neutropénies de grade 3-4) (Gagne et coll., 2002; Gao et coll., 2013; Levesque et coll., 2013; Liu et coll., 2014b; Chen et coll., 2015a).

D'autres facteurs pouvant contribuer à la variabilité interindividuelle de la voie de glucuronidation ont été identifiés, dont des processus épigénétiques. Par exemple, le statut

de méthylation des gènes *UGT* est connu pour affecter leur expression (Gagnon et coll., 2006; Belanger et coll., 2010; Oda et coll., 2014; Schioth et coll., 2016; Oeser et coll., 2018). Des études récentes font également état d'une régulation des enzymes UGT2B15 et 2B17 par des microARN, un processus qui serait associé à la progression du cancer de la prostate (Wijayakumara et coll., 2015; Margaillan et coll., 2016). La phosphorylation des enzymes UGT a également été identifiée comme nécessaire à l'activité glucuronosyltransférase, notamment pour les enzymes UGT1A1, 1A3, 1A6, 2B7 et 2B15 (Basu et coll., 2003; Basu et coll., 2005; Basu et coll., 2008; Mitra et coll., 2009; Chakraborty et coll., 2012; Riches et Collier, 2015; Xiao et coll., 2015).

Des travaux récents soutiennent également que les UGT pourraient jouer un rôle dans la résistance au traitement, notamment dans le cas des agents anticancéreux ribavarine, cytarabine et fludarabine (Gruber et coll., 2013; Zahreddine et coll., 2014). De plus, la littérature soutient que les niveaux d'expression des UGT sont altérés en présence de néoplasie, soulevant la possibilité d'une implication de ces protéines dans les modifications métaboliques survenant au niveau tumoral (Giuliani et coll., 2005; Lepine et coll., 2010; Bellemare et coll., 2011; Cengiz et coll., 2015; Lu et coll., 2015; Margaillan et coll., 2015a; Margaillan et coll., 2016; Yang et coll., 2017). En ce sens, une association entre les niveaux d'expression des UGT et la progression tumorale a été observée, notamment dans le cancer de la prostate et en leucémie lymphoïde chronique (Gruber et coll., 2013; Belledant et coll., 2016; Bhoi et coll., 2016; Li et coll., 2016). Dans les deux cas, l'expression des UGT est augmentée et associée à un mauvais pronostic, en absence de traitement pharmacologique, soulevant le fait que la surexpression de cette voie enzymatique pourrait favoriser la progression tumorale via la perturbation de métabolites oncogéniques. Cependant, les mécanismes moléculaires précis sont pour le moment peu connus.

La variabilité de cette voie métabolique entraine donc des conséquences pathologiques et pharmacologiques notables, puisque tout processus influençant la capacité de glucuronidation d'un individu a le potentiel d'influencer l'exposition à de nombreuses molécules, incluant des molécules endogènes, et d'en moduler les effets sur l'organisme. Ces processus incluent non seulement la variabilité génétique, le sexe (Gallagher et coll., 2010), l'âge (particulièrement les nouveau-nés) (Miyagi et Collier, 2007; Knibbe et coll., 2009; Zuppa et coll., 2011; Smits et coll., 2013) et les interactions médicamenteuses (Kiang et coll., 2005; Uchaipichat et coll., 2013), mais également les processus d'épissage alternatif, qui peuvent mener à une modification de la quantité d'enzymes actives produite

ou encore à la production de variants alternatifs possédant de nouvelles propriétés biologiques. Parmi ces propriétés, le laboratoire a été le premier à rapporter la capacité d'isoformes UGT issues de l'épissage alternatif à moduler négativement l'activité de l'enzyme canonique, notamment via des interactions protéines-protéines (section suivante).

2.1.2. Nouveaux évènements d'épissage et interactions protéine-protéine

L'épissage alternatif est un déterminant majeur de l'expression génique, puisqu'il permet d'une part de produire une grande diversité de protéines fonctionnellement distinctes à partir d'un nombre restreint de gènes, et d'autre part d'influencer les niveaux d'expression des différentes isoformes produites en respectant une spécificité tissulaire propre à chacune (Pineda et Bradley, 2018). Les conséquences de l'épissage alternatif sur les différents ARNm produits sont variées, parfois subtiles et indétectables, alors qu'à l'inverse, elles peuvent mener à une perte de fonction complète, à une localisation subcellulaire différente et à la production de nouvelles protéines ayant des fonctions biologiques distinctes des protéines natives (Caridi et coll., 2014; Haeusgen et coll., 2014; Tan et coll., 2014).

Notre laboratoire a découvert un nouvel exon du gène *UGT1* – identifié exon 5b en contraste avec l'exon 5 connu, renommé 5a – dans la région 3' du gène et impliqué dans un nouvel évènement d'épissage. L'utilisation de ce nouvel exon entraîne la formation de 18 nouveaux transcrits nommés v2 (exon 5b) et v3 (exons 5b-5a), possédant le même cadre de lecture et produisant 9 nouvelles protéines UGT1A de 45 kDa, nommées isoformes 2 ou i2 (**Figure 9**). Le domaine transmembranaire en C-terminal, normalement codé par l'exon 5a, est absent et remplacé par une séquence de 10 acides aminés (RKKQQSGRQM) codée par l'exon 5b. Les protéines i2 partagent la même extrémité amino-terminale que les isoformes i1, qui comprend un peptide signal, de même que des sites de liaison au substrat et au co-substrat. De plus, contrairement aux enzymes i1, les protéines alternatives i2 semblent partiellement localisée au cytoplasme en plus de leur présence au RE, probablement en raison de la délétion d'une partie du domaine transmembranaire permettant leur rétention au RE (Girard et coll., 2007; Levesque et coll., 2007).

Du point de vue enzymatique, les protéines i2 sont dépourvues d'activité transférase en présence d'UDP-GlcA en essai *in vitro* (Girard et coll., 2007; Levesque et coll., 2007). Les isoformes i2 sont détectées dans plusieurs tissus, dont le côlon, le foie, l'intestin, l'œsophage et le rein (Girard et coll., 2007; Bellemare et coll., 2011). En fait, les isoformes i2 sont co-exprimées dans les mêmes tissus et structures tissulaires que les enzymes i1

mais se retrouvent parfois seules à y être exprimées. Par exemple, l'UGT1A1_i2 est présente au rein alors que l'enzyme UGT1A1 y est absente (Levesque et coll., 2007). Lorsque les protéines i2 et les enzymes i1 sont co-exprimées dans les cellules eucaryotes, l'activité UGT est diminuée de l'ordre de 15 à 79%, dépendamment de l'enzyme et du substrat testés. Ces données suggèrent que les protéines i2 agissent comme modulateurs négatifs de l'activité de glucuronidation et ce, par interactions protéine-protéine au RE, menant à la production de complexes i1-i2 inactifs (Bellemare et coll., 2010a; Bellemare et coll., 2010b; Rouleau et coll., 2013a; Rouleau et coll., 2013b). Cette observation est en lien avec les travaux précédents de la littérature indiquant que les UGT ont la capacité d'interagir entre elles, modifiant ainsi l'activité, la régio-sélectivité ou même la spécificité des enzymes impliquées *in vitro* (Operana et Tukey, 2007; Finel et Kurkela, 2008; Ishii et coll., 2010b). D'ailleurs, la répression de l'expression endogène des formes i2 par interférence à l'ARN dans un modèle cellulaire de côlon (HT115) supporte cette notion : l'activité UGT1A est augmentée de façon significative à la suite d'une déplétion partielle (50%) de l'ensemble de protéines i2, que ce soit par répression transitoire des i2 par siRNA (Bellemare et coll., 2010c) ou de façon stable en utilisant un shRNA ciblant l'exon 5b (Rouleau et coll., 2014). Ces données supportent le rôle des protéines alternatives i2 dans la modulation de l'activité de glucuronidation effectuée par les enzymes UGT1A.

Des évènements d'épissage entraînant une troncation en C-terminal ont également été identifiés pour le gène *UGT2B7* (Menard et coll., 2013a). De façon similaire aux protéines UGT1A_i2, ces évènements d'épissage mènent aussi à une répression de l'activité des enzymes UGT2B7_i1, soutenant la capacité des protéines alternatives UGT à réguler l'activité des enzymes canoniques via des interactions protéine-protéine. Or, des travaux récents du laboratoire, utilisant l'enrichissement des ARN UGT et le séquençage à haut débit, ont identifié de nouveaux événements d'épissage des UGT (Tourancheau et coll., 2016). Les séquences des transcrits identifiées coderaient pour des protéines affichant des troncations en N- ou C-terminal, incorporant des exons supplémentaires, ou encore sautant des exons ou des parties de ceux-ci. Ces modifications dans les domaines protéiques des UGT pourraient conférer de nouvelles propriétés aux protéines alternatives, dont les répercussions sur le métabolisme cellulaire sont encore inconnues. Parmi les objectifs de la thèse, je me suis penché sur certains de ces variants alternatifs.

3. Hypothèses de recherche et objectifs

Les UGT font partie des mécanismes permettant de réguler la biodisponibilité et l'action de nombreux métabolites cellulaires. Ces mêmes voies sont impliquées dans les mécanismes de défense contre les composés d'origine exogène, c'est-à-dire la biotransformation des xénobiotiques, incluant les médicaments. Il est également reconnu que plusieurs substrats des enzymes UGT, telles les hormones thyroïdiennes et stéroïdiennes, entraînent une modification de l'expression de nombreux gènes via l'activation de récepteurs nucléaires et autres voies de signalisation, ou encore affectent les mécanismes d'épissage alternatif (Satoh et coll., 2014; Dago et coll., 2015). Or, la voie des UGT elle-même, ainsi que plusieurs autres voies métaboliques, sont régulées par les récepteurs nucléaires et autres voies de signalisation, établissant des boucles de rétroaction (Anderson et coll., 2012; Bhat-Nakshatri et coll., 2013; Hu et coll., 2014). Par exemple, Maglich et coll. (2004) ont montré que chez la souris, l'activation de CAR par une restriction calorique ou des activateurs pharmacologiques entrainait une augmentation de l'expression des enzymes ugt1a1, sult1a1 et sult2a1, causant une diminution des niveaux d'hormones thyroïdiennes circulantes, alors que des spécimens CAR double délétant ($CAR^{-/-}$) conservaient des niveaux faibles de ces enzymes et des concentrations élevées d'hormones thyroïdiennes. Or, la perte de poids de ces souris $CAR^{-/-}$ suite à une restriction calorique était deux fois plus importante que celle des souris contrôles non délétées en raison des niveaux élevés d'hormones thyroïdiennes. Ce phénomène est d'autant plus intéressant considérant que les hormones thyroïdiennes régulent positivement l'expression de CAR (Bing et coll., 2014). Ces boucles de régulation soulèvent ainsi la possibilité que la perturbation de la voie des UGT puisse avoir de conséquences plus étendues que celles de contrôler les concentrations intracellulaires des substrats de ces enzymes. **Une première hypothèse de recherche** stipule que la modulation de l'expression des UGT mènerait à des perturbations métaboliques au-delà des substrats de ces enzymes.

Le métabolisme cellulaire est également modifié de façon importante par diverses conditions pathologiques telles que le cancer, une condition impliquant un remodelage important des programmes d'expression et d'épissage des gènes et ayant une influence importante sur les concentrations cellulaires d'une multitude de métabolites (Chen et Weiss, 2015). Par exemple, ces modifications métaboliques entrainent souvent un avantage prolifératif pour les cellules cancéreuses, permettant une synthèse accrue de constituants cellulaires (discuté en introduction) (Oltean et Bates, 2014; de Alteriis et coll., 2018). À ce

jour, peu d'études se sont intéressées à l'implication potentielle de la voie des UGT dans la progression tumorale, bien que leur rôle dans le métabolisme de plusieurs traitements anticancéreux et d'oncométabolites ait été démontré par différents groupes (Lien et coll., 1989; Innocenti et coll., 2001; Wen et coll., 2007; Balliet et coll., 2009; Peer et coll., 2012; Wang et coll., 2013b). Plusieurs évidences, dont certaines issues des travaux précédents du laboratoire, suggèrent que la voie des UGT est perturbée soit à la hausse ou à la baisse dans plusieurs types de cancer et ce, en fonction du type histologique et du stade d'évolution de la maladie (Giuliani et coll., 2005; Lepine et coll., 2010; Bellemare et coll., 2011; Nadeau et coll., 2011; Gruber et coll., 2013; Lu et coll., 2015; Margaillan et coll., 2015a; Belledant et coll., 2016; Tourancheau et coll., 2016; Yang et coll., 2017), ainsi que suite au traitement pharmacologique (Gruber et coll., 2013; Zahreddine et coll., 2014).

De par leur rôle clé dans le maintien de l'homéostasie cellulaire, et suite à divers stimuli, il est possible que des changements dans l'expression des UGT entrainent des modifications métaboliques en faveur (ou défaveur) de la progression tumorale et de la résistance aux agents anticancéreux. Ces métabolites pourraient être des substrats des UGT, mais ceux-ci pourraient également être issus d'autres voies métaboliques. Cette notion est soutenue par les travaux précédents du laboratoire indiquant un rôle de perturbateur métabolique pour certaines protéines alternatives dérivées des gènes *UGT* humains, qui semblent interagir non seulement avec les enzymes UGT pour en moduler l'activité, mais également avec des protéines d'autres voies métaboliques. En effet, une première étude montre que les isoformes alternatives du gène *UGT1A*, les protéines UGT1A_i2, modulent l'activité de la voie de défense contre les espèces oxygénées réactives (ROS) en interagissant avec l'enzyme catalase (Rouleau et coll., 2014). Cette capacité des UGT à interagir via des interactions protéine-protéine est soutenue par quelques observations d'autres groupes démontrant que les enzymes UGT interagissent avec d'autres enzymes de la biotransformation des xénobiotiques, telles que les CYP, entraînant une modification de l'activité de ces partenaires *in vitro* (Taura et coll., 2000; Fremont et coll., 2005; Ishii et coll., 2007; Fujiwara et Itoh, 2014; Ishii et coll., 2014; Nakamura et coll., 2016). Ces notions appuient la première hypothèse et en soulèvent une **seconde**, stipulant que les enzymes et les protéines alternatives UGT puissent faire partie de réseaux d'interactions protéiques, possiblement distincts en partie l'un de l'autre, entrainant des modifications significatives du métabolisme cellulaire dans certains contextes. D'ailleurs, les travaux du laboratoire montrent que les variants alternatifs possèdent des structures protéiques différentes :

certains variants ont des domaines protéiques tronqués, alors que d'autres présentent de nouvelles séquences peptidiques tout en conservant les principaux domaines caractéristiques d'une enzyme UGT (Tourancheau et coll., 2016). Ces différences pourraient permettre une localisation cellulaire distincte et un réseau d'interaction divergent, entrainant des conséquences métaboliques propres à chacune des protéines UGT. D'autre part, ces changements du métabolisme sont susceptibles d'entraîner des modifications phénotypiques au niveau cellulaire, notamment dans un contexte tumoral et possiblement dans la physiologie normale de la cellule. Cette **troisième hypothèse** a également constitué l'objet de nos travaux.

En lien avec ces hypothèses, **nos objectifs étaient :**

1) Étudier les changements métaboliques associés à une modification de la voie des UGT, incluant des enzymes parmi les plus caractérisées et abondantes, ainsi que de nouvelles protéines alternatives, dont le rôle est moins bien connu;

2) Établir le réseau d'interaction protéique, ou l'interactome, des protéines UGT;

3) Caractériser les effets potentiels d'une modification de l'expression des UGT sur le phénotype cellulaire, au-delà de la perturbation de l'activité de glucuronidation.

4. Méthodologie et importance des articles dans la démarche scientifique

L'étude approfondie du métabolisme global, ou métabolome, est rendue possible par l'émergence d'outils de métabolomique, qui permettent la quantification simultanée d'une grande quantité de métabolites. Bien entendu, les différentes approches et méthodes pour l'étude des métabolites endogènes produits par le corps humain et présents dans les cellules, tissus et fluides corporels comportent des avantages et inconvénients (**Tableau 3**). En lien avec le premier objectif du projet, qui visait à détailler de façon systématique les perturbations métaboliques associées aux UGT, la métabolomique non-ciblée par spectrométrie de masse a été retenue. Cette approche a mené à l'identification et la quantification de métabolites intracellulaires dans différents modèles *in vitro*. Ce choix méthodologique constitue une approche novatrice dans le domaine, puisqu'aucune étude n'a rapporté les conséquences métaboliques globales d'une modification de l'expression des UGT. Les études actuelles portent essentiellement sur des classes de molécules

précises souvent reconnues pour être des substrats des UGT (Harrington et coll., 2006; Richardson et Klaassen, 2010; Chen et coll., 2017; Zhou et coll., 2017).

Tableau 3. Sommaires des avantages et inconvénients des principales approches utilisées pour l'analyse de métabolites lors d'études métabolomiques.

	Avantages	Désavantages
Approches		
Métabolomique ciblée	- Permet la quantification absolue des métabolites - L'identité des métabolites détectés est connue	- Nombre relativement restreint de métabolites investigués, selon la méthode
Métabolomique non-ciblée	- Grande quantité de métabolites détectés	- Quantification relative des métabolites - Comporte souvent beaucoup de métabolites inconnus - Base de données de référence variable entre les laboratoires
Techniques		
Chromatographie liquide (LC) couplée à la spectrométrie de masse en tandem (MS/MS)	- Nécessite peu ou pas de modifications chimiques (ex. dérivatisation) des métabolites pré-analyse - Détecte une très grande quantité des molécules - Sensibilité généralement supérieure à la GC et au RMN ^{1}H	- Nécessite souvent la préparation de l'échantillon pré-chromatographie (précipitation des protéines, extraction liquide-liquide ou sur colonne) - Susceptible à la suppression du signal par la matrice - Méthode de séparation chromatographique simple ou complexe à temps variable
Chromatographie gazeuse (GC) couplée à la MS/MS	- Signal plus stable dans le temps - Résolution supérieure à la LC - Mieux adaptée pour les molécules volatiles et non-polaires	- Nécessite souvent la préparation de l'échantillon pré-chromatographie (précipitation des protéines, extraction liquide-liquide ou sur colonne) - Nécessite souvent la dérivatisation de molécules non-volatiles - Sensibilité parfois inférieure à la LC-MS/MS dépendant de la molécule -Ne permet pas l'analyse d'échantillons à très haut débit
Résonance magnétique nucléaire du proton (RMN ^{1}H)	- Ne détruit pas l'échantillon - Détecte et quantifie les métabolites simultanément - Nécessite peu de préparation de l'échantillon	- Sensibilité inférieure à la MS - Temps d'acquisition et d'analyse plus long que la MS - Spectrogrammes complexes - Appareillage très couteux

Afin de questionner l'effet d'une perturbation de la voie des UGT sur le métabolome et le phénotype cellulaire, nous avons opté pour l'étude de modèles cellulaires. Cette approche nous est d'abord apparue nécessaire afin de caractériser les effets plus spécifiques aux protéines UGT (enzymes versus protéines alternatives) dans des modèles cellulaires reconnus du domaine, avant de pouvoir l'étudier éventuellement à un niveau plus complexe *in vivo*. Dans un premier temps, la lignée HEK293, dérivée de rein humain embryonnaire et dépourvue d'expression UGT, a été utilisée. Des lignées stables exprimant les enzymes UGT1A1 et UGT2B7 ont été créées puisque ces isoenzymes possèdent toutes deux une grande diversité de substrats et qu'elles représentent une proportion importante des transcrits et protéines UGT exprimés dans les principaux organes du métabolisme des médicaments (Guillemette et coll., 2014). Parallèlement, des lignées exprimant les variants alternatifs de ces enzymes ont également été investiguées et ce, afin de discerner, par métabolomique non ciblée, les effets potentiels des enzymes de ceux des protéines alternatives sur le métabolisme cellulaire. Ces travaux se trouvent dans le Chapitre 2, intitulé « **Glucuronosyltransferase protein expression alters cellular metabolome** ». Cette étude est la première à rapporter une perturbation significative du métabolisme global de la cellule en présence d'une expression accrue d'enzymes et de protéines UGT humaines. Les voies perturbées se sont avérées plus vastes que celles anticipées, puisqu'elles s'étendent à des molécules qui ne sont probablement pas toutes des substrats des UGT, incluant plusieurs classes de lipides, des acides aminés, des acides nucléiques et des intermédiaires de la glycolyse et du cycle des acides tricarboxyliques.

Il a été observé par immunohistochimie dans une étude précédente que l'expression des protéines alternatives UGT1A_i2 était diminuée dans une proportion importante de tumeurs de cancer du côlon comparativement au tissu péritumoral normal (Bellemare et coll., 2011). Afin de mimer cette répression, nous avons utilisé une lignée cellulaire de cancer du côlon exprimant de façon endogène les produits du gène *UGT1A*. Le modèle cellulaire HT115 a été sélectionné car celui-ci exprime les protéines alternatives UGT1A de manière significative, en plus d'afficher un ratio d'expression enzyme/protéine alternative similaire à celui observé dans les tissus humains. Nous avons ainsi établi une lignée stable dont les protéines alternatives UGT1A ont été réprimées par interférence à l'ARN, via des courts ARN en forme d'épingle à cheveux (shRNA) dirigés contre la séquence spécifique à ces variants. Une répression stable de 90% de l'expression protéique a été obtenue pour ce modèle cellulaire. Pour cette étude, nos travaux se sont portés sur la caractérisation du

métabolome (obj.1), en plus de s'intéresser à l'interaction avec un nouveau partenaire protéique de la voie de la glycolyse, fréquemment perturbée en cancer (obj.2), et aux conséquences de la répression des UGT1A alternatives sur le phénotype cellulaire (obj.3). Les résultats de ces travaux sont présentés au Chapitre 4, intitulé « **Cross-talk between alternatively spliced UGT1A isoforms and colon cancer cell metabolism** ». Ces travaux sont novateurs car ils présentent les premières évidences d'une interrelation entre le métabolisme cellulaire et les protéines alternatives UGT dans un contexte néoplasique.

Avec ces premières évidences appuyant l'hypothèse des réseaux d'interactions protéiques et afin de répondre plus particulièrement au deuxième objectif, l'interactome des UGT dans les principaux tissus dans lesquels ces protéines sont abondantes a été caractérisé. La plupart des études favorisent une approche méthodologique basée sur l'expression de protéines étiquettes afin d'élucider ces réseaux d'interaction. Cette approche est notamment limitée par l'utilisation d'un type cellulaire en particulier et une expression exogène de la protéine d'intérêt dont la séquence a été modifiée par l'ajout d'un peptide étiquette.

Dans un contexte physiologique, les tissus, de même que les cellules qui les composent, présentent des profils d'expression protéique distincts afin d'assurer les fonctions biologiques qui leurs sont propres. Or, ces fonctions complexes sont soutenues par des réseaux d'interactions protéiques fonctionnels dont les composantes dépendent de l'environnement protéique, c'est-à-dire l'identité et l'abondance des protéines. Ces réseaux constituent l'interactome endogène. Ainsi, afin de valider notre hypothèse, nous avons favorisé une approche basée sur l'interactome endogène tissulaire plutôt que celui d'un type cellulaire en particulier. Nous avons utilisé un anticorps dirigé contre les protéines UGT par opposition à l'expression d'une protéine UGT couplée à un peptide étiquette. L'approche favorisée offre l'avantage de pouvoir étudier l'interactome de façon non-biaisée dans un environnement protéique physiologique où les différentes protéines sont exprimées à des niveaux physiologiques; en opposition avec l'autre méthode. L'utilisation d'un ensemble de tissus (*pool*) provenant de divers individus offre aussi la possibilité de s'affranchir des variances interindividuelles associées à l'expression des partenaires potentiels des UGT.

L'amélioration des outils moléculaires, de bio-informatique et de spectrométrie de masse ont mené à une progression rapide de la protéomique dans les dernières années, permettant la caractérisation systématique de réseaux d'interactions protéiques. Différentes techniques permettent d'étudier les interactions protéiques **(Tableau 4)**. Au moment où mes

travaux ont été entrepris, la purification d'affinité sur bille couplée à la spectrométrie de masse était la méthode la plus adaptée pour caractériser de façon non-ciblée un interactome endogène tel celui des UGT. Cette méthode à haut débit permet l'identification de plusieurs partenaires de façon simultanée, une approche qui se distingue de celles utilisées par les quelques groupes ayant étudié les interactions protéiques des UGT. De plus, ces auteurs ont exploré les interactions potentielles de façon individuelle, c'est-à-dire un partenaire à la fois (Taura et coll., 2000; Ghosh et coll., 2001; Fremont et coll., 2005; Ishii et coll., 2007; Operana et Tukey, 2007; Ishii et coll., 2014). Notre approche est donc non biaisée et s'effectue dans un contexte physiologique.

N'utilisant pas de protéines de fusion ou d'étiquettes peptidiques, l'étude de l'interactome endogène est cependant limitée par la spécificité des anticorps, une limite significative dans le domaine. En effet, l'obtention d'un anticorps spécifique représente un défi de taille pour les UGT puisque ces protéines présentent une très forte homologie de séquence, dépassant les 97% pour les membres d'une même sous-famille et partageant plus de 50% d'homologie entre les familles *UGT1* et *UGT2* (Nair et coll., 2015; Tourancheau et coll., 2016). Peu d'anticorps sont disponibles commercialement et s'ils le sont, leur caractérisation est souvent très minimale. Dans le cas des protéines alternatives, aucun anticorps n'est disponible commercialement. De plus, pour les isoformes alternatives et les enzymes dérivées du gène *UGT1*, qui ont fait l'objet de notre étude, seulement la séquence issue de l'exon terminal diffère et permet de distinguer les enzymes des protéines alternatives. Pour les enzymes, une séquence codant pour 95 résidus situés en C-terminal a permis la création d'un peptide immunogène dans cette région et de produire un anticorps spécifique, reconnaissant seulement les enzymes UGT1A (Bellemare et coll., 2011). Celui-ci est spécifique aux enzymes UGT1A et ne reconnaît pas les enzymes UGT2B. De façon similaire, un anticorps ciblant une séquence immunogène issue des 10 peptides distinguant les protéines alternatives UGT1A_i2 a été créé. Celui-ci est spécifique aux protéines alternatives et ne reconnaît pas les enzymes UGT1A (Bellemare et coll., 2010c).

Ces anticorps ont été utilisés pour identifier les partenaires endogènes des enzymes et protéines alternatives UGT1A dans des extraits dérivés de plusieurs individus provenant des principaux organes dans lesquels ces protéines sont abondantes, soit le foie, le rein et l'intestin. Certains de ces partenariats ont ensuite été validés dans des modèles cellulaires exprimant les UGT1A et leurs partenaires. Ces travaux sont présentés au Chapitre 3: « **Endogenous protein interactome of human UDP-glucuronosyltransferases exposed**

by untargeted proteomics ». Ce travail porte sur les enzymes UGT1A alors que l'interactome de leurs protéines alternatives est présenté au Chapitre 4. Ces travaux ont mis en lumière l'étendu de l'interactome des enzymes et protéines alternatives dérivés du gène *UGT1*, identifiant non seulement des partenaires impliqués dans la fonction de détoxication tout comme les UGT, mais également dans plusieurs autres voies métaboliques, incluant la glycolyse, la gluconéogenèse et le métabolisme des lipides, dont plusieurs sont perturbées en présence de cancer, tel que discuté en introduction.

S'appuyant sur les modifications métaboliques observées et l'interactome des UGT, nous avons par la suite caractérisé les répercussions phénotypiques d'une modification de l'expression des UGT et ce, en lien avec l'objectif 3 et dans un contexte de cancer. En effet, la littérature soutient que les modifications métaboliques, tout comme les interactions protéiques, influencent le phénotype cellulaire, dont la prolifération et la migration cellulaires, l'activité énergétique, etc., et que ces mécanismes permettent à la cellule cancéreuse de s'adapter, de proliférer et de se propager (Xu et coll., 2011; Granata et coll., 2014; Yang et coll., 2014b; Chen et coll., 2015b; Hussain et coll., 2016; Park et coll., 2016; Andrzejewski et coll., 2017; Yan et coll., 2017; Zhao et coll., 2018). Les essais fonctionnels ont été menés en utilisant différents essais cellulaires courants en laboratoire, notamment des essais de prolifération cellulaire, adhésion cellulaire et un suivi en temps réel des flux métaboliques. Les résultats de ces travaux de recherche sont présentés dans les chapitres suivants, dans une séquence permettant de reconnaître des fonctions cellulaires additionnelles possibles aux protéines UGT, au-delà de leur activité enzymatique utilisant le co-substrat UDP-GlcA.

Tableau 4. Description des différentes méthodes disponibles pour l'étude des interactomes protéiques.

Approche et brève description	Avantages et inconvénients
Purification d'affinité Immunoprécipitation et purification de l'appât et de ses partenaires avec un anticorps. Les protéines immuno-précipitées sont ensuite digérées et analysées par spectrométrie de masse.	- Technique à haut débit - Ne nécessite pas de modifier génétiquement la cible - Artéfacts possibles dus à la spécificité de l'anticorps et/ou la lyse des cellules - Détecte seulement les interactions robustes
Étiquetage protéique dépendant de la proximité Ajout d'un marqueur, telle la biotine, sur les protéines à proximité de l'appât (par ex. BioID). Les protéines ainsi marquées sont enrichies grâce à une purification utilisant la streptavidine couplée à un support solide. Les protéines sont ensuite digérées et analysées par spectrométrie de masse.	- Technique à haut débit - Détecte les interactions faibles/transitoires - Permet d'inférer la localisation cellulaire - Ne discrimine pas les interactions directes et indirectes - Nécessite la création d'un appât fusionné à une autre enzyme - Ne peut être utilisé que dans des modèles cellulaires

Essai de ligation dépendant de la proximité Utilisation d'anticorps secondaires, couplés à des amorces, qui reconnaissent des anticorps primaires dirigés contre l'appât et son partenaire. Lorsqu'en forte proximité, les amorces permettent l'amplification d'un brin d'ADN, détecté via des sondes fluorescentes.	- Permet de visualiser l'interaction des partenaires protéiques par microscopie - Technique à faible débit - Nécessite des anticorps très spécifiques, telles les anti-étiquettes peptidiques
Résonance de la fluorescence par transfert d'énergie Stimulation photonique d'un fluorochrome couplé à l'appât, qui par proximité transfert son énergie au fluorochrome du partenaire, possédant une longueur d'onde d'émission différente	- Permet de visualiser la localisation des partenaires protéiques par microscopie - Technique à faible débit - Nécessite l'utilisation de modèles cellulaires spécifiques aux partenaires étudiés

Adapté de Che et Khavari (2017)

Toujours en lien avec l'objectif 3, et supportant un rôle plus étendu des UGT, nous avons caractérisé les répercussions phénotypiques issues d'une modification de l'expression d'autres types de variants alternatifs. Ainsi, nous avons investigué les protéines alternatives d'UGT2B10 représentant une proportion appréciable du transcriptome du gène UGT2B10 au foie, atteignant les 50%. Les protéines variantes d'UGT2B10 présentent une insertion d'exon, à l'intérieur du cadre de lecture, dans la section terminale du transcrit. L'ajout de tels segments peptidiques, correspondants à 10 et 65 acides aminés pour les protéines alternatives isoformes 4 et 5 dérivés du gène *UGT2B10*, pourraient conférer de nouvelles propriétés biologiques. Ceux-ci se situent à proximité du domaine de liaison au co-substrat et des peptides signalétiques permettant la rétention de la protéine au réticulum endoplasmique. Ces travaux sont présentés au Chapitre 5, intitulé « **Posttranscriptional regulation of UGT2B10 hepatic expression and activity by alternative splicing** ». Les données ont révélé une interaction entre l'enzyme UGT2B10 et ses protéines alternatives (obj.2), dont l'expression entraine des répercussions significatives qui semblent dépendre du type cellulaire (obj.3). De plus, ces travaux ont permis de mettre à jour une induction différentielle de l'expression des transcrits alternatifs au détriment de l'expression de l'enzyme à la suite d'un traitement pharmacologique, influençant possiblement la capacité métabolique cellulaire en réponse à des stimuli.

L'implication de ces travaux novateurs dans le domaine est significative considérant que plusieurs autres protéines alternatives UGT, découvertes par le laboratoire (Tourancheau et coll., 2016; Tourancheau et coll., 2018), pourraient comporter des fonctions similaires ou divergentes à celles observées pour les variants étudiés dans cette thèse. La découverte d'une diversité importante d'isoformes UGT s'appuie sur l'utilisation du séquençage à haut débit, qui a permis de quantifier l'ensemble des transcrits UGT (transcriptome des UGT),

incluant ceux présents en moindre abondance. Ces travaux s'appuient également sur un travail précédent réalisé par le laboratoire, qui avait comme objectif de reconstruire le transcriptome des principaux tissus métaboliques (foie, rein, côlon et intestin) à partir de séquençage ciblé. La technique utilisée a également permis de produire des lectures de séquences plus longues (de 450 nucléotides en moyenne), permettant un meilleur alignement des séquences et la construction des transcrits hautement homologues dérivés des gènes *UGT*. Une approche similaire avait été utilisée pour les gènes d'histocompatibilité *HLA*, partageant aussi un très haut degré d'homologie et étant l'objet de nombreux évènements d'épissage alternatif (Bentley et coll., 2009). Ces travaux, présentés au Chapitre 6 et intitulés « **Divergent Expression and Metabolic Functions of Human Glucuronosyltransferases through Alternative Splicing** », présentent l'étendue du transcriptome alternatif *UGT* humain, en plus d'explorer les conséquences d'une expression de variants alternatifs sur le métabolisme cellulaire (obj.1) et les modifications du phénotype (obj.3) en lien avec les objectifs de la thèse. Ce travail met également en lumière la nécessité de poursuivre ces recherches, car peu d'UGT alternatifs ont été caractérisés à ce jour, malgré la contribution significative des travaux de cette thèse.

Chapitre 2 : « Glucuronosyltransferase protein expression alters cellular metabolome »

Résumé

Les UGT sont des enzymes ubiquitaires essentielles à l'homéostasie de nombreuses molécules endogènes. Nos travaux récents ont révélé un transcriptome étendu et un interactome complexe pour les protéines UGT humaines, supportant leur potentielle connexion avec le métabolisme cellulaire. Nous avons utilisé une approche métabolomique non-ciblée pour investiguer les changements métaboliques associés à l'expression des UGT. Les enzymes UGT1A1 et UGT2B7 ont été étudiées, toutes deux abondantes au foie et démontrant une grande diversité de substrat. Leurs protéines alternatives dérivées de l'épissage, présentant des différences structurelles majeures et possédant de nouvelles séquences peptidiques dans le cadre de lecture, ont aussi été exprimées de façon stable dans des cellules UGT-négatives. Un total de 615 métabolites de toutes classes a été quantifié dans les lysats cellulaires. Nous avons observé des profils métaboliques divergents entre les isoformes UGT, ainsi que des changements dans les concentrations de métabolites n'étant pas des substrats des UGT. Près de 20 sentiers métaboliques sont modifiés par l'expression des enzymes UGT, incluant des glucides, des acides nucléiques et des lipides. Des précurseurs du co-substrat UDP-GlcA sont altérés dans ces cellules, appartenant notamment à la glycolyse et la voie de synthèse des pyrimidines. De plus, des lipides bioactifs tels que l'acide arachidonique et des endocannabinoïdes sont grandement enrichis, jusqu'à 13.3 fois plus élevés ($P < 0.01$). Les protéines UGT2B7 induisent des modifications significatives dans les intermédiaires de la voie de la créatine, tandis que l'expression des protéines UGT1A promeut l'accumulation de métabolites en amont de complexe OGDC, notamment des métabolites des acides aminés à branche ramifiée et du cycle des acides tricarboxyliques. Ces changements sont plus importants pour la protéine alternative UGT1A1, qui interagit avec OGDHL, une sous-unité du complexe OGDC. Cette étude élargit nos connaissances des voies métaboliques associées à l'expression et à l'activité des UGT, supportant une vaste connexion entre la voie de glucuronidation et les autres voies métaboliques.

ORIGINAL ARTICLE IN PREPARATION FOR PUBLICATION

Glucuronosyltransferase protein expression alters cellular metabolome

Yannick Audet-Delage[1], Michèle Rouleau[1], Lyne Villeneuve[1], Chantal Guillemette[1,2]

[1]Pharmacogenomics Laboratory, Centre Hospitalier Universitaire (CHU) de Québec Research Center and Faculty of Pharmacy, Laval University, Québec, Canada.

[2]Canada Research Chair in Pharmacogenomics

Corresponding author:

Chantal Guillemette, Ph.D. Canada Research Chair in Pharmacogenomics

CHU de Québec Research Center, R4720, 2705 Boul. Laurier, Québec, Canada, G1V 4G2

Phone: (418) 654-2296

Email: chantal.guillemette@crchudequebec.ulaval.ca

Running title: Cellular metabolome associated with UGT

Word count:

Abstract: 250

Intro: 582

MM: 1096

Results: 1354

Discussion: 1104

Table: 1

Figures: 6

Supplementary material: 2 tables, 1 figure

Context

- UGTs are ubiquitous enzymes central to homeostasis of endobiotics
- Their regulation through a variety of mechanisms allows a response to cellular signals and environmental changes
- We hypothesized that UGT expression affects other cellular pathways and has consequences on the cellular metabolome

Highlights

- Untargeted metabolomics exposed 19 biochemical pathways perturbed by UGT1A1 and UGT2B7 expression.
- Cellular concentrations of nucleotide sugar precursors, pyrimidine nucleosides as well as bioactive lipids were significantly changed.
- Divergent metabolic alterations were noted between UGT isoforms.
- Findings expand our knowledge of biochemical changes beyond known substrates associated with UGT expression and highlight a broad connectivity with cell metabolism.

Abstract

Nucleotide sugar-dependent glucuronosyltransferases (UGTs) are ubiquitous enzymes critical to the homeostasis of numerous endogenous metabolites and xenobiotics detoxification. Our recent investigations revealed complex transcriptome and interactome landscapes for human UGTs, potentially expanding their connectivity to cell metabolism. Non-targeted metabolomics was applied to portray metabolic changes caused by UGT expression. We studied the abundant hepatic bilirubin-conjugating UGT1A1 and UGT2B7 enzymes, exhibiting broad substrate specificity. Their alternative (alt.) splicing-derived isoforms showing major structural differences and novel in-frame sequences were also stably expressed in UGT-negative cells. A total of 615 metabolites from all major metabolite classes were quantified in cell lysates. Divergent metabolic profiles were noted between UGT isoforms and changes in levels of metabolites were observed beyond known UGT substrates. Nearly 20 biochemical routes were modified by UGT enzyme expression, including carbohydrates, nucleic acids and lipids. Precursors of the co-substrate UDP-glucuronic acid (UDP-GlcA) were changed, with significant variations in glycolysis and pyrimidine pathways. Bioactive lipids such as arachidonic acid and endocannabinoids were also highly enriched in these cells, up to 13.3-fold ($P < 0.01$). For UGT2B7 proteins, significant variations for creatine pathway metabolites were observed. In contrast, UGT1A1 proteins promoted the accumulation of metabolites upstream of the mitochondrial oxoglutarate dehydrogenase complex (OGDC), namely branched-chain amino acids (BCAA) and tricarboxylic acid cycle (TCA) metabolites. These changes were more pronounced for alt. UGT1A1, which interacts with the OGDC component OGDHL. This study expands our knowledge of biochemical pathways associated with UGT expression and supports an extensive connectivity between UGTs and other cellular metabolic processes.

Introduction

Maintenance of cellular homeostasis relies on a variety of biosynthetic and catabolic pathways, and involves a plethora of biomolecules. The glucuronidation pathway is one of these key metabolic processes that participate in the regulation of bioactive molecules, inactivating them through the addition of glucuronic acid, a sugar moiety derived from the co-substrate UDP-glucuronic acid (UDP-GlcA) (1). This metabolic reaction is catalyzed by uridine diphospho-glucuronosyltransferases (UGT) and leads to an increase polarity of the aglycone, promoting excretion of the glucuronide product through bile and urine (1, 2). UGT enzymes are involved in the elimination of drugs from all classes, toxins and other xenobiotics disturbing various cellular processes. Endobiotics from diverse metabolic routes participating in a variety of cellular processes are also inactivated by UGTs, including bilirubin (the product of heme catabolism), neurotransmitters such as serotonin, as well as steroid and thyroid hormones and various bioactive lipids (3).

Our knowledge of transcriptional, translational and post-translational regulation of UGT metabolism is constantly expanding (1, 4-6). Many endobiotic UGT substrates are involved in signal transduction pathways that control key transcription factors acting as major regulators of gene expression programs (3, 6). This mechanism is primary used by cells to control its metabolic state by modulating expression levels of enzyme-coding genes including UGTs, which allows to respond to signals and environmental changes (3). Allosteric regulation by small molecules as control loops as well as by protein interactions resulting namely in conformational changes also affect UGT functions (7-11). Biochemical studies further support that homomeric and heteromeric UGT-UGT interactions can modulate the substrate selectivity of a UGT enzyme as well as catalytic rates of a variety of glucuronidation reactions (12). Our recent examination of the endogenous UGT interactome in human tissues further exposed the ability of UGT to interact with other enzymatic systems such as cytochromes P450 and dehydrogenases as well as enzymes related to bioenergetics and lipid metabolism (1, 13, 14). Alternative splicing has recently emerged as another key process involved in the regulation of UGT expression and activity (14-18). A comprehensive quantification of the UGT transcriptome based on high-throughput RNA sequencing identified over 130 diverse novel UGT variants with nearly a fifth comprising in-frame sequences that may create distinct structural and functional features (15, 19). According to functional assays, some of these alternate (alt.) UGT isoforms were found to inhibit or induce glucuronidation activity. Moreover, alt. UGT1A isoforms were found to

interact with various protein partners, perhaps partially distinct from those of UGT enzymes (1, 13, 14). However, the contribution of UGT network connectivity on the cell metabolome remains unclear, as is the role that these complexes may play in regulating the bioavailability of endobiotics.

We hypothesized that a potential functional interplay between UGTs and other cellular pathways has consequences on the cellular metabolome, possibly beyond the control of metabolites known as UGT substrates. To examine changes in intracellular metabolite concentrations induced by UGT expression, we used non-targeted metabolomics and stably expressed selected human UGT proteins in a UGT-negative mammalian cell model, the human kidney cell line HEK293. We focused on two of the most studied UGT enzymes, the bilirubin-conjugating enzyme UGT1A1 and UGT2B7 exhibiting broad substrate specificity. We also included their alternative isoforms exhibiting major structural differences and novel in-frame sequences, namely the shorter UGT1A1 protein with an in-frame C-terminal sequence UGT1A1_i2, and the longer UGT2B7 protein with an internal in-frame peptide sequence, UGT2B7_i8 (**Fig.1**) (17, 19). Our findings expand knowledge of biochemical changes associated with UGT expression and highlight an important connectivity with cell metabolism.

Materials and Methods

Cell culture and metabolomics

HEK293 were cultured in standard conditions, i.e. DMEM medium with 4.5 g/L glucose, 2 mM glutamine, 1 mM sodium pyruvate, 10% fetal bovine serum, as well as 100 IU penicillin and 100 µg/mL streptamycin. Cells stably expressing the UGT1A1 enzyme, its alternative isoform UGT1A1_i2, the UGT2B7 enzyme, its alternative isoform UGT2B7_i8 or the parental plasmid vector as a control were generated as described (15, 17). Protein expression was maintained using appropriate selection antibiotics supplemented to culture media, i.e. G418 (1 mg/mL, Life Technologies Inc., Burlington, ON, Canada) or blasticidin (10 mg/mL, Wisent Bioproducts, St-Bruno, QC, Canada). For metabolomics analyses, cell pellets (10-15x10^6 cells) were rinsed with 1 mL ice-cold PBS and centrifuged (5 minutes, 525 *xg*), flash-frozen on dry ice, then stored at -80°C until shipment to Metabolon (Morrisville, NC, USA). Five biological replicates were prepared for each cell model. Metabolomics profiling was conducted by Metabolon Inc. based on ultra-high-performance liquid chromatography-mass spectrometry (UPLC-MS/MS) (20). Proteins were removed from samples by methanol-

induced precipitation and centrifugation. Each sample extract was divided into five fractions for analyses using four methods: two for analysis by two separate reverse phase (RP)/UPLC-MS/MS methods with different solvent gradients and analyzed in positive ion mode electrospray ionization (ESI), one for analysis by RP/UPLC-MS/MS with negative ion mode ESI, one for analysis by hydrophilic interaction chromatography (HILIC) UPLC-MS/MS with negative ion mode ESI, and one sample was reserved for backup. Several types of controls were analyzed in concert with the experimental samples. Each reconstitution solvent contained a series of standards at fixed concentrations to ensure injection and chromatographic consistency. Raw data was extracted, peak-identified and QC processed using Metabolon's hardware and software. Compounds were identified by comparison to library entries of purified standards or recurrent unknown entities. Data were normalized for protein concentration and log-transformed before being subjected to the analysis of variance (ANOVA). Metabolites displaying a *P*-value under 0.05 were considered significant.

UGT enzymatic assays

Cellular extracts enriched in endoplasmic reticulum membranes (i.e. microsomes) were generated as follow: cells from confluent 15 cm petri dishes were scraped and resuspended in microsome buffer [4 mM potassium phosphate buffer pH7.0, 20% glycerol]. Samples were frozen at -80°C for at least 16 hours before being thawed on ice. Samples were sonicated on ice and centrifuged (20 min, 16 000 x*g*, 4°C). Supernatants were collected and centrifuged (1 hour, 100 000 x*g*, 4°C) to concentrate cellular extracts. Pellets were resuspended in microsome buffer and quantified using a bicinchoninic acid assay (ThermoFisher Scientific, Ottawa, ON, Canada). Microsomes (20 µg) were incubated with bilirubin (10 µM; Sigma, Oakville, ON, Canada), estradiol (E_2, 100 µM; Steraloid, Newport, RI, USA), zidovudine (AZT, 300 µM; Sigma), 7-ethyl-10-hydroxy-camptothecin (SN-38, 200 µM; obtained as previously (5)) or arachidonic acid (AA, 100 µM; Cayman Chemical, Ann Arbor, MI, USA) in assay buffer (50 mM Tris-HCl pH 7.5, 10 mM $MgCl_2$, 5 µg/mL pepstatin, 0.5 µg/mL leupeptin, 2 mM UDP-GlcA, 20 µg/mL alamethicin) at 37°C. Reactions were stopped with methanol, centrifuged (13 000 x*g*, 10 minutes, 4°C) and store at -20°C until MS analysis. Glucuronides were quantified by LC-MS/MS and according to published methods for bilirubin (18), E_2 (21), AZT (22) and SN-38 (23). Arachidonic acid glucuronide was detected with an API 6500 (Sciex, Concord, Canada), operated in multiple reaction monitoring (MRM) mode and equipped with a turbo ion-spray source. ESI was performed in negative ion mode. The chromatographic system consisted of a Nexera (Shimadzu Scientific

instruments, Inc., Columbia, MD, USA) equipped with a Synergie RP-Hydro 4.0 µm packing material, 100 X 4.6 mm (Phenomenex, Torrance, CA, USA). The mobile phases were 35% water 1 mM ammonium formate (A) and 65% methanol 1 mM ammonium formate (B) at a flow rate of 0.9 ml/min. The initial conditions were of 75% B, followed by a linear gradient up to 90% B in 5 minutes. This concentration was held for 2 minutes and then re-equilibrated to initial conditions over 3 minutes. The MRM transition used for analysis was 479.2 $\rightarrow$ 303.1 m/z. The resolution used in those methods for Q1 and Q3 was Unit/Unit. HPLC and MS were controlled through Analyst Software (v1.6.1, AB Sciex LP, Concord, ON, Canada).

Fatty acid synthesis assay

Fatty acid synthase (FASN) activity was based on a published protocol (25). Briefly, HEK293 cells from two confluent 15 cm petri dishes were scraped and rinsed with ice-cold PBS. After centrifugation (525 x*g*, 5 minutes), cells were resuspended in lysis buffer (50 mM Tris-HCl pH 7.4, 1 mM EDTA, 150 mM NaCl and cOmplete Protease inhibitor [Sigma]). Cell suspensions were homogenized on ice using a microtip sonicator and a dounce homogenizer. Samples were centrifuged (14 000 x*g*, 15 minutes, 4°C) and supernatants were quantified using a Bradford assay. Assays were conducted with 100 µg of protein in an assay buffer (200 mM potassium phosphate buffer pH 6.6, 1 mM DTT, 1 mM EDTA, 240 µM NADPH and 30 µM acetyl-CoA). Malonyl-CoA was added to a final concentration of 50 µM. NADPH oxidation rate was monitored during 10 minutes at λ=340 nm with a TECAN M1000 Pro (Morrisville, TN, USA).

Gene expression analysis

Flash-frozen cell pellets were obtained as above. RNA extraction was carried out using the RNeasy Plus Mini Kit (Qiagen Inc., Toronto, ON, Canada) as per the manufacturer's protocol. Reverse transcriptase and qPCR were conducted as previously reported (15). Primer sequences are listed in **Supplementary Table 1**. Data were analyzed using the $\Delta\Delta$Ct method (25).

Co-immunoprecipitation

Co-immunoprecipitations (Co-IPs) to confirm OGDHL partnership with UGT1A1 alternative protein were carried out on cell lysates from HEK293 cells stably expressing UGT1A1_i2-V5-His and in which OGDHL-Myc-DDK (Origene, Rockville, MD, USA) was transfected

using Lipofectamine 3000 (Life Technologies Inc.). Co-IPs were conducted as described (13). Briefly, proteins were crosslinked with 0.125% paraformaldehyde (Sigma) during 10 minutes at 37°C. Crosslink reaction was stopped with glycine (125 mM, pH 3.0) for 5 minutes at room temperature. Cells were rinsed twice with PBS and lysed in 1 mL of lysis buffer (175 mM Tris-HCl pH 7.4, 150 mM NaCl, 1% Igepal [Sigma], 1 mM DTT, cOmplete Protease Inhibitor) for 1 hour at 4°C. Lysates were homogenized using 18G and 20G needles. After centrifugation (6000 x*g*, 10 minutes), the lysates were split and mixed with Protein A/G magnetic beads (Life Technologies Inc.) pre-incubated with either goat anti-V5 antibody (Bio-Techne Canada, Oakville, ON, Canada) or goat anti-IgG (R&D Systems, Inc., Minneapolis, MN, USA). After incubation (2 hours, 4°C), beads were rinsed thrice with lysis buffer and subjected to SDS-PAGE. Proteins were detected by immunoblotting using mouse anti-V5 (1:20 000, Life Technologies Inc.) and goat anti-Flag M2 (1:10 000, Sigma) antibodies.

Results

Validation of cell models

The full-length canonical UGT1A1 and UGT2B7 enzymes were stably expressed in the UGT-negative cell line HEK293 (**Fig.1**). Selected alternative UGT proteins were also studied and included the shorter UGT1A1_i2 (alt. UGT1A1) and the longer UGT2B7_i8 (alt. UGT2B7) proteins. The alt. UGT1A1 lacks the canonical sequence of 99 amino acids comprising the trans-membrane domain and a short cytosolic charged tail (encoded by exon 5a) replaced by a truncated C-terminus encoding a unique sequence of 10 amino acids derived from the exon 5b (**Fig.1A)**. Its molecular weight corresponds to approximately 45 kDa, as confirmed by western blotting. The alt. UGT2B7 has a unique 32-residue in-frame internal region derived from the novel exon 2b, residing at the interface between the N-terminal substrate-binding domain and the C-terminal co-substrate–binding domain leading to an apparent molecular mass of 62 kDa (**Fig.1A**). The enzymatic functionality of UGT proteins was confirmed in standard *in vitro* UGT assays using microsomal fractions derived from HEK293 cells incubated in the presence of the co-substrate UDP-GlcA and known substrates. UGT1A1 and UGT2B7 enzymes displayed significant transferase activity for bilirubin, AA, estradiol and SN-38 (**Fig.1B**), and estradiol, AZT and AA (**Fig.1C**), respectively. In these enzymatic assay conditions, detectable activity was noticed for the

UGT2B7_i8 isoform whereas glucuronide formation was not detected for UGT1A1_i2 (**Fig.1B-C**), consistent with previous reports (18, 20).

UGT expression induced significant changes in the cellular metabolome

An unbiased metabolomics analysis of cell lysates allowed the examination of 615 metabolites (**Supplementary Table 2**). Compared to control cells, the levels of 276 metabolites were significantly altered in cells expressing the UGT1A1 canonical enzyme (176 increased and 100 decreased), and 345 metabolites in cells expressing the UGT2B7 enzyme (228 increased and 117 decreased) (**Fig.2A**). Overall, all four UGT proteins produced significant changes in pyrimidine metabolism and glycolysis (**Table 1**; **Supplementary Figure 1**). Compared to control cells, the levels of 2'-deoxycytidine and uracil as well as glucose, mannose and fructose, along with several glycolytic intermediates, were the most severely changed (by -100 to 18-fold) (**Table 1**). Pathway enrichment analysis further revealed that 19 biochemical routes, including carbohydrate, nucleotide and lipid pathways, were altered by the expression of the UGT1A1 and UGT2B7 enzymes (**Fig.2B**). Common changes included 190 metabolites and most notably glucose-6-phosphate, mannose-6-phosphate and arachidonic acid (AA) (**Table 1)**.

Alt. UGT1A1 expression modified the levels of 207 cellular metabolites (97 increased and 110 decreased; **Fig.2C**), with 127 metabolites (61%) being also altered in UGT1A1 enzyme-expressing cells. Of those, 94 metabolites (48 increased and 46 decreased) were concordantly affected in both cell models, representing 45% and 34% of metabolites altered by alt. and enzyme UGT1A1 expression, respectively. The levels of 292 metabolites (184 increased and 108 decreased) were perturbed by alt. UGT2B7, including 198 metabolites (68%) in common with UGT2B7 enzyme-expressing cells (**Fig.2D**). Of these, 147 metabolites were similarly modified (101 increased and 46 decreased)**.**

Nucleotide sugar precursors were significantly altered

Consistent with the utilization of UDP-GlcA as a co-substrate by UGT enzymes, cellular levels of metabolites related to its synthesis were modified in enzyme-expressing cells, including glycolysis, pentose-phosphate, pyrimidine synthesis, and hexosamine synthesis pathways (**Fig.3**). For example, the levels of orotate, orotidine and uridine-5'-monophosphate (UMP) metabolites from the pyrimidine synthesis pathway were up to 3.6-fold higher ($P < 0.01$) in UGT enzyme-expressing cells when compared to control cells

(**Fig.3**). Expression of the UGT2B7 enzyme also induced elevated levels of N-carbamoyl aspartate (9.0-fold; *P* = 0.004), a metabolite resulting from a committed step of pyrimidine synthesis. In addition, metabolites from pathways competing with UDP-GlcA synthesis were severely depleted in the presence of UGT enzymes. For example, glycolytic and pentose phosphate intermediates such as Glc/Fru-1-6-BP, glycerate-3-phosphate, phosphoenolpyruvate and 6-phosphogluconate were decreased by -2.6 to -12.5-fold. Although to a lesser extent, some of the glycolytic and pyrimidine synthesis intermediates were also altered by the expression of the alt. UGT1A1 protein (**Fig.3**). In contrast, most of these metabolic intermediates were elevated in cells expressing the alt. UGT2B7 protein, including UDP-GlcA (1.6-fold; *P* = 0.004) and several glycolytic intermediates (**Fig.3**).

Changes specific to UGT isoforms

In cell models expressing UGT1A1 and UGT2B7 enzymes, several classes of lipids, and most particularly bioactive lipids such as AA, were among the most modified metabolites (**Fig.2B**), with higher levels by 5.4 and 13.3-fold (*P* < 0.001) in UGT1A1 and UGT2B7 cells, respectively, compared to control cells (**Fig.4A**). Numerous polyunsaturated fatty acids (PUFAs) and endocannabinoids were significantly enriched in UGT enzyme-expressing cells when compared to control cells. The monoacylglycerol (MAG) 2-arachidonoylglycerol (2-AG) was significantly higher in UGT1A1 and UGT2B7 enzyme-expressing cells by 5.5 and 2.8-fold (*P* < 0.001), respectively (**Fig.4A**). In line, increased mRNA expression of *PLA2G4A*, encoding an enzyme releasing AA from phospholipids, and lower expression of *MAGL*, coding for an enzyme catalyzing MAG hydrolysis, were observed in both UGT enzyme-expressing cells (**Fig.4B**). In addition to 2-AG, other endocannabinoid molecules also accumulated in enzyme-expressing cells (**Fig.4C**). This was also consistent with a significantly decreased expression of *FAAH,* which encodes the fatty acid amide hydrolase, the main enzyme catabolizing these bioactive lipids (**Fig.4D**).

For UGT1A1-expressing cells, we further observed a decreased expression of genes encoding cannabinoid receptors, including the G-protein coupled receptor *CNR1* (-2.9-fold; *P* < 0.001) and the transient receptor potential cation channel *TRPV1* (-1.7-fold; *P* < 0.001) (**Fig.5A-B**). Downstream targets of the cannabinoid system were also decreased, such as mRNA expression (-1.4-fold, *P* < 0.001) and activity (-1.9-fold, *P* < 0.01) of the fatty acid synthase (FASN) enzyme, determined by an *in vitro* assay measuring the oxidation rate of NADPH upon addition of malonyl-CoA (**Fig.5C-D**). A slight decreased in the expression of

endocannabinoid-targeted nuclear receptors *PPARD* was observed with no significant modifications for *PPARA* and *PPARG*. We also perceived a modest but constant decrease in expression of genes coding for PPAR-regulated mitochondrial and peroxisomal enzymes (**Fig.5A-B**), suggesting that these nuclear receptors were repressed. This change in gene expression was specific to cells expressing the UGT1A1 enzyme, as it remained near control levels in cells expressing the alt. UGT1A1 (**Supplementary Table 2**).

For UGT2B7-expressing cells, specific metabolic changes were connected to the creatine pathway. Levels of guanidinoacetate, a metabolite resulting from a committed step of creatine synthesis, were depleted by -3.8 and -1.4-fold ($P < 0.05$) in cells expressing the enzyme and the alt. UGT2B7 protein, respectively (**Fig.6A**). Supporting the induction of this pathway in UGT2B7-expressing cell models, levels of the downstream metabolite creatinine were 1.2-fold higher ($P < 0.01$) in both cell models when compared to control. Elevation of creatine and creatine-P were also noted in alt. UGT2B7 cells, whereas these metabolites were unaltered in UGT2B7 enzyme-expressing cells. Enzymatic conversion of guanidinoacetate to creatine requires the simultaneous transformation of S-adenosylmethionine (SAM) into S-adenosylhomocysteine (SAH) by guanidinoacetate N-methyltransferase (GAMT). In line with an increased GAMT activity, SAH levels were enriched by up to 2.0-fold ($P < 0.05$) in UGT2B7-expressing cells. This is supported by an elevated expression of GAMT by up to 2.0-fold ($P<0.05$) in these cells (**Fig.6B**). In contrast, few of these metabolites were significantly modified in cells expressing UGT1A1 proteins (**Supplementary Table 2**).

Evidence of a functional interaction leading to changes in metabolite levels

Mitochondrial branched-chain keto acids, i.e. 3-methyl-2-oxovalerate, 4-methyl-2-oxopentanoate and 3-methyl-2-oxobutyrate, derived from branched-chain amino acids (BCAA), were particularly more abundant in alt. UGT1A1 expressing cells by up to 5.9-fold ($P < 0.001$) when compared to control cells. TCA cycle metabolites, namely citrate, isocitrate and oxoglutarate, were also higher in these cells (by 1.6 to 2.5-fold; $P < 0.01$; **Fig.6C**). These changes were much less significant for the UGT1A1 enzyme, whereas UGT2B7 protein expressions led to their depletion, suggesting a differential effect of the UGT proteins on mitochondrial metabolism. Altered BCAA and TCA cycle metabolites are located upstream of the oxoglutarate dehydrogenase complex (OGDC), among which protein partners of the UGT1As were previously identified by untargeted proteomics experiments in human tissues

(14). While no interaction between the UGT1A1 enzyme and the OGDC component oxoglutarate dehydrogenase-like (OGDHL) protein was detected (**Fig.6D**), we observed a protein-protein interaction between the alt. UGT1A1 and OGDHL. This supports the possibility that metabolic changes might be caused by a functional interaction between this member of the OGDC complex and the alt. UGT1A1 protein (**Fig.6E**).

Discussion

Our study reveals that UGT protein expression triggers significant changes in cellular metabolism beyond known UGT substrates, including alterations in the levels of major macromolecular groups. These changes were observed for all four UGT proteins included in the study and comprised those in carbohydrates, nucleotides and bioactive lipids pathways.

Notably, UGT enzyme expression induced significant modifications in the pyrimidine metabolism and glycolysis, suggesting a diversion of these intermediates to support UDP-GlcA co-substrate synthesis. Previous lines of evidence implied a limited availability of UDP-GlcA when exposed to important amounts of UGT substrates (26-29), while our data indicate that UGT expression induces modifications in this pathway in the absence of UGT substrate supplementation (i.e. normal growth media supplemented with serum). An increased pyrimidine metabolism may also reflect a metabolic rewiring to repress UGT activity, as nucleotides represent endogenous allosteric inhibitors (30, 31). Certain UGT enzymes, including UGT2B7, are capable of using UDP-Glc as a co-substrate (32-34). Coherent with a potential increased usage of downstream-related metabolites such as UDP-Glc, depletion in early glycolytic intermediates (e.g. mannose-6-phosphate and glucose-6-phosphate) was observed in UGT2B7 enzyme-expressing cells. Metabolic flux analysis would help examine more closely the effects of UGT expression on these pathways. In addition, the absolute quantification of UDP-sugars with some sharing the same mass-to-charge (*m/z*) ratio in MS such as UDP-Glc / UDP-galactose, and UDP-GlcA / UDP-galacturonic acid, would provide a more accurate quantification.

Additional biochemical routes affected by UGT expression were related to lipid pathways, including the bioactive lipid AA and endocannabinoids. For instance, expression of UGT1A1 and UGT2B7 enzymes induced a significant elevation of AA levels. The opposite would have been expected since our data and a previous report identified AA as a substrate of several UGTs including UGT1A1 and UGT2B7 (35). It remains unclear how AA accumulates within

cells and it may involve a regulatory feedback loop. A previous study showed that AA supplementation induces a repression of UGT1A1 expression in the hepatic model HepG2, which endogenously express this isoenzyme (36). It may also engage PPAR signaling, as lower expression of several peroxisomal and mitochondrial PPAR targets involved in mitochondrial fatty acid beta-oxidation were noticed in UGT1A1 enzyme-expressing cells. Moreover, we previously observed an accumulation of lipid droplets induced by UGT1A expression (13), a process reflecting storage of energy-rich fatty acids as well as bioactive lipids (37, 38), and which potentially involved protein-protein interactions (13). Another report further supports a key role of UGTs in maintaining lipid homeostasis, with an effect on the proliferation of cancer cells (39). An impact of UGT on gene expression and cell metabolism was also observed in a humanized mouse model (*hUGT1*). For instance, (40) reported that the loss of UGT1A functionality in liver resulted in significant alterations in the expression of gene pathways such as those linked to hormones, fatty acids and pyrimidine metabolism. Accordingly, the interconnection between lipid metabolism and the UGT pathway seems more complex than being related to substrates for these enzymes, and likely involves signaling events and modifications of gene expression triggered by bioactive lipids, as well as protein-protein interactions.

In support of functional protein interactions involving UGTs, we demonstrated a protein-protein interaction between the alt. UGT1A1 protein and OGDHL, a component of the OGDC enzyme complex and a key control point in the citric acid cycle often bypassed in cancer cells (41-45). It is plausible that this partnership may explain, at least in part, changes in the levels of TCA cycle intermediates and BCAA metabolites observed in cells overexpressing the alt. UG1A1 protein. Consistent with this notion, our previous work using an alt. UGT1A-depleted cancer cell model showed a shift in energy metabolism, increasing cell dependency on glucose at the expense of oxidative phosphorylation, likely dependent on a functional interaction of UGT1A proteins with the pyruvate kinase M2 (PKM2) enzyme (14). These two protein partners of the alt. UGT1A1 protein are key regulators of energy metabolism, which could be linked to the capacity of UGTs to induce a redirection of carbon skeletons as discussed above. In fact, when compared to UGT1A1 enzyme-expressing cells, those expressing the alt. UGT1A1 displayed similar alterations for several abovementioned metabolic pathways (glycolysis, pyrimidine synthesis and bioactive lipid metabolism), and could be instigated by common protein interactors (1, 13, 14). By these interactions, we also exposed that alt. UGT1A proteins, but not UGT1A enzymes, interfere with oligomeric

complex formation necessary for scavenging activity of catalase and peroxiredoxin (1). OGDC activity is linked to an increased ROS formation in mitochondria (46, 47), upholding a role for alt. UGT1A proteins in ROS metabolism. Besides, UGT1A1 is a key regulator of oxidative stress through controlling the homeostasis of the antioxidant bilirubin, implying a potential role of UGT expression in oxidative stress-related diseases (48).

Isoform-specific interactions are thus expected to induce, to a certain extent, different metabolic changes that may be related to their divergent primary structure and/or subcellular localisation (19). Supporting this notion, expression of the structurally divergent alt. UGT2B7 caused distinct metabolic profiles for several pathways, notably for glycolytic intermediates and nucleotide sugar precursors, which could result from protein partners interacting with its unique peptide sequence. We also previously observed that in contrast to the canonical enzyme, the expression of the alt. UGT2B7 increased cellular adhesion while reducing proliferation, supporting a distinct role for alt. proteins on cellular metabolism (15).

The human HEK293 embryonic kidney cell model was selected for our study because the UGT pathway is inactive due to the lack of endogenous UGT expression (**Fig.1**) (49). This allowed us to better delineate the effects of individual UGT protein on the cell metabolome since most available human immortalized cell lines express multiple UGTs including enzymes and some forms of alt. UGTs (50, 51). Profiling cell culture media could have helped better portray the effects of UGT expression since glucuronide derivatives as well as many other metabolic intermediates are excreted by cells into the medium (52, 53). Limitations of the study include the fact that most of known signalling molecules inactivated by UGTs were not part of the panel of metabolites detected by MS, including many hormones. Moreover, relative metabolite quantification hinders our capacity to compare metabolite levels with other studies, an inherent limitation of untargeted metabolomics analyses. Our study represents an extensive portrait of cellular metabolites changed by UGT expression that also resulted in changes in gene expression. We are currently exploiting these data for the discovery of endogenous substrates of UGT proteins, a strategy that has been successful for organic anion transporters (54). The glucuronidation pathway emerges as a potential regulatory process used by cells to control the activity of their metabolic networks, with broad consequences on cell metabolite levels.

Acknowledgements

We would like to thank Andréa Fournier for her technical support for cell culture and Patrick Caron and Véronique Turcotte for their contribution to glucuronide quantification by MS. We also acknowledge the financial support of the Canadian Institutes for Health Research [CIHR FRN-142318]. YAD received a studentship from the *Fonds de Recherche du Québec Santé* (FRQS). CG is holder of a Tier I Canada Research Chair in Pharmacogenomics.

Declaration of interest

The authors declare that they have no conflict of interest.

References

(1) Guillemette C, Levesque E, Rouleau M. Pharmacogenomics of human uridine diphospho-glucuronosyltransferases and clinical implications. Clinical pharmacology and therapeutics. 2014;96:324-39.
(2) Rowland A, Miners JO, Mackenzie PI. The UDP-glucuronosyltransferases: their role in drug metabolism and detoxification. The international journal of biochemistry & cell biology. 2013;45:1121-32.
(3) Bock KW. Roles of human UDP-glucuronosyltransferases in clearance and homeostasis of endogenous substrates, and functional implications. Biochemical pharmacology. 2015;96:77-82.
(4) Riches Z, Collier AC. Posttranscriptional regulation of uridine diphosphate glucuronosyltransferases. Expert opinion on drug metabolism & toxicology. 2015;11:949-65.
(5) Gagnon JF, Bernard O, Villeneuve L, Tetu B, Guillemette C. Irinotecan inactivation is modulated by epigenetic silencing of UGT1A1 in colon cancer. Clinical cancer research : an official journal of the American Association for Cancer Research. 2006;12:1850-8.
(6) Hu DG, Meech R, McKinnon RA, Mackenzie PI. Transcriptional regulation of human UDP-glucuronosyltransferase genes. Drug metabolism reviews. 2014;46:421-58.
(7) Nishimura Y, Maeda S, Ikushiro S, Mackenzie PI, Ishii Y, Yamada H. Inhibitory effects of adenine nucleotides and related substances on UDP-glucuronosyltransferase: structure-effect relationships and evidence for an allosteric mechanism. Biochimica et biophysica acta. 2007;1770:1557-66.
(8) Yokota H, Ando F, Iwano H, Yuasa A. Inhibitory effects of uridine diphosphate on UDP-glucuronosyltransferase. Life sciences. 1998;63:1693-9.
(9) van der Knaap JA, Verrijzer CP. Undercover: gene control by metabolites and metabolic enzymes. Genes & development. 2016;30:2345-69.
(10) Takeda S, Ishii Y, Iwanaga M, Mackenzie PI, Nagata K, Yamazoe Y, et al. Modulation of UDP-glucuronosyltransferase function by cytochrome P450: evidence for the alteration of UGT2B7-catalyzed glucuronidation of morphine by CYP3A4. Molecular pharmacology. 2005;67:665-72.
(11) Ishii Y, Koba H, Kinoshita K, Oizaki T, Iwamoto Y, Takeda S, et al. Alteration of the function of the UDP-glucuronosyltransferase 1A subfamily by cytochrome P450 3A4: different susceptibility for UGT isoforms and UGT1A1/7 variants. Drug metabolism and disposition: the biological fate of chemicals. 2014;42:229-38.
(12) Fujiwara R, Yokoi T, Nakajima M. Structure and Protein-Protein Interactions of Human UDP-Glucuronosyltransferases. Front Pharmacol. 2016;7:388.
(13) Rouleau M, Audet-Delage Y, Desjardins S, Rouleau M, Girard-Bock C, Guillemette C. Endogenous Protein Interactome of Human UDP-Glucuronosyltransferases Exposed by Untargeted Proteomics. Front Pharmacol. 2017;8:23.
(14) Audet-Delage Y, Rouleau M, Rouleau M, Roberge J, Miard S, Picard F, et al. Cross-Talk between Alternatively Spliced UGT1A Isoforms and Colon Cancer Cell Metabolism. Molecular pharmacology. 2017;91:167-77.

(15) Rouleau M, Tourancheau A, Girard-Bock C, Villeneuve L, Vaucher J, Duperre AM, et al. Divergent Expression and Metabolic Functions of Human Glucuronosyltransferases through Alternative Splicing. Cell reports. 2016;17:114-24.
(16) Menard V, Collin P, Margaillan G, Guillemette C. Modulation of the UGT2B7 enzyme activity by C-terminally truncated proteins derived from alternative splicing. Drug metabolism and disposition: the biological fate of chemicals. 2013;41:2197-205.
(17) Girard H, Levesque E, Bellemare J, Journault K, Caillier B, Guillemette C. Genetic diversity at the UGT1 locus is amplified by a novel 3' alternative splicing mechanism leading to nine additional UGT1A proteins that act as regulators of glucuronidation activity. Pharmacogenetics and genomics. 2007;17:1077-89.
(18) Levesque E, Girard H, Journault K, Lepine J, Guillemette C. Regulation of the UGT1A1 bilirubin-conjugating pathway: role of a new splicing event at the UGT1A locus. Hepatology. 2007;45:128-38.
(19) Tourancheau A, Margaillan G, Rouleau M, Gilbert I, Villeneuve L, Levesque E, et al. Unravelling the transcriptomic landscape of the major phase II UDP-glucuronosyltransferase drug metabolizing pathway using targeted RNA sequencing. The pharmacogenomics journal. 2016;16:60-70.
(20) Evans AM, DeHaven CD, Barrett T, Mitchell M, Milgram E. Integrated, nontargeted ultrahigh performance liquid chromatography/electrospray ionization tandem mass spectrometry platform for the identification and relative quantification of the small-molecule complement of biological systems. Analytical chemistry. 2009;81:6656-67.
(21) Lepine J, Bernard O, Plante M, Tetu B, Pelletier G, Labrie F, et al. Specificity and regioselectivity of the conjugation of estradiol, estrone, and their catecholestrogen and methoxyestrogen metabolites by human uridine diphospho-glucuronosyltransferases expressed in endometrium. The Journal of clinical endocrinology and metabolism. 2004;89:5222-32.
(22) Belanger AS, Caron P, Harvey M, Zimmerman PA, Mehlotra RK, Guillemette C. Glucuronidation of the antiretroviral drug efavirenz by UGT2B7 and an in vitro investigation of drug-drug interaction with zidovudine. Drug metabolism and disposition: the biological fate of chemicals. 2009;37:1793-6.
(23) Gagne JF, Montminy V, Belanger P, Journault K, Gaucher G, Guillemette C. Common human UGT1A polymorphisms and the altered metabolism of irinotecan active metabolite 7-ethyl-10-hydroxycamptothecin (SN-38). Molecular pharmacology. 2002;62:608-17.
(24) Vazquez-Martin A, Colomer R, Brunet J, Lupu R, Menendez JA. Overexpression of fatty acid synthase gene activates HER1/HER2 tyrosine kinase receptors in human breast epithelial cells. Cell proliferation. 2008;41:59-85.
(25) Livak KJ, Schmittgen TD. Analysis of relative gene expression data using real-time quantitative PCR and the 2(-Delta Delta C(T)) Method. Methods (San Diego, Calif). 2001;25:402-8.
(26) Bray BJ, Rosengren RJ. Retinol potentiates acetaminophen-induced hepatotoxicity in the mouse: mechanistic studies. Toxicology and applied pharmacology. 2001;173:129-36.

(27) Gregus Z, Madhu C, Goon D, Klaassen CD. Effect of galactosamine-induced hepatic UDP-glucuronic acid depletion on acetaminophen elimination in rats. Dispositional differences between hepatically and extrahepatically formed glucuronides of acetaminophen and other chemicals. Drug metabolism and disposition: the biological fate of chemicals. 1988;16:527-33.
(28) Hjelle JJ. Hepatic UDP-glucuronic acid regulation during acetaminophen biotransformation in rats. The Journal of pharmacology and experimental therapeutics. 1986;237:750-6.
(29) Kultti A, Pasonen-Seppanen S, Jauhiainen M, Rilla KJ, Karna R, Pyoria E, et al. 4-Methylumbelliferone inhibits hyaluronan synthesis by depletion of cellular UDP-glucuronic acid and downregulation of hyaluronan synthase 2 and 3. Experimental cell research. 2009;315:1914-23.
(30) Grancharov K, Naydenova Z, Lozeva S, Golovinsky E. Natural and synthetic inhibitors of UDP-glucuronosyltransferase. Pharmacology & therapeutics. 2001;89:171-86.
(31) Ishii Y, Nurrochmad A, Yamada H. Modulation of UDP-glucuronosyltransferase activity by endogenous compounds. Drug metabolism and pharmacokinetics. 2010;25:134-48.
(32) Mackenzie P, Little JM, Radominska-Pandya A. Glucosidation of hyodeoxycholic acid by UDP-glucuronosyltransferase 2B7. Biochemical pharmacology. 2003;65:417-21.
(33) Buchheit D, Dragan CA, Schmitt EI, Bureik M. Production of ibuprofen acyl glucosides by human UGT2B7. Drug metabolism and disposition: the biological fate of chemicals. 2011;39:2174-81.
(34) Chau N, Elliot DJ, Lewis BC, Burns K, Johnston MR, Mackenzie PI, et al. Morphine glucuronidation and glucosidation represent complementary metabolic pathways that are both catalyzed by UDP-glucuronosyltransferase 2B7: kinetic, inhibition, and molecular modeling studies. The Journal of pharmacology and experimental therapeutics. 2014;349:126-37.
(35) Little JM, Kurkela M, Sonka J, Jantti S, Ketola R, Bratton S, et al. Glucuronidation of oxidized fatty acids and prostaglandins B1 and E2 by human hepatic and recombinant UDP-glucuronosyltransferases. Journal of lipid research. 2004;45:1694-703.
(36) Caputo M, Zirpoli H, Torino G, Tecce MF. Selective regulation of UGT1A1 and SREBP-1c mRNA expression by docosahexaenoic, eicosapentaenoic, and arachidonic acids. Journal of cellular physiology. 2011;226:187-93.
(37) Herms A, Bosch M, Ariotti N, Reddy BJ, Fajardo A, Fernandez-Vidal A, et al. Cell-to-cell heterogeneity in lipid droplets suggests a mechanism to reduce lipotoxicity. Current biology : CB. 2013;23:1489-96.
(38) Bozza PT, Bakker-Abreu I, Navarro-Xavier RA, Bandeira-Melo C. Lipid body function in eicosanoid synthesis: an update. Prostaglandins, leukotrienes, and essential fatty acids. 2011;85:205-13.
(39) Dates CR, Fahmi T, Pyrek SJ, Yao-Borengasser A, Borowa-Mazgaj B, Bratton SM, et al. Human UDP-Glucuronosyltransferases: Effects of altered expression in breast and pancreatic cancer cell lines. Cancer biology & therapy. 2015;16:714-23.

(40) Nguyen N, Bonzo JA, Chen S, Chouinard S, Kelner MJ, Hardiman G, et al. Disruption of the ugt1 locus in mice resembles human Crigler-Najjar type I disease. The Journal of biological chemistry. 2008;283:7901-11.
(41) Bunik V, Mkrtchyan G, Grabarska A, Oppermann H, Daloso D, Araujo WL, et al. Inhibition of mitochondrial 2-oxoglutarate dehydrogenase impairs viability of cancer cells in a cell-specific metabolism-dependent manner. Oncotarget. 2016;7:26400-21.
(42) Vincent EE, Sergushichev A, Griss T, Gingras MC, Samborska B, Ntimbane T, et al. Mitochondrial Phosphoenolpyruvate Carboxykinase Regulates Metabolic Adaptation and Enables Glucose-Independent Tumor Growth. Molecular cell. 2015;60:195-207.
(43) Yang C, Ko B, Hensley CT, Jiang L, Wasti AT, Kim J, et al. Glutamine oxidation maintains the TCA cycle and cell survival during impaired mitochondrial pyruvate transport. Molecular cell. 2014;56:414-24.
(44) Schell JC, Olson KA, Jiang L, Hawkins AJ, Van Vranken JG, Xie J, et al. A role for the mitochondrial pyruvate carrier as a repressor of the Warburg effect and colon cancer cell growth. Molecular cell. 2014;56:400-13.
(45) Sen T, Sen N, Noordhuis MG, Ravi R, Wu TC, Ha PK, et al. OGDHL is a modifier of AKT-dependent signaling and NF-kappaB function. PloS one. 2012;7:e48770.
(46) Chalker J, Gardiner D, Kuksal N, Mailloux RJ. Characterization of the impact of glutaredoxin-2 (GRX2) deficiency on superoxide/hydrogen peroxide release from cardiac and liver mitochondria. Redox biology. 2018;15:216-27.
(47) Sherrill JD, Kc K, Wang X, Wen T, Chamberlin A, Stucke EM, et al. Whole-exome sequencing uncovers oxidoreductases DHTKD1 and OGDHL as linkers between mitochondrial dysfunction and eosinophilic esophagitis. JCI Insight. 2018;3:e99922.
(48) Fujiwara R, Haag M, Schaeffeler E, Nies AT, Zanger UM, Schwab M. Systemic regulation of bilirubin homeostasis: Potential benefits of hyperbilirubinemia. Hepatology. 2018;67:1609-19.
(49) Dietmair S, Hodson MP, Quek L-E, Timmins NE, Gray P, Nielsen LK. A Multi-Omics Analysis of Recombinant Protein Production in Hek293 Cells. PloS one. 2012;7:e43394.
(50) Bellemare J, Rouleau M, Harvey M, Tetu B, Guillemette C. Alternative-splicing forms of the major phase II conjugating UGT1A gene negatively regulate glucuronidation in human carcinoma cell lines. The pharmacogenomics journal. 2010;10:431-41.
(51) Nakamura A, Nakajima M, Yamanaka H, Fujiwara R, Yokoi T. Expression of UGT1A and UGT2B mRNA in human normal tissues and various cell lines. Drug metabolism and disposition: the biological fate of chemicals. 2008;36:1461-4.
(52) Jarvinen E, Troberg J, Kidron H, Finel M. Selectivity in the Efflux of Glucuronides by Human Transporters: MRP4 Is Highly Active toward 4-Methylumbelliferone and 1-Naphthol Glucuronides, while MRP3 Exhibits Stereoselective Propranolol Glucuronide Transport. Molecular pharmaceutics. 2017;14:3299-311.
(53) Jarvinen E, Deng F, Kidron H, Finel M. Efflux transport of estrogen glucuronides by human MRP2, MRP3, MRP4 and BCRP. The Journal of steroid biochemistry and molecular biology. 2018;178:99-107.

(54) Yee SW, Giacomini MM, Hsueh CH, Weitz D, Liang X, Goswami S, et al. Metabolomic and Genome-wide Association Studies Reveal Potential Endogenous Biomarkers for OATP1B1. Clinical pharmacology and therapeutics. 2016;100:524-36.

Table 1. Top 6 up and down modulated metabolites in UGT-expressing cells.

Cell line	Pathway	Metabolite	Fold Change	P-value
UGT1A1	Glycolysis, Gluconeogenesis, and Pyruvate Metabolism	Isobar: fructose 1,6-diphosphate, glucose 1,6-diphosphate, myo-inositol 1,4 or 1,3-diphosphate	-12.5	4.4E-08
	Fructose, Mannose and Galactose Metabolism	mannose-6-phosphate	-9.1	8.6E-05
	Glycolysis, Gluconeogenesis, and Pyruvate Metabolism	glucose 6-phosphate	-5.3	9.4E-05
	Pentose Phosphate Pathway	6-phosphogluconate	-5.3	5.8E-05
	Glycolysis, Gluconeogenesis, and Pyruvate Metabolism	3-phosphoglycerate	-5.0	2.0E-06
	Glycolysis, Gluconeogenesis, and Pyruvate Metabolism	dihydroxyacetone phosphate (DHAP)	-5.0	5.8E-08
	Glycerolipid Metabolism	glycerophosphoglycerol	5.4	1.4E-10
	Polyunsaturated Fatty Acid (n3 and n6)	arachidonate (20:4n6)	5.4	2.7E-08
	Monoacylglycerol	1-arachidonylglycerol (20:4)	5.5	5.9E-08
	Purine Metabolism, Adenine containing	adenine	5.5	2.4E-10
	Pyrimidine Metabolism, Cytidine containing	2'-deoxycytidine	5.6	9.8E-06
	Polyamine Metabolism	N1,N12-diacetylspermine	5.9	1.0E-04
UGT2B7	Fructose, Mannose and Galactose Metabolism	mannose-6-phosphate	-20.0	5.9E-11
	Pyrimidine Metabolism, Cytidine containing	2'-deoxycytidine	-20.0	5.1E-10
	Polyamine Metabolism	N1,N12-diacetylspermine	-14.3	2.2E-06
	Polyamine Metabolism	N(1)-acetylspermine	-9.1	1.1E-07
	Glycolysis, Gluconeogenesis, and Pyruvate Metabolism	glucose 6-phosphate	-6.3	3.9E-07
	Nicotinate and Nicotinamide Metabolism	adenosine 5'-diphosphoribose (ADP-ribose)	-6.3	4.1E-06
	Polyunsaturated Fatty Acid (n3 and n6)	arachidonate (20:4n6)	13.3	6.5E-09
	Glutathione Metabolism	cysteine-glutathione disulfide	14.5	8.3E-07
	Pyrimidine Metabolism, Thymine containing	5,6-dihydrothymine	19.5	3.6E-09
	Methionine, Cysteine, SAM and Taurine Metabolism	cystine	21.0	1.4E-09
	Pyrimidine Metabolism, Thymine containing	thymine	26.1	7.3E-09
	Pyrimidine Metabolism, Uracil containing	uracil	28.3	1.9E-08

alt. UGT1A1	Plasmalogen	1-(1-enyl-stearoyl)-2-linoleoyl-GPE (P-18:0/18:2)*	-6.3	1.1E-06
	Polyamine Metabolism	putrescine	-4.3	8.8E-08
	Glycolysis, Gluconeogenesis, and Pyruvate Metabolism	Isobar: fructose 1,6-diphosphate, glucose 1,6-diphosphate, myo-inositol 1,4 or 1,3-diphosphate	-4.0	7.4E-05
	Pentose Phosphate Pathway	6-phosphogluconate	-3.6	8.0E-04
	Polyamine Metabolism	N-acetylputrescine	-3.6	9.1E-07
	Glycolysis, Gluconeogenesis, and Pyruvate Metabolism	dihydroxyacetone phosphate (DHAP)	-3.4	1.7E-06
	Leucine, Isoleucine and Valine Metabolism	3-methyl-2-oxovalerate	5.5	7.3E-07
	Leucine, Isoleucine and Valine Metabolism	4-methyl-2-oxopentanoate	5.8	2.1E-06
	Leucine, Isoleucine and Valine Metabolism	3-methyl-2-oxobutyrate	5.9	1.6E-06
	Diacylglycerol	palmitoleoyl-oleoyl-glycerol (16:1/18:1) [1]*	6.9	4.9E-05
	Diacylglycerol	diacylglycerol (12:0/18:1, 14:0/16:1, 16:0/14:1) [1]*	8.0	5.7E-07
	Pyrimidine Metabolism, Cytidine containing	2'-deoxycytidine	13.5	1.1E-07
alt. UGT2B7	Pyrimidine Metabolism, Cytidine containing	2'-deoxycytidine	-100.0	1.0E-13
	Diacylglycerol	diacylglycerol (12:0/18:1, 14:0/16:1, 16:0/14:1) [1]*	-7.7	2.2E-03
	Pyrimidine Metabolism, Cytidine containing	cytidine	-7.1	5.7E-07
	Pyrimidine Metabolism, Cytidine containing	5-methylcytidine	-7.1	9.8E-06
	Polyamine Metabolism	N1,N12-diacetylspermine	-6.7	2.0E-04
	Endocannabinoid	N-oleoyltaurine	-3.8	7.9E-06
	Polyunsaturated Fatty Acid (n3 and n6)	mead acid (20:3n9)	4.5	6.4E-06
	Pentose Phosphate Pathway	6-phosphogluconate	4.6	1.8E-07
	Pyrimidine Metabolism, Thymine containing	3-aminoisobutyrate	4.8	1.1E-12
	Pyrimidine Metabolism, Uracil containing	uracil	5.5	3.0E-04
	Plasmalogen	1-(1-enyl-stearoyl)-2-linoleoyl-GPE (P-18:0/18:2)*	6.1	1.8E-07
	Glycolysis, Gluconeogenesis, and Pyruvate Metabolism	glucose	18.2	5.7E-07

Figure Legends

Figure 1. Expression and activity of UGT enzymes and alt. proteins in UGT-negative HEK293 cells. A) Schematic representation of splicing events in *UGT1* and *UGT2B* genes, leading to the UGT1A1 and UGT2B7 canonical enzymes (full lines). The UGT1A1_i2 alternative protein (alt. UGT1A1) possess a truncated C-terminal, resulting from a stop codon located in the exon 5b, whereas the UGT2B7_i8 alternative protein (alt. UGT2B7) has an in-frame insertion of 32 amino acids encoded by the exon 2b. Stable expression and glucuronidation activity of UGT1A1 (B) and UGT2B7 (C) enzymes (enz.) or alternative proteins (alt.) in HEK293 cells. Expression was revealed by immunoblotting of microsomal fractions of UGT-expressing cell models and control cells (Ctr). UGT1A1 and UGT2B7 enzymes displayed enzymatic activity toward typical substrates of these isoenzymes. Assays were conducted with microsomal extracts of each cell model incubated with bilirubin, arachidonic acid (AA), estradiol (E_2), SN-38 or zidovudine (AZT). All substrates are reported in pmol/mg prot/h (right axis), except for bilirubin and AA ($1x10^3$ area/mg prot/h; left axis). No activity was detected in Ctr cells (not shown).

Figure 2. UGT expression induces significant perturbations of metabolite levels. Using an unbiased metabolomic approach, we showed that UGT expression modified intracellular metabolite concentrations in comparison to control cells. A) Common and divergent changes in metabolite levels ($P<0.05$) for enzyme-expressing models are displayed in the Venn diagram (Upper panel), while the scatter plot (Lower panel) shows the log2 fold change (Log2 FC) of metabolites significantly altered in both cell models. Numbers of metabolites in each quadrant are displayed. B) Pathway enrichment analysis revealed perturbations common to UGT1A1 and UGT2B7. Displayed pathways were enriched in both cell models with an enrichment score > 1 and comprised at least 3 metabolites. C) Venn diagram of common and divergent changes in metabolite levels ($P<0.05$) for UGT1A1 and alt. UGT1A1 models (left). The scatter plot shows the Log2 FC of metabolites altered in both cell models (right). D) Common and divergent changes in metabolite levels ($P<0.05$) for UGT2B7 and alt. UGT2B7 models are displayed in the Venn diagram (left). The scatter plot shows the log2 FC of metabolites altered in both conditions. Pathway enrichment analysis for E) and F) are displayed in Supplementary Figure 1. Cells were cultured in standard conditions, as described in the Methods. Metabolites were categorized according to Metabolon proprietary database. The complete list of metabolites and their quantification are provided in Supplementary Table 2.

Figure 3. Metabolic precursors of UDP-GlcA synthesis are modified by UGT expression. Several metabolites of the pyrimidine, glycolytic and pentose phosphate pathways are preferentially altered in UGT enzyme-expressing cells. Fold changes (FC) relative to control cells are provided in the heatmap. Non-significant metabolites are displayed in white. Note that glucose and pyruvate were supplemented by the medium. NCA, N-carbamoyl aspartate; DHO, dihydroorotate; UMP, uridine monophosphate; UDP, uridine-diphosphate; UTP, uridine triphosphate; Glc, glucose; Glc-6-P, glucose-6-phosphate; Glc-1-P, glucose-1-phosphate; UDP-Glc, UDP-glucose; UDP-GlcA, UDP-glucuronic acid; Fru, fructose; Fru-6-P, fructose-6-phosphate; GlcN-6P, glucosamine-6-phosphate; GlcNAc-6-P, N-acetyl-glucosamine-6-phosphate; GlcNAc-1-P, N-acetyl-glucosamine-1-phosphate; UDP-GlcNAc, UDP-N-acetyl-glucosamine; Man-6-P, Mannose-6-phosphate; Glc/Fru-1-6-BP, glucose/fructose-1-6-bisphosphate; PEP, phosphoenolpyruvate.

Figure 4. UGT1A1 and UGT2B7 enzymes induce an accumulation of bioactive lipids. A) Arachidonic acid (AA; C20:4n6) and its precursors, 1-arachidonoylglycerol (1-AG) and 2-AG, are elevated in cells expressing UGT1A1 and UGT2B7 enzymes, whereas the levels of these metabolites are almost unaffected by the expression of alt. UGT1A1 and alt. UGT2B7 (Supplemental Table 2). MAG, monoacylglycerol; DAG, diacylglycerol; GPC, glycerophosphocholine; GPE, glycerophosphoethanolamine; GPI, glycerophosphoinositol; GPS, glycerophosphoserine; LPA, lysophosphatidic acid. MAGL, monoacylglycerol lipase; DAGLB, diacylglycerol lipase B; PLA2G4A, cytosolic phospholipase A2 group IVA. Lipid species are detailed in parentheses. B) The accumulation of AA is linked to an increased expression of *PLA2G4A* and repressed expression of *MAGL* in enzyme-expressing cells, as detected by reverse-transcriptase-quantitative-PCR (RT-qPCR). DAGLB expression did not correlate with levels of AA-containing lipids. mRNA fold change (FC) over control (Ctr) cells is displayed. C) Enrichment of endocannabinoids in UGT enzyme-expressing cells. D) The expression of the fatty acid amide hydrolase (*FAAH)*, catalyzing the hydrolysis of endocannabinoids, was decreased in enzyme-expressing cells. Metabolite fold changes (FC) relative to control cells are provided in heatmaps. Non-significant metabolites are displayed in white. ***P<0.001, **P<0.01, *P<0.05.

Figure 5. The cannabinoid system is downregulated in cells expressing UGT1A1 enzyme and its alt. protein. A) Scheme of the endocannabinoid system in HEK293 cells, including cannabinoid receptors (*CNR1*, *TRPV1*), peroxisome proliferator-activated

receptors (PPARs) and PPAR targets. B) Gene expression of the endocannabinoid system in HEK293 cells expressing UGT1A1 enzyme and alt. UGT1A1. Expression of most genes is perturbed in both cell models and preferentially reduced in UGT1A1 enzyme-expressing cells. Cells expressing the UGT1A1 enzyme have lower fatty-acid synthase (FASN) C) expression and D) activity than control cells, as detected by an assay measuring NADPH oxidation upon malonyl-CoA addition. EHHADH, Enoyl-CoA Hydratase And 3-Hydroxyacyl CoA Dehydrogenase; ACAA, Acetyl-CoA Acyltransferase; ECH1, Enoyl-CoA Hydratase 1; CPT1A, Carnitine Palmitoyltransferase 1A. ***P<0.001, **P<0.01, *P<0.05, $^{\dagger}P$<0.1.

Figure 6. Specific metabolic changes induced by UGT expression. A) Expression of UGT2B7 proteins is associated with elevated metabolites of the creatine pathway. Fold changes (FC) relative to control cells are provided in the heatmap. Non-significant metabolites are displayed in white. SAM, S-adenosyl-methionine; SAH, S-adenosyl-homocysteine; DMGly, dimethyl-glycine; GAMT, guanidinoacetate methyltransferase. **B)** GAMT mRNA expression are increased in cells expressing UGT2B7 proteins when compared to control cells. **C)** Metabolites upstream from the oxoglutarate dehydrogenase complex (OGDC) in the TCA cycle are elevated in cells expressing UGT1A1 proteins. Branched-chain keto acids (BCKA) are also enriched in alt. UGT1A1 cells. **D)** Co-immunoprecipitations (co-IPs) revealed no interaction between UGT1A1 and the oxoglutarate dehydrogenase-like (OGDHL) protein, a key regulator of the OGDC. **E)** The alt. UGT1A1 interacts with OGDHL, as detected by co-IP. Co-IPs were conducted using anti-myc (UGT1A1) or anti-V5 (alt.UGT1A1) and control IgG antibodies. Western blots were revealed with in-house anti-UGT1A (RC-71; for UGT1A1), anti-V5 (for alt. UGT1A1) or anti-Flag (for OGDHL) antibodies.

Figure 1

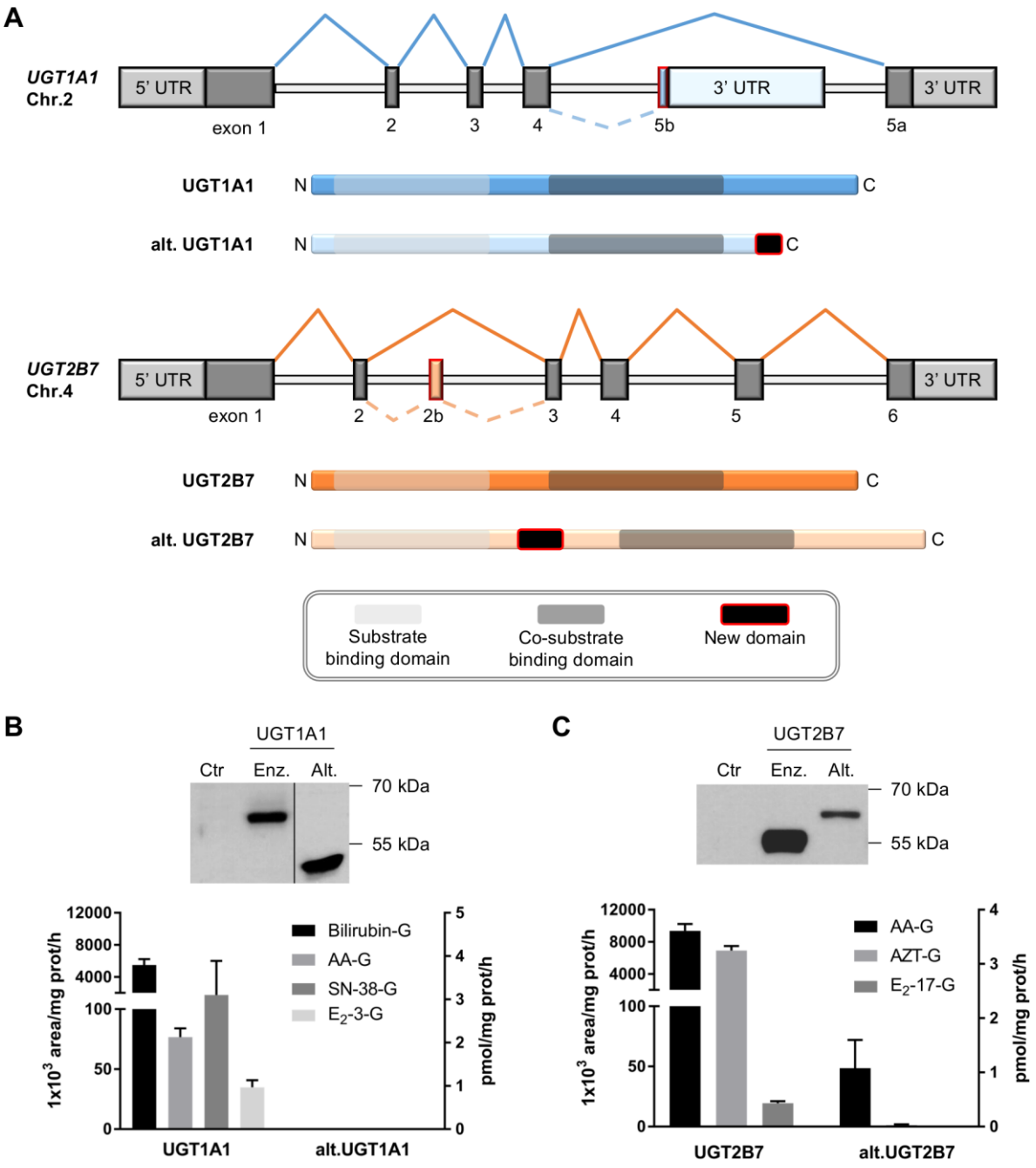
A
UGT1A1
Chr.2
5' UTR
3' UTR
3' UTR
exon 1
2
3
4
5b
5a
UGT1A1
N
C
alt. UGT1A1
N
C
UGT2B7
Chr.4
5' UTR
3' UTR
exon 1
2
2b
3
4
5
6
UGT2B7
N
C
alt. UGT2B7
N
C
Substrate binding domain
Co-substrate binding domain
New domain
B
UGT1A1
Ctr
Enz.
Alt.
70 kDa
55 kDa
1x10³ area/mg prot/h
pmol/mg prot/h
Bilirubin-G
AA-G
SN-38-G
E2-3-G
UGT1A1
alt.UGT1A1
C
UGT2B7
Ctr
Enz.
Alt.
70 kDa
55 kDa
1x10³ area/mg prot/h
pmol/mg prot/h
AA-G
AZT-G
E2-17-G
UGT2B7
alt.UGT2B7

Figure 2

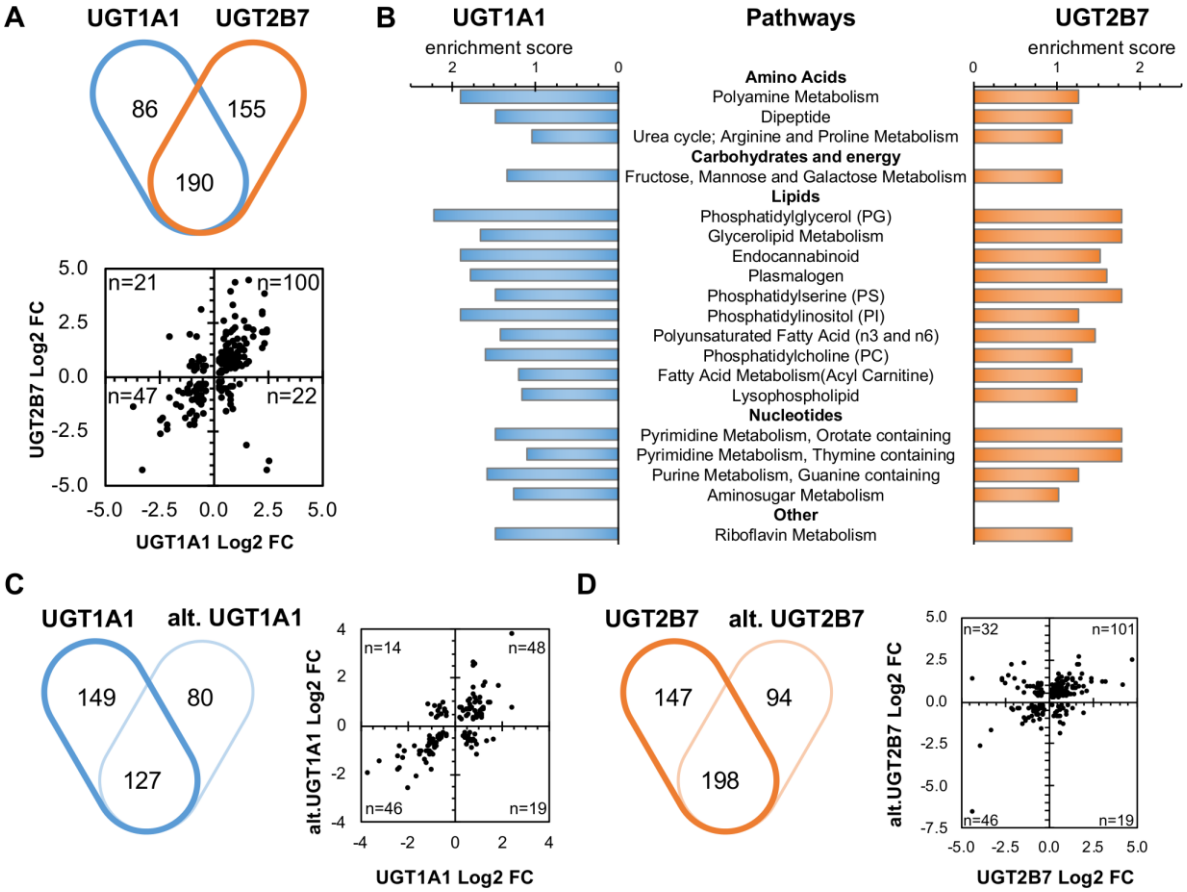
A
UGT1A1
UGT2B7
86
155
190
n=21
n=100
n=47
n=22
UGT2B7 Log2 FC
UGT1A1 Log2 FC
B
UGT1A1
enrichment score
Pathways
UGT2B7
enrichment score
Amino Acids
Polyamine Metabolism
Dipeptide
Urea cycle; Arginine and Proline Metabolism
Carbohydrates and energy
Fructose, Mannose and Galactose Metabolism
Lipids
Phosphatidylglycerol (PG)
Glycerolipid Metabolism
Endocannabinoid
Plasmalogen
Phosphatidylserine (PS)
Phosphatidylinositol (PI)
Polyunsaturated Fatty Acid (n3 and n6)
Phosphatidylcholine (PC)
Fatty Acid Metabolism(Acyl Carnitine)
Lysophospholipid
Nucleotides
Pyrimidine Metabolism, Orotate containing
Pyrimidine Metabolism, Thymine containing
Purine Metabolism, Guanine containing
Aminosugar Metabolism
Other
Riboflavin Metabolism
C
UGT1A1
alt. UGT1A1
149
80
127
n=14
n=48
n=46
n=19
alt.UGT1A1 Log2 FC
UGT1A1 Log2 FC
D
UGT2B7
alt. UGT2B7
147
94
198
n=32
n=101
n=46
n=19
alt.UGT2B7 Log2 FC
UGT2B7 Log2 FC

Figure 3

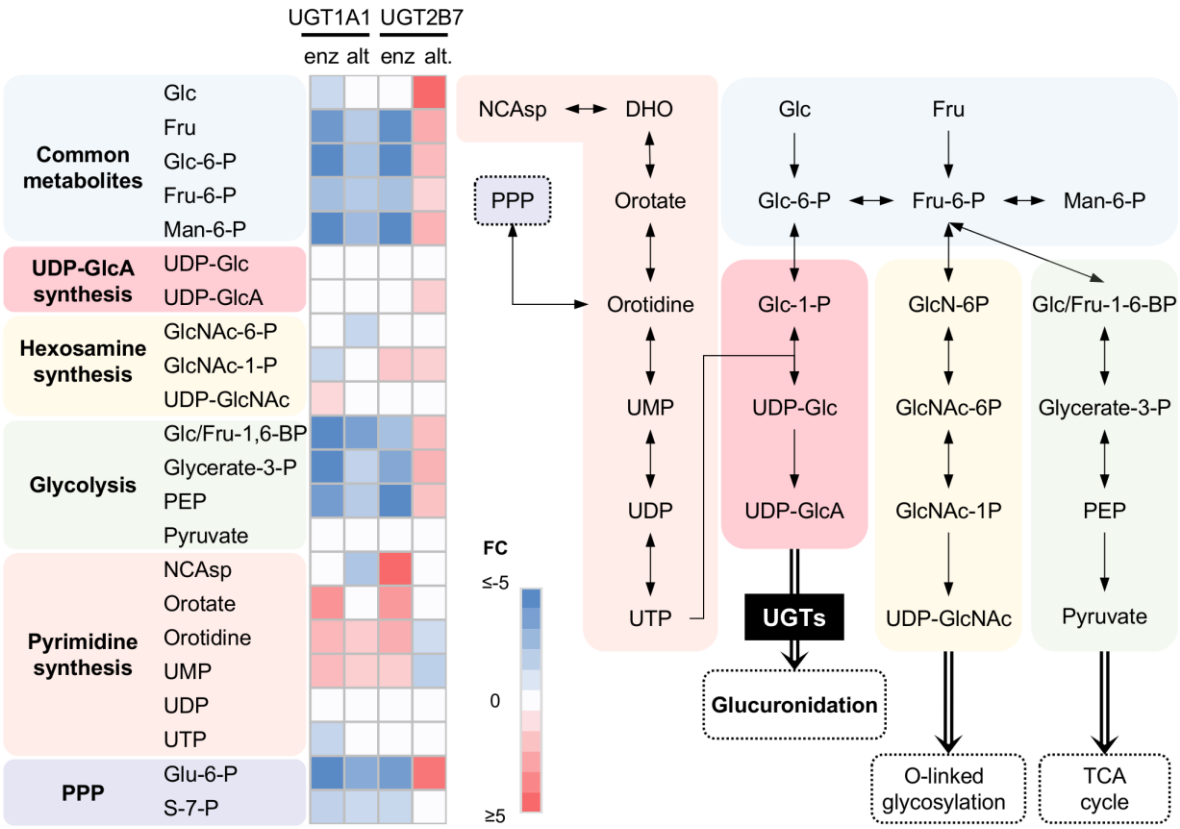
UGT1A1
UGT2B7
enz
alt
enz
alt.
Common metabolites
Glc
Fru
Glc-6-P
Fru-6-P
Man-6-P
UDP-GlcA synthesis
UDP-Glc
UDP-GlcA
Hexosamine synthesis
GlcNAc-6-P
GlcNAc-1-P
UDP-GlcNAc
Glycolysis
Glc/Fru-1,6-BP
Glycerate-3-P
PEP
Pyruvate
Pyrimidine synthesis
NCAsp
Orotate
Orotidine
UMP
UDP
UTP
PPP
Glu-6-P
S-7-P
FC
≤-5
0
≥5
NCAsp
DHO
PPP
Orotate
Orotidine
UMP
UDP
UTP
Glc
Fru
Glc-6-P
Fru-6-P
Man-6-P
Glc-1-P
UDP-Glc
UDP-GlcA
GlcN-6P
GlcNAc-6P
GlcNAc-1P
UDP-GlcNAc
Glc/Fru-1-6-BP
Glycerate-3-P
PEP
Pyruvate
UGTs
Glucuronidation
O-linked glycosylation
TCA cycle

Figure 4

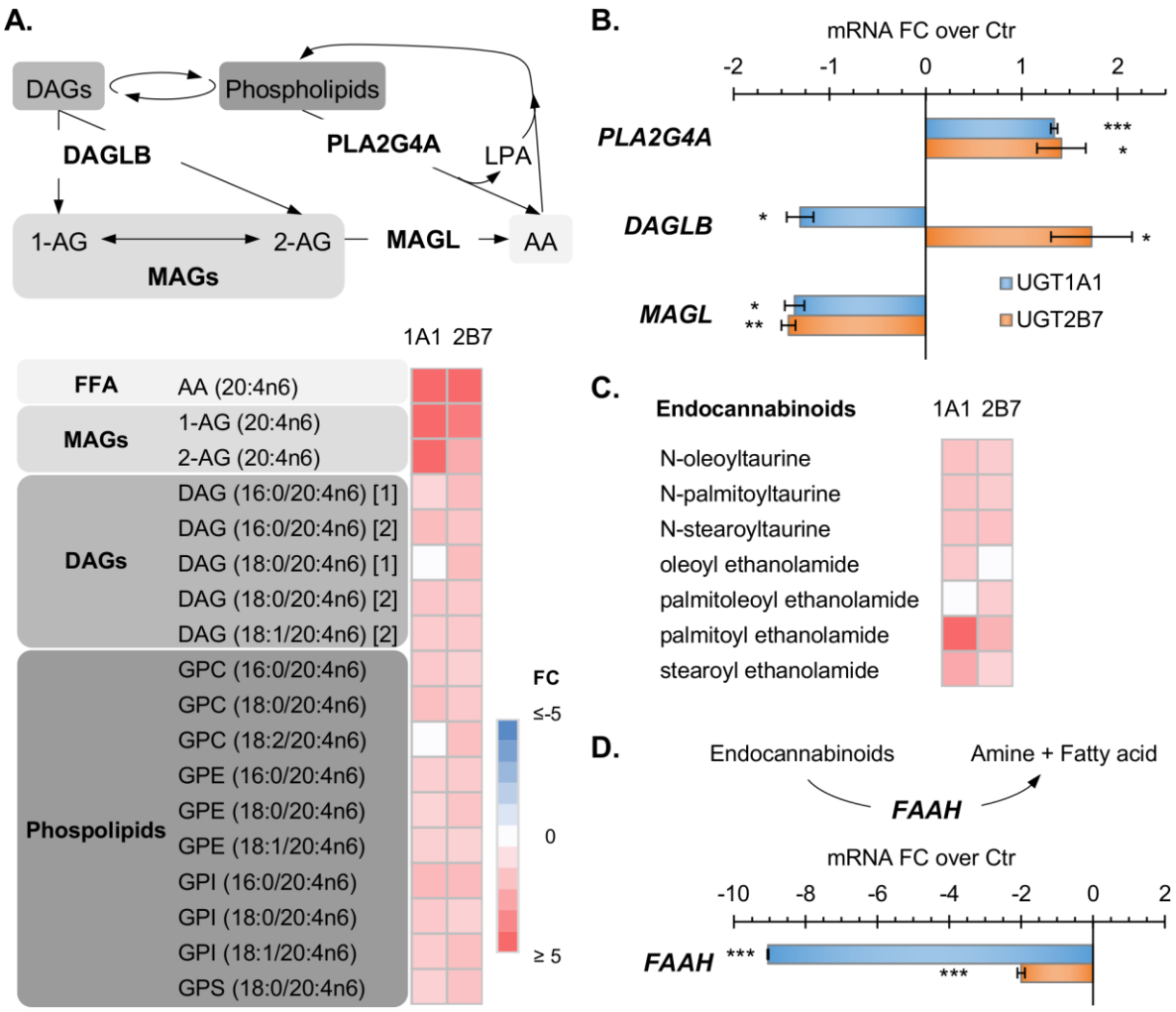
A.
DAGs
Phospholipids
DAGLB
PLA2G4A
LPA
1-AG
2-AG
MAGL
AA
MAGs
1A1 2B7
FFA
AA (20:4n6)
MAGs
1-AG (20:4n6)
2-AG (20:4n6)
DAGs
DAG (16:0/20:4n6) [1]
DAG (16:0/20:4n6) [2]
DAG (18:0/20:4n6) [1]
DAG (18:0/20:4n6) [2]
DAG (18:1/20:4n6) [2]
Phospolipids
GPC (16:0/20:4n6)
GPC (18:0/20:4n6)
GPC (18:2/20:4n6)
GPE (16:0/20:4n6)
GPE (18:0/20:4n6)
GPE (18:1/20:4n6)
GPI (16:0/20:4n6)
GPI (18:0/20:4n6)
GPI (18:1/20:4n6)
GPS (18:0/20:4n6)
FC
≤-5
0
≥ 5
B.
mRNA FC over Ctr
-2
-1
0
1
2
PLA2G4A
DAGLB
MAGL
UGT1A1
UGT2B7
C.
Endocannabinoids
1A1 2B7
N-oleoyltaurine
N-palmitoyltaurine
N-stearoyltaurine
oleoyl ethanolamide
palmitoleoyl ethanolamide
palmitoyl ethanolamide
stearoyl ethanolamide
D.
Endocannabinoids
Amine + Fatty acid
FAAH
mRNA FC over Ctr
-10
-8
-6
-4
-2
0
2
FAAH

Figure 5

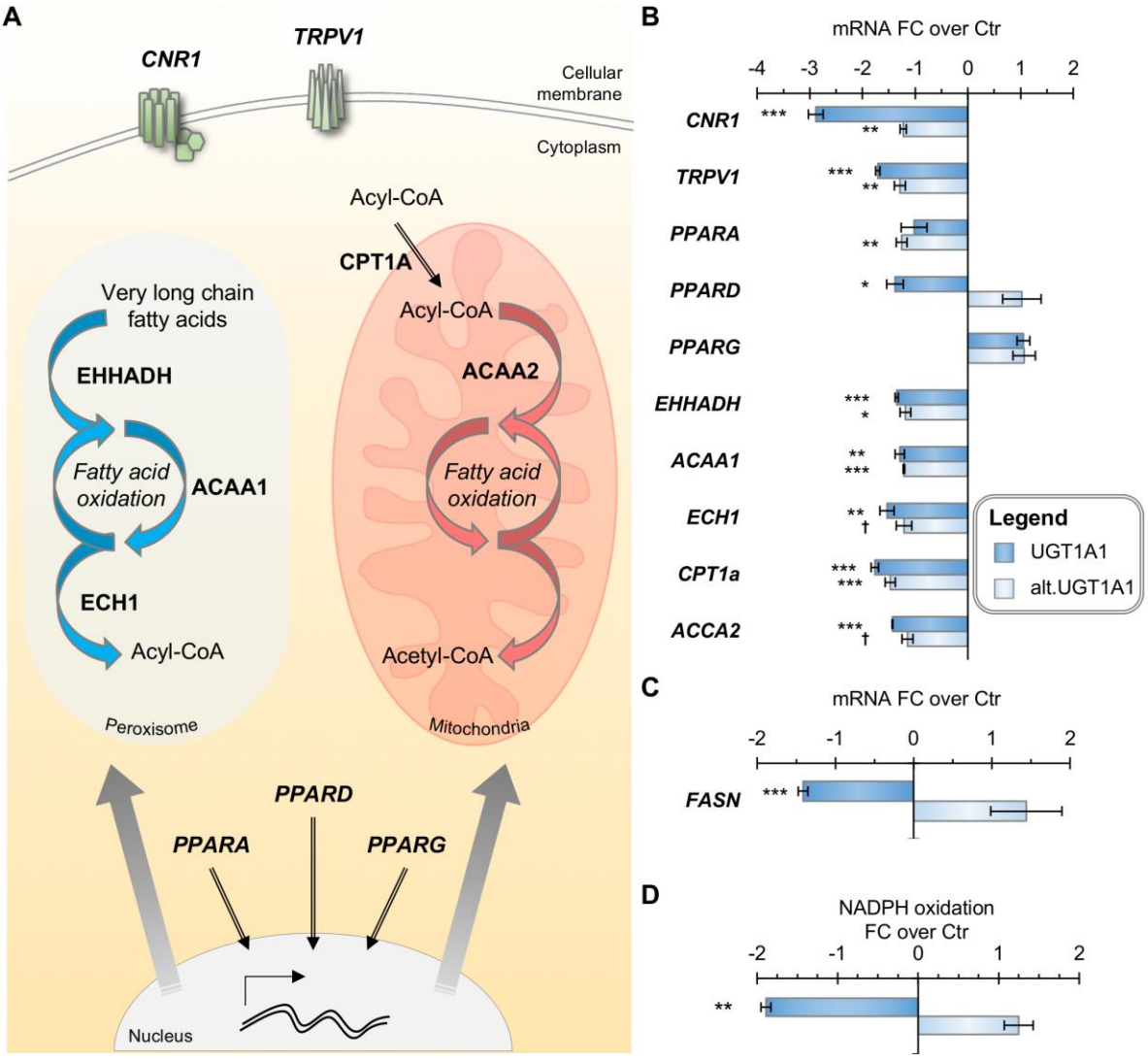
A
CNR1
TRPV1
Cellular membrane
Cytoplasm
Acyl-CoA
CPT1A
Very long chain fatty acids
EHHADH
Fatty acid oxidation
ACAA1
ECH1
Acyl-CoA
Peroxisome
Acyl-CoA
ACAA2
Fatty acid oxidation
Acetyl-CoA
Mitochondria
PPARD
PPARA
PPARG
Nucleus
B
mRNA FC over Ctr
-4 -3 -2 -1 0 1 2
CNR1
TRPV1
PPARA
PPARD
PPARG
EHHADH
ACAA1
ECH1
CPT1a
ACCA2
Legend
UGT1A1
alt.UGT1A1
C
mRNA FC over Ctr
-2 -1 0 1 2
FASN
D
NADPH oxidation
FC over Ctr
-2 -1 0 1 2

Figure 6

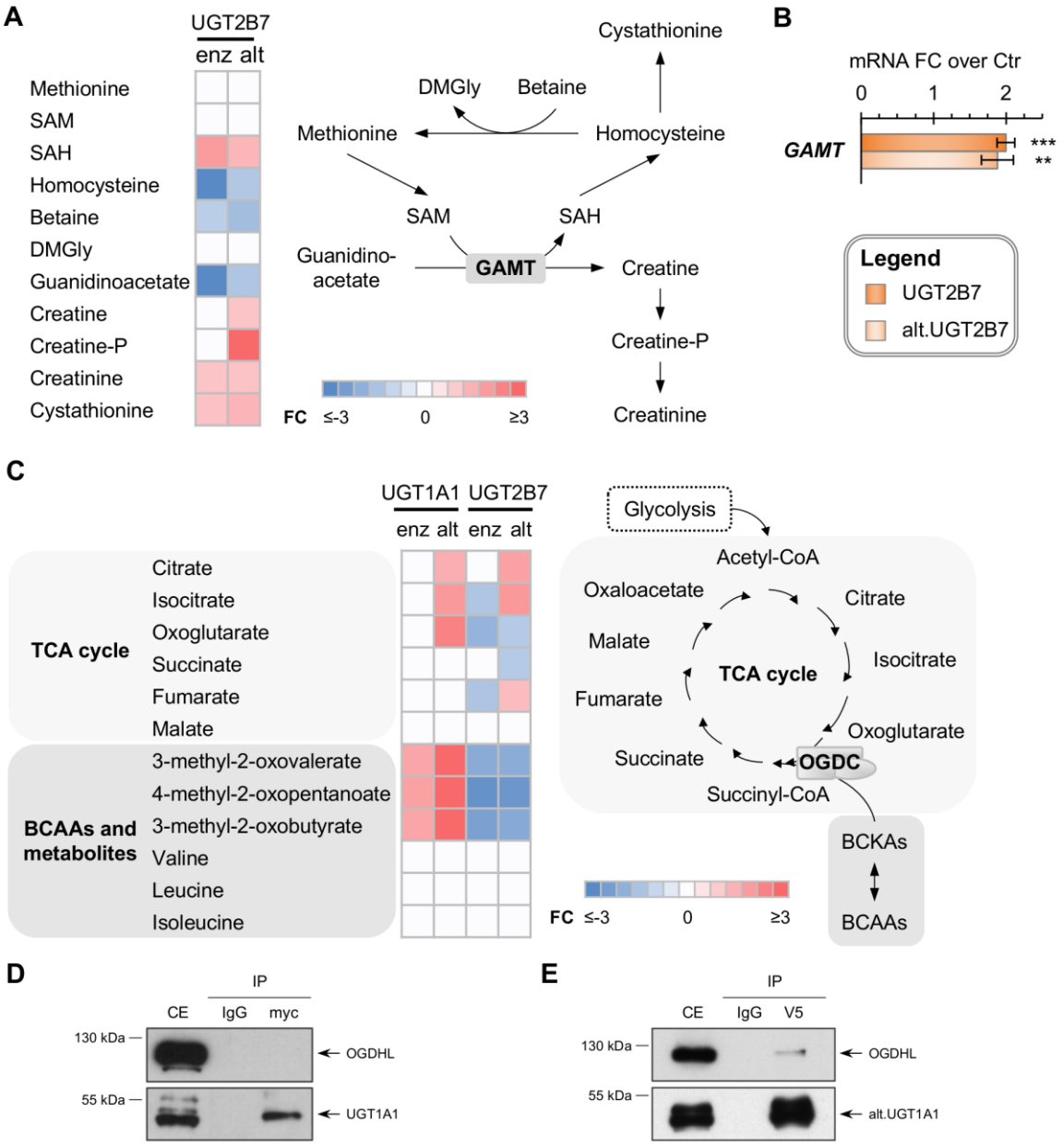
A
UGT2B7
enz alt
Methionine
SAM
SAH
Homocysteine
Betaine
DMGly
Guanidinoacetate
Creatine
Creatine-P
Creatinine
Cystathionine
Cystathionine
DMGly
Betaine
Methionine
Homocysteine
SAM
SAH
Guanidino-
acetate
GAMT
Creatine
Creatine-P
Creatinine
FC ≤-3 0 ≥3
B
mRNA FC over Ctr
0 1 2
GAMT
***
**
Legend
UGT2B7
alt.UGT2B7
C
UGT1A1 UGT2B7
enz alt enz alt
TCA cycle
Citrate
Isocitrate
Oxoglutarate
Succinate
Fumarate
Malate
BCAAs and metabolites
3-methyl-2-oxovalerate
4-methyl-2-oxopentanoate
3-methyl-2-oxobutyrate
Valine
Leucine
Isoleucine
Glycolysis
Acetyl-CoA
Oxaloacetate
Citrate
Malate
TCA cycle
Isocitrate
Fumarate
Oxoglutarate
Succinate
OGDC
Succinyl-CoA
BCKAs
BCAAs
FC ≤-3 0 ≥3
D
IP
CE IgG myc
130 kDa
55 kDa
OGDHL
UGT1A1
E
IP
CE IgG V5
130 kDa
55 kDa
OGDHL
alt.UGT1A1

Supplementary Material

Supplementary Table 1. Primers for gene expression analysis by qPCR.

Gene	Primer Sequences
PLA2G4A	F- ACTGCACAATGCCCTTTACC R- CGGGAGCCATAAAAGTACCA
DAGLB	F- TGCTTCATCAGCAACAGGAC R- CAGCAGTCACCACCAATCC
MAGL	F- ATGCAGAAAGACTACCCTGGGC R- TTATTCCGAGAGAGCACGC
FAAH	F- AAGGTGATTTCGTGGACCCC R- CCAGCCGAACGAGACTTCAT
PPARA	F- GCTGGTGTATGACAAGTGCG R- TCTTGGCATTCGTCCAAAACG
PPARD	F- CTTCCAGCAGCTACACAGACCTC R- TACTGGCACTTGTTGCGGTT
PPARG	F- AGATGACAGCGACTTGGCAATA R- AGGGCTTGTAGCAGGTTGTCT
CNR1	F- GATGCGAAGGGATTGCCCC R- GATGGTGCGGAAGGTGGTAT
CNR2	F- CCACCCACAACACAACCCAAAG R- GCTGTCTTCTGGGGACCACT
TRPV1	F- GGGTACACACCTGATGGCAA R- GCCTGAAACTCTGCTTGACC
ACAA1	F- GAGATCAATGAGGCCTTTGC R- GATGCACATGGACACCACTC
ECH1	F- GGGATAGTGGCTTCTCGCAG R- CCAGTGAGGCGAAGGCTAAT
EHHADH	F- GTGAAGGAGCTTGGTGGTGT R- AAAAGAAGTGGGTGCCAATG
CPT1a	F- AGATGAGTCGTGCCACCAAG R- CCACCAGTCGCTCACGTAAT
HADHB	F- TAATCATGGCGGAGGAAAAG R- CCAAAATCTGACCCGAGAAA
ACAA2	F- GGCTGTTGAGAGGAGTTTGG R- GGCTGTGCTCTGAATGATGA

Supplementary Figure 1

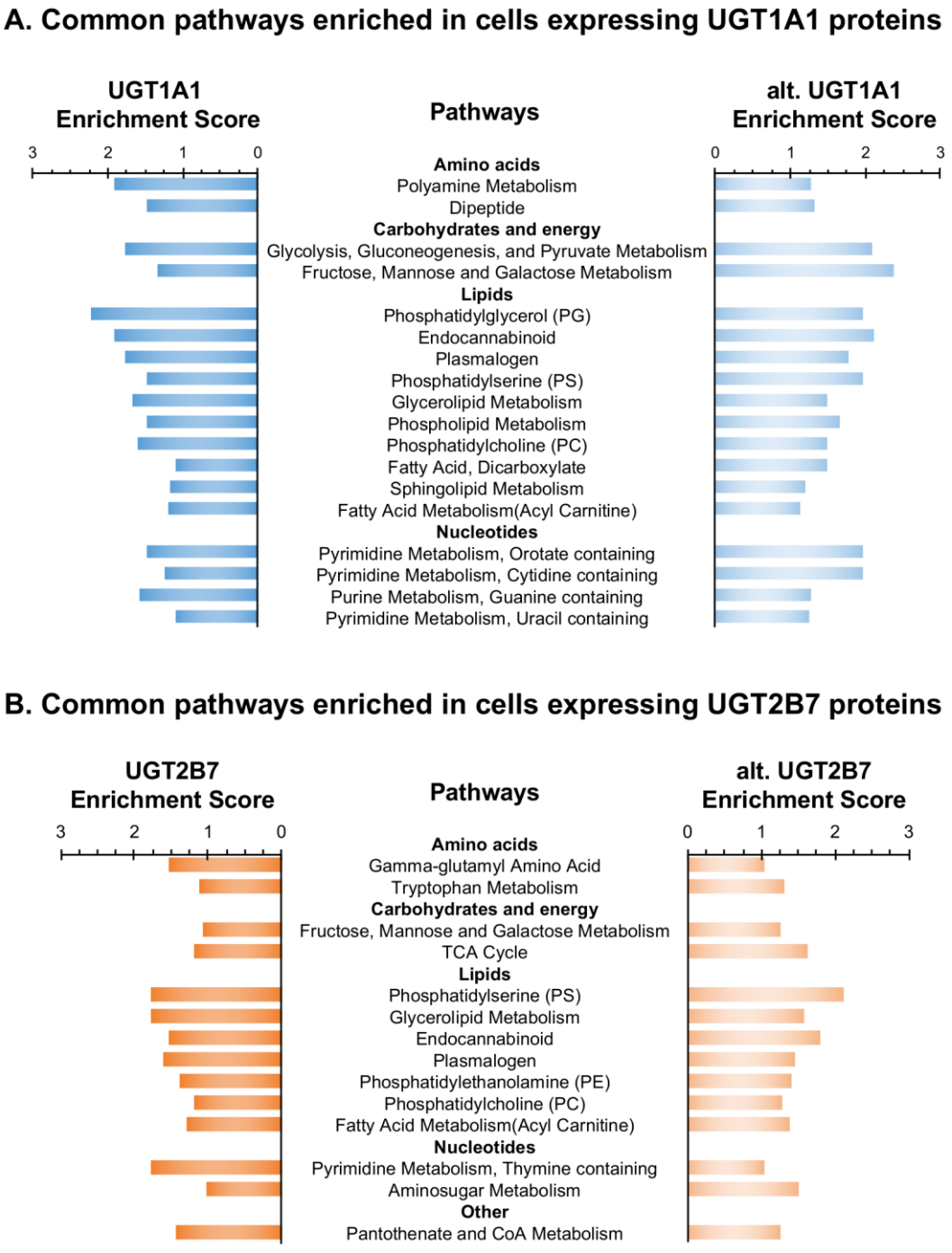

Supplementary Figure 1. Pathway enrichment analysis revealed perturbations common to **A)** UGT1A1 and **B)** UGT2B7 enzymes and alt. proteins. Displayed pathways were enriched in both cell models with an enrichment score > 1 and comprised at least 3 metabolites. Metabolites were categorized according to Metabolon proprietary database.

Chapitre 3 : « Endogenous protein interactome of human UDP-glucuronosyltransferases exposed by untargeted proteomics »

Résumé

Le métabolisme de conjugaison médié par les UGT influence significativement la biodisponibilité et la réponse biologique à des substrats endogènes et exogènes de ces enzymes, incluant des médicaments. Les UGT participent à la régulation de l'homéostasie cellulaire en limitant le stress induit par des molécules toxiques, et en contrôlant la signalisation hormonale. La glucuronidation est hautement régulée tant au niveau génomique, transcriptionnel, post-transcriptionnel que post-traductionnel. Le réseau d'interaction protéique des UGT, ayant le potentiel d'influencer l'activité de glucuronidation, a cependant été peu étudié. Nous avons investigué l'interactome endogène des enzymes UGT1A dans les principaux tissus du métabolisme des médicaments, où l'expression de ces enzymes est plus prévalente, en utilisant une approche protéomique non-biaisée. L'analyse par spectrométrie de masse de complexes protéiques UGT purifiés par affinité dans le foie, les reins et les intestins a identifié un réseau d'interactions complexe, reliant les enzymes UGT à de nombreuses voies métaboliques. Nous avons identifié plusieurs protéines importantes pour la pharmacologie, tels que des transférases (incluant les UGT2), des transporteurs et des déshydrogénases, supportant l'existence d'une coordination de la réponse cellulaire à des petites molécules lipophiles et des médicaments. De plus, nous avons observé des regroupements d'enzymes fonctionnellement liées parmi les partenaires des enzymes UGT1A, notamment dans la béta-oxydation des lipides, la glycolyse et la gluconéogenèse. Plusieurs de ces partenariats sont validés par co-immunoprécipitation et par co-localisation en microscopie confocale. En support d'une interaction fonctionnelle, nous avons observé une accumulation de gouttelettes lipidiques dans un modèle cellulaire rénal exprimant l'enzyme UGT1A9. Ces travaux représentent les premières preuves d'une interaction entre la voie de glucuronidation et le métabolisme bioénergétique.

Endogenous protein interactome of human UDP-glucuronosyltransferases exposed by untargeted proteomics

Michèle Rouleau, Yannick Audet-Delage, Sylvie Desjardins, Mélanie Rouleau, Camille Girard-Bock and Chantal Guillemette*

Pharmacogenomics Laboratory, Canada Research Chair in Pharmacogenomics, Centre Hospitalier Universitaire (CHU) de Québec Research Center and Faculty of Pharmacy, Laval University, G1V 4G2, Québec, Canada

*Corresponding author:

Chantal Guillemette, Ph.D.

Canada Research Chair in Pharmacogenomics

Pharmacogenomics Laboratory, CHU de Québec Research Center, R4720

2705 Boul. Laurier, Québec, Canada, G1V 4G2

Tel. (418) 654-2296 Fax. (418) 654-2298

E-mail: Chantal.Guillemette@crchudequebec.ulaval.ca

Running title: Human UGT1A interaction network

Number of: Pages: 26

Tables: 2

Figures: 5

References: 62

Supplemental Tables: 7

Supplemental Figures: 5

Number of words: Total: 7882

Abstract: 229

Introduction: 549

Results: 1309

Discussion: 1403

Body Text: 3261

Abbreviations: AP: affinity purification; UGT, UDP-glucuronosyltransferases; IP, immuno-precipitation; PPIs, protein-protein interactions; UDP-GlcA, Uridine diphospho-glucuronic acid; ER, endoplasmic reticulum; MS, mass spectrometry.

Keywords: UGT; Proteomics; Protein-protein interaction; Affinity purification; Mass spectrometry; Metabolism; Human tissues;

Abstract

The conjugative metabolism mediated by UDP-glucuronosyltransferase enzymes (UGTs) significantly influences the bioavailability and biological responses of endogenous molecule substrates and xenobiotics including drugs. UGTs participate in the regulation of cellular homeostasis by limiting stress induced by toxic molecules, and by controlling hormonal signaling networks. Glucuronidation is highly regulated at genomic, transcriptional, post-transcriptional and post-translational levels. However, the UGT protein interaction network, which is likely to influence glucuronidation, has received little attention. We investigated the endogenous protein interactome of human UGT1A enzymes in main drug metabolizing non-malignant tissues, where UGT expression is most prevalent, using an unbiased proteomics approach. Mass spectrometry analysis of affinity-purified UGT1A enzymes and associated protein complexes in liver, kidney and intestine tissues revealed an intricate interactome linking UGT1A enzymes to multiple metabolic pathways. Several proteins of pharmacological importance such as transferases (including UGT2 enzymes), transporters and dehydrogenases were identified, upholding a potential coordinated cellular response to small lipophilic molecules and drugs. Furthermore, a significant cluster of functionally related enzymes involved in fatty acid β-oxidation, as well as in the glycolysis and glycogenolysis pathways were enriched in UGT1A enzymes complexes. Several partnerships were confirmed by co-immunoprecipitations and co-localization by confocal microscopy. An enhanced accumulation of lipid droplets in a kidney cell model overexpressing the UGT1A9 enzyme supported the presence of a functional interplay. Our work provides unprecedented evidence for a functional interaction between glucuronidation and bioenergetic metabolism.

Introduction

UDP-glucuronosyltransferases (UGTs) are well known for their crucial role in the regulation of cellular homeostasis, by limiting stress induced by toxic drugs, other xenobiotics and endogenous lipophilic molecules, and by controlling the hormonal signaling network (Rowland et al., 2013; Guillemette et al., 2014). UGTs coordinate the transfer of the sugar moiety of their co-substrate UDP-glucuronic acid (UDP-GlcA) to amino, hydroxyl and thiol groups on a variety of lipophilic molecules, thereby reducing their bioactivity and facilitating their excretion. In humans, nine UGT1A and ten UGT2 enzymes constitute the main glucuronidating enzymes. UGTs are found in nearly all tissues, each UGT displaying a specific tissue-expression profile, and are most abundant in the liver, kidney and gastrointestinal tract, where drug metabolism is highly active. These membrane-bound enzymes localized in the endoplasmic reticulum (ER) share between 55 and 97 % sequence identity, thus displaying substrate specificity and some overlapping substrate preferences (Rowland et al., 2013; Guillemette et al., 2014; Tourancheau et al., 2016). For instance, the alternative first exons of the single *UGT1* gene produce the nine UGT1A enzymes with distinct N-terminal substrate binding domains but common C-terminal UDP-GlcA-binding and transmembrane domains. The seven UGT2B enzymes and UGT2A3 are encoded by eight distinct genes, whereas UGT2A1 and UGT2A2 originate from a single gene by a UGT1A-like, alternative exon 1 strategy. However, similar to UGT1As, substrate binding domains of UGT2 enzymes are more divergent than their C-terminal domains.

Genetic variations, epigenetic regulation, as well as posttranscriptional and translational modifications, all contribute to the modulation of UGT conjugation activity, thereby influencing an individual's response to pharmacologic molecules and the bioactivity of endogenous molecules (Guillemette et al., 2010; Ramirez et al., 2010; Guillemette et al., 2014; Hu et al., 2014; Dluzen and Lazarus, 2015). For instance, genetic lesions at the *UGT1* locus that impair UGT1A1 expression or activity result in transient or fatal hyperbilirubinemia, characterizing Gilbert and Crigler-Najjar syndromes, respectively (Costa, 2006).

Several lines of evidence support protein-protein interactions (PPIs) among UGTs and with other enzymes of pharmacological importance (Taura et al., 2000; Fremont et al., 2005; Takeda et al., 2005a; Takeda et al., 2005b; Ishii et al., 2007; Takeda et al., 2009; Ishii et al., 2014) (Operana and Tukey, 2007). These interactions may also significantly influence UGT enzymatic activity (Bellemare et al., 2010b; Menard et al., 2013; Ishii et al., 2014; Fujiwara

et al., 2016). In addition, interactions of UGT proteins with some anti-oxidant enzymes that have been recently uncovered have raised the interesting concept of alternative functions of UGTs in cells (Rouleau et al., 2014). However, most studies have been conducted in cell-based systems with overexpression of tagged UGTs and little evidence in human tissues supports the extent of this mechanism and its physiological significance.

PPIs are essential to cell functions including responses to extracellular and intracellular stimuli, protein subcellular distribution, enzymatic activity, and stability. Understanding molecular interaction networks in specific biological contexts is therefore highly informative of protein functions. We aimed to gain insight on the endogenous protein interaction network of UGT1A enzymes by applying an unbiased proteomics approach in main drug metabolizing human tissues. In doing so, we provide support to a potential coordinated cellular response to small lipophilic molecules and drugs. Importantly, a potential functional interplay between UGT1A enzymes and those of bioenergetic pathways also emerges from this exhaustive endogenous interaction network.

Materials and methods

UGT1A enzyme antibodies – The anti-UGT1A rabbit polyclonal antibody (#9348) that specifically recognizes UGT1A enzymes, and not the alternative UGT1A variant isoforms 2, has been described (Bellemare et al., 2011). Purification was performed using the biotinylated immunogenic peptide (K_{520}KGRVKKAHKSKTH_{533}; Genscript, Piscataway, NJ, USA) and streptavidin magnetic beads (Genscript) per the manufacturer's instructions. Antibodies (3 ml) were incubated O/N at 4°C with peptide-streptavidin beads, and then washed with PBS to remove unbound immunoglobulins. UGT1A-specific antibodies were eluted using glycine (0.125 M, pH 2.9), and rapidly buffered with Tris pH 8.0. Purified antibodies were subsequently concentrated using a centrifugal filter unit (cut off 3 kDa; Millipore (Fisher Scientific), Ottawa, ON) to a final volume of 1 ml.

Affinity purification of endogenous UGT1A enzymes and their interacting partners in human tissues and a UGT1A expressing cellular model – Human liver, kidney and intestine S9 fractions comprised of ER and associated membranes as well as cytosolic cellular content (Xenotech LLC, Lenexa, KS, USA) were from 50, 4 and 13 donors, respectively. This study was reviewed by the local ethics committee and was exempt given that anonymized human tissues were from a commercial source. Human colon cancer HT-29 cells (ATCC, Manassas, VA, USA) were grown in DMEM supplemented with 10% fetal

bovine serum (Wisent, St-Bruno, QC, Canada), 50 mg/ml streptomycin, 100 IU/ml penicillin, at 37°C in a humidified incubator with 5% CO_2 as recommended by ATCC. Immunoprecipitations (IP) were conducted according to standard procedures (Savas et al., 2011; Ruan et al., 2012), with at least three independent replicates per sample source. For each sample, 1 mg protein was lysed in 1 ml lysis buffer A (final concentration: 50 mM Tris-HCl pH 7.4, 150 mM NaCl, 0.3% deoxycholic acid, 1% Igepal CA-630 (Sigma-Aldrich), 1 mM EDTA, Complete protease inhibitor (Roche, Laval, QC, Canada)) for 45 min on ice. This buffer included deoxycholate to enhance membrane solubilization and stringency of immunoprecipitation conditions. Lysates were then homogenized by pipetting up and down through fine needles (18G followed by 20G) 10–20 times on ice. Lysates were cleared of debris by centrifugation for 15 min at 13,000 *g*. UGT1A enzymes were immunoprecipitated from cleared lysates with 4 µg of purified anti-UGT1A for 1 h at 4°C with end-over-end agitation. After addition of protein G–coated magnetic beads (200 µl Dynabeads, Life Technologies, Burlington, ON), lysates were incubated O/N at 4°C. Beads were washed three times with 1 ml lysis buffer A and subsequently processed for mass spectrometry (MS) analysis, as described below. Control IPs were conducted in similar conditions using 4 µg normal rabbit IgGs (Sigma-Aldrich) per protein sample. The inclusion of 150 mM NaCl and 0.3% deoxycholate ensured stringent wash conditions.

Liquid chromatography-MS/MS identification of UGT1A interacting partners – Protein complexes bound to magnetic beads were washed 5 times with 20 mM ammonium bicarbonate (1 ml). Tryptic digestion and desalting was performed as described (Rouleau et al., 2016). Briefly, bead-bound proteins were digested in 10 µg/µl trypsin for 5 hrs at 37°C. The tryptic digest was recovered, dried, and resuspended in 30 µl sample buffer (3% acetonitrile, 0.1% trifluoroacetic acid, 0.5% acetic acid). Peptides were desalted on a C18 Empore filter (ThermoFisher Scientific), dried out, resuspended in 10 µl 0.1% formic acid and analyzed using high-performance liquid chromatography-coupled MS/MS on a LTQ linear ion trap-mass spectrometer equipped with a nanoelectrospray ion source (Thermo Electron, San Jose, CA, USA) or on a triple-quadrupole time-of-flight mass spectrometer (TripleTOF 5600, AB Sciex, Concord, ON) as described (Rouleau et al., 2014). Data files were submitted for simultaneous searches using Protein Pilot version 4 software (AB Sciex) utilizing the Paragon and Progroup algorithms (Shilov). The RAW or MGF file created by Protein Pilot was used to search with Mascot (Matrix Science, London, UK; version 2.4.1). Mascot was set up to search against the human protein database (Uniref May 2012; 204083

entries) supplemented with a complete human UGT protein sequence database comprised of common UGT coding variations and protein sequences of newly discovered alternatively spliced UGT isoforms (assembled in-house (November 2013; 882 entries). Mascot analysis was conducted using the following settings: tryptic peptides, fragment and parent ion tolerance of 0.100 Da, deamidation of asparagine and glutamine and oxidation of methionine specified as variable modifications, deisotoping was not performed, two missed cleavage were allowed. Mass spectra were also searched in a reversed database (decoy) to evaluate the false discovery rate (FDR). On-beads digestion and MS analyses were performed by the proteomics platform of the CHU de Québec Research Center. The MS proteomics data have been deposited to the ProteomeXchange Consortium (http://proteomecentral.proteomexchange.org) via the PRIDE partner repository with the dataset identifier PXD000295.

Identification of proteins in Scaffold (version 4.6.1; Proteome Software, Portland, OR) was carried out using two sets of criteria: 1- for UGT proteins, 95% peptide and protein probability, and 1 unique peptide were used, considering the high level of sequence identity among the proteins in this family. For the same reason of high sequence identity, each identified peptide was manually assigned to the proper UGT protein or to the common UGT sequence (**Supplementary Table 1**). 2- For UGT1A interacting proteins, specificity threshold was set to 95% peptide and protein probability and a minimum of 2 unique peptides. Proteins that contained similar peptides and could not be differentiated based on MS/MS analysis alone were grouped to satisfy the principles of parsimony. Detailed proteomics datasets are provided in **Supplementary Tables 4-7**.

Confidence scores of each UGT1A-protein interaction were determined using the computational tools provided online at http://crapome.org (Choi et al., 2011). Spectral counts for each identified protein were normalized to the length of the protein and total number of spectra in the experiment. Two empirical scores (FC-A and more stringent FC-B) and one probability score (SAINT) (Mellacheruvu et al., 2013) were then calculated based on normalized spectral counts of identified proteins in UGT1A immunoprecipitation samples compared to our matching control immunoprecipitation samples (CRAPome Workflow 3). Confidence score calculations were conducted separately for each tissue, with the following analysis options: FC-A: Default parameters; FC-B: User controls, stringent background estimation, geometric combining replicates; SAINT: User Controls, Average - best 2

Combining replicates, 10 Virtual controls and default SAINT options. Confidence scores for all UGT1A interaction partners are given in **Supplementary Table 2**.

Bioinformatics tools and data analysis – The common external contaminants keratins and trypsin were manually removed from the lists of interacting proteins prior to pathway enrichment analysis. UGT1A interacting partners were classified according to KEGG pathways (update November 12, 2016) using ClueGO and CluePedia Apps (v2.3.2) in Cytoscape 3.4 (Bindea et al., 2009; Bindea et al., 2013). Enrichment was determined based on a two-sided hypergeometric statistical test and a Bonferroni step down correction method. Only enriched pathways with P <0.05 and a Kappa score threshold of 0.4 were considered. The following optional criteria were also used for the search: minimum # genes = 4, minimum 2% genes. The UGT1A interactome was generated using Cytoscape basic tools. Because protein annotations based on tools such as KEGG and Gene Ontology are partial, the UGT1A interactome was subsequently manually extended to include significant UGT1A interactors that were absent in the original output but involved in enriched pathways, per their Uniprot entries (www.uniprot.org) and literature mining. Details are included in the legend of **Fig.3**.

Validation of protein-protein interactions by co-IP and immunofluorescence (IF) – HEK293 cells stably expressing the human enzyme UGT1A9-myc/his (a pool of cells) were used (Bellemare et al., 2010a). Expression and glucuronidation activity of the tagged UGT1A9 in this model have been described and were similar to the untagged enzyme (Bellemare et al., 2010a). In the current study, only the myc tag served for UGT1A9 detection and the his tag was not exploited. Cells were transfected with Lipofectamine 2000 (Life Technologies) to transiently express tagged protein partners. HA-ACOT8 and FLAG-SH3KBP1 were kindly provided by Dr Ming-Derg Lai (National Cheng Kung University, Taiwan (Hung et al., 2014)) and Dr Mark McNiven (Mayo Clinic, Rochester, MN (Schroeder et al., 2010)) respectively. The PHKA2-myc-FLAG expression construct was purchased from OriGene (Rockville, MD, USA).

Co-IP: HEK293 cells (3 x 10^5 cells plated in 10 cm dishes) were harvested 40 hrs post-transfection. Cells were washed three times with PBS, lysed in 800 µl lysis buffer B (50 mM Tris-HCl pH 7.4, 150 mM NaCl, 1 % Igepal, 1 mM DTT, complete protease inhibitor) for 1 h at 4°C and subsequently homogenized and centrifuged as described above. Immunoprecipitation with purified anti-UGT1A antibodies (2 µg) or control rabbit IgG (2 µg)

and 50 µl Protein-G magnetic beads was as above. Protein complexes were washed three times in lysis buffer B and eluted in Laemmli sample buffer by heating at 95°C for 5 min. Eluates were subjected to SDS-PAGE, and the presence of interacting partners was revealed by immunoblotting using anti-tag antibodies specified in figures and legends: anti-myc (clone 4A6, EMD Millipore, Etobicoke, ON, Canada; 1:5000), anti-FLAG (clone M2, Sigma-Aldrich, St-Louis, MO, USA; 1:20 000) and anti-HA (Y-11, Santa Cruz Biotechnologies, Dallas, TX, USA; 1:500).

IF: HEK293 cells (2 x 10^5 cells per well of 6-well plates) grown on coverslips were harvested 36 hrs post-transfection and processed for IF, as described (Rouleau et al., 2016). ACOT8 was detected with anti-HA (1:500), SH3KBP1 with anti-FLAG (1:1500), UGT1A9-myc/his with anti-myc (1:200) or purified anti-UGT1A (1:500), and with secondary goat anti-rabbit, goat anti-mouse or donkey anti-mouse respectively, conjugated to either AlexaFluor 488 or 594 (1:1000; Invitrogen). Immunofluorescence images were acquired on a LSM510 META NLO laser scanning confocal microscope (Zeiss, Toronto, ON, Canada). Zen 2009 software version 5.5 SP1 (Zeiss) was used for image acquisitions.

Quantification of lipid droplets – HEK293 cells grown on coverslips were fixed in 3.7% formaldehyde (Sigma) for 30 min at RT. Cells were then gently washed three times with PBS and incubated for 10 minutes in 0.4 µg/mL Nile Red (Sigma). After being rinsed three times, coverslips were mounted on glass slides using Fluoromount (Sigma) as a mounting medium. Images were acquired on a Wave FX-Borealis (Quorum Technologies, Guelph, ON, Canada) - Leica DMI 6000B (Clemex Technologies inc., Longueil, QC, Canada) confocal microscope, with a 491 nm laser and 536 nm filter. Z-stacks were acquired every 0.15 µm. Stacks were analyzed using ImageJ (v1.51f; U.S. National Institutes of Health, Bethesda, MD, USA) and the 3-D Object Counter plugin (Bolte and Cordelieres, 2006). Results are derived from 3 independent experiments and more than 140 cells per experiment were analyzed for each condition. Fluorescence images were acquired on an LSM 510 microscope as above.

Results

Endogenous UGT1A enzymes associate with several other metabolic proteins in non-malignant human tissues

The endogenous interactome of human UGT1A enzymes was established in three major metabolic tissues, namely liver, kidney and intestine from pools of 4 to 50 donors, using S9 tissue fractions comprised of ER and associated membranes as well as cytosolic cellular content (**Fig.1**). IPs were conducted with an antibody specific to the C-terminal region common to the nine human UGT1A enzymes, thereby allowing affinity purification of all UGT1A enzymes expressed in studied tissues (**Fig.1A**). This antibody was shown by western blotting to lack affinity for alternatively spliced UGT1A isoform 2 proteins derived from the same human *UGT1* gene locus (Bellemare et al., 2011). The experimental approach to establish the endogenous UGT1A enzymes interactome using the anti-UGT1A enzymes antibody is presented in **Fig.1B**.

Multiple UGT1A enzymes were immunopurified from each tissue in line with their documented expression profile (**Fig.2**). The list of specific UGT1A enzymes immunoprecipitated from each tissue was established based on their unique N-terminal peptide sequences, whereas multiple additional peptides corresponding to the common C-terminal half of the UGT1A proteins and thereby common to all UGT1A enzymes were also observed (**Fig.2B, Supplementary Fig.1**; **Supplementary Table 1**).

Spectral counts for unique peptides provided a quantitative appreciation of immunoprecipitated UGT1A (**Fig.2A**). UGT1A1 and UGT1A4 were the most abundant UGT1As in hepatic IPs, whereas UGT1A1 and UGT1A10 were predominantly immunopurified from the intestine and UGT1A9 from the kidney (**Fig.2A, Supplementary Table 1**). UGT1A9 (n=51 spectra) was far more abundant than UGT1A6 (n=2 spectra) in the kidney whereas UGT1A10 (n=194 spectra) predominated over most other UGT1A in the intestine, although all UGT1A enzymes were identified besides UGT1A7 and UGT1A9. These metrics indicated that an exhaustive immunoprecipitation of UGT1As from each tissue was achieved.

UGT1A interaction network and functional annotation

A total of 9 independent AP-MS datasets (4 liver, 3 kidney and 2 intestine replicates of control and UGT1A AP-MS) efficiently immunoprecipitated UGT1A enzymes and associated proteins. Mass spectra were assigned to specific proteins using Mascot and Scaffold software. A list of UGT1A-interacting proteins was created based on the analysis of total spectral counts assigned to each identified protein in each replicate to obtain empirical (FC-B) and probability (SAINT) confidence scores (**Supplementary Table 2**). Using a FC-B

score threshold of 1.42, we reported a total of 148 proteins forming endogenous interactions with UGT1A enzymes in the three surveyed human tissues (31 in the liver, 70 in the kidney and 77 in the intestine) (**Fig.1B, Supplementary Table 2**). This FC-B threshold was selected based on the validated protein partner having the lowest probability score, corresponding to PHKA2 in the intestine (see below). This approach was chosen because of the inherent difficulty to obtain similar replicate datasets with AP-MS from tissues, especially in intestine, a variability highly penalized in the SAINT scoring algorithm (**Supplementary Fig.2**). To further strengthen the UGT1A interactome in the gastrointestinal tract, we also conducted three more replicate AP-MS experiments of endogenous UGT1A enzymes with the human colon cancer cell line HT-29, expressing high levels of UGT1As. The intestinal UGT expression profile is well represented in HT-29 cells, with UGT1A1, UGT1A6, UGT1A8 and UGT1A10 immunoprecipitated in similar proportions (**Supplementary Table 1**). Using the FC-B threshold used for tissues (1.42), 125 interaction partners were selected for further analysis. Of those, 44 proteins were common with those immunoprecipitated in non-malignant tissue samples, including 26 common with the intestine dataset (**Fig.1B, Supplementary Fig.3**). UGT1A protein partners with highest significance scores are given in **Table 1** whereas a complete list of immunoprecipitated protein partners is provided in **Supplementary Table 2**.

To portray the global functions enriched in the UGT1A interactome, the UGT1A protein partners from the three surveyed tissues were classified per the KEGG pathway database. Structural proteins such as tubulins, myosins, actin, as well as multiple ribosomal protein subunits (RPL/RPS proteins) and other RNA-binding proteins involved in mRNA splicing (e.g. heterogeneous ribonucleotide proteins (hnRNPs) and serine/arginine-rich splicing factors (SRSF) proteins) were significant classes of proteins immunoprecipitated with UGT1As. However, because these proteins are frequently non-specifically enriched in AP-MS experiments (Mellacheruvu et al., 2013), the specificity of interactions with UGT1A will require validation and will not be discussed further.

The interactome of UGT1A enzymes is characterized by numerous metabolic proteins playing roles in detoxification and bioenergetic pathways (**Fig.3**). They include the UGT2 glucuronosyltransferases UGT2A3, UGT2B4, UGT2B7 and UGT2B17, the glutathione S-transferase GSTA1, glycine N-acyltransferase GLYAT, the alcohol dehydrogenase ALDH2 and the antioxidant enzymes PRDX1 and PRDX2 (full protein names are provided in **Table 2**). Given their functions in line with high scoring proteins, ADH1B and PRDX3 were also

included in the final interactome, having confidence interaction scores just below threshold (FC-B=1.37; **Supplementary Fig.2**). Similarly, cytochrome P450 CYP3A4 was included because also observed in liver tissue with a single high confidence peptide and a previously observed interaction partner (Fremont et al., 2005; Ishii et al., 2014). Enzymes of the lipid metabolism pathway were also significantly represented and most particularly several peroxisomal and mitochondrial proteins involved in fatty acid β-oxidation, namely ACOT8, ECH1, CPT1A, and ACAA2. To encompass all potential protein partners involved in lipid metabolism, a pathway that was functionally validated at a later stage (see below), relevant but slightly lower scoring proteins were incorporated in the final interactome, namely SCP2, ACSL1, EHHADH, ACAT1, and ECHS1 (FC-B=1.38-1.19; **Supplementary Fig.2**). Finally, the glycolysis/pyruvate and glycogenolysis metabolic pathways were also significantly enriched, given the high number of immunoprecipitated UGT1A partners in these pathways. Several other protein partners, including transporters (SLC25A5, SLC25A13 and SLC34A2) and proteins participating in vesicular trafficking (RALGAPA1, RALGAPA2, RALGAPB and GBF1) were also immunoprecipitated from tissues and may represent important partners (**Table 1, Fig.3**). The interaction network of UGT1A enzymes established in the HT-29 cell model was consistent with that built from tissues, with enrichments in xenobiotic and bioenergetics metabolic pathways. Several transporters, anti-oxidant, lipid metabolism, glycolytic/glycogen metabolic enzymes and vesicular trafficking proteins were all significantly identified in AP-MS on cells, as in tissues (**Supplementary Table 2**), further supporting the significance of the endogenous interactome of UGT1A enzymes.

Experimental validation of selected UGT1A partners

Using the non-malignant kidney model cell line HEK293 (a UGT negative model) stably expressing a myc/his-tagged UGT1A9 enzyme, selected partnerships with enzymes of bioenergetic cellular pathways were confirmed by a co-IP/immunodetection approach. The peroxisomal acyl-coenzyme A thioesterase ACOT8, involved in fatty acid β-oxidation, and the cytosolic phosphorylase b kinase regulatory subunit A2 (PHKA2), involved in glycogen degradation, were selected based on their significant enrichment in more than one tissue (ACOT8 in kidney, intestine and HT-29; PHKA2 in all 4 matrices). The cytosolic SH3 domain-containing kinase-binding protein 1, also known as cbl-interacting protein of 85 kDa (SH3KBP1/CIN85), an adaptor protein regulating membrane trafficking and receptor signaling, was also chosen as a representative protein partner of the vesicular trafficking pathway, given its identification in the kidney and HT-29 datasets. After transient expression

of selected partners as tagged proteins in the kidney cell model stably expressing UGT1A9, each of the candidate partners was specifically enriched by an IP of UGT1A (**Fig.4A**). Likelihood of a physical interaction of ACOT8 and CIN85 with UGT1A enzymes was further supported by their partial co-localization with UGT1A9 detected by IF and confocal microscopy (**Fig.4B**).

Influence of UGT1A on cellular lipid droplets

Pathway enrichment analysis identified several proteins involved in lipid metabolism and suggested a possible functional implication of UGT1A enzymes in this pathway. This was explored by measuring levels of lipid droplet in HEK293 cells stably expressing or not the UGT1A9 enzyme. Lipid droplets, cytoplasmic organelles that constitute a store of neutral lipids such as triacylglycerides, were labeled with Nile Red and counted. This analysis revealed that the number of lipid droplets per cell was significantly higher in UGT1A9-expressing cells relative to control cells (by 7.5 fold, $P<0.001$), whereas average size and staining intensity of lipid droplets were similar between UGT negative and UGT1A9-expressing HEK293 cells **(Fig.5)**.

Discussion

Defining protein interaction networks is a key step towards a better understanding of functional crosstalk among cellular pathways. In the current work, we established the endogenous interactome of key metabolic UGT1A enzymes in three relevant human tissues. Data suggest an interplay between UGT1A enzymes regulating the glucuronidation pathway and enzymes involved in multiple cellular energetic pathways, most notably with lipid and glucose/glycogen metabolism. This interactome considerably expands what was known about UGT1A protein interactions in the literature (reviewed by (Ishii et al., 2010; Fujiwara et al., 2016)) and public databases (3 interactions among UGT1A enzymes reported in STRING database (http://string-db.org/), none in the iRefWEB database (http://wodaklab.org/iRefWeb/), accessed November 9, 2016).

One of our study's strength relies on the use of an unbiased approach targeting endogenous proteins in non-malignant human tissues, as opposed to most studies that used the overexpression of an exogenous tagged protein expressed in a cellular model (Taura et al., 2000; Takeda et al., 2005a; Takeda et al., 2005b; Fujiwara et al., 2007a; Fujiwara et al., 2007b; Kurkela et al., 2007; Takeda et al., 2009; Fujiwara et al., 2010). In addition, profiles

of immunoprecipitated UGT1A enzymes replicated well their known tissue distribution, and spectral peptide counting further reflected the relative abundance of these UGT1A enzymes previously established by mass spectrometry-based multiple reaction monitoring and RNA-sequencing (Fallon et al., 2013a; Fallon et al., 2013b; Sato et al., 2014; Margaillan et al., 2015a; Margaillan et al., 2015b; Tourancheau et al., 2016). Of note, our data support the notion that both UGT1A8 and UGT1A10 enzymes are expressed in the intestine, as peptides unique to each UGT were detected (**Fig.2**; **Supplementary Table 1**) (Strassburg et al., 2000; Sato et al., 2014; Fujiwara et al., 2016; Troberg et al., 2016). Moreover, two peptides specific to the UGT1A5 enzyme sequence were detected in the intestine, albeit at low levels (1 spectrum for each peptide) relative to other expressed UGT1As, providing evidence for its intestinal expression at the protein level (**Supplementary Fig.4**).

We provide unprecedented data on protein-protein interactions within the UGT family, namely between UGT1A and UGT2A3 enzymes and/or UGT2B family members. UGT1A-UGT2 interactions were observed in the liver (UGT2B4 and UGT2B7), in the kidney (UGT2B7) and in the intestine (UGT2B7, UGT2B17 and UGT2A3), and reflect the expression profiles of these UGT2 enzymes (Harbourt et al., 2012; Fallon et al., 2013a; Fallon et al., 2013b; Sato et al., 2014; Margaillan et al., 2015a; Margaillan et al., 2015b; Tourancheau et al., 2016). Our current study offers a representative view of the endogenous UGT1A enzyme interactome in relevant drug metabolizing tissues. Findings are consistent with the interactions between several UGT1A enzymes and UGT2B7 detected in microsomes from liver tissues (Fremont et al., 2005; Fujiwara and Itoh, 2014) and when overexpressed in heterologous cell model systems as tagged proteins (Kurkela et al., 2007; Operana and Tukey, 2007; Fujiwara et al., 2010; Ishii et al., 2010; Ishii et al., 2014; Liu et al., 2016). In addition, other transferases and anti-oxidant PRDX1, PRDX2 and PRDX3 enzymes were also found associated with UGT1A enzymes. The interaction network is also in line with a model favoring detoxifying enzymes acting in a “metabolosome”, i.e. a complex of xenobiotic-metabolizing enzymes and associated transport proteins regulating drug and xenobiotics inactivation and elimination (Taura et al., 2000; Takeda et al., 2005a; Takeda et al., 2005b; Akizawa et al., 2008; Takeda et al., 2009; Mori et al., 2011; Fujiwara and Itoh, 2014; Ishii et al., 2014; Rouleau et al., 2014; Fujiwara et al., 2016).

The significant number of peroxisomal and mitochondrial enzymes regulating fatty acid β-oxidation identified in protein complexes with UGT1A enzymes hinted towards a potential involvement of UGT1A in regulating lipid metabolism. The higher number of lipid droplets, a

reservoir of neutral lipids (such as fatty acids, sterol esters and phospholipids) (Thiam et al., 2013), in the UGT negative kidney cell model HEK293 overexpressing UGT1A9 lends support to this hypothesis. This observation is reminiscent of higher levels of lipid bodies induced by the overexpression of the peroxisomal ACOT8 protein, a confirmed UGT1A protein partner (Ishizuka et al., 2004). A modulation of lipid storage levels by overexpression of the UGT2B7 enzyme was also recently uncovered in breast and pancreatic cancer cell line models (Dates et al., 2015). This potential functional link between UGTs and lipid metabolism is intriguing and may be independent of the glucuronidation of some bioactive lipids previously reported (Turgeon et al., 2003). The underlying mechanism(s) of increased lipid droplets and the potential involvement of protein complexes comprised of UGT1A enzymes thus remain to be addressed and are aspects that fall beyond the scope of this study.

While UGT1A are ER-resident enzymes, their presence in other subcellular compartments such as the mitochondria is suggested by their co-localization with markers of several organelles (Rouleau et al., 2016). An intimate connection between ER, mitochondria, peroxisomes, and lipid droplets is also well recognized (Currie et al., 2013; Schrader et al., 2015). This is consistent with the significant number of peroxisomal and mitochondrial proteins interacting with ER-resident UGT1A enzymes. Indeed, peroxisomes and lipid droplets are ER-derived substructures, whereas interactions between the ER and mitochondria at the so-called mitochondria-associated ER membranes are gaining recognition as important sites of ER-mitochondria crosstalk where regulation of calcium signaling, lipid transport and tricarboxylic acid cycle take place (Hayashi et al., 2009; Tabak et al., 2013; Lodhi and Semenkovich, 2014; Pol et al., 2014).

The UGT1A interaction network exposes multiple links with enzymes of bioenergetic pathways. Besides lipids, glycogen catabolism as well as glycolytic and tricarboxylic acid cycle pathways may be influenced by the interactions of UGT1A with several subunits of the phosphorylase b UGT1A enzymes and glycolytic/TCA cycle enzymes. It could be envisioned that UGT1A enzymes participate in the regulation of metabolite levels to prevent the toxic impact of excess concentrations of basic constituents, a hypothesis that remains to be addressed. Interestingly, mice with a disrupted *UGT1* gene locus (*UGT1*$^{-/-}$ mice) are short-lived, dying within 1 week of birth. Whereas hyperbilirubinemia induced by UGT1A1 deficiency appears largely responsible for early death, highly perturbed hepatic expression of genes involved in general cellular metabolic function, and notably those of starch, sugar

and fatty acid metabolism was also observed in *UGT1*$^{-/-}$ mice, also supporting a contribution of UGT1A enzymes in those metabolic pathways (Nguyen et al., 2008). Rodent cell models from UGT1A-deficient mice or Gunn rats may constitute valuable models to investigate the interplay between UGT1A enzymes and global metabolic pathways.

One of the limitations of this study is that it examines complexes in which UGT1A enzymes reside and it does not provide information on direct interactions of UGT1A with proteins. Approaches such as proximity ligation and fluorescence resonance energy transfer approaches are necessary to move forward with a better understanding of direct protein interactions and the domains involved. It is well documented that UGTs, like numerous metabolic enzymes, homo- and hetero-oligomerize with other UGTs (Fujiwara et al., 2007a; Kurkela et al., 2007; Operana and Tukey, 2007; Bellemare et al., 2010b). It is therefore conceivable that UGT1A enzymes influence the activity of other metabolic enzymes by direct interactions that could alter the stoichiometry or composition of metabolic protein complexes. In turn, interactions of UGT1A enzymes with other metabolic enzymes may influence the glucuronidation pathway and thus contribute to the variable conjugation rates of individuals. This notion is supported by the altered activity of several UGT1A enzymes by CYP3A4 demonstrated in cell-based systems (Ishii et al., 2014). As well, the antagonistic or stimulatory functions of interactions among UGT1A and UGT2 enzymes, or with alternatively spliced isoforms, are consistent with a potential mode of regulation of UGTs by PPI (Fujiwara et al., 2007a; Bellemare et al., 2010b; Bushey and Lazarus, 2012; Rouleau et al., 2014; Rouleau et al., 2016).

In summary, we established an effective affinity purification method coupled to mass spectrometry for the enrichment and identification of protein complexes interacting with endogenous UGT1A enzymes. We successfully applied this approach to UGT1A enzymes expressed in drug metabolizing tissues and a UGT positive cell model to uncover an interaction map linking glucuronidation enzymes to other metabolic proteins involved in detoxification, as well as in the regulation of bioenergetic molecules (lipids and carbohydrates). Our data also support physical and functional interactions between ER and other subcellular compartments. The crosstalk among cellular metabolic functions exposed in this work warrants future investigations to address the impact of UGT1A-protein interactions on detoxification functions of UGT1A enzymes and of UGT1A enzymes on global metabolic cellular functions.

References

Akizawa, E., Koiwai, K., Hayano, T., Maezawa, S., Matsushita, T., and Koiwai, O. (2008). Direct binding of ligandin to uridine 5'-diphosphate glucuronosyltransferase 1A1. *Hepatol Res* 38, 402-409.

Bellemare, J., Rouleau, M., Girard, H., Harvey, M., and Guillemette, C. (2010a). Alternatively spliced products of the UGT1A gene interact with the enzymatically active proteins to inhibit glucuronosyltransferase activity in vitro. *Drug Metab Dispos* 38, 1785-1789.

Bellemare, J., Rouleau, M., Harvey, M., and Guillemette, C. (2010b). Modulation of the human glucuronosyltransferase UGT1A pathway by splice isoform polypeptides is mediated through protein-protein interactions. *J Biol Chem* 285, 3600-3607.

Bellemare, J., Rouleau, M., Harvey, M., Popa, I., Pelletier, G., Tetu, B., and Guillemette, C. (2011). Immunohistochemical expression of conjugating UGT1A-derived isoforms in normal and tumoral drug-metabolizing tissues in humans. *J Pathol* 223, 425-435.

Bindea, G., Galon, J., and Mlecnik, B. (2013). CluePedia Cytoscape plugin: pathway insights using integrated experimental and in silico data. *Bioinformatics* 29, 661-663.

Bindea, G., Mlecnik, B., Hackl, H., Charoentong, P., Tosolini, M., Kirilovsky, A., Fridman, W.H., Pages, F., Trajanoski, Z., and Galon, J. (2009). ClueGO: a Cytoscape plug-in to decipher functionally grouped gene ontology and pathway annotation networks. *Bioinformatics* 25, 1091-1093.

Bolte, S., and Cordelieres, F.P. (2006). A guided tour into subcellular colocalization analysis in light microscopy. *J Microsc* 224, 213-232.

Bushey, R.T., and Lazarus, P. (2012). Identification and functional characterization of a novel UDP-glucuronosyltransferase 2A1 splice variant: potential importance in tobacco-related cancer susceptibility. *J Pharmacol Exp Ther* 343, 712-724.

Choi, H., Larsen, B., Lin, Z.Y., Breitkreutz, A., Mellacheruvu, D., Fermin, D., Qin, Z.S., Tyers, M., Gingras, A.C., and Nesvizhskii, A.I. (2011). SAINT: probabilistic scoring of affinity purification-mass spectrometry data. *Nat Methods* 8, 70-73.

Costa, E. (2006). Hematologically important mutations: bilirubin UDP-glucuronosyltransferase gene mutations in Gilbert and Crigler-Najjar syndromes. *Blood Cells Mol Dis* 36, 77-80.

Currie, E., Schulze, A., Zechner, R., Walther, T.C., and Farese, R.V., Jr. (2013). Cellular fatty acid metabolism and cancer. *Cell Metab* 18, 153-161.

Dates, C.R., Fahmi, T., Pyrek, S.J., Yao-Borengasser, A., Borowa-Mazgaj, B., Bratton, S.M., Kadlubar, S.A., Mackenzie, P.I., Haun, R.S., and Radominska-Pandya, A. (2015). Human UDP-Glucuronosyltransferases: Effects of altered expression in breast and pancreatic cancer cell lines. *Cancer Biol Ther* 16, 714-723.

Dluzen, D.F., and Lazarus, P. (2015). MicroRNA regulation of the major drug-metabolizing enzymes and related transcription factors. *Drug Metab Rev* 47, 320-334.

Fallon, J.K., Neubert, H., Goosen, T.C., and Smith, P.C. (2013a). Targeted precise quantification of 12 human recombinant uridine-diphosphate glucuronosyl transferase 1A and 2B isoforms using nano-ultra-high-performance liquid chromatography/tandem mass spectrometry with selected reaction monitoring. *Drug Metab Dispos* 41, 2076-2080.

Fallon, J.K., Neubert, H., Hyland, R., Goosen, T.C., and Smith, P.C. (2013b). Targeted quantitative proteomics for the analysis of 14 UGT1As and -2Bs in human liver using NanoUPLC-MS/MS with selected reaction monitoring. *J Proteome Res* 12, 4402-4413.

Fremont, J.J., Wang, R.W., and King, C.D. (2005). Coimmunoprecipitation of UDP-glucuronosyltransferase isoforms and cytochrome P450 3A4. *Mol Pharmacol* 67, 260-262.

Fujiwara, R., and Itoh, T. (2014). Extensive protein-protein interactions involving UDP-glucuronosyltransferase (UGT) 2B7 in human liver microsomes. *Drug Metab Pharmacokinet* 29, 259-265.

Fujiwara, R., Nakajima, M., Oda, S., Yamanaka, H., Ikushiro, S., Sakaki, T., and Yokoi, T. (2010). Interactions between human UDP-glucuronosyltransferase (UGT) 2B7 and UGT1A enzymes. *J Pharm Sci* 99, 442-454.

Fujiwara, R., Nakajima, M., Yamanaka, H., Katoh, M., and Yokoi, T. (2007a). Interactions between human UGT1A1, UGT1A4, and UGT1A6 affect their enzymatic activities. *Drug Metab Dispos* 35, 1781-1787.

Fujiwara, R., Nakajima, M., Yamanaka, H., Nakamura, A., Katoh, M., Ikushiro, S., Sakaki, T., and Yokoi, T. (2007b). Effects of coexpression of UGT1A9 on enzymatic activities of human UGT1A isoforms. *Drug Metab Dispos* 35, 747-757.

Fujiwara, R., Yokoi, T., and Nakajima, M. (2016). Structure and Protein-Protein Interactions of Human UDP-Glucuronosyltransferases. *Front Pharmacol* 7, 388.

Guillemette, C., Levesque, E., Harvey, M., Bellemare, J., and Menard, V. (2010). UGT genomic diversity: beyond gene duplication. *Drug Metab Rev* 42, 24-44.

Guillemette, C., Levesque, E., and Rouleau, M. (2014). Pharmacogenomics of human uridine diphospho-glucuronosyltransferases and clinical implications. *Clin Pharmacol Ther* 96, 324-339.

Harbourt, D.E., Fallon, J.K., Ito, S., Baba, T., Ritter, J.K., Glish, G.L., and Smith, P.C. (2012). Quantification of human uridine-diphosphate glucuronosyl transferase 1A isoforms in liver, intestine, and kidney using nanobore liquid chromatography-tandem mass spectrometry. *Anal Chem* 84, 98-105.

Hayashi, T., Rizzuto, R., Hajnoczky, G., and Su, T.P. (2009). MAM: more than just a housekeeper. *Trends Cell Biol* 19, 81-88.

Hu, D.G., Meech, R., McKinnon, R.A., and Mackenzie, P.I. (2014). Transcriptional regulation of human UDP-glucuronosyltransferase genes. *Drug Metab Rev* 46, 421-458.

Hung, Y.H., Chan, Y.S., Chang, Y.S., Lee, K.T., Hsu, H.P., Yen, M.C., Chen, W.C., Wang, C.Y., and Lai, M.D. (2014). Fatty acid metabolic enzyme acyl-CoA thioesterase 8 promotes the development of hepatocellular carcinoma. *Oncol Rep* 31, 2797-2803.

Ishii, Y., Iwanaga, M., Nishimura, Y., Takeda, S., Ikushiro, S., Nagata, K., Yamazoe, Y., Mackenzie, P.I., and Yamada, H. (2007). Protein-protein interactions between rat hepatic cytochromes P450 (P450s) and UDP-glucuronosyltransferases (UGTs): evidence for the functionally active UGT in P450-UGT complex. *Drug Metab Pharmacokinet* 22, 367-376.

Ishii, Y., Koba, H., Kinoshita, K., Oizaki, T., Iwamoto, Y., Takeda, S., Miyauchi, Y., Nishimura, Y., Egoshi, N., Taura, F., Morimoto, S., Ikushiro, S., Nagata, K., Yamazoe, Y., Mackenzie, P.I., and Yamada, H. (2014). Alteration of the function of the UDP-glucuronosyltransferase 1A subfamily by cytochrome P450 3A4: different susceptibility for UGT isoforms and UGT1A1/7 variants. *Drug Metab Dispos* 42, 229-238.

Ishii, Y., Takeda, S., and Yamada, H. (2010). Modulation of UDP-glucuronosyltransferase activity by protein-protein association. *Drug Metab Rev* 42, 145-158.

Ishizuka, M., Toyama, Y., Watanabe, H., Fujiki, Y., Takeuchi, A., Yamasaki, S., Yuasa, S., Miyazaki, M., Nakajima, N., Taki, S., and Saito, T. (2004). Overexpression of human acyl-CoA thioesterase upregulates peroxisome biogenesis. *Exp Cell Res* 297, 127-141.

Kurkela, M., Patana, A.S., Mackenzie, P.I., Court, M.H., Tate, C.G., Hirvonen, J., Goldman, A., and Finel, M. (2007). Interactions with other human UDP-glucuronosyltransferases attenuate the consequences of the Y485D mutation on the activity and substrate affinity of UGT1A6. *Pharmacogenet Genomics* 17, 115-126.

Liu, Y.Q., Yuan, L.M., Gao, Z.Z., Xiao, Y.S., Sun, H.Y., Yu, L.S., and Zeng, S. (2016). Dimerization of human uridine diphosphate glucuronosyltransferase allozymes 1A1 and 1A9 alters their quercetin glucuronidation activities. *Sci Rep* 6, 23763.

Lodhi, I.J., and Semenkovich, C.F. (2014). Peroxisomes: a nexus for lipid metabolism and cellular signaling. *Cell Metab* 19, 380-392.

Margaillan, G., Rouleau, M., Fallon, J.K., Caron, P., Villeneuve, L., Turcotte, V., Smith, P.C., Joy, M.S., and Guillemette, C. (2015a). Quantitative profiling of human renal UDP-glucuronosyltransferases and glucuronidation activity: a comparison of normal and tumoral kidney tissues. *Drug Metab Dispos* 43, 611-619.

Margaillan, G., Rouleau, M., Klein, K., Fallon, J.K., Caron, P., Villeneuve, L., Smith, P.C., Zanger, U.M., and Guillemette, C. (2015b). Multiplexed Targeted Quantitative Proteomics Predicts Hepatic Glucuronidation Potential. *Drug Metab Dispos* 43, 1331-1335.

Mellacheruvu, D., Wright, Z., Couzens, A.L., Lambert, J.P., St-Denis, N.A., Li, T., Miteva, Y.V., Hauri, S., Sardiu, M.E., Low, T.Y., Halim, V.A., Bagshaw, R.D., Hubner, N.C., Al-Hakim, A., Bouchard, A., Faubert, D., Fermin, D., Dunham, W.H., Goudreault, M., Lin, Z.Y., Badillo, B.G., Pawson, T., Durocher, D., Coulombe, B., Aebersold, R., Superti-Furga, G., Colinge, J., Heck, A.J., Choi, H., Gstaiger, M., Mohammed, S., Cristea, I.M., Bennett, K.L., Washburn, M.P., Raught, B., Ewing, R.M., Gingras, A.C., and Nesvizhskii, A.I. (2013). The CRAPome: a contaminant repository for affinity purification-mass spectrometry data. *Nat Methods* 10, 730-736.

Menard, V., Collin, P., Margaillan, G., and Guillemette, C. (2013). Modulation of the UGT2B7 enzyme activity by C-terminally truncated proteins derived from alternative splicing. *Drug Metab Dispos* 41, 2197-2205.

Mori, Y., Kiyonaka, S., and Kanai, Y. (2011). Transportsomes and channelsomes: are they functional units for physiological responses? *Channels (Austin)* 5, 387-390.

Nguyen, N., Bonzo, J.A., Chen, S., Chouinard, S., Kelner, M.J., Hardiman, G., Belanger, A., and Tukey, R.H. (2008). Disruption of the ugt1 locus in mice resembles human Crigler-Najjar type I disease. *J Biol Chem* 283, 7901-7911.

Operana, T.N., and Tukey, R.H. (2007). Oligomerization of the UDP-glucuronosyltransferase 1A proteins: homo- and heterodimerization analysis by fluorescence resonance energy transfer and co-immunoprecipitation. *J Biol Chem* 282, 4821-4829.

Pol, A., Gross, S.P., and Parton, R.G. (2014). Review: biogenesis of the multifunctional lipid droplet: lipids, proteins, and sites. *J Cell Biol* 204, 635-646.

Ramirez, J., Ratain, M.J., and Innocenti, F. (2010). Uridine 5'-diphospho-glucuronosyltransferase genetic polymorphisms and response to cancer chemotherapy. *Future Oncol* 6, 563-585.

Rouleau, M., Roberge, J., Bellemare, J., and Guillemette, C. (2014). Dual roles for splice variants of the glucuronidation pathway as regulators of cellular metabolism. *Mol Pharmacol* 85, 29-36.

Rouleau, M., Tourancheau, A., Girard-Bock, C., Villeneuve, L., Vaucher, J., Duperre, A.M., Audet-Delage, Y., Gilbert, I., Popa, I., Droit, A., and Guillemette, C. (2016). Divergent Expression and Metabolic Functions of Human Glucuronosyltransferases through Alternative Splicing. *Cell Rep* 17, 114-124.

Rowland, A., Miners, J.O., and Mackenzie, P.I. (2013). The UDP-glucuronosyltransferases: their role in drug metabolism and detoxification. *Int J Biochem Cell Biol* 45, 1121-1132.

Ruan, H.B., Han, X., Li, M.D., Singh, J.P., Qian, K., Azarhoush, S., Zhao, L., Bennett, A.M., Samuel, V.T., Wu, J., Yates, J.R., 3rd, and Yang, X. (2012). O-GlcNAc transferase/host cell factor C1 complex regulates gluconeogenesis by modulating PGC-1alpha stability. *Cell Metab* 16, 226-237.

Sato, Y., Nagata, M., Tetsuka, K., Tamura, K., Miyashita, A., Kawamura, A., and Usui, T. (2014). Optimized methods for targeted peptide-based quantification of human uridine 5'-diphosphate-glucuronosyltransferases in biological specimens using liquid chromatography-tandem mass spectrometry. *Drug Metab Dispos* 42, 885-889.

Savas, J.N., Stein, B.D., Wu, C.C., and Yates, J.R., 3rd (2011). Mass spectrometry accelerates membrane protein analysis. *Trends Biochem Sci* 36, 388-396.

Schrader, M., Godinho, L.F., Costello, J.L., and Islinger, M. (2015). The different facets of organelle interplay-an overview of organelle interactions. *Front Cell Dev Biol* 3, 56.

Schroeder, B., Weller, S.G., Chen, J., Billadeau, D., and McNiven, M.A. (2010). A Dyn2-CIN85 complex mediates degradative traffic of the EGFR by regulation of late endosomal budding. *EMBO J* 29, 3039-3053.

Strassburg, C.P., Kneip, S., Topp, J., Obermayer-Straub, P., Barut, A., Tukey, R.H., and Manns, M.P. (2000). Polymorphic gene regulation and interindividual variation of UDP-glucuronosyltransferase activity in human small intestine. *J Biol Chem* 275, 36164-36171.

Tabak, H.F., Braakman, I., and van der Zand, A. (2013). Peroxisome formation and maintenance are dependent on the endoplasmic reticulum. *Annu Rev Biochem* 82, 723-744.

Takeda, S., Ishii, Y., Iwanaga, M., Mackenzie, P.I., Nagata, K., Yamazoe, Y., Oguri, K., and Yamada, H. (2005a). Modulation of UDP-glucuronosyltransferase function by cytochrome P450: evidence for the alteration of UGT2B7-catalyzed glucuronidation of morphine by CYP3A4. *Mol Pharmacol* 67, 665-672.

Takeda, S., Ishii, Y., Iwanaga, M., Nurrochmad, A., Ito, Y., Mackenzie, P.I., Nagata, K., Yamazoe, Y., Oguri, K., and Yamada, H. (2009). Interaction of cytochrome P450 3A4 and UDP-glucuronosyltransferase 2B7: evidence for protein-protein association and possible involvement of CYP3A4 J-helix in the interaction. *Mol Pharmacol* 75, 956-964.

Takeda, S., Ishii, Y., Mackenzie, P.I., Nagata, K., Yamazoe, Y., Oguri, K., and Yamada, H. (2005b). Modulation of UDP-glucuronosyltransferase 2B7 function by cytochrome P450s in vitro: differential effects of CYP1A2, CYP2C9 and CYP3A4. *Biol Pharm Bull* 28, 2026-2027.

Taura, K.I., Yamada, H., Hagino, Y., Ishii, Y., Mori, M.A., and Oguri, K. (2000). Interaction between cytochrome P450 and other drug-metabolizing enzymes: evidence for an association of CYP1A1 with microsomal epoxide hydrolase and UDP-glucuronosyltransferase. *Biochem Biophys Res Commun* 273, 1048-1052.

Thiam, A.R., Farese, R.V., Jr., and Walther, T.C. (2013). The biophysics and cell biology of lipid droplets. *Nat Rev Mol Cell Biol* 14, 775-786.

Tourancheau, A., Margaillan, G., Rouleau, M., Gilbert, I., Villeneuve, L., Levesque, E., Droit, A., and Guillemette, C. (2016). Unravelling the transcriptomic landscape of the major phase II UDP-glucuronosyltransferase drug metabolizing pathway using targeted RNA sequencing. *Pharmacogenomics J* 16, 60-70.

Troberg, J., Jarvinen, E., Ge, G.B., Yang, L., and Finel, M. (2016). UGT1A10 Is a High Activity and Important Extrahepatic Enzyme: Why Has Its Role in Intestinal Glucuronidation Been Frequently Underestimated? *Mol Pharm*.

Turgeon, D., Chouinard, S., Belanger, P., Picard, S., Labbe, J.F., Borgeat, P., and Belanger, A. (2003). Glucuronidation of arachidonic and linoleic acid metabolites by human UDP-glucuronosyltransferases. *J Lipid Res* 44, 1182-1191.

Acknowledgements

The authors would like to thank Dr MD Lai (National Cheng Kung University, Taiwan) and Dr MA McNiven (Mayo Clinic, Rochester, USA) for the gift of reagents, Mario Harvey, Lyne Villeneuve and Joannie Roberge for technical assistance, Sylvie Bourassa at the Proteomics Platform of CHU de Québec Research Center for mass spectrometry analysis, and France Couture for artwork.

This work was supported by the Natural Sciences and Engineering Research Council of Canada (342176-2012). YAD received a Ph.D. studentship award from the Fonds de Recherche Santé-Québec, MeR received a Canadian Institutes for Health Research Frederick Banting and Charles Best Graduate Scholarship award, CGB received a studentship from the Fonds de l'Enseignement et de la Recherche of the Faculty of Pharmacy of Laval University.

C.G. holds a Tier I Canada Research Chair in Pharmacogenomics.

Competing financial interests

The authors declare no conflict of interest

Author contributions

Conceptualization: CG; Methodology, MiR, MeR, YAD, CG; Investigation, MeR, YAD, CGB, SD; Formal Analysis, MiR, MeR, YAD, CGB, SD, CG. Writing – Review & Editing, All authors; Visualization, MiR, YAD, CG; Supervision, MiR, CG; Funding Acquisition, CG.

Table 1: Top 10 UGT1A interaction partners[1] for each tissue based on confidence score.

Liver				Kidney				Intestine			
Protein name[2]	coverage (%)[3]	Total spectral counts[4]	FC_B score	Protein name[2]	coverage (%)[3]	Total spectral counts[4]	FC_B score	Protein name[2]	coverage (%)[3]	Total spectral counts[4]	FC_B score
PHKB	36	193	28.55	TOP2B	16	53	5.93	ATP5A1	13	8	4.91
PHKA2	34	180	26.62	PFKL	24	35	4.68	UGT2A3	24	61	4.63
PHKG2	40	68	10.49	TRA2B	24	36	4.21	**GBF1**	12	60	4.60
PRDX2	47	55	7.62	ATP5A1	33	32	4.10	**SLC25A5**	35	54	4.37
UGT2B7	19	31	5.53	**PRDX2**	41	50	3.60	RALGAPB	13	51	4.26
PRDX1	35	25	3.42	**PRDX1**	44	39	3.08	**PRDX2**	24	46	4.06
ECH1	28	17	2.61	HSPA8	30	21	2.70	**PRDX1**	31	45	4.01
SLC25A5	17	9	2.20	SLC34A2	16	17	2.66	RALGAPA2	6	29	3.28
GBF1	4	9	2.15	ACCA2	43	21	2.30	**ECH1**	30	21	2.84
UGT2B4	11	12	1.98	ASS1	42	21	2.22	PDIA3	5	3	2.82

[1] Excluding common IP protein contaminants (structural, ribosomal and RNA-binding proteins).
[2] Proteins in bold were identified in the 3 tissues.
[3]Total coverage calculated with peptides identified in all replicates (n=4, 3 and 2 for the liver, kidney and intestine, respectively).
[4]Total spectral counts of all replicates.

Table 2: Complete names of UGT1A protein partners

Protein names[1]	
Abbreviation	**Complete name**
ACAA2	3-ketoacyl-CoA thiolase, mitochondrial
ACAT1/SOAT1	Sterol O-acyltransferase 1
ACOT8	Acyl-coenzyme A thioesterase 8
ACSL1	Long-chain-fatty-acid--CoA ligase 1
ADH1B	Alcohol dehydrogenase 1B
ALDH2	Aldehyde dehydrogenase, mitochondrial
ALDH6A1	Methylmalonate-semialdehyde dehydrogenase [acylating], mitochondrial
ASS1	Argininosuccinate synthase
ATP5A1	ATP synthase subunit alpha, mitochondrial
CALM1	Calmodulin
CPT1A	Carnitine O-palmitoyltransferase 1, liver isoform
CYP3A4	Cytochrome P450 3A4
ECH1	Delta(3,5)-Delta(2,4)-dienoyl-CoA isomerase, mitochondrial
ECHS1	Enoyl-CoA hydratase, mitochondrial
EHHADH	Peroxisomal bifunctional enzyme
GAPDH	Glyceraldehyde-3-phosphate dehydrogenase
GBF1	Golgi-specific brefeldin A-resistance guanine nucleotide exchange factor 1
GLYAT	Glycine N-acyltransferase
GSTA1	Glutathione S-transferase A1
HSPA8	Heat shock cognate 71 kDa protein
IDH2	Isocitrate dehydrogenase [NADP], mitochondrial
ITPR2	Inositol 1,4,5-trisphosphate receptor type 2
PC	Pyruvate carboxylase, mitochondrial
PCK2	Phosphoenolpyruvate carboxykinase [GTP], mitochondrial
PDIA3	Protein disulfide-isomerase A3
PFKL	ATP-dependent 6-phosphofructokinase, liver type
PHKA2	Phosphorylase b kinase regulatory subunit alpha, liver isoform
PHKB	Phosphorylase b kinase regulatory subunit beta
PHKG2	Phosphorylase b kinase gamma catalytic chain, liver/testis isoform
PKM	Pyruvate kinase
PRDX1	Peroxiredoxin-1
PRDX2	Peroxiredoxin-2
PRDX3	Peroxiredoxin-3
RALGAPA1	Ral GTPase-activating protein subunit alpha-1
RALGAPA2	Ral GTPase-activating protein subunit alpha-2
RALGAPB	Ral GTPase-activating protein subunit beta
SCP2	Non-specific lipid-transfer protein
SH3KBP1	SH3 domain-containing kinase-binding protein 1

SLC25A13	Calcium-binding mitochondrial carrier protein Aralar2
SLC25A5	ADP/ATP translocase 2
SLC34A2	Sodium-dependent phosphate transport protein 2B
TOP2B	DNA topoisomerase 2-beta
TRA2B	Transformer-2 protein homolog beta

[1]Protein names are according to Uniprot (www.uniprot.org; accessed Dec.21, 2016)

Figure legends

Figure 1. UGT1A interaction network investigated by untargeted proteomics. (A) The nine UGT1A enzymes are distinguished by the amino acid sequence of their substrate binding domain (unique peptides) whereas they share identical C-terminal co-substrate and transmembrane domains (common peptides). The anti-UGT1A antibody used in this study was raised against a C-terminal peptide common to all nine UGT1A enzymes but does not recognize the main spliced alternative isoforms 2 or UGT1A_i2s. (B) Experimental approach to establish endogenous UGT1A protein interactomes in drug metabolizing tissues and in the colon cancer cell model HT-29. Immunoprecipitation of UGT1A enzymes was conducted with the anti-UGT1A antibody. The numbers of common and unique UGT1A protein partners identified by mass spectrometry and above confidence threshold are represented in the Venn diagrams. Datasets were established on a minimum of two biological replicates. A Venn diagram for the 4 matrices is presented in **Supplementary Figure 2.** A list of proteins in each group is provided in **Supplementary Table 3.**

Figure 2. Quantitative overview of UGT1A enzymes immunoprecipitated from each tissue. Identification of immunoprecipitated UGT1A enzymes was based on the detection of peptides unique to specified UGT1A enzymes. (A) The quantitative assessment of each immunoprecipitated UGT1A is given by the total number of spectral counts for peptides unique to each UGT1A identified by mass spectrometry. Total spectral counts for peptides common to all UGT1A enzymes (Liver: 465; Kidney: 67; Intestine: 1561) were not considered in the quantitative assessment of specific UGT1As. (B) For each tissue, the number of peptides unique to each UGT1A identified by MS/MS analysis is represented in ring charts. Detailed quantification and unique/common UGT1A peptides identified are presented in **Supplementary Table 1**.

Figure 3. UGT1A interaction network in drug metabolizing tissues. UGT1A interacting proteins were classified according to KEGG pathways with ClueGO/CluePedia (Bindea et al., 2009; Bindea et al., 2013). Node size is representative of pathway enrichment significance. Interactome was enhanced with significant interaction partners not part of KEGG pathways that are functionally related based on Uniprot and literature. These proteins are not linked to nodes but are grouped according to global functions. Structural proteins, ribosomal protein subunits and other RNA-binding proteins involved in mRNA splicing are not shown but were significantly enriched in UGT1A IPs. Full protein names are provided in

Table 2. Complete lists of UGT1A interacting proteins are provided in **Supplementary Table 2**.

Figure 4. Validation of selected protein interactions by immunoprecipitation and immunofluorescence in a UGT negative kidney cell model. (A) Immunoprecipitation (IP) of UGT1A9, with purified anti-UGT1A antibodies, was conducted in HEK293-UGT1A9_myc/his transiently transfected with the indicated protein partner. UGT1A was immunodetected with anti-myc, whereas protein partners were detected with anti-tag antibodies as specified below immunoblots. Control IPs were conducted with normal rabbit immunoglobulins (IgG). Lysates (IP input) are shown as references. (B) Co-localization of UGT1A9 and the protein partners ACOT8 and SH3KBP1/CIN85 assessed by immunofluorescence in HEK293-UGT1A9_myc/his transiently transfected with specified partners. Confocal microscope images are representative of three independent experiments. Partial co-localization is detected by yellow labelling in merged images. Insets present enlargements of boxed regions in merged images. Bar = 20 µm.

Figure 5. Accumulation of cellular lipid droplets in UGT1A9 expressing HEK293 cells. **(**A) Representative images of lipid droplets (green fluorescence) stained with Nile Red in HEK293-UGT1A9_myc-his or control HEK cells (stably transfected with the empty pcDNA3.1 vector – UGT negative cells). Bar = 20 µm. (B) Average number of lipid droplets per cell stably expressing UGT1A9 or control HEK cells. Lipid droplets per cell were counted in at least 140 cells per condition and averaged (n=3 independent experiments).

Figure 1

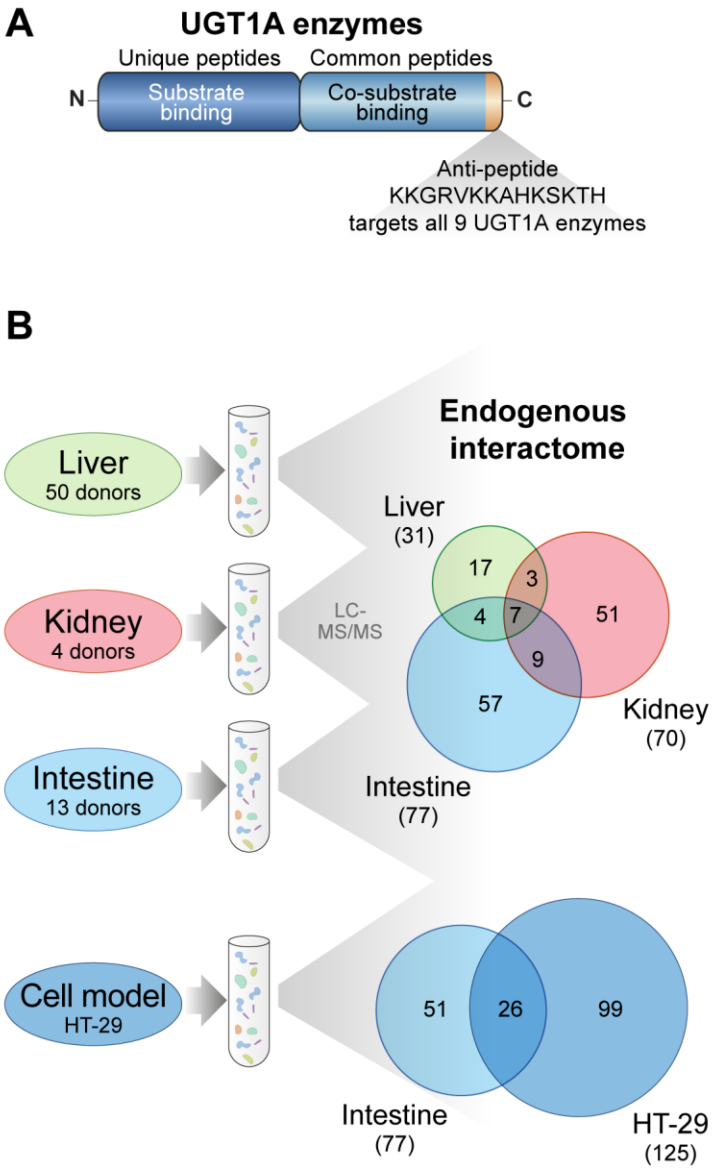
A
UGT1A enzymes
Unique peptides
Common peptides
N
Substrate binding
Co-substrate binding
C
Anti-peptide
KKGRVKKAHKSKTH
targets all 9 UGT1A enzymes
B
Liver
50 donors
Kidney
4 donors
Intestine
13 donors
Cell model
HT-29
LC-MS/MS
Endogenous interactome
Liver
(31)
17
3
4
7
51
9
57
Kidney
(70)
Intestine
(77)
51
26
99
Intestine
(77)
HT-29
(125)

Figure 2

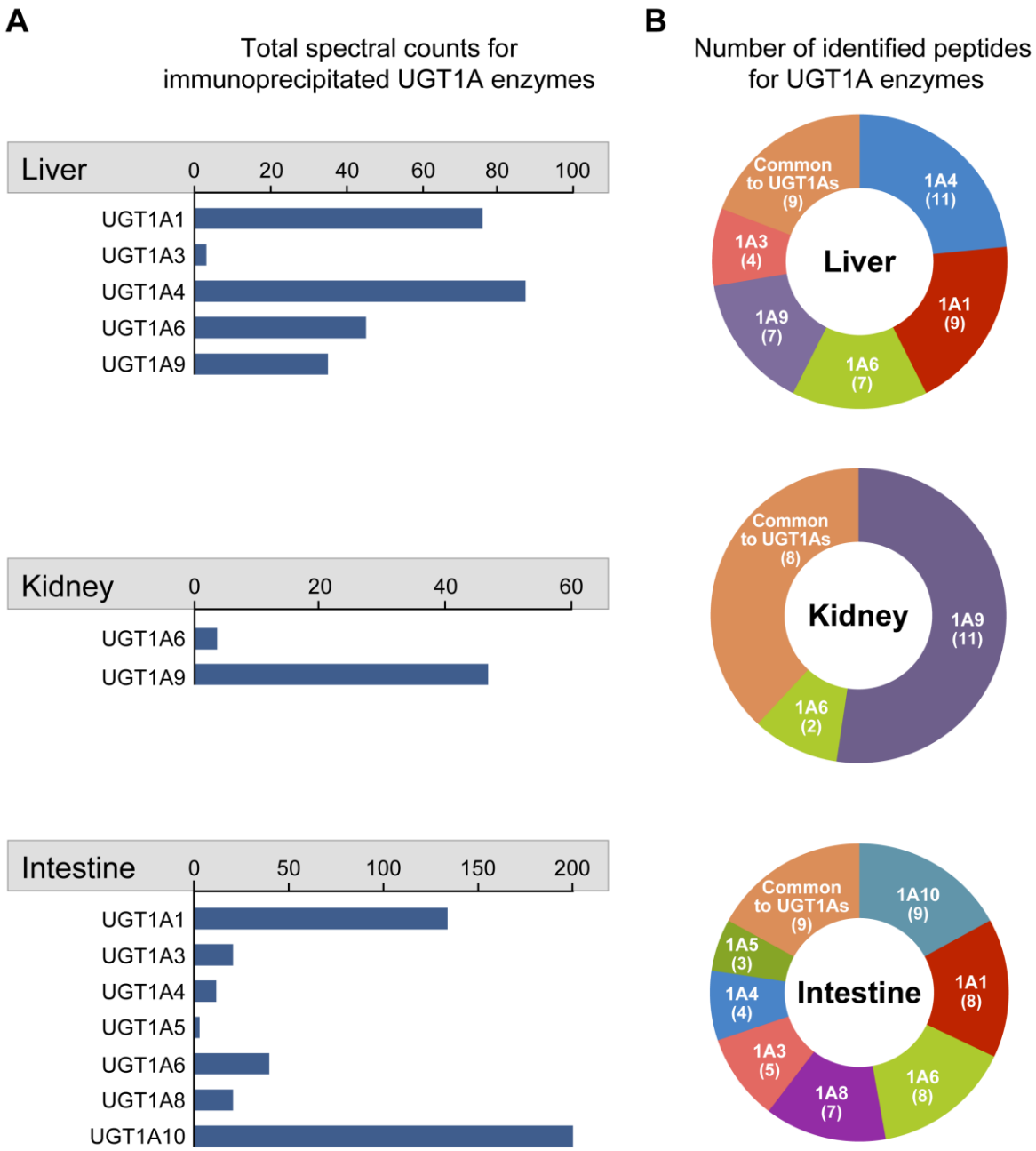
A
Total spectral counts for immunoprecipitated UGT1A enzymes
Liver
0
20
40
60
80
100
UGT1A1
UGT1A3
UGT1A4
UGT1A6
UGT1A9
Kidney
0
20
40
60
UGT1A6
UGT1A9
Intestine
0
50
100
150
200
UGT1A1
UGT1A3
UGT1A4
UGT1A5
UGT1A6
UGT1A8
UGT1A10
B
Number of identified peptides for UGT1A enzymes
Common to UGT1As (9)
1A4 (11)
1A3 (4)
Liver
1A1 (9)
1A9 (7)
1A6 (7)
Common to UGT1As (8)
Kidney
1A9 (11)
1A6 (2)
Common to UGT1As (9)
1A10 (9)
1A5 (3)
1A1 (8)
1A4 (4)
Intestine
1A3 (5)
1A6 (8)
1A8 (7)

Figure 3

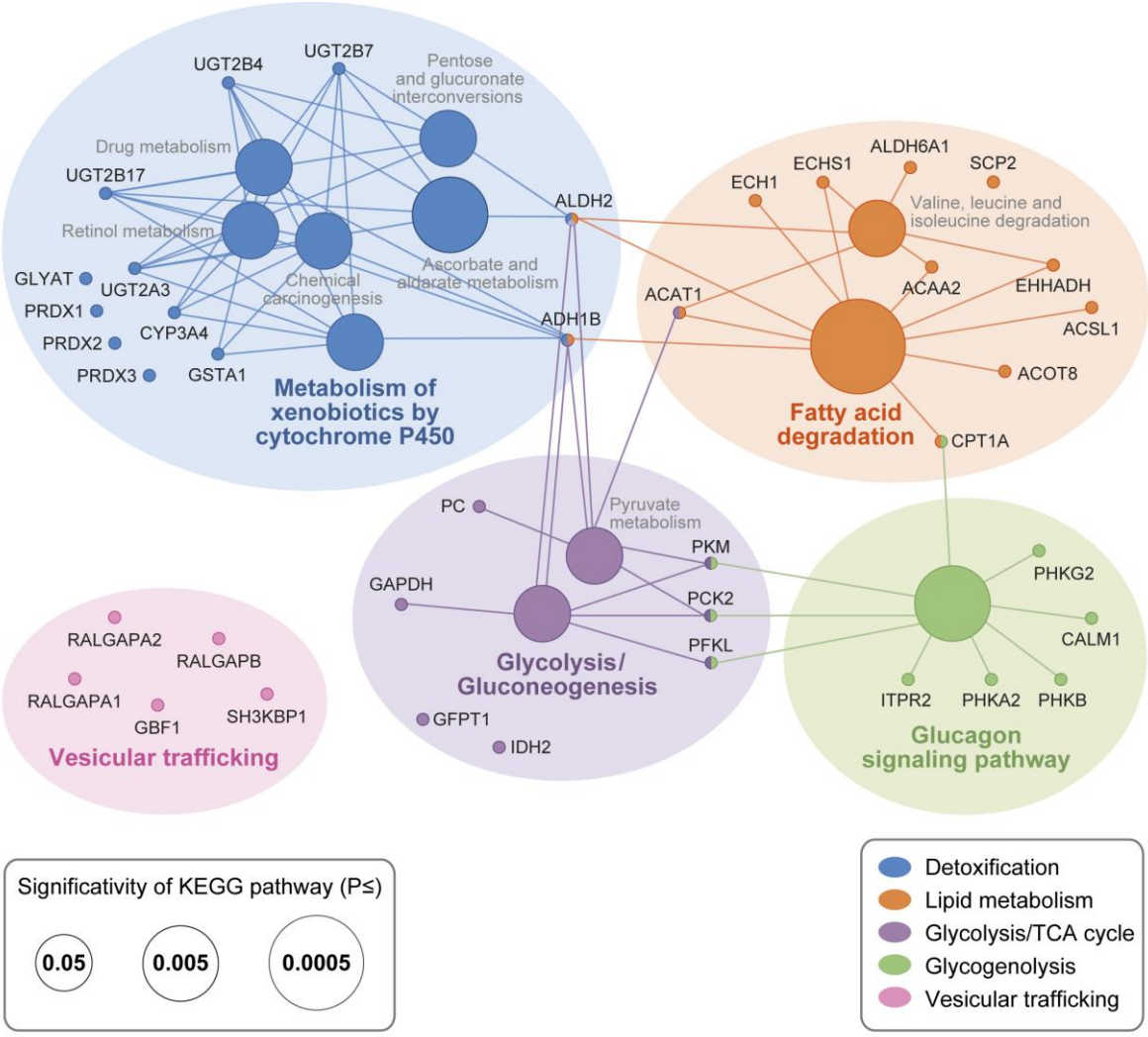
UGT2B4
UGT2B7
Pentose and glucuronate interconversions
Drug metabolism
UGT2B17
Retinol metabolism
GLYAT
UGT2A3
PRDX1
CYP3A4
PRDX2
PRDX3
GSTA1
Chemical carcinogenesis
Ascorbate and aldarate metabolism
ALDH2
ADH1B
Metabolism of xenobiotics by cytochrome P450
ALDH6A1
ECHS1
SCP2
ECH1
Valine, leucine and isoleucine degradation
ACAT1
ACAA2
EHHADH
ACSL1
ACOT8
Fatty acid degradation
CPT1A
PC
Pyruvate metabolism
PKM
GAPDH
PCK2
PFKL
Glycolysis/ Gluconeogenesis
GFPT1
IDH2
PHKG2
CALM1
ITPR2
PHKA2
PHKB
Glucagon signaling pathway
RALGAPA2
RALGAPB
RALGAPA1
GBF1
SH3KBP1
Vesicular trafficking
Significativity of KEGG pathway (P≤)
0.05
0.005
0.0005
Detoxification
Lipid metabolism
Glycolysis/TCA cycle
Glycogenolysis
Vesicular trafficking

Figure 4

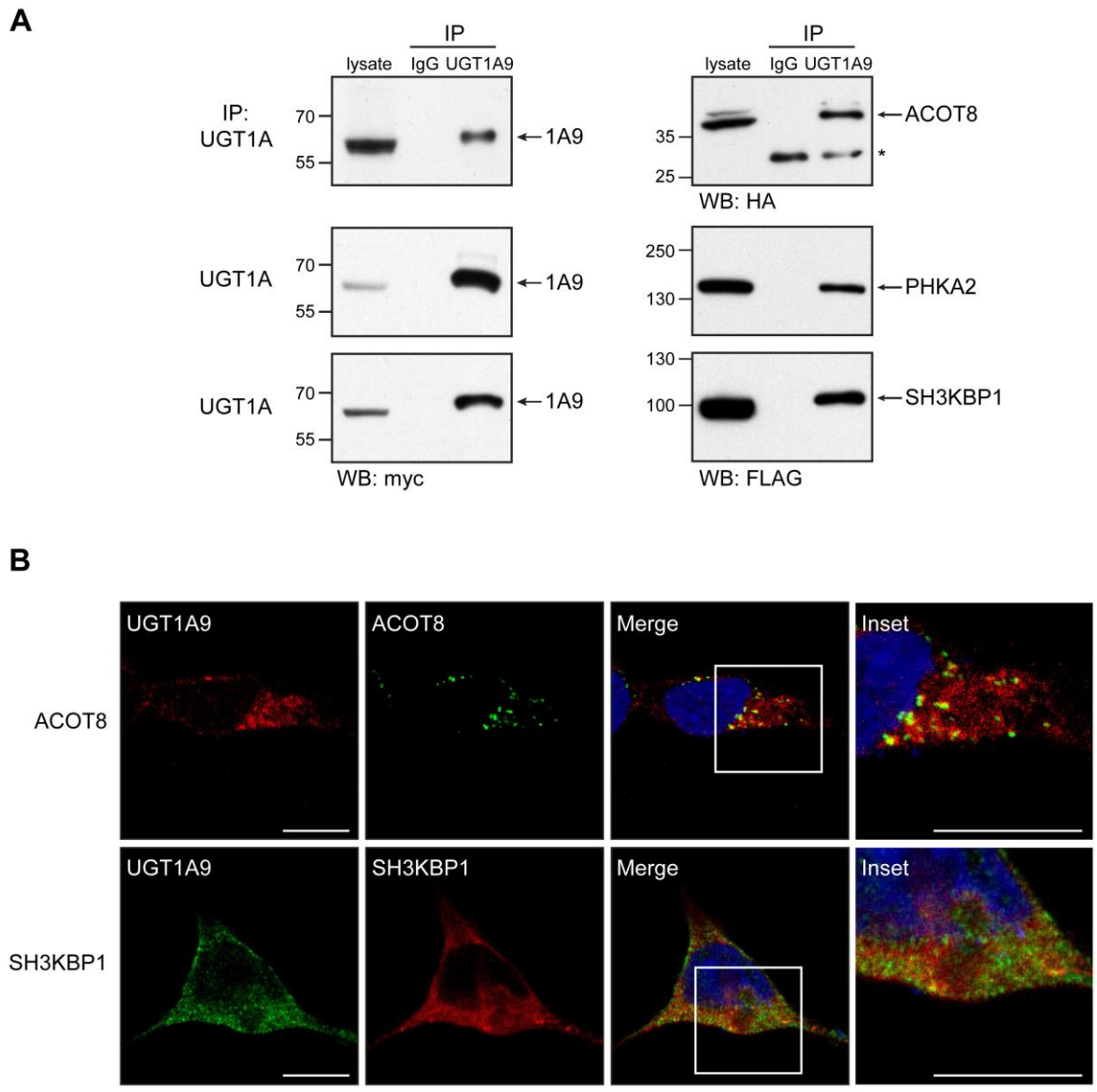
A
IP
lysate
IgG
UGT1A9
IP:
UGT1A
70
55
1A9
WB: myc
35
25
ACOT8
*
WB: HA
250
130
PHKA2
100
SH3KBP1
WB: FLAG
B
ACOT8
SH3KBP1
UGT1A9
ACOT8
Merge
Inset
SH3KBP1

Figure 5

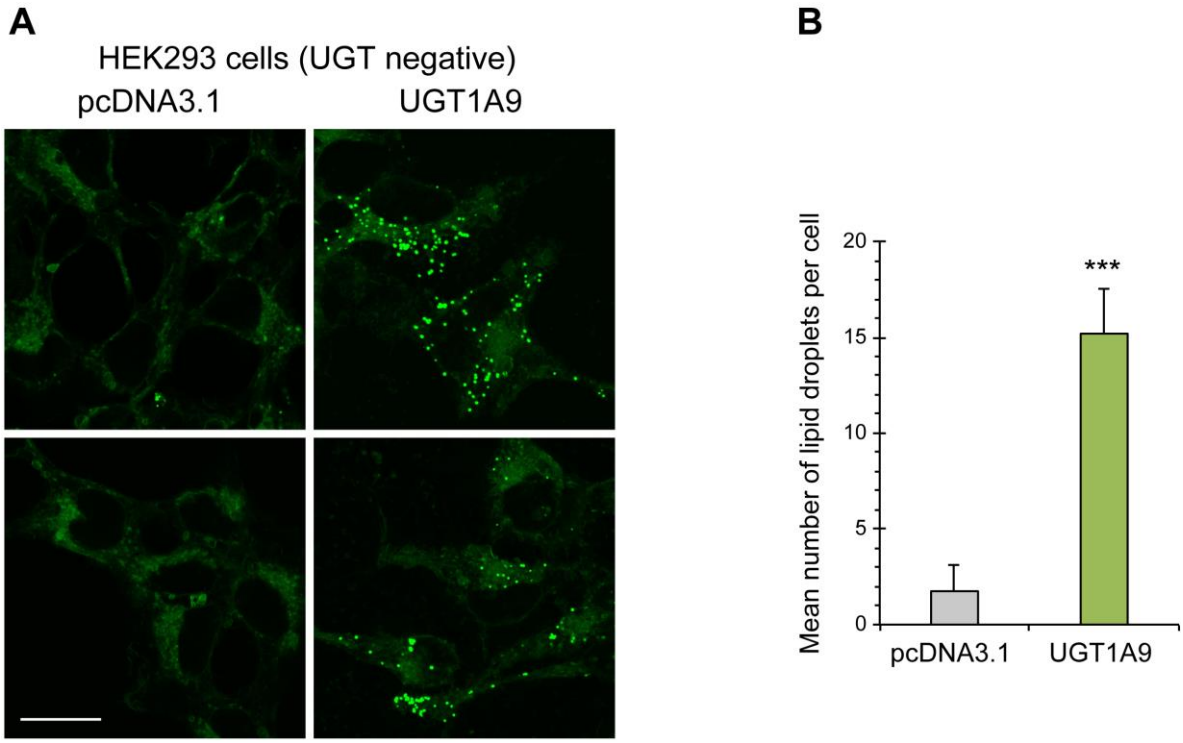
A
HEK293 cells (UGT negative)
pcDNA3.1
UGT1A9
B
Mean number of lipid droplets per cell
20
15
10
5
0
***
pcDNA3.1
UGT1A9

Chapitre 4 : « Cross-talk between alternatively spliced UGT1A isoforms and colon cancer cell metabolism »

Résumé

L'épissage alternatif du locus *UGT1* humain produit des isoformes alternatives UDP-glucuronosyltransférase i2 (UGT1A_i2), qui contrôlent l'activité de glucuronidation via des interactions protéine-protéine. Notre hypothèse stipulait que les protéines UGT1A_i2 sont impliquées dans un réseau complexe d'interactions protéiques, les connectant à de nombreuses autres voies métaboliques dont l'activité serait affectée. Ceci est supporté par une analyse d'enrichissement de voies métaboliques, basée sur des données protéomiques et ayant identifié plusieurs partenaires protéiques potentiels des protéines UGT1A_i2, notamment l'enzyme clé de la glycolyse pyruvate kinase (PKM), impliquée dans le métabolisme cellulaire cancéreux et la croissance tumorale. Le partenariat entre UGT1A_i2 et PKM2 est confirmé par co-immunoprécipitation dans le modèle cellulaire de cancer du côlon HT115, et est supporté par la co-localisation partielle des deux protéines. Supportant un rôle fonctionnel à cette interaction, la déplétion des protéines UGT1A_i2 dans les cellules HT115 augmente l'effet Warburg, favorisant l'activité glycolytique au détriment de l'activité mitochondriale tout en promouvant l'accumulation du lactate extracellulaire. La métabolomique non-ciblée identifie aussi une altération significative de 58 métabolites intracellulaires, incluant des intermédiaires métaboliques dérivés de la glycolyse et du cycle des acides tricarboxyliques. Ces changements métaboliques sont associés à une augmentation du potentiel de migration. La pertinence de ces observations est supportée par la répression en ARN messager des UGT1A_i2 dans des tumeurs de côlon comparées aux tissus sains adjacents. Les protéines alternatives UGT1A feraient donc partie de l'ensemble des voies métaboliques impliquées dans la biologie du cancer, contribuant au phénotype oncogénique du cancer du côlon. Ces découvertes révèlent de nouvelles fonctions des UGT, en marge de leur activité transférase.

Crosstalk between alternatively spliced UGT1A isoforms and colon cancer cell metabolism

Yannick Audet-Delage, Michèle Rouleau, Mélanie Rouleau, Joannie Roberge, Stéphanie Miard, Frédéric Picard, Bernard Têtu and Chantal Guillemette

Pharmacogenomics Laboratory, Centre Hospitalier Universitaire de Québec (CHU de Québec) Research Center and Faculty of Pharmacy, Laval University, Québec, Canada (YAD, MiR, MeR, JR, CG).

Centre de recherche de l'Institut universitaire de cardiologie et de pneumologie de Québec (CRIUCPQ), Laval University, Québec, QC, Canada (SM, FP)

Centre Hospitalier Universitaire de Québec (CHU de Québec) Research Center and Faculty of Medicine, Laval University, Québec, Canada (BT)

Running Title: Alternative UGT1A and cancer cell metabolism

CORRESPONDING AUTHOR:

Chantal Guillemette, Ph.D. Canada Research Chair in Pharmacogenomics

CHU de Québec Research Center, R4720, 2705 Boul. Laurier, Québec, Canada, G1V 4G2. Phone: (418) 654-2296

Email: chantal.guillemette@crchudequebec.ulaval.ca

Number of:

Abstract: 243 words

Introduction: 1024

Material and Methods: 1671

Results: 764

Discussion: 1555

Tables: 0

Figures: 6

Supplemental Figures: 2

Supplemental Tables: 2

List of abbreviations:

CAT, catalase; co-IP, co-immunoprecipitation; CTR, control; ECAR, extracellular acidification rate; FBS, fetal bovine serum; FCCP, trifluoromethoxy carbonylcyanide phenylhydrazone; i1, isoform 1; i2, isoform 2; KD, knockdown; OCR, oxygen consumption rate; OXPHOS, mitochondrial oxidative phosphorylation; PBS, phosphate buffered saline; PKM, pyruvate kinase; PRDX1, peroxiredoxin 1; RQ, relative quantities; UDPGlcA: UDP-glucuronic acid; UGT, UDP-glucuronosyltransferase; TCA, tricarboxylic acid cycle

Abstract

Alternative splicing at the human glucuronosyltransferase 1 gene locus (UGT1) produces alternate isoforms UGT1A_i2s that control glucuronidation activity through protein-protein interactions. Here, we hypothesized that UGT1A_i2s function into a complex protein network connecting other metabolic pathways with influence on cancer cell metabolism. This is based on a pathway enrichment analysis of proteomic data that identified several high-confidence candidate interaction proteins of UGT1A_i2 proteins in human tissues, namely the rate-limiting enzyme of glycolysis pyruvate kinase (PKM), which plays a critical role in cancer cell metabolism and tumor growth. The partnership of UGT1A_i2 and PKM2 was confirmed by co-immunoprecipitation in the HT115 colon cancer cells and was supported by a partial co-localization of these two proteins. In support of a functional role for this partnership, depletion of UGT1A_i2 proteins in HT115 cells enforced the Warburg effect with higher glycolytic rate at the expense of mitochondrial respiration, and led to lactate accumulation. Untargeted metabolomics further revealed a significantly altered cellular content of 58 metabolites including many intermediates derived from the glycolysis and TCA cycle pathways. These metabolic changes were associated with a greater migration potential. The potential relevance of our observations is supported by the down-regulation of UGT1A_i2s mRNA in colon tumors compared to normal tissues. Alternate UGT1A variants may thus be part of the expanding compendium of metabolic pathways involved in cancer biology directly contributing to the oncogenic phenotype of colon cancer cells. Findings uncover new aspects of UGT functions diverging from their transferase activity.

Introduction

The uridine diphospho-glucuronosyltransferases (UGTs) are critical enzymes involved in drug and carcinogen metabolism as well as in the homeostasis of a wide range of endogenous molecules such as bilirubin, steroids and lipids (Rouleau et al., 2014; Rowland et al., 2013). UGT enzymes catalyze the transfer of the sugar moiety of uridine diphospho-glucuronic acid (UDPGlcA) to numerous lipophilic substrates, and this reaction leads to inactivation and favors elimination of metabolites through bile and urine. Together with other metabolizing enzymes and transporters, UGTs are increasingly recognized as key determinants of the interindividual variability in pharmacokinetic and pharmacodynamic outcomes of clinically important drugs (Stingl et al., 2014). Findings also reveal that metabolic alterations in the glucuronidation pathway may determine the degree of exposure of an individual to toxic or carcinogenic substances over a long period determining individual susceptibility to diseases such as cancer, as well as its progression (Rouleau et al., 2014).

Alternative splicing is a powerful mean of controlling gene expression but also creates novel proteins with distinct structural and functional features (Biamonti et al., 2014). Extensive analysis of human UGT genomic sequences by our group uncovered a new class of UGT alternate isoforms derived from the UGT1 locus. Novel transcripts are created by the inclusion of an alternative terminal exon (exon 5b) that leads to the production of nine shorter UGT1A proteins called isoforms 2 (or i2s) (Girard et al., 2007; Levesque et al., 2007). Expression analyses revealed that UGT1A enzymes (referred to as isoforms 1 or i1s) and alternate UGT1A_i2s are co-produced in the same tissue structures of the liver, kidney, stomach, intestine and colon (Bellemare et al., 2011). The presence of exon 5b in the mRNA sequence causes a premature end of translation, and produces nine alternate UGT1A_i2s with different N-terminal regions (encoded by different exons 1) and lacking the transmembrane domain but comprising ten novel C-terminal amino acids (R435KKQQSGRQM444). As a consequence, these alternate proteins lack transferase function with UDPGlcA but gain new biologic activity by negatively modulating cellular glucuronidation through direct protein-protein interaction with UGT1A enzymes. This represents a new mode of regulation of the UGT metabolic pathway (Bellemare et al., 2010a; Rouleau et al., 2014).

Alternative splicing was shown to produce isoforms with vastly different interaction profiles (Yang et al., 2016). Literature supports oligomerization of UGT enzymes and with other

proteins such as cytochrome P450 (Miyauchi et al., 2015; Rouleau et al., 2014). It raises the possibility of other cellular functions for alternate UGT1A proteins and perhaps, in disease processes like cancer. Indeed, the human protein interactome is of pivotal importance in the regulation of biological systems and was shown to contribute to different pathologies, particularly cancer (Mitsopoulos et al., 2015; Yang et al., 2016). These interactions are considered as promising therapeutic targets with selected protein–protein interaction inhibitors that have reached clinical development (Scott et al., 2016). Previous untargeted proteomic experiments with human liver and kidney normal tissues revealed a partnership between UGT1A_i2s and enzymes of the scavenging pathway such as catalase (CAT) and peroxiredoxin (PRDX). By these interactions, UGT1A_i2 proteins likely interfere with oligomeric complex formation necessary for scavenging activity of CAT and PRDX (Rouleau et al., 2014). Other proteins were identified as partners of UGT1A_i2s in human tissues, using an antibody that recognized all nine alternative UGT1A_i2 proteins but not the nine UGT1A enzymes, including the multifunctional protein pyruvate kinase (PKM). PKM plays a critical role in cancer cell metabolism and tumor growth (Gupta and Bamezai, 2010). However, the potential influence of this crosstalk remains unknown. Besides, it also remains undefined which of the nine UGT1A_i2 proteins interact with these other proteins. We thus postulated that UGT1A_i2s might interact with PKM and influence its activity with potential consequences on cancer cell phenotypes given the role the PKM enzyme in the metabolic remodelling of cancer cells.

Cancer cells present a distinct metabolic phenotype also known as the Warburg effect (Li and Zhang, 2016; Warburg et al., 1927). In this context, the splice variant of pyruvate kinase M2 (PKM2) has received great attention as the major PKM isoform expressed by dividing cancer cells (Anastasiou et al., 2012; Israelsen and Vander Heiden, 2015; Taniguchi et al., 2015). In contrast, PKM1 is more abundant in healthy quiescent cells (Bluemlein et al., 2011; Zhan et al., 2015). PKM2 is a rate limiting glycolytic enzyme and a key metabolic regulator, whereas a clear picture of its function in cancer is still unresolved (Israelsen and Vander Heiden, 2015). PKM2 favors aerobic glycolysis, in which glucose is preferentially catabolized to lactate, rather than fully metabolized to carbon dioxide via mitochondrial oxidative phosphorylation (OXPHOS) (Christofk et al., 2008a). This process provides cancer cells with energy and precursors for the synthesis of nucleic acids, amino acids, and lipids to support cell division. Recent data indicate that overexpression of PKM2 in colon tumors connote poor outcome, as it is associated with advanced tumor stage and lymph node metastasis,

and is essential for the aerobic glycolysis of colon cancer cells in vitro (Cui and Shi, 2015; Yang et al., 2014; Yang et al., 2015; Zhou et al., 2012).

In this work, we sought to expose potential metabolic and phenotypic changes associated with UGT1A_i2 proteins in a colon cancer cell model HT115, in which PKM2 is expressed in addition to several different UGT1A proteins, including UGT1A enzymes and alternative i2 isoforms. We initially confirmed the direct interaction of UGT1A_i2s with pyruvate kinase by co-immunoprecipitation (co-IP) in HT115 cell lysates. Compared to normal colon tissues, downregulation of UGT1A_i2s mRNA expression was established in colon tumors by quantitative PCR and RNA sequencing. Metabolic alterations associated with depletion of UGT1A_i2 protein levels stably induced by shRNA (targeting the exon 5b region common to all UGT1A_i2s) were then investigated by complementary approaches including untargeted metabolomics and extracellular flux assays to monitor glycolysis and oxidative phosphorylation. Findings reveal for the first time a significant remodelling of energy metabolism and cellular content of several metabolic intermediates in UGT1A_i2s depleted cancer cells, likely partially explained by a direct interaction with PKM2. These metabolic changes are further associated with a greater migration potential, suggesting that alternate UGT1A proteins might contribute to the oncogenic phenotype of colon cancer cells.

Materials and Method

Immunofluorescence

HT115 cells were obtained from the European Collection of Cell Cultures (Salisbury, UK) and grown as described (Bellemare et al., 2010b). Cells grown on coverslips to 60% confluence were fixed with 4% formaldehyde (Sigma, Oakville, ON, Canada) for 15 min at room temperature, and permeabilized with 0.5% TX-100 (Sigma) for 5 min. All solutions were prepared in phosphate-buffered saline (PBS). Cells were incubated for 1h30 at RT with primary antibodies diluted in 1% fetal bovine serum (FBS). Primary antibodies were anti-PKM2 (1:500; #3198S, Cell Signaling, Danvers, MA, USA) and the custom mouse monoclonal anti-i2s (1:100; #4C5E7; GenScript, Piscataway, NJ, USA) described in Rouleau et al. (Rouleau et al., 2016). Detection was made with donkey anti-mouse Alexa Fluor 488 (Life Technologies Inc., Burlington, ON, Canada) and goat anti-rabbit Alexa Fluor 594 (Cell Signaling) antibodies on a LSM510 META NLO laser scanning confocal microscope (Zeiss, Toronto, ON, Canada). Images were acquired with the Zen 2009

software (v.5.5 SP1; Zeiss) and were analyzed with ImageJ (v2.0.0; U.S. National Institutes of Health, Bethesda, MD, USA).

Immunoprecipitation and pathway enrichment analysis

Proteomics experiments in commercial pools of human liver and kidney tissues were conducted according to a previous study (Rouleau et al., 2014). Data have been deposited in the PRIDE database under the accession number PXD000295. Briefly, immunoprecipitation was carried out using 1 mg total protein lysate of human liver or kidney S9 fractions (cytosol and microsomes) (Xenotech, Lenexa, KS, USA) with 4 µg anti-UGT1A_i2 #4863 antibody and Protein G–coated magnetic beads (Dynabeads; Life Technologies) for 15 hours at 4°C. Proteins were identified by mass spectrometry using a TripleTOF 5600 after on-beads trypsin digestion. Pathway enrichment analysis was performed with Cytoscape v3.3.0, using ClueGo v2.2.3 and CluePedia v1.2.3 apps (Bindea et al., 2013; Bindea et al., 2009; Shannon et al., 2003). Pathways were retrieved from the KEGG database (updated on January 15, 2016) and an enrichment/depletion two-sided hypergeometric test with the Bonferroni step down correction method was applied. All presented protein partners were part of a significantly enriched pathway (q-value<0.05).

Detection of protein expression and complexes

Co-immunoprecipitations (co-IPs) to confirm partnership with PKM2 were conducted on HT115 cell lysates using the anti-UGT1A_i2s (#4863) and the anti-UGT1A_i1s (#9348) as described (Rouleau et al., 2014). Protein complexes were subjected to SDS-PAGE and detected by Western blotting with UGT1A_i2s (#4863), biotinylated UGT1A_i1 (#9348), and PKM2 (#3198S, Cell Signaling) antibodies. Protein expression was also detected by Western blot. To monitor protein integrity and phosphorylation status, cells were lysed in Tris buffered solution (175 mM Tris pH 7.4, 150 mM NaCl, 1% Igepal, 1mM DTT) supplemented with Complete protease inhibitor (Roche, Laval, Qc, Canada) and phosSTOP (Sigma). Proteins were revealed using anti-PKM1 (#7067P, Cell Signaling), anti-PKM2 (Cell Signaling), anti-phospho-PKM2 Y105 (#3827; Cell Signaling) and anti-phospho-PKM2 S37 (#11456; Signalway Antibody; College Park, MD, USA). PKM2 dimers and tetramers were crosslinked according to (Wang et al., 2014). Briefly, cell were lysed in PBS (pH 7.4) containing 0.5% Triton X-100 for 30 min, then centrifuged at 16 000 *xg* for 20 min to remove debris. Lysates were then diluted to 4 mg/mL and glutaraldehyde (final concentration 0.0035%) was added to permanently crosslink proteins. After 2 min of incubation at RT, the

crosslinking reaction was stopped using Tris pH 8.0 (final concentration 50 mM). Finally, protein complexes were subjected to SDS-PAGE and revealed using anti-PKM2 (Cell Signaling).

Metabolic profiling of HT115 colon cancer cells

Metabolic profiles were established for two HT115 cell lines, a reference HT115 cell line (CTR) and a HT115 cell line in which the expression of UGT1A_i2 proteins were stably repressed (>90%) using a shRNA specific to the exon 5b of *UGT1A* (KD) (Rouleau et al., 2014). Cell lines were grown for a maximum of 15 passages and periodically tested for mycoplasmas. Cells were seeded at 2 x 10^6 cells in a 10 cm petri dish and allowed to adhere and proliferate for four days, with one growth medium change after two days. Cells were trypsinized, centrifuged and counted, before being washed twice with ice-cold PBS and frozen on dry ice. Mass spectrometry analyses were performed by the West Coast Metabolomics Center (UC Davis, Davis, CA, USA) as reported (Fiehn et al., 2010; Fiehn et al., 2008). Data were normalized for cell count and log-transformed prior to testing for statistical differences using two-sided Student's t-tests.

The analysis of extracellular flux was achieved on a Seahorse XF^e24 using glycolysis and mitochondria stress kits according to the manufacturer's instructions (Seahorse Bioscience, MA, USA). For the glycolysis stress kit, 100 µL of cells at 2.0 x 10^6 cells/mL were seeded in the dedicated plates, and allowed to adhere for two hours in the incubator before adding 150 µL of pre-warmed culture medium. Cells were grown overnight, rinsed twice with 1 mL Seahorse XF Base Medium (Seahorse Bioscience) supplemented with 4 mM glutamine, and a final volume of 450 µL of the medium was added. Cells were incubated for 1 hour at 37°C and 100% humidity in a non-CO_2 incubator. Test compounds were reconstituted in glutamine-supplemented Seahorse XF Base Medium, according to instructions. A total of 75 µL of this medium was loaded in the injection plate port 'A', while glucose was added in 'B', oligomycin in 'C' and 2-deoxyglucose in 'D'. Three measure phases were done for each condition, constituted of three minutes of mixing, two minutes of waiting and three minutes of measuring. For the mitochondria stress kit, a similar protocol was used, except that the Seahorse XF Base Medium was supplemented with both 4 mM glutamine and 4 g/L of glucose, and injection ports were loaded as follows: assay medium in 'A', oligomycin in 'B', trifluoromethoxy carbonylcyanide phenylhydrazone (FCCP) in 'C' and rotenone/antimycin A

in ‘D’. Data were normalized for protein content. Number of replicates and independent experiments are specified in the figure legend.

Lactate was quantified with a Lactate Colorimetric/Fluorometric Assay Kit (BioVision, Milpitas, CA, USA). Cells were seeded at 0.6 x 10^6 cells per well in a 6-well plate for 48 hours, rinsed twice with fresh medium and 3 mL of medium was added per well. Medium was sampled at 0, 60, 120 and 180 min and immediately frozen on dry ice. Cells were then trypsinized and counted. A perchloric acid deproteinization kit (BioVision) was used prior to sample dilution and lactate dosage. Fluorescence (Ex/Em = 535/590 nm) was measured on a TECAN M-1000 (Tecan US Inc., Morrisville, NC, USA). Samples were measured in duplicate for each time point. Results represent the mean of two independent experiments and differences were assessed by Student’s two-sided T-tests.

Cellular phenotypes

For proliferation assays, HT115 cells were monitored for 8 days and counted using a TC10 automated cell counter (Bio-Rad, Hercules, California, USA) after addition of Trypan Blue (Sigma). Live cell proliferation assays were conducted on the xCELLigence DP system according to the manufacturer instructions (ACEA Biosciences Inc., San Diego, CA, USA). Cells were seeded in E-plates (6.0 x 10^4 cells/well) and monitored every five min for the first four hours, and every 15 min for five days, with the culture medium being changed every 48 hours. In deprivation assays, cells were washed three times with the experimental culture medium before seeding. For glucose deprivation, cells grew in reconstituted glucose free DMEM medium (Sigma), supplemented with 15% FBS (Wisent Bioproducts, St-Bruno, QC, Canada) and 5.6 mM glucose (Sigma). For glutamine deprivation, cells grew in DMEM supplemented with 15% dialyzed FBS and glutamine (Wisent Bioproducts) at a concentration of 0.75 mM or 4 mM. Conditions for serine/glycine deprivation were adapted from (Maddocks et al., 2013). Briefly, MEM medium (Life Technologies) was supplemented with 15% dialyzed FBS, 25 mM glucose (Sigma), 4 mM glutamine and MEM vitamins (Life Technologies). Cells grew either in 0.4 mM serine (Sigma) and glycine (MP Biomedicals, Solon, OH, USA) or in absence of those. Doubling time was calculated with the RTCA Software 2.0 (ACEA Biosciences Inc.), using two points within the exponential proliferation phase. Data are derived from two independent experiments performed at least in triplicate. Differences were assessed with Student’s two-sided T-tests.

Adhesion assays were conducted with the ECM 545 adhesion array kit (Millipore Inc., Billerica, MA, USA), according to the manufacturer's instructions. Each well was seeded with 5 X 10^4 cells in 100 µL of assay buffer. Cells were allowed to adhere for two hours and then rinsed 3 times with the assay buffer. Along with the provided lysis buffer, CyQuant GR DNA dye was added to each well and lysates were transferred in a black plate for fluorescence reading at specified wavelength, i.e. 485 nm (excitation) and 530 nm (emission), on a TECAN M-1000. Data are derived from three independent experiments performed in triplicate and differences were assessed with the two-sided Student's T-tests.

Wound healing assays were conducted using ibidi culture inserts (Minitube Canada, Ingersoll, ON, Canada). Cells were seeded at 9.8 x 10^4 cells/well in a 6-well plate with complete media, and allowed to adhere for 6-8 hours. Cells were then serum-starved overnight and complete media was given 24 hours prior to removal of inserts. Migration was monitored every 24 hours on an inverted Diaphot (Nikon) microscope equipped with a 10X objective and a QICAM (QImaging, Burnaby, BC, Canada) video camera. Five microscopic fields per wound were recorded and the wound area was determined by tracing its contours using ImageJ v1.48. Data are derived from three independent experiments performed in duplicate, and each analyzed independently by two investigators. Differences were assessed with the two-sided Student's T-tests.

mRNA quantification

Human colon tissues (n=6) from primary tumors and paired peritumoral normal tissues were analyzed by reverse transcription and quantitative PCR and are expressed in Relative Quantities (RQ) (Margaillan et al., 2015). RT-qPCR were performed using *UGT1A* specific primers for variants 2/3 (encoding UGT1A_i2s) as described (Bellemare et al., 2010b). Each participant provided written consent, and the local ethic committee approved the study. RNA sequencing data (GSE80463) are from a previous study (Rouleau et al., submitted) and were collected from three pools of colon tissues, each containing total RNA from 5 individuals (normal tissues) or 3 individuals (tumor tissues).

Results

Interaction of UGT1A_i2 proteins with PKM2 in colon cancer HT115 cells

Proteomics experiments in human liver and kidney tissues were conducted according to a previous study (**Fig.1A**). The complete list of identified partners in both tissues is provided (**Supplemental Tables 1 and 2**) based on a previous report (Rouleau et al., 2014). A pathway enrichment analysis of alternate UGT1A_i2 protein partners identified several enzymes linked to pyruvate metabolism, citrate metabolism and glycolysis pathway, including pyruvate kinase involved in glycolysis (**Fig.1B**). We validated the interaction with pyruvate kinase by co-IP in the HT115 cell model that expresses endogenous PKM2, UGT1A_i2s as well as UGT1A_i1 enzymes. These experiments confirmed that PKM2 interacts specifically with the UGT1A_i2 proteins but not with UGT1A_i1 enzymes in HT115 cells (**Fig.1C**). Since PKM2 primarily localized in the cytoplasm (Wang et al., 2014), we then sought to establish the cellular distribution of alternate UGT1A_i2 proteins along with PKM2 **(Fig.1D)**. A subset of UGT1A_i2s co-localized with PKM2 and supports the potential of UGT1A_i2s to interact with PKM2 in this cellular context.

Depletion of UGT1A_i2s enhances glycolytic activity and lactate production but reduces mitochondrial respiration in living colon cancer HT115 cells.

We next assessed the potential influence of UGT1A_i2s on glycolysis and compared HT115 colon cancer cells expressing low (KD) and high (reference or control) UGT1A_i2 levels (**Fig.2A**) (Rouleau et al., 2014). Given that PKM2 and PKM1 expression is similar in both cell models (**Supplemental Fig. 1**), we postulated that the cellular content in alternate UGT1A_i2s could affect PKM2 activity thereby modifying glucose metabolism to produce lactate, the end product of glycolysis. The accumulation of lactate by 57% (P=0.029; **Fig.2B**) in cell medium of KD cells compared to control cells supports a functional impact of UGT1A_i2s on PKM2 activity. We then used an extracellular flux analyzer to measure extracellular acidification rate (ECAR) and oxygen consumption rate (OCR) in living HT115 cells, which reflects glycolytic activity and mitochondrial respiration, respectively. A higher glycolytic activity in the UGT1A_i2s depleted cells was observed as evidenced by a 27% ECAR elevation after addition of glucose to the medium. The maximal glycolytic capacity (measured after addition of oligomycin) was also elevated by 30%, upholding greater utilization of the glycolysis pathway compared to control cells (**Fig.2C,D**). In an assay challenging the mitochondrial capacity and measuring OCR, we detected a lower activity in

KD cells supported by lower baseline (-27%) and lower maximal mitochondrial respiration rates (-39%; after addition of FCCP) in these cells compared to control cells (**Fig.2E,F**). Thus, repression of endogenous UGT1A_i2 levels led to higher glycolytic rate at the expense of mitochondrial respiration.

Depletion of UGT1A_i2s induces broad metabolic changes in colon cancer HT115 cells and a greater migration potential.

Given the changes in the energetic pathway induced by depletion of endogenous UGT1A_i2 levels, we extended these studies to global cell metabolism using untargeted metabolomics. A significant effect in the cellular levels of 58 metabolites was observed including many intermediates derived from the glycolysis and TCA cycle pathways. These metabolites include unknown (n=34; data not shown) and known (n=24) metabolites (**Fig.3,4**). Specifically, higher levels of glucose, fructose and citrate were observed, as well as decreased serine and glutamine cellular contents (**Fig.3B**). Lower levels of several amino acids and some of their metabolites in KD cells were also noted (**Fig.3,4**). These metabolic changes were not associated with differences in cell growth assessed by cell counts, or doubling time determined by a live cell proliferation assay in normal culture conditions or after deprivation of main extracellular carbon sources, glucose and glutamine (**Supplemental Fig.2**). A modest change was noted upon deprivation of the non-essential amino acids serine and glycine (13% longer doubling time; $P<0.05$; **Fig.5A,B**). However, KD cells had a significant greater migration potential (wound closure: 72%; $P<0.05$) compared to control cells (50%) (**Fig.5C-E**). Using an array of extracellular matrix proteins, data further showed a modest but significantly reduced adhesion capacity for KD cells toward collagen I (13%), laminin (10%) and tenascin (11%), compared to control cells (**Fig.5F**).

Downregulation of UGT1A_i2s mRNA expression in colon tumors compared to normal tissues

To evaluate the potential relevance of our observations using the HT115 model in which endogenous UGT1A_i2 levels were depleted, we studied UGT1A_i2s expression in colon tumors compared to normal tissues. Quantitative PCR expression of the alternative mRNA variants (*v2/v3)* encoding UGT1A_i2 proteins assessed in primary colon tumors and paired peritumoral normal tissues revealed that most tumors (4/6; 67%) had a reduced UGT1A_i2s expression compared to normal tissues (**Fig.6A**). This observation was further confirmed

using RNA sequencing data generated from an independent set of colon samples (Fold change = -20.5; *P*<0.05; **Fig.6B**).

Discussion

It is now well established that there is a strong and multifaceted connection between cell metabolism and cancer (Li and Zhang, 2016; Vander Heiden et al., 2009), while alternative splice variants of many cancer-related genes directly contribute to the oncogenic phenotype (Oltean and Bates, 2014). We showed that depletion of UGT1A_i2 proteins in the colon cancer cell model HT115 enforces the Warburg effect, modifies levels of cellular metabolic intermediates and impacts migration properties. These metabolic and phenotypic changes may be explained, at least in part, by the interaction between UGT1A_i2s and PKM2, a key enzyme of the glycolysis pathway. Since glycolysis-related pathways determine cellular energy level, redox homeostasis and ability to proliferate (Vander Heiden et al., 2011), it is plausible that alternate UGT1A_i2 proteins play a role in oncogenic phenotypes. In support, the metabolic adaptation of cancer cells, which oxidize carbohydrates at a reduced rate even in the presence of oxygen, was shown to be greater in the absence of UGT1A_i2 proteins, suggesting a functional role of its interaction with the glycolytic enzyme PKM2. The production of excess amounts of lactate released from cancer cells also supports this notion. The *in vivo* relevance of our observations was further supported by a severely decreased UGT1A_i2s expression in colon tumors compared to normal tissues established by quantitative PCR and RNA sequencing, and in few specimens by IHC (Bellemare et al., 2011), in line with a potential role of alternate UGT1A proteins in tumor cell biology.

Previous studies have linked energy metabolism to colon cancer progression, and as a rate-limiting enzyme of glycolysis, PKM2 has been investigated (Li et al., 2014; Lunt et al., 2015; Yang et al., 2014; Zhou et al., 2012). Zhou et al (Zhou et al., 2012) have reported an upregulation of PKM2 in colorectal cancer, and that its knockdown suppressed the proliferation and migration of colon cancer RKO cells. Other findings indicated that the activity of PKM2 is pivotal for the fate of pyruvate: the highly active PKM2 tetramer (high pyruvate kinase activity) leads to pyruvate oxidation in the TCA cycle, whereas the less active PKM2 dimer (low pyruvate kinase activity) enhances the conversion of pyruvate into lactate by the lactate dehydrogenase and favors synthesis of cell constituents (Anastasiou et al., 2012; Christofk et al., 2008a). Our analysis of extracellular flux in real-time uncovered an enhanced glycolytic activity and a lower OXPHOS capacity for KD cells, which is in

accordance with a rerouting of carbohydrates toward lactate instead of TCA cycle. We also observed accumulation of lactate in KD cell medium, further suggesting that the presence of UGT1A_i2 proteins interferes with the glycolytic pathway. Given that PKM2 and PKM1 expression is similar in both cell models (**Supplemental Fig. 1A**), we investigated the status of PKM2 phosphorylation and oligomerization. Phosphorylation of PKM2 at position Y_{105}, favoring lactate production by the less active dimeric PKM2 conformation, was slightly enhanced in KD relative to control cells (**Supplemental Fig.1A**) whereas the PKM2 tetramer/dimer ratios were similar between the two model cell lines, unsupportive of a modulation of PKM2 oligomeric state by UGT1A_i2s (**Supplemental Fig.1B**). PKM2 may also be involved in other functions in tumorigenesis and metastasis, since PKM2 was shown to act in the nucleus by regulating gene expression (Wang et al., 2014; Yang et al., 2012). However, our previous analysis of global gene expression in HT115 cell lines suggest that the KD of UGT1A_i2s does not induce significant perturbations in gene expression of glycolytic enzymes or of other metabolic pathways, including genes modulated by PKM2 and reported to modulate migration and epithelial-mesenchymal transition (Hamabe et al., 2014; Rouleau et al., 2014; Yang et al., 2014). Consistently, levels of phospho-PKM2 (position S_{37}) involved in nuclear translocation and functions of PKM2, were not altered by a KD of UGT1A_i2s (**Supplemental Fig.1**). Therefore, it may be envisioned that the interaction between PKM2 and alternate UGT1A_i2 proteins might influence PKM2 allosteric regulation. In line with this notion, similar functional interactions of PKM2 with other proteins such as the promyelocytic leukemia (PML) tumor suppressor protein, the prolactin receptor, and the phosphoprotein (pp60src)-associated protein kinase of Rous sarcoma virus led to reduced pyruvate kinase activity through allosteric regulation (Christofk et al., 2008b; Gao et al., 2013; Glossmann et al., 1981; Mazurek et al., 2001; Presek et al., 1980; Shimada et al., 2008; Varghese et al., 2010). Whether this could be mediated by direct interactions with phosphorylated UGT1A_i2s *(Basu et al., 2003; Basu et al., 2005; Volak and Court, 2010)* or by a UGT1A_i2-dependent modulation of interactions between PKM2 and other allosteric modulators will necessitate additional investigations. From a therapeutic perspective PKM2 expression and activity can be regulated by inhibitors and activators that have been tested *in vitro* and *in vivo* (Dong et al., 2016).

The greater migration potential provoked by UGT1A_i2s KD in HT115 cells is in line with a shift from oxidative metabolism to aerobic glycolysis reported in more aggressive colon cancer cells (Hussain et al., 2016). Consistent with our observation that lactate accumulates

in the medium of UGT1A_i2s KD compared to control cells; this oncometabolite was shown to act not only as a potent fuel (oxidative) but also function as a signalling molecule to stimulate tumor angiogenesis (Doherty and Cleveland, 2013). Moreover, the mitochondrial oxidative metabolism is viewed as a critical suppressor of metastasis and thus, lower OXPHOS activity may help promote metastasis (Lu et al., 2015). Cell migration is an early requirement for tumor metastasis (Findlay et al., 2014), but is a complex phenomenon that involves cycling of adhesion and cell detachment (Kurniawan et al., 2016; Pankova et al., 2010; Tozluoglu et al., 2013). Strongly adherent cells may increase their migration capacity through a decrease of their adhesion to extracellular matrix. While subtle, we observed a differential adhesion capacity of KD cells, namely for laminin, a non-collagenous extracellular matrix critical in colon cancer and linked to tumor angiogenesis, epithelial-mesenchymal transition and metastasis (Guess et al., 2009; Kitayama et al., 1999; Simon-Assmann et al., 2011). Accordingly, this observation may partially explain the differential migration phenotype between low and high UGT1A_i2 expressing cell lines.

A potential limitation is the fact that metabolomics data were derived from a single time-point, and thus represent the sum of numerous metabolic reactions that occurred in a 48-hour period. The cellular content of several metabolic intermediates from the glycolysis and TCA cycle pathways was changed in UGT1A_i2-depleted HT115 cells compared to control cells and are unlikely explained solely by the protein-protein interaction between UGT1A_i2s and PKM2. Additional partnerships observed by proteomics, such as those with enzymes of the gluconeogenesis and TCA cycle that require additional validation by co-IP, may also underlie these observations. Of note, data revealed a globally reduced pool of glucogenic amino acids in KD cells. This is consistent with the enhanced glycolytic potential induced by the KD and with the identification of additional i2 protein partners associated with gluconeogenesis, for instance pyruvate carboxylase (PC) and phosphoenolpyruvate carboxykinase (PCK1 and PCK2). Furthermore, the lower serine levels in KD cells compared to CTR suggested that the *de novo* serine synthesis pathway, critical for cancer cell proliferation and metabolism (Mehrmohamadi and Locasale, 2015; Yoon et al., 2015), might be perturbed. We thus expected that serine and glycine deprivation would increase the metabolic pressure on glycolysis through a deviation of its intermediates. Although modest, a significantly decreased cellular proliferation for KD cells was observed in these conditions, compared to control cells. It remains unknown whether a specific UGT1A_i2 protein or several of those expressed in the HT115 cell model trigger the observed effects

given that all UGT1A_i2s were simultaneously repressed by shRNA. Additional cell models need to be established to further investigate our initial findings.

To the best of our knowledge, this is the first identification of a functional link between the UGT pathway and energy metabolism implying that alternate UGT1A proteins might be regulators of PKM2 with consequences on cancer cell metabolism and phenotype. It may be unexpected that a depletion of alternate UGT1A_i2s is sufficient to alter the metabolic program of colon cancer cells given the numerous, redundant, and efficacious mechanisms in place to limit pyruvate oxidation in cancer cells. In the face of these counteracting mechanisms, the metabolic effects of UGT1A_i2s depletion are rather impressive and may be explained in part by an interaction with the key glycolytic and multifunctional enzyme PKM2, and most likely with other metabolic enzymes. Although there was no change in UDPGlcA cell content between the two cell models, another possibility could involve the allosteric modulation by UDPGlcA and/or other UDP-sugars, as reported for other glycolytic enzymes (Wu et al., 2006). It also remains to be demonstrated whether UGT1A_i2s possess enzyme activity by utilizing other UDP-sugars for instance. Alternatively, the effects observed on metabolism could be mediated through an impact on endogenous levels of key metabolic molecules that are unknown substrates of UGT enzymes repressed by UGT1A_i2s. Findings thus support that alternate UGT1A proteins are potential metabolic regulators of cancer cell metabolism and that they may contribute to the oncogenic phenotype of colon cancer cells. We conclude that alternate UGT proteins may be part of the expanding compendium of metabolic pathways involved in cancer biology. However, further investigations of UGT1A alternate proteins in cancer metabolism are required, as the crosstalk between global cell metabolism and the UGT pathway may likely constitute a key vulnerability in cancer cells that could be exploited.

Conflict of interest

The authors have declared that no conflict of interest exists.

Acknowledgments

We would like to acknowledge Lyne Villeneuve, Andréa Fournier, Patrick Caron and Véronique Turcotte for technical support. We acknowledge the support from Michèle Orain for help with handling of human tissues.

Authorship contributions

Participated in research design: Mi Rouleau, Guillemette

Conducted experiments: Audet-Delage, Me Rouleau, Roberge

Contributed new reagents or analytic tools: Miard, Picard, Têtu

Performed data analysis: Audet-Delage, Mi Rouleau, Me Rouleau, Roberge, Miard, Guillemette

Wrote or contributed to the writing of the manuscript: Audet-Delage, Mi Rouleau, Me Rouleau, Guillemette

Footnotes

a) This work was supported by the Canadian Institutes of Health [CIHR MOP-142318] and the Natural Sciences and Engineering Research Council of Canada [NSERC 342176-2012]. YAD received studentship awards from Centre de Recherche en Endocrinologie Moléculaire et Oncologique et Génomique Humaine (CREMOGH), Laval University and Fonds de Recherche du Québec – Santé (FRQS). MeR and JR received studentship awards from CIHR. CG holds a Canada Research Chair in Pharmacogenomics (Canadian Research Chair Program).

b) Part of the initial data was presented at the Integrating Metabolism and Tumor Biology Keystone meeting held January 13-17, 2015 in Vancouver (BC, Canada).

References

Anastasiou D, Yu Y, Israelsen WJ, Jiang JK, Boxer MB, Hong BS, Tempel W, Dimov S, Shen M, Jha A, Yang H, Mattaini KR, Metallo CM, Fiske BP, Courtney KD, Malstrom S, Khan TM, Kung C, Skoumbourdis AP, Veith H, Southall N, Walsh MJ, Brimacombe KR, Leister W, Lunt SY, Johnson ZR, Yen KE, Kunii K, Davidson SM, Christofk HR, Austin CP, Inglese J, Harris MH, Asara JM, Stephanopoulos G, Salituro FG, Jin S, Dang L, Auld DS, Park HW, Cantley LC, Thomas CJ and Vander Heiden MG (2012) Pyruvate kinase M2 activators promote tetramer formation and suppress tumorigenesis. *Nat Chem Biol* **8**: 839-847.

Basu NK, Kole L and Owens IS (2003) Evidence for phosphorylation requirement for human bilirubin UDP-glucuronosyltransferase (UGT1A1) activity. *Biochem Biophys Res Commun* **303**: 98-104.

Basu NK, Kovarova M, Garza A, Kubota S, Saha T, Mitra PS, Banerjee R, Rivera J and Owens IS (2005) Phosphorylation of a UDP-glucuronosyltransferase regulates substrate specificity. *Proc Natl Acad Sci U S A* **102**: 6285-6290.

Bellemare J, Rouleau M, Girard H, Harvey M and Guillemette C (2010a) Alternatively spliced products of the UGT1A gene interact with the enzymatically active proteins to inhibit glucuronosyltransferase activity in vitro. *Drug Metab Dispos* **38**: 1785-1789.

Bellemare J, Rouleau M, Harvey M, Popa I, Pelletier G, Tetu B and Guillemette C (2011) Immunohistochemical expression of conjugating UGT1A-derived isoforms in normal and tumoral drug-metabolizing tissues in humans. *J Pathol* **223**: 425-435.

Bellemare J, Rouleau M, Harvey M, Tetu B and Guillemette C (2010b) Alternative-splicing forms of the major phase II conjugating UGT1A gene negatively regulate glucuronidation in human carcinoma cell lines. *Pharmacogenomics J* **10**: 431-441.

Biamonti G, Catillo M, Pignataro D, Montecucco A and Ghigna C (2014) The alternative splicing side of cancer. *Semin Cell Dev Biol* **32**: 30-36.

Bindea G, Galon J and Mlecnik B (2013) CluePedia Cytoscape plugin: pathway insights using integrated experimental and in silico data. *Bioinformatics* **29**: 661-663.

Bindea G, Mlecnik B, Hackl H, Charoentong P, Tosolini M, Kirilovsky A, Fridman WH, Pages F, Trajanoski Z and Galon J (2009) ClueGO: a Cytoscape plug-in to decipher functionally grouped gene ontology and pathway annotation networks. *Bioinformatics* **25**: 1091-1093.

Bluemlein K, Gruning NM, Feichtinger RG, Lehrach H, Kofler B and Ralser M (2011) No evidence for a shift in pyruvate kinase PKM1 to PKM2 expression during tumorigenesis. *Oncotarget* **2**: 393-400.

Christofk HR, Vander Heiden MG, Harris MH, Ramanathan A, Gerszten RE, Wei R, Fleming MD, Schreiber SL and Cantley LC (2008a) The M2 splice isoform of pyruvate kinase is important for cancer metabolism and tumour growth. *Nature* **452**: 230-233.

Christofk HR, Vander Heiden MG, Wu N, Asara JM and Cantley LC (2008b) Pyruvate kinase M2 is a phosphotyrosine-binding protein. *Nature* **452**: 181-186.

Cui R and Shi XY (2015) Expression of pyruvate kinase M2 in human colorectal cancer and its prognostic value. *Int J Clin Exp Pathol* **8**: 11393-11399.

Doherty JR and Cleveland JL (2013) Targeting lactate metabolism for cancer therapeutics. *J Clin Invest* **123**: 3685-3692.

Dong G, Mao Q, Xia W, Xu Y, Wang J, Xu L and Jiang F (2016) PKM2 and cancer: The function of PKM2 beyond glycolysis. *Oncol Lett* **11**: 1980-1986.

Fiehn O, Garvey WT, Newman JW, Lok KH, Hoppel CL and Adams SH (2010) Plasma metabolomic profiles reflective of glucose homeostasis in non-diabetic and type 2 diabetic obese African-American women. *PLoS One* **5**: e15234.

Fiehn O, Wohlgemuth G, Scholz M, Kind T, Lee DY, Lu Y, Moon S and Nikolau B (2008) Quality control for plant metabolomics: reporting MSI-compliant studies. *Plant J* **53**: 691-704.

Findlay VJ, Wang C, Watson DK and Camp ER (2014) Epithelial-to-mesenchymal transition and the cancer stem cell phenotype: insights from cancer biology with therapeutic implications for colorectal cancer. *Cancer Gene Ther* **21**: 181-187.

Gao X, Wang H, Yang JJ, Chen J, Jie J, Li L, Zhang Y and Liu ZR (2013) Reciprocal regulation of protein kinase and pyruvate kinase activities of pyruvate kinase M2 by growth signals. *J Biol Chem* **288**: 15971-15979.

Girard H, Levesque E, Bellemare J, Journault K, Caillier B and Guillemette C (2007) Genetic diversity at the UGT1 locus is amplified by a novel 3' alternative splicing mechanism leading to nine additional UGT1A proteins that act as regulators of glucuronidation activity. *Pharmacogenet Genomics* **17**: 1077-1089.

Glossmann H, Presek P and Eigenbrodt E (1981) Association of the src-gene product of Rous sarcoma virus with a pyruvate-kinase inactivation factor. *Mol Cell Endocrinol* **23**: 49-63.

Guess CM, Lafleur BJ, Weidow BL and Quaranta V (2009) A decreased ratio of laminin-332 beta3 to gamma2 subunit mRNA is associated with poor prognosis in colon cancer. *Cancer Epidemiol Biomarkers Prev* **18**: 1584-1590.

Gupta V and Bamezai RN (2010) Human pyruvate kinase M2: a multifunctional protein. *Protein Sci* **19**: 2031-2044.

Hamabe A, Konno M, Tanuma N, Shima H, Tsunekuni K, Kawamoto K, Nishida N, Koseki J, Mimori K, Gotoh N, Yamamoto H, Doki Y, Mori M and Ishii H (2014) Role of pyruvate kinase M2 in transcriptional regulation leading to epithelial-mesenchymal transition. *Proc Natl Acad Sci U S A* **111**: 15526-15531.

Hussain A, Qazi AK, Mupparapu N, Guru SK, Kumar A, Sharma PR, Singh SK, Singh P, Dar MJ, Bharate SB, Zargar MA, Ahmed QN, Bhushan S, Vishwakarma RA and Hamid A (2016) Modulation of glycolysis and lipogenesis by novel PI3K selective molecule represses tumor angiogenesis and decreases colorectal cancer growth. *Cancer Lett* **374**: 250-260.

Israelsen WJ and Vander Heiden MG (2015) Pyruvate kinase: Function, regulation and role in cancer. *Semin Cell Dev Biol* **43**: 43-51.

Kitayama J, Nagawa H, Tsuno N, Osada T, Hatano K, Sunami E, Saito H and Muto T (1999) Laminin mediates tethering and spreading of colon cancer cells in physiological shear flow. *Br J Cancer* **80**: 1927-1934.

Kurniawan NA, Chaudhuri PK and Lim CT (2016) Mechanobiology of cell migration in the context of dynamic two-way cell-matrix interactions. *J Biomech* **49**: 1355-1368.

Levesque E, Girard H, Journault K, Lepine J and Guillemette C (2007) Regulation of the UGT1A1 bilirubin-conjugating pathway: role of a new splicing event at the UGT1A locus. *Hepatology* **45**: 128-138.

Li L, Zhang Y, Qiao J, Yang JJ and Liu ZR (2014) Pyruvate kinase M2 in blood circulation facilitates tumor growth by promoting angiogenesis. *J Biol Chem* **289**: 25812-25821.

Li Z and Zhang H (2016) Reprogramming of glucose, fatty acid and amino acid metabolism for cancer progression. *Cell Mol Life Sci* **73**: 377-392.

Lu J, Tan M and Cai Q (2015) The Warburg effect in tumor progression: mitochondrial oxidative metabolism as an anti-metastasis mechanism. *Cancer Lett* **356**: 156-164.

Lunt SY, Muralidhar V, Hosios AM, Israelsen WJ, Gui DY, Newhouse L, Ogrodzinski M, Hecht V, Xu K, Acevedo PN, Hollern DP, Bellinger G, Dayton TL, Christen S, Elia I, Dinh AT, Stephanopoulos G, Manalis SR, Yaffe MB, Andrechek ER, Fendt SM and Vander Heiden MG (2015) Pyruvate kinase isoform expression alters nucleotide synthesis to impact cell proliferation. *Mol Cell* **57**: 95-107.

Maddocks OD, Berkers CR, Mason SM, Zheng L, Blyth K, Gottlieb E and Vousden KH (2013) Serine starvation induces stress and p53-dependent metabolic remodelling in cancer cells. *Nature* **493**: 542-546.

Margaillan G, Rouleau M, Fallon JK, Caron P, Villeneuve L, Turcotte V, Smith PC, Joy MS and Guillemette C (2015) Quantitative profiling of human renal UDP-glucuronosyltransferases and glucuronidation activity: a comparison of normal and tumoral kidney tissues. *Drug Metab Dispos* **43**: 611-619.

Mazurek S, Zwerschke W, Jansen-Durr P and Eigenbrodt E (2001) Metabolic cooperation between different oncogenes during cell transformation: interaction between activated ras and HPV-16 E7. *Oncogene* **20**: 6891-6898.

Mehrmohamadi M and Locasale JW (2015) Context dependent utilization of serine in cancer. *Mol Cell Oncol* **2**: e996418.

Mitsopoulos C, Schierz AC, Workman P and Al-Lazikani B (2015) Distinctive Behaviors of Druggable Proteins in Cellular Networks. *PLoS Comput Biol* **11**: e1004597.

Miyauchi Y, Nagata K, Yamazoe Y, Mackenzie PI, Yamada H and Ishii Y (2015) Suppression of Cytochrome P450 3A4 Function by UDP-Glucuronosyltransferase 2B7 through a Protein-Protein Interaction: Cooperative Roles of the Cytosolic Carboxyl-Terminal Domain and the Luminal Anchoring Region. *Mol Pharmacol* **88**: 800-812.

Oltean S and Bates DO (2014) Hallmarks of alternative splicing in cancer. *Oncogene* **33**: 5311-5318.

Pankova K, Rosel D, Novotny M and Brabek J (2010) The molecular mechanisms of transition between mesenchymal and amoeboid invasiveness in tumor cells. *Cell Mol Life Sci* **67**: 63-71.

Presek P, Glossmann H, Eigenbrodt E, Schoner W, Rubsamen H, Friis RR and Bauer H (1980) Similarities between a phosphoprotein (pp60src)-associated protein kinase of Rous sarcoma virus and a cyclic adenosine 3':5'-monophosphate-independent protein kinase that phosphorylates pyruvate kinase type M2. *Cancer Res* **40**: 1733-1741.

Rouleau M, Roberge J, Bellemare J and Guillemette C (2014) Dual roles for splice variants of the glucuronidation pathway as regulators of cellular metabolism. *Mol Pharmacol* **85**: 29-36.

Rouleau M, Tourancheau A, Girard-Bock C, Villeneuve L, Vaucher J, Duperre AM, Audet-Delage Y, Gilbert I, Popa I, Droit A and Guillemette C (2016) Divergent Expression and Metabolic Functions of Human Glucuronosyltransferases through Alternative Splicing. *Cell reports* **17**: 114-124.

Rowland A, Miners JO and Mackenzie PI (2013) The UDP-glucuronosyltransferases: their role in drug metabolism and detoxification. *Int J Biochem Cell Biol* **45**: 1121-1132.

Scott DE, Bayly AR, Abell C and Skidmore J (2016) Small molecules, big targets: drug discovery faces the protein-protein interaction challenge. *Nat Rev Drug Discov* **15**: 533-550.

Shannon P, Markiel A, Ozier O, Baliga NS, Wang JT, Ramage D, Amin N, Schwikowski B and Ideker T (2003) Cytoscape: a software environment for integrated models of biomolecular interaction networks. *Genome Res* **13**: 2498-2504.

Shimada N, Shinagawa T and Ishii S (2008) Modulation of M2-type pyruvate kinase activity by the cytoplasmic PML tumor suppressor protein. *Genes Cells* **13**: 245-254.

Simon-Assmann P, Orend G, Mammadova-Bach E, Spenle C and Lefebvre O (2011) Role of laminins in physiological and pathological angiogenesis. *Int J Dev Biol* **55**: 455-465.

Stingl JC, Bartels H, Viviani R, Lehmann ML and Brockmoller J (2014) Relevance of UDP-glucuronosyltransferase polymorphisms for drug dosing: A quantitative systematic review. *Pharmacol Ther* **141**: 92-116.

Taniguchi K, Ito Y, Sugito N, Kumazaki M, Shinohara H, Yamada N, Nakagawa Y, Sugiyama T, Futamura M, Otsuki Y, Yoshida K, Uchiyama K and Akao Y (2015) Organ-specific PTB1-associated microRNAs determine expression of pyruvate kinase isoforms. *Sci Rep* **5**: 8647.

Tozluoglu M, Tournier AL, Jenkins RP, Hooper S, Bates PA and Sahai E (2013) Matrix geometry determines optimal cancer cell migration strategy and modulates response to interventions. *Nat Cell Biol* **15**: 751-762.

Vander Heiden MG, Cantley LC and Thompson CB (2009) Understanding the Warburg effect: the metabolic requirements of cell proliferation. *Science* **324**: 1029-1033.

Vander Heiden MG, Lunt SY, Dayton TL, Fiske BP, Israelsen WJ, Mattaini KR, Vokes NI, Stephanopoulos G, Cantley LC, Metallo CM and Locasale JW (2011) Metabolic pathway alterations that support cell proliferation. *Cold Spring Harb Symp Quant Biol* **76**: 325-334.

Varghese B, Swaminathan G, Plotnikov A, Tzimas C, Yang N, Rui H and Fuchs SY (2010) Prolactin inhibits activity of pyruvate kinase M2 to stimulate cell proliferation. *Mol Endocrinol* **24**: 2356-2365.

Volak LP and Court MH (2010) Role for protein kinase C delta in the functional activity of human UGT1A6: implications for drug-drug interactions between PKC inhibitors and UGT1A6. *Xenobiotica* **40**: 306-318.

Wang HJ, Hsieh YJ, Cheng WC, Lin CP, Lin YS, Yang SF, Chen CC, Izumiya Y, Yu JS, Kung HJ and Wang WC (2014) JMJD5 regulates PKM2 nuclear translocation and reprograms HIF-1alpha-mediated glucose metabolism. *Proc Natl Acad Sci U S A* **111**: 279-284.

Warburg O, Wind F and Negelein E (1927) The Metabolism of Tumors in the Body. *J Gen Physiol* **8**: 519-530.

Wu C, Khan SA, Peng LJ and Lange AJ (2006) Roles for fructose-2,6-bisphosphate in the control of fuel metabolism: beyond its allosteric effects on glycolytic and gluconeogenic enzymes. *Advances in enzyme regulation* **46**: 72-88.

Yang P, Li Z, Fu R, Wu H and Li Z (2014) Pyruvate kinase M2 facilitates colon cancer cell migration via the modulation of STAT3 signalling. *Cell Signal* **26**: 1853-1862.

Yang P, Li Z, Wang Y, Zhang L, Wu H and Li Z (2015) Secreted pyruvate kinase M2 facilitates cell migration via PI3K/Akt and Wnt/beta-catenin pathway in colon cancer cells. *Biochem Biophys Res Commun* **459**: 327-332.

Yang W, Zheng Y, Xia Y, Ji H, Chen X, Guo F, Lyssiotis CA, Aldape K, Cantley LC and Lu Z (2012) ERK1/2-dependent phosphorylation and nuclear translocation of PKM2 promotes the Warburg effect. *Nat Cell Biol* **14**: 1295-1304.

Yang X, Coulombe-Huntington J, Kang S, Sheynkman GM, Hao T, Richardson A, Sun S, Yang F, Shen YA, Murray RR, Spirohn K, Begg BE, Duran-Frigola M, MacWilliams A, Pevzner SJ, Zhong Q, Trigg SA, Tam S, Ghamsari L, Sahni N, Yi S, Rodriguez MD, Balcha D, Tan G, Costanzo M, Andrews B, Boone C, Zhou XJ, Salehi-Ashtiani K, Charloteaux B, Chen AA, Calderwood MA, Aloy P, Roth FP, Hill DE, Iakoucheva LM, Xia Y and Vidal M (2016) Widespread Expansion of Protein Interaction Capabilities by Alternative Splicing. *Cell* **164**: 805-817.

Yoon S, Kim JG, Seo AN, Park SY, Kim HJ, Park JS, Choi GS, Jeong JY, Jun do Y, Yoon GS and Kang BW (2015) Clinical Implication of Serine Metabolism-Associated Enzymes in Colon Cancer. *Oncology* **89**: 351-359.

Zhan C, Yan L, Wang L, Ma J, Jiang W, Zhang Y, Shi Y and Wang Q (2015) Isoform switch of pyruvate kinase M1 indeed occurs but not to pyruvate kinase M2 in human tumorigenesis. *PLoS One* **10**: e0118663.

Zhou CF, Li XB, Sun H, Zhang B, Han YS, Jiang Y, Zhuang QL, Fang J and Wu GH (2012) Pyruvate kinase type M2 is upregulated in colorectal cancer and promotes proliferation and migration of colon cancer cells. *IUBMB Life* **64**: 775-782.

Figures legends

Figure 1. Interaction between UGT1A_i2s and energy metabolism-related proteins. A) Experimental scheme of the affinity purification/mass spectrometry identification of UGT1A_i2 endogenous protein partners. Peptide coordinates are those of UGT1A1. **B)** Pathway enrichment analysis, according to KEGG, of proteins immunprecipitated with UGT1A_i2s. Main metabolic pathways are 'Citrate Cycle (TCA cycle)' and 'Tryptophan Metabolism'. Enriched pathways related to TCA cycle (kappa>0.4) through protein sharing are indicated by blue circles. Circle sizes are proportional to the number of proteins identified within each pathway. A selection of significantly enriched pathways (*q*-value<0.05) and their proteins is shown. **C)** PKM2 endogenously interacts with UGT1A_i2 alternate proteins in HT115 cells, but not with UGT1A_i1 enzymes. Immunoprecipitation (IP) was carried out from a whole HT115 cell lysate (HT115) and revealed by western blotting (WB) using antibodies specific to indicated proteins. **D)** UGT1A_i2 alternate proteins co-localize with PKM2 in HT115 cells. Fluorescence intensity profiles are given for the cross-section (dashed line in the merge panel). The scale bar represents 5 µm.

Figure 2. Remodelling of the energy metabolism in UGT1A_i2s depleted HT115 (KD) cells compared to control (CTR) cells. A) HT115 colon cancer cell models. UGT1A_i2s expression is stably depleted (KD) by a shRNA specific to exon 5b. Control cells (CTR) carry a non-targeting shRNA. Upper panel: Depletion of i2s does not affect i1 enzymes expression. Lower panel: i2s are depleted by 90% in KD cells. Multiple protein bands reflect expression of several of the nine UGT1A_i2 proteins in HT115 cells. First two lanes: lysates from HEK293 cells (UGT negative) overexpressing i1 and i2 demonstrate specificity of anti-UGT1A_i1s (#9348) and anti-UGT1A_i2s (#4C5E7). **B)** Lactate formation in growth medium of HT115 cells over time, corrected for baseline and normalized by cell count. Data (mean ± SD) are derived from at least two independent experiments performed in duplicate. **C)** Glycolytic profile of KD cells. Extracellular acidification rates (ECAR) were measured by extracellular flux using the glycolysis stress kit. Representative profiles from three independent experiments performed in triplicate are shown. Injection of compounds during the assay is highlighted. **D)** Relative glycolytic and maximal glycolytic capacity, extracted from time points with the highest response, during the glycolysis stress assay, to glucose and oligomycin, respectively. Data (mean ± SD) are derived from three independent experiments performed in triplicate and were normalized for protein concentration. **E)** Mitochondrial respiration profile of KD cells. Oxygen consumption rates (OCR) were

measured by extracellular flux using the mitochondria stress kit. Representative profiles from three independent experiments performed in triplicate. Injection of compounds during the assay is highlighted. **F)** Relative basal and maximal mitochondrial respiration, extracted from the last basal time point and the time point with the highest response to FCCP during the mitochondria stress assay, respectively. Data (mean ± SD) are derived from three independent experiments performed in triplicate and were normalized for protein concentration. * $P<0.05$; ** $P<0.01$; *** $P<0.001$.

Figure 3. Untargeted metabolomics analysis of UGT1A_i2s-depleted HT115 cells (KD) and control (CTR) cells. A) Cellular levels of known metabolites (n=144) are shown. Dotted lines represent a 20% fold change (FC). **B)** Known metabolites (n=24) significantly altered in HT115 KD cells compared to control cells.

Figure 4. Depletion of UGT1A_i2s perturbs glycolysis, TCA cycle and amino acids. Relative levels (arbitrary units) of selected metabolites in HT115 CTR and KD cells are given in the context of bioenergetic pathways. Glucose-6-Phosphate (G-6-P), Fructose-6-P (F-6-P), Fructose1-6-Bisphosphate (F-1-6-BP), Glyceraldehyde-3-Phosphate (GA-3-P), Glyceraldehyde (GA), Fructose-1-Phosphate (F-1-P), Dihydroxyacetone phosphate (DHAP), Glycerate-3-Phosphate (G-3-P), Phosphoenolpyruvate (PEP), 2-oxoglutarate (2-OG). The pink background highlights the TCA cycle and the blue background highlights amino acids. CTR: control cells; KD: UGT1A_i2s-depleted cells. Data normalized for cell count. * $P<0.05$; ** $P<0.01$.

Figure 5. Proliferation, migration and adhesion of HT115 cells. A) Live-cell proliferation assay of HT115 cell models with or without deprivation of serine (S) and glycine (G), as detected by an impedance-based system. Graph of a representative experiment is shown. **B)** Doubling time ratio between growth with S/G (dark bars) and without S/G (light bars) for each cell line. Data represent values of 2 independent experiments. Proliferation data in basal conditions and with glucose or glutamine deprivation are shown in Supplemental Fig. 2. **C)** HT115 UGT1A_i2s-depleted cells (KD) have an increased migration potential. Representative images of cells in a wound healing assay at wound induction (t_0) and 24 hrs post-wounding (t_{24}). Image enlargement: 10X. **D)** Wound area (arbitrary units) of images shown in C were measured using ImageJ. **E)** Relative wound closure was calculated from three wound healing assays performed in triplicate and analyzed independently by two investigators. **F)** Decreased adhesion of HT115 KD cells relative to CTR. An extracellular

matrix assay detected a lower adhesion profile for Collagen I (Col I), Laminin (Lam) and Tenascin (Ten) in KD cells. Other matrices: Collagen II (Col II); Collagen IV (Col IV); Fibronectin (Fibro); Vitronectin (Vitro); and Bovine Serum Albumin (BSA, as negative control). Mean ± SEM. n=3 independent experiments performed in triplicate. * $P<0.05$; ** $P<0.01$; *** $P<0.001$.

Figure 6. **Expression of alternative mRNA variants *v2/v3*, encoding UGT1A_i2 proteins, is drastically reduced in human colon tumoral tissues. A)** Relative quantity (RQ) of alternative mRNA variants (*v2/v3)* expression in colon tumors compared to paired peritumoral normal tissues detected by quantitative PCR in 6 clinical samples. **B)** Quantification of mRNAs encoding UGT1A_i2 proteins by RNA sequencing (GSE80463) in normal and tumoral colon tissues. FPKM: Fragments Per Kilobase of transcript per Million mapped reads.

Figure 1

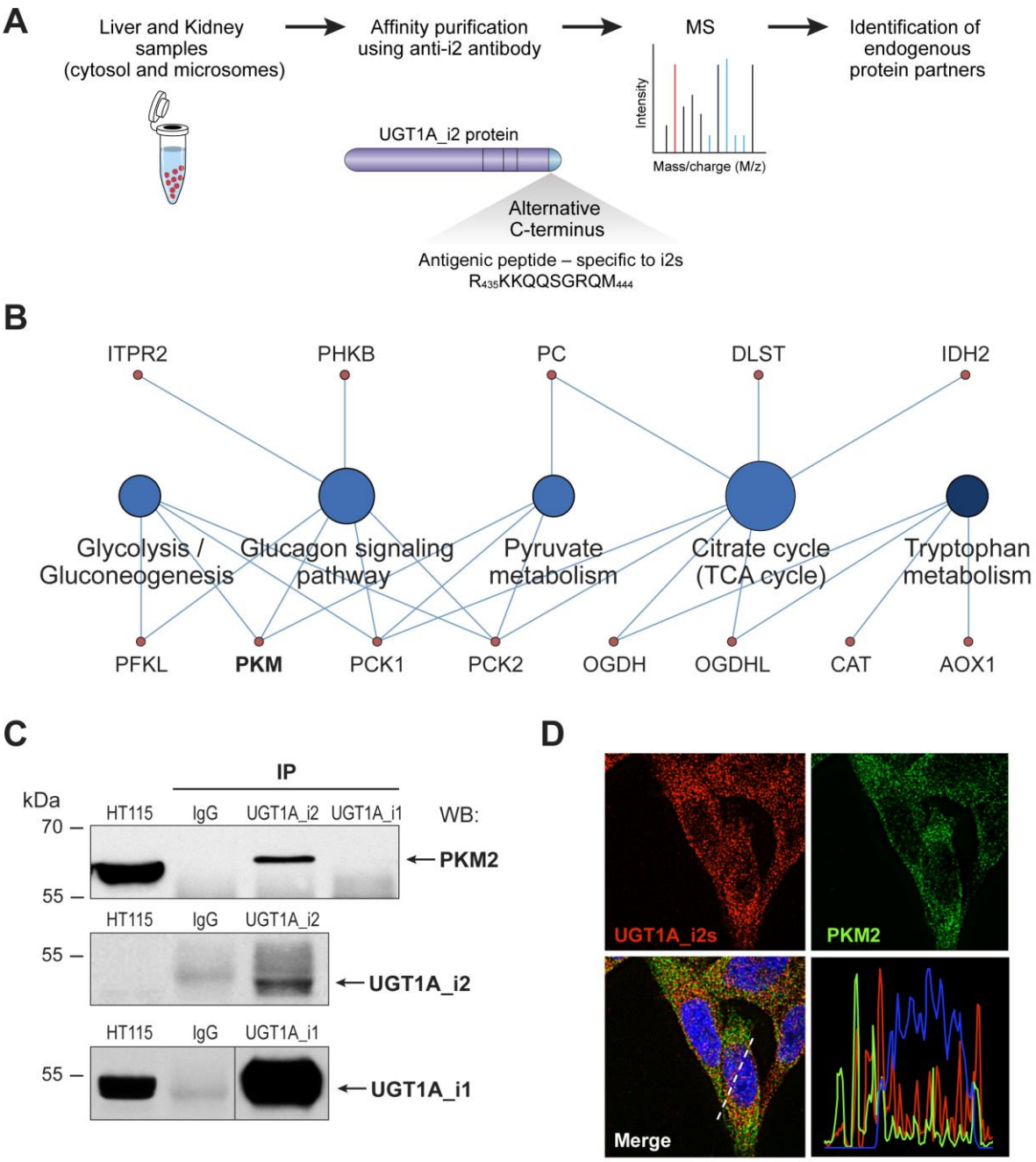
A
Liver and Kidney samples (cytosol and microsomes)
Affinity purification using anti-i2 antibody
MS
Identification of endogenous protein partners
Intensity
Mass/charge (M/z)
UGT1A_i2 protein
Alternative C-terminus
Antigenic peptide – specific to i2s
R435KKQQSGRQM444
B
ITPR2
PHKB
PC
DLST
IDH2
Glycolysis / Gluconeogenesis
Glucagon signaling pathway
Pyruvate metabolism
Citrate cycle (TCA cycle)
Tryptophan metabolism
PFKL
PKM
PCK1
PCK2
OGDH
OGDHL
CAT
AOX1
C
IP
kDa
HT115
IgG
UGT1A_i2
UGT1A_i1
WB:
70
55
PKM2
UGT1A_i2
UGT1A_i1
D
UGT1A_i2s
PKM2
Merge

Figure 2

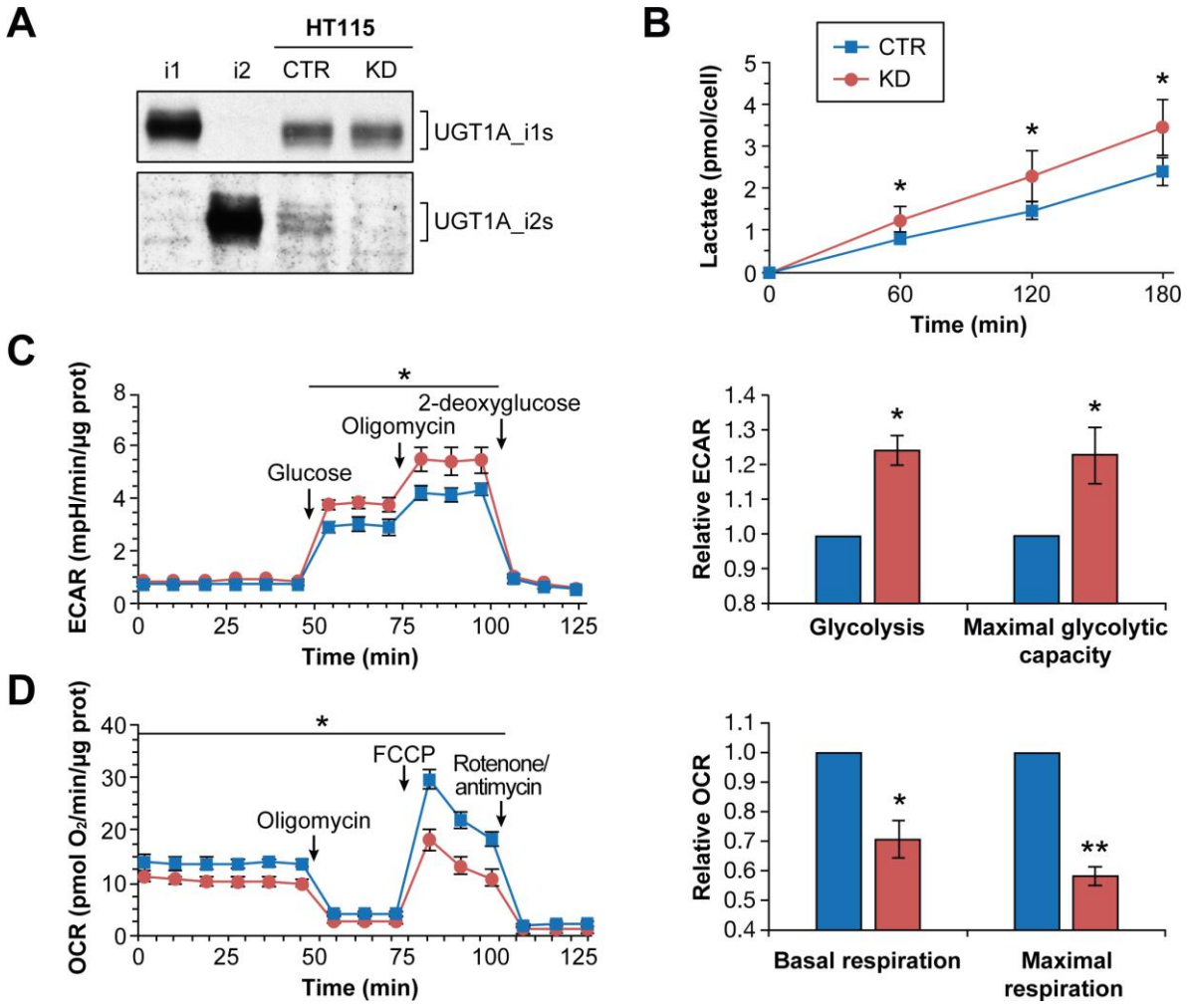
A
HT115
i1
i2
CTR
KD
UGT1A_i1s
UGT1A_i2s
B
CTR
KD
Lactate (pmol/cell)
Time (min)
C
ECAR (mpH/min/µg prot)
Glucose
Oligomycin
2-deoxyglucose
Time (min)
Relative ECAR
Glycolysis
Maximal glycolytic capacity
D
OCR (pmol O2/min/µg prot)
Oligomycin
FCCP
Rotenone/ antimycin
Time (min)
Relative OCR
Basal respiration
Maximal respiration

Figure 3

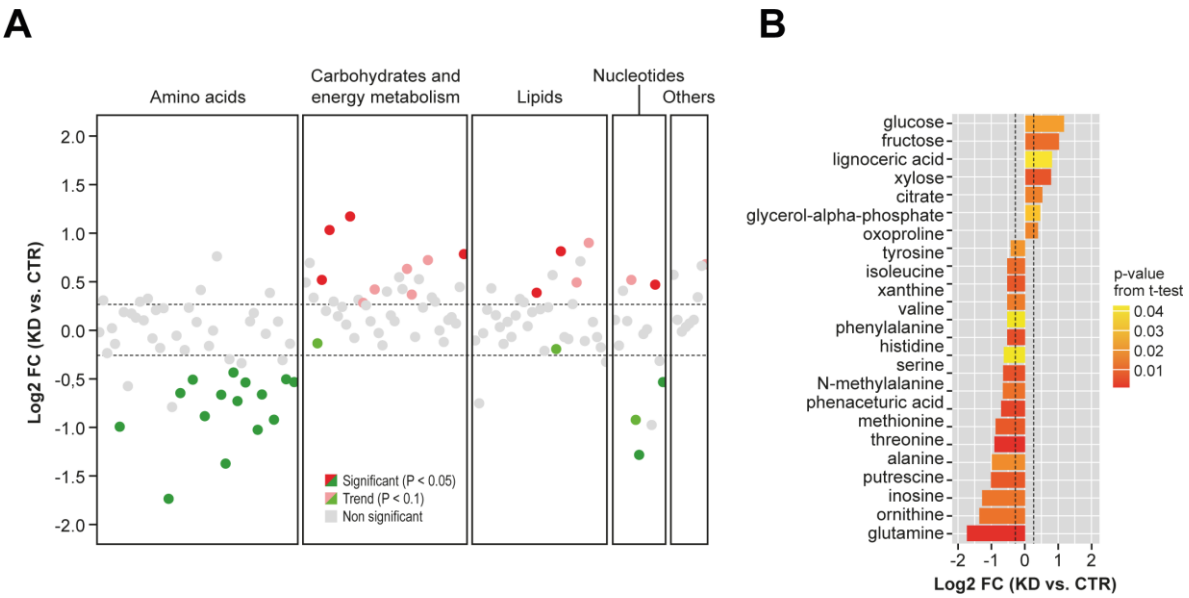
A
Amino acids
Carbohydrates and energy metabolism
Lipids
Nucleotides
Others
Log2 FC (KD vs. CTR)
2.0
1.5
1.0
0.5
0.0
-0.5
-1.0
-1.5
-2.0
Significant (P < 0.05)
Trend (P < 0.1)
Non significant
B
glucose
fructose
lignoceric acid
xylose
citrate
glycerol-alpha-phosphate
oxoproline
tyrosine
isoleucine
xanthine
valine
phenylalanine
histidine
serine
N-methylalanine
phenaceturic acid
methionine
threonine
alanine
putrescine
inosine
ornithine
glutamine
-2
-1
0
1
2
Log2 FC (KD vs. CTR)
p-value from t-test
0.04
0.03
0.02
0.01

Figure 4

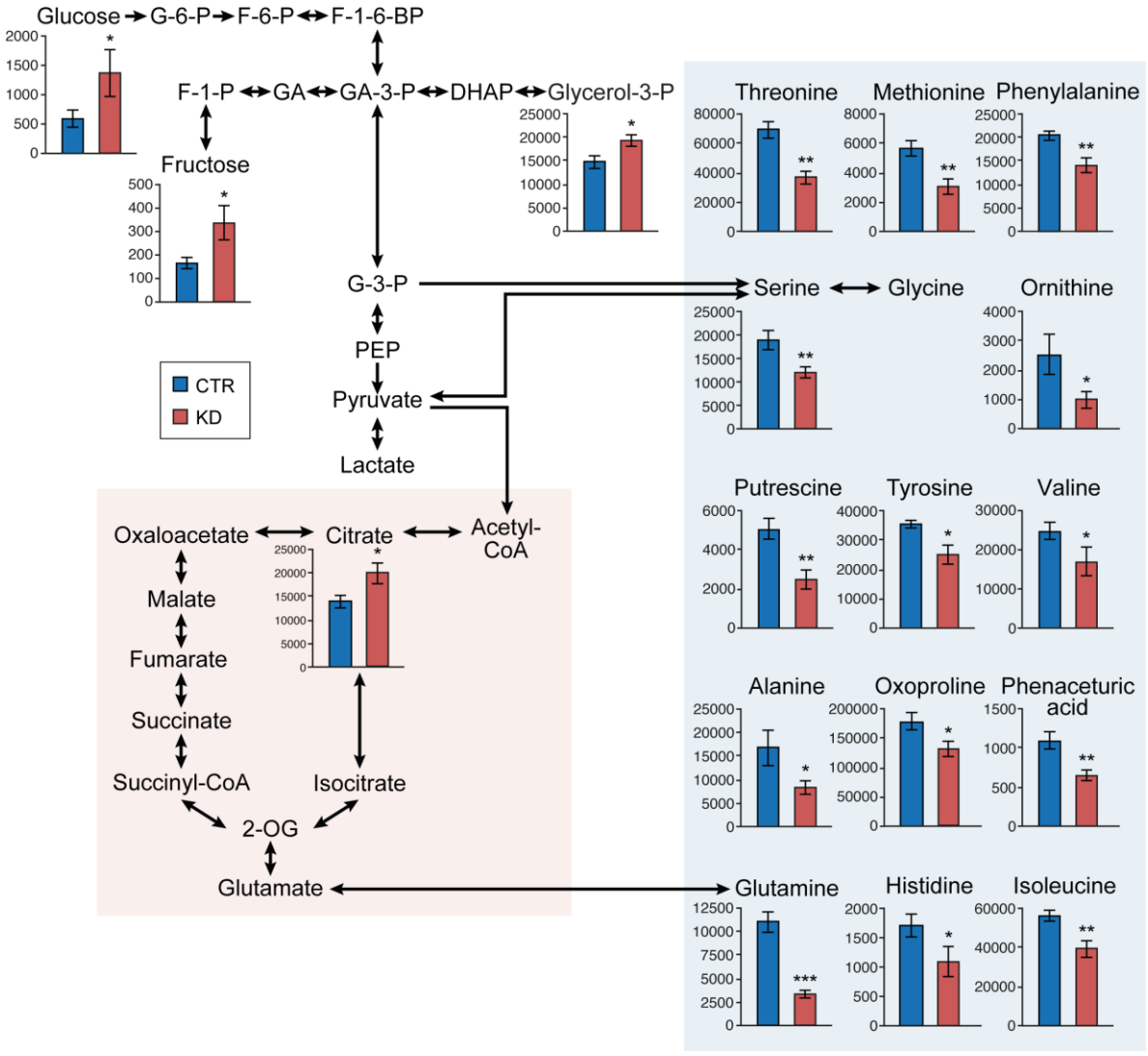
Glucose
G-6-P
F-6-P
F-1-6-BP
F-1-P
GA
GA-3-P
DHAP
Glycerol-3-P
Fructose
G-3-P
PEP
Pyruvate
Lactate
CTR
KD
Oxaloacetate
Citrate
Acetyl-CoA
Malate
Fumarate
Succinate
Succinyl-CoA
Isocitrate
2-OG
Glutamate
Threonine
Methionine
Phenylalanine
Serine
Glycine
Ornithine
Putrescine
Tyrosine
Valine
Alanine
Oxoproline
Phenaceturic acid
Glutamine
Histidine
Isoleucine

Figure 5

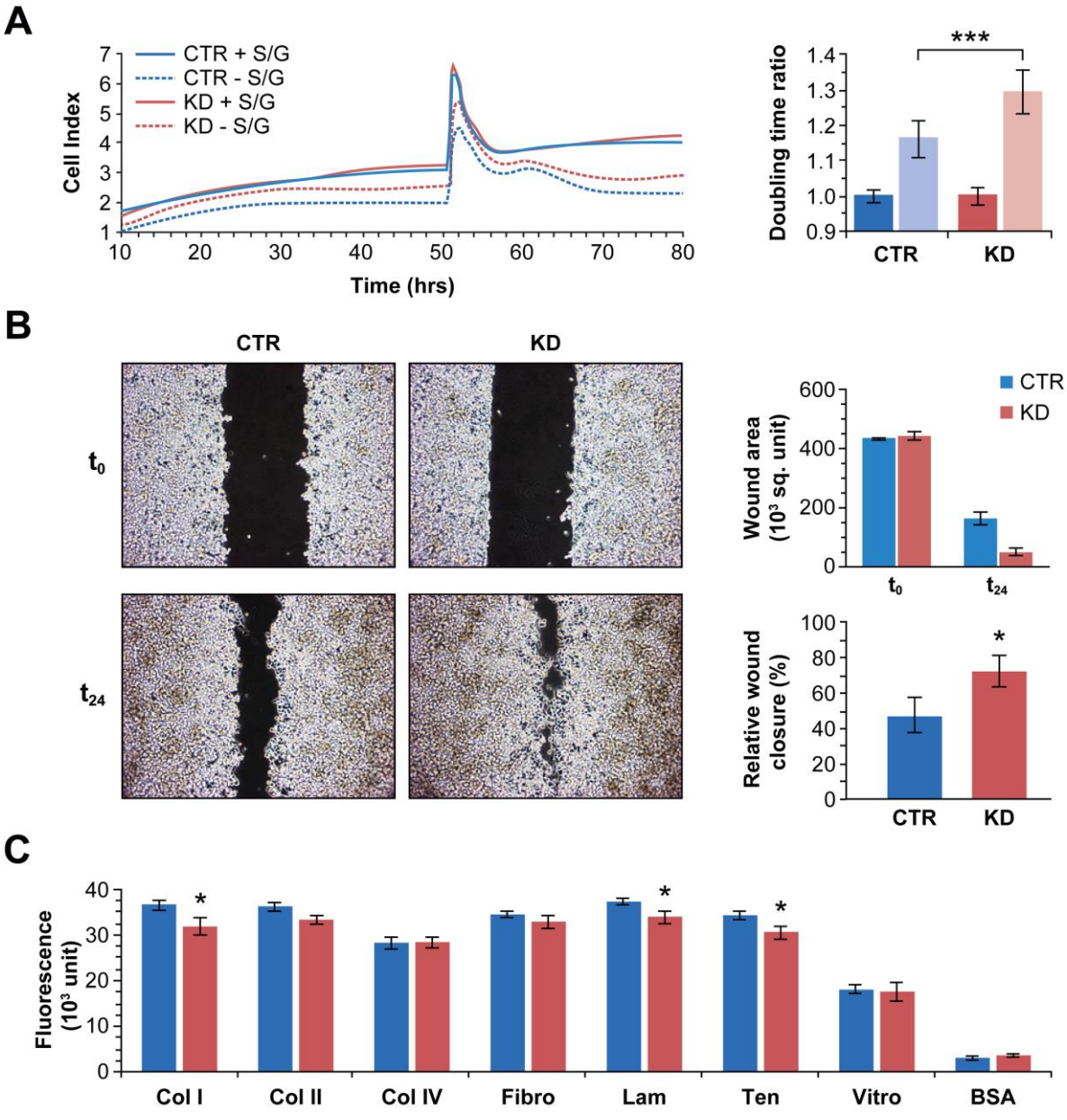
A
CTR + S/G
CTR - S/G
KD + S/G
KD - S/G
Cell Index
Time (hrs)
Doubling time ratio
***
CTR
KD
B
CTR
KD
t0
t24
Wound area (10³ sq. unit)
Relative wound closure (%)
*
C
Fluorescence (10³ unit)
Col I
Col II
Col IV
Fibro
Lam
Ten
Vitro
BSA

Figure 6

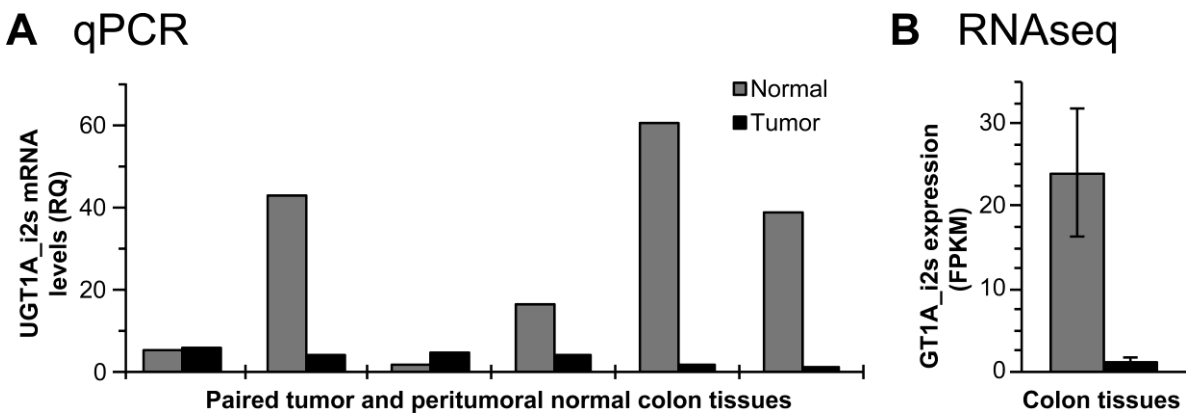
A qPCR
B RNAseq
Normal
Tumor
UGT1A_i2s mRNA levels (RQ)
0
20
40
60
Paired tumor and peritumoral normal colon tissues
GT1A_i2s expression (FPKM)
0
10
20
30
Colon tissues

Supplemental Data

Supplemental Figure 1

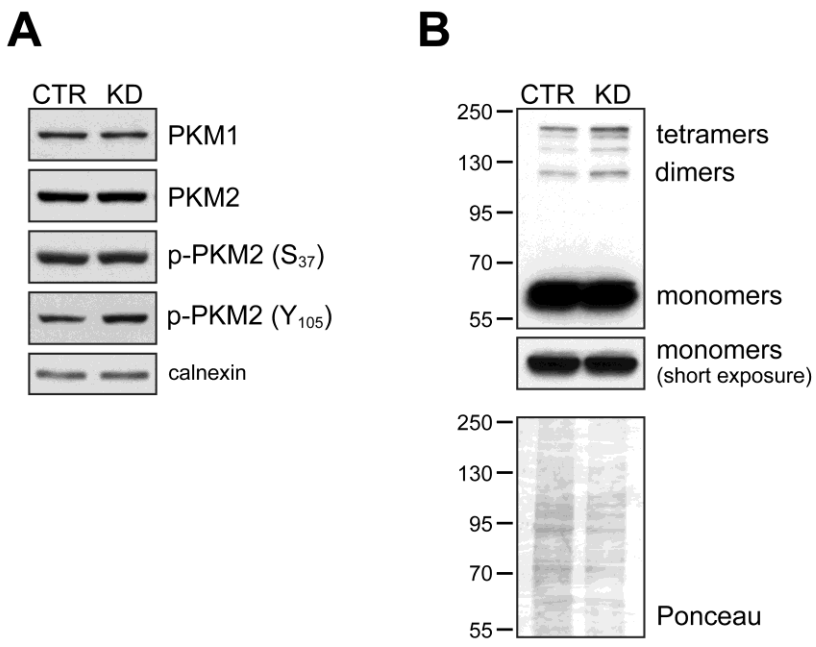

Supplemental Figure 1. Influence of UGT1A_i2 on the expression, phosphorylation and oligomerization of pyruvate kinase. **(A)** In HT115 cell models, the expression of PKM1 and PKM2 and the phosphorylation of PKM2 on S37 are not affected by the repression UGT1A_i2s (KD) compared to control HT115 cells (CTR) whereas phosphorylation on Y105 is slightly enhanced (1.37 fold; *P*=0.26). Data are representative of at least three experiments. Whole cell lysates were probed with specified antibodies by immunoblotting. Calnexin was used as a loading control. (B) Oligomerization status of PKM2 in HT115 cell models assessed by immunoblotting after glutaraldehyde cross-linking of cell extracts. Data are representative of at least four experiments. Ponceau S staining of the membrane was used as a loading control. Tetramer/dimer ratios were 2.02 for KD and 2.00 for CTR cells.

Supplemental Figure 2

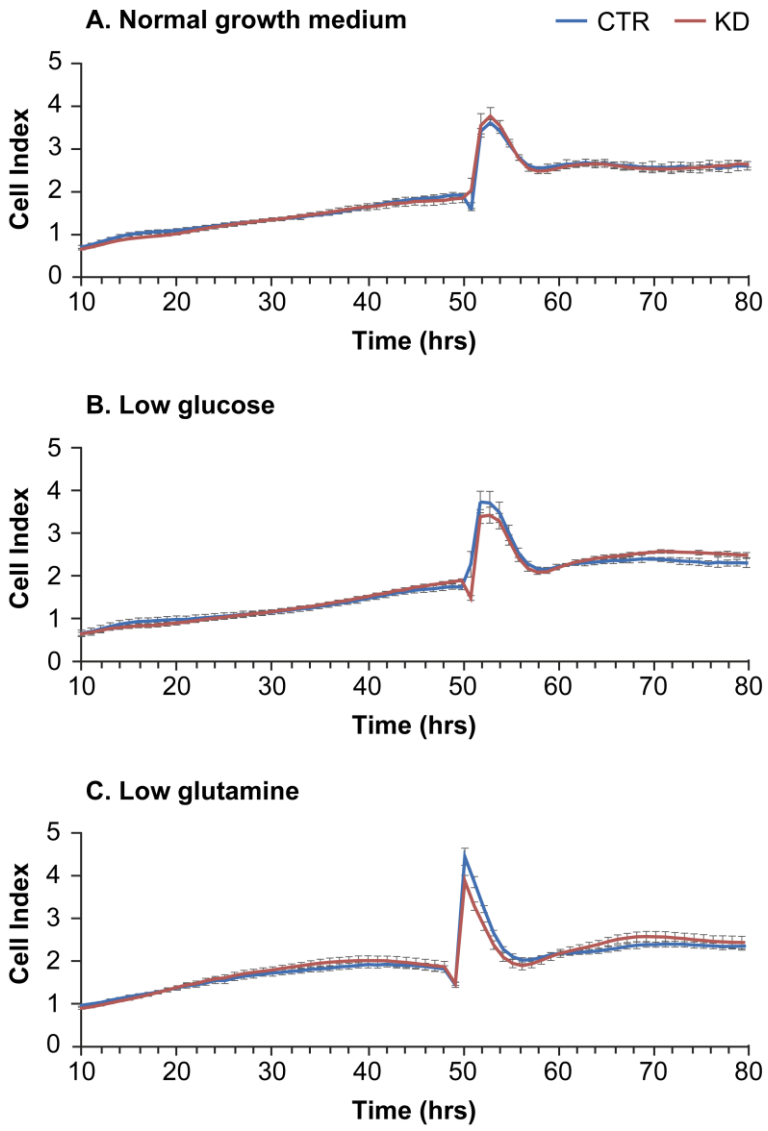

Supplemental Figure 2. The proliferation of HT115 cell models is not affected by a knockdown of UGT1A_i2s expression. Live cell proliferation of HT115 in **A.** normal growth conditions (25 mM glucose, 4 mM glutamine) **B.** low glucose medium (5.6 mM) and **C**. low glutamine medium (0.75 mM). Data presented are representative of 3 experiments done in triplicate.

Supplemental Table 1. Protein partners of UGT1A_i2s identified in the liver.

Identified Proteins	Accession #	Unique Peptide	Total spectral count	Coverage (%)
UGT1A†	O60656	4	7	11.9
ACY1	Q03154	3	5	12.0
AOX1	Q06278	2	3	1.6
BOK	Q9UMX3	2	3	11.3
CAT	P04040	9	17	24.1
CLU	P10909	2	2	15.5
CPSF7	Q8N684	2	2	6.6
DBT	P11182	4	5	10.6
DLST	P36957	15	52	40.8
EEF1D	P29692	4	6	19.5
FN3K	Q9H479	2	3	10.0
GNB2L1	P63244	4	8	20.5
HDLBP	Q00341	5	6	5.2
HP1BP3	Q5SSJ5	3	3	12.3
HRG	P04196	3	4	8.6
ITPR2	Q14571	7	12	2.8
OGDH	Q02218	21	43	27.4
OGDHL	Q9ULD0	8	24	16.8
PCK1	P35558	2	7	5.8
PFN1	P07737	2	2	20.0
PHKB	Q93100	2	2	2.7
PKM	P14618	4	4	13.0
PRDX6	P30041	2	4	17.0
PRPF8	Q6P2Q9	2	2	2.1
REPS1	Q96D71	2	2	4.3
SEC23A	Q15436	2	3	4.6
SEC62	Q99442	2	3	25.7
SNX9	Q9Y5X1	3	4	4.7
SORBS2	O94875	2	6	1.9
SULT1B1	O43704	2	2	11.6
TTN	Q8WZ42	3	3	9.0
UGT2B4	P06133	3	10	10.0

†No peptide allowed specification of the isoform. Proteins related to energy metabolism are indicated in bold. Complete data are available in the PRIDE database, accession PXD000295.

Supplemental Table 2. Protein partners of UGT1A_i2s identified in the kidney.

Identified proteins	Accession #	Unique Peptide	Total spectral count	Coverage (%)
UGT1A†		4	4	11.8
ABHD14B	Q96IU4	2	2	17.1
ACSL1	P33121	2	2	2.9
ATP5A1	P25705-2	11	11	28.0
Beta actin variant	Q53G76	16	26	56.8
CAT	P04040	2	2	5.3
CHMP4B	Q9H444	3	4	15.6
CKAP4	Q07065	18	19	40.7
CLU	P10909	4	4	10.0
COL6A3	P12111	9	11	5.0
CTSB	P07858	2	2	10.6
Isoform CRA_a	D3DPI2	3	3	12.6
DBT	P11182	3	3	8.7
DDX5	P17844	3	3	8.0
DPYSL2	Q16555	2	2	5.2
EML3	Q32P44	5	5	7.7
FGA	P02671	20	35	27.5
FGB	P02675	6	6	18.5
FLNA	P21333	6	6	2.8
FLOT1	O75955	2	2	4.0
Formyltetrahydrofolate dehydrogenase isoform a variant	Q53HP5	5	5	7.7
GSTA2	P09210	2	2	9.0
HIST1H2AA	Q96QV6	7	10	40.5
HIST1H4A	P62805	2	3	29.1
HP	Q6NSB4	3	3	10.0
HSP90AB1	P08238	4	4	7.5
HSPA1A	P08107	7	7	13.4
HSPA5	P11021	2	3	5.4
HSPA8	P11142	5	7	14.6
HSPA9	P38646	2	2	3.0
HSPD1	P10809	5	6	9.1
IDH2	P48735	5	5	15.3
ITPR2	Q14571	8	8	4.2
KIF5B	P33176	15	15	20.6
KLC1	Q07866	4	4	8.1
KLC4	Q9NSK0	2	2	4.8
LMNA	P02545	4	4	7.1
MCCC2	Q9HCC0	3	3	8.2
MGST2	Q99735	3	5	19.0
MYH11	P35749	2	2	2.7
MYH9	P35579	9	9	7.2
MYL6	P60660	3	3	16.0
MYO6	Q9UM54	2	2	3.7
PC	P11498	6	7	7.1
PCBP1	Q15365	4	4	18.3
PCK1	P35558	4	4	7.7

PCK2	Q16822	3	4	7.3
PFKL	P17858-2	11	11	18.3
PRDX2	P32119	2	2	14.6
RPL14	Q6IPH7	4	6	22.7
SEC16A	O15027	3	3	1.8
SRSF10	O75494-5	2	2	9.7
SRSF3	P84103	2	2	21.0
TLN1	Q5TCU6	2	2	1.2
TRA2B	P62995	4	4	15.6
UMOD	P07911	4	4	7.4
VIM	P08670	3	4	9.0
XPO5	Q9HAV4	2	2	4.7
XRCC5	P13010	2	2	6.2
XRCC6	P12956	6	6	10.8

[†]No peptide allowed specification of the isoform. Proteins related to energy metabolism are indicated in bold. Complete data are available in the PRIDE database, accession PXD000295.

Chapitre 5 : « Posttranscriptional regulation of UGT2B10 hepatic expression and activity by alternative splicing »

Résumé

L'enzyme de détoxication UGT2B10 est spécialisée dans la N-glucuronidation de plusieurs drogues et xénobiotiques. Ses substrats incluent des amines tertiaires aliphatiques et des amines hétérocycliques, tels que les carcinogènes du tabac et plusieurs antidépresseurs et antipsychotiques. Nous avons émis l'hypothèse que l'épissage alternatif constitue un moyen de réguler l'expression et l'activité de l'UGT2B10. Nous avons établi le transcriptome de cette enzyme dans des tissus normaux et tumoraux provenant de plusieurs individus. L'analyse de 50 foies normaux et 44 hépatocarcinomes montre une forte expression en UGT avec une dizaine de transcrits représentant la moitié de tous les transcrits UGT2B10. Une classe abondante de transcrits alternatifs incorpore une nouvelle séquence exonique et mène à deux protéines alternatives possédant une nouvelle séquence de 10 et 65 acides aminés en C-terminal. Leur expression hépatique varie grandement entre les individus, est 3.5 fois plus élevée dans le tissu tumoral et corrèle avec l'expression de l'enzyme canonique. Des preuves de leur traduction dans le foie ont été obtenues par spectrométrie de masse. Dans des modèles cellulaires, ces protéines co-localisent avec l'enzyme et influencent la conjugaison de l'amitriptyline et de la lévomédétomidine en réprimant ou en activant (40-70%; $P < 0.01$) l'activité transférase et ce, différemment selon l'UGT présente. De plus, nous avons démontré un remodelage de l'épissage alternatif de l'UGT2B10 induit par des composés pharmacologiques dans le modèle de foie HepaRG, où l'expression de variants alternatifs est favorisée au détriment de l'expression de la forme canonique. Nos découvertes supportent une contribution significative de l'épissage alternatif dans la régulation de l'UGT2B10 dans le foie, pouvant impacter l'activité enzymatique.

Posttranscriptional regulation of UGT2B10 hepatic expression and activity by alternative splicing

Adrien Labriet, Eric P. Allain, Michèle Rouleau, Yannick Audet-Delage, Lyne Villeneuve and Chantal Guillemette

Pharmacogenomics Laboratory, Centre Hospitalier Universitaire (CHU) de Québec Research Center – Université Laval, Québec, QC, Canada and Faculty of Pharmacy, Université Laval, Québec, Canada

Canada Research Chair in Pharmacogenomics (CG)

Short title: Regulation of UGT2B10 by alternative splicing

Corresponding Author:

Chantal Guillemette, Ph.D.

Pharmacogenomics Laboratory

CHU de Québec Research Center – Univesité Laval

2705 Boul. Laurier, R4701.5

Québec, Canada, G1V 4G2

Tel. (418) 654-2296

E-mail: Chantal.Guillemette@crchudequebec.ulaval.ca

Abstract: 248 words

Introduction: 722

Material and Methods: 1811

Results: 1566

Discussion: 1686

Body text: 5785

References: 60

Number of:

Tables: 0

Figures: 7

Supplemental Tables: 1

Supplemental Figures: 6

Non-standard abbreviations:

AS: Alternative splicing, ER: Endoplasmic reticulum, MS-MRM: Mass spectrometry – multiple reaction monitoring, RT-PCR: Reverse transcription – PCR, RNA-seq: RNA sequencing, TPM: transcripts per million, UDP-GlcA: UDP-glucuronic acid, UGT: UDP-glucuronosyltransferases

Abstract

The detoxification enzyme UDP-glucuronosyltransferase UGT2B10 is specialized in the N-linked glucuronidation of many drugs and xenobiotics. Preferred substrates possess tertiary aliphatic amines and heterocyclic amines such as tobacco carcinogens and several anti-depressants and anti-psychotics. We hypothesized that alternative splicing (AS) constitutes a mean to regulate steady state levels of UGT2B10 and enzyme activity. We established the transcriptome of *UGT2B10* in normal and tumoral tissues of multiple individuals. Highest expression was in the liver, where ten AS transcripts represented 50% of the *UGT2B10* transcriptome in 50 normal livers and 44 hepatocellular carcinomas. One abundant class of transcripts involves a novel exonic sequence and leads to two alternative (alt.) variants with novel in-frame C-termini of 10 or 65 amino acids. Their hepatic expression was highly variable among individuals, correlated with canonical transcript levels, and was 3.5-fold higher in tumors. Evidence for their translation in liver tissues was acquired by mass spectrometry. In cell models, they co-localized with the enzyme and influenced the conjugation of amitriptyline and levomedetomidine by repressing or activating the enzyme (40-70%; $P<0.01$), in a cell context-specific manner. A high turnover rate for the alt. proteins, regulated by the proteasome, was observed in contrast to the more stable UGT2B10 enzyme. Moreover, a drug-induced remodelling of *UGT2B10* splicing was demonstrated in the HepaRG hepatic cell model, which favored alt. variants expression over the canonical transcript. Our findings support a significant contribution of AS in the regulation of UGT2B10 expression in the liver with an impact on enzyme activity.

Introduction

N-linked glucuronidation is an important inactivation route for amine-containing drugs and xenobiotics (Kaivosaari et al., 2011; Kato et al., 2013). Two of the 19 UDP-glucuronosyltransferases (UGTs), UGT2B10 and UGT1A4, are the main drivers of N-linked glucuronidation (Chen et al., 2008a; Kerdpin et al., 2009; Kato et al., 2013). Long described as an orphan UGT, the discovery that UGT2B10 is crucial for the detoxification of tobacco carcinogens has raised much attention and rationalized the importance to characterize this unique UGT (Chen et al., 2007; Kaivosaari et al., 2007; Chen et al., 2008b; Berg et al., 2010; Murphy et al., 2014). UGT2B10 is one of the main liver UGT enzymes, based on mRNA (quantitative PCR and deep RNA-sequencing data) and protein levels (quantitative mass spectrometry–based proteomics data) (Court et al., 2012; Fallon et al., 2013; Margaillan et al., 2015; Tourancheau et al., 2017). Expression has also been reported in the breast, testis, gallbladder, tongue and tonsils although at much lower levels than hepatic expression (Haakensen et al., 2010; Jones and Lazarus, 2014).

UGT2B10 displays a preference for tertiary aliphatic amines and heterocyclic amines. These structures are found in several clinically used drugs such as antihistamines, anti-psychotics and anti-depressants including several of the tricyclic class such as imipramine and amitriptyline (Kaivosaari et al., 2008; Kaivosaari et al., 2011; Kato et al., 2013; Kazmi et al., 2015; Pattanawongsa et al., 2016) whereas endogenous substrates have yet to be identified. Although UGT1A4 substrate preference significantly overlaps with that of UGT2B10, the latter presents a greater affinity and clearance for many tertiary cyclic amines at therapeutic concentration (Kato et al., 2013). One structural determinant of the specificity towards amine substrates may be the residues Pro40 of UGT1A4 and Leu34 of UGT2B10 located in their substrate binding domain, a position that is otherwise a strictly conserved histidine residue (His40, coordinates of UGT1A1) in all human UGTs (Kerdpin et al., 2009).

Genetic studies in smokers have established a direct link between single nucleotide polymorphisms (SNPs) at the *UGT2B10* gene locus (4q13.2), UGT2B10 activity and metabolism of nicotine and cotinine (Chen et al., 2007; Chen et al., 2012; Murphy et al., 2014; Patel et al., 2015; Ware et al., 2016; Murphy, 2017). Two relatively frequent polymorphisms are associated with significant decreased nicotine and cotinine glucuronidation in humans. One variant creates the missense Asp67Tyr coding variant (rs61750900) that abolishes UGT2B10 glucuronidation activity (Chen et al., 2007), while the

other variant (rs116294140/rs2942857) alters the splice acceptor site between intron 2 and exon 3, and is thought to create an unstable mRNA (Murphy et al., 2014; Fowler et al., 2015). Consistently, individuals homozygous for either of these SNPs have very low to undetected nicotine and cotinine glucuronides in urine, further indicating that UGT2B10 is the main UGT responsible for glucuronidation of nicotine and cotinine (Chen et al., 2007; Murphy et al., 2014). It also supports the main role of this detoxification pathway in tobacco carcinogenesis. These genetic variations display an important ethnic bias. Whereas the Asp67Tyr variation is most frequent in Caucasians (nearly 10%) (Chen et al., 2007; Murphy et al., 2014), the splice variant rs2942857 prevails in approximately 35% of African Americans and in up to 50% of subjects of African origins (NCBI; Murphy et al., 2014). Of interest, the splice variant was also reported to affect the metabolism of the antipsychotic preclinical drug RO5263397 whose main clearance route is N-glucuronidation (Fowler et al., 2015). It is thus likely that these SNPs also affect the glucuronidation of prescribed drugs conjugated by UGT2B10 such as amitriptyline (Kaivosaari et al., 2008; Kato et al., 2013).

Recent studies by our group revealed that alternative splicing (AS) largely expands the UGT transcriptome (Tourancheau et al., 2016; Tourancheau et al., 2017). In turn, alternative (alt.) isoforms modulate the activity of UGT enzymes, suggesting that AS programs may contribute to interindividual variability in xenobiotics metabolism and cancer susceptibility (Bellemare et al., 2010b; Menard et al., 2013; Rouleau et al., 2014; Rouleau et al., 2016). Given the clinical importance of UGT2B10, by virtue of its detoxification functions towards tobacco by-products, anti-depressors and anti-psychotics, we hypothesized that AS represents a mean to regulate steady-state levels of UGT2B10 mRNA and enzyme activity. The goal of this study was to investigate in more details the expression of UGT2B10 and evaluate the influence of alternative isoforms on the metabolic functions of UGT2B10.

Materials and Methods

Analysis of UGT2B10 mRNA expression

To carefully analyze *UGT2B10* expression and AS patterns, raw RNA sequencing (RNA-seq) data were downloaded from public databases and realigned to the recently established UGT transcriptome (Tourancheau et al., 2016; GTEx (http://www.gtexportal.org/home/) and TCGA (https://gdc.cancer.gov/)). RNA-seq datasets were obtained from dbGaP at http://www.ncbi.nlm.nih.gov/gap through dbGaP accession number phs000424.v6.p1;

project ID 13346. The GTEx normal liver data (downloaded on June 7, 2017) were from 50 healthy individuals [29 males; 18 females; 3 unknown; median age: 55 years old (range 21-69 years old), mostly Caucasians]. The TCGA cancer liver data (downloaded on August 22, 2017), all hepatocellular carcinoma, were from 44 individuals [29 males, 15 females; median age: 62 years old (range 18-82 years old), 16 Caucasians, 22 Asians, and 5 African-Americans]. GTEx RNA-seq data of bladder (n=6), breast (n=51), colon (n=49), lung (n=48), kidney (n=35) prostate (n=50), and skin (n=53) were similarly obtained. HepaRG RNA-seq data (GSE 71446, accessed March 9, 2017; (Li et al., 2015)) were downloaded from the NCBI Gene expression omnibus database. For each individual RNA-seq data, quality of FASTQ files was assessed with FastQC before quality trimming with Trimmomatic v0.36 (Bolger et al., 2014). UGT transcript quantification was done with trimmed reads from each sample and a custom UGT transcript annotation (Tourancheau et al., 2016) using Kallisto v0.43 (Bray et al., 2016). Data (counts) was then upper-quantile normalized and further adjusted using housekeeping genes as described (de Jonge et al., 2007) using the EDASeq and RUVSeq packages for R version 3.2.2. Differential expression of UGT isoforms was assessed using the edgeR package for R. Normalized counts were then converted to counts per million (CPM) or transcripts per million (TPM) using transcript length. Reverse Transcription-PCR (RT-PCR) analysis of *UGT2B10* transcripts was as described (Tourancheau et al., 2016), using primer sequences provided in Table S1. The Basic Local Alignment Search Tool (BLAST) of the National Center for Biotechnology Information (NCBI, https://blast.ncbi.nlm.nih.gov/Blast.cgi) served to search sequence similarity between the novel UGT2B10 sequences and other genes in humans and other species. The Protein BLAST (blastp) suite was used to search "Non-redundant protein sequences" and "Reference proteins" whereas Translated nucleotide (tblastn) suite was used to search the "Nucleotide collection" and "Reference RNA sequences" with the unique amino acid sequences of alt. proteins.

Expression vectors and human cell models (HEK293 and HepG2)

To study alt. trancripts and proteins, expression vectors were produced from the *UGT2B10_v1* pcDNA6 construct (Beaulieu et al., 1998) using the Q5 Site-Directed Mutagenesis kit (New England Biolabs Ltd., Whitby, ON, Canada). Sequences of purified primers used for mutagenesis are provided in Supplemental Table 1. UGT2B10_v1 coding sequence was also cloned in the pcDNA3.1 vector to produce co-expression cell models (below). All constructs were verified by Sanger sequencing. For the expression of alt.

proteins tagged with V5-his (for immunoprecipitations studies), the stop codon of each coding sequence cloned in the pcDNA6 vector was removed using the Q5 Site-Directed Mutagenesis kit to permit in-frame V5-his expression.

HEK293 and HepG2 cell lines were obtained from the American Type Culture Collection (Manassas, VA, USA) and grown as described (Levesque et al., 1997; Menard et al., 2013). HEK293 cells (UGT negative; 2 x 10^6 cells in a 10 cm-plate) were transfected with 1 µg of each construct using Effectene (Qiagen, Toronto, ON, Canada), and HepG2 cells (UGT positive; 1 x 10^7 cells) were transfected with 20 µg of each construct by electroporation with the Neon Transfection System (Invitrogen, ThermoFisher Scientific, Ottawa, ON, Canada) as per manufacturers' instructions. HEK293 cells stably expressing the UGT2B10 cDNAs were established by supplementing cell culture media with blasticidin (Wisent, St-Bruno, QC, Canada; 10 µg/ml). Clones were selected based on UGT2B10 expression detected by immunoblotting with antibodies specified below. HEK293 cells co-expressing UGT2B10_v1 (encoding the canonical enzyme) and alt. UGT2B10 (with novel sequences in C-termini) were established by subsequent transfection of HEK293 clones expressing alt. sequences with the UGT2B10_v1-pcDNA3.1 construct and selection with G418 (Invitrogen, 1 mg/ml). HepG2 cells, which express UGT2B10_v1 endogenously, were transfected with the constructs expressing alt. variants and clone selection was with blasticidin. Control HEK293 and HepG2 cells were produced by transfection with the parental vector pcDNA6 and selection as above.

Analysis of protein expression

Antibodies. The rabbit polyclonal anti-UGT2B10 #1845 produced in-house against GST-UGT2B11 (aa 60-140) by Dr Alain Bélanger's group (Chouinard et al., 2006), was used for the immunodetection of UGT2B10 in HepG2 (1:5000) and HEK293 (1:10 000) cell models. Our analysis revealed that this antibody detects UGT2B10, UGT2B11 and less efficiently UGT2B28 (Supplemental Figure 1). The monoclonal anti-UGT2B10 antibody (Abcam ab57685) was used for immunoprecipitation in human liver. Cell compartment-specific antibodies used for immunofluorescence (IF) were anti-58K Golgi protein (1:100; ab27043, Abcam Inc., Toronto, ON, Canada), anti-protein disulfide isomerase (PDI: 1:100; ab2792, Abcam) for the ER, and anti-lamin (1:200; sc-376248, Santa Cruz Biotechnology, Dallas, TX, USA). DNA was stained with DRAQ5 (1:2000; ThermoFisher Scientific). Anti-calnexin was from Enzo Life Sciences (Farmingdale, NY, USA; ADI-SPA-860; 1:5000).

Mass spectrometry – multiple reaction monitoring (MS-MRM). Detection of peptides unique to alt. UGT2B10 was as described (Rouleau et al., 2016) with minor modifications. Briefly, human liver S9 fraction (8 mg protein; Xenotech LLC, Lenexa, KS, USA) was lysed for 45 min on ice in a total volume of 4 ml Lysis Buffer containing 0.05 M Tris-HCl pH 7.4, 0.15 M NaCl, 1% (w/v) Igepal CA-630 (Sigma-Aldrich), 1 mM dithiothreitol, and Complete protease inhibitor cocktail (Roche, Laval, QC, Canada). Lysates were centrifuged for 15 min at 13,000 *g*, and UGT2B10 was immunoprecipitated with 10 µg of the monoclonal anti-UGT2B10 (Abcam ab57685) for 1 h at 4°C on an orbital shaker. Protein complexes were captured by an overnight incubation at 4°C with Protein G–coated magnetic beads (200 µl Dynabeads, ThermoFisher Scientific). Beads were washed in lysis buffer and with 50 mM ammonium bicarbonate and stored at −20°C until analysis. Tryptic digests of UGT2B10 were prepared and analyzed by MS-coupled multiple reaction monitoring on a 6500 QTRAP hybrid triple quadrupole/linear ion trap mass spectrometer (Sciex, Concord, ON, Canada) as described (Rouleau et al., 2016). Briefly, MS analyses were conducted with an ionspray voltage of 2500 V in positive ion mode. Peptides were desalted on a 200 µm × 6 mm chip trap ChromXP C18 column, 3 µm (Eksigent, Sciex), at 2 µl/min solvent A (0.1% formic acid). Peptides were then eluted at a flow rate of 1 µl/min with a 30-min linear gradient from 5 to 40% solvent B (acetonitrile with 0.1% formic acid) and a 10-min linear gradient from 40 to 95% solvent B. MRM-MS analyses were performed using the four most intense transitions for each of the target peptides for the light and heavy forms. The UGT2B10 signature peptides were detected in tryptic digests of the immunoprecipitated UGT2B10 samples, and peptide identity was confirmed by co-injection of isotopically labeled [^{13}C6,^{15}N2]Lys and [^{13}C6,^{15}N4]Arg synthetic peptides (Pierce Protein Biotechnology, ThermoFisher Scientific).

Glucuronidation assays – For enzymatic assays in intact cells (*in situ* assays), two cell models were employed (HEK293 and HepG2 cells). Cells were seeded in 24-well plates (HEK293: 8 x 10^4 cells/well, HepG2: 2.25 x 10^5 cells/well). Assays were initiated 72 h after seeding by replacing the culture medium with fresh medium (1 ml/well) containing a UGT2B10 substrate (amitriptyline, 7.5 µM and 150 µM; levomedetomidine, 7.5 µM and 75 µM). All substrates were obtained from Sigma-Aldrich. Cells were incubated for 4 h, media were then collected and stored at −20°C until glucuronide (G) quantification by high-performance liquid chromatography tandem mass spectrometry. Assays were replicated in at least two independent experiments in triplicates. Separation of amitriptyline and levomedetomidine was performed onto an ACE Phenyl column 3 µM packing material, 100

× 4.6 mm (Canadian Life Science, ON, Canada). Isocratic condition with 70% methanol/30% water/3 mM ammonium formate with a flow rate of 0.9 ml/min was used to elute amitriptyline-G. A linear gradient was used to elute levomedetomidine-G, with 5% methanol/95% water/1 mM ammonium formate as initial conditions followed by a 10 min-linear gradient to 90% methanol/10% water/ 1 mM ammonium formate. The glucuronides were quantified by tandem mass spectrometry (API 6500; Biosystems-Sciex, Concord, ON, Canada). The following mass ion transitions (m/z) were used: 377.1 → 201.1 for levomedetomidine-G and 454.2 → 191.1 for amitriptyline-G. Glucuronidation activity (area/hour/mg protein/UGT level) was normalized for the expression of the UGT2B10 enzyme in each cell model, determined by densitometry scanning of band intensity on immunoblots with antibody #1845. Cycloheximide glucuronidation assays were conducted using microsomes isolated from human liver (Xenotech LLC), HepG2-pcDNA6 described above, commercial supersomes expressing UGT1A and UGT2B isoenzymes (Corning, Woburn, MA, USA), and microsomes of UGT2B11-expressing HEK293 prepared in-house as described (Lepine et al., 2004). Glucuronidation assays were conducted at 37°C using 20 µg membrane proteins and a final concentration of 200 µM cycloheximide (Sigma-Aldrich). Cycloheximide-G quantification was conducted as specified above for the UGT2B10 substrates, using a linear gradient with 10% methanol/90% water/1 mM ammonium formate as the initial conditions followed by a linear gradient to 85% methanol/15% water/ 1 mM ammonium formate in 5 min.

Immunofluorescence – Subcellular distribution of UGT2B10 enzyme and alternative isoforms was carried out in HEK293 cells stably expressing either protein and detected with the anti-UGT2B10 antibody #1845 (1:1000) as described (Rouleau et al., 2016).

Immunoprecipitation - Stable HEK293 *UGT2B10_v1* cells (2 x 10^6 cells) were seeded in 10 cm-plates and transiently transfected with alt. UGT2B10 V5-tagged constructs (3 µg) using Effectene as per manufacturer's instructions (Qiagen). 36 h post-transfection, cells were processed for cross-linking and immunoprecipitation with the polyclonal anti-V5 (1:600; NB600-380; Novus Biologicals) as described (Rouleau et al., 2016).

Protein and mRNA stability in cell models - HEK293 cell models were seeded in 6-well plates (4 x 10^5 cells/well) and grown for 48 h. HepG2 cell models were seeded in 6-well plates (1.5 x 10^6 cells/well) and grown for 24 h. Cells were rinsed and incubated for 16h with media containing 1 µM MG132 (Calbiochem, EMD Millipore, Etobicoke, ON, Canada) or vehicle (DMSO). Cells were harvested and protein extracts were prepared in Lysis Buffer. Cells

were lysed for 30 min on a rotation unit, homogenized by pipetting up and down through fine needles (18G and 20G, 10 times each) on ice and cleared by centrifugation for 15 min at 13,000 *g* prior to analysis by immunoblotting using anti-UGT2B10 #1845. Duplicate cell samples were harvested for RNA extraction and RT-PCR analysis of UGT2B10 variants as described (Rouleau et al., 2016). Assays were done twice. UGT2B10 proteins half-lives were determined by treatment with cycloheximide (20 ug/ml) for 0-16 h as described (Turgeon et al., 2003). Cells were washed in PBS, collected and lysed by scraping in Lysis Buffer, prior to analysis by immunoblotting.

Assessment of the glycosylation status of UGT2B10 proteins expressed in HEK293 cells - Microsomes (20 µg proteins) prepared from HEK293 stably expressing each UGT2B10 isoform were treated with Endo H and O-glycosidase obtained from New England Biolabs Inc. (Ipswich, MA, USA) as described (Girard-Bock et al., 2016). Assays were performed in two independent experiments.

Results

UGT2B10 gene expression predominates in human liver and is regulated by alternative splicing

For a quantitative assessment of UGT2B10 expression, we performed a realignment of public GTEX and TCGA RNA-seq data from human tissue samples to the fully annotated UGT variant sequence database. This database was created based on RNA-seq experiments previously conducted with several human tissues (Tourancheau et al., 2016). Data indicated that the UGT2B10 transcriptome is comprised of one canonical and 10 alt. transcripts arising from the single *UGT2B10* gene. The UGT2B10 alt. transcripts are created by partial intronization of exon 1-2, exon skipping of exon 4-6 and inclusion of novel terminal exons 6b or 6c. UGT2B10 transcripts and encoded isoforms are depicted in **Figure 1**. Data revealed *UGT2B10* as one of the highest expressed UGTs in normal liver samples whereas variants arising from alternative splicing represented nearly 50% of the *UGT2B10* hepatic transcriptome (**Figure 2A**). Some variant classes were remarkably abundant, at levels comparable to those of the canonical *UGT2B10_v1* transcript encoding the UGT2B10 enzyme, namely those with N-terminal truncations and with novel C-terminal sequences (**Figure 2A**). Total *UGT2B10* expression was 2.15-fold (*P*=0.013) higher in hepatocellular carcinoma (HCC; n=44) relative to normal livers (n=50), and was highly variable among

individuals (coefficients of variation of 93 to 117%) (**Figure 2B**). In contrast to the high hepatic levels, expression of *UGT2B10* in other normal tissues surveyed was much lower, with values below 1 TPM in the bladder, breast, colon, kidney, lung, prostate, and skin (data not shown).

Alternative splicing creates UGT2B10 variants with novel in-frame C-terminal sequences detected in human liver at the protein level

Splicing events generating *UGT2B10* transcripts (*n9* and *n10*) harbouring novel C-terminal sequences were of particular interest for this study. These alt. variants are produced by intronization of parts of the canonical exon 6 and inclusion of a novel exon 6c (**Figure 1**). These AS events appeared specific to human and were not noted in other species based on BLAST searches in the non-redundant nucleotide collection and RNA Reference sequence databases. Transcripts were abundant in human livers and were 3.5 fold higher in hepatic tumors relative to normal tissues. They represented on average 15% of total *UGT2B10* expression in normal liver tissues and 25% in HCC tissues (**Figure 2A-B**). The considerable interindividual variability for these alt. transcripts was higher than for the total and canonical *UGT2B10* hepatic expression. We also noted a significant positive correlation between the expression of the canonical and alt. transcripts (ρ=0.854-0.915, $P \leq 0.001$) (**Figure 2C**).

The putative UGT2B10 proteins encoded by these alt. transcripts are referred to as UGT2B10 isoforms 4 and 5, named i4 and i5 respectively. They are predicted to retain both the substrate and the co-substrate (UDP-GlcA) binding domains coupled to a novel alt. C-sequence (**Figure 1**). Isoform 4 lacks the 43 C-terminal amino acids including the transmembrane domain and the positively charged C-terminal tail of the UGT2B10 enzyme that are replaced by 10 novel amino acids encoded by exon 6c **(Figure 3A)**. As for isoform 5, because a smaller portion of exon 6 is intronized, the encoded protein is predicted to retain 18 of the 24 transmembrane domain residues and to be extended by 65 novel amino acids, of which half are encoded by a frame-shift in exon 6, and half by exon 6c (**Figure 1, 3A**).

Validation of endogenous protein expression was possible for UGT2B10_i5 through the identification of a unique peptide sequence by targeted mass spectrometry-multiple reaction monitoring (MRM) of liver UGT2B10 immunoprecipitated from multiple donors (**Figure**

3B,C). This result is in line with the detection of the corresponding transcripts by PCR in human livers (**Supplemental Figure 2A**). The endogenous expression of UGT2B10_i4 could not be addressed by this approach given the short and hydrophobic nature of the C-terminal unique sequence.

Alternative isoforms with novel C-terminal sequences co-localized with the UGT2B10 enzyme and modified its activity *in vitro*

The alt. UGT2B10 isoforms were stably expressed in the embryonic kidney cell line HEK293, devoid of endogenous UGT expression, alone or with the canonical UGT2B10 enzyme. As well, their expression was examined in the liver cell model HepG2 that expresses endogenously the UGT2B10 enzyme and conjugates substrates of the enzyme such as amitriptyline and levomedetomidine. We initially confirmed protein expression using immunoblot and immunofluorescence experiments using an anti-UGT2B10 antibody (#1845) that targets amino acids encoded by exon 1 and therefore recognizes the three UGT2B10 isoforms (**Figure 4A**). Indeed, we detected UGT2B10_i4 and UGT2B10_i5, near their predicted molecular weights (MW) of 57 and 66 kDa in cell models (**Figure 4A**).

The subcellular distribution of each protein was examined in the HEK293 models where the canonical and alt. proteins were detected and largely restricted to an endoplasmic reticulum (ER) localization. This was confirmed by the co-localization with the ER marker protein disulfide isomerase (PDI) (**Figure 4B**). Each isoform also displayed minor perinuclear and Golgi localization (**Supplemental Figure 3**). The glycosylation status of each protein was studied by subjecting microsomes from HEK293 cell models to Endo H glycosidase, which cleaves N-linked sugars on asparagine acquired by ER-resident enzymes, and to O-glycosidase, which removes serine and threonine O-linked complex sugars acquired in the Golgi. Each UGT2B10 protein was sensitive to Endo H treatment, revealed by the shift to a higher mobility protein band upon treatment (**Figure 4C**). In contrast, their mobility was not affected by a treatment with O-glycosidase.

Enzymatic assays in intact cells were subsequently conducted in the hepatic cell model HepG2 that expresses the endogenous UGT2B10 enzyme. Compared to the reference cell line (stably transfected with pcDNA6), expression of alt. UGT2B10_i4 isoform enhanced glucuronidation of the UGT2B10 enzyme with two drug substrates, amitriptyline and levomedetomidine, by 1.5 to 2 fold (**Figure 5A,B**). In turns, the presence of alt. UGT2B10_i5

significantly impaired the glucuronidation of amitriptyline and tended to reduce that of levomedetomidine as well, by 20-25%. Glucuronidation assays conducted with the UGT negative cells HEK293 stably expressing either alt. UGT2B10 isoforms revealed no transferase activity for amitriptyline and levomedetomidine. When co-expressed with the UGT2B10 enzyme, we observed a significant inhibition by 23 to 65% of glucuronidation activity by HEK293 cells in the presence of the alt. i4 or i5 proteins (**Figure 5A,B**). Since we observed a co-localization of alt. isoforms and the UGT2B10 enzyme in the ER, we addressed their potential interaction as a possible regulatory mechanism. Immunoprecipitations were conducted with an anti-V5 epitope antibody using cell models stably expressing the UGT2B10 enzyme and transiently expressing either alt. isoform tagged with the V5 epitope. The UGT2B10 enzyme was immunoprecipitated with each alt. isoform, indicating their ability to form complexes (**Figure 5C**).

Alternative isoforms have shorter half-lives than the UGT2B10 enzyme and are targeted for degradation by the proteasome

Protein stability was evaluated in both cell models. The UGT2B10 enzyme displayed a half-life over 16 hours in both HEK293 (exogenous expression) and HepG2 (endogenous expression) cell models whereas the alt. isoforms displayed superior turnover rates. The alt. UGT2B10_ i5 was the least stable, with short half-lives of 1.9 and 0.7 hours in HEK293 and HepG2, respectively (**Figure 6A**). The turnover rate of isoform i4 differed between the two cell models, and was 11.5 hours in HEK293 but much shorter in HepG2 (1.5 hours). We noted in HepG2 cells a significant recovery of alt. proteins expression, even rising above those of non-treated cells by 16h after initiation of the cycloheximide treatment. This was not observed for the UGT2B10 enzyme, nor for any of the UGT2B10 proteins in HEK293 cells. This observation implied a possible inactivation in HepG2 cells, which was confirmed by the detection of two glucuronides of cycloheximide (G1 and G2) with HepG2 microsomes (**Supplemental Figure 5**). This was further validated using microsomal fractions of pooled human livers and UGT supersomes. In these experiments, UGT1A9 and UGT2B7 most efficiently glucuronidated cycloheximide (G1 and G2), whereas UGT1A3 and UGT1A4 (G1) as well as UGT1A1 and UGT2B4 (G1 and G2) also conjugated some cycloheximide (**Supplemental Figure 5**), with some of them detected in HepG2 cells and not in the HEK293 cell model. As a consequence, this may lead to an inaccurate assessment of UGT proteins half-lives using this approach in the HepG2 model.

Accordingly, the difference in protein stability between the UGT2B10 enzyme and alt. proteins was further addressed by proteasomal inhibition. Whereas the enzyme levels were nearly unperturbed by inhibition of the ubiquitin-proteasome system, alt. UGT2B10 and more particularly isoform i5, were stabilized, indicating that they were degraded via the ubiquitin-proteasome system. Proteasomal inhibition for 16 h increased the ratio of alt. isoform / UGT2B10 enzyme in HepG2 liver cell models, whereas stabilization was more modest in HEK293 (**Figure 6B**). Increased levels of alt. isoforms were not derived from enhanced transcription, verified at the mRNA level (**Supplemental Figure 2B).**

Differential induction of UGT2B10 alternative transcripts in liver cells by phenobarbital and a CAR agonist

HepaRG cells constitute a good surrogate system to study hepatic functions and response to drug treatments. An analysis of public HepaRG RNA-seq data (Li et al., 2015) with the exhaustive UGT transcriptome revealed an expression of canonical and alt. *UGT2B10* in comparable proportions to the human liver (not shown). In HepaRG cells treated with the constitutive androstane receptor (CAR) agonist CITCO, a significant and preferential induction of the alt. UGT2B10 transcripts (1.4 fold, P=0.003) occurred, whereas the enzyme-coding *v1* transcript was not significantly altered (**Figure 7**). Phenobarbital did not significantly induce expression of *UGT2B10* in wild type HepaRG cells. In contrast, in HepaRG cells with a CAR knock-out, alt. transcripts were significantly upregulated by 1.8 fold (P≤0.001) by phenobarbital, and 1.4 fold (P=0.011) by the CAR agonist, whereas *v1* was not significantly perturbed (**Figure 7**).

Discussion

The recent expansion of the pharmacogene transcriptome by AS has shed light on a novel mechanism regulating drug metabolism and clearance (Bellemare et al., 2010a; Bellemare et al., 2010b; Guillemette et al., 2010; Guillemette et al., 2014; Rouleau et al., 2014; Chhibber et al., 2016; Rouleau et al., 2016; Tourancheau et al., 2016; Tourancheau et al., 2017). Our study of the *UGT2B10* transcriptome, encoding a key detoxification enzyme specialized in N-glucuronidation of multiple harmful xenobiotics (Kaivosaari et al., 2007; Kaivosaari et al., 2011; Kato et al., 2013), demonstrated that AS accounts for a large proportion of *UGT2B10* gene expression and especially in the liver. This observation held true in liver tumors, where *UGT2B10* expression was enhanced by two-fold in hepatocellular

carcinoma. Indeed, our analysis of next-generation sequencing data revealed that *UGT2B10* expression prevails in the liver whereas in all other tissues surveyed, including the lung, its expression was low to undetected. This is consistent with the expression determined at the RNA level in several human tissues, including those of the aerodigestive tract (Ohno and Nakajin, 2011; Court et al., 2012; Jones and Lazarus, 2014). It supports that a main detoxification site of UGT2B10-dependent N-glucuronidation is the liver, where UGT2B10 is one of the most abundant UGT enzyme based on proteomics data (Fallon et al., 2013; Sato et al., 2014; Margaillan et al., 2015). Besides, AS also provides an explanation for the multiple observations reporting a lack of correlation between mRNA and protein expression, such as in hepatocellular carcinoma where the RNA expression remained equivalent between tumor tissues and adjacent normal tissues whereas glucuronidation activity was drastically decreased (Lu et al., 2015).

With a focus on one abundant class of hepatic alt. *UGT2B10* variants containing a novel 3' terminal exon that were confirmed at the protein level in human liver samples and in heterologous expression models, we expose their regulated expression and influence on UGT2B10 enzyme activity *in vitro*. In fact, the transcriptional regulation of *UGT2B10* has been poorly studied. A response element for the bile acid sensing farnesoyl X receptor (FXR) was recently uncovered in the *UGT2B10* promoter region and participated in the induction of *UGT2B10* by the FXR agonists GW4064 and chenodeoxycholic acid (Lu et al., 2017a). In the cell model HepaRG, a surrogate to human primary hepatocytes in drug metabolism studies (Antherieu et al., 2012), RNA-seq data revealed drug-induced regulation of the *UGT2B10* transcriptome by both the constitutive androstane receptor (CAR) and pregnane X receptor (PXR). The superior induction of alt. *UGT2B10* by CAR and PXR agonists observed herein, especially in HepaRG cells devoid of CAR expression, further raises the possibility of a PXR-dependent remodelling of splicing events at the *UGT2B10* locus that may significantly influence UGT2B10 detoxification activity. Whether other receptors such as FXR, previously reported to regulate *UGT2B10* transcription (Lu et al., 2017a), also influence splicing remain to be addressed. When expressed in human cells, alt. UGT2B10 acted as regulators of the glucuronidation activity of the UGT2B10 enzyme, possibly conveyed by heterologous complexes formed between the enzyme and alternative proteins; a regulatory mechanism documented for other human UGTs (Bushey and Lazarus, 2012; Menard et al., 2013; Rouleau et al., 2014; Rouleau et al., 2016). Our findings further suggest a cell-specific influence given that in HepG2 cells, an increased N-glucuronidation of the

UGT2B10 substrates amitriptyline and levomedetomidine by the endogenous enzyme was observed, in contrast with a repression of enzyme activity in HEK293 cells. The endogenous expression of additional UGTs other than UGT2B10 in HepG2 cells and different protein turnover rates could be among factors influencing their functions. Likewise, the impact of AS on UGT2B10 activity has been documented previously by findings of a common polymorphism (rs116294140) that disrupts a splice site in exon 3 and introduces a premature stop codon possibly triggering non-sense mRNA decay (Fowler et al., 2015). This polymorphism, particularly more frequent among African Americans, significantly reduced N-glucuronidation of drugs such as RO5263397 as well as nicotine and cotinine (Murphy et al., 2014; Fowler et al., 2015). In fact, occurrence of this splice site variant as well as the coding variant Asp67Tyr (rs61750900) were estimated to collectively explain over 24% of interindividual variability in cotinine glucuronidation (Patel et al., 2015). Our results support that alternative splicing at the *UGT2B10* locus may be a major factor contributing to this variability in the constitutive expression of the gene, with a potential impact on responses to substrates of the UGT2B10 pathway.

The alternate UGT2B10 proteins with novel in-frame C-terminal sequences are predicted to include the entire putative catalytic domain (Radominska-Pandya et al., 2010), although their enzyme activity could not be confirmed in standard *in vitro* assay conditions when expressed in HEK293 human cells. This could be due to an inadequate topology of the alt. proteins essential for enzyme function. *In silico* analysis of the novel exonic sequence with NCBI BLAST tools did not reveal a match with other nucleotide or amino acid sequences of any organism. The splicing event at the *UGT2B10* locus appears specific to humans. This is consistent with the low to undetectable activity towards preferred UGT2B10 substrates such as N-heterocyclic amines and aliphatic tertiary amines in most primates and other mammals, suggesting that *UGT2B10* expression occurs preferentially in humans (Kaivosaari et al., 2007; Kaivosaari et al., 2008; Zhou et al., 2010; Lu et al., 2017b). The novel appended amino acid sequence encoded in the alternative frame by exon 6 is however related to that of putative alternative variants of several other human proteins including CLCN3 (chloride exchange transporter 3), ALG9 (alpha-1, 2-mannosyltransferase), and CHFR (E3-ubiquitin ligase) supporting that the new sequence may encode a conserved domain (**Supplemental Figure 6**).

As for subcellular localization, our immunofluorescence data indicated that the alt. isoforms, partially or completely lacking the transmembrane domain and devoid of the positively

charged lysine tail (**Figure 3**) are nonetheless ER-resident proteins when expressed in HEK293 human cells. Although studied in a limited set of UGTs, the high sequence similarity of ER retention elements among UGTs supports a common ER retention mechanism. ER residency of UGT enzymes is mediated by at least four protein regions: the N-terminal signal peptide, a short hydrophobic patch in the N-terminal substrate binding domain, the C-terminal transmembrane region and the cytoplasmic dilysine motif containing the ER retention signal "KXKXX" (K, lysines, X, any amino acids) (Jackson et al., 1993; Ciotti et al., 1998; Ouzzine et al., 1999; Barre et al., 2005). In line with our observations, these structural features may be partially redundant, as none appears strictly essential to ER retention. The Endo H sensitivity and lack of sensitivity towards O-glycosidase for each of the UGT2B10 enzyme and alt. UGT2B10 also support ER residency. Consistent with their co-localization, the potential of alt. UGT2B10 to interact with the UGT2B10 enzyme suggests that this may be a mechanism underlying their regulatory function.

The preferential stabilization of alt. isoforms by proteasomal inhibition and their shorter half-lives relative to the UGT2B10 enzyme suggest that distinct pathways may govern the turnover of alt. isoforms and the enzyme. This also suggests that a small variation in RNA levels has the potential to affect AS protein expression level. The significant abundance of alt. transcripts encoding these proteins may indicate that hepatic cells are poised to adapt levels of regulatory isoforms in response to various endogenous or exogenous stimuli. This is supported by the preferential mRNA expression of alternates in HepaRG cells treated with nuclear receptors agonists. While the structural determinants of UGT protein stability are scarcely known, mechanisms modulating UGT turnover may significantly contribute to the regulation of their detoxifying functions, a well-documented aspect for some drug metabolizing CYPs (Zhukov and Ingelman-Sundberg, 1999; Kim et al., 2016 and references therein). When expressed in the HEK293 model, half-lives of UGTs were more than 12-16 hours for UGT2B4, UGT2B7, UGT2B10 and UGT2B15 whereas UGT1A1 and UGT2B17 were more labile with half-lives less than 3 hours (Turgeon et al., 2001; Rouleau et al., 2016); this study). However, given that cycloheximide is glucuronidated by several UGT enzymes as demonstrated herein, alt. UGT protein half-lives established by translational inhibition with this compound in cells expressing UGTs likely constitute an inaccurate estimate that will be influenced by the enzymes expressed.

A limitation of our study is the lack of detection of alt. UGT2B10 by immunoblotting in pooled liver microsomes from 50 individuals using the polyclonal anti-UGT2B10 antibody #1845.

Their expression varied widely among individuals (CV of 155%), with some having no or barely detectable hepatic alt. *UGT2B10* variants. Levels of alt. proteins in our human liver pool may be too low for detection by immunoblotting. In contrast, the detection of alt. UGT2B10 by MS-MRM was performed following an immunoprecipitation step that enriched UGT2B10, thus improving the sensitivity of detection. The high turnover rate of the alt. proteins, as observed in the two cell models, may also influence our ability to detect them in human livers by immunoblotting. Additional experiments are required to ascertain the expression of alt. UGT2B10 proteins in individual human liver samples and their expression ratio relative to the UGT2B10 enzyme.

In conclusion, our study reveals that AS creates a diversified *UGT2B10* transcriptome and represents half of the UGT2B10 expression in the human liver, with a wide interindividual variability. Alternate UGT2B10 proteins may significantly influence the UGT2B10-dependent detoxification of amine-containing drugs such as anti-psychotic and tobacco metabolites and are expected to modulate endogenous substrates of the UGT2B10 enzyme, which are currently unknown. Our study further highlights a long-term stability of the UGT2B10 enzyme that contrasts with the lability of alt. proteins, the latter being regulated by proteasomal degradation. Most interestingly, we further expose a preferential induction by PXR and CAR inducers of alt. *UGT2B10* with novel in-frame C-terminal sequences in hepatic cells, implying a fine regulation of the AS process by xenosensing transcription factors. Our study highlights an important regulatory role of AS in UGT2B10 expression and detoxification functions that may explain part of the significant variability in N-glucuronidation, largely mediated by the UGT2B10 pathway in the liver. We thus believe that interindividual differences in the clinical response to UGT2B10 substrates are likely to be understood through the AS process affecting both the constitutive and inducible expression of UGT2B10.

Acknowledgements

Authors wish to thank Dr H. Wang and B. Mackowiak (U. of Maryland) for their collaboration with the HepaRG data and Patrick Caron, Véronique Turcotte, Anne-Marie Duperré, Camille Girard-Bock and Andréa Fournier for their technical assistance. We also thank the Proteomics Platform of the CHU de Québec Research Center for their services.

Authorship contribution

Participated in research design: Labriet, Allain, Rouleau, Audet-Delage, Guillemette

Conducted experiments: Labriet, Allain, Audet-Delage, Villeneuve

Performed data analysis: Labriet, Allain, Rouleau, Audet-Delage, Villeneuve, Guillemette

Wrote or contributed to the writing of the manuscript: Labriet, Rouleau, Guillemette

Financial disclosure

All authors declare they have no competing interest

References

Antherieu S, Chesne C, Li R, Guguen-Guillouzo C, and Guillouzo A (2012) Optimization of the HepaRG cell model for drug metabolism and toxicity studies. *Toxicol In Vitro* **26:**1278-1285.

Barre L, Magdalou J, Netter P, Fournel-Gigleux S, and Ouzzine M (2005) The stop transfer sequence of the human UDP-glucuronosyltransferase 1A determines localization to the endoplasmic reticulum by both static retention and retrieval mechanisms. *FEBS J* **272:**1063-1071.

Beaulieu M, Levesque E, Hum DW, and Belanger A (1998) Isolation and characterization of a human orphan UDP-glucuronosyltransferase, UGT2B11. *Biochem Biophys Res Commun* **248:**44-50.

Bellemare J, Rouleau M, Girard H, Harvey M, and Guillemette C (2010a) Alternatively spliced products of the UGT1A gene interact with the enzymatically active proteins to inhibit glucuronosyltransferase activity in vitro. *Drug Metab Dispos* **38:**1785-1789.

Bellemare J, Rouleau M, Harvey M, and Guillemette C (2010b) Modulation of the human glucuronosyltransferase UGT1A pathway by splice isoform polypeptides is mediated through protein-protein interactions. *J Biol Chem* **285:**3600-3607.

Berg JZ, Mason J, Boettcher AJ, Hatsukami DK, and Murphy SE (2010) Nicotine metabolism in African Americans and European Americans: variation in glucuronidation by ethnicity and UGT2B10 haplotype. *J Pharmacol Exp Ther* **332:**202-209.

Bolger AM, Lohse M, and Usadel B (2014) Trimmomatic: a flexible trimmer for Illumina sequence data. *Bioinformatics* **30:**2114-2120.

Bray NL, Pimentel H, Melsted P, and Pachter L (2016) Near-optimal probabilistic RNA-seq quantification. *Nat Biotechnol* **34:**525-527.

Bushey RT and Lazarus P (2012) Identification and functional characterization of a novel UDP-glucuronosyltransferase 2A1 splice variant: potential importance in tobacco-related cancer susceptibility. *J Pharmacol Exp Ther* **343:**712-724.

Chen G, Blevins-Primeau AS, Dellinger RW, Muscat JE, and Lazarus P (2007) Glucuronidation of nicotine and cotinine by UGT2B10: loss of function by the UGT2B10 Codon 67 (Asp>Tyr) polymorphism. *Cancer Res* **67:**9024-9029.

Chen G, Dellinger RW, Gallagher CJ, Sun D, and Lazarus P (2008a) Identification of a prevalent functional missense polymorphism in the UGT2B10 gene and its association with UGT2B10 inactivation against tobacco-specific nitrosamines. *Pharmacogenet Genomics* **18:**181-191.

Chen G, Dellinger RW, Sun D, Spratt TE, and Lazarus P (2008b) Glucuronidation of tobacco-specific nitrosamines by UGT2B10. *Drug Metab Dispos* **36:**824-830.

Chen G, Giambrone NE, and Lazarus P (2012) Glucuronidation of trans-3'-hydroxycotinine by UGT2B17 and UGT2B10. *Pharmacogenet Genomics* **22:**183-190.

Chhibber A, French CE, Yee SW, Gamazon ER, Theusch E, Qin X, Webb A, Papp AC, Wang A, Simmons CQ, Konkashbaev A, Chaudhry AS, Mitchel K, Stryke D, Ferrin TE, Weiss ST, Kroetz DL, Sadee W, Nickerson DA, Krauss RM, George AL, Schuetz EG, Medina MW, Cox NJ, Scherer SE, Giacomini KM, and Brenner SE (2016) Transcriptomic variation of pharmacogenes in multiple human tissues and lymphoblastoid cell lines. *Pharmacogenomics J. In press.*

Chouinard S, Pelletier G, Belanger A, and Barbier O (2006) Isoform-specific regulation of uridine diphosphate-glucuronosyltransferase 2B enzymes in the human prostate: differential consequences for androgen and bioactive lipid inactivation. *Endocrinology* **147:**5431-5442.

Ciotti M, Cho JW, George J, and Owens IS (1998) Required buried alpha-helical structure in the bilirubin UDP-glucuronosyltransferase, UGT1A1, contains a nonreplaceable phenylalanine. *Biochemistry* **37:**11018-11025.

Court MH, Zhang X, Ding X, Yee KK, Hesse LM, and Finel M (2012) Quantitative distribution of mRNAs encoding the 19 human UDP-glucuronosyltransferase enzymes in 26 adult and 3 fetal tissues. *Xenobiotica* **42:**266-277.

de Jonge HJ, Fehrmann RS, de Bont ES, Hofstra RM, Gerbens F, Kamps WA, de Vries EG, van der Zee AG, te Meerman GJ, and ter Elst A (2007) Evidence based selection of housekeeping genes. *PLoS One* **2:**e898.

Fallon JK, Neubert H, Hyland R, Goosen TC, and Smith PC (2013) Targeted quantitative proteomics for the analysis of 14 UGT1As and -2Bs in human liver using NanoUPLC-MS/MS with selected reaction monitoring. *J Proteome Res* **12:**4402-4413.

Fowler S, Kletzl H, Finel M, Manevski N, Schmid P, Tuerck D, Norcross RD, Hoener MC, Spleiss O, and Iglesias VA (2015) A UGT2B10 splicing polymorphism common in african populations may greatly increase drug exposure. *J Pharmacol Exp Ther* **352:**358-367.

Girard-Bock C, Benoit-Biancamano MO, Villeneuve L, Desjardins S, and Guillemette C (2016) A Rare UGT2B7 Variant Creates a Novel N-Glycosylation Site at Codon 121 with Impaired Enzyme Activity. *Drug Metab Dispos* **44:**1867-1871.

Guillemette C, Levesque E, Harvey M, Bellemare J, and Menard V (2010) UGT genomic diversity: beyond gene duplication. *Drug Metab Rev* **42:**24-44.

Guillemette C, Levesque E, and Rouleau M (2014) Pharmacogenomics of human uridine diphospho-glucuronosyltransferases and clinical implications. *Clin Pharmacol Ther* **96:**324-339.

Haakensen VD, Biong M, Lingjaerde OC, Holmen MM, Frantzen JO, Chen Y, Navjord D, Romundstad L, Luders T, Bukholm IK, Solvang HK, Kristensen VN, Ursin G, Borresen-Dale AL, and Helland A (2010) Expression levels of uridine 5'-diphospho-glucuronosyltransferase genes in breast tissue from healthy women are associated with mammographic density. *Breast Cancer Res* **12:**R65.

Jackson MR, Nilsson T, and Peterson PA (1993) Retrieval of transmembrane proteins to the endoplasmic reticulum. *J Cell Biol* **121:**317-333.

Jones NR and Lazarus P (2014) UGT2B gene expression analysis in multiple tobacco carcinogen-targeted tissues. *Drug Metab Dispos* **42:**529-536.

Kaivosaari S, Finel M, and Koskinen M (2011) N-glucuronidation of drugs and other xenobiotics by human and animal UDP-glucuronosyltransferases. *Xenobiotica* **41:**652-669.

Kaivosaari S, Toivonen P, Aitio O, Sipila J, Koskinen M, Salonen JS, and Finel M (2008) Regio- and stereospecific N-glucuronidation of medetomidine: the differences between UDP glucuronosyltransferase (UGT) 1A4 and UGT2B10 account for the complex kinetics of human liver microsomes. *Drug Metab Dispos* **36:**1529-1537.

Kaivosaari S, Toivonen P, Hesse LM, Koskinen M, Court MH, and Finel M (2007) Nicotine glucuronidation and the human UDP-glucuronosyltransferase UGT2B10. *Mol Pharmacol* **72:**761-768.

Kato Y, Izukawa T, Oda S, Fukami T, Finel M, Yokoi T, and Nakajima M (2013) Human UDP-glucuronosyltransferase (UGT) 2B10 in drug N-glucuronidation: substrate screening and comparison with UGT1A3 and UGT1A4. *Drug Metab Dispos* **41:**1389-1397.

Kazmi F, Barbara JE, Yerino P, and Parkinson A (2015) A long-standing mystery solved: the formation of 3-hydroxydesloratadine is catalyzed by CYP2C8 but prior glucuronidation of desloratadine by UDP-glucuronosyltransferase 2B10 is an obligatory requirement. *Drug Metab Dispos* **43:**523-533.

Kerdpin O, Mackenzie PI, Bowalgaha K, Finel M, and Miners JO (2009) Influence of N-terminal domain histidine and proline residues on the substrate selectivities of human UDP-glucuronosyltransferase 1A1, 1A6, 1A9, 2B7, and 2B10. *Drug Metab Dispos* **37:**1948-1955.

Kim SM, Wang Y, Nabavi N, Liu Y, and Correia MA (2016) Hepatic cytochromes P450: structural degrons and barcodes, posttranslational modifications and cellular adapters in the ERAD-endgame. *Drug Metab Rev* **48:**405-433.

Lepine J, Bernard O, Plante M, Tetu B, Pelletier G, Labrie F, Belanger A, and Guillemette C (2004) Specificity and regioselectivity of the conjugation of estradiol, estrone, and their catecholestrogen and methoxyestrogen metabolites by human uridine diphospho-glucuronosyltransferases expressed in endometrium. *J Clin Endocrinol Metab* **89:**5222-5232.

Levesque E, Beaulieu M, Green MD, Tephly TR, Belanger A, and Hum DW (1997) Isolation and characterization of UGT2B15(Y85): a UDP-glucuronosyltransferase encoded by a polymorphic gene. *Pharmacogenetics* **7:**317-325.

Li D, Mackowiak B, Brayman TG, Mitchell M, Zhang L, Huang SM, and Wang H (2015) Genome-wide analysis of human constitutive androstane receptor (CAR) transcriptome in wild-type and CAR-knockout HepaRG cells. *Biochem Pharmacol* **98:**190-202.

Lu D, Wang S, Xie Q, Guo L, and Wu B (2017a) Transcriptional Regulation of Human UDP-Glucuronosyltransferase 2B10 by Farnesoid X Receptor in Human Hepatoma HepG2 Cells. *Mol Pharm* **14:**2899-2907.

Lu D, Xie Q, and Wu B (2017b) N-glucuronidation catalyzed by UGT1A4 and UGT2B10 in human liver microsomes: Assay optimization and substrate identification. *J Pharm Biomed Anal* **145:**692-703.

Lu L, Zhou J, Shi J, Peng XJ, Qi XX, Wang Y, Li FY, Zhou FY, Liu L, and Liu ZQ (2015) Drug-Metabolizing Activity, Protein and Gene Expression of UDP-Glucuronosyltransferases Are Significantly Altered in Hepatocellular Carcinoma Patients. *PLoS One* **10:**e0127524.

Margaillan G, Rouleau M, Klein K, Fallon JK, Caron P, Villeneuve L, Smith PC, Zanger UM, and Guillemette C (2015) Multiplexed Targeted Quantitative Proteomics Predicts Hepatic Glucuronidation Potential. *Drug Metab Dispos* **43:**1331-1335.

Menard V, Collin P, Margaillan G, and Guillemette C (2013) Modulation of the UGT2B7 enzyme activity by C-terminally truncated proteins derived from alternative splicing. *Drug Metab Dispos* **41:**2197-2205.

Murphy SE (2017) Nicotine Metabolism and Smoking: Ethnic Differences in the Role of P450 2A6. *Chem Res Toxicol* **30:**410-419.

Murphy SE, Park SS, Thompson EF, Wilkens LR, Patel Y, Stram DO, and Le Marchand L (2014) Nicotine N-glucuronidation relative to N-oxidation and C-oxidation and UGT2B10 genotype in five ethnic/racial groups. *Carcinogenesis* **35:**2526-2533.

NCBI dbSNP build 151 accessed Dec. 8, 2017 https://www.ncbi.nlm.nih.gov/projects/SNP/snp_ref.cgi

Ohno S and Nakajin S (2011) Quantitative analysis of UGT2B28 mRNA expression by real-time RT-PCR and application to human tissue distribution study. *Drug Metab Lett* **5:**202-208.

Ouzzine M, Magdalou J, Burchell B, and Fournel-Gigleux S (1999) An internal signal sequence mediates the targeting and retention of the human UDP-glucuronosyltransferase 1A6 to the endoplasmic reticulum. *J Biol Chem* **274:**31401-31409.

Patel YM, Stram DO, Wilkens LR, Park SS, Henderson BE, Le Marchand L, Haiman CA, and Murphy SE (2015) The contribution of common genetic variation to nicotine and

cotinine glucuronidation in multiple ethnic/racial populations. *Cancer Epidemiol Biomarkers Prev* **24:**119-127.

Pattanawongsa A, Nair PC, Rowland A, and Miners JO (2016) Human UDP-Glucuronosyltransferase (UGT) 2B10: Validation of Cotinine as a Selective Probe Substrate, Inhibition by UGT Enzyme-Selective Inhibitors and Antidepressant and Antipsychotic Drugs, and Structural Determinants of Enzyme Inhibition. *Drug Metab Dispos* **44:**378-388.

Radominska-Pandya A, Bratton SM, Redinbo MR, and Miley MJ (2010) The crystal structure of human UDP-glucuronosyltransferase 2B7 C-terminal end is the first mammalian UGT target to be revealed: the significance for human UGTs from both the 1A and 2B families. *Drug Metab Rev* **42:**133-144.

Rath A, Glibowicka M, Nadeau VG, Chen G, and Deber CM (2009) Detergent binding explains anomalous SDS-PAGE migration of membrane proteins. *Proc Natl Acad Sci U S A* **106:**1760-1765.

Rouleau M, Roberge J, Bellemare J, and Guillemette C (2014) Dual roles for splice variants of the glucuronidation pathway as regulators of cellular metabolism. *Mol Pharmacol* **85:**29-36.

Rouleau M, Tourancheau A, Girard-Bock C, Villeneuve L, Vaucher J, Duperre AM, Audet-Delage Y, Gilbert I, Popa I, Droit A, and Guillemette C (2016) Divergent Expression and Metabolic Functions of Human Glucuronosyltransferases through Alternative Splicing. *Cell Rep* **17:**114-124.

Sato Y, Nagata M, Tetsuka K, Tamura K, Miyashita A, Kawamura A, and Usui T (2014) Optimized methods for targeted peptide-based quantification of human uridine 5'-diphosphate-glucuronosyltransferases in biological specimens using liquid chromatography-tandem mass spectrometry. *Drug Metab Dispos* **42:**885-889.

Tourancheau A, Margaillan G, Rouleau M, Gilbert I, Villeneuve L, Levesque E, Droit A, and Guillemette C (2016) Unravelling the transcriptomic landscape of the major phase II UDP-glucuronosyltransferase drug metabolizing pathway using targeted RNA sequencing. *Pharmacogenomics J* **16:**60-70.

Tourancheau A, Rouleau M, Guauque-Olarte S, Villeneuve L, Gilbert I, Droit A, and Guillemette C (2017) Quantitative profiling of the UGT transcriptome in human drug-metabolizing tissues. *Pharmacogenomics J*. *In press.*

Turgeon D, Carrier JS, Levesque E, Hum DW, and Belanger A (2001) Relative enzymatic activity, protein stability, and tissue distribution of human steroid-metabolizing UGT2B subfamily members. *Endocrinology* **142:**778-787.

Turgeon D, Chouinard S, Belanger P, Picard S, Labbe JF, Borgeat P, and Belanger A (2003) Glucuronidation of arachidonic and linoleic acid metabolites by human UDP-glucuronosyltransferases. *J Lipid Res* **44:**1182-1191.

Ware JJ, Chen X, Vink J, Loukola A, Minica C, Pool R, Milaneschi Y, Mangino M, Menni C, Chen J, Peterson RE, Auro K, Lyytikainen LP, Wedenoja J, Stiby AI, Hemani G, Willemsen G, Hottenga JJ, Korhonen T, Heliovaara M, Perola M, Rose RJ, Paternoster L, Timpson N, Wassenaar CA, Zhu AZ, Davey Smith G, Raitakari OT, Lehtimaki T, Kahonen M, Koskinen S, Spector T, Penninx BW, Salomaa V, Boomsma DI, Tyndale RF, Kaprio J, and Munafo MR (2016) Genome-Wide Meta-Analysis of Cotinine Levels in Cigarette Smokers Identifies Locus at 4q13.2. *Sci Rep* **6:**20092.

Zhou D, Guo J, Linnenbach AJ, Booth-Genthe CL, and Grimm SW (2010) Role of human UGT2B10 in N-glucuronidation of tricyclic antidepressants, amitriptyline, imipramine, clomipramine, and trimipramine. *Drug Metab Dispos* **38:**863-870.

Zhukov A and Ingelman-Sundberg M (1999) Relationship between cytochrome P450 catalytic cycling and stability: fast degradation of ethanol-inducible cytochrome P450

2E1 (CYP2E1) in hepatoma cells is abolished by inactivation of its electron donor NADPH-cytochrome P450 reductase. *Biochem J* **340 (Pt 2):**453-458.

Footnotes

This work was supported by the Canadian Institutes of Health Research [FRN-42392]; and the Canada Research Chair in Pharmacogenomics (Tier I); AL and EPA were supported by graduate scholarships from the "Fonds d'enseignement et de recherche" (FER) of the Faculty of pharmacy, Laval University (graduate scholarship); YAD was supported by a graduate scholarship from the "Fonds de Recherche en Santé du Québec". The Genotype-Tissue Expression (GTEx) Project was supported by the Common Fund of the Office of the Director of the National Institutes of Health, and by National Cancer Institute (NCI), National Human Genome Research Institute (NHGRI), National Heart, Lung, and Blood Institute, National Institute on Drug Abuse, National Institute of Mental Health, and National Institute of Neurological Disorders and Stroke and The Cancer Genome Atlas (TCGA) is managed by the NCI and NHGRI (http://cancergenome.nih.gov).

Figure legends

Figure 1. Schematic overview of *UGT2B10* mRNA transcripts and encoded proteins. *Top*. The UGT2B10 gene is comprised of 6 canonical exons and 2 alternative exons 6b and 6c. *Bottom*. The canonical *UGT2B10_v1* transcript encodes the UGT2B10_i1 enzyme. Alternative splicing produces 3 classes of variants, with N-terminal or C-terminal truncations, and novel C-terminal sequence. The N-terminally truncated *UGT2B10_n3 and _n4* variants are reported in the NCBI RefSeq UGT2B10 gene entry (https://www.ncbi.nlm.nih.gov/gene/7365) to encode, respectively, isoforms i3 and i2 in RefSeq. Consequently, the isoform encoded by the transcripts *n9* and *n10* were named i4 and i5 respectively. Exons are represented by colored boxes and skipped exons by dashed boxes. Thinner parts of exons 1 and 6 represent untranslated regions. UGT2B10 is the UGT2B with the largest 3'untranslated region and only the first 279 of 1424 nucleotides of exon 6 are coding in the canonical mRNA. Note that the predicted molecular weight of mature proteins is smaller by 2.5 kDa due to the cleavage of the signal peptide.

Figure 2. **Alternative splicing diversifies the hepatic *UGT2B10* transcriptome.** A. Relative levels of canonical (*v1*) and alt. transcript classes in the normal human liver and in hepatocellular carcinoma. The ΔC-term+new sequence class is predominantly comprised of *n9* and *n10* transcripts whereas transcript *n8* represented less than 2% in normal and tumor tissues. B. Interindividual variability in *UGT2B10* expression for all transcripts (Total), canonical (*v1*) and alt. transcripts (*n9/n10*). Boxes represent 25-75 percentiles, whiskers 10-90 percentiles. Median is indicated by the horizontal line and mean by a "+". CV, coefficient of variation; FC, fold change; N: normal tissues; T: tumor tissues; TPM: transcripts per million. C. Correlation between *UGT2B10_v1* and *n9/n10* expression in normal livers and hepatocellular carcinoma. All expression data were derived by a realignement of RNA-Seq data from GTEx (n = 50) and TCGA (n = 44) to the fully annotated UGT variant sequence (Tourancheau et al., 2016).

Figure 3. **Alternate UGT2B10 protein is expressed in the human liver. A.** C-terminal amino acid sequences of the UGT2B10 enzyme (i1) and alt. isoforms i4 and i5. Sequences unique to each alt. proteins are italicized. TMD: transmembrane domain; K: ER retention signal. **B.** Experimental approach for the detection of UGT2B10_i5 by immunoprecipitation and multiple reaction monitoring (MRM). **C.** The common UGT2B10 peptide NSWNFK (left) and the alt. specific peptide LLGSSNNPPILASQR (right) were detected in tryptic digests of

UGT2B10 immunoprecipitated from human liver samples (upper chromatograms). The chromatograms of control peptides (lower chromatograms) labelled with stable isotopes mixed with the immunopurified UGT2B10 confirmed the identity of i1 and i5 peptides. Representative chromatograms are shown (n = 2).

Figure 4. Interaction of UGT2B10 isoforms in the ER. **A.** Stable expression of UGT2B10 alternative isoforms in HEK293 and HepG2 cell models. UGT2B10 was detected in microsomal fractions of each cell model (20 µg proteins) and of human liver (L) using the anti-UGT2B10 antibody. The expression ratio of the UGT2B10 enzyme relative to alt. isoforms is estimated to more than 4 fold in each model. Note that the apparent molecular weight of the enzyme was lower than predicted, likely explained by the influence of the hydrophobic amino acids in the transmembrane domains (TMD) that perturb the interactions with SDS and the shape of the denatured protein (Rath et al., 2009). **B.** UGT2B10 enzyme and alt. isoforms (i4 and i5) co-localized with the ER marker protein disulfide isomerase (PDI). Merged images of UGT2B10 proteins labelled with anti-UGT2B10 (green), PDI (red), and nuclei (blue) are shown. Separate images and co-localization with other subcellular markers are shown in **Supplemental Figure 3**. Bar = 10 µm. **C.** Glycosylation status of the UGT2B10 enzyme and alt. proteins. UGT2B10 proteins in microsomes from HEK293 cell models subjected to endoglycosidase H (Endo H) or O-glycosidase were detected by immunoblotting.

Figure 5. The alternative UGT2B10 isoforms modulate the glucuronidation activity of the UGT2B10 enzyme. A-B. *In situ* cell glucuronidation assays of amitriptyline and levomedetomidine in HEK293 and HepG2 cell models that co-express the alt. isoforms i4 an i5. Activity is presented relative to that in cells expressing only the UGT2B10 enzyme (control). Assays were conducted twice in triplicates. *t*, $P \leq 0.1$; *, $P \leq 0.05$; **, $P \leq 0.01$; ***, $P \leq 0.001$. **C.** Co-immunoprecipitation of the UGT2B10 enzyme with alt. isoforms i4 and i5 expressed in HEK293. Alternative isoforms were C-terminally tagged with the epitope V5 and immunoprecipitated (IP) with the anti-V5 antibody.

Figure 6. Stability of UGT2B10 proteins. A. The half-life of UGT2B10 proteins was determined by translational inhibition with cycloheximide (CHX) in HEK293 and HepG2 cell models. Protein levels were measured by densitometry scanning of immunoblots from two independent assays and are expressed as % of untreated cells. Half-lives were averaged from the two independent assays. A representative experiment is shown. An independent

replicate assay is presented in **Supplemental Figure 4. B.** UGT2B10 alternative isoforms are stabilized by proteasomal inhibition. HEK293 and HepG2 cell models were exposed to vehicle only (DMSO; lane "-") or MG132 (1 µM; lanes "+") for 16 h. UGT2B10 was detected by immunoblotting total cell lysates (40 µg) with anti-UGT2B10.

Figure 7. Differential induction of alt. UGT2B10 by phenobarbital and a CAR agonist in HepaRG cells. Expression data of *UGT2B10* canonical and alt. transcripts *n9* and *n10* (encoding i4 and i5) in HepaRG cells wild type (WT) or with a knock-out of the constitutive androstane recetor (CAR KO) were obtained from the public RNA-seq data GSE 71446. Cells were treated either with vehicle (DMSO), phenobarbital (PB, 1 mM) or the CAR agonist CITCO (1 µM) for 24 h as described (Li et al., 2015). **, $P \leq 0.01$; ***, $P \leq 0.001$.

Figure 1

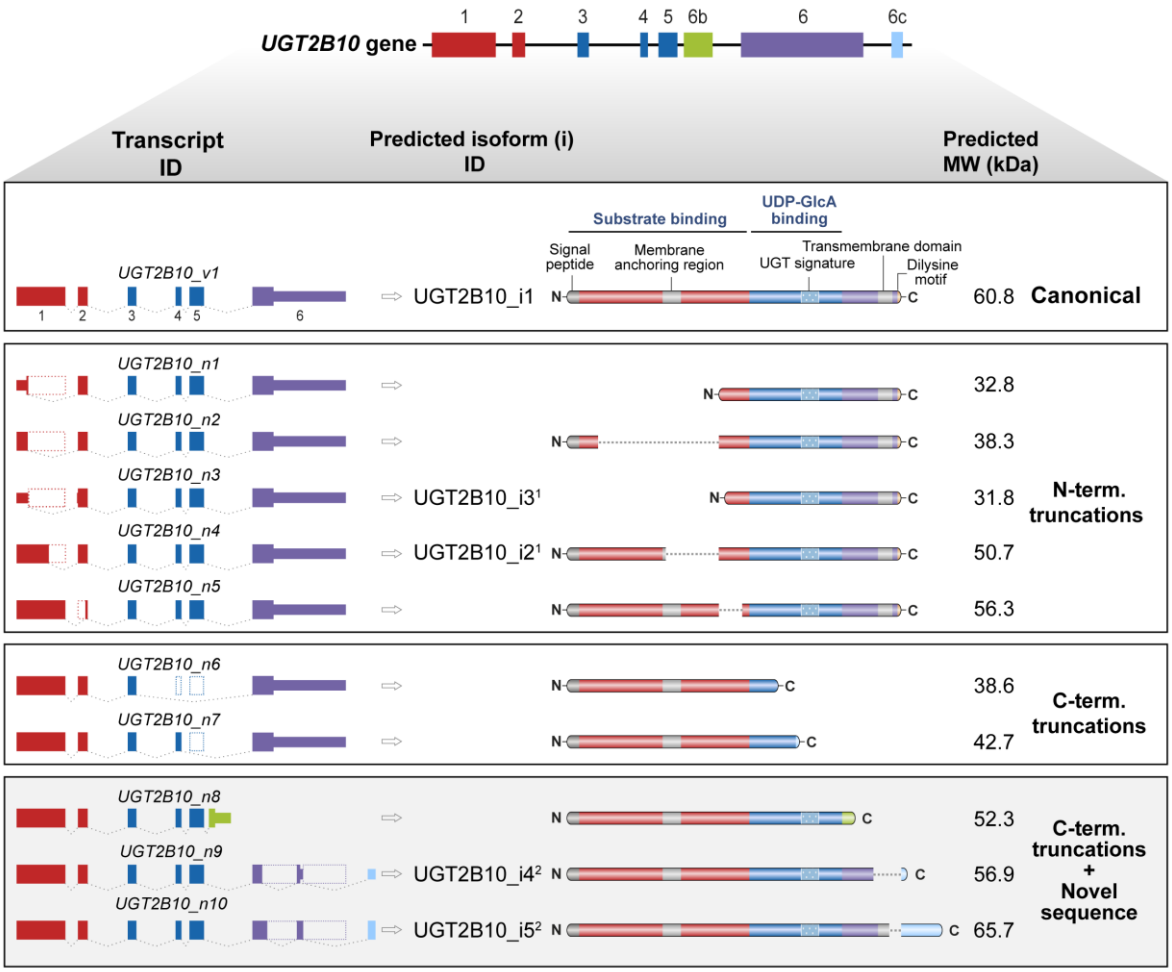

[1]Nomenclature from RefSeq *Homo sapiens* annotation release 108 (https://www.ncbi.nlm.nih.gov/gene/7365)
[2]Nomenclature from Tourancheau et al. (2017)

☐ Focus of this study

Figure 2

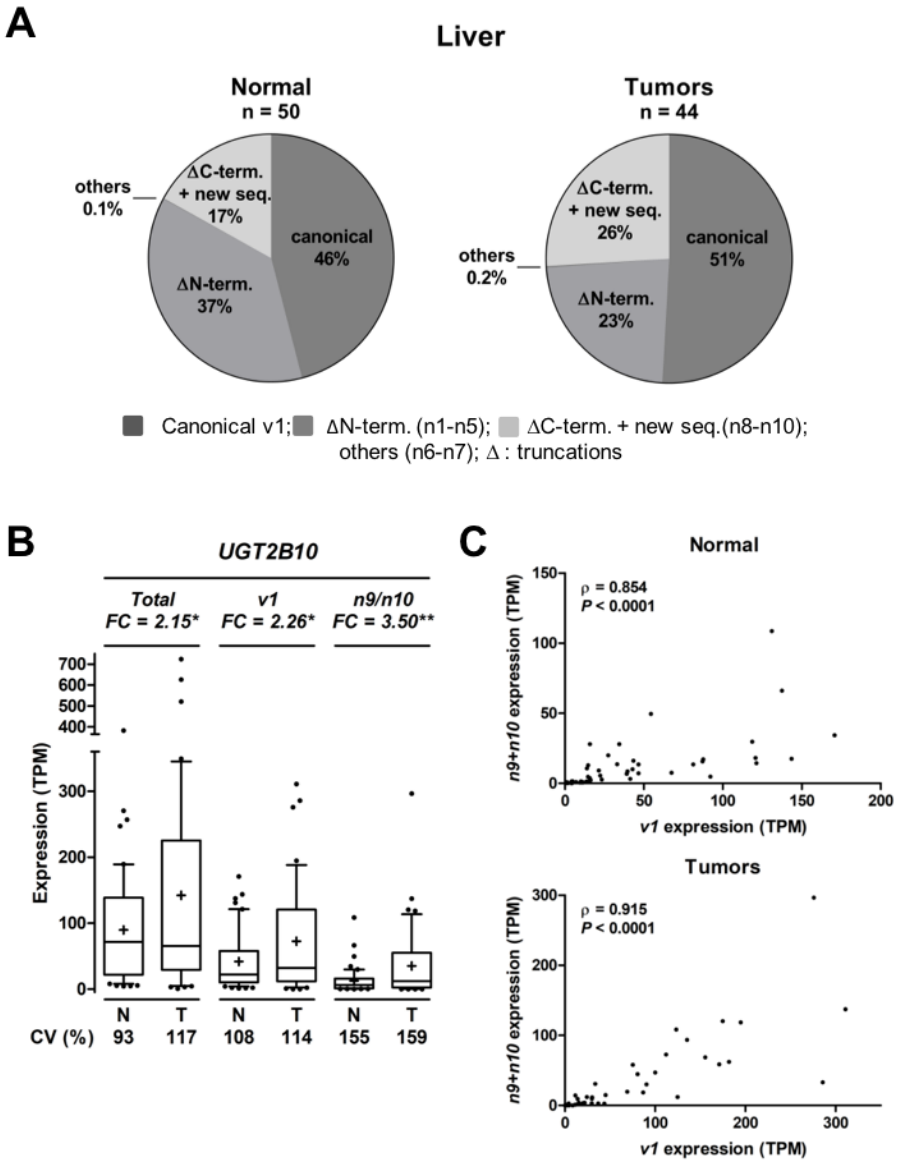
A
Liver
Normal
n = 50
others 0.1%
ΔC-term. + new seq. 17%
canonical 46%
ΔN-term. 37%
Tumors
n = 44
others 0.2%
ΔC-term. + new seq. 26%
canonical 51%
ΔN-term. 23%
Canonical v1; ΔN-term. (n1-n5); ΔC-term. + new seq.(n8-n10); others (n6-n7); Δ : truncations
B
UGT2B10
Total FC = 2.15*
v1 FC = 2.26*
n9/n10 FC = 3.50**
Expression (TPM)
CV (%) 93 117 108 114 155 159
C
Normal
ρ = 0.854
P < 0.0001
n9+n10 expression (TPM)
v1 expression (TPM)
Tumors
ρ = 0.915
P < 0.0001
n9+n10 expression (TPM)
v1 expression (TPM)

Figure 3

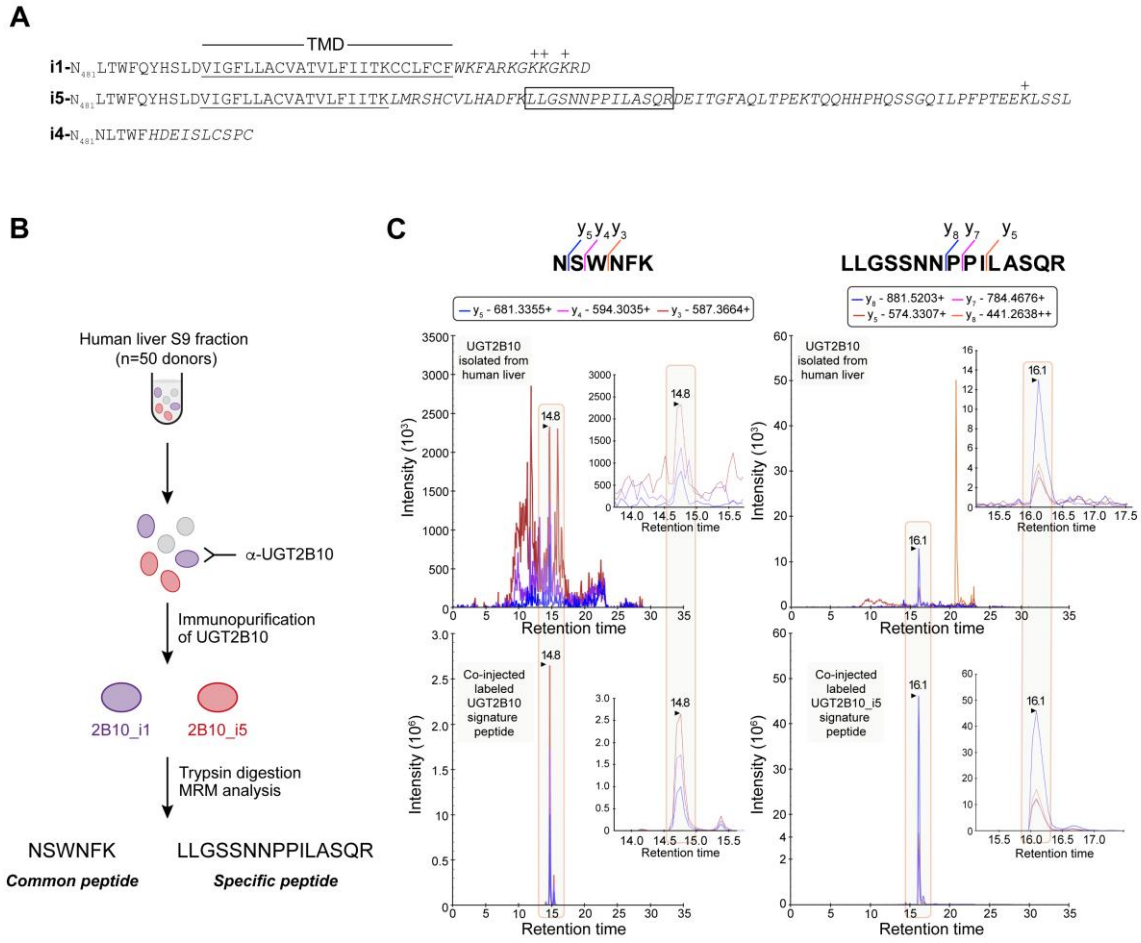
A
TMD
i1-N481LTWFQYHSLDVIGFLLACVATVLFIITKCCLFCFWKFARKGKKGKRD
i5-N481LTWFQYHSLDVIGFLLACVATVLFIITKLMRSHCVLHADFKLLGSNNPPILASQRDEITGFAQLTPEKTQQHHPHQSSGQILPFPTEEKLSSL
i4-N481NLTWFHDEISLCSPC
B
Human liver S9 fraction
(n=50 donors)
α-UGT2B10
Immunopurification
of UGT2B10
2B10_i1
2B10_i5
Trypsin digestion
MRM analysis
NSWNFK
Common peptide
LLGSSNNPPILASQR
Specific peptide
C
NSWNFK
LLGSSNNPPILASQR
UGT2B10
isolated from
human liver
Co-injected
labeled
UGT2B10
signature
peptide
Co-injected
labeled
UGT2B10_i5
signature
peptide
Intensity
Retention time
14.8
16.1

Figure 4

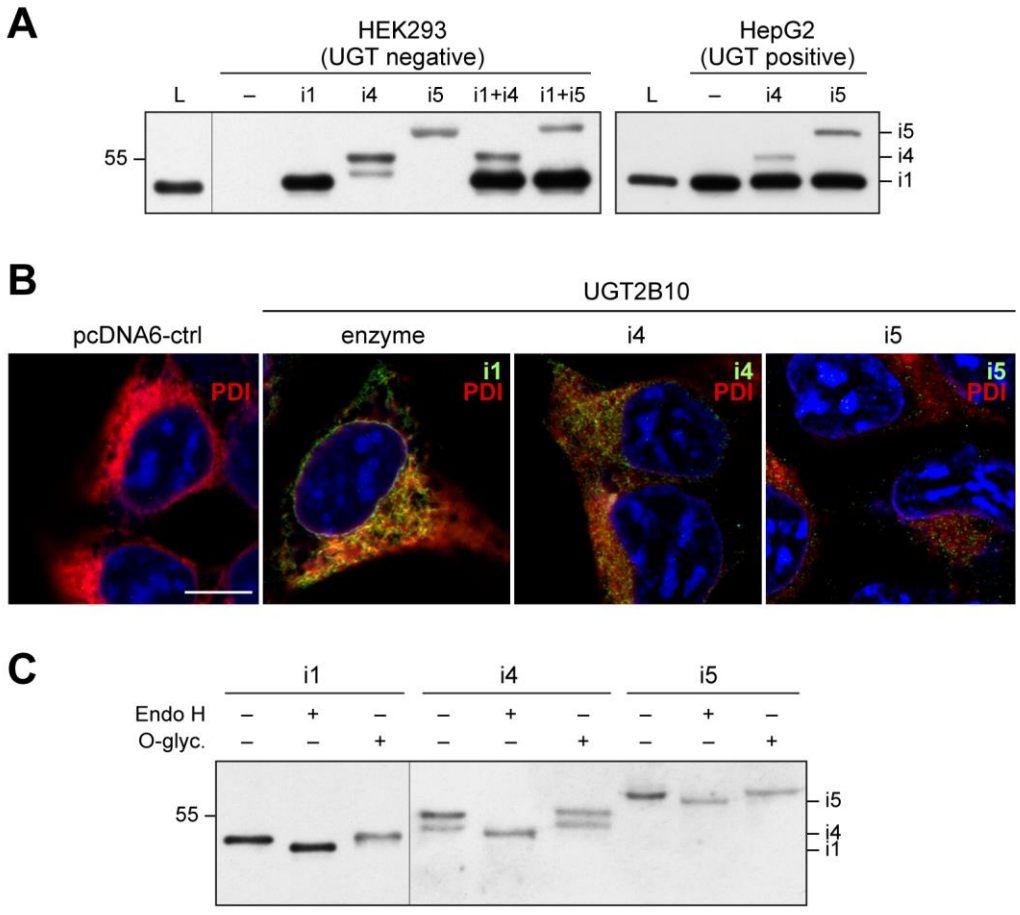
A
HEK293
(UGT negative)
HepG2
(UGT positive)
L
–
i1
i4
i5
i1+i4
i1+i5
L
–
i4
i5
55
i5
i4
i1
B
UGT2B10
pcDNA6-ctrl
enzyme
i4
i5
PDI
i1
PDI
i4
PDI
i5
PDI
C
i1
i4
i5
Endo H
O-glyc.
55
i5
i4
i1

Figure 5

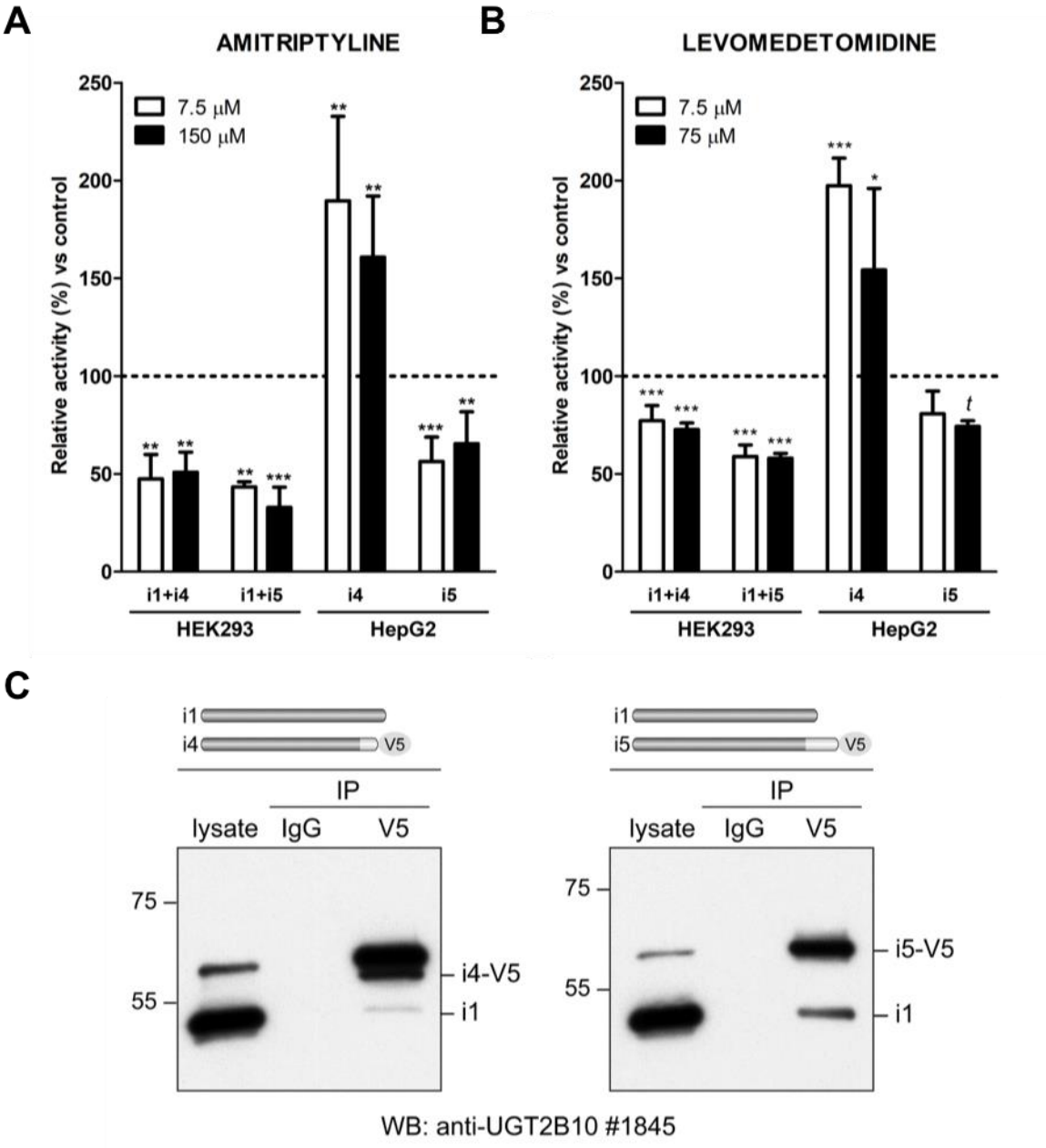
A
AMITRIPTYLINE
7.5 μM
150 μM
Relative activity (%) vs control
250
200
150
100
50
0
i1+i4
i1+i5
i4
i5
HEK293
HepG2
B
LEVOMEDETOMIDINE
7.5 μM
75 μM
Relative activity (%) vs control
i1+i4
i1+i5
i4
i5
HEK293
HepG2
C
i1
i4
V5
i5
IP
lysate
IgG
V5
75
55
i4-V5
i5-V5
i1
WB: anti-UGT2B10 #1845

Figure 6

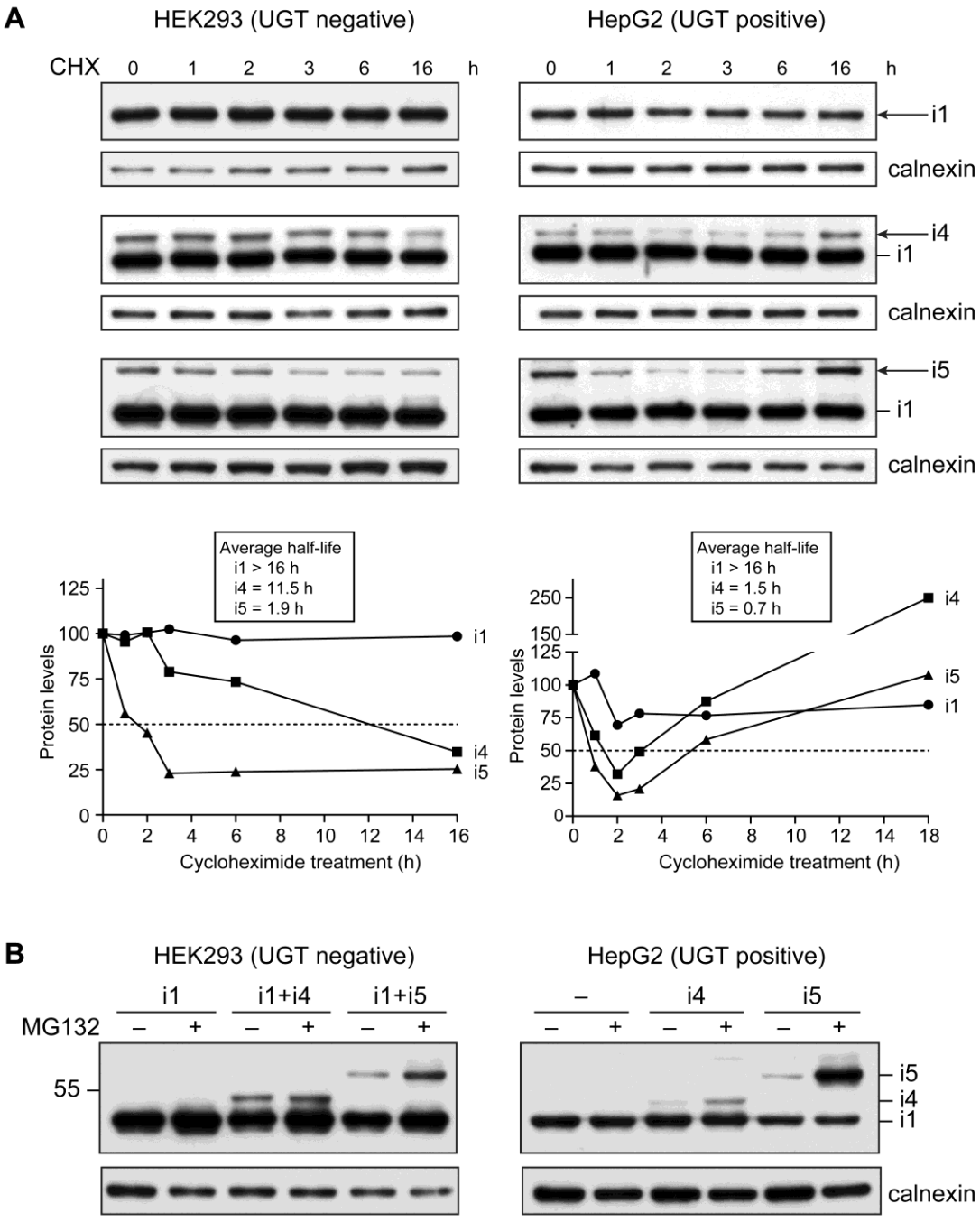
A
HEK293 (UGT negative)
HepG2 (UGT positive)
CHX
0 1 2 3 6 16 h
i1
calnexin
i4
i5
Average half-life
i1 > 16 h
i4 = 11.5 h
i5 = 1.9 h
Average half-life
i1 > 16 h
i4 = 1.5 h
i5 = 0.7 h
Protein levels
Cycloheximide treatment (h)
B
HEK293 (UGT negative)
HepG2 (UGT positive)
i1
i1+i4
i1+i5
i4
i5
MG132
55

Figure 7

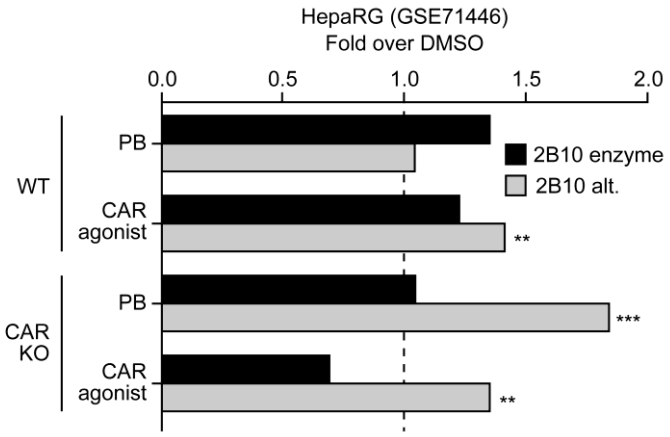
HepaRG (GSE71446)
Fold over DMSO
0.0
0.5
1.0
1.5
2.0
WT
PB
CAR agonist
CAR KO
PB
CAR agonist
2B10 enzyme
2B10 alt.
**
***
**

Supplementary Material

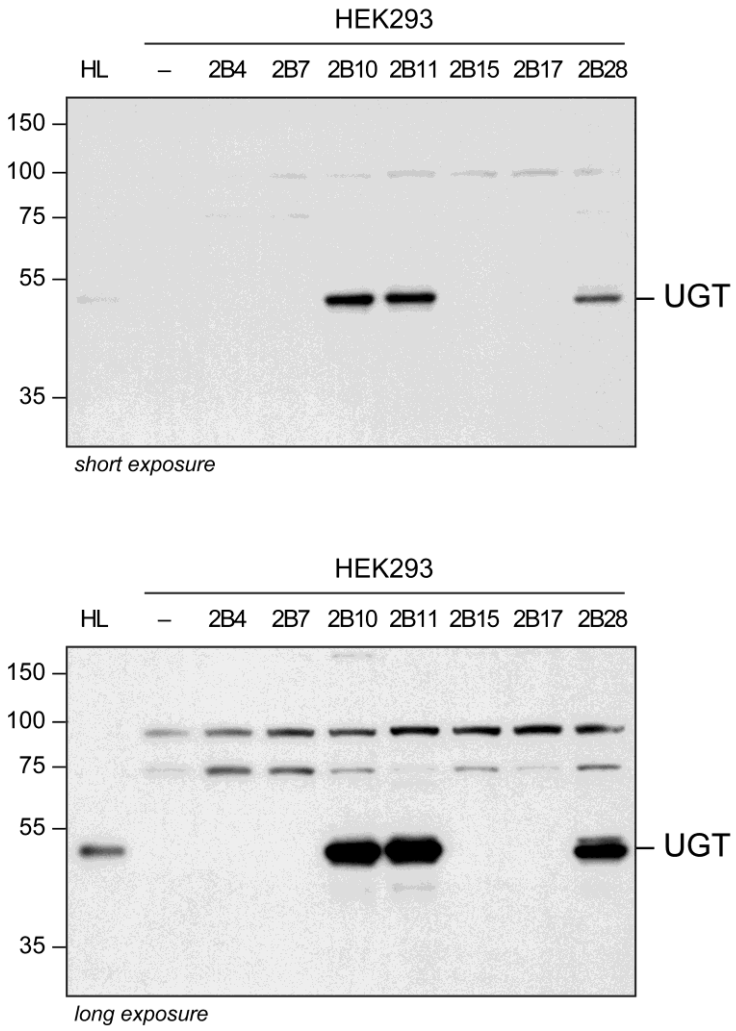

Supplemental Figure 1. Specificity of anti-UGT2B10 #1845 for human UGT enzymes. The microsomal fraction prepared from HEK293 cells (UGT negative) stably expressing each of the seven UGT2B enzymes or transfected with the empty vector pcDNA6 (-) was probed with the anti-UGT2B10 to demonstrate specificity. HL, human liver microsomes. Short and long exposures of the same immunoblot is provided to ascertain specificity.

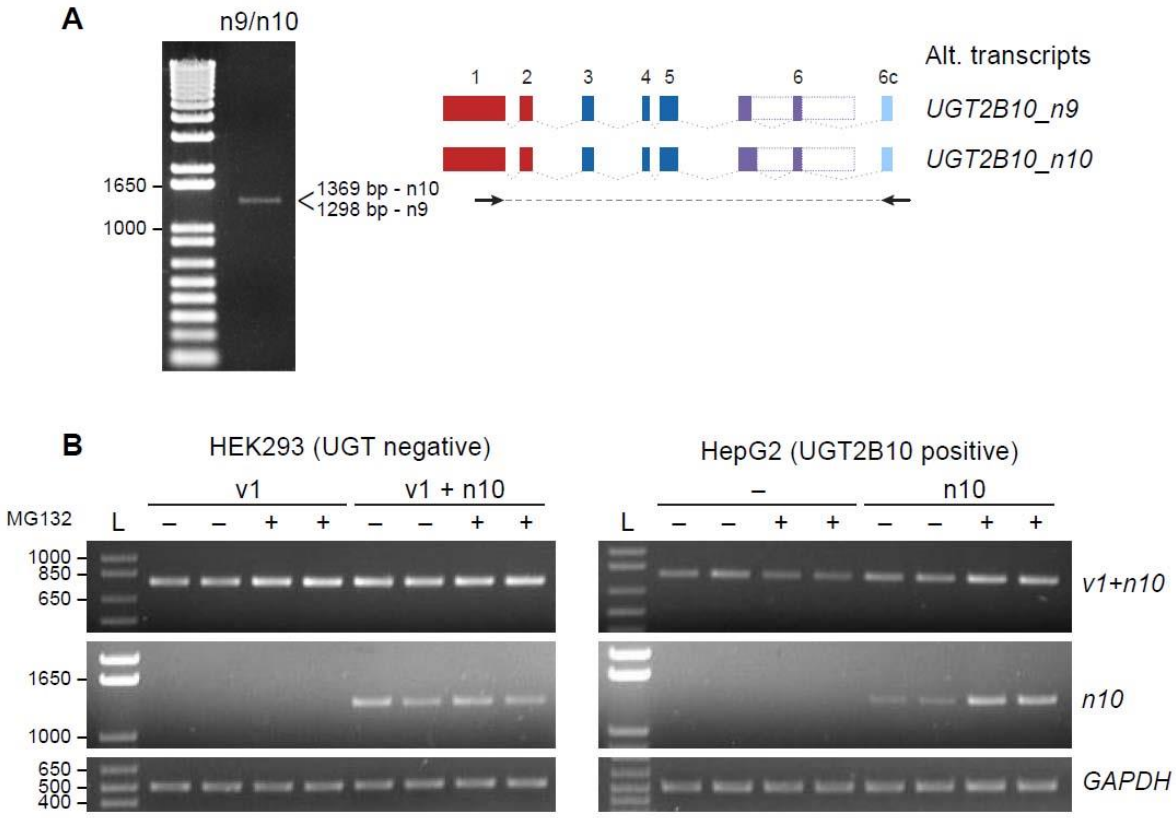

Supplemental Figure 2. RT-PCR amplification of *UGT2B10* transcripts. **A.** Validation of *UGT2B10_n9* and *UGT2B10_n10* expression in human liver. Primers (arrows; 4203F and 4211R) were located in exon 1 and in exon 6c common to both variants. PCR products corresponding to *n9* and *n10* could not be distinguished because they differed by only 71 base pairs (bp). The identity of PCR products as n9 and n10 was verified by Sanger sequencing. **B.** RT-PCR detection of transcripts in cell models exposed to MG132. PCR strategies specified on the right either amplified both *v1* and *n10* or only *n10*. GAPDH served as a positive and loading control. L: molecular weight ladder.

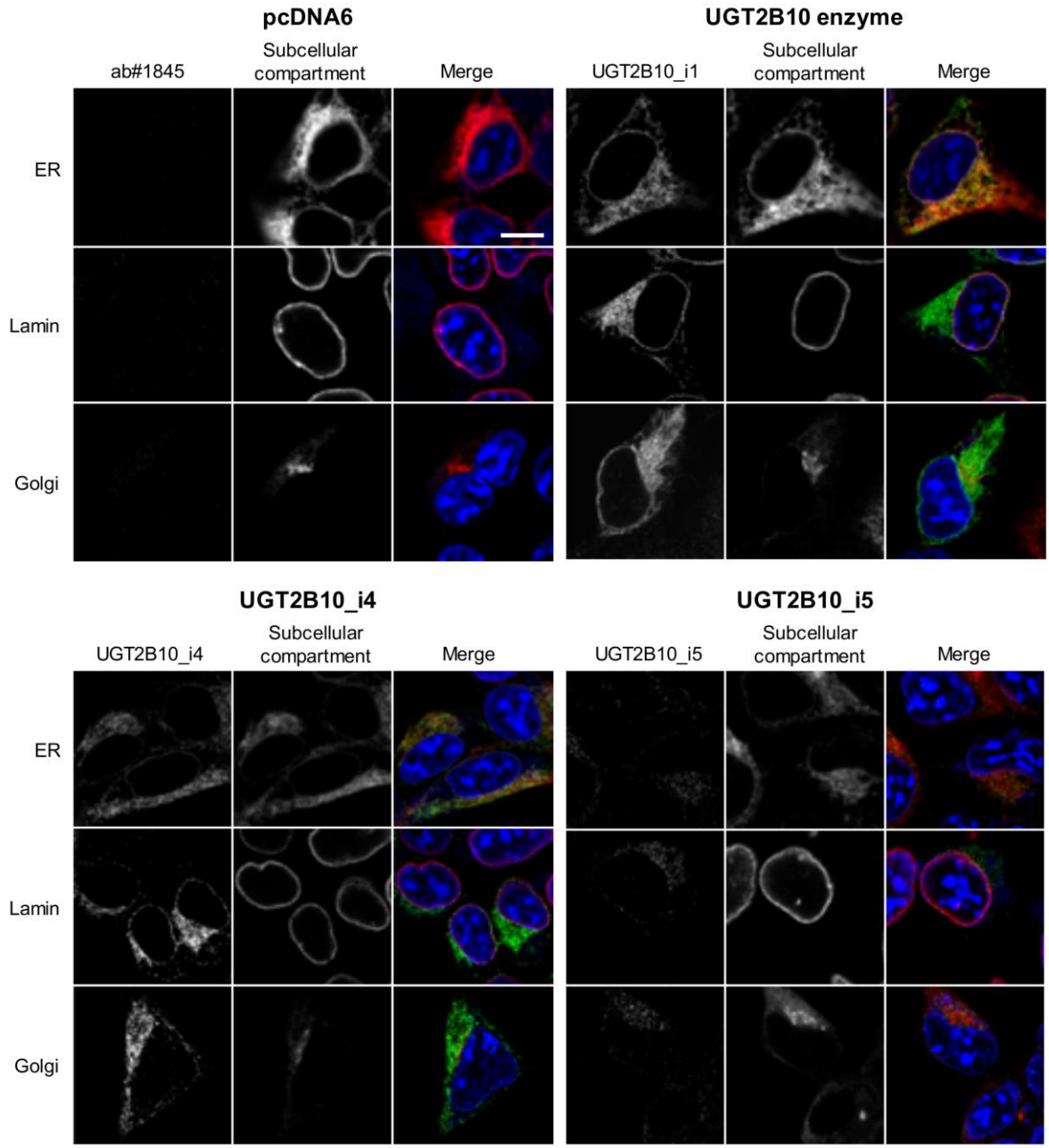

Supplemental Figure 3. Subcellular localization of UGT2B10 and alternative isoforms expressed in HEK293. UGT2B10 proteins were detected with #1845, and cellular compartments with specific markers as described in Materials and Methods. In merged images, nuclei are stained with DRAQ5. Bar represents 10 µm. Control HEK293 cells were transfected with the empty vector pcDNA6.

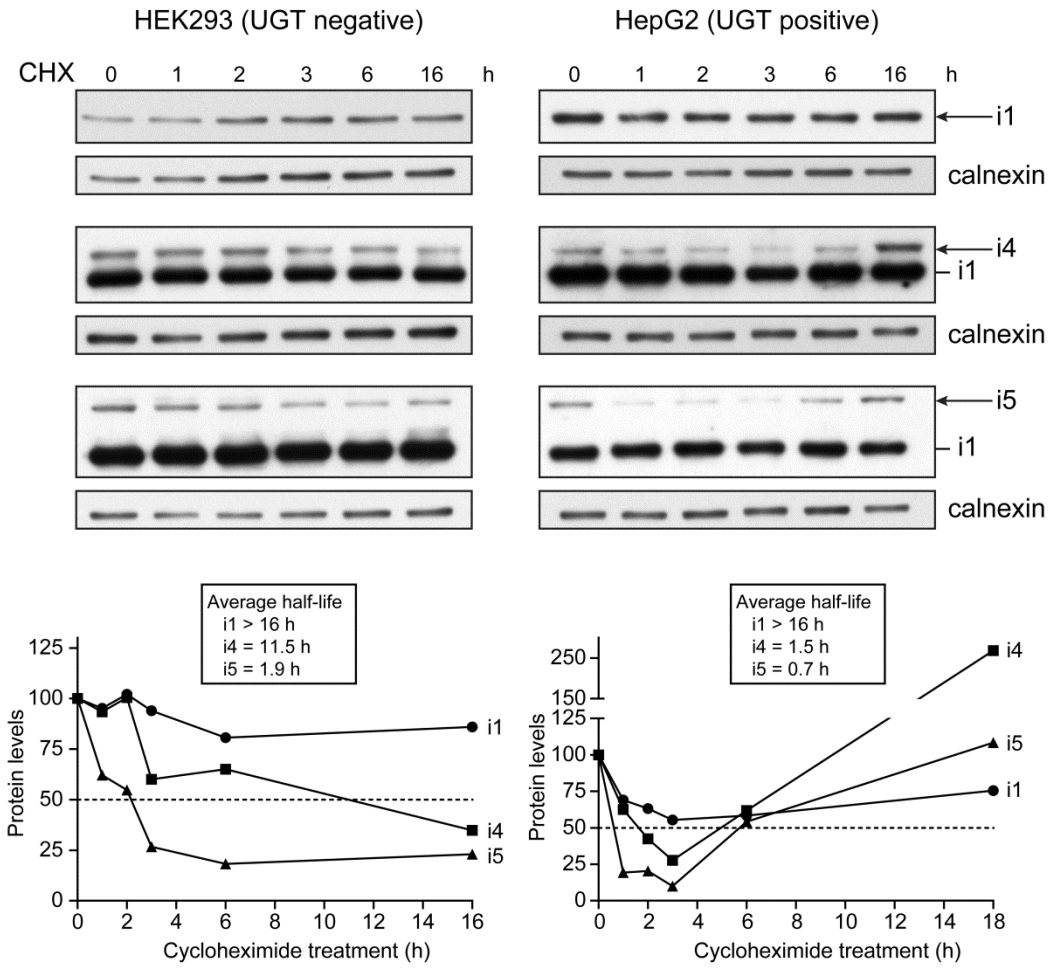

Supplemental Figure 4. Stability of UGT2B10 proteins - Replicate assay. The half-life of UGT2B10 proteins were determined by translational inhibition with cycloheximide (CHX) in HEK293 and HepG2 cell models. Protein levels were measured by densitometry scanning of immunoblots from two independent assays. Half-lives were averaged from the two biological replicates. Related to Fig.6A.

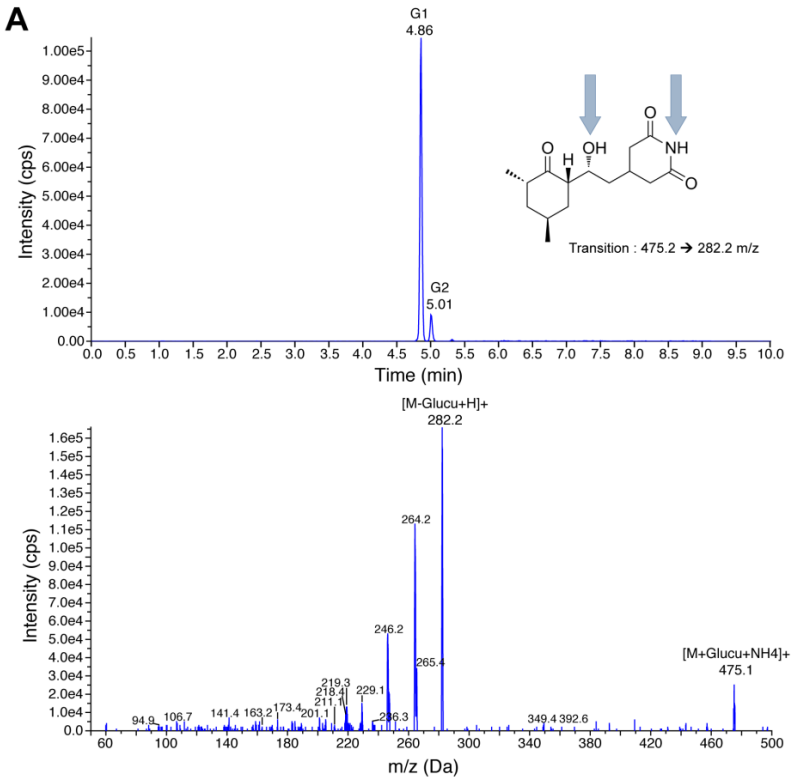

B

	Cycloheximide (area/h/µg protein)	
	G1	**G2**
Human Liver	202917	10234
HepG2	5901	582
UGT1A1	177	1
UGT1A3	68	-
UGT1A4	8	-
UGT1A6	-	-
UGT1A9	215208	1247
UGT2B4	278	5
UGT2B7	135573	8016
UGT2B10	-	-
UGT2B11	-	-

G : glucuronide;
- : below limit of detection

Supplemental Figure 5. Analysis of cycloheximide glucuronidation by high-performance liquid chromatography tandem mass spectrometry. **A**. Human liver microsomes produced two cycloheximide glucuronides (G1 and G2). Representative chromatograms of cycloheximide glucuronides (top) and their fragmentation pattern (bottom). Putative glucuronidation sites are indicated by blue arrows in the chemical structure of cycloheximide. **B**. Glucuronidation activity of microsomes from human liver, HepG2 pcDNA6, HEK-UGT2B11 and of commercial UGT supersomes. Two independent assays were conducted in triplicate.

```
UGT2B10_i5              510  lmrSHcVlhAdfKLLGSnNPPiLASQrdEITGfaqltpektqq  48
SP|P51790-5|CLCN3_i4      6  lgeSHyVvQAGLqLLGSSNPPaLASQvAEITGthytmtnggsi  47
SP|Q96EP1-3|CHFR_i3     135  emvpccVAQAGLKLLGSSdPPTLASQSIvITGsggggispkgs  57
NP_001339349|ALG9_ii    401  asrSqfVAQAGLKLLGSSNPPTsASQnIGITGlshrawpltsp  60
XP_011508885|MITD1_iX5  150  qtgfHhVAQAGLKLLGSSsPPTLASQSAGITGMshctqphyly  52
                             * :* ::****  **  ***   ***
```

Supplemental Figure 6. Sequence similarity of the UGT2B10_i5 unique sequence with other alt. human proteins. A BLASTp search with the unique C-terminal UGT2B10_i5 amino acid sequence revealed a conserved region encoded by the frame shift in exon 6 (boxed). asterisk: conserved amino acid; colon: conservative substitution. Alignment was produced with the Clustal Omega tool available at www.Uniprot.org.

Table S1. Primers used in this study.

Target	Primer	Sequence (5' to 3')
Cloning		
UGT2B10_ n9	4238F	TGTTCTCCATGCTGACTCGAGTCTAGAGGGCCC
	4239R	CAATGAGATCTCATCATGGAACCAGGTGAGGTTG
UGT2B10_n10	4240F	AACAATCCTCCCATTTTAGCATCCCAAAGGGATGAGATTACAGGTTTTGCTCGAGTCTAGAGGGCCC
	4241R	TGAGCCCAGGAGTTTGAAATCAGCATGGAGAACACAATGAGATCTCATCAACTTTGTGATGATAAATAGCACGG
	4242F	TGGACAAATTCTTCCATTTCCTACAGAGGAAAAACTTTCTTCATTATAACTCGAGTCTAGAGGGCCC
	4243R	GAGCTCTGATGAGGATGGTGTTGTTGTGTTTTCTCTGGAGTCAGTTGTGCAAAACCTGTAATCTCATCCCTTTG
Validation		
v1, n9, n10		
Exon 1	1894F	AGATTTGACATCGTTTTTGCAGATGCTTA
Exon 4	1895R	CCTTCATGTGAGCAATATTATCAGGTTGATCAAA
n9, n10		
Exon 1	4203F	GTTAAGAGATTGTCAGAAATTCA
Exon 6c	4211R	TCTCTGGAGTCAGTTGTGC
GAPDH	1904F	TGGGTGTGAACCATGAG
	1905R	CCCAGCGTCAAAGGTGG

Chapitre 6 : « Divergent Expression and Metabolic Functions of Human Glucuronosyltransferases through Alternative Splicing »

Résumé

Le maintien de l'homéostasie cellulaire et la détoxication des xénobiotiques sont médiés par 19 enzymes UGT, encodées par 10 gènes et formant la voie de glucuronidation. Le séquençage en profondeur de l'ARN dans les principaux organes du métabolisme des médicaments a révélé une expansion substantielle du transcriptome UGT par l'épissage alternatif, où les variants représentent de 20% à 60% de l'expression des transcrits canoniques. Près d'un cinquième des variants incluent une insertion d'exon dans le cadre de lecture qui pourrait créer des différences structurales et fonctionnelles. Des essais cellulaires ont révélé des fonctions biologiques pour ces protéines alternatives des UGT. Certaines isoformes inhibent ou induisent l'inactivation de médicaments et d'hormones stéroïdiennes, en plus de perturber le métabolisme cellulaire global (voies énergétiques, acides aminés, nucléotides), l'adhésion et la prolifération cellulaire. Ces travaux soutiennent l'importance biologique de l'expression des protéines alternatives UGT et leur potentiel d'agir comme régulateur du métabolisme.

Divergent expression and metabolic functions of human glucuronosyltransferases through alternative splicing

Michèle Rouleau[1], Alan Tourancheau[1], Camille Girard-Bock[1], Lyne Villeneuve[1], Jonathan Vaucher[2], Anne-Marie Duperré[1], Yannick Audet-Delage[1], Isabelle Gilbert[1], Ion Popa[2], Arnaud Droit[2], Chantal Guillemette[1¥]

[1]Pharmacogenomics Laboratory, Centre Hospitalier Universitaire (CHU) de Québec Research Center, Québec, QC, Canada and Faculty of Pharmacy, Laval University, Québec, Canada, G1V 4G2

[2]Faculty of Medicine, Laval University, Québec, Canada, G1V 0A6

[¥]Canada Research Chair in Pharmacogenomics

Corresponding Author/Lead Contact:

Chantal Guillemette, Ph.D.
Canada Research Chair in Pharmacogenomics
Pharmacogenomics Laboratory
CHU de Québec Research Center
2705 Blvd. Laurier, R4720
Québec, Canada, G1V 4G2
Tel. (418) 654-2296
E-mail: Chantal.Guillemette@crchudequebec.ulaval.ca

Summary

Maintenance of cellular homeostasis and xenobiotic detoxification is mediated by 19 human UDP-glucuronosyltransferase enzymes (UGTs) encoded by 10 genes that comprise the glucuronidation pathway. Deep RNA sequencing of major metabolic organs exposes a substantial expansion of the UGT transcriptome by alternative splicing, with variants representing 20 to 60% of canonical transcript expression. Nearly a fifth of expressed variants comprise in-frame sequences that may create distinct structural and functional features. Follow up cell-based assays reveal biological functions for these alternative UGT proteins. Some isoforms were found to inhibit or induce inactivation of drugs and steroids in addition to perturbing global cell metabolism (energy, amino acids, nucleotides), cell adhesion and proliferation. This work highlights the biological relevance of alternative UGT expression, which we propose increases protein diversity through evolution of metabolic regulators from specific enzymes.

Introduction

Human glycosyltransferases utilize different sugar nucleotide donors to regulate a wide variety of cellular processes (Breton et al., 2012; De Bruyn et al., 2015; Guillemette et al., 2004; Little et al., 2004; Rowland et al., 2013). One large family of membrane-associated uridine diphospho-glucuronosyltransferases (UGTs) employ uridine diphospho-glucuronic acid (UDPGA) to conjugate a variety of small-molecule acceptors and catalyze the most important metabolic pathway for the human body's elimination of both endogenous and exogenous lipophilic molecules. These endoplasmic reticulum (ER) resident type I membrane proteins transfer the sugar moiety of the co-substrate UDPGA to the nucleophilic functional group of their substrates to promote, in most cases, their inactivation and elimination. Glucuronidation affects bioactivity and bioavailability of harmful xenobiotics, chemicals, and drugs from food, the environment, or pharmacological treatments. In parallel, glucuronidation maintains the homoeostasis of the heme-breakdown product bilirubin, multiple endogenous hormones, secondary metabolites, and other endobiotics (Bock, 2015; Guillemette, 2003; Radominska-Pandya et al., 1999; Wells et al., 2004).

In humans, 10 genes encode 19 canonical UGT enzymes (isoform 1s or i1s) that display remarkable plasticity. For example, a single *UGT1* gene on chromosome 2q37 encodes nine UGT1A enzymes through usage of individual alternative promoters and first exons, whereas 10 UGT2 enzymes (three UGT2A and seven UGT2B) are synthesized from nine independent genes clustered on chromosome 4q13 (Mackenzie et al., 2005). Although amino acid sequences among UGTs are highly similar, substrate specificity is dictated by the slightly more divergent first (UGT1) or first/second (UGT2) exons that encode the N-terminal half of each enzyme. UGTs are found in nearly all human tissues and display tissue- and cell type–specific expression, but they are most abundant in metabolically highly active organs such as the liver, kidney, and intestine (Court et al., 2012; Margaillan et al., 2015a; Margaillan et al., 2015b; Rowland et al., 2013).

Alternative splicing (AS) is a key mechanism in the control of gene expression, transcriptomes, and protein diversity, with over 90% of human multi-exon genes undergoing AS regulation before forming mature transcript isoforms (Wang et al., 2008). The important contributions of AS to an individual’s response to endogenous and exogenous molecules, including drugs, and the link to various human diseases are

emerging but remain largely unknown (Gamazon and Stranger, 2014; Garcia-Blanco et al., 2004; Oltean and Bates, 2014). Our recent work established that AS expands the coding capacity of human *UGT*s, allowing over 180 canonical and alternative *UGT* transcripts in various tissues involved in drug metabolism as well as hormone-dependent tissues (Tourancheau et al., 2016). Thus, a large genetic diversity characterizes the transcriptome landscape of human *UGT*s and implies a functional diversification of the UGT proteome that remains unexplored.

In this study, we applied targeted next-generation RNA sequencing (CaptureSeq) (Clark et al., 2015; Mercer et al., 2012) to quantify the UGT transcriptome and expression of alternative transcripts in the liver, kidney, and gastrointestinal tissues, which are most relevant to the metabolic functions of this crucial enzymatic pathway. We further addressed tissue-specific protein expression as well as the function of selected UGT isoforms where in-frame sequences have been introduced using cell-based assays combined with untargeted metabolomics (**Fig. 1**). Our findings reveal a complex expression pattern of UGT alternative variants and distinct functional properties, including antagonizing and inducing UGT transferase function, likely through protein–protein interaction, while inducing substantial rewiring of cell metabolism that affects cellular behavior.

Results

AS contributes to quantitative profiles of the UGT transcriptome in human metabolic tissues

A quantitative transcriptome analysis of all 10 human *UGT1* and *UGT2* genes was conducted in pooled samples of normal liver, kidney, and intestine/colon tissues as well as in tumors originating from the kidney and the intestine/colon. A CaptureSeq approach was used to achieve sufficient sequencing depth and ensure the fullest coverage of alternative UGT variants. Reads were mapped to the human genome sequence (hg19) complemented with the recently published comprehensive human UGT transcriptome (Tourancheau et al., 2016) (**Fig. 1**). The data revealed that AS contributes substantially to the UGT transcriptome landscape, affecting each expressed *UGT1* and *UGT2* gene in a tissue-specific manner, and the AS products are significantly altered in neoplastic tissues (**Fig. 2A, B**). Alternatively spliced species were abundant in normal tissues, representing

an average of 19, 24, and 34% of the total UGT expression in liver, intestine/colon, and kidney, respectively (**Fig. 2C**). In intestine/colon and kidney tumor tissues, these levels were strikingly elevated to an average of 33 and 61%, respectively. Changes in liver cancer could not be assessed owing to the lack of availability of hepatic tumors. The abundance and tissue-specific expression of several alternative transcripts supports a physiologically relevant role in the surveyed tissues.

Diverse structural features of alternative UGT isoforms

A common structural organization is shared by the 19 known human UGT1 and UGT2 enzymes, each encoded by a canonical mRNA variant v1. An N-terminal signal peptide and a C-terminal transmembrane region direct the substrate and UDPGA co-substrate-binding domains and catalytic site of each mature protein to the luminal side of the ER (**Fig. 3A**). Based on these structural features, 164 expressed non-v1 alternative transcripts were classified into five categories (**Fig. 3B)**. Nearly half of expressed alternative UGT variants lacked a sequence encoding the substrate-binding domain (N-terminal), frequently due to truncation or skipping of exon 1, and this alteration was especially frequent among *UGT2* transcripts. In the absence of the N-terminal substrate-binding domain, the encoded proteins would be expected to lack transferase activity. Another prominently expressed class of variants that constituted over one-third of alternative variants lacked part or all of the exons encoding the C-terminal co-substrate domain. Remarkably, over 20% of the expressed variants comprised introduction of in-frame sequences. The domain organization and sequences of the putative isoforms imply that several may have different subcellular distribution, substrate specificity, or catalytic activity and thus could have altered biological functions.

Functional diversity of selected alternate UGTs containing in-frame sequences

Shorter UGT1 isoforms with an alternative C-terminal sequence have antagonistic functions.

A single *UGT1* locus encodes half of the human UGT enzymes, i.e., 9 UGT1A enzymes. It is well established that mature transcripts encoding each UGT1A enzyme include only one of the different *UGT1* exon-1 sequences associated with four downstream exons common to all UGT1A enzymes (i1s). A splicing event involving the use of an alternative 3′-terminal exon (exon 5b) generates three categories of *UGT1* transcripts, namely the

canonical *v1* (exon 5a) and alternative *v2* (exon 5b) and *v3* (exons 5b and 5a) (**Fig. 4A**). Our CaptureSeq data and those of an independent RNA sequencing (RNA-Seq) study revealed significant expression of *v2*/*v3*, with these transcripts representing between 9 and 20% of canonical *UGT1A* transcripts in normal tissues and high interindividual variability (**Fig. S1A, B**). In kidney and intestine/colon tumor tissues, v2/v3 constituted between 19 and 23% of *UGT1A_v1* expression. Because of a stop codon in exon 5b, the alternative *v2/v3* variants both encode shorter, 45-kDa isoform 2 proteins (i2s) lacking the C-terminal 99 amino acid residues encoded by exon 5a that comprise the membrane-spanning domain and the short cytosolic charged tail. In alternate UGT1A_i2 proteins, this sequence is replaced by a charged 10-residue C-terminal sequence not found in any other human proteins. The functions of i2s were studied in the HEK293 human embryonic kidney cell line, in which endogenous UGTs are not detected. UGT1A1_i2 had a remarkably long half-life compared with that of UGT1A1_i1 (11.6 h versus 1.3 h), whereas co-expression of the two isoforms did not alter their respective half-lives (**Fig. 4B**). *In situ* enzymatic assays in intact cells supported the notion that UGT1A1_i2 lacks transferase activity; rather, it has an antagonist role, leading to a significant reduction in UGT1A1_i1-mediated glucuronidation of the anti-cancer agent SN-38 (the active metabolite of irinotecan; −73.5%; $P < 0.001$) and the endogenous substrate estradiol (E_2; –75%; $P < 0.001$) (**Fig. 4C**). These antagonistic effects of i2 are consistent with the co-immunoprecipitation (IP) of UGT1A_i2 with UGT1A_i1 (**Fig. 4D**) as well as with the co-localization of both isoforms in the ER as assessed by immunofluorescence (IF; **Fig. 4E**) and in cells of human tissues by immunohistochemistry (IHC: **Fig. 4F**). The data also indicated that UGT1A proteins are distributed in other subcellular compartments (**Fig. S2**). In colon tissues, i1 and i2 co-localized at surface epithelial cells and in intestinal gland (crypt) cells, whereas in liver tissues the two isoforms co-localized in hepatocytes.

A UGT2B7 isoform with a spacer domain enhances drug inactivation and provokes remodeling of cellular metabolism and phenotypic changes.

An alternative full-length *UGT2B7_n4* transcript, confirmed by PCR analysis as containing an introduced sequence, exon 2b (**Fig. S3A**), encodes an alternate UGT2B7 protein termed isoform 8 (UGT2B7_i8) that has a unique 32-residue in-frame internal region residing at the interface between the N-terminal substrate-binding domain and the C-terminal co-substrate–binding domain (**Fig. 5A**). CaptureSeq data analysis revealed that expression of exon 2b–containing transcripts in three pools of three liver samples was low

compared with the canonical transcript **(Fig. S1C)**. However, the analysis of an independent RNA-Seq dataset derived from 18 different individuals indicated that the UGT2B7_i8-encoding transcript represents up to 75% of the canonical UGT2B7 transcripts, with an average coefficient of variation of 350% **(Fig. S1D)**. Similar patterns of expression were noted in the kidney, with a greater proportion of UGT2B7_i8-encoding transcript in kidney tumors relative to the canonical transcript. The encoded UGT2B7_i8 had a significant half-life of ~6 h that is not affected when co-expressed with the i1 protein, which has a half-life of 12 h (**Fig. S3B**). Expression of the encoded i8 protein along with UGT2B7 in human liver was further established in hepatocytes using an i8-specific antibody, supporting the expression data of the alternative isoform and its partial co-localization with UGT2B7_i1 (**Fig. 5B**). Staining was also observed in smooth muscle cells of hepatic arteries as well as in the same structures of esophageal, breast, uterine, testicular, and skeletal muscle tissues (data not shown), suggesting a potential unique cell type–specific expression of UGT2B7_i8 that deserves further investigation. Endogenous alternate protein expression was also corroborated by the detection of peptides specific to the sequence encoded by exon 2b in human liver samples using a targeted mass spectrometry (MS) approach (**Fig. S4**).

UGT-negative (HEK293) and UGT-positive (HepG2) cell models were established to study cellular functions of this UGT2B7 isoform and to reproduce the expression observed in tissues (i8 < i1). We could not detect the formation of glucuronide from zidovudine (AZT), the probe substrate of the UGT2B7 enzyme, in UGT2B7_i8-expressing HEK293 cells. However, the co-expression of UGT2B7_i8 and UGT2B7_i1 induced 1.3- and 2.1-fold increases in the formation of the glucuronide in HEK293 and HepG2 cells, respectively, implying a UGT-activating function (**Fig. 5C**). The potential of UGT2B7_i8 and UGT2B7_i1 proteins to interact was further supported by co-IP experiments and by their co-localization in the ER and may underlie the induction in glucuronidation activity (**Fig. 5D-E**). Untargeted metabolic profiling of the HEK293 and HepG2 cell models further revealed that the levels of a vast array of cellular metabolites were significantly altered in cells overexpressing UGT2B7_i8 compared with control cells (**Fig. 5F; Table S1**). Despite the distinctive basal metabolomes of the kidney and liver cell models, expression of UGT2B7_i8 induced remarkable accumulation of multiple amino acids in both cell types, with glutamine level being most altered. Most purines and pyrimidines were reduced upon i8 expression in HEK cells, whereas several glycolytic and TCA cycle intermediates were

significantly reduced in HepG2 cells (**Fig. 5F, Table S1**). These alterations in numerous metabolites essential for cell growth were associated with 3.5-fold enhanced adhesion but 3.7-fold slower proliferation in HEK293 cells overexpressing UGT2B7_i8 compared with control cells (**Fig. 5G**). In support of a specific effect of the UGT2B7_i8 protein, adhesion and proliferation of HEK293 cells overexpressing UGT2B7_i1 were similar to the control cells despite higher expression of i1 than i8.

Discussion

Our findings reveal large differences in the levels of naturally occurring alternative mRNAs transcribed from *UGT* loci in major metabolic tissues and demonstrate that these alternate transcripts are expressed in a tissue-specific manner, with remodeling of the UGT transcriptome in cancer tissues. Among this large collection of alternative UGT variants, expression of selected alternately spliced isoforms with in-frame sequences was confirmed at the protein level in human tissues such as the liver and colon. In cell-based assays, alternate UGT proteins were shown to differentially regulate the glucuronidation pathway by inhibiting or promoting the inactivation of drugs and hormones, likely through protein–protein interactions. We also uncovered that the alternate UGT isoforms have functions distinct from the canonical glucuronidation function, and these appear to broadly affect global metabolism, which results in changes in cell behavior. These findings imply that this transcriptome diversity expands the proteome and biological functions of human UGTs, likely playing crucial roles in multiple cellular processes.

Our targeted CaptureSeq approach allowed high-resolution, quantitative evaluation of *UGT* expression in the liver, kidney, and intestine/colon. A strength of our study is the mapping of RNA sequencing short reads on the exhaustive human *UGT* transcriptome recently established (Tourancheau et al., 2016), leading to precise assignment of reads to the appropriate *UGT* loci and transcript reconstruction than previously possible. This work revealed that alternative *UGT* mRNAs constitute an appreciable proportion of the total UGT transcriptome in the surveyed tissues, representing 19 to 60% of all *UGT* mRNAs. In line with this, there are many examples in the literature of protein functional expansion created by AS, among which the human tRNA synthetases and brain neurexins are remarkable recent examples (Lo et al., 2014; Treutlein et al., 2014). Our data further indicate that UGT AS programs are constitutive in normal tissues, implying that these events are associated with normal biological processes. This observation was also

validated in an independent RNA-Seq dataset not captured for UGT sequences (Chhibber et al., 2016). These findings support a role for AS in controlling coordinated cellular responses induced by small molecules and exposure to xenobiotics, including drugs of various classes. Given the key role played by UGTs in cellular homeostasis by inactivation of a variety of endogenous lipophilic cellular constituents, one can envision that expression of alternative UGTs may be triggered by the cellular environment and/or stimuli such as hormones and lipids (Dates et al., 2015; Hu et al., 2014). Expression of alternative UGTs is also highly likely to be triggered by exogenous stimuli and toxic xenobiotics that are common substrates of UGTs (Hu et al., 2014). It remains unknown if other enzymes involved in parallel cellular and drug-metabolism functions diversify their expression profiles and functional complexity through splice variants. A recent study indicated that this might be the case for a vast majority (>70%) of factors in drug-related pathways, such as cytochromes P450 and other transferases (Chhibber et al., 2016). However, the regulation and functional consequences of AS events for these clinically important pharmacogenes remain undefined.

We estimate that only a small fraction of the UGT variants we quantified may undergo nonsense-mediated mRNA decay according to the 50-bp rule (Popp and Maquat, 2013), and therefore most observed *UGT* transcripts likely have the potential to be translated. Multiple distinct features characterize putative UGT isoforms, including truncated substrate or co-substrate-binding domains and distinctive in-frame sequences. We provide evidence that AS may represent a potential mechanism to modify canonical UGT function and to produce alternative UGT isoforms with introduced domains and divergent functions. Our findings with the *UGT1A* and *UGT2B7* transcripts, which encode, respectively, a shorter protein with an in-frame C-terminal sequence and a longer protein with an internal peptide sequence introduced, clearly support this notion. At the transcript level, *UGT1A* and *UGT2B7* expression shows high interindividual variability in the liver and kidney. Specific antibodies raised against the peptide sequences not found in canonical UGTs or any other known proteins labeled several human tissues (IHC). Co-localization of alternate isoforms with canonical UGTs in the same cell types, such as hepatocytes, was evident, even though relative abundance could not be deduced. According to functional assays in intact proliferating cells, both UGT1A1_i2 and UGT2B7_i8 lack the ability to transfer a glucuronic acid moiety to the typical substrates of the canonical enzymes and therefore would be enzymatically null. Alternate UGT1A_i2s

contain complete binding sites for both the substrate and co-substrate and a C-terminal dilysine motif encoded by the new terminal exon, but they lack the transmembrane-binding domain, which likely affects membrane topology and conformation and thus UGT activity. In contrast, UGT2B7_i8 contains all UGT domains but also an internal 32-residue sequence that potentially disrupts the coordination of co-substrate-to-substrate S_N2 transfer of the glucuronic acid for typical UGT2B7 substrates, such as AZT, as observed in this study. Alternatively, this region may also potentially adapt to a different set of substrates, changing substrate specificity compared with the canonical UGT2B7 enzyme that conjugates a wide variety of lipophilic metabolites and is involved in the clearance of ~25% of common medications (Guillemette et al., 2014; Stingl et al., 2014). A larger set of substrates, as well as co-substrates such as UDP-glucose, that are metabolized by UGT2B7 in addition to UDPGA (Chau et al., 2014), needs to be tested to determine whether the alternative UGT isoforms are truly enzymatically null.

When co-expressed with UGTs in human tissues and cells, alternate UGTs either inhibited or activated cellular glucuronide formation, significantly affecting inactivation of drugs and hormones. To our knowledge, a UGT acting as an inducer/activator of the glucuronidation pathway has not been reported before. Previous investigations by our group and others indicate that UGTs form oligomeric complexes (Ishii et al., 2010; Operana and Tukey, 2007; Rouleau et al., 2013). The immunofluorescence evidence of close proximity in the ER membrane and co-IP data strongly suggest that the modulatory effects of the UGT1A and UGT2B7 alternative isoforms are caused by direct protein-protein interactions with their cognate UGT enzymes, and perhaps other UGTs, leading to a mixture of active and inactive complexes (Ishii et al., 2010; Operana and Tukey, 2007; Rouleau et al., 2013). Given the enhanced stability of at least some alternative isoforms relative to the canonical UGTs, as shown for UGT1A1_i2, the impact of alternative isoforms on cellular glucuronidation activity is likely greater than anticipated from mRNA expression levels. We suggest that AS hampers or potentiates canonical UGT functions. This likely helps coordinate and fine-tune cellular responses to numerous endogenous and exogenous stimuli, with the potential to affect drug responses and disease development and progression, especially tumorigenesis, given the altered ratio of alternative/canonical variant expression and the large interindividual variability in their expression.

Our functional investigations of the UGT2B7_i8 variant provide further evidence that alternative isoforms have extended metabolic functions that affect global cell metabolism,

suggesting that they may be part of multi-enzyme complexes of a core metabolic network. The biological relevance of a metabolic shift induced by expression of UGT2B7_i8 alone warrants further characterization, but our data also suggest that the glucuronidation pathway and primary cell metabolism (e.g., amino acids and nucleotides) are interrelated enzymatic processes. Whether dimerization/oligomerization and/or glucuronidation of alternative endogenous substrates link the biological activity of these isoforms with cell metabolism remains to be addressed. Furthermore, UGT2B7_i8 expression is functionally linked to modulation of cell adhesion and proliferation, supporting the conclusion that UGTs substantially impact multiple cellular processes.

Conclusions

This study provides a comprehensive quantitative portrait of hepatic, renal, and gastrointestinal UGT transcriptomes and reveals the abundance of alternate UGT variants, which clearly expand the UGT proteome. A first biological consequence of altering the UGT transcriptome was emphasized by the functional characterization of alternative isoforms with in-frame sequences introduced, which were found to antagonize or induce cellular glucuronidation, thus affecting inactivation of drugs and sex hormones. This study also raises the exciting possibility that different UGTs may exhibit biological functions independent of glucuronic acid transferase activity. Alternate isoform expression induced drastic shifts in multiple metabolic pathways and modified cellular phenotypes, suggesting crosstalk between various enzymatic pathways and UGTs that could serve to maintain cellular homeostasis and increase cell fitness. The broader regulatory and functional relevance of such an extensive splicing program remains to be fully characterized. We expect that this work will enable the exploration of human UGT-mediated metabolism and its potentially extended role in health and disease.

Experimental Procedures

RNA samples, sequencing, and mRNA expression

UGT expression was characterized in normal tissue samples from 9 liver, 9 kidney, and 15 intestine and colon samples as well as in samples from 9 kidney, and 9 intestine and colon tumor tissues of mixed-gender origin. For each tissue, equivalent amounts of total RNA from at least three samples were pooled, and three pools per tissue type were prepared and used for production of sequencing libraries. UGT sequences were enriched from paired-end bar-coded cDNA libraries with UGT capture (Tourancheau et al., 2016). Libraries were sequenced on an Illumina HiSeq 2500 system (McGill University and Génome Québec Innovation Center, Montreal, QC, Canada). Trimmed reads were aligned with the splice-aware software TopHat2 on the UCSC hg19 reference genome with annotation provided by Illumina iGenome combined with the complete annotated human UGT loci described recently by our group (Tourancheau et al., 2016). The average normalized expression of replicates is provided throughout the text. Detailed library construction, sequence analysis, and validation of *UGT2B7_n4* expression by reverse transcription-PCR and Sanger sequencing are described in Supplemental Experimental Procedures.

Expression of *UGT1A* and *UGT2B7* variants was examined in 18 normal liver and 18 normal kidney samples in the RNA-Seq dataset from the Pharmacogenomics Research Network (Chhibber et al., 2016) accessed from the GEO accession number GSE70503. Alignment of reads on the complete human UGT transcriptome and quantification using Cufflinks are described in Supplemental Experimental Procedures.

Cell models

HT115 cells expressing endogenous UGT1A isoforms and HEK293 cell models expressing myc- or V5-tagged UGT1A1 isoforms have been described previously (Bellemare et al., 2010a; Rouleau et al., 2014). The pool of HEK293 cells stably expressing *UGT2B7_v1* was established by supplementing cell culture media with G418 (Invitrogen, 1 mg/ml). The pool of HEK293 cells co-expressing *UGT2B7_v1* and *UGT2B7_n4* (corresponding to the exon 2b encoding transcript) was established by subsequent transfection of HEK-2B7_v1 with the UGT2B7_n4 construct (with or without a V5 tag) and selection with blasticidin (Wisent, 10 µg/ml). The HEK293 cell model

expressing UGT2B7_i1 and UGT2B7_i8-V5 was used only to demonstrate protein-protein interactions by IP. HepG2 cells, which express *UGT2B7_v1* endogenously but not *UGT2B7_n4*, were transfected with the UGT2B7_n4 construct (without tag), and the pool was established with blasticidin selection. Control HEK293 and HepG2 cells were produced by transfection with the parental vectors and selection as above.

Analysis of protein expression

Antibodies. UGT2B7 polyclonal antibody was from ProteinTech Group (16661-1-AP; western blotting (WB): 1:5000; IHC: 1:800; IF: 1:500) and monoclonal antibody was from Abcam (ab57685; IP: 1:100; Abcam, Toronto, ON, Canada; note that ab57685 is sold as an anti-UGT2B10 antibody but it also recognizes UGT2B7 (Fig. S5)). The purified pan-UGT1A polyclonal antibody (RC-71; WB: 1:1000), purified UGT1A_i1 polyclonal antibody (#9348; IHC and IF: 1:1000; IP: 1:200), and purified UGT1A_i2 antibody (#4863; IHC: 1:1000) have been described (Albert et al., 1999; Bellemare et al., 2011). UGT1A_i2 (#4C5E7; IF: 1:100) and UGT2B7_i8 (IF and IHC: 1:1000) antibodies were custom made (Genscript, Piscataway, NJ, USA). Anti-V5 (WB: 1:5000) and anti-myc (clone 4A6, WB: 1:5000) were from Invitrogen (Life Technologies, Burlington, Canada) and EMD Millipore (Etobicoke, ON, Canada), respectively. Cell compartment–specific antibodies used in IF were: anti-58K Golgi protein (1:100; ab27043; Abcam), anti-protein disulfide isomerase (PDI: 1:100; ab2792; Abcam) for the ER, anti-cytochrome c (1:300; cat #12963S; Cell Signaling Technology) for the mitochondria; DNA was stained with Hoechst 33342 (1:1500; Sigma) or DRAQ5 (1:2000; Life Technologies Inc.). Production of antibodies against variants is detailed in Supplemental Experimental Procedures.

mRNA and protein stability of UGT1A and UGT2B7. Cells were treated with 20 µg/ml cycloheximide for 0–16 h and collected at various time points as described (Turgeon et al., 2001). Cell homogenates (20 µg protein) prepared in phosphate-buffered saline containing 0.5 mM dithiothreitol were analyzed by WB with RC-71 (UGT1A) or anti-UGT2B7 from ProteinTech.

IF. Detection of endogenous UGT1A_i1 and _i2 in HT115 cells was as described (Bellemare et al., 2010b). Stably expressed UGT2B7_i1 and UGT2B7_i8 in the HEK cell models were detected with anti-2B7 16661-1-AP.

IHC. Paraffin-embedded tissue blocks were available for individual patients. The institutional board approved the study, and written consent was given by all patients concerning the use of their tissues for research purposes. Serial sections (5 µm) were deparaffinized, rehydrated, and processed using the IDetect SuperStain HRP polymer kit (Empire Genomics, Buffalo, NY, USA) with an overnight incubation of tissues at 4°C with primary antibodies. Control sections were incubated with the anti-UGT2B7_i8 preadsorbed for 3 h at room temperature with an excess of the immunogenic peptide (2 µM) to ascertain labeling specificity.

IP. HEK293 UGT1A-tagged cell models were grown to confluency in 10-cm culture dishes, washed, scraped into 800 µl lysis buffer/dish, and immunoprecipitated as described in Supplemental Experimental Procedures using anti-UGT1A_i1 or control rabbit IgG. For UGT2B7_i8 IP, HEK293 cells grown in two 15-cm dishes were scraped and cross-linked with 0.125% formaldehyde for 10 min at 37°C then quenched with 0.125 M glycine. Cells were collected by centrifugation prior to lysis in 1 ml lysis buffer and IP as described in Supplemental Experimental Procedures.

MS-coupled multiple reaction monitoring. Tryptic digests of UGT2B7 immunoprecipitated from human liver S9 fractions were analyzed by MS-coupled multiple reaction monitoring on a 6500QTRAP hybrid triple quadrupole/linear ion trap mass spectrometer (Sciex, Concord, ON, Canada). The UGT2B7 signature peptide ADVWLIR and the UGT2B7_i8-specific peptide LDSFNTGWINK were detected in tryptic digests of the immunoprecipitated UGT2B7 samples, and peptide identity was confirmed by co-injection of isotopically labeled [^{13}C6,^{15}N2]Lys and [^{13}C6,^{15}N4]Arg synthetic peptides.

Cell adhesion and proliferation. HEK293 and HepG2 cells (pool of control cells or cells stably expressing *UGT2B7_n4*) plated in E-view PET 16-well plates (10,000 cells/well, four replicates/experiment, n = 3) were monitored in real time on an Xcelligence DP system (ACEA Biosciences Inc., San Diego, CA, USA). Doubling time was determined with the RTCA software 2.0 (ACEA Biosciences Inc.) using normalized cell index values between the 20 and 45 h time points. Alternatively, HEK293 and HepG2 cells were plated in 6-well plates (125,000 HEK cells/well; 100,000 HepG2 cells/well), incubated for specified times, and counted with a TC-10 automated cell counter (Bio-Rad) at 48, 72 and 96 h after plating. Cell media were replaced after the 48 h time point.

Metabolic functions

In situ glucuronidation assays. HEK293 and HepG2 cells (control cells or cells stably expressing *UGT2B7_v1*, *UGT2B7_n4* or both, as stated in the figure legends) were seeded in 24-well plates (HEK293: 80,000 cells/well, HepG2: 125,000 cells/well). Assays were initiated 72 h after seeding by replacing the culture medium with fresh medium (1 ml/well) containing a labeled UGT substrate probe (for UGT1A1: 5 µM SN-38 prepared by hydrolysis of irinotecan-HCl (McKesson, ON, Canada) and/or 25 µM estradiol (Steraloids, Newport, RI, USA); for UGT2B7: AZT (Sigma-Aldrich, St. Louis, MO, USA)). Cells were incubated for 4 h, and the media were collected and stored at −20°C until glucuronide assessment by MS-based analysis as described (Belanger et al., 2009; Lepine et al., 2004). Briefly, for AZT-G, the culture media were diluted 1:3 with 25% aqueous methanol solution containing AZT-d3-G standard (Toronto Research Chemicals, Toronto, ON, Canada) prior to analysis as described (Belanger et al., 2009).

Untargeted metabolomics analysis. HEK293 and HepG2 cells (stable pool of control cells or cells expressing *UGT2B7_n4*) were plated in 10-cm culture dishes (1.5 million HEK cells/dish; 3.5 million HepG2 cells/dish) and grown for 96 h, with a change to fresh medium after the first 48 h. Cells were harvested by trypsinization, counted, rinsed twice in ice-cold phosphate-buffered saline, snap-frozen on dry ice, and stored at −80°C until extraction for metabolomics analysis. Untargeted global metabolite profiling was conducted on triplicate samples at the West Coast Metabolomics Center (University of California at Davis) as described (Fiehn et al., 2008). Relative quantification data provided as normalized peak heights were further normalized for cell counts in each sample and expressed as fold change ratios of mean metabolite levels in the cells expressing variant UGT2B7 versus control cells. Details about the data analysis are provided in Supplemental Experimental Procedures.

Competing Interests

The authors have no conflicts of interest to disclose.

Author contributions

Conceptualization: MR, CG; Methodology: MR, CG; Investigation: MR, AT, CGB, LV, AMD, YAD, IG, AD, CG; Validation: MR, AT, CGB, LV, JV, IP, AD, CG; Writing – Original

Draft: MR, CG; Writing – Review & Editing: MR, AT, CGB, LV, JV, AMD, YAD, IG, IP, AD, CG; Supervision: MR, CG; Project administration: CG; Funding Acquisition: CG

Accession numbers

RNA sequencing data are available in the GEO database (GSE80463)

Acknowledgements

We acknowledge Patrick Caron and Véronique Turcotte for their contribution to the mass spectrometry analysis of glucuronide metabolites, Sylvie Desjardins for contributing to IP experiments, Andréa Fournier for contributing to the adhesion and proliferation experiments, Joannie Roberge and Hugo Girard for contributing to the protein stability experiments, Sandra Guauque-Olarte for GEO submission of RNA sequencing data, Johanne Ouellet and Michèle Orain for contributing to the IHC analysis, Isabelle Kelly from the Proteomics platform at the CHU de Québec Research Center for support with the multiple reaction monitoring analysis, France Couture for artwork, and Dr. Éric Lévesque for helpful discussion.

This work was financially supported by grants from the Canadian Institutes for Health Research (MOP-42392 and MOP-142318), the Natural Sciences and Engineering Research Council of Canada (342176-2012), and a Canadian Research Chair in Pharmacogenomics to CG (Tier I). CGB holds an FER studentship award from the Faculty of Pharmacy of Laval University. YAD received studentship funding from the Centre de Recherche en Endocrinologie Moléculaire et Oncologique et Génomique Humaine, Laval University and Fonds de Recherche du Québec – Santé.

References

Albert, C., Vallee, M., Beaudry, G., Belanger, A., and Hum, D.W. (1999). The monkey and human uridine diphosphate-glucuronosyltransferase UGT1A9, expressed in steroid target tissues, are estrogen-conjugating enzymes. Endocrinology *140*, 3292-3302.

Belanger, A.S., Caron, P., Harvey, M., Zimmerman, P.A., Mehlotra, R.K., and Guillemette, C. (2009). Glucuronidation of the antiretroviral drug efavirenz by UGT2B7 and an in vitro investigation of drug-drug interaction with zidovudine. Drug Metab Dispos *37*, 1793-1796.

Bellemare, J., Rouleau, M., Harvey, M., and Guillemette, C. (2010a). Modulation of the human glucuronosyltransferase UGT1A pathway by splice isoform polypeptides is mediated through protein-protein interactions. J Biol Chem *285*, 3600-3607.

Bellemare, J., Rouleau, M., Harvey, M., Popa, I., Pelletier, G., Tetu, B., and Guillemette, C. (2011). Immunohistochemical expression of conjugating UGT1A-derived isoforms in normal and tumoral drug-metabolizing tissues in humans. J Pathol *223*, 425-435.

Bellemare, J., Rouleau, M., Harvey, M., Tetu, B., and Guillemette, C. (2010b). Alternative-splicing forms of the major phase II conjugating UGT1A gene negatively regulate glucuronidation in human carcinoma cell lines. Pharmacogenomics J *10*, 431-441.

Bock, K.W. (2015). Roles of human UDP-glucuronosyltransferases in clearance and homeostasis of endogenous substrates, and functional implications. Biochem Pharmacol *96*, 77-82.

Breton, C., Fournel-Gigleux, S., and Palcic, M.M. (2012). Recent structures, evolution and mechanisms of glycosyltransferases. Curr Opin Struct Biol *22*, 540-549.

Chau, N., Elliot, D.J., Lewis, B.C., Burns, K., Johnston, M.R., Mackenzie, P.I., and Miners, J.O. (2014). Morphine glucuronidation and glucosidation represent complementary metabolic pathways that are both catalyzed by UDP-glucuronosyltransferase 2B7: kinetic, inhibition, and molecular modeling studies. J Pharmacol Exp Ther *349*, 126-137.

Chhibber, A., French, C.E., Yee, S.W., Gamazon, E.R., Theusch, E., Qin, X., Webb, A., Papp, A.C., Wang, A., Simmons, C.Q.*, et al.* (2016). Transcriptomic variation of pharmacogenes in multiple human tissues and lymphoblastoid cell lines. Pharmacogenomics J. *On line*: February 9, 2016; doi:10.1038/tpj.2015.93

Clark, M.B., Mercer, T.R., Bussotti, G., Leonardi, T., Haynes, K.R., Crawford, J., Brunck, M.E., Cao, K.A., Thomas, G.P., Chen, W.Y.*, et al.* (2015). Quantitative gene profiling of long noncoding RNAs with targeted RNA sequencing. Nat Methods *12*, 339-342.

Court, M.H., Zhang, X., Ding, X., Yee, K.K., Hesse, L.M., and Finel, M. (2012). Quantitative distribution of mRNAs encoding the 19 human UDP-glucuronosyltransferase enzymes in 26 adult and 3 fetal tissues. Xenobiotica *42*, 266-277.

Dates, C.R., Fahmi, T., Pyrek, S.J., Yao-Borengasser, A., Borowa-Mazgaj, B., Bratton, S.M., Kadlubar, S.A., Mackenzie, P.I., Haun, R.S., and Radominska-Pandya, A. (2015). Human UDP-Glucuronosyltransferases: Effects of altered expression in breast and pancreatic cancer cell lines. Cancer Biol Ther *16*, 714-723.

De Bruyn, F., Maertens, J., Beauprez, J., Soetaert, W., and De Mey, M. (2015). Biotechnological advances in UDP-sugar based glycosylation of small molecules. Biotechnol Adv *33*, 288-302.

Fiehn, O., Wohlgemuth, G., Scholz, M., Kind, T., Lee do, Y., Lu, Y., Moon, S., and Nikolau, B. (2008). Quality control for plant metabolomics: reporting MSI-compliant studies. Plant J *53*, 691-704.

Gamazon, E.R., and Stranger, B.E. (2014). Genomics of alternative splicing: evolution, development and pathophysiology. Hum Genet *133*, 679-687.
Garcia-Blanco, M.A., Baraniak, A.P., and Lasda, E.L. (2004). Alternative splicing in disease and therapy. Nat Biotechnol *22*, 535-546.
Guillemette, C. (2003). Pharmacogenomics of human UDP-glucuronosyltransferase enzymes. Pharmacogenomics J *3*, 136-158.
Guillemette, C., Belanger, A., and Lepine, J. (2004). Metabolic inactivation of estrogens in breast tissue by UDP-glucuronosyltransferase enzymes: an overview. Breast Cancer Res *6*, 246-254.
Guillemette, C., Levesque, E., and Rouleau, M. (2014). Pharmacogenomics of human uridine diphospho-glucuronosyltransferases and clinical implications. Clin Pharmacol Ther *96*, 324-339.
Hu, D.G., Meech, R., McKinnon, R.A., and Mackenzie, P.I. (2014). Transcriptional regulation of human UDP-glucuronosyltransferase genes. Drug Metab Rev *46*, 421-458.
Ishii, Y., Takeda, S., and Yamada, H. (2010). Modulation of UDP-glucuronosyltransferase activity by protein-protein association. Drug Metab Rev *42*, 145-158.
Lepine, J., Bernard, O., Plante, M., Tetu, B., Pelletier, G., Labrie, F., Belanger, A., and Guillemette, C. (2004). Specificity and regioselectivity of the conjugation of estradiol, estrone, and their catecholestrogen and methoxyestrogen metabolites by human uridine diphospho-glucuronosyltransferases expressed in endometrium. J Clin Endocrinol Metab *89*, 5222-5232.
Little, J.M., Kurkela, M., Sonka, J., Jantti, S., Ketola, R., Bratton, S., Finel, M., and Radominska-Pandya, A. (2004). Glucuronidation of oxidized fatty acids and prostaglandins B1 and E2 by human hepatic and recombinant UDP-glucuronosyltransferases. J Lipid Res *45*, 1694-1703.
Lo, W.S., Gardiner, E., Xu, Z., Lau, C.F., Wang, F., Zhou, J.J., Mendlein, J.D., Nangle, L.A., Chiang, K.P., Yang, X.L.*, et al.* (2014). Human tRNA synthetase catalytic nulls with diverse functions. Science *345*, 328-332.
Mackenzie, P.I., Bock, K.W., Burchell, B., Guillemette, C., Ikushiro, S., Iyanagi, T., Miners, J.O., Owens, I.S., and Nebert, D.W. (2005). Nomenclature update for the mammalian UDP glycosyltransferase (UGT) gene superfamily. Pharmacogenet Genomics *15*, 677-685.
Margaillan, G., Rouleau, M., Fallon, J.K., Caron, P., Villeneuve, L., Turcotte, V., Smith, P.C., Joy, M.S., and Guillemette, C. (2015a). Quantitative profiling of human renal UDP-glucuronosyltransferases and glucuronidation activity: a comparison of normal and tumoral kidney tissues. Drug Metab Dispos *43*, 611-619.
Margaillan, G., Rouleau, M., Klein, K., Fallon, J.K., Caron, P., Villeneuve, L., Smith, P.C., Zanger, U.M., and Guillemette, C. (2015b). Multiplexed Targeted Quantitative Proteomics Predicts Hepatic Glucuronidation Potential. Drug Metab Dispos *43*, 1331-1335.
Mercer, T.R., Gerhardt, D.J., Dinger, M.E., Crawford, J., Trapnell, C., Jeddeloh, J.A., Mattick, J.S., and Rinn, J.L. (2012). Targeted RNA sequencing reveals the deep complexity of the human transcriptome. Nat Biotechnol *30*, 99-104.
Oltean, S., and Bates, D.O. (2014). Hallmarks of alternative splicing in cancer. Oncogene *33*, 5311-5318.
Operana, T.N., and Tukey, R.H. (2007). Oligomerization of the UDP-glucuronosyltransferase 1A proteins: homo- and heterodimerization analysis by fluorescence resonance energy transfer and co-immunoprecipitation. J Biol Chem *282*, 4821-4829.

Popp, M.W., and Maquat, L.E. (2013). Organizing principles of mammalian nonsense-mediated mRNA decay. Annu Rev Genet *47*, 139-165.

Radominska-Pandya, A., Czernik, P.J., Little, J.M., Battaglia, E., and Mackenzie, P.I. (1999). Structural and functional studies of UDP-glucuronosyltransferases. Drug Metab Rev *31*, 817-899.

Rouleau, M., Collin, P., Bellemare, J., Harvey, M., and Guillemette, C. (2013). Protein-protein interactions between the bilirubin-conjugating UDP-glucuronosyltransferase UGT1A1 and its shorter isoform 2 regulatory partner derived from alternative splicing. Biochem J *450*, 107-114.

Rouleau, M., Roberge, J., Bellemare, J., and Guillemette, C. (2014). Dual roles for splice variants of the glucuronidation pathway as regulators of cellular metabolism. Mol Pharmacol *85*, 29-36.

Rowland, A., Miners, J.O., and Mackenzie, P.I. (2013). The UDP-glucuronosyltransferases: their role in drug metabolism and detoxification. Int J Biochem Cell Biol *45*, 1121-1132.

Stingl, J.C., Bartels, H., Viviani, R., Lehmann, M.L., and Brockmoller, J. (2014). Relevance of UDP-glucuronosyltransferase polymorphisms for drug dosing: A quantitative systematic review. Pharmacol Ther *141*, 92-116.

Tourancheau, A., Margaillan, G., Rouleau, M., Gilbert, I., Villeneuve, L., Levesque, E., Droit, A., and Guillemette, C. (2016). Unravelling the transcriptomic landscape of the major phase II UDP-glucuronosyltransferase drug metabolizing pathway using targeted RNA sequencing. Pharmacogenomics J *16*, 60-70.

Treutlein, B., Gokce, O., Quake, S.R., and Sudhof, T.C. (2014). Cartography of neurexin alternative splicing mapped by single-molecule long-read mRNA sequencing. Proc Natl Acad Sci U S A *111*, E1291-1299.

Turgeon, D., Carrier, J.S., Levesque, E., Hum, D.W., and Belanger, A. (2001). Relative enzymatic activity, protein stability, and tissue distribution of human steroid-metabolizing UGT2B subfamily members. Endocrinology *142*, 778-787.

Wang, E.T., Sandberg, R., Luo, S., Khrebtukova, I., Zhang, L., Mayr, C., Kingsmore, S.F., Schroth, G.P., and Burge, C.B. (2008). Alternative isoform regulation in human tissue transcriptomes. Nature *456*, 470-476.

Wells, P.G., Mackenzie, P.I., Chowdhury, J.R., Guillemette, C., Gregory, P.A., Ishii, Y., Hansen, A.J., Kessler, F.K., Kim, P.M., Chowdhury, N.R.*, et al.* (2004). Glucuronidation and the UDP-glucuronosyltransferases in health and disease. Drug Metab Dispos *32*, 281-290.

Figure Legends

Figure 1: Profiling the UGT transcriptome and characterization of UGT isoforms: an overview of the experimental design. The UGT transcriptome in the main drug metabolizing organs (≥9 samples per tissue) was quantified by RNA-Seq after a targeted capture step. The complete human UGT sequence annotation (Tourancheau et al., 2016) enabled precise mapping of reads to canonical and alternative transcripts. Expression and functional analysis of mRNA variants and predicted protein isoforms were conducted by multiple approaches. MS: mass spectrometry; IF: immunofluorescence; IHC: immunohistochemistry.

Figure 2: Tissue-specific expression of canonical and alternative *UGT* transcripts. Venn diagrams showing the large diversity in expression patterns between tissues (**A**) and between healthy and tumor tissues (**B**). Total number of canonical (v1) UGTs and alternative variants (alt) are given for each tissue. Values in the Venn diagrams represent number of alternative transcripts (alt) expressed above 600 fragments per kilobase of transcript per million mapped reads in CaptureSeq. **C**. Average quantitative expression of alternative transcripts in healthy and tumor tissues. Proportion of alternative transcripts represents total expression of alternative transcripts relative to total v1 expression in each tissue. See also Fig. S1.

Figure 3: Structural organization of UGT enzymes and alternative isoforms. A. Schematic of functional domains and structural organization of UGT enzymes in the endoplasmic reticulum (ER). The bulk of the substrate-binding (red) and co-substrate-binding (blue) domains lie on the luminal side of the ER. The transmembrane domain (grey segment) positions the positively charged tail (orange, ++) on the cytoplasmic side of the ER. **B**. Quantification of alternative UGT levels classified on the basis of truncated regions and inclusion of sequences predicted from alternative transcript expression levels. N-term: N-terminal; C-term: C-terminal.

Figure 4. Functional characterization of alternate UGT1A_i2. A. The nine well-characterized UGT1A_v1 transcripts are produced from splicing of alternative exon 1s to the common exons 2–5a (blue lines) at the single *UGT1* locus and encode the nine UGT1A_i1 enzymes. The *UGT1A_v2* and *UGT1A_v3* transcripts (nine of each type) arise from the use of alternative exon 5b, without or with exon 5a, respectively (green lines).

UGT1A_v2 and *_v3* transcripts encode the same nine UGT1A_i2 proteins, because exon 5b includes a stop codon. UGT1A_i2 and UGT1A_i1 are distinguishable by their divergent C-termini. The UGT1A_i2-specific antibody is directed towards the unique i2 amino acid sequence (green box). Domains are organized as in Fig. 3A. **B**. UGT1A_i2s have a longer protein half-life compared with UGT1A_i1. *Top panel*: Protein levels of UGT1A1_i1, UGT1A1_i2 or both in the HEK293 cell models were measured at different times after treatment with cycloheximide using a pan-UGT1A antibody recognizing both isoforms. *Lower panel*: Densitometric quantification of UGT1A protein level is expressed as a function of time after cycloheximide treatment. Data are presented as means + SD. **C**. The HEK293 cell models (UGT negative) were developed to express UGT1A1_i1, UGT1A1_i2, or both isoforms. *In situ* cell assays demonstrate that glucuronidation of SN-38 and estradiol (E_2) by UGT1A1_i1 is impaired by the co-expression of UGT1A1_i2 (n = 2 independent assays in triplicate). UGT1A1_i2 did not catalyze glucuronidation of these substrates. Activity was normalized to UGT1A1_i1 level. Data are presented as means + SD, ***P<0.001, Student's *t*-test. **D**. Interactions between UGT1A_i1 and i2. IP of i1 from HEK cell lysates with the specific anti-i1 co-purifies UGT1A_i2. Lanes "ctr" served as markers for i1 and i2 protein mobility and detection. **E**. Endogenous UGT1A_i1 and i2 co-localize in the endoplasmic reticulum (ER) of colorectal cancer HT115 cells. Protein disulfide isomerase (PDI) is an ER marker, whereas Hoechst (H) labels nuclei. Fluorescence intensity profiles are given for cross-sections (dashed lines). See also Fig. S2 for a comparison of co-localization with multiple specific subcellular markers including the ER. Scale bars: 10 µm. **F.** Immunohistochemical investigation of UGT1A_i1 and I2 in consecutive sections of normal human liver and colon tissues. H: hepatocytes; PV: portal vein; IG: intestinal gland; L: lumen; LP: lamina propria; SE: surface epithelium. Scale bars: 200 µm.

Figure 5. **Functional characterization of UGT2B7_i8. A**. Alternative splicing at the *UGT2B7* locus. The canonical *UGT2B7_v1* transcript excludes the exon 2b (blue lines) and encodes **the** UGT2B7_i1 enzyme, whereas *UGT2B7_n4* includes exon 2b (green region, line and boxed sequence) that extends the coding sequence to produce UGT2B7_i8. Anti-2B7_i8 was raised against the underlined immunogenic peptide. **B**. Immunohistochemical investigation of i8 expression in normal liver tissues. *Left*: UGT2B7_i1, labeled by the commercial antibody against UGT2B7, is expressed predominantly in hepatocytes but not in hepatic arteries or bile ducts. *Center*: The purified

anti-i8 specifically and strongly labels smooth muscle cells of hepatic arteries whereas hepatocytes are weakly labeled and bile ducts are unlabeled. *Right*: Labeling is impaired by preadsorption of anti-2B7_i8 with the immunogenic peptide prior to tissue labeling, demonstrating specificity of staining with anti-2B7_i8. Representative images from consecutive sections of two liver tissues are shown. BD: bile ducts; H: hepatocytes; HA: hepatic arteries; PV: portal vein. Scale bars: 200 µm. **C.** Metabolic alterations associated with the expression of UGT2B7_i8. HEK293 kidney and HepG2 liver cell models (expressing endogenous UGTs, including UGT2B7) were developed. UGT2B7_i8 has an apparent molecular mass of 62 kDa, slightly larger than that the UGT2B7_i1 enzyme (55 kDa), as expected, upon analysis of the microsomal fractions (20 µg) from each cell model. L: Human liver microsomes, as a positive control. *In situ* glucuronidation activity towards the UGT2B7-specific substrate zidovudine (AZT) was enhanced by co-expression of UGT2B7_i1 and the i8 isoform in both cell models (HEK293, n = 4 assays; HepG2, n = 3 assays, in triplicate). UGT2B7_i8 did not have glucuronidation activity with AZT as a substrate. Activity was normalized to UGT2B7_i1 level. Data are presented as means + SD, ***P<0.001, Student's *t*-test. **D**. Interactions between UGT2B7_i8 and i1. IP of i8 from cell lysates of HEK293 cells co-expressing UGT2B7_i1 and tagged UGT2B7_i8-V5 with anti-V5 co-purifies UGT2B7_i1. **E.** UGT2B7_i1 and i8 co-localize in the endoplasmic reticulum (ER). Each UGT2B7 variant protein stably expressed in HEK293 cells co-localizes with the ER marker protein disulfide isomerase (PDI). Fluorescence intensity profiles are given for cross-sections (dashed lines). Scale bars: 10 µm. **F**. Cellular metabolic profiles reveal an important modulation of levels of amino acids and nucleotides induced by UGT2B7_i8 expression in HEK293 and HepG2 cell models. Data points for which the coefficient of variation exceeded 50% were omitted for clarity. Detailed metabolomics data are given in **Table S1**. **G.** UGT2B7_i8 enhanced adhesion but reduced the proliferation rate of HEK293 cells. *Left* Real-time cell adhesion was measured by electrical impedance (cell index) (n=2 independent assays in quadruplicate; significantly different for all time points). *Right* Proliferation was assessed by cell counts (n=2 independent assays in triplicate) and doubling time was determined from real time cell index data. Data are presented as means + SD, **P<0.01, ***P<0.001, Student's *t*-test. See also Fig. S3 and S4.

Figure 1

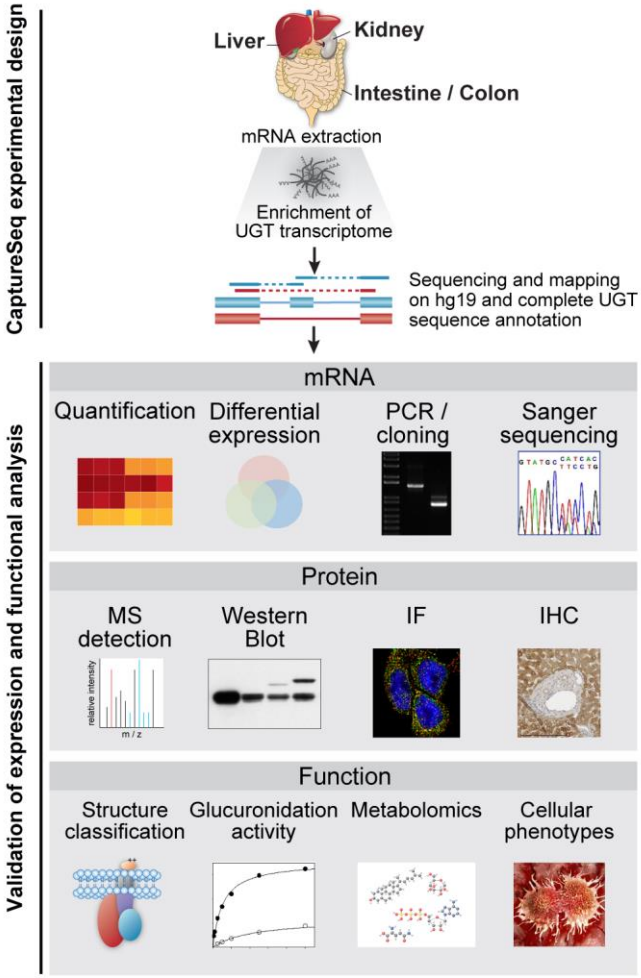
CaptureSeq experimental design
Liver
Kidney
Intestine / Colon
mRNA extraction
Enrichment of UGT transcriptome
Sequencing and mapping on hg19 and complete UGT sequence annotation
Validation of expression and functional analysis
mRNA
Quantification
Differential expression
PCR / cloning
Sanger sequencing
Protein
MS detection
Western Blot
IF
IHC
relative intensity
m / z
Function
Structure classification
Glucuronidation activity
Metabolomics
Cellular phenotypes

Figure 2

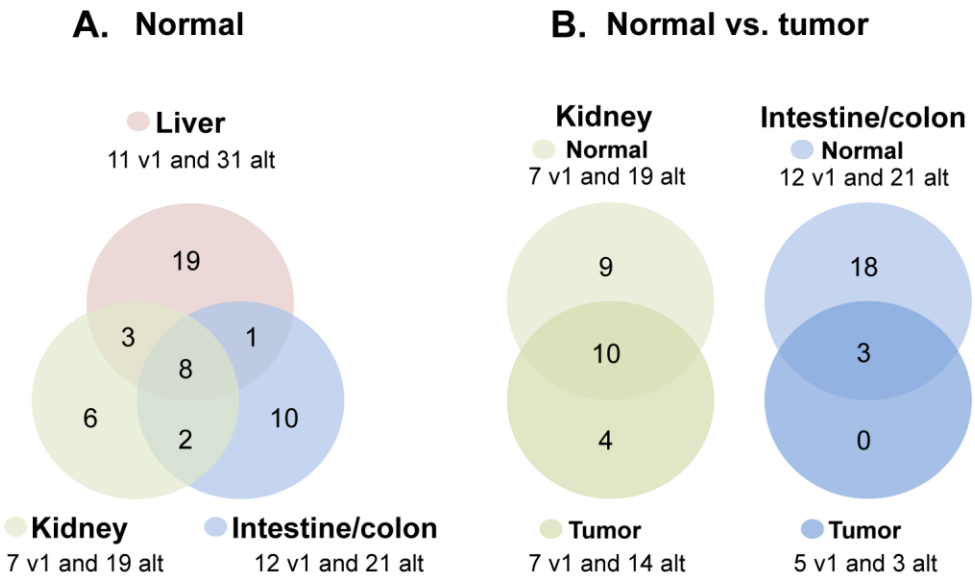
A. Normal
Liver
11 v1 and 31 alt
19
3
1
8
6
10
2
Kidney
7 v1 and 19 alt
Intestine/colon
12 v1 and 21 alt
B. Normal vs. tumor
Kidney
Normal
7 v1 and 19 alt
9
10
4
Tumor
7 v1 and 14 alt
Intestine/colon
Normal
12 v1 and 21 alt
18
3
0
Tumor
5 v1 and 3 alt

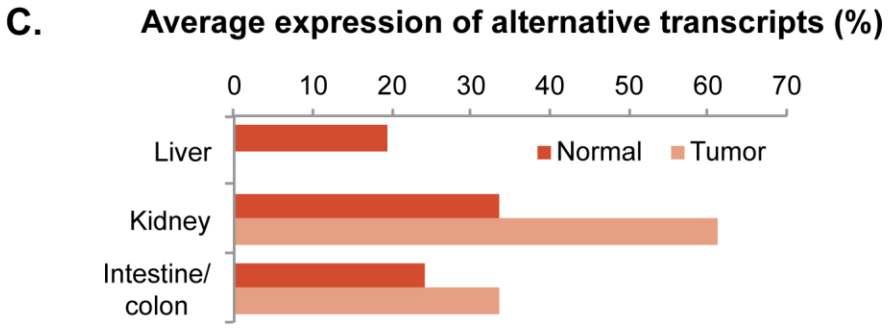
C. Average expression of alternative transcripts (%)
0
10
20
30
40
50
60
70
Liver
Kidney
Intestine/
colon
Normal
Tumor

Figure 3

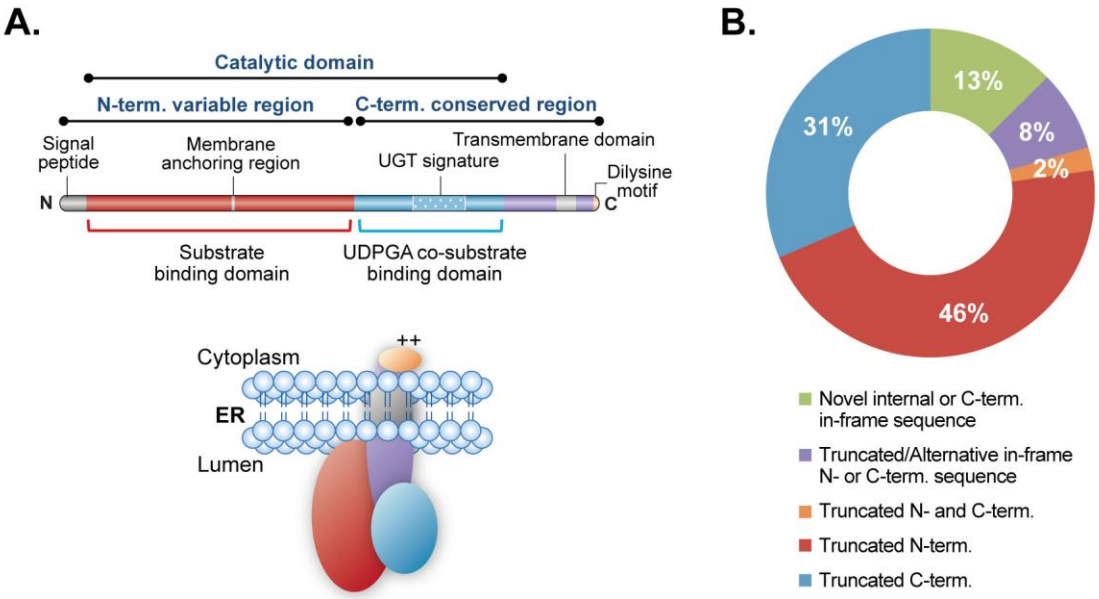
A.
Catalytic domain
N-term. variable region
C-term. conserved region
Signal peptide
Membrane anchoring region
UGT signature
Transmembrane domain
Dilysine motif
N
C
Substrate binding domain
UDPGA co-substrate binding domain
Cytoplasm
++
ER
Lumen
B.
13%
8%
2%
46%
31%
Novel internal or C-term. in-frame sequence
Truncated/Alternative in-frame N- or C-term. sequence
Truncated N- and C-term.
Truncated N-term.
Truncated C-term.

Figure 4

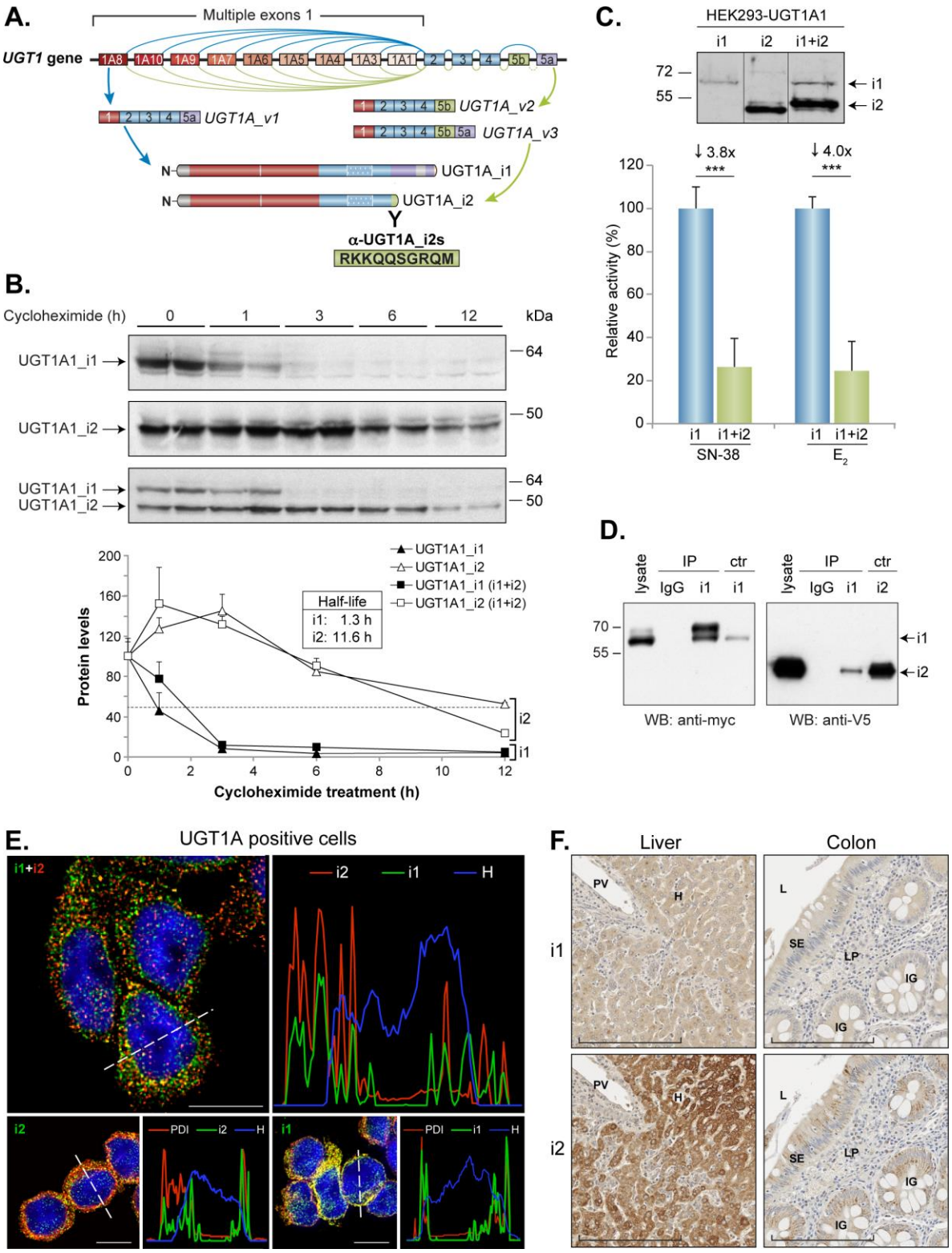
A.
Multiple exons 1
UGT1 gene
1A8 1A10 1A9 1A7 1A6 1A5 1A4 1A3 1A1 2 3 4 5b 5a
UGT1A_v1
UGT1A_v2
UGT1A_v3
UGT1A_i1
UGT1A_i2
α-UGT1A_i2s
RKKQQSGRQM
B.
Cycloheximide (h) 0 1 3 6 12 kDa
UGT1A1_i1
UGT1A1_i2
64
50
Protein levels
Half-life
i1: 1.3 h
i2: 11.6 h
Cycloheximide treatment (h)
C.
HEK293-UGT1A1
i1 i2 i1+i2
72
55
↓ 3.8x
↓ 4.0x
***
Relative activity (%)
SN-38
E2
D.
lysate IP IgG i1 ctr i1
lysate IP IgG i1 ctr i2
WB: anti-myc
WB: anti-V5
E.
UGT1A positive cells
i1+i2
i2 i1 H
PDI i2 H
PDI i1 H
F.
Liver
Colon
PV
H
L
SE
LP
IG

Figure 5

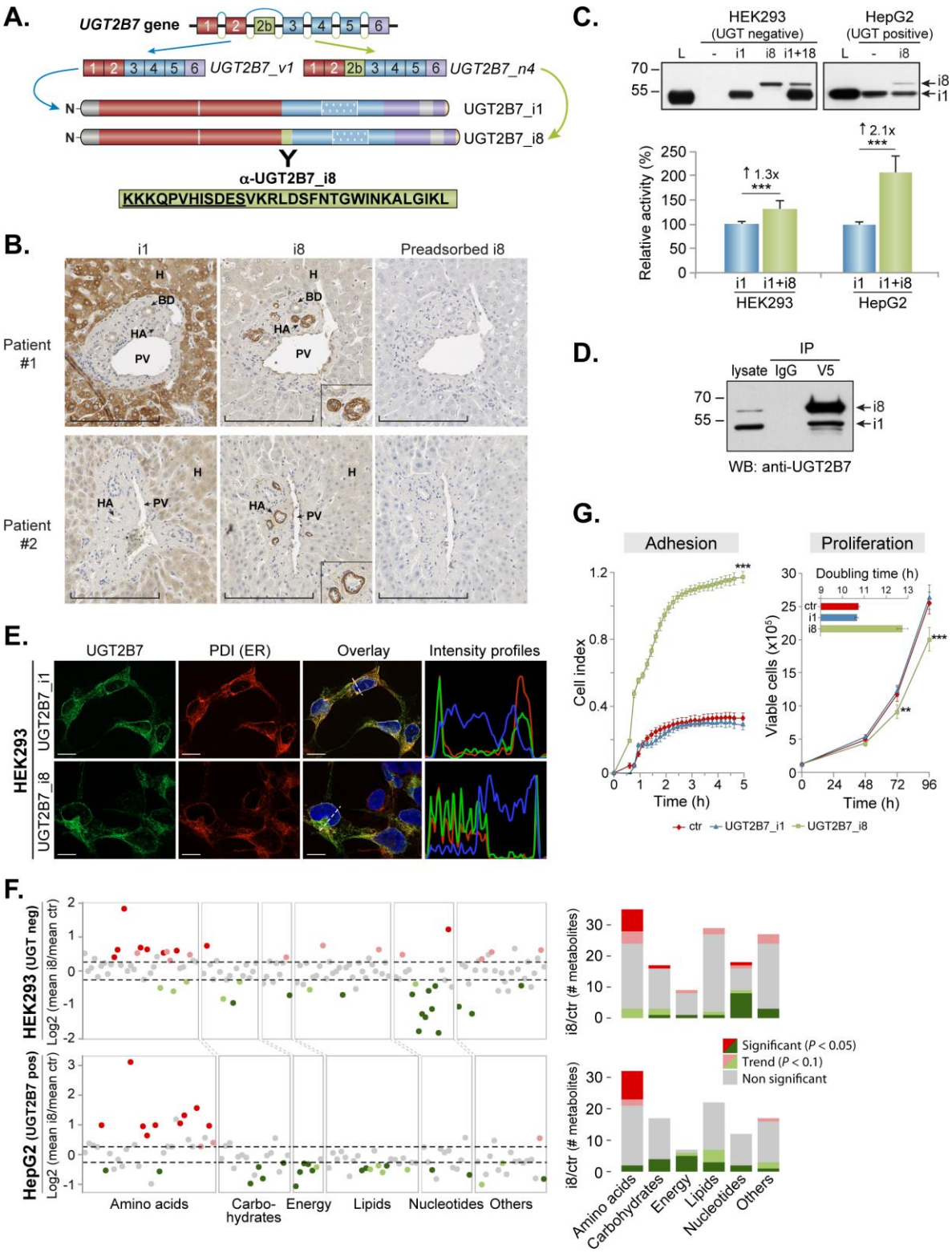
A.
UGT2B7 gene
UGT2B7_v1
UGT2B7_n4
UGT2B7_i1
UGT2B7_i8
α-UGT2B7_i8
KKKQPVHISDESVKRLDSFNTGWINKALGIKL
B.
i1
i8
Preadsorbed i8
Patient #1
Patient #2
H
BD
HA
PV
C.
HEK293 (UGT negative)
HepG2 (UGT positive)
L
i1
i8
i1+18
Relative activity (%)
1.3x
2.1x
HEK293
HepG2
D.
IP
lysate
IgG
V5
WB: anti-UGT2B7
E.
UGT2B7
PDI (ER)
Overlay
Intensity profiles
HEK293
UGT2B7_i1
UGT2B7_i8
F.
HEK293 (UGT neg)
HepG2 (UGT2B7 pos)
Log2 (mean i8/mean ctr)
Amino acids
Carbo-hydrates
Energy
Lipids
Nucleotides
Others
i8/ctr (# metabolites)
Significant (P < 0.05)
Trend (P < 0.1)
Non significant
G.
Adhesion
Proliferation
Cell index
Time (h)
Doubling time (h)
Viable cells (x10⁵)
ctr
UGT2B7_i1
UGT2B7_i8

Supplementary Material

Figure S1 related to Figure 2

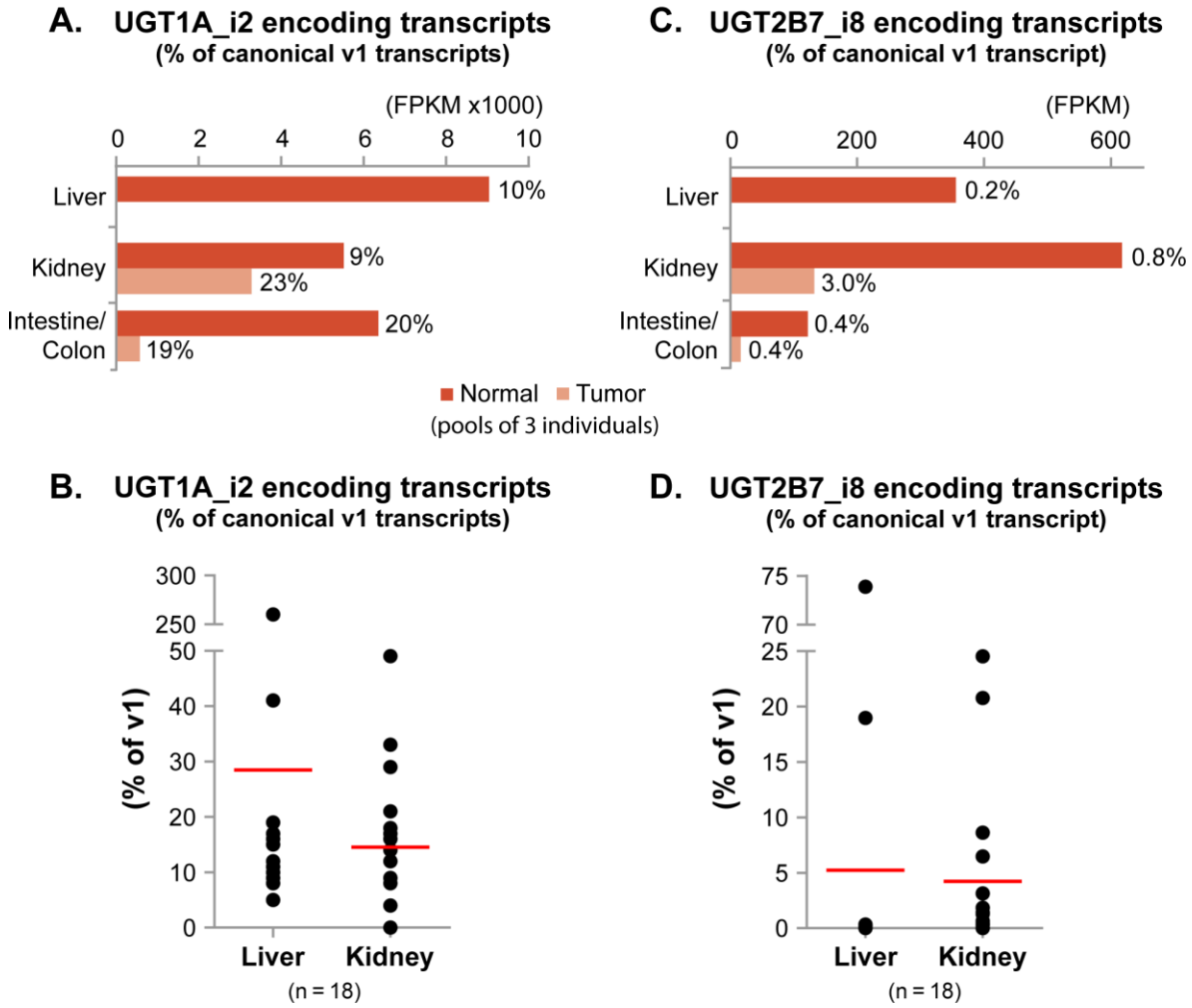

Figure S1: RNA-Seq expression data for canonical and alternative UGT variants, Related to Figure 2.

Figure S2 related to Figure 4

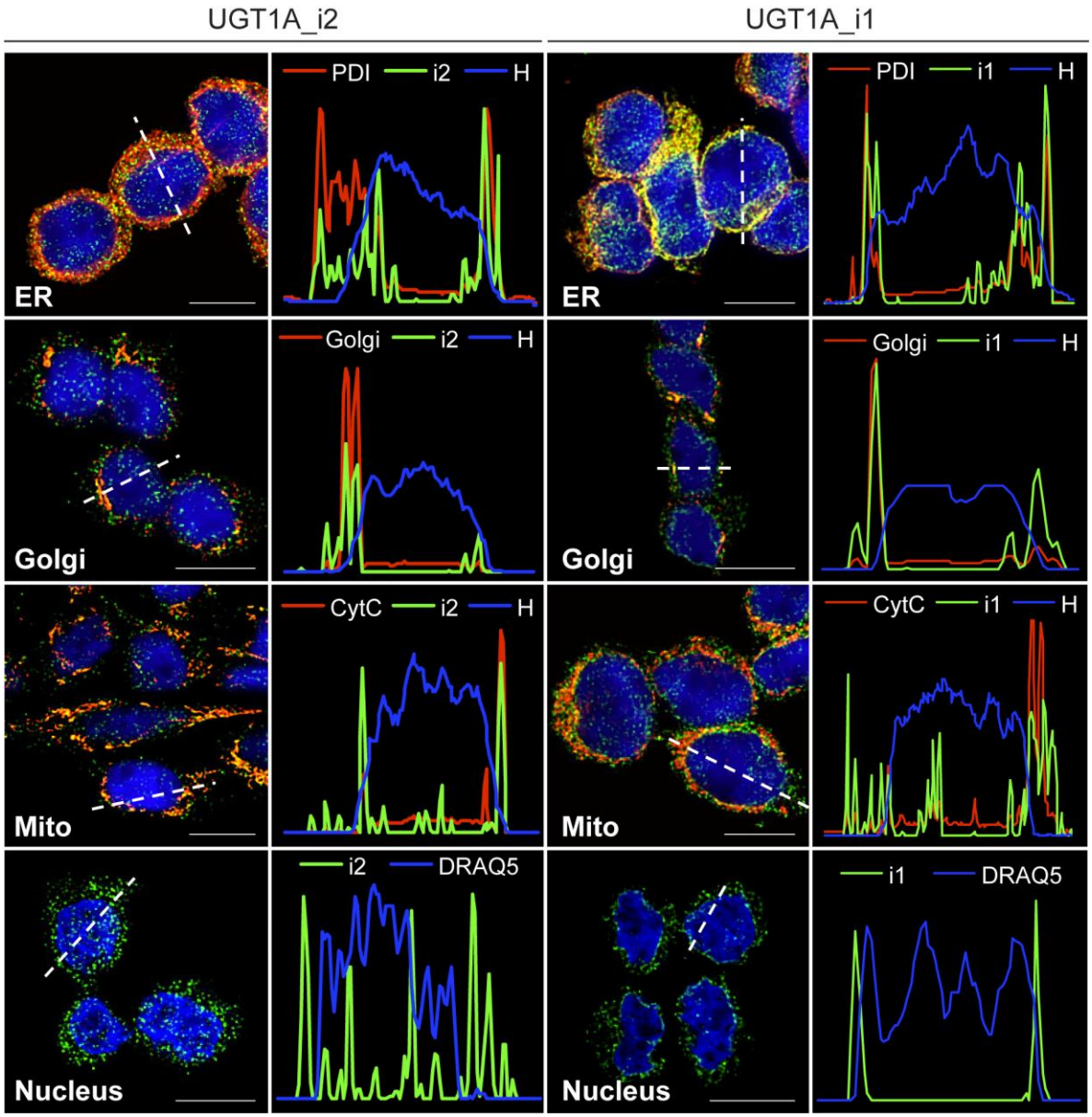

Figure S2: Subcellular distribution of UGT1A_i1 and UGT1A_i2 isoforms, Related to Figure 4E.

Figure S3 related to Figure 5

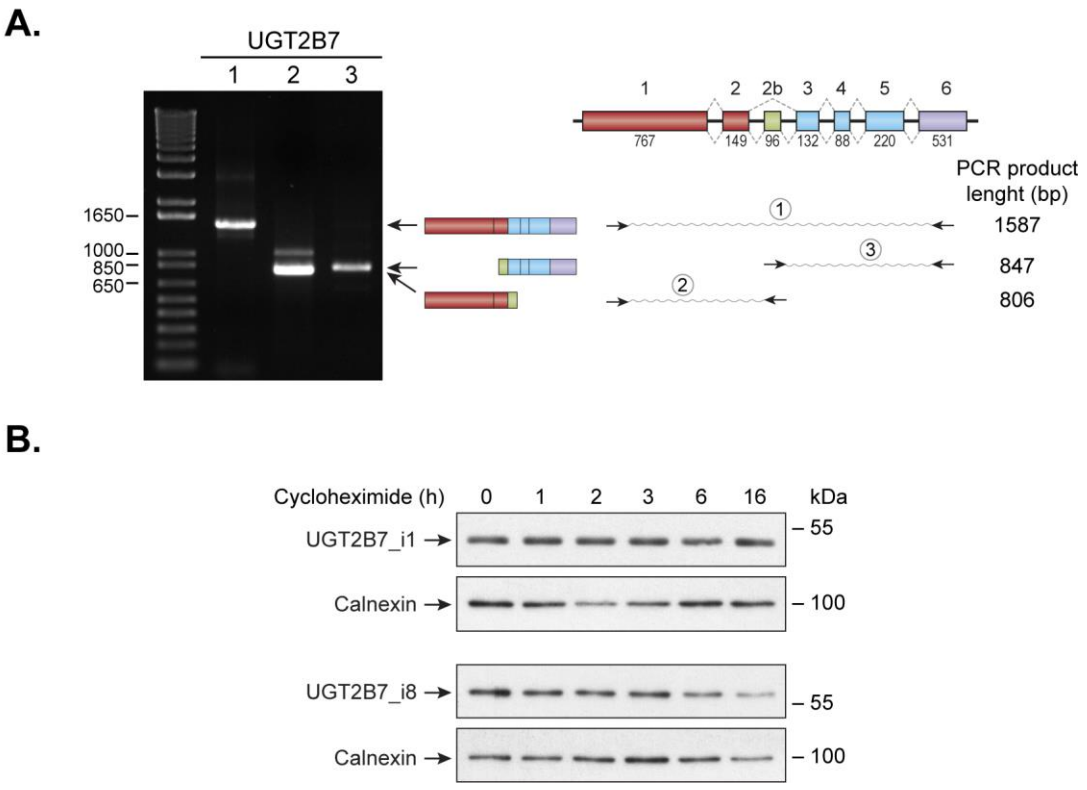

Figure S3: Validation of UGT2B7_i8 encoding transcript and protein stability, Related to Figure 5.

Figure S4 related to Figure 5

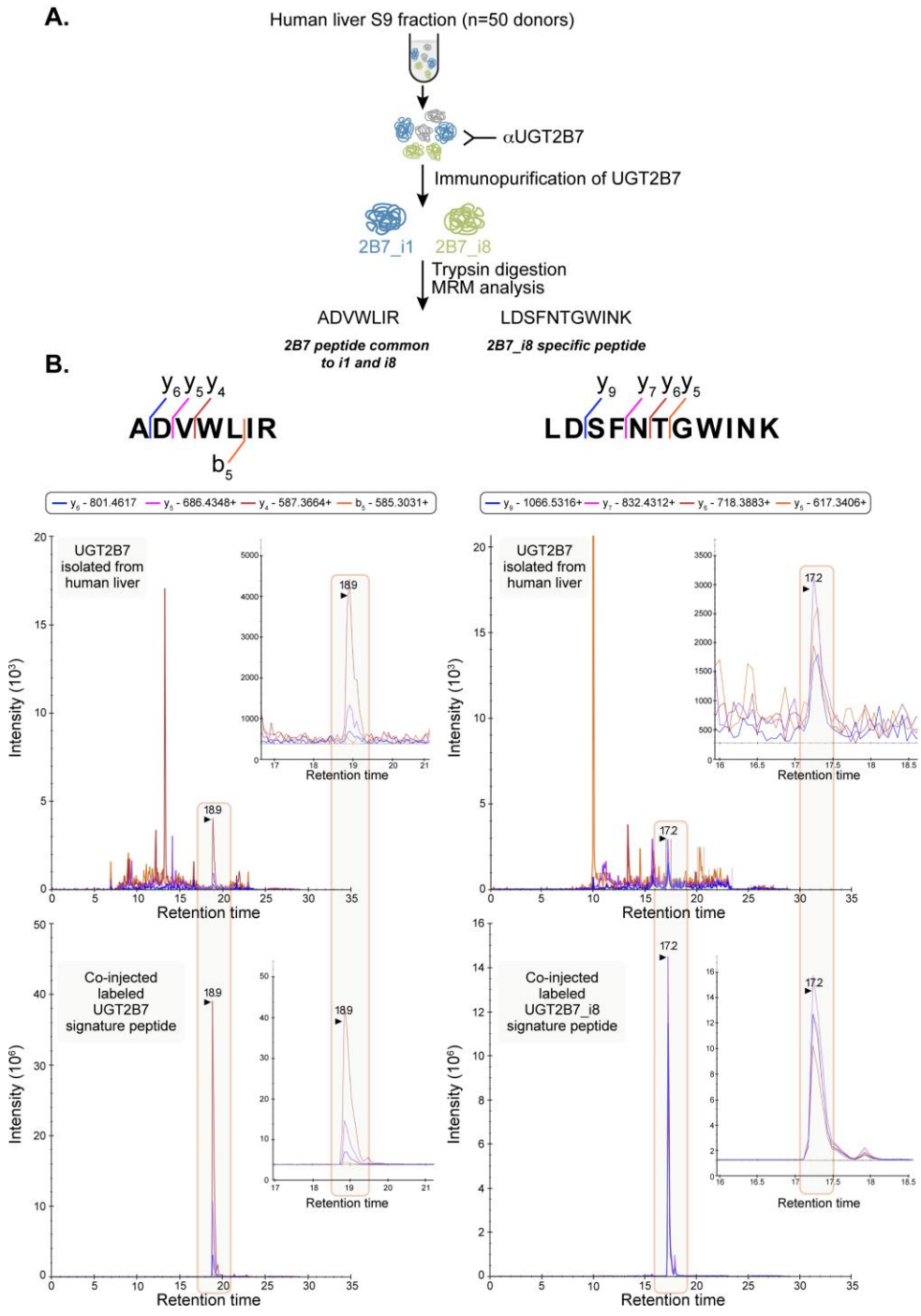

Figure S4: Detection of UGT2B7_i8 in human liver tissues by mass spectrometry, Related to Figure 5.

Figure S5 related to Figure S4

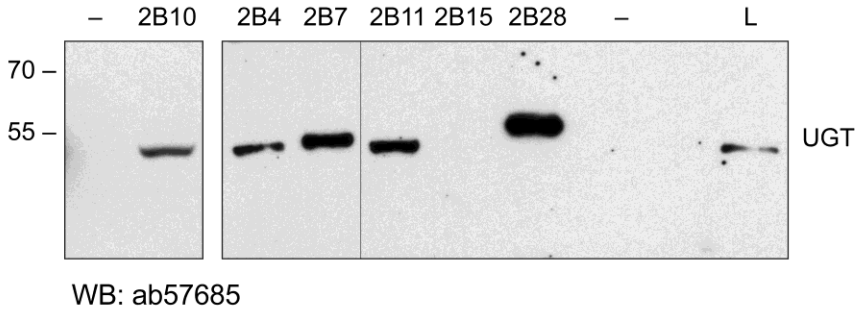

Figure S5: Specificity of the antibody ab57685 for human UGT2B proteins, Related to Experimental Procedures and Figure S4.

Discussion

En lien avec les objectifs de recherche, les travaux présentés dans cette thèse identifient de nombreux changements dans les concentrations intracellulaires de métabolites à la suite de changements dans la voie UGT. Ces métabolites sont impliqués dans plusieurs voies métaboliques et incluent des molécules qui ne sont pas des substrats documentés des enzymes UGT. Puisque les UGT sont connues pour interagir avec d'autres protéines, nous avons également caractérisé l'interactome endogène de ces enzymes ainsi que de certains de leurs variants alternatifs, révélant plusieurs similitudes, mais également des divergences dans l'identité des partenaires protéiques. Nous avons mis en évidence certains changements de phénotype, comme la migration et l'adhésion cellulaire des cellules cancéreuses, étant associés à une modification de l'expression des protéines UGT. Ces résultats supportent les hypothèses initiales de recherche et suggèrent l'existence d'une interconnexion plus étendue et complexe entre le métabolisme cellulaire et la voie de glucuronidation.

Des changements dans la voie des UGT entrainent des perturbations métaboliques étendues

Le premier objectif de cette thèse visait à étudier les changements métaboliques associés à une modification de la voie des UGT, incluant des enzymes parmi les plus caractérisées et abondantes, ainsi que de nouvelles protéines alternatives, dont le rôle est moins bien connu. À cette fin, nous avons exprimé des protéines UGT dans un modèle cellulaire n'exprimant pas ces enzymes de façon endogène (environnement UGT négatif; cellules HEK293), en plus de réprimer ou de surexprimer les protéines UGT dans des modèles exprimant ces protéines de façon endogène (environnement UGT positif; cellules HT115 et HepG2). Nous avons ensuite quantifié les métabolites intracellulaires dans ces modèles par une approche métabolomique non-dirigée; des analyses réalisées dans deux centres reconnus (Metabolon® et *West Coast Metabolomics Center*).

Les travaux présentés dans le premier article montrent l'étendue des modifications de nombreux métabolites cellulaires associées à l'expression de protéines UGT. Pour cette étude, les enzymes UGT1A1 et UGT2B7, ainsi que leurs variants alternatifs UGT1A1_i2 et UGT2B7_i8, ont été exprimés dans le modèle HEK293, révélant une modification des niveaux intracellulaires d'intermédiaires métaboliques variés appartenant à toutes classes

de biomolécules. Ces résultats sont en phase avec ceux présentés aux chapitres 4 et 6, dans lesquels l'expression des variants alternatifs UGT1A_i2 et UGT2B7_i8 a été modifiée dans les modèles HT115 et HepG2, respectivement. Dans l'ensemble, l'étude des changements métaboliques associés à une modification de l'expression des UGT supporte qu'une modification de l'expression de ces protéines entraine un remodelage des intermédiaires métaboliques des voies énergétiques, des acides nucléiques, des acides aminés et des lipides bioactifs. Au niveau fonctionnel, ces modifications dans les concentrations de métabolites intracellulaires pourraient contribuer à contrôler l'activité de nombreuses voies métaboliques, incluant la voie de glucuronidation. Cette régulation de l'activité pourrait se produire via plusieurs mécanismes, discutés plus bas, incluant 1) une modulation des niveaux de co-substrats des enzymes UGT (UDP-GlcA et UDP-Glc), 2) une régulation allostérique des enzymes par les endobiotiques, 3) une modification des conditions physico-chimiques membranaires ou 4) d'autres mécanismes de régulation indirects, telles les boucles de rétroaction.

Puisque l'activité UGT nécessite un co-substrat pour l'activité de conjugaison, il est attendu qu'une modulation des niveaux de co-substrat puisse influencer l'activité de glucuronidation si les concentrations de ce co-substrat deviennent limitantes. En ce sens, la littérature soutient que les niveaux d'UDP-GlcA sont limitants lors d'une exposition accrue à certains substrats des UGT, causant ainsi des toxicités néfastes (Gregus et coll., 1988; Braun et coll., 1997; Kultti et coll., 2009). Par exemple, Bray et Rosengren (2001) rapporte que les niveaux hépatiques d'UDP-GlcA diminuent de plus de trois fois, passant de ~250 µM à ~80 µM, chez des souris traitées avec une forte dose d'acétaminophène. Ces concentrations d'UDP-GlcA sont similaires à celles observées chez l'humain (Cappiello et coll., 1991) et correspondent environ à la constante d'affinité (K_m) moyenne du co-substrat pour les enzymes UGT1A humaines exprimées dans le foie (50-500 µM) (Luukkanen et coll., 2005). Or, nos travaux supportent que les niveaux des précurseurs du co-substrat UDP-GlcA appartenant à la voie glycolytique (glucose-6-phosphate, mannose-6-phosphate, fructose-6-phosphate) sont jusqu'à 20 fois inférieurs dans les cellules exprimant les UGT et ce, même en absence de supplémentation en substrat (condition de culture cellulaire normale, sans ajout de substrat exogène). Nos données supposent donc que ces intermédiaires représenteraient possiblement une étape limitante pour la synthèse d'UDP-GlcA. Afin de tester cette hypothèse, il serait possible de quantifier les glucuronides formés par des cellules supplémentées avec ces

intermédiaires glycolytiques, et de comparer cette quantité avec celle formée par des cellules non-supplémentées. Si ces intermédiaires glycolytiques représentent véritablement une étape limitante, nous devrions détecter moins de composés glucuronidés dans les cellules non supplémentées, reflétant la pénurie de co-substrat. Ces expériences permettraient de mieux comprendre les mécanismes régulant les niveaux intracellulaires d'UDP-GlcA et ultimement, de contrôler la disponibilité de ce co-substrat pour la réaction de glucuronidation.

En dehors de réguler les niveaux d'UDP-GlcA, les modifications métaboliques observées dans nos échantillons pourraient également refléter des mécanismes de contrôle allostérique de l'activité UGT. En effet, plusieurs métabolites endogènes sont identifiés dans la littérature comme étant de tels modulateurs de la voie de glucuronidation (Ishii et coll., 2010a). Par exemple, certains intermédiaires puriques et pyrimidiques sont associés à une répression allostérique de l'activité UGT, tel que l'UDP et le CTP (Koster et Noordhoek, 1983; Yokota et coll., 1998; Fujiwara et coll., 2008). Bien que les niveaux de ces deux métabolites ne soient pas altérés dans nos modèles cellulaires, nos travaux indiquent que les niveaux de plusieurs intermédiaires pyrimidiques en amont de ceux-ci sont augmentés dans les cellules exprimant les enzymes UGT, supportant un potentiel rôle de régulation via cette voie. D'autres molécules régulatrices, telles que l'ATP, le NADP+, des acyl-CoA, etc., pourraient être impliquées dans la régulation allostérique des UGT. Cependant, les niveaux intracellulaires de ces autres molécules régulatrices sont inconnus, nous empêchant de faire une analyse systématique de ces régulateurs endogènes. Afin de déterminer leur importance dans le contrôle de la voie de glucuronidation, il serait donc pertinent de développer une méthode analytique précise et reproductible, c'est-à-dire avec une courbe-étalon et des standards internes, afin de quantifier l'entièreté de ces molécules. Les niveaux de ces dernières pourraient alors être mis en corrélation avec l'activité de glucuronidation, ce qui nous permettrait de caractériser de façon systématique la contribution de ces molécules dans la régulation endogène de l'activité de la voie de glucuronidation.

La littérature soutient que la voie de glucuronidation pourrait aussi être affectée par les propriétés physico-chimiques des membranes entourant les enzymes; une modification des concentrations de certains lipides dans les essais enzymatiques *in vitro* étant associée à une modulation de l'activité de glucuronidation (Winsnes, 1972; Erickson et coll., 1978; Hochman et Zakim, 1983; 1984; Ishii et coll., 2010a; Liu et Coughtrie, 2017).

Parmi les diverses catégories de lipides, les acides gras polyinsaturés sont parmi ceux affectant le plus l'activité de la voie de glucuronidation (Shibuya et coll., 2013). Ces effets pourraient se produire via les propriétés physiques et biochimiques nombreuses de ces molécules, dont une modulation des niveaux cause une altération dans le transport d'ions et de substrats, ainsi que dans les interactions protéiques à la membrane (Zhang et coll., 2012; Schaefer et coll., 2016; Jeromson et coll., 2018; Sullivan et coll., 2018). Or, nous avons observé qu'une modification de l'expression des protéines UGT a pour conséquence de fortement augmenter les niveaux de plusieurs acides gras polyinsaturés dans nos modèles. L'accumulation de ces lipides pourrait ainsi refléter des processus métaboliques visant à moduler l'activité de glucuronidation. Supportant la capacité des UGT à modifier la composition lipidique des cellules, l'équipe de Dates et coll. (2015) a d'ailleurs observé une accumulation de lipides suite à une surexpression d'enzymes UGT dans des modèles de cancer du sein et du pancréas. En effet, l'expression des UGT2B4, UGT2B7 et UGT2B15 a pour conséquence d'augmenter la quantité de lipides intracellulaires contenus sous forme de gouttelettes lipidiques, une forme de stockage riche en lipides bioactifs (Bozza et coll., 2011; Dates et coll., 2015). Cependant, l'identité exacte des lipides accumulés était inconnue dans leurs échantillons, ainsi que l'influence de l'accumulation de ces lipides sur l'activité de glucuronidation. Dans l'ensemble, ces observations supportent la nécessité d'étudier davantage la relation entre les lipides intracellulaires et les UGT, puisque celle-ci pourrait être impliquée dans certaines maladies, incluant des cancers (Dates et coll., 2015) et la stéatose hépatique, caractérisée par une accumulation de lipides au foie en conséquence d'une exposition à certains médicaments, dont des substrats des UGT (Amacher et Chalasani, 2014).

Il est également possible que les modifications dans les concentrations de métabolites intracellulaires reflètent la participation de ces molécules à des boucles de rétroaction potentiellement impliquées dans le contrôle de leurs niveaux et de l'expression des UGT. Par exemple, nos données ont identifié l'acide arachidonique (AA) comme étant l'un des métabolites les plus fortement accumulés suite à l'expression des UGT1A1 et UGT2B7. Or, ces enzymes sont connues pour conjuguer cet acide gras (Little et coll., 2004). Par ailleurs, Caputo et coll. (2011) ont montré que supplémenter des cellules HepG2 en AA menait à une répression de l'expression en ARN messager de l'UGT1A1. Il appert donc qu'une forte expression d'UGT1A1 cause une augmentation des niveaux d'AA, et que de fortes concentrations d'AA entraînent une diminution de l'expression de l'UGT1A1 dans

des modèles exprimant cette enzyme de façon endogène. Il serait cependant nécessaire de mieux caractériser cette boucle de rétroaction. Quels sont les mécanismes impliqués dans cette boucle de régulation? Comment celle-ci affecte l'activité de la voie de glucuronidation, incluant l'expression des autres isoenzymes et isoformes UGT? Comment l'activité de la voie de glucuronidation affecte les niveaux d'AA? Pour répondre à ces questions, il serait pertinent de caractériser l'activité enzymatique et l'expression des UGT et de leurs variants alternatifs à la suite d'une supplémentation en AA, dans des modèles exprimant ces protéines de façon endogène, telles les cellules HepG2 ou HepaRG®. Complémentairement, il serait aussi approprié 1) de modifier l'expression des UGT et de leurs isoformes dans ces modèles et de quantifier les lipides polyinsaturés; et 2) de moduler l'activité de PLA2, essentiel au relargage de l'acide arachidonique à partir des phospholipides, afin de valider les effets de l'AA endogène sur l'expression et l'activité UGT. Ces expériences permettraient de caractériser de façon approfondie la boucle de rétroaction impliquant l'AA et les UGT, ainsi que le rôle de la voie de glucuronidation sur le contrôle des niveaux d'AA. Une meilleure connaissance de cette interconnexion permettrait éventuellement un meilleur contrôle de cette boucle de rétroaction, qui semble notamment impliquée dans les cas d'hyperbilirubinémie néonatale (Shibuya et coll., 2013).

L'approche métabolomique non-dirigée que nous avons retenue a permis d'observer des modifications dans les niveaux de métabolites impliqués dans de nombreuses voies métaboliques et ce, suite à une modification de l'expression des UGT. Ceci a été rendu possible grâce à la grande diversité de molécules quantifiées par cette approche. Cette grande diversité d'analytes apporte cependant un certain désavantage : elle rend difficile l'utilisation d'une courbe étalon pour l'entièreté des molécules, rendant la quantification relative, plutôt qu'absolue. Bien que la validité des expériences demeure, il est cependant difficile de comparer certains résultats obtenus entre deux séries d'expériences et entre les deux plateformes reconnues que nous avons utilisées, c'est-à-dire *Metabolon*® et *West Coast Metabolomics Center*. La disparité dans l'identité de certains métabolites identifiés par les deux plateformes complique également la comparaison de certains résultats entre deux séries d'expériences. Notons aussi l'absence de quantification pour certaines molécules clés du métabolisme cellulaire, telles les hormones stéroïdiennes et thyroïdiennes, reconnues comme étant des substrats des UGT. Ces facteurs combinés limitent quelque peu notre capacité à caractériser certains effets plus spécifiques des

divers UGT étudiés dans plusieurs modèles. Malgré tout, nos études identifient clairement des modifications similaires pour de nombreuses voies métaboliques, supportant la validité de nos observations.

Il importe de souligner les forces et les limitations associées à notre étude du métabolome dans des modèles *in vitro* de lignées cellulaires. Représentant une force de nos études, nous avons utilisé des modèles cellulaires avec différents environnements protéiques. Le modèle HEK293, UGT négatif, a permis d'observer les changements métaboliques associés à une enzyme ou une isoforme alternative UGT pour les nombreuses voies métaboliques présentes dans ce modèle, sans interférence des autres protéines UGT endogènes. D'un autre côté, les modèles HT115 et HepG2, exprimant de façon endogène certaines isoformes UGT, ont permis de caractériser les interactions entre les différentes isoformes alternatives et enzymes UGT, ainsi qu'avec les nombreuses voies métaboliques présentes dans ces modèles. Les protéines UGT ont été exprimées de façon stable dans ces modèles cultivés dans des conditions de culture standards, afin de mieux caractériser l'interrelation entre les UGT et le métabolisme cellulaire de base à l'équilibre; en opposition avec l'étude dynamique des flux métaboliques en réponse à des stimuli externes ou du microenvironnement. La méthode sélectionnée semblait une première étape adéquate afin de répondre aux objectifs, quoique la seconde approche constituerait certainement l'objet de recherches futures.

Une limite des études métabolomiques à l'aide de modèles cellulaires repose sur le choix de la méthode de récolte et de normalisation des échantillons, deux facteurs pouvant influencer les résultats d'études métabolomiques selon une étude récente (Muschet et coll., 2016). Afin de minimiser ces effets, notre laboratoire a utilisé une seule méthode pour récolter les échantillons pour le métabolomique, c'est-à-dire par trypsinisation des cellules. Cependant, la normalisation des résultats métabolomiques a varié selon les standards des plateformes utilisées, s'appuyant sur le nombre de cellules (*West Coast Metabolomics Center*; Chapitres 4 et 6), ou sur la concentration protéique (Metabolon®; Chapitre 2). Bien que le compte cellulaire montre le plus faible coefficient de variation entre les réplicats, la normalisation par la concentration protéique est généralement bien corrélée au nombre de cellules lorsque ce dernier est élevé (plus d'un million de cellules), tel que dans nos échantillons (Silva et coll., 2013; Muschet et coll., 2016). Néanmoins, une seule méthode de normalisation devrait être utilisée dans les prochaines études afin

d’éviter un biais potentiel relié à la normalisation des métabolites issus d’échantillons cellulaires.

Finalement, il est important de souligner le caractère novateur de nos travaux. En effet, ceux-ci sont les premiers à rapporter une perturbation significative du métabolisme global de la cellule suite à une modification de l’expression des enzymes et protéines alternatives UGT humaines. Nous avons ainsi observé des modifications dans les niveaux de métabolites impliqués dans de nombreux sentiers métaboliques, exposant non seulement l’ampleur des mécanismes de régulation pouvant contrôler l’activité de glucuronidation, mais révélant également l’étendue des transformations métaboliques pouvant résulter d’une modification de l’activité de la voie glucuronidation. Nos travaux supportent qu’une meilleure connaissance de l’interconnexion entre le métabolisme cellulaire et la voie de glucuronidation permettrait de mieux comprendre les déterminants de l’activité de cette voie et du métabolisme cellulaire, et potentiellement de pouvoir les influencer. Est-ce que certains métabolites identifiés dans nos travaux pourraient représenter des biomarqueurs de l’activité de glucuronidation chez l’individu? Est-ce que certains intermédiaires métaboliques pourraient être modulés chez l’humain pour adapter la réponse aux médicaments? Ces questions restent en suspens, mais y répondre représenterait de grandes avancées dans le domaine.

Les protéines UGT font partie de réseaux d’interactions protéiques complexes et affectent l’activité de certains partenaires

Tel que mentionné en introduction, certaines des répercussions métaboliques associées à une modification de l’expression des UGT pourraient en fait découler de la capacité de ces protéines à interagir avec des protéines impliquées dans d’autres voies métaboliques. Notre second objectif visait ainsi à établir le réseau d’interaction protéique, ou l’interactome, des protéines UGT. Utilisant la purification d’affinité couplée à la spectrométrie de masse, nous avons identifié un nombre important d’interacteurs protéiques potentiels des enzymes de la famille UGT1A, ainsi que de leurs variants alternatifs UGT1A_i2, tel que présenté aux chapitres 3 et 4, respectivement. Nos résultats supportent que l’interactome endogène des enzymes UGT1A inclut non seulement des partenaires du métabolisme des xénobiotiques, mais également de la glycolyse et la gluconéogenèse, de l’oxydation des acides gras, de la signalisation du glucagon, ainsi

que du trafic vésiculaire. De façon similaire, nos résultats supportent que les UGT1A_i2 peuvent interagir avec plusieurs protéines de la glycolyse, du cycle des acides tricarboxyliques, de la signalisation du glucagon et du métabolisme du tryptophane. Avant ces travaux, seulement quelques interacteurs des enzymes UGT1A avaient été identifiés, notamment des protéines UGT et des CYP (abordé en introduction), alors que certaines enzymes du métabolisme des ROS avaient été identifiées comme partenaires des UGT1A_i2, telles que la catalase et la peroxiredoxine (Rouleau et coll., 2014). Nos travaux exposent donc un interactome étendu pour les enzymes et protéines UGT1A, dont les implications sur le métabolisme cellulaire et sur la voie de glucuronidation demeurent inconnues, malgré la contribution des travaux de cette thèse.

Dans un premier temps, il importe de souligner la similitude des voies métaboliques auxquelles appartiennent les partenaires des enzymes et des protéines alternatives UGT1A. Cette observation est cohérente avec la grande homologie que partage ces deux types de protéines, se différenciant seulement par leur portion C-terminale (Girard et coll., 2007). Parmi les interacteurs communs des enzymes et des protéines UGT1A, nous retrouvons plusieurs enzymes impliquées dans les voies énergétiques. Or, nous avons également observé des changements métaboliques similaires associés à l'expression de l'enzyme UGT1A1 et de sa protéine alternative dans les voies glycolytiques. Ainsi, le partenariat des UGT avec les différentes protéines impliquées dans les voies énergétiques pourrait supporter le remodelage des intermédiaires métaboliques impliqués dans la synthèse du co-substrat UDP-GlcA, ou encore la synthèse d'autres régulateurs allostériques endogènes (Ishii et coll., 2010a). D'autres expériences sont cependant nécessaires pour mieux comprendre ces phénomènes. À cette fin, des régulateurs allostériques endogènes pourraient être supplémentés aux cellules dans le but d'altérer l'activité des partenaires des UGT. Par exemple, le fructose-1,6-bisphosphate est connu pour activer l'enzyme phosphofructokinase, un partenaire potentiel des UGT1A qui est situé à une étape charnière de la glycolyse (Yi et coll., 2012). On pourrait ainsi supplémenter ce métabolite aux cellules afin d'activer la glycolyse au détriment de la synthèse d'UDP-GlcA. Il serait attendu qu'un tel traitement diminuerait les concentrations d'UDP-GlcA intracellulaires, et du coup de l'activité de glucuronidation, confirmant ainsi le rôle clé de ce partenaire dans le contrôle de la voie de glucuronidation.

La confirmation des partenariats constitue une étape cruciale dans l'étude d'un l'interactome. En ce sens, nous avons validé plusieurs partenaires des enzymes UGT1A

par co-immunprécipitation en utilisant des protéines arborant des peptides étiquettes, tels que ACOT8, SH3KBP1 et PHKA2. Cette approche a pour avantage de confirmer la spécificité des partenariats, puisqu'elle repose sur l'utilisation d'anticorps différents de ceux utilisés lors des purifications d'affinité pour la protéomique, en plus d'être réalisée dans un modèle cellulaire différent. De plus, une co-localisation partielle entre les UGT et les partenaires ACOT8 et SH3KPB1 a été observée par microscopie confocale, appuyant davantage le potentiel d'interaction entre les partenaires.

Au niveau fonctionnel, plusieurs de nos observations supportent l'existence de répercussions métaboliques découlant de ces interactions protéiques entre les UGT et leurs partenaires. Par exemple, l'accumulation de gouttelettes lipidiques a été observée dans un modèle exprimant l'enzyme UGT1A9, indiquant un remodelage du métabolisme des lipides (Chapitre 3). Or, plusieurs partenaires protéiques des enzymes UGT1A sont impliqués dans l'oxydation des acides gras, incluant ACOT8, un partenaire validé de l'enzymes UGT1A9_i1. De plus, notre étude du métabolome suite à une expression des enzyme UGT1A a identifié une modification des niveaux de plusieurs dérivés lipidiques pouvant contribuer à l'accumulation des gouttelettes lipidiques (Chapitre 2), tels les phospholipides et les acylglycérols incorporant l'AA (Bozza et coll., 2011). Ainsi, nos données issues de l'étude du métabolome et de l'interactome des UGT1A coïncident, et sont supportées par des observations phénotypiques, renforçant la justesse de nos observations.

Nos résultats supportent également que les interactions entre les protéines alternatives UGT1A_i2 et leurs partenaires entraînent des changements dans le métabolome. Ainsi, une interaction entre OGDHL et UGT1A1_i2 a été validée dans le modèle HEK293 (Chapitre 2). Cette observation fait écho aux données métabolomiques montrant que les intermédiaires situés en aval du complexe OGDC, dont OGDHL fait partie, s'accumulent dans les cellules exprimant ce variant alternatif. De plus, une interaction spécifique entre les UGT1A_i2 et PKM2 est validée dans le modèle de cancer du côlon HT115, où aucune interaction entre les UGT1A_i1 et PKM2 n'est détectée. Bien que les deux types d'isoformes UGT1A soient exprimés dans ce modèle, nos données supportent que le métabolisme énergétique puisse être affecté par la répression des UGT1A_i2, potentiellement via une modification de l'activité PKM2. Ces deux partenaires des UGT1A_i2 sont des protéines clés du métabolisme énergétique (Mazurek, 2011; Sen et coll., 2012). Ces observations soutiennent ainsi que les protéines alternatives UGT1A_i2

joueraient un rôle de régulateur métabolique, dont l'action serait médiée par les interactions protéine-protéine; puisque aucune activité transférase avec le co-substrat UDP-GlcA n'a été détectée à ce jour pour ces variants alternatifs. De plus, le fait que PKM2 soit un partenaire spécifique aux UGT1A_i2 démontre la capacité de ces protéines à induire des effets métaboliques distincts de ceux des enzymes. L'existence de tels partenaires spécifiques peut notamment découler de la différence de séquence peptidique de ces protéines alternatives en comparaison avec les enzymes canoniques. Effectivement, la séquence et/ou la structure tridimensionnelle des UGT1A_i2 pourraient leur permettre d'interagir avec d'autres protéines, puisque celles-ci pourraient présenter/omettre des régions promouvant les interactions protéine-protéine. Toutefois, très peu d'informations sont connues sur la topologie des UGT, en dehors d'une partie du domaine catalytique de l'UGT2B7 (Miley et coll., 2007). Soutenant l'existence d'interactions différentielles pour les protéines alternatives UGT1A_i2, des travaux précédents du laboratoire avaient révélé que certains domaines peptidiques étaient nécessaires à l'homo-oligomérisation des enzymes, alors qu'ils ne l'étaient pas pour l'oligomérisation des protéines alternatives (Rouleau et coll., 2013a). Par ailleurs, la localisation subcellulaire des protéines alternatives UGT1A_i2 semble diverger de celle des enzymes UGT1A_i1 (Chapitre 6). Ainsi, nos travaux soutiennent que ces protéines sont partiellement localisées en dehors du RE, une localisation différentielle qui leur permettrait d'interagir avec des partenaires protéiques autres que ceux des enzymes canoniques, incluant des partenaires clés du métabolisme énergétique.

Dans l'ensemble, nos travaux expandent considérablement l'interactome endogène des protéines UGT1A, les situant au cœur d'un réseau d'interaction complexe entraînant possiblement plusieurs changements métaboliques. Cependant, d'autres études sont nécessaires pour mieux caractériser le rôle de ces interactions dans le contrôle du métabolisme cellulaire et ce, dans plusieurs contextes. En outre, la plupart des partenaires n'ont été validés que dans un seul modèle cellulaire, et puisque l'environnement protéique fluctue grandement d'un type cellulaire à l'autre, il est fort possible que les changements causés par ces interactions soient différents (Buljan et coll., 2012). Par ailleurs, certains interacteurs communs pourraient être le fruit d'interactions indirectes avec la cible des immunoprécipitations. En effet, les UGT1A_i1 sont connus pour interagir avec les protéines alternatives UGT1A_i2. Or, les extraits tissulaires utilisés pour faire les analyses protéomiques présentent une expression des deux types d'isoforme UGT1A. Ainsi, il est

possible que les partenaires identifiés lors des immunoprécipitations des enzymes soient en fait des partenaires des protéines alternatives, et vice versa. C'est pourquoi la validation des partenaires par l'utilisation de techniques complémentaires, comme nous l'avons fait, est essentielle. De plus, d'autres systèmes expérimentaux pourraient être considérés pour la validation des partenariats. Par exemple, les essais de ligation dépendants de la proximité (voir le Tableau 4 pour une description de la technique) constitueraient une approche adéquate pour valider les interactions protéiques. En effet, cette approche n'émet du signal que lorsque les protéines sont en très forte proximité[1] l'une de l'autre, permettant donc d'éviter une partie du bruit de fond inhérent à la détection des protéines via des anticorps couplés à des fluorophores. Le laboratoire établit actuellement cette approche, qui permettra une meilleure évaluation du potentiel d'interaction des partenaires avec les UGT.

Les travaux présentés dans cette thèse supportent par ailleurs une interaction entre l'enzyme UGT2B7 et son variant alternatif UGT2B7_i8 (Chapitre 6). À l'instar de de la co-expression des UGT1A_i1 et UGT1A_i2, la co-expression de l'enzyme et de la protéine alternative UGT2B7 induit des changements dans l'activité de glucuronidation. La co-expression de ces deux isoformes apporte une augmentation de l'activité UGT, telle que détectée par des essais enzymatiques en cellules intactes. La séquence unique de l'UGT2B7_i8 semble ainsi lui conférer cette fonction, qui se produirait vraisemblablement par des interactions protéiques. Toutefois, l'influence de cette séquence sur l'interactome de l'UGT2B7_i8 est inconnue, car les interactomes endogènes de ce variant alternatif et de son enzyme n'ont pas encore été investigués et ce, malgré la contribution majeure de l'UGT2B7 dans la voie de glucuronidation et l'expression importante de ce variant alternatif dans certains tissus (Guillemette et coll., 2014; Margaillan et coll., 2015b; Tourancheau et coll., 2018).

Dans le même ordre d'idée, nos travaux supportent également l'existence d'interactions protéiques entre l'UGT2B10 et ses variants alternatifs UGT2B10_i4 et UGT2B10_i5 (Chapitre 5). Ces variants alternatifs, possédant chacun une séquence additionnelle dans leur portion C-terminale, semblent également en mesure de moduler l'activité

[1] La distance maximale entre les protéines doit être inférieure à 40 nm selon les notes d'application du *Duolink*® *Proximity Ligation Assay* de Sigma-Aldrich®. https://www.sigmaaldrich.com/technical-documents/protocols/biology/duolink-troubleshooting-guide.html; consulté le 16 juin 2018.

enzymatique de l'UGT2B10. Cependant, les effets de ces protéines alternatives semblent dépendants du contexte cellulaire, puisque nous avons observé une diminution de l'activité pour certains substrats dans la lignée HEK293 (UGT négatif), et une augmentation de l'activité pour ces mêmes substrats dans le modèle HepG2 (UGT positif). Ces observations apportent ainsi une complexité supplémentaire aux modulations entraînées par les interactions hétéro-oligomériques des UGT. En effet, celles-ci supportent que l'environnement cellulaire puisse impacter la façon dont de ces interactions module l'activité UGT. Est-ce seulement la présence des enzymes UGT endogènes qui influencent cette modulation, ou est-elle médiée par des interactions avec d'autres protéines ou des métabolites? D'autres études sont nécessaires pour répondre à ces questions et caractériser l'influence de l'environnement protéique et métabolique cellulaire sur la régulation de l'activité de la voie de glucuronidation. Répondre à ces questions est d'autant plus important lorsqu'on considère que l'environnement cellulaire (Li et coll., 2018), de même que l'épissage alternatif des protéines, sont fortement modifiés lors de néoplasies (Chen et Weiss, 2015; Yang et coll., 2016), ce qui pourrait non-seulement affecter l'activité de glucuronidation, mais également toutes les voies y étant associées.

Changements phénotypiques associés aux protéines UGT

En lien avec les observations précédentes, nous avons cherché à déterminer si ces changements dans le métabolisme cellulaire ont un effet sur le phénotype cellulaire, au-delà de la perturbation de l'activité de glucuronidation. Nos travaux sont les premiers à rapporter de telles conséquences phénotypiques suite à une modulation de l'expression de protéines alternatives des UGT. En effet, nos travaux indiquent que la répression stable des protéines UGT1A_i2 dans les cellules de cancer du côlon HT115 mène à une augmentation du potentiel migratoire de ces cellules. Ce phénotype est relié à une plus faible adhésion de ces cellules pour diverses matrices extracellulaires, incluant le collagène de type I, la laminine et la ténascine (Chapitre 4). De plus, la répression des UGT1A_i2 est associée à une augmentation de l'activité glycolytique au détriment de l'activité mitochondriale dans le même modèle cellulaire. Ces résultats supportent que les cellules tumorales de côlon voient leur potentiel d'agressivité augmenté par une répression des protéines alternatives UGT1A_i2. Ces résultats font suite à la démonstration que la répression des UGT1A_i2 peut mener à une augmentation de la résistance des cellules HT115 à l'agent thérapeutique SN-38 (Rouleau et coll., 2014).

Dans l'ensemble, ces travaux soutiennent qu'une répression des niveaux de ces protéines serait favorable à la progression tumorale.

Nos données supportent également qu'une répression des protéines alternatives UGT1A_i2 dans la lignée HT115 sensibilise les cellules à une déprivation en sérine et glycine. Quoiqu'ils ne soient pas considérés comme des oncométabolites à proprement parler, la littérature supporte que certains acides aminés seraient cependant essentiels au métabolisme tumoral (Labuschagne et coll., 2014; Ananieva et Wilkinson, 2018). Cette observation soulève la question suivante : est-ce que les traitements antinéoplasiques reposant sur des cibles associées à ces acides aminés verraient leurs effets potentialisés par une répression des UGT1A_i2? Pour répondre à cette question, il serait pertinent d'étudier la sensibilité de nos cellules aux agents thérapeutiques ciblant ces voies, comme le 5-fluorouracile et le méthotrexate, déjà utilisés dans le traitement du cancer colorectal (Myte et coll., 2017). Par ailleurs, les données métabolomiques soutiennent que les concentrations de plusieurs autres acides aminés sont également perturbées dans ce modèle. Considérant que ceux-ci peuvent représenter des réservoirs de groupements chimiques actifs (Labuschagne et coll., 2014; Yang et coll., 2014a; Baggott et Tamura, 2015; Knott et coll., 2018), le traçage métabolique de ces groupements pourrait assurément nous renseigner sur le devenir de ceux-ci. De tels résultats permettraient potentiellement la découverte de nouvelles cibles thérapeutiques, qui pourraient être exploitées par la suite. Une approche similaire a été utilisée pour les voies utilisant la glutamine, démontrant le fort potentiel de cette approche (Zhang et coll., 2014).

Ces observations doivent cependant être répliquées dans d'autres contextes. La validation de ces observations nécessite toutefois la création de modèles expérimentaux supplémentaires. Or, le laboratoire s'est heurté à plusieurs obstacles lors de la création de tels modèles. En effet, la région disponible pour le design d'un court ARN en forme d'épingle à cheveux spécifique aux isoformes UGT1A_i2 est réduite, limitant le nombre de candidats disponibles (Rouleau et coll., 2014). Bien que nous ayons obtenu une efficacité de répression aux alentours de 90% au niveau protéique dans le modèle HT115, cette efficacité était souvent moindre dans les autres modèles testés. De plus, l'expression initiale des enzymes et de protéines alternatives UGT1A dans les modèles cellulaires doit être représentative des niveaux d'expression relatifs de ces isoformes dans le côlon, c'est-à-dire environ deux fois plus d'enzymes que de protéines alternatives (Girard et coll., 2007). Finalement, la répression des protéines alternatives UGT1A_i2 dans le modèle

cellulaire ne doit pas altérer l'expression des enzymes, puisque cela rendrait impossible la différentiation des effets causés spécifiquement par les protéines alternatives. Au vu des résultats obtenus dans le modèle HT115, les efforts pour établir d'autres modèles réprimés en UGT1A_i2 devraient cependant être poursuivis.

La pertinence de nos observations est néanmoins supportée par le fait que les protéines alternatives UGT1A_i2 sont réprimées dans les tumeurs de côlon, à l'instar de notre modèle cellulaire. Puisque la répression des protéines UGT1A_i2 est associée à un phénotype plus agressif dans notre modèle, il est donc possible que celles-ci soient impliquées dans la progression de cette maladie. Afin de valider cette hypothèse, il faudrait corréler l'expression de ces protéines avec la progression tumorale. Malheureusement, en raison du génome de référence omettant les protéines alternatives UGT, leur expression n'est pas disponible a priori dans les bases de données publiques, telle celle du consortium *The Cancer Genome Atlas* (TCGA). Afin d'évaluer l'expression de ces protéines alternatives, les lectures issues de séquençage à haut débit doivent être réalignées sur un génome de référence bonifié par nos travaux pour ces loci UGT (Tourancheau et coll., 2016). Afin d'avoir un meilleur portrait de l'expression des protéines alternatives dans les tissus tumoraux, un tel réalignement a récemment été entrepris par le laboratoire, notamment pour des échantillons dérivés de tumeurs colorectales. À terme, il sera donc possible d'investiguer l'expression des protéines alternatives en lien avec la progression tumorale et ce, pour plusieurs types de cancer.

La contribution potentielle des protéines alternatives dans le métabolisme cellulaire est mise en relief par les travaux présentés au Chapitre 5. En effet, des données de séquençage à haut débit supportent une induction différentielle des enzymes et des protéines alternatives dérivées du gène *UGT2B10* à la suite d'une activation pharmacologique du récepteur CAR. Ces résultats impliquent que les protéines alternatives UGT sont sous le contrôle d'éléments de régulation différents de ceux des enzymes et donc, que leur expression puisse être finement régulée. Cette découverte est d'autant plus importante lorsqu'on considère la grande diversité des protéines alternatives rapportées au Chapitre 6. Ces travaux soutiennent par ailleurs que d'autres isoformes alternatives peuvent induire des modifications phénotypiques, au-delà des UGT1A_i2. Ceci a été observé pour la protéine UGT2B7_i8, dont l'expression dans les cellules HEK293 entraîne une forte augmentation de l'adhésion cellulaire, tout en diminuant la prolifération. Ces résultats supportent ainsi la nécessité d'investiguer les enzymes et les

protéines alternatives faiblement exprimées, puisque ces effets ont été observés malgré une expression relativement faible de cette protéine alternative dans le modèle cellulaire.

Conclusion

Les travaux présentés dans cette thèse soutiennent l'existence d'une interconnexion entre le métabolisme cellulaire et la voie de glucuronidation. Ceci est supporté par l'observation de nombreuses modifications dans les concentrations de métabolites intracellulaires associées à une modification de l'expression des UGT, mais également par l'étendue de l'interactome de ces protéines. Les voies métaboliques identifiées par nos travaux comme étant associées à la voie de glucuronidation pourraient en fait être des mécanismes de régulation de cette voie agissant via divers processus directs ou indirects, incluant la régulation allostérique et des boucles de rétroaction. Ces hypothèses demeurent toutefois à être testées, ainsi que la capacité de ces processus à être altérés. Néanmoins, nos données supportent que par cette interrelation avec le métabolisme cellulaire, les protéines UGT pourraient être impliquées dans la progression de certaines maladies, notamment des néoplasies.

Une meilleure connaissance des répercussions métaboliques associées à la voie de glucuronidation, et réciproquement, les modifications métaboliques affectant l'activité de cette voie, permettra ainsi de comprendre l'implication de la voie de glucuronidation dans la progression tumorale. L'expression de ces protéines pourrait constituer un biomarqueur, autant pour la réponse aux traitements impliquant la voie de glucuronidation, que pour le pronostic du patient. La poursuite de ces travaux pourrait notamment mener à la découverte de nouvelles cibles thérapeutiques visant à réguler l'activité de la voie de glucuronidation, ou encore à une meilleure modélisation de l'activité de cette voie en fonction de l'environnement cellulaire, le tout dans l'optique de développer une médecine personnalisée.

Bibliographie

Abu El Maaty, M.A., Alborzinia, H., Khan, S.J., Buttner, M., and Wolfl, S. (2017). 1,25(OH)2D3 disrupts glucose metabolism in prostate cancer cells leading to a truncation of the TCA cycle and inhibition of TXNIP expression. *Biochim Biophys Acta* 1864**,** 1618-1630.

Ajdzanovic, V., Mojic, M., Maksimovic-Ivanic, D., Bulatovic, M., Mijatovic, S., Milosevic, V., and Spasojevic, I. (2013). Membrane fluidity, invasiveness and dynamic phenotype of metastatic prostate cancer cells after treatment with soy isoflavones. *J Membr Biol* 246**,** 307-314.

Amacher, D.E., and Chalasani, N. (2014). Drug-induced hepatic steatosis. *Semin Liver Dis* 34**,** 205-214.

Amelio, I., Cutruzzola, F., Antonov, A., Agostini, M., and Melino, G. (2014). Serine and glycine metabolism in cancer. *Trends Biochem Sci* 39**,** 191-198.

Ananieva, E.A., and Wilkinson, A.C. (2018). Branched-chain amino acid metabolism in cancer. *Curr Opin Clin Nutr Metab Care* 21**,** 64-70.

Anderson, E.M., Del Valle-Pinero, A.Y., Suckow, S.K., Nolan, T.A., Neubert, J.K., and Caudle, R.M. (2012). Morphine and MK-801 administration leads to alternative N-methyl-D-aspartate receptor 1 splicing and associated changes in reward seeking behavior and nociception on an operant orofacial assay. *Neuroscience* 214**,** 14-27.

Ando, M., Ando, Y., Sekido, Y., Ando, M., Shimokata, K., and Hasegawa, Y. (2002). Genetic polymorphisms of the UDP-glucuronosyltransferase 1A7 gene and irinotecan toxicity in Japanese cancer patients. *Jpn J Cancer Res* 93**,** 591-597.

Andrzejewski, S., Klimcakova, E., Johnson, R.M., Tabaries, S., Annis, M.G., Mcguirk, S., Northey, J.J., Chenard, V., Sriram, U., Papadopoli, D.J., Siegel, P.M., and St-Pierre, J. (2017). PGC-1alpha Promotes Breast Cancer Metastasis and Confers Bioenergetic Flexibility against Metabolic Drugs. *Cell Metab* 26**,** 778-787 e775.

Astuti, D., Latif, F., Dallol, A., Dahia, P.L., Douglas, F., George, E., Skoldberg, F., Husebye, E.S., Eng, C., and Maher, E.R. (2001). Gene mutations in the succinate dehydrogenase subunit SDHB cause susceptibility to familial pheochromocytoma and to familial paraganglioma. *Am J Hum Genet* 69**,** 49-54.

Audet-Delage, Y., Gregoire, J., Caron, P., Turcotte, V., Plante, M., Ayotte, P., Simonyan, D., Villeneuve, L., and Guillemette, C. (2018a). Estradiol metabolites as biomarkers of endometrial cancer prognosis after surgery. *J Steroid Biochem Mol Biol* 178**,** 45-54.

Audet-Delage, Y., Rouleau, M., Rouleau, M., Roberge, J., Miard, S., Picard, F., Tetu, B., and Guillemette, C. (2017). Cross-Talk between Alternatively Spliced UGT1A Isoforms and Colon Cancer Cell Metabolism. *Mol Pharmacol* 91**,** 167-177.

Audet-Delage, Y., Villeneuve, L., Gregoire, J., Plante, M., and Guillemette, C. (2018b). Identification of Metabolomic Biomarkers for Endometrial Cancer and Its Recurrence after Surgery in Postmenopausal Women. *Front Endocrinol (Lausanne)* 9**,** 87.

Audet-Walsh, E., Dufour, C.R., Yee, T., Zouanat, F.Z., Yan, M., Kalloghlian, G., Vernier, M., Caron, M., Bourque, G., Scarlata, E., Hamel, L., Brimo, F., Aprikian, A.G., Lapointe, J., Chevalier, S., and Giguere, V. (2017). Nuclear mTOR acts as a transcriptional integrator of the androgen signaling pathway in prostate cancer. *Genes Dev* 31**,** 1228-1242.

Baggott, J.E., and Tamura, T. (2015). Folate-Dependent Purine Nucleotide Biosynthesis in Humans. *Adv Nutr* 6**,** 564-571.

Balliet, R.M., Chen, G., Gallagher, C.J., Dellinger, R.W., Sun, D., and Lazarus, P. (2009). Characterization of UGTs active against SAHA and association between SAHA glucuronidation activity phenotype with UGT genotype. *Cancer Res* 69**,** 2981-2989.

Barua, A.B., and Sidell, N. (2004). Retinoyl beta-glucuronide: a biologically active interesting retinoid. *J Nutr* 134**,** 286S-289S.

Basu, N.K., Kole, L., Basu, M., Chakraborty, K., Mitra, P.S., and Owens, I.S. (2008). The major chemical-detoxifying system of UDP-glucuronosyltransferases requires regulated phosphorylation supported by protein kinase C. *J Biol Chem* 283**,** 23048-23061.

Basu, N.K., Kole, L., and Owens, I.S. (2003). Evidence for phosphorylation requirement for human bilirubin UDP-glucuronosyltransferase (UGT1A1) activity. *Biochem Biophys Res Commun* 303**,** 98-104.

Basu, N.K., Kovarova, M., Garza, A., Kubota, S., Saha, T., Mitra, P.S., Banerjee, R., Rivera, J., and Owens, I.S. (2005). Phosphorylation of a UDP-glucuronosyltransferase regulates substrate specificity. *Proc Natl Acad Sci U S A* 102**,** 6285-6290.

Bauer, D.E., Hatzivassiliou, G., Zhao, F., Andreadis, C., and Thompson, C.B. (2005). ATP citrate lyase is an important component of cell growth and transformation. *Oncogene* 24**,** 6314-6322.

Belanger, A.S., Tojcic, J., Harvey, M., and Guillemette, C. (2010). Regulation of UGT1A1 and HNF1 transcription factor gene expression by DNA methylation in colon cancer cells. *BMC Mol Biol* 11**,** 9.

Belledant, A., Hovington, H., Garcia, L., Caron, P., Brisson, H., Villeneuve, L., Simonyan, D., Tetu, B., Fradet, Y., Lacombe, L., Guillemette, C., and Levesque, E. (2016). The UGT2B28 Sex-steroid Inactivation Pathway Is a Regulator of Steroidogenesis and Modifies the Risk of Prostate Cancer Progression. *Eur Urol* 69**,** 601-609.

Bellemare, J., Rouleau, M., Girard, H., Harvey, M., and Guillemette, C. (2010a). Alternatively spliced products of the UGT1A gene interact with the enzymatically active proteins to inhibit glucuronosyltransferase activity in vitro. *Drug Metab Dispos* 38**,** 1785-1789.

Bellemare, J., Rouleau, M., Harvey, M., and Guillemette, C. (2010b). Modulation of the human glucuronosyltransferase UGT1A pathway by splice isoform polypeptides is mediated through protein-protein interactions. *J Biol Chem* 285**,** 3600-3607.

Bellemare, J., Rouleau, M., Harvey, M., Popa, I., Pelletier, G., Tetu, B., and Guillemette, C. (2011). Immunohistochemical expression of conjugating UGT1A-derived isoforms in normal and tumoral drug-metabolizing tissues in humans. *J Pathol* 223**,** 425-435.

Bellemare, J., Rouleau, M., Harvey, M., Tetu, B., and Guillemette, C. (2010c). Alternative-splicing forms of the major phase II conjugating UGT1A gene negatively regulate glucuronidation in human carcinoma cell lines. *Pharmacogenomics J* 10**,** 431-441.

Benito, A., Polat, I.H., Noe, V., Ciudad, C.J., Marin, S., and Cascante, M. (2017). Glucose-6-phosphate dehydrogenase and transketolase modulate breast cancer cell metabolic reprogramming and correlate with poor patient outcome. *Oncotarget* 8**,** 106693-106706.

Bentley, G., Higuchi, R., Hoglund, B., Goodridge, D., Sayer, D., Trachtenberg, E.A., and Erlich, H.A. (2009). High-resolution, high-throughput HLA genotyping by next-generation sequencing. *Tissue Antigens* 74**,** 393-403.

Bhat-Nakshatri, P., Song, E.K., Collins, N.R., Uversky, V.N., Dunker, A.K., O'malley, B.W., Geistlinger, T.R., Carroll, J.S., Brown, M., and Nakshatri, H. (2013). Interplay between estrogen receptor and AKT in estradiol-induced alternative splicing. *BMC Med Genomics* 6**,** 21.

Bhoi, S., Baliakas, P., Cortese, D., Mattsson, M., Engvall, M., Smedby, K.E., Juliusson, G., Sutton, L.A., and Mansouri, L. (2016). UGT2B17 expression: a novel prognostic marker within IGHV-mutated chronic lymphocytic leukemia? *Haematologica* 101**,** e63-65.

Bing, Y., Zhu, S., Jiang, K., Dong, G., Li, J., Yang, Z., Yang, J., and Yue, J. (2014). Reduction of thyroid hormones triggers down-regulation of hepatic CYP2B through nuclear receptors CAR and TR in a rat model of acute stroke. *Biochem Pharmacol* 87**,** 636-649.

Bock, K.W. (2012). Human UDP-glucuronosyltransferases: feedback loops between substrates and ligands of their transcription factors. *Biochem Pharmacol* 84**,** 1000-1006.

Bock, K.W. (2015). Roles of human UDP-glucuronosyltransferases in clearance and homeostasis of endogenous substrates, and functional implications. *Biochem Pharmacol* 96**,** 77-82.

Boland, M.L., Chourasia, A.H., and Macleod, K.F. (2013). Mitochondrial dysfunction in cancer. *Front Oncol* 3**,** 292.

Borin, T.F., Angara, K., Rashid, M.H., Achyut, B.R., and Arbab, A.S. (2017). Arachidonic Acid Metabolite as a Novel Therapeutic Target in Breast Cancer Metastasis. *Int J Mol Sci* 18.

Bosio, A., Binczek, E., Le Beau, M.M., Fernald, A.A., and Stoffel, W. (1996). The human gene CGT encoding the UDP-galactose ceramide galactosyl transferase (cerebroside synthase): cloning, characterization, and assignment to human chromosome 4, band q26. *Genomics* 34**,** 69-75.

Bosma, P.J., Chowdhury, J.R., Bakker, C., Gantla, S., De Boer, A., Oostra, B.A., Lindhout, D., Tytgat, G.N., Jansen, P.L., Oude Elferink, R.P., and Et Al. (1995). The genetic basis of the reduced expression of bilirubin UDP-glucuronosyltransferase 1 in Gilbert's syndrome. *N Engl J Med* 333**,** 1171-1175.

Bozza, P.T., Bakker-Abreu, I., Navarro-Xavier, R.A., and Bandeira-Melo, C. (2011). Lipid body function in eicosanoid synthesis: an update. *Prostaglandins Leukot Essent Fatty Acids* 85**,** 205-213.

Braun, L., Kardon, T., Puskas, F., Csala, M., Banhegyi, G., and Mandl, J. (1997). Regulation of glucuronidation by glutathione redox state through the alteration of UDP-glucose supply originating from glycogen metabolism. *Arch Biochem Biophys* 348**,** 169-173.

Bray, B.J., and Rosengren, R.J. (2001). Retinol potentiates acetaminophen-induced hepatotoxicity in the mouse: mechanistic studies. *Toxicol Appl Pharmacol* 173**,** 129-136.

Brown, I., Cascio, M.G., Rotondo, D., Pertwee, R.G., Heys, S.D., and Wahle, K.W. (2013). Cannabinoids and omega-3/6 endocannabinoids as cell death and anticancer modulators. *Prog Lipid Res* 52**,** 80-109.

Buljan, M., Chalancon, G., Eustermann, S., Wagner, Gunter p., Fuxreiter, M., Bateman, A., and Babu, M.M. (2012). Tissue-Specific Splicing of Disordered Segments that Embed Binding Motifs Rewires Protein Interaction Networks. *Molecular Cell* 46**,** 871-883.

Burchell, B., Brierley, C.H., and Rance, D. (1995). Specificity of human UDP-glucuronosyltransferases and xenobiotic glucuronidation. *Life Sci* 57**,** 1819-1831.

Burchell, B., and Coughtrie, M.W. (1989). UDP-glucuronosyltransferases. *Pharmacol Ther* 43**,** 261-289.

Burns, J.S., and Manda, G. (2017). Metabolic Pathways of the Warburg Effect in Health and Disease: Perspectives of Choice, Chain or Chance. *Int J Mol Sci* 18**,** 2755.

Cappiello, M., Giuliani, L., and Pacifici, G.M. (1991). Distribution of UDP-glucuronosyltransferase and its endogenous substrate uridine 5'-diphosphoglucuronic acid in human tissues. *European Journal of Clinical Pharmacology* 41**,** 345-350.

Caputo, M., Zirpoli, H., Torino, G., and Tecce, M.F. (2011). Selective regulation of UGT1A1 and SREBP-1c mRNA expression by docosahexaenoic, eicosapentaenoic, and arachidonic acids. *J Cell Physiol* 226**,** 187-193.

Caridi, G., Dagnino, M., Erdeve, O., Di Duca, M., Yildiz, D., Alan, S., Atasay, B., Arsan, S., Campagnoli, M., Galliano, M., and Minchiotti, L. (2014). Congenital analbuminemia caused by a novel aberrant splicing in the albumin gene. *Biochem Med (Zagreb)* 24**,** 151-158.

Casos, K., Siguero, L., Fernandez-Figueras, M.T., Leon, X., Sarda, M.P., Vila, L., and Camacho, M. (2011). Tumor cells induce COX-2 and mPGES-1 expression in microvascular endothelial cells mainly by means of IL-1 receptor activation. *Microvasc Res* 81**,** 261-268.

Cavalieri, E.L., and Rogan, E.G. (2016). Depurinating estrogen-DNA adducts, generators of cancer initiation: their minimization leads to cancer prevention. *Clin Transl Med* 5**,** 12.

Cengiz, B., Yumrutas, O., Bozgeyik, E., Borazan, E., Igci, Y.Z., Bozgeyik, I., and Oztuzcu, S. (2015). Differential expression of the UGT1A family of genes in stomach cancer tissues. *Tumour Biol* 36**,** 5831-5837.

Chakraborty, S.K., Basu, N.K., Jana, S., Basu, M., Raychoudhuri, A., and Owens, I.S. (2012). Protein kinase Calpha and Src kinase support human prostate-distributed dihydrotestosterone-metabolizing UDP-glucuronosyltransferase 2B15 activity. *J Biol Chem* 287**,** 24387-24396.

Che, Y., and Khavari, P.A. (2017). Research Techniques Made Simple: Emerging Methods to Elucidate Protein Interactions through Spatial Proximity. *J Invest Dermatol* 137**,** e197-e203.

Chen, J., and Weiss, W.A. (2015). Alternative splicing in cancer: implications for biology and therapy. *Oncogene* 34**,** 1-14.

Chen, S., Laverdiere, I., Tourancheau, A., Jonker, D., Couture, F., Cecchin, E., Villeneuve, L., Harvey, M., Court, M.H., Innocenti, F., Toffoli, G., Levesque, E., and Guillemette, C. (2015a). A novel UGT1 marker associated with better tolerance against irinotecan-induced severe neutropenia in metastatic colorectal cancer patients. *Pharmacogenomics J* 15**,** 513-520.

Chen, S., Lu, W., Yueh, M.F., Rettenmeier, E., Liu, M., Paszek, M., Auwerx, J., Yu, R.T., Evans, R.M., Wang, K., Karin, M., and Tukey, R.H. (2017). Intestinal NCoR1, a regulator of epithelial cell maturation, controls neonatal hyperbilirubinemia. *Proc Natl Acad Sci U S A* 114**,** E1432-E1440.

Chen, Z., Wang, Z., Guo, W., Zhang, Z., Zhao, F., Zhao, Y., Jia, D., Ding, J., Wang, H., Yao, M., and He, X. (2015b). TRIM35 Interacts with pyruvate kinase isoform M2 to suppress the Warburg effect and tumorigenicity in hepatocellular carcinoma. *Oncogene* 34**,** 3946-3956.

Cho, E.S., Cha, Y.H., Kim, H.S., Kim, N.H., and Yook, J.I. (2018). The Pentose Phosphate Pathway as a Potential Target for Cancer Therapy. *Biomol Ther (Seoul)* 26**,** 29-38.

Chouinard, S., Pelletier, G., Belanger, A., and Barbier, O. (2004). Cellular specific expression of the androgen-conjugating enzymes UGT2B15 and UGT2B17 in the human prostate epithelium. *Endocr Res* 30**,** 717-725.

Christofk, H.R., Vander Heiden, M.G., Harris, M.H., Ramanathan, A., Gerszten, R.E., Wei, R., Fleming, M.D., Schreiber, S.L., and Cantley, L.C. (2008). The M2 splice isoform of pyruvate kinase is important for cancer metabolism and tumour growth. *Nature* 452**,** 230-233.

Ciotti, M., Cho, J.W., George, J., and Owens, I.S. (1998). Required buried alpha-helical structure in the bilirubin UDP-glucuronosyltransferase, UGT1A1, contains a nonreplaceable phenylalanine. *Biochemistry* 37**,** 11018-11025.

Collins, R.R.J., Patel, K., Putnam, W.C., Kapur, P., and Rakheja, D. (2017). Oncometabolites: A New Paradigm for Oncology, Metabolism, and the Clinical Laboratory. *Clin Chem* 63**,** 1812-1820.

Cory, J.G., and Cory, A.H. (2006). Critical roles of glutamine as nitrogen donors in purine and pyrimidine nucleotide synthesis: asparaginase treatment in childhood acute lymphoblastic leukemia. *In Vivo* 20**,** 587-589.

Cosentino, C., Grieco, D., and Costanzo, V. (2011). ATM activates the pentose phosphate pathway promoting anti-oxidant defence and DNA repair. *EMBO J* 30**,** 546-555.

Court, M.H. (2010). Interindividual variability in hepatic drug glucuronidation: studies into the role of age, sex, enzyme inducers, and genetic polymorphism using the human liver bank as a model system. *Drug Metab Rev* 42**,** 209-224.

Court, M.H., Duan, S.X., Von Moltke, L.L., Greenblatt, D.J., Patten, C.J., Miners, J.O., and Mackenzie, P.I. (2001). Interindividual variability in acetaminophen glucuronidation by human liver microsomes: identification of relevant acetaminophen UDP-glucuronosyltransferase isoforms. *J Pharmacol Exp Ther* 299**,** 998-1006.

Court, M.H., Zhu, Z., Masse, G., Duan, S.X., James, L.P., Harmatz, J.S., and Greenblatt, D.J. (2017). Race, Gender, and Genetic Polymorphism Contribute to Variability in Acetaminophen Pharmacokinetics, Metabolism, and Protein-Adduct Concentrations in Healthy African-American and European-American Volunteers. *J Pharmacol Exp Ther* 362**,** 431-440.

Dago, D.N., Scafoglio, C., Rinaldi, A., Memoli, D., Giurato, G., Nassa, G., Ravo, M., Rizzo, F., Tarallo, R., and Weisz, A. (2015). Estrogen receptor beta impacts hormone-induced alternative mRNA splicing in breast cancer cells. *BMC Genomics* 16**,** 367.

Dahlin, D.C., and Nelson, S.D. (1982). Synthesis, decomposition kinetics, and preliminary toxicological studies of pure N-acetyl-p-benzoquinone imine, a proposed toxic metabolite of acetaminophen. *J Med Chem* 25**,** 885-886.

Dang, L., White, D.W., Gross, S., Bennett, B.D., Bittinger, M.A., Driggers, E.M., Fantin, V.R., Jang, H.G., Jin, S., Keenan, M.C., Marks, K.M., Prins, R.M., Ward, P.S., Yen, K.E., Liau, L.M., Rabinowitz, J.D., Cantley, L.C., Thompson, C.B., Vander Heiden, M.G., and Su, S.M. (2009). Cancer-associated IDH1 mutations produce 2-hydroxyglutarate. *Nature* 462**,** 739-744.

Dates, C.R., Fahmi, T., Pyrek, S.J., Yao-Borengasser, A., Borowa-Mazgaj, B., Bratton, S.M., Kadlubar, S.A., Mackenzie, P.I., Haun, R.S., and Radominska-Pandya, A. (2015). Human UDP-Glucuronosyltransferases: Effects of altered expression in breast and pancreatic cancer cell lines. *Cancer Biol Ther* 16**,** 714-723.

De Alteriis, E., Carteni, F., Parascandola, P., Serpa, J., and Mazzoleni, S. (2018). Revisiting the Crabtree/Warburg effect in a dynamic perspective: a fitness advantage against sugar-induced cell death. *Cell Cycle* 17**,** 688-701.

Deberardinis, R.J., and Chandel, N.S. (2016). Fundamentals of cancer metabolism. *Sci Adv* 2**,** e1600200.

Deberardinis, R.J., Lum, J.J., Hatzivassiliou, G., and Thompson, C.B. (2008a). The biology of cancer: metabolic reprogramming fuels cell growth and proliferation. *Cell Metab* 7**,** 11-20.

Deberardinis, R.J., Mancuso, A., Daikhin, E., Nissim, I., Yudkoff, M., Wehrli, S., and Thompson, C.B. (2007). Beyond aerobic glycolysis: transformed cells can engage in glutamine metabolism that exceeds the requirement for protein and nucleotide synthesis. *Proc Natl Acad Sci U S A* 104**,** 19345-19350.

Deberardinis, R.J., Sayed, N., Ditsworth, D., and Thompson, C.B. (2008b). Brick by brick: metabolism and tumor cell growth. *Curr Opin Genet Dev* 18**,** 54-61.

Dong, A.N., Tan, B.H., Pan, Y., and Ong, C.E. (2018). Cytochrome P450 genotype-guided drug therapies: an update on current states. *Clin Exp Pharmacol Physiol*.

Erickson, R.H., Zakim, D., and Vessey, D.A. (1978). Preparation and properties of a phospholipid-free form of microsomal UDP-glucuronyltransferase. *Biochemistry* 17**,** 3706-3711.

Evans, W.E., and Relling, M.V. (1999). Pharmacogenomics: translating functional genomics into rational therapeutics. *Science* 286**,** 487-491.

Fajardo, V.A., Mcmeekin, L., and Leblanc, P.J. (2011). Influence of phospholipid species on membrane fluidity: a meta-analysis for a novel phospholipid fluidity index. *J Membr Biol* 244**,** 97-103.

Fantin, V.R., St-Pierre, J., and Leder, P. (2006). Attenuation of LDH-A expression uncovers a link between glycolysis, mitochondrial physiology, and tumor maintenance. *Cancer Cell* 9**,** 425-434.

Feng, D., Zhao, T., Yan, K., Liang, H., Liang, J., Zhou, Y., Zhao, W., and Ling, B. (2017). Gonadotropins promote human ovarian cancer cell migration and invasion via a cyclooxygenase 2-dependent pathway. *Oncol Rep* 38**,** 1091-1098.

Ferrucci, L.M., Sinha, R., Huang, W.Y., Berndt, S.I., Katki, H.A., Schoen, R.E., Hayes, R.B., and Cross, A.J. (2012). Meat consumption and the risk of incident distal colon and rectal adenoma. *Br J Cancer* 106**,** 608-616.

Finel, M., and Kurkela, M. (2008). The UDP-glucuronosyltransferases as oligomeric enzymes. *Curr Drug Metab* 9**,** 70-76.

Frances, B., Gout, R., Monsarrat, B., Cros, J., and Zajac, J.M. (1992). Further evidence that morphine-6 beta-glucuronide is a more potent opioid agonist than morphine. *J Pharmacol Exp Ther* 262**,** 25-31.

Fremont, J.J., Wang, R.W., and King, C.D. (2005). Coimmunoprecipitation of UDP-glucuronosyltransferase isoforms and cytochrome P450 3A4. *Mol Pharmacol* 67**,** 260-262.

Fujiwara, R., and Itoh, T. (2014). Extensive protein-protein interactions involving UDP-glucuronosyltransferase (UGT) 2B7 in human liver microsomes. *Drug Metab Pharmacokinet* 29**,** 259-265.

Fujiwara, R., Nakajima, M., Yamanaka, H., Katoh, M., and Yokoi, T. (2008). Product inhibition of UDP-glucuronosyltransferase (UGT) enzymes by UDP obfuscates the inhibitory effects of UGT substrates. *Drug Metab Dispos* 36**,** 361-367.

Gagne, J.F., Montminy, V., Belanger, P., Journault, K., Gaucher, G., and Guillemette, C. (2002). Common human UGT1A polymorphisms and the altered metabolism of irinotecan active metabolite 7-ethyl-10-hydroxycamptothecin (SN-38). *Mol Pharmacol* 62**,** 608-617.

Gagnon, J.F., Bernard, O., Villeneuve, L., Tetu, B., and Guillemette, C. (2006). Irinotecan inactivation is modulated by epigenetic silencing of UGT1A1 in colon cancer. *Clin Cancer Res* 12**,** 1850-1858.

Gallagher, C.J., Balliet, R.M., Sun, D., Chen, G., and Lazarus, P. (2010). Sex differences in UDP-glucuronosyltransferase 2B17 expression and activity. *Drug Metab Dispos* 38**,** 2204-2209.

Gao, J., Zhou, J., Li, Y., Peng, Z., Li, Y., Wang, X., and Shen, L. (2013). Associations between UGT1A1*6/*28 polymorphisms and irinotecan-induced severe toxicity in Chinese gastric or esophageal cancer patients. *Med Oncol* 30**,** 630.

Gerstner, S., Glasemann, D., Pfeiffer, E., and Metzler, M. (2008). The influence of metabolism on the genotoxicity of catechol estrogens in three cultured cell lines. *Mol Nutr Food Res* 52**,** 823-829.

Ghosh, S.S., Sappal, B.S., Kalpana, G.V., Lee, S.W., Chowdhury, J.R., and Chowdhury, N.R. (2001). Homodimerization of human bilirubin-uridine-diphosphoglucuronate glucuronosyltransferase-1 (UGT1A1) and its functional implications. *J Biol Chem* 276**,** 42108-42115.

Girard, H., Levesque, E., Bellemare, J., Journault, K., Caillier, B., and Guillemette, C. (2007). Genetic diversity at the UGT1 locus is amplified by a novel 3' alternative splicing mechanism leading to nine additional UGT1A proteins that act as regulators of glucuronidation activity. *Pharmacogenet Genomics* 17**,** 1077-1089.

Girard, H., Thibaudeau, J., Court, M.H., Fortier, L.C., Villeneuve, L., Caron, P., Hao, Q., Von Moltke, L.L., Greenblatt, D.J., and Guillemette, C. (2005). UGT1A1 polymorphisms are important determinants of dietary carcinogen detoxification in the liver. *Hepatology* 42**,** 448-457.

Giuliani, L., Ciotti, M., Stoppacciaro, A., Pasquini, A., Silvestri, I., De Matteis, A., Frati, L., and Agliano, A.M. (2005). UDP-glucuronosyltransferases 1A expression in human urinary bladder and colon cancer by immunohistochemistry. *Oncol Rep* 13**,** 185-191.

Go, R.E., Hwang, K.A., and Choi, K.C. (2015). Cytochrome P450 1 family and cancers. *J Steroid Biochem Mol Biol* 147**,** 24-30.

Gong, Q.H., Cho, J.W., Huang, T., Potter, C., Gholami, N., Basu, N.K., Kubota, S., Carvalho, S., Pennington, M.W., Owens, I.S., and Popescu, N.C. (2001). Thirteen UDPglucuronosyltransferase genes are encoded at the human UGT1 gene complex locus. *Pharmacogenetics* 11**,** 357-368.

Grabner, G.F., Zimmermann, R., Schicho, R., and Taschler, U. (2017). Monoglyceride lipase as a drug target: At the crossroads of arachidonic acid metabolism and endocannabinoid signaling. *Pharmacol Ther* 175**,** 35-46.

Granata, A., Nicoletti, R., Tinaglia, V., De Cecco, L., Pisanu, M.E., Ricci, A., Podo, F., Canevari, S., Iorio, E., Bagnoli, M., and Mezzanzanica, D. (2014). Choline kinase-alpha by regulating cell aggressiveness and drug sensitivity is a potential druggable target for ovarian cancer. *Br J Cancer* 110**,** 330-340.

Gregus, Z., Madhu, C., Goon, D., and Klaassen, C.D. (1988). Effect of galactosamine-induced hepatic UDP-glucuronic acid depletion on acetaminophen elimination in rats. Dispositional differences between hepatically and extrahepatically formed glucuronides of acetaminophen and other chemicals. *Drug Metab Dispos* 16**,** 527-533.

Gruber, M., Bellemare, J., Hoermann, G., Gleiss, A., Porpaczy, E., Bilban, M., Le, T., Zehetmayer, S., Mannhalter, C., Gaiger, A., Shehata, M., Fleiss, K., Skrabs, C., Levesque, E., Vanura, K., Guillemette, C., and Jaeger, U. (2013). Overexpression of uridine diphospho glucuronosyltransferase 2B17 in high-risk chronic lymphocytic leukemia. *Blood* 121**,** 1175-1183.

Guillemette, C. (2003). Pharmacogenomics of human UDP-glucuronosyltransferase enzymes. *Pharmacogenomics J* 3**,** 136-158.

Guillemette, C., Levesque, E., Harvey, M., Bellemare, J., and Menard, V. (2010). UGT genomic diversity: beyond gene duplication. *Drug Metab Rev* 42**,** 24-44.

Guillemette, C., Levesque, E., and Rouleau, M. (2014). Pharmacogenomics of human uridine diphospho-glucuronosyltransferases and clinical implications. *Clin Pharmacol Ther* 96**,** 324-339.

Guillemette, C., Millikan, R.C., Newman, B., and Housman, D.E. (2000). Genetic polymorphisms in uridine diphospho-glucuronosyltransferase 1A1 and association with breast cancer among African Americans. *Cancer Res* 60**,** 950-956.

Haeusgen, W., Tueffers, L., Herdegen, T., and Waetzig, V. (2014). Map2k4delta - identification and functional characterization of a novel Map2k4 splice variant. *Biochim Biophys Acta* 1843**,** 875-884.

Hanahan, D., and Weinberg, R.A. (2011). Hallmarks of cancer: the next generation. *Cell* 144**,** 646-674.

Hardwick, R.N., Ferreira, D.W., More, V.R., Lake, A.D., Lu, Z., Manautou, J.E., Slitt, A.L., and Cherrington, N.J. (2013). Altered UDP-glucuronosyltransferase and sulfotransferase expression and function during progressive stages of human nonalcoholic fatty liver disease. *Drug Metab Dispos* 41**,** 554-561.

Harrington, W.R., Sengupta, S., and Katzenellenbogen, B.S. (2006). Estrogen regulation of the glucuronidation enzyme UGT2B15 in estrogen receptor-positive breast cancer cells. *Endocrinology* 147**,** 3843-3850.

Hatzivassiliou, G., Zhao, F., Bauer, D.E., Andreadis, C., Shaw, A.N., Dhanak, D., Hingorani, S.R., Tuveson, D.A., and Thompson, C.B. (2005). ATP citrate lyase inhibition can suppress tumor cell growth. *Cancer Cell* 8**,** 311-321.

He, X., and Feng, S. (2015). Role of Metabolic Enzymes P450 (CYP) on Activating Procarcinogen and their Polymorphisms on the Risk of Cancers. *Curr Drug Metab* 16**,** 850-863.

Heidelberger, C., Chaudhuri, N.K., Danneberg, P., Mooren, D., Griesbach, L., Duschinsky, R., Schnitzer, R.J., Pleven, E., and Scheiner, J. (1957). Fluorinated pyrimidines, a new class of tumour-inhibitory compounds. *Nature* 179**,** 663-666.

Hensley, C.T., Wasti, A.T., and Deberardinis, R.J. (2013). Glutamine and cancer: cell biology, physiology, and clinical opportunities. *J Clin Invest* 123**,** 3678-3684.

Hochman, Y., and Zakim, D. (1983). A comparison of the kinetic properties of two different forms of microsomal UDPglucuronyltransferase. *J Biol Chem* 258**,** 4143-4146.

Hochman, Y., and Zakim, D. (1984). Studies of the catalytic mechanism of microsomal UDP-glucuronyltransferase. Alpha-glucuronidase activity and its stimulation by phospholipids. *J Biol Chem* 259**,** 5521-5525.

Hong, W., Cai, P., Xu, C., Cao, D., Yu, W., Zhao, Z., Huang, M., and Jin, J. (2018). Inhibition of Glucose-6-Phosphate Dehydrogenase Reverses Cisplatin Resistance in Lung Cancer Cells via the Redox System. *Front Pharmacol* 9**,** 43.

Hrycay, E.G., and Bandiera, S.M. (2015). Monooxygenase, peroxidase and peroxygenase properties and reaction mechanisms of cytochrome P450 enzymes. *Adv Exp Med Biol* 851**,** 1-61.

Hu, D.G., Meech, R., Mckinnon, R.A., and Mackenzie, P.I. (2014). Transcriptional regulation of human UDP-glucuronosyltransferase genes. *Drug Metab Rev* 46**,** 421-458.

Huang, C., and Mcconathy, J. (2013). Radiolabeled amino acids for oncologic imaging. *J Nucl Med* 54**,** 1007-1010.

Hui, Y., Yasuda, S., Liu, M.Y., Wu, Y.Y., and Liu, M.C. (2008). On the sulfation and methylation of catecholestrogens in human mammary epithelial cells and breast cancer cells. *Biol Pharm Bull* 31**,** 769-773.

Hussain, A., Qazi, A.K., Mupparapu, N., Guru, S.K., Kumar, A., Sharma, P.R., Singh, S.K., Singh, P., Dar, M.J., Bharate, S.B., Zargar, M.A., Ahmed, Q.N., Bhushan, S., Vishwakarma, R.A., and Hamid, A. (2016). Modulation of glycolysis and lipogenesis by novel PI3K selective molecule represses tumor angiogenesis and decreases colorectal cancer growth. *Cancer Lett* 374**,** 250-260.

Innocenti, F., Iyer, L., Ramirez, J., Green, M.D., and Ratain, M.J. (2001). Epirubicin glucuronidation is catalyzed by human UDP-glucuronosyltransferase 2B7. *Drug Metab Dispos* 29**,** 686-692.

Ishii, Y., Iwanaga, M., Nishimura, Y., Takeda, S., Ikushiro, S., Nagata, K., Yamazoe, Y., Mackenzie, P.I., and Yamada, H. (2007). Protein-protein interactions between rat hepatic cytochromes P450 (P450s) and UDP-glucuronosyltransferases (UGTs): evidence for the functionally active UGT in P450-UGT complex. *Drug Metab Pharmacokinet* 22**,** 367-376.

Ishii, Y., Koba, H., Kinoshita, K., Oizaki, T., Iwamoto, Y., Takeda, S., Miyauchi, Y., Nishimura, Y., Egoshi, N., Taura, F., Morimoto, S., Ikushiro, S., Nagata, K., Yamazoe, Y., Mackenzie, P.I., and Yamada, H. (2014). Alteration of the function of the UDP-glucuronosyltransferase 1A subfamily by cytochrome P450 3A4: different susceptibility for UGT isoforms and UGT1A1/7 variants. *Drug Metab Dispos* 42**,** 229-238.

Ishii, Y., Nurrochmad, A., and Yamada, H. (2010a). Modulation of UDP-glucuronosyltransferase activity by endogenous compounds. *Drug Metab Pharmacokinet* 25**,** 134-148.

Ishii, Y., Takeda, S., and Yamada, H. (2010b). Modulation of UDP-glucuronosyltransferase activity by protein-protein association. *Drug Metab Rev* 42**,** 145-158.

Iyer, L., Das, S., Janisch, L., Wen, M., Ramirez, J., Karrison, T., Fleming, G.F., Vokes, E.E., Schilsky, R.L., and Ratain, M.J. (2002). UGT1A1*28 polymorphism as a determinant of irinotecan disposition and toxicity. *Pharmacogenomics J* 2**,** 43-47.

Iyer, L., King, C.D., Whitington, P.F., Green, M.D., Roy, S.K., Tephly, T.R., Coffman, B.L., and Ratain, M.J. (1998). Genetic predisposition to the metabolism of irinotecan (CPT-11). Role of uridine diphosphate glucuronosyltransferase isoform 1A1 in the glucuronidation of its active metabolite (SN-38) in human liver microsomes. *J Clin Invest* 101**,** 847-854.

Izukawa, T., Nakajima, M., Fujiwara, R., Yamanaka, H., Fukami, T., Takamiya, M., Aoki, Y., Ikushiro, S., Sakaki, T., and Yokoi, T. (2009). Quantitative analysis of UDP-glucuronosyltransferase (UGT) 1A and UGT2B expression levels in human livers. *Drug Metab Dispos* 37**,** 1759-1768.

Izyumov, D.S., Avetisyan, A.V., Pletjushkina, O.Y., Sakharov, D.V., Wirtz, K.W., Chernyak, B.V., and Skulachev, V.P. (2004). "Wages of fear": transient threefold decrease in intracellular ATP level imposes apoptosis. *Biochim Biophys Acta* 1658**,** 141-147.

Jackman, A.L., Taylor, G.A., Gibson, W., Kimbell, R., Brown, M., Calvert, A.H., Judson, I.R., and Hughes, L.R. (1991). ICI D1694, a quinazoline antifolate thymidylate synthase inhibitor that is a potent inhibitor of L1210 tumor cell growth in vitro and in vivo: a new agent for clinical study. *Cancer Res* 51**,** 5579-5586.

Jacobs, E.T., Van Pelt, C., Forster, R.E., Zaidi, W., Hibler, E.A., Galligan, M.A., Haussler, M.R., and Jurutka, P.W. (2013). CYP24A1 and CYP27B1 polymorphisms modulate vitamin D metabolism in colon cancer cells. *Cancer Res* 73**,** 2563-2573.

Jamin, E.L., Riu, A., Douki, T., Debrauwer, L., Cravedi, J.P., Zalko, D., and Audebert, M. (2013). Combined genotoxic effects of a polycyclic aromatic hydrocarbon (B(a)P) and an heterocyclic amine (PhIP) in relation to colorectal carcinogenesis. *PLoS One* 8**,** e58591.

Jeromson, S., Mackenzie, I., Doherty, M.K., Whitfield, P.D., Bell, G., Dick, J., Shaw, A., Rao, F.V., Ashcroft, S.P., Philp, A., Galloway, S.D.R., Gallagher, I., and Hamilton, D.L. (2018). Lipid remodeling and an altered membrane-associated proteome may drive the differential effects of EPA and DHA treatment on skeletal muscle glucose uptake and protein accretion. *Am J Physiol Endocrinol Metab* 314**,** E605-e619.

Ji, L., Gupta, M., and Feldman, B.J. (2016). Vitamin D Regulates Fatty Acid Composition in Subcutaneous Adipose Tissue Through Elovl3. *Endocrinology* 157**,** 91-97.

Jiraskova, A., Novotny, J., Novotny, L., Vodicka, P., Pardini, B., Naccarati, A., Schwertner, H.A., Hubacek, J.A., Puncocharova, L., Smerhovsky, Z., and Vitek, L. (2012). Association of serum bilirubin and promoter variations in HMOX1 and UGT1A1 genes with sporadic colorectal cancer. *Int J Cancer* 131**,** 1549-1555.

Jonas, S.K., Benedetto, C., Flatman, A., Hammond, R.H., Micheletti, L., Riley, C., Riley, P.A., Spargo, D.J., Zonca, M., and Slater, T.F. (1992). Increased activity of 6-phosphogluconate dehydrogenase and glucose-6-phosphate dehydrogenase in purified cell suspensions and single cells from the uterine cervix in cervical intraepithelial neoplasia. *Br J Cancer* 66**,** 185-191.

Kiang, T.K., Ensom, M.H., and Chang, T.K. (2005). UDP-glucuronosyltransferases and clinical drug-drug interactions. *Pharmacol Ther* 106**,** 97-132.

Kilburn, D.G., Lilly, M.D., and Webb, F.C. (1969). The energetics of mammalian cell growth. *J Cell Sci* 4**,** 645-654.

Knibbe, C.A., Krekels, E.H., Van Den Anker, J.N., Dejongh, J., Santen, G.W., Van Dijk, M., Simons, S.H., Van Lingen, R.A., Jacqz-Aigrain, E.M., Danhof, M., and Tibboel, D. (2009). Morphine glucuronidation in preterm neonates, infants and children younger than 3 years. *Clin Pharmacokinet* 48**,** 371-385.

Knott, S.R.V., Wagenblast, E., Khan, S., Kim, S.Y., Soto, M., Wagner, M., Turgeon, M.O., Fish, L., Erard, N., Gable, A.L., Maceli, A.R., Dickopf, S., Papachristou, E.K., D'santos, C.S., Carey, L.A., Wilkinson, J.E., Harrell, J.C., Perou, C.M., Goodarzi, H., Poulogiannis, G., and Hannon, G.J. (2018). Asparagine bioavailability governs metastasis in a model of breast cancer. *Nature* 554**,** 378-381.

Koppenol, W.H., Bounds, P.L., and Dang, C.V. (2011). Otto Warburg's contributions to current concepts of cancer metabolism. *Nat Rev Cancer* 11**,** 325-337.

Koster, A.S., and Noordhoek, J. (1983). Kinetic properties of the rat intestinal microsomal 1-naphthol:UDP-glucuronosyl transferase. Inhibition by UDP and UDP-N-acetylglucosamine. *Biochim Biophys Acta* 761**,** 76-85.

Kuhajda, F.P., Jenner, K., Wood, F.D., Hennigar, R.A., Jacobs, L.B., Dick, J.D., and Pasternack, G.R. (1994). Fatty acid synthesis: a potential selective target for antineoplastic therapy. *Proc Natl Acad Sci U S A* 91**,** 6379-6383.

Kultti, A., Pasonen-Seppanen, S., Jauhiainen, M., Rilla, K.J., Karna, R., Pyoria, E., Tammi, R.H., and Tammi, M.I. (2009). 4-Methylumbelliferone inhibits hyaluronan synthesis by depletion of cellular UDP-glucuronic acid and downregulation of hyaluronan synthase 2 and 3. *Exp Cell Res* 315**,** 1914-1923.

Labriet, A., Allain, E.P., Rouleau, M., Audet-Delage, Y., Villeneuve, L., and Guillemette, C. (2018). Post-transcriptional Regulation of UGT2B10 Hepatic Expression and Activity by Alternative Splicing. *Drug Metab Dispos* 46**,** 514-524.

Labuschagne, C.F., Van Den Broek, N.J., Mackay, G.M., Vousden, K.H., and Maddocks, O.D. (2014). Serine, but not glycine, supports one-carbon metabolism and proliferation of cancer cells. *Cell Rep* 7**,** 1248-1258.

Lepine, J., Audet-Walsh, E., Gregoire, J., Tetu, B., Plante, M., Menard, V., Ayotte, P., Brisson, J., Caron, P., Villeneuve, L., Belanger, A., and Guillemette, C. (2010). Circulating estrogens in endometrial cancer cases and their relationship with tissular expression of key estrogen biosynthesis and metabolic pathways. *J Clin Endocrinol Metab* 95**,** 2689-2698.

Lepine, J., Bernard, O., Plante, M., Tetu, B., Pelletier, G., Labrie, F., Belanger, A., and Guillemette, C. (2004). Specificity and regioselectivity of the conjugation of estradiol, estrone, and their catecholestrogen and methoxyestrogen metabolites by human uridine diphospho-glucuronosyltransferases expressed in endometrium. *J Clin Endocrinol Metab* 89**,** 5222-5232.

Levesque, E., Belanger, A.S., Harvey, M., Couture, F., Jonker, D., Innocenti, F., Cecchin, E., Toffoli, G., and Guillemette, C. (2013). Refining the UGT1A haplotype associated with irinotecan-induced hematological toxicity in metastatic colorectal cancer patients treated with 5-fluorouracil/irinotecan-based regimens. *J Pharmacol Exp Ther* 345**,** 95-101.

Levesque, E., Girard, H., Journault, K., Lepine, J., and Guillemette, C. (2007). Regulation of the UGT1A1 bilirubin-conjugating pathway: role of a new splicing event at the UGT1A locus. *Hepatology* 45**,** 128-138.

Li, H., Xie, N., Chen, R., Verreault, M., Fazli, L., Gleave, M.E., Barbier, O., and Dong, X. (2016). UGT2B17 Expedites Progression of Castration-Resistant Prostate Cancers by Promoting Ligand-Independent AR Signaling. *Cancer Res* 76**,** 6701-6711.

Li, J.N., Mahmoud, M.A., Han, W.F., Ripple, M., and Pizer, E.S. (2000). Sterol regulatory element-binding protein-1 participates in the regulation of fatty acid synthase expression in colorectal neoplasia. *Exp Cell Res* 261**,** 159-165.

Li, X., Egervari, G., Wang, Y., Berger, S.L., and Lu, Z. (2018). Regulation of chromatin and gene expression by metabolic enzymes and metabolites. *Nat Rev Mol Cell Biol*.

Lien, E.A., Solheim, E., Lea, O.A., Lundgren, S., Kvinnsland, S., and Ueland, P.M. (1989). Distribution of 4-hydroxy-N-desmethyltamoxifen and other tamoxifen metabolites in human biological fluids during tamoxifen treatment. *Cancer Res* 49**,** 2175-2183.

Liston, H.L., Markowitz, J.S., and Devane, C.L. (2001). Drug glucuronidation in clinical psychopharmacology. *J Clin Psychopharmacol* 21**,** 500-515.

Little, J.M., Kurkela, M., Sonka, J., Jantti, S., Ketola, R., Bratton, S., Finel, M., and Radominska-Pandya, A. (2004). Glucuronidation of oxidized fatty acids and prostaglandins B1 and E2 by human hepatic and recombinant UDP-glucuronosyltransferases. *J Lipid Res* 45**,** 1694-1703.

Liu, W., Ramirez, J., Gamazon, E.R., Mirkov, S., Chen, P., Wu, K., Sun, C., Cox, N.J., Cook, E., Jr., Das, S., and Ratain, M.J. (2014a). Genetic factors affecting gene transcription and catalytic activity of UDP-glucuronosyltransferases in human liver. *Hum Mol Genet* 23**,** 5558-5569.

Liu, X., Cheng, D., Kuang, Q., Liu, G., and Xu, W. (2014b). Association of UGT1A1*28 polymorphisms with irinotecan-induced toxicities in colorectal cancer: a meta-analysis in Caucasians. *Pharmacogenomics J* 14**,** 120-129.

Liu, Y., and Coughtrie, M.W.H. (2017). Revisiting the Latency of Uridine Diphosphate-Glucuronosyltransferases (UGTs)-How Does the Endoplasmic Reticulum Membrane Influence Their Function? *Pharmaceutics* 9.

Lu, L., Zhou, J., Shi, J., Peng, X.J., Qi, X.X., Wang, Y., Li, F.Y., Zhou, F.Y., Liu, L., and Liu, Z.Q. (2015). Drug-Metabolizing Activity, Protein and Gene Expression of UDP-Glucuronosyltransferases Are Significantly Altered in Hepatocellular Carcinoma Patients. *PLoS One* 10**,** e0127524.

Lum, J.J., Bauer, D.E., Kong, M., Harris, M.H., Li, C., Lindsten, T., and Thompson, C.B. (2005). Growth factor regulation of autophagy and cell survival in the absence of apoptosis. *Cell* 120**,** 237-248.

Luu-The, V., Ferraris, C., Duche, D., Belanger, P., Leclaire, J., and Labrie, F. (2007). Steroid metabolism and profile of steroidogenic gene expression in Episkin: high similarity with human epidermis. *J Steroid Biochem Mol Biol* 107**,** 30-36.

Luukkanen, L., Taskinen, J., Kurkela, M., Kostiainen, R., Hirvonen, J., and Finel, M. (2005). Kinetic characterization of the 1A subfamily of recombinant human UDP-glucuronosyltransferases. *Drug Metab Dispos* 33**,** 1017-1026.

M. Gagne, L., Boulay, K., Topisirovic, I., Huot, M.E., and Mallette, F.A. (2017). Oncogenic Activities of IDH1/2 Mutations: From Epigenetics to Cellular Signaling. *Trends Cell Biol* 27**,** 738-752.

Mackenzie, P.I., Rogers, A., Treloar, J., Jorgensen, B.R., Miners, J.O., and Meech, R. (2008). Identification of UDP glycosyltransferase 3A1 as a UDP N-acetylglucosaminyltransferase. *J Biol Chem* 283**,** 36205-36210.

Mackie, K. (2008). Cannabinoid receptors: where they are and what they do. *J Neuroendocrinol* 20 Suppl 1**,** 10-14.

Maddocks, O.D.K., Athineos, D., Cheung, E.C., Lee, P., Zhang, T., Van Den Broek, N.J.F., Mackay, G.M., Labuschagne, C.F., Gay, D., Kruiswijk, F., Blagih, J., Vincent, D.F., Campbell, K.J., Ceteci, F., Sansom, O.J., Blyth, K., and Vousden, K.H. (2017). Modulating the therapeutic response of tumours to dietary serine and glycine starvation. *Nature* 544**,** 372-376.

Maglich, J.M., Watson, J., Mcmillen, P.J., Goodwin, B., Willson, T.M., and Moore, J.T. (2004). The nuclear receptor CAR is a regulator of thyroid hormone metabolism during caloric restriction. *J Biol Chem* 279**,** 19832-19838.

Marcotorchino, J., Tourniaire, F., Astier, J., Karkeni, E., Canault, M., Amiot, M.J., Bendahan, D., Bernard, M., Martin, J.C., Giannesini, B., and Landrier, J.F. (2014). Vitamin D protects against diet-induced obesity by enhancing fatty acid oxidation. *J Nutr Biochem* 25**,** 1077-1083.

Margaillan, G., Levesque, E., and Guillemette, C. (2016). Epigenetic regulation of steroid inactivating UDP-glucuronosyltransferases by microRNAs in prostate cancer. *J Steroid Biochem Mol Biol* 155**,** 85-93.

Margaillan, G., Rouleau, M., Fallon, J.K., Caron, P., Villeneuve, L., Turcotte, V., Smith, P.C., Joy, M.S., and Guillemette, C. (2015a). Quantitative profiling of human renal UDP-glucuronosyltransferases and glucuronidation activity: a comparison of normal and tumoral kidney tissues. *Drug Metab Dispos* 43**,** 611-619.

Margaillan, G., Rouleau, M., Klein, K., Fallon, J.K., Caron, P., Villeneuve, L., Smith, P.C., Zanger, U.M., and Guillemette, C. (2015b). Multiplexed Targeted Quantitative Proteomics Predicts Hepatic Glucuronidation Potential. *Drug Metab Dispos* 43**,** 1331-1335.

Mazurek, S. (2011). Pyruvate kinase type M2: a key regulator of the metabolic budget system in tumor cells. *Int J Biochem Cell Biol* 43**,** 969-980.

Mcgrath, M., Lepine, J., Lee, I.M., Villeneuve, L., Buring, J., Guillemette, C., and De Vivo, I. (2009). Genetic variations in UGT1A1 and UGT2B7 and endometrial cancer risk. *Pharmacogenet Genomics* 19**,** 239-243.

Medes, G., Thomas, A., and Weinhouse, S. (1953). Metabolism of neoplastic tissue. IV. A study of lipid synthesis in neoplastic tissue slices in vitro. *Cancer Res* 13**,** 27-29.

Medina, M.A. (2001). Glutamine and cancer. *J Nutr* 131**,** 2539S-2542S; discussion 2550S-2531S.

Meech, R., and Mackenzie, P.I. (1998). Determinants of UDP glucuronosyltransferase membrane association and residency in the endoplasmic reticulum. *Arch Biochem Biophys* 356**,** 77-85.

Meech, R., Mubarokah, N., Shivasami, A., Rogers, A., Nair, P.C., Hu, D.G., Mckinnon, R.A., and Mackenzie, P.I. (2015). A novel function for UDP glycosyltransferase 8: galactosidation of bile acids. *Mol Pharmacol* 87**,** 442-450.

Menard, V., Collin, P., Margaillan, G., and Guillemette, C. (2013a). Modulation of the UGT2B7 enzyme activity by C-terminally truncated proteins derived from alternative splicing. *Drug Metab Dispos* 41**,** 2197-2205.

Menard, V., Levesque, E., Chen, S., Eap, O., Joy, M.S., Ekstrom, L., Rane, A., and Guillemette, C. (2013b). Expression of UGT2B7 is driven by two mutually exclusive promoters and alternative splicing in human tissues: changes from prenatal life to adulthood and in kidney cancer. *Pharmacogenet Genomics* 23**,** 684-696.

Menendez, J.A., and Lupu, R. (2007). Fatty acid synthase and the lipogenic phenotype in cancer pathogenesis. *Nat Rev Cancer* 7**,** 763-777.
Miley, M.J., Zielinska, A.K., Keenan, J.E., Bratton, S.M., Radominska-Pandya, A., and Redinbo, M.R. (2007). Crystal structure of the cofactor-binding domain of the human phase II drug-metabolism enzyme UDP-glucuronosyltransferase 2B7. *J Mol Biol* 369**,** 498-511.
Miller, P.E., Lazarus, P., Lesko, S.M., Cross, A.J., Sinha, R., Laio, J., Zhu, J., Harper, G., Muscat, J.E., and Hartman, T.J. (2013). Meat-related compounds and colorectal cancer risk by anatomical subsite. *Nutr Cancer* 65**,** 202-226.
Mitchell, J.A., and Kirkby, N.S. (2018). Eicosanoids, prostacyclin and cyclooxygenase in the cardiovascular system. *Br J Pharmacol*.
Mitra, P.S., Basu, N.K., and Owens, I.S. (2009). Src supports UDP-glucuronosyltransferase-2B7 detoxification of catechol estrogens associated with breast cancer. *Biochem Biophys Res Commun* 382**,** 651-656.
Miyagi, S.J., and Collier, A.C. (2007). Pediatric development of glucuronidation: the ontogeny of hepatic UGT1A4. *Drug Metab Dispos* 35**,** 1587-1592.
Moreno-Sanchez, R., Rodriguez-Enriquez, S., Marin-Hernandez, A., and Saavedra, E. (2007). Energy metabolism in tumor cells. *FEBS J* 274**,** 1393-1418.
Moscovitz, J.E., Kalgutkar, A.S., Nulick, K., Johnson, N., Lin, Z., Goosen, T.C., and Weng, Y. (2018). Establishing Transcriptional Signatures to Differentiate PXR-, CAR-, and AhR-Mediated Regulation of Drug Metabolism and Transport Genes in Cryopreserved Human Hepatocytes. *J Pharmacol Exp Ther* 365**,** 262-271.
Muschet, C., Moller, G., Prehn, C., De Angelis, M.H., Adamski, J., and Tokarz, J. (2016). Removing the bottlenecks of cell culture metabolomics: fast normalization procedure, correlation of metabolites to cell number, and impact of the cell harvesting method. *Metabolomics* 12**,** 151.
Myte, R., Gylling, B., Haggstrom, J., Schneede, J., Magne Ueland, P., Hallmans, G., Johansson, I., Palmqvist, R., and Van Guelpen, B. (2017). Untangling the role of one-carbon metabolism in colorectal cancer risk: a comprehensive Bayesian network analysis. *Sci Rep* 7**,** 43434.
Nadeau, G., Bellemare, J., Audet-Walsh, E., Flageole, C., Huang, S.P., Bao, B.Y., Douville, P., Caron, P., Fradet, Y., Lacombe, L., Guillemette, C., and Levesque, E. (2011). Deletions of the androgen-metabolizing UGT2B genes have an effect on circulating steroid levels and biochemical recurrence after radical prostatectomy in localized prostate cancer. *J Clin Endocrinol Metab* 96**,** E1550-1557.
Nagao, M., Wakabayashi, K., Ushijima, T., Toyota, M., Totsuka, Y., and Sugimura, T. (1996). Human exposure to carcinogenic heterocyclic amines and their mutational fingerprints in experimental animals. *Environ Health Perspect* 104 Suppl 3**,** 497-501.
Nagar, S., and Remmel, R.P. (2006). Uridine diphosphoglucuronosyltransferase pharmacogenetics and cancer. *Oncogene* 25**,** 1659-1672.
Nair, P.C., Meech, R., Mackenzie, P.I., Mckinnon, R.A., and Miners, J.O. (2015). Insights into the UDP-sugar selectivities of human UDP-glycosyltransferases (UGT): a molecular modeling perspective. *Drug Metab Rev* 47**,** 335-345.
Nakamura, A., Nakajima, M., Yamanaka, H., Fujiwara, R., and Yokoi, T. (2008). Expression of UGT1A and UGT2B mRNA in human normal tissues and various cell lines. *Drug Metab Dispos* 36**,** 1461-1464.
Nakamura, T., Yamaguchi, N., Miyauchi, Y., Takeda, T., Yamazoe, Y., Nagata, K., Mackenzie, P.I., Yamada, H., and Ishii, Y. (2016). Introduction of an N-Glycosylation Site into UDP-Glucuronosyltransferase 2B3 Alters Its Sensitivity to Cytochrome P450 3A1-Dependent Modulation. *Front Pharmacol* 7**,** 427.
Niwa, T., Murayama, N., Imagawa, Y., and Yamazaki, H. (2015). Regioselective hydroxylation of steroid hormones by human cytochromes P450. *Drug Metab Rev* 47**,** 89-110.
Oda, S., Fukami, T., Yokoi, T., and Nakajima, M. (2014). Epigenetic regulation of the tissue-specific expression of human UDP-glucuronosyltransferase (UGT) 1A10. *Biochem Pharmacol* 87**,** 660-667.
Oeser, S.G., Bingham, J.P., and Collier, A.C. (2018). Regulation of Hepatic UGT2B15 by Methylation in Adults of Asian Descent. *Pharmaceutics* 10.

Ohno, S., and Nakajin, S. (2009). Determination of mRNA expression of human UDP-glucuronosyltransferases and application for localization in various human tissues by real-time reverse transcriptase-polymerase chain reaction. *Drug Metab Dispos* 37**,** 32-40.

Oltean, S., and Bates, D.O. (2014). Hallmarks of alternative splicing in cancer. *Oncogene* 33**,** 5311-5318.

Operana, T.N., and Tukey, R.H. (2007). Oligomerization of the UDP-glucuronosyltransferase 1A proteins: homo- and heterodimerization analysis by fluorescence resonance energy transfer and co-immunoprecipitation. *J Biol Chem* 282**,** 4821-4829.

Pace, S., Sautebin, L., and Werz, O. (2017). Sex-biased eicosanoid biology: Impact for sex differences in inflammation and consequences for pharmacotherapy. *Biochem Pharmacol* 145**,** 1-11.

Pacheco, P.R., Brilhante, M.J., Ballart, C., Sigalat, F., Polena, H., Cabral, R., Branco, C.C., and Mota-Vieira, L. (2009). UGT1A1, UGT1A6 and UGT1A7 genetic analysis: repercussion for irinotecan pharmacogenetics in the Sao Miguel Island Population (Azores, Portugal). *Mol Diagn Ther* 13**,** 261-268.

Park, S.H., Ozden, O., Liu, G., Song, H.Y., Zhu, Y., Yan, Y., Zou, X., Kang, H.J., Jiang, H., Principe, D.R., Cha, Y.I., Roh, M., Vassilopoulos, A., and Gius, D. (2016). SIRT2-Mediated Deacetylation and Tetramerization of Pyruvate Kinase Directs Glycolysis and Tumor Growth. *Cancer Res* 76**,** 3802-3812.

Patel, K.D., Davison, J.S., Pittman, Q.J., and Sharkey, K.A. (2010). Cannabinoid CB(2) receptors in health and disease. *Curr Med Chem* 17**,** 1393-1410.

Peer, C.J., Sissung, T.M., Kim, A., Jain, L., Woo, S., Gardner, E.R., Kirkland, C.T., Troutman, S.M., English, B.C., Richardson, E.D., Federspiel, J., Venzon, D., Dahut, W., Kohn, E., Kummar, S., Yarchoan, R., Giaccone, G., Widemann, B., and Figg, W.D. (2012). Sorafenib is an inhibitor of UGT1A1 but is metabolized by UGT1A9: implications of genetic variants on pharmacokinetics and hyperbilirubinemia. *Clin Cancer Res* 18**,** 2099-2107.

Pertwee, R.G., Howlett, A.C., Abood, M.E., Alexander, S.P., Di Marzo, V., Elphick, M.R., Greasley, P.J., Hansen, H.S., Kunos, G., Mackie, K., Mechoulam, R., and Ross, R.A. (2010). International Union of Basic and Clinical Pharmacology. LXXIX. Cannabinoid receptors and their ligands: beyond CB(1) and CB(2). *Pharmacol Rev* 62**,** 588-631.

Phan, L.M., Yeung, S.C., and Lee, M.H. (2014). Cancer metabolic reprogramming: importance, main features, and potentials for precise targeted anti-cancer therapies. *Cancer Biol Med* 11**,** 1-19.

Pineda, J.M.B., and Bradley, R.K. (2018). Most human introns are recognized via multiple and tissue-specific branchpoints. *Genes Dev* 32**,** 577-591.

Radominska-Pandya, A., Czernik, P.J., Little, J.M., Battaglia, E., and Mackenzie, P.I. (1999). Structural and functional studies of UDP-glucuronosyltransferases. *Drug Metab Rev* 31**,** 817-899.

Ramachandran, A., and Jaeschke, H. (2017). Mechanisms of acetaminophen hepatotoxicity and their translation to the human pathophysiology. *J Clin Transl Res* 3**,** 157-169.

Reeves, D.A., Mu, H., Kropachev, K., Cai, Y., Ding, S., Kolbanovskiy, A., Kolbanovskiy, M., Chen, Y., Krzeminski, J., Amin, S., Patel, D.J., Broyde, S., and Geacintov, N.E. (2011). Resistance of bulky DNA lesions to nucleotide excision repair can result from extensive aromatic lesion-base stacking interactions. *Nucleic Acids Res* 39**,** 8752-8764.

Richardson, T.A., and Klaassen, C.D. (2010). Disruption of thyroid hormone homeostasis in Ugt1a-deficient Gunn rats by microsomal enzyme inducers is not due to enhanced thyroxine glucuronidation. *Toxicol Appl Pharmacol* 248**,** 38-44.

Riches, Z., and Collier, A.C. (2015). Posttranscriptional regulation of uridine diphosphate glucuronosyltransferases. *Expert Opin Drug Metab Toxicol* 11**,** 949-965.

Riganti, C., Gazzano, E., Polimeni, M., Aldieri, E., and Ghigo, D. (2012). The pentose phosphate pathway: an antioxidant defense and a crossroad in tumor cell fate. *Free Radic Biol Med* 53**,** 421-436.

Ritter, J.K., Chen, F., Sheen, Y.Y., Tran, H.M., Kimura, S., Yeatman, M.T., and Owens, I.S. (1992). A novel complex locus UGT1 encodes human bilirubin, phenol, and other UDP-glucuronosyltransferase isozymes with identical carboxyl termini. *J Biol Chem* 267**,** 3257-3261.

Rogan, E.G., Badawi, A.F., Devanesan, P.D., Meza, J.L., Edney, J.A., West, W.W., Higginbotham, S.M., and Cavalieri, E.L. (2003). Relative imbalances in estrogen metabolism and conjugation in breast tissue of women with carcinoma: potential biomarkers of susceptibility to cancer. *Carcinogenesis* 24**,** 697-702.

Rouleau, M., Audet-Delage, Y., Desjardins, S., Rouleau, M., Girard-Bock, C., and Guillemette, C. (2017). Endogenous Protein Interactome of Human UDP-Glucuronosyltransferases Exposed by Untargeted Proteomics. *Front Pharmacol* 8**,** 23.

Rouleau, M., Collin, P., Bellemare, J., Harvey, M., and Guillemette, C. (2013a). Protein-protein interactions between the bilirubin-conjugating UDP-glucuronosyltransferase UGT1A1 and its shorter isoform 2 regulatory partner derived from alternative splicing. *Biochem J* 450**,** 107-114.

Rouleau, M., Roberge, J., Bellemare, J., and Guillemette, C. (2014). Dual roles for splice variants of the glucuronidation pathway as regulators of cellular metabolism. *Mol Pharmacol* 85**,** 29-36.

Rouleau, M., Roberge, J., Falardeau, S.A., Villeneuve, L., and Guillemette, C. (2013b). The relative protein abundance of UGT1A alternative splice variants as a key determinant of glucuronidation activity in vitro. *Drug Metab Dispos* 41**,** 694-697.

Rouleau, M., Tourancheau, A., Girard-Bock, C., Villeneuve, L., Vaucher, J., Duperre, A.M., Audet-Delage, Y., Gilbert, I., Popa, I., Droit, A., and Guillemette, C. (2016). Divergent Expression and Metabolic Functions of Human Glucuronosyltransferases through Alternative Splicing. *Cell Rep* 17**,** 114-124.

Rowland, A., Miners, J.O., and Mackenzie, P.I. (2013). The UDP-glucuronosyltransferases: their role in drug metabolism and detoxification. *Int J Biochem Cell Biol* 45**,** 1121-1132.

Sano, Y., Kogashiwa, Y., Araki, R., Enoki, Y., Ikeda, T., Yoda, T., Nakahira, M., and Sugasawa, M. (2018). Correlation of Inflammatory Markers, Survival, and COX2 Expression in Oral Cancer and Implications for Prognosis. *Otolaryngol Head Neck Surg* 158**,** 667-676.

Santos, C.R., and Schulze, A. (2012). Lipid metabolism in cancer. *FEBS J* 279**,** 2610-2623.

Satoh, T., Katano-Toki, A., Tomaru, T., Yoshino, S., Ishizuka, T., Horiguchi, K., Nakajima, Y., Ishii, S., Ozawa, A., Shibusawa, N., Hashimoto, K., Mori, M., and Yamada, M. (2014). Coordinated regulation of transcription and alternative splicing by the thyroid hormone receptor and its associating coregulators. *Biochem Biophys Res Commun* 451**,** 24-29.

Schaefer, M.B., Schaefer, C.A., Schifferings, S., Kuhlmann, C.R., Urban, A., Benscheid, U., Fischer, T., Hecker, M., Morty, R.E., Vadasz, I., Herold, S., Witzenrath, M., Seeger, W., Erdogan, A., and Mayer, K. (2016). N-3 vs. n-6 fatty acids differentially influence calcium signalling and adhesion of inflammatory activated monocytes: impact of lipid rafts. *Inflamm Res* 65**,** 881-894.

Schioth, H.B., Bostrom, A., Murphy, S.K., Erhart, W., Hampe, J., Moylan, C., and Mwinyi, J. (2016). A targeted analysis reveals relevant shifts in the methylation and transcription of genes responsible for bile acid homeostasis and drug metabolism in non-alcoholic fatty liver disease. *BMC Genomics* 17**,** 462.

Sen, T., Sen, N., Noordhuis, M.G., Ravi, R., Wu, T.C., Ha, P.K., Sidransky, D., and Hoque, M.O. (2012). OGDHL is a modifier of AKT-dependent signaling and NF-kappaB function. *PLoS One* 7**,** e48770.

Shaw, R.J., Kosmatka, M., Bardeesy, N., Hurley, R.L., Witters, L.A., Depinho, R.A., and Cantley, L.C. (2004). The tumor suppressor LKB1 kinase directly activates AMP-activated kinase and regulates apoptosis in response to energy stress. *Proc Natl Acad Sci U S A* 101**,** 3329-3335.

Shibuya, A., Itoh, T., Tukey, R.H., and Fujiwara, R. (2013). Impact of fatty acids on human UDP-glucuronosyltransferase 1A1 activity and its expression in neonatal hyperbilirubinemia. *Scientific Reports* 3**,** 2903.

Sidell, N., Sawatsri, S., Connor, M.J., Barua, A.B., Olson, J.A., and Wada, R.K. (2000). Pharmacokinetics of chronically administered all-trans-retinoyl-beta-glucuronide in mice. *Biochim Biophys Acta* 1502**,** 264-272.

Silva, L.P., Lorenzi, P.L., Purwaha, P., Yong, V., Hawke, D.H., and Weinstein, J.N. (2013). Measurement of DNA Concentration as a Normalization Strategy for Metabolomic Data from Adherent Cell Lines. *Analytical Chemistry* 85**,** 9536-9542.

Skierka, J.M., Kotzer, K.E., Lagerstedt, S.A., O'kane, D.J., and Baudhuin, L.M. (2013). UGT1A1 genetic analysis as a diagnostic aid for individuals with unconjugated hyperbilirubinemia. *J Pediatr* 162**,** 1146-1152, 1152 e1141-1142.

Sledzinski, P., Zeyland, J., Slomski, R., and Nowak, A. (2018). The current state and future perspectives of cannabinoids in cancer biology. *Cancer Med* 7**,** 765-775.

Smits, A., Verbesselt, R., Kulo, A., Naulaers, G., De Hoon, J., and Allegaert, K. (2013). Urinary metabolites after intravenous propofol bolus in neonates. *Eur J Drug Metab Pharmacokinet* 38**,** 97-103.

Stephen, R.L., Gustafsson, M.C., Jarvis, M., Tatoud, R., Marshall, B.R., Knight, D., Ehrenborg, E., Harris, A.L., Wolf, C.R., and Palmer, C.N. (2004). Activation of peroxisome proliferator-activated receptor delta stimulates the proliferation of human breast and prostate cancer cell lines. *Cancer Res* 64**,** 3162-3170.

Sticova, E., and Jirsa, M. (2013). New insights in bilirubin metabolism and their clinical implications. *World J Gastroenterol* 19**,** 6398-6407.

Stingl, J.C., Bartels, H., Viviani, R., Lehmann, M.L., and Brockmoller, J. (2014). Relevance of UDP-glucuronosyltransferase polymorphisms for drug dosing: A quantitative systematic review. *Pharmacol Ther* 141**,** 92-116.

Sugatani, J., Nishitani, S., Yamakawa, K., Yoshinari, K., Sueyoshi, T., Negishi, M., and Miwa, M. (2005). Transcriptional regulation of human UGT1A1 gene expression: activated glucocorticoid receptor enhances constitutive androstane receptor/pregnane X receptor-mediated UDP-glucuronosyltransferase 1A1 regulation with glucocorticoid receptor-interacting protein 1. *Mol Pharmacol* 67**,** 845-855.

Sullivan, E.M., Pennington, E.R., Green, W.D., Beck, M.A., Brown, D.A., and Shaikh, S.R. (2018). Mechanisms by Which Dietary Fatty Acids Regulate Mitochondrial Structure-Function in Health and Disease. *Adv Nutr* 9**,** 247-262.

Swinnen, J.V., Vanderhoydonc, F., Elgamal, A.A., Eelen, M., Vercaeren, I., Joniau, S., Van Poppel, H., Baert, L., Goossens, K., Heyns, W., and Verhoeven, G. (2000). Selective activation of the fatty acid synthesis pathway in human prostate cancer. *Int J Cancer* 88**,** 176-179.

Tan, D., Chen, K.E., Deng, C., Tang, P., Huang, J., Mansour, T., Luben, R.A., and Walker, A.M. (2014). An N-terminal splice variant of human Stat5a that interacts with different transcription factors is the dominant form expressed in invasive ductal carcinoma. *Cancer Lett* 346**,** 148-157.

Taura, K.I., Yamada, H., Hagino, Y., Ishii, Y., Mori, M.A., and Oguri, K. (2000). Interaction between cytochrome P450 and other drug-metabolizing enzymes: evidence for an association of CYP1A1 with microsomal epoxide hydrolase and UDP-glucuronosyltransferase. *Biochem Biophys Res Commun* 273**,** 1048-1052.

Tchernof, A., Levesque, E., Beaulieu, M., Couture, P., Despres, J.P., Hum, D.W., and Belanger, A. (1999). Expression of the androgen metabolizing enzyme UGT2B15 in adipose tissue and relative expression measurement using a competitive RT-PCR method. *Clin Endocrinol (Oxf)* 50**,** 637-642.

Teasdale, R.D., and Jackson, M.R. (1996). Signal-mediated sorting of membrane proteins between the endoplasmic reticulum and the golgi apparatus. *Annu Rev Cell Dev Biol* 12**,** 27-54.

Tedeschi, P.M., Markert, E.K., Gounder, M., Lin, H., Dvorzhinski, D., Dolfi, S.C., Chan, L.L., Qiu, J., Dipaola, R.S., Hirshfield, K.M., Boros, L.G., Bertino, J.R., Oltvai, Z.N., and Vazquez, A. (2013). Contribution of serine, folate and glycine metabolism to the ATP, NADPH and purine requirements of cancer cells. *Cell Death Dis* 4**,** e877.

Tomlinson, I.P., Alam, N.A., Rowan, A.J., Barclay, E., Jaeger, E.E., Kelsell, D., Leigh, I., Gorman, P., Lamlum, H., Rahman, S., Roylance, R.R., Olpin, S., Bevan, S., Barker, K., Hearle, N., Houlston, R.S., Kiuru, M., Lehtonen, R., Karhu, A., Vilkki, S., Laiho, P., Eklund, C., Vierimaa, O., Aittomaki, K., Hietala, M., Sistonen, P., Paetau, A., Salovaara, R., Herva, R., Launonen, V., Aaltonen, L.A., and Multiple Leiomyoma, C. (2002). Germline mutations in FH predispose to dominantly inherited uterine fibroids, skin leiomyomata and papillary renal cell cancer. *Nat Genet* 30**,** 406-410.

Tourancheau, A., Margaillan, G., Rouleau, M., Gilbert, I., Villeneuve, L., Levesque, E., Droit, A., and Guillemette, C. (2016). Unravelling the transcriptomic landscape of the major phase II UDP-glucuronosyltransferase drug metabolizing pathway using targeted RNA sequencing. *Pharmacogenomics J* 16**,** 60-70.

Tourancheau, A., Rouleau, M., Guauque-Olarte, S., Villeneuve, L., Gilbert, I., Droit, A., and Guillemette, C. (2018). Quantitative profiling of the UGT transcriptome in human drug-metabolizing tissues. *Pharmacogenomics J* 18**,** 251-261.

Travan, L., Lega, S., Crovella, S., Montico, M., Panontin, E., and Demarini, S. (2014). Severe neonatal hyperbilirubinemia and UGT1A1 promoter polymorphism. *J Pediatr* 165**,** 42-45.

Tripathi, S.P., Bhadauriya, A., Patil, A., and Sangamwar, A.T. (2013). Substrate selectivity of human intestinal UDP-glucuronosyltransferases (UGTs): in silico and in vitro insights. *Drug Metab Rev* 45**,** 231-252.

Uchaipichat, V., Suthisisang, C., and Miners, J.O. (2013). The glucuronidation of R- and S-lorazepam: human liver microsomal kinetics, UDP-glucuronosyltransferase enzyme selectivity, and inhibition by drugs. *Drug Metab Dispos* 41**,** 1273-1284.

Van Dorp, E.L., Morariu, A., and Dahan, A. (2008). Morphine-6-glucuronide: potency and safety compared with morphine. *Expert Opin Pharmacother* 9**,** 1955-1961.

Vander Heiden, M.G., Cantley, L.C., and Thompson, C.B. (2009). Understanding the Warburg effect: the metabolic requirements of cell proliferation. *Science* 324**,** 1029-1033.

Vander Heiden, M.G., Chandel, N.S., Schumacker, P.T., and Thompson, C.B. (1999). Bcl-xL prevents cell death following growth factor withdrawal by facilitating mitochondrial ATP/ADP exchange. *Mol Cell* 3**,** 159-167.

Vander Heiden, M.G., Lunt, S.Y., Dayton, T.L., Fiske, B.P., Israelsen, W.J., Mattaini, K.R., Vokes, N.I., Stephanopoulos, G., Cantley, L.C., Metallo, C.M., and Locasale, J.W. (2011). Metabolic pathway alterations that support cell proliferation. *Cold Spring Harb Symp Quant Biol* 76**,** 325-334.

Wallace, D.C. (2012). Mitochondria and cancer. *Nat Rev Cancer* 12**,** 685-698.

Wang, J., Wu, X., Kamat, A., Barton Grossman, H., Dinney, C.P., and Lin, J. (2013a). Fluid intake, genetic variants of UDP-glucuronosyltransferases, and bladder cancer risk. *Br J Cancer* 108**,** 2372-2380.

Wang, L.Z., Ramirez, J., Yeo, W., Chan, M.Y., Thuya, W.L., Lau, J.Y., Wan, S.C., Wong, A.L., Zee, Y.K., Lim, R., Lee, S.C., Ho, P.C., Lee, H.S., Chan, A., Ansher, S., Ratain, M.J., and Goh, B.C. (2013b). Glucuronidation by UGT1A1 is the dominant pathway of the metabolic disposition of belinostat in liver cancer patients. *PLoS One* 8**,** e54522.

Wang, Z.Q., Faddaoui, A., Bachvarova, M., Plante, M., Gregoire, J., Renaud, M.C., Sebastianelli, A., Guillemette, C., Gobeil, S., Macdonald, E., Vanderhyden, B., and Bachvarov, D. (2015). BCAT1 expression associates with ovarian cancer progression: possible implications in altered disease metabolism. *Oncotarget* 6**,** 31522-31543.

Warburg, O. (1956a). On respiratory impairment in cancer cells. *Science* 124**,** 269-270.

Warburg, O. (1956b). On the origin of cancer cells. *Science* 123**,** 309-314.

Warburg, O. (1956c). [Origin of cancer cells]. *Oncologia* 9**,** 75-83.

Warburg, O., Wind, F., and Negelein, E. (1927). The Metabolism of Tumors in the Body. *J Gen Physiol* 8**,** 519-530.

Weinhouse, S. (1976). The Warburg hypothesis fifty years later. *Z Krebsforsch Klin Onkol Cancer Res Clin Oncol* 87**,** 115-126.

Wen, Z., Tallman, M.N., Ali, S.Y., and Smith, P.C. (2007). UDP-glucuronosyltransferase 1A1 is the principal enzyme responsible for etoposide glucuronidation in human liver and intestinal microsomes: structural characterization of phenolic and alcoholic glucuronides of etoposide and estimation of enzyme kinetics. *Drug Metab Dispos* 35**,** 371-380.

Wijayakumara, D.D., Hu, D.G., Meech, R., Mckinnon, R.A., and Mackenzie, P.I. (2015). Regulation of Human UGT2B15 and UGT2B17 by miR-376c in Prostate Cancer Cell Lines. *J Pharmacol Exp Ther* 354**,** 417-425.

Winsnes, A. (1972). Kinetic properties of different forms of hepatic UDPglucuronyltransferase. *Biochim Biophys Acta* 284**,** 394-405.

Wright, J.C., Prigot, A., Wright, B., Weintraub, S., and Wright, L.T. (1951). An evaluation of folic acid antagonists in adults with neoplastic diseases: a study of 93 patients with incurable neoplasms. *J Natl Med Assoc* 43**,** 211-240.

Xiao, Y., Yao, Y., Jiang, H., Lu, C., Zeng, S., and Yu, L. (2015). Regulation of uridine diphosphate-glucuronosyltransferase 1A3 activity by protein phosphorylation. *Biopharm Drug Dispos* 36**,** 520-528.

Xu, W., Yang, H., Liu, Y., Yang, Y., Wang, P., Kim, S.H., Ito, S., Yang, C., Wang, P., Xiao, M.T., Liu, L.X., Jiang, W.Q., Liu, J., Zhang, J.Y., Wang, B., Frye, S., Zhang, Y., Xu, Y.H., Lei, Q.Y., Guan, K.L., Zhao,

S.M., and Xiong, Y. (2011). Oncometabolite 2-hydroxyglutarate is a competitive inhibitor of alpha-ketoglutarate-dependent dioxygenases. *Cancer Cell* 19**,** 17-30.

Yan, X.L., Zhang, X.B., Ao, R., and Guan, L. (2017). Effects of shRNA-Mediated Silencing of PKM2 Gene on Aerobic Glycolysis, Cell Migration, Cell Invasion, and Apoptosis in Colorectal Cancer Cells. *J Cell Biochem* 118**,** 4792-4803.

Yang, C., Ko, B., Hensley, C.T., Jiang, L., Wasti, A.T., Kim, J., Sudderth, J., Calvaruso, M.A., Lumata, L., Mitsche, M., Rutter, J., Merritt, M.E., and Deberardinis, R.J. (2014a). Glutamine oxidation maintains the TCA cycle and cell survival during impaired mitochondrial pyruvate transport. *Mol Cell* 56**,** 414-424.

Yang, P., Li, Z., Fu, R., Wu, H., and Li, Z. (2014b). Pyruvate kinase M2 facilitates colon cancer cell migration via the modulation of STAT3 signalling. *Cell Signal* 26**,** 1853-1862.

Yang, X., Coulombe-Huntington, J., Kang, S., Sheynkman, G.M., Hao, T., Richardson, A., Sun, S., Yang, F., Shen, Y.A., Murray, R.R., Spirohn, K., Begg, B.E., Duran-Frigola, M., Macwilliams, A., Pevzner, S.J., Zhong, Q., Trigg, S.A., Tam, S., Ghamsari, L., Sahni, N., Yi, S., Rodriguez, M.D., Balcha, D., Tan, G., Costanzo, M., Andrews, B., Boone, C., Zhou, X.J., Salehi-Ashtiani, K., Charloteaux, B., Chen, A.A., Calderwood, M.A., Aloy, P., Roth, F.P., Hill, D.E., Iakoucheva, L.M., Xia, Y., and Vidal, M. (2016). Widespread Expansion of Protein Interaction Capabilities by Alternative Splicing. *Cell* 164**,** 805-817.

Yang, X., Peng, X., and Huang, J. (2018). Inhibiting 6-phosphogluconate dehydrogenase selectively targets breast cancer through AMPK activation. *Clin Transl Oncol*.

Yang, Z.Z., Li, L., Xu, M.C., Ju, H.X., Hao, M., Gu, J.K., Jim Wang, Z.J., Jiang, H.D., Yu, L.S., and Zeng, S. (2017). Brain-derived neurotrophic factor involved epigenetic repression of UGT2B7 in colorectal carcinoma: A mechanism to alter morphine glucuronidation in tumor. *Oncotarget* 8**,** 29138-29150.

Yi, W., Clark, P.M., Mason, D.E., Keenan, M.C., Hill, C., Goddard, W.A., 3rd, Peters, E.C., Driggers, E.M., and Hsieh-Wilson, L.C. (2012). Phosphofructokinase 1 glycosylation regulates cell growth and metabolism. *Science* 337**,** 975-980.

Yokota, H., Ando, F., Iwano, H., and Yuasa, A. (1998). Inhibitory effects of uridine diphosphate on UDP-glucuronosyltransferase. *Life Sci* 63**,** 1693-1699.

Yoon, S., Lee, M.Y., Park, S.W., Moon, J.S., Koh, Y.K., Ahn, Y.H., Park, B.W., and Kim, K.S. (2007). Up-regulation of acetyl-CoA carboxylase alpha and fatty acid synthase by human epidermal growth factor receptor 2 at the translational level in breast cancer cells. *J Biol Chem* 282**,** 26122-26131.

Zahreddine, H.A., Culjkovic-Kraljacic, B., Assouline, S., Gendron, P., Romeo, A.A., Morris, S.J., Cormack, G., Jaquith, J.B., Cerchietti, L., Cocolakis, E., Amri, A., Bergeron, J., Leber, B., Becker, M.W., Pei, S., Jordan, C.T., Miller, W.H., and Borden, K.L. (2014). The sonic hedgehog factor GLI1 imparts drug resistance through inducible glucuronidation. *Nature* 511**,** 90-93.

Zhang, H., Zhou, L., Shi, W., Song, N., Yu, K., and Gu, Y. (2012). A mechanism underlying the effects of polyunsaturated fatty acids on breast cancer. *Int J Mol Med* 30**,** 487-494.

Zhang, J., Ahn, W.S., Gameiro, P.A., Keibler, M.A., Zhang, Z., and Stephanopoulos, G. (2014). 13C isotope-assisted methods for quantifying glutamine metabolism in cancer cells. *Methods Enzymol* 542**,** 369-389.

Zhang, L., and Han, J. (2017). Branched-chain amino acid transaminase 1 (BCAT1) promotes the growth of breast cancer cells through improving mTOR-mediated mitochondrial biogenesis and function. *Biochem Biophys Res Commun* 486**,** 224-231.

Zhao, X., Zhao, L., Yang, H., Li, J., Min, X., Yang, F., Liu, J., and Huang, G. (2018). Pyruvate kinase M2 interacts with nuclear sterol regulatory element-binding protein 1a and thereby activates lipogenesis and cell proliferation in hepatocellular carcinoma. *J Biol Chem* 293**,** 6623-6634.

Zheng, Y.H., Hu, W.J., Chen, B.C., Grahn, T.H., Zhao, Y.R., Bao, H.L., Zhu, Y.F., and Zhang, Q.Y. (2016). BCAT1, a key prognostic predictor of hepatocellular carcinoma, promotes cell proliferation and induces chemoresistance to cisplatin. *Liver Int* 36**,** 1836-1847.

Zhou, X., Zheng, Z., Xu, C., Wang, J., Min, M., Zhao, Y., Wang, X., Gong, Y., Yin, J., Guo, M., Guo, D., Zheng, J., Zhang, B., and Yin, X. (2017). Disturbance of Mammary UDP-Glucuronosyltransferase Represses Estrogen Metabolism and Exacerbates Experimental Breast Cancer. *J Pharm Sci* 106**,** 2152-2162.

Zu, X.L., and Guppy, M. (2004). Cancer metabolism: facts, fantasy, and fiction. *Biochem Biophys Res Commun* 313**,** 459-465.

Zuppa, A.F., Hammer, G.B., Barrett, J.S., Kenney, B.F., Kassir, N., Mouksassi, S., and Royal, M.A. (2011). Safety and population pharmacokinetic analysis of intravenous acetaminophen in neonates, infants, children, and adolescents with pain or Fever. *J Pediatr Pharmacol Ther* 16**,** 246-261.

Annexe 1 : « Estradiol metabolites as biomarkers of endometrial cancer prognosis after surgery »

Résumé

Le cancer de l'endomètre (CE) est le cancer gynécologique le plus prévalent après la ménopause. Définir les profils stéroïdiens pourrait aider à la prédiction du risque de récidive après hystérectomie, qui demeure limitée en raison d'un manque de biomarqueurs fiables. Nous avons mesuré les niveaux des précurseurs surrénaliens, d'androgènes, d'estrogènes parents et de catéchols estrogènes chez 246 femmes postménopausées nouvellement diagnostiquées, et dont le sérum a été récolté avant le chirurgie et un mois après celle-ci. Nous avons examiné les associations entre les hormones stéroïdiennes et le statut de CE en incluant 100 femmes post-ménopausées en santé. Les niveaux stéroïdiens ont été analysés en relation avec les caractéristiques clinico-pathologiques, la récidive et la survie globale. La durée de suivi moyenne est de 65.5 mois, et 26 patientes ont récidivé après la chirurgie, pour un taux d'incidence de la récidive à 10.6% (6.4% pour le type I et 29.5% pour le type II). La récidive et la survie globale sont reliées à une maladie plus agressive, mais pas à l'indice de masse corporelle. Les niveaux préopératoires d'estriol (E_3) et d'estrone-sulfate (E_1-S) sont inversement associés à la récidive dans des modèles de régression logistique multivariée (Risque relatif [RR] de 0.31, P = 0.039, et de 3.01, P = 0.024; respectivement). Les niveaux de tous les stéroïdes diminuent considérablement après la chirurgie, s'approchant de ceux des femmes en santé, à l'exception du 4-méthoxy-E_2 (4-MeO-E_2), dont les niveaux postopératoires augmentaient de 35% et étaient associés à une diminution de 68% du risque de récidive (RR = 0.32, P = 0.015). Les concentrations d'hormones stéroïdiennes sont plus élevées dans les cas de cancer des deux types histologiques, supportant leurs effets mitogènes. Le précurseur ostrogénique E_1-S, le métabolite anticancéreux 4-MeO-E_2 et le E_3, qui présente une activité ostrogénique agoniste et antagoniste et des effets immunologiques, sont de potentiels facteurs pronostiques indépendants.

Estradiol Metabolites as Biomarkers of Endometrial Cancer Prognosis After Surgery

Yannick Audet-Delage[1], Jean Grégoire[2], Patrick Caron[1], Véronique Turcotte[1], Marie Plante[2], Pierre Ayotte[3], David Simonyan[4], Lyne Villeneuve[1] and Chantal Guillemette[1,5]

[1]Centre Hospitalier Universitaire de Québec (CHU de Québec) Research Center and Faculty of Pharmacy, Laval University, Québec, Canada.

[2]Gynecologic Oncology Service, CHU de Québec, and Department of Obstetrics, Gynecology, and Reproduction, Faculty of Medicine, Laval University, Québec, Canada.

[3]CHU de Québec Research Center, and Department of Social and Preventive Medicine, Faculty of Medicine, Laval University, Québec, Canada.

[4]Statistical and Clinical Research Platform, CHU de Québec Research Center, Québec, Canada.

[5]Canada Research Chair in Pharmacogenomics.

Short title: Estradiol metabolites as EC prognostic markers

Correspondence and reprint requests should be addressed to: Chantal Guillemette, Ph.D., CHU de Québec Research Center, R4720, 2705 Boul. Laurier, Québec, QC, Canada, G1V 4G2. Tel: 1-418-654-2296

Email: chantal.guillemette@crchudequebec.ulaval.ca

Abstract

Endometrial cancer (EC) is the most common gynecologic malignancy prevailing after menopause. Defining steroid profiles may help predict the risk of recurrence after hysterectomy, which remains limited due to the lack of reliable markers. Adrenal precursors, androgens, parent estrogens and catechol estrogen metabolites were measured by mass spectrometry (MS) in preoperative serums and those collected one month after hysterectomy from 246 newly diagnosed postmenopausal EC cases. We also examined the associations between steroid hormones and EC status by including 110 healthy postmenopausal women. Steroid concentrations were analyzed in relation to clinicopathological features, recurrence and overall survival (OS). The mean follow-up time was 65.5 months and 26 patients experienced relapse after surgery for a recurrence incidence of 10.6% (6.4% Type I and 29.5% Type II). Recurrence and OS were related to a more aggressive disease but not linked to body mass index. Preoperative levels of estriol (E_3) and estrone-sulfate (E_1-S) were inversely associated with recurrence in a multivariate logistic regression analysis (Hazard ratios (HRs) of 0.31, *P*=0.039 and 3.01, *P*=0.024; respectively). All circulating steroids declined considerably after surgery almost reaching those of healthy women, except 4-methoxy-E_2 (4MeO-E_2) for which postoperative levels increased by 35% and were associated to a 68% decreased risk of recurrence (HR=0.32, *P*=0.015). Women diagnosed with both histological types of EC present significantly higher levels of steroids, in support of their mitogenic effects. The estrogen precursor E_1-S, the anticancer metabolite 4MeO-E_2, and E_3 that exert mixed antagonist and agonist estrogenic activities and immunological effects, are potential independent prognostic factors.

Keywords: Catechol estrogens, Mass spectrometry, Endometrial cancer, Recurrence.

1. Introduction

Endometrial cancer (EC) is the most common gynecologic cancer and the fourth most frequent neoplasm in women in North America, predominantly occurring in postmenopausal women. Furthermore, EC is the only gynecologic cancer with a rising incidence and mortality [1]. Curative surgery, alone or combined with adjuvant radiation therapy, is performed when cancer is limited to the uterus. However, a subset of EC patients experience recurrence, shorter survival and display inadequate response rates to cytotoxic chemotherapy [2]. The prognosis of EC is determined primarily by disease stage, grade and histologic subtype, reinforcing the need to explore novel prognostic markers.

EC is a heterogeneous disease comprising two types based on histology. The most common type, which accounts for nearly 80% of cases, is the endometrioid or Type I adenocarcinoma, associated with unopposed estrogen stimulation and generally has good prognosis. Type II is nonendometrioid that includes serous, clear cell, mixed carcinoma, with higher-grade histology and carries an adverse prognosis. Studies originally described Type I EC as estrogen-dependent whereas Type II was not. However, recent studies indicate that steroid hormones may play a significant etiological role in both types [3]. EC prevails after menopause when ovaries have ceased to secrete potent estrogens. Obesity is a known risk factor of EC [4] and this may be partly related to the fact that adipose tissue represents a major source of estrogen synthesis in postmenopausal women, actively converting adrenal and androgen precursors to estrogens resulting in increased serum bioavailable estradiol (E_2) [5,6]. Previous work by our group and others has revealed that the potent estrogen E_2 primarily derive from conversion of estrone-sulfate (E_1-S) in EC tumors rather than aromatization of androgens by the aromatase (CYP19), which has barely detectable expression levels in EC cells [7-10]. Besides, E_2 and E_1 may be converted into numerous biologically active derivatives with varying mitogenic and genotoxic properties by the action of various cytochrome P450 and catechol-O-methyl transferase enzymes [11]. This metabolism involves the irreversible hydroxylation (OH) at the C-2, C-4, or C-16 positions of the steroid ring and the methylation of C-2 or C-4 hydroxyl group. The latter prevents formation of mutagenic catechol quinones derived from hydroxyl estrogens that form stable and depurinating DNA adducts. In vitro and in vivo studies further support that 2-methoxyestradiol (2-MeOE_2) has strong anticancer activity [12,13]. In addition, these metabolites can be converted to their inactive sulfate and glucuronide conjugates. Recent studies have assessed the risk of EC in relation to steroid hormones, yet none have explored their association with prognosis [4,14].

In a cohort of 246 postmenopausal women undergoing hysterectomy for a newly diagnosed endometrial cancer, we analyzed the levels of 27 steroids in serums collected the morning of surgery and one month after surgery. Steroid measures included the assessment of endogenous concentrations of adrenal precursors, androgens, potent estrogens and catechol estrogens using sensitive and specific mass spectrometry (MS) validated assays. Our primary goal was to evaluate the association between circulating steroid levels, clinicopathological features and the risk of recurrence after surgery. A group of 110 healthy postmenopausal women was also included to examine the association between steroid hormones and EC status.

2.Materials and Methods

2.1. Study populations

All participants provided a written informed consent for their participation to the study and the use of their specimens. The current study was reviewed and approved by our institutional review boards. Recruitment of healthy postmenopausal women, as well as specimen collection and treatments, have been described elsewhere [15]. Briefly, women were recruited in a mammography clinic in Quebec City (QC, Canada) between July 2003 and March 2004. To be eligible, women had to: 1) be of postmenopausal status, 2) have no history of health problems related to steroid hormone metabolism, 3) have no history of hepatic, thyroid, or adrenal diseases, and 4) have not taken hormone replacement therapy (HRT) during the three months preceding enrolment. Recruitment methods and specimen collection of EC cases have been described [16]. Participants were all recruited at the Hôtel-Dieu de Québec Hospital (Québec City), between 2002 and 2013. All women were of postmenopausal status, undergoing surgery for EC (hysterectomy and bilateral salpingo-oophorectomy) and had not taken HRT in the three weeks prior to surgery. Blood samples were collected the morning of surgery and one month after surgery as part of a follow-up appointment. Samples were immediately processed, separated in aliquots and stored at -80°C until analysis. EC recurrence was ascertained by computerized tomography scan. For both cohorts, demographic and anthropometric data were collected through nurse-administered questionnaires, whereas information regarding drug use (including oral contraceptive and HRT) and obstetric history were collected at the same time. A pathologist assessed the histopathological characteristics of the hysterectomy specimen. Systematic assembling and review of medical records was performed by one of the treating gynecologic oncologist (J.G.).

2.2. Reagents and material

Parent estrogens standards were purchased from USP reference standard (Rockville, MD, USA), while other steroids were purchased from Steraloids (Newport, RI, USA). Deuterated standards were from C/D/N Isotopes (Montréal, QC, Canada), except d3-DHEA, which was synthesized by the Organic Synthesis Service of the CHU de Québec Research Center (Québec, QC, Canada). All chemicals and solvents used in this study were HPLC or reagent grade. Methanol, chlorobutane, dichloromethane, ethyl acetate and acetone were purchased from VWR (Montréal, QC, Canada). Ascorbic acid, sodium bicarbonate, β-glucuronidase/sulfatase (*Helix Pomentia* Type HP-2) and dansyl chloride were purchased from Sigma (Oakville, ON, Canada).

2.3. Steroids and SHBG quantification

Steroids and SHBG were quantified using validated methods [16,17]. Internal standards (deuterated steroids) were added to samples and quality controls were included in each run. The measured steroids and their limits of quantification were as follows: dehydroepiandrosterone (DHEA; 100 pg/mL); androstenediol (5-diol; 50 pg/mL); testosterone (30 pg/mL); dihydrotestosterone (DHT; 10 pg/mL); androsterone (ADT; 50 pg/mL); estrone (E_1; 5 pg/mL); estradiol (E_2; 1 pg/mL); androstenedione (4-dione; 50 pg/mL); ADT-glucuronide (ADT-G; 1 ng/mL); androstane-3□, 17□-diol 3-glucuronide (3□-diol-3G; 0.25 ng/mL); 3□-diol-17-G (0.25 ng/mL); DHEA-sulfate (DHEA-S; 0.075 mg/mL); estrone-sulfate (E_1-S; 0.075 ng/mL). Briefly, gas-chromatography (GC) coupled to mass spectrometry (MS) were used to quantify levels of DHEA, ADT, 5-diol, 4-dione,

testosterone, DHT, E_1 and E_2 using 250 µL of serum, while liquid-chromatography (LC) tandem MS was used for conjugated steroids using 20 µL for sulfates and 100 µL for glucuronides in two independent assays. All metabolite coefficients of variation (CV) were <10% and no samples had undetectable hormone levels.

We also measured 14 catechol estrogens with another MS-based assays, namely i) catechol 2OH: 2-hydroxyestrone (2-OHE_1), 2-hydroxyestradiol (2-OHE_2), ii) catechol 4OH: 4-hydroxyestrone (4-OHE_1), 4-hydroxyestradiol (4-OHE_2), iii) catechol 16OH: estriol (E_3), 16α-hydroxyestrone (16α-OHE_1), 16-ketoestradiol (16-ketoE_2), 16-epiestriol (16-epiE_3), and 17-epiestriol (17-epiE_3), and iv) catechol MeO: 2-methoxyestrone (2-$MeOE_1$), 2-methoxyestradiol (2-$MeOE_2$), 2-hydroxyestrone-3-methyl ether (3-$MeOE_1$), 4-methoxyestrone (4-$MeOE_1$) and 4-methoxyestradiol (4-$MeOE_2$). The quantification method was performed after some adjustments (described below) by stable isotope dilution LC/MS-MS based on method published by Xu *et al* [18] , which detected 13 catechol estrogens in addition to E_1 and E_2 and used 500 µL for a reported lower limit of quantification (LLOQ) of 8 pg/mL. In our study, we used 250 uL of serum for extraction to measure 14 catechol estrogens with a LLOQ of 5 pg/mL (corresponding to 16.56-18.52 pmol/L depending on the estrogen metabolite). LLOQ was defined as the minimum value at which the ratio of signal-to-noise was ≥5:1. Also, values of catechol estrogens observed below LLOQ (even if detected above the limit of detection) were considered as undetected. To measure total catechol estrogens corresponding to the sum of conjugated plus unconjugated forms, β-glucuronidase/sulfatase was included in sample preparation. Briefly, catechol estrogens were extracted from 250 µL of serum with ethyl acetate:chlorobutane (25:75, v/v) and evaporated to dryness. Derivatization was conducted with dansyl chloride (0.5 mg/mL final in 50% acetone and 50 mM sodium bicarbonate, pH 9.0). Samples were heated for 5 minutes at 60°C, mixed with 15 volumes of water:methanol (80:20, v/v) and loaded on pre-conditioned Strata X 60 mg SPE columns (Phenomenex, Torrance, CA, USA). After being washed with water and water:methanol (10:90, v/v), catechol estrogens were eluted with dichloromethane:methanol (50:50, v/v). Eluates were evaporated to dryness at 45°C under nitrogen gas, reconstituted in 100 µL of acetone:water (75:25, v/v) and injected into a high performance liquid chromatograph (HPLC) Waters (Milford, MA, USA). The chromatographic separation was achieved with an Synergie RP Hydro column containing 2.5 µm packing material, 100 X 3 mm (Phenomenex, Torrance, USA). The mobile phases consisted of water with 0.0375% formic acid (solvent A) and MeOH with 0.0375% formic acid (solvent B). The flow rate was 0.5 ml/min. The analytes were eluted with the following program: 0-8 min, isocratic 22.5% B; 8-18 min, linear gradient 22.5-35% B; 18-23 min, isocratic 35% B; 23-23.1 min, linear gradient 35-95% B; 23.1-28 min, isocratic 95% B; 28.0-28.1 min, linear gradient 95-22.5% B and 28.1-33 min, isocratic 22.5% B. Catechol estrogens were detected with an API5500 QTRAP MS (Concord, ON, Canada) equipped with a turbo ion-spray source set in positive ion mode, and operated in multiple reaction monitoring mode (MRM). Electrospray ionization was performed with an ionization voltage of 5500 V, declustering potential voltage of 180 V, collision energy of 42 V, and a heater probe temperature of 650°C. The catechol estrogens were detected using the following mass transitions: E3, 16-epi-E_3 and 17-epi-E_3: 522.3 to 171.0; 16-keto-E_2 and 16OH-E_1: 520.3 to 171.0; 2MeO-E_2 and 4MeO-E_2: 536.1 to 171.0; 2MeO-E_1, 3MeO-E_1 and 4MeO-E_1: 534.1 to 171.0; 2OH-E_1 and 4OH-E_1: 753.3 to 170.0; 2OH-E_2 and 4OH-E_2: 755.3 to 170.0. Quality controls were prepared in non-adsorbed serum samples to obtain low, medium or high analyte concentrations and were included in each run, along with a seven-point calibration curve prepared by spiking, as well as blanks. All catechol estrogen metabolites coefficients of variation were below 10%.

2.4. Statistical analyses

Statistics were conducted using SAS Statistical Software v.9.2 (SAS Institute, Cary, NC, USA) and SPSS Statistics v.23 (IBM Corporation, Armonk, NY, USA). Age and body mass index (BMI) between cases and controls were compared with Student's *t*-test. For analysis of nominal data, chi-square (χ^2) tests were conducted, and the Fisher's exact test was applied when required. Odds of EC were assessed using binary logistic regressions to calculate odds ratios (ORs) and 95% confidence intervals (95% CIs). Backward stepwise (likelihood ratio) was used for the selection of covariates included in the final model, in which hormone concentrations (categorized upon tertiles or the median when specified) were added. For assessment of risk of recurrence, a similar method was used, with the median level of EC cases as the category threshold. For survival and recurrence analyses, patients were also categorized as low or high risk of poor prognosis, based on histological types (T) and grade (G): TI-G1 or TI-G2 were considered at low risk, whereas TII and TI-G3 were considered at high risk [19]. Differences in steroid concentrations between groups were assessed using the analysis of covariance (ANCOVA) on log-transformed data, and untransformed data are presented to facilitate understanding. Fold changes were calculated upon the median of each group. For pairwise comparison of more than two groups, the Tukey-Kramer *post hoc* test was used. The hormone variation between paired blood samples (preoperative and postoperative samples were available for 187 cases) was analyzed using Wilcoxon signed rank test, whereas variation between groups was compared by ANCOVA on the difference of paired preoperative and postoperative levels (log-transformed). The overall survival (OS) (all-cause mortality) was estimated with the Kaplan-Meier method and tested using log-rank test, while Cox regressions were used for further adjustments using backward stepwise (likelihood ratio) for the selection of covariates. Cancer-specific survival could not be not analyzed. Because of the exploratory nature of the study and the significant interrelations between circulating steroids, two-sided *P*-values were considered statistically significant at $P<0.05$, without adjustment for multiplicity. Covariates adjustments are specified in figure and table legends.

3. Results

3.1. A cohort of 246 postmenopausal EC cases treated by hysterectomy

We studied a cohort of 246 postmenopausal EC cases prospectively recruited at a single center and all treated by hysterectomy performed for curative intent. Most cases (82%) presented with a Type I adenocarcinoma and 18% were histologically characterized by serous, clear cell, mucinous, or mixed carcinoma; combined as Type II (**Table 1**). The mean follow-up time after recruitment was 65.5 months and 26 patients experienced recurrence after surgery for a recurrence incidence of 10.6%. (6.4% Type I and 29.5% Type II). The estimated 5-year recurrence incidence was of nearly 10% (n=24 cases). Of note, the majority of Type I cases who experienced relapse (12 out of the 13) were of low-grade and particularly of grade 2 (67%), whereas for Type II, 82% recurrent cases were of grade 3. EC relapse and OS were related to a more aggressive disease (myoinvasive tumors, presence of metastatic nodes) but not BMI (**Table 2**). Only OS was associated with age (HR=1.08, 95% CI=1.04-1.12; $P<0.001$ for OS).

3.2. Estradiol metabolites are associated with recurrence and survival

In serum samples collected on the morning of surgery and one month later, we initially profiled 13 unconjugated (using gas chromatography-mass spectrometry (GC-MS)) and

conjugated (using liquid chromatography-mass spectrometry (LC-MS/MS)) steroids including adrenal precursors (DHEA, DHEA-S, 4-dione, 5-diol), androgens (testosterone, DHT, ADT, ADT-G, 3α-diol-3G, 3α-diol-17G) and parent estrogens (E_1-S, E_1, E_2) (**Fig.1**). Steroid hormones were detected above the LLOQ for all cases. None of these steroids measured prior or after surgery were associated with clinicopathological characteristics, i.e. histological type, grade, stage, lymph-vascular space invasion and metastases. Consistent with the notion that adipose tissue is a major source of estrogens in postmenopausal women; E_2 levels were 3.3-fold higher in obese EC cases (P<0.001) compared to those of normal weight **(Fig.2a).** A similar trend was observed for the other parent estrogens E_1-S and E_1. This observation is in line with the significant association between BMI and low-grade (1 and 2) endometrial tumors ($\chi^2_{df=4}$=28.9, P<0.001), mainly characterizing Type I adenocarcinomas. In contrast, for both Type I and Type II cases, circulating levels of adrenal precursors and androgens were not significantly associated with obesity, except for levels of 3□-diol glucuronide metabolites derived from the potent androgen dihydrotestosterone (DHT) (**Supplemental Table 3**).

LC-MS/MS–based analysis was also used to profile 14 catechol estrogen derivatives in preoperative and postoperative serums of EC cases. Note that only steroid concentrations accurately measured above the LLOQ of 5 pg/mL were considered as detectable. Detection rates are presented in **Table 3** and were similar in preoperative and postoperative serums. In particular, four metabolites were most abundant and detected in more than 60% of EC cases, namely E_3, 2OH-E_1, 2MeO-E_1 and 4MeO-E_2. As observed for the parent estrogens E_1 and E_2, levels of these catechol estrogens were significantly affected by BMI, except 4MeO-E_2, which remained constant across BMI categories (**Fig.2b**). In relation to clinicopathological characteristics, a significant association was only observed for E_3, which levels were 1.6-fold lower in myoinvasive tumors (≥50%) compared to less myoinvasive tumors (<50%) (21.0 vs 33.2 pg/mL, P=0.011; adjusted for age and BMI). Compared to cases with preoperative E_3 levels below median (≤30.5 pg/mL), those with higher levels (>30.5 pg/mL) were less likely to experience recurrence after surgery (Log-rank P=0.001) during the 5 years following diagnostic; an association that remained significant in the fully adjusted model for all available follow-up (HR=0.27, 95% CI=0.09-0.80; P=0.018; **Fig.3a; Supplemental Table 4**). Preoperative levels of E_3 were also linked to an improved OS, as shown by the Kaplan-Meier curves for OS within 5 years post surgery (Log-rank P=0.002; **Fig.3b**) and for all available follow-up (Log-rank P=0.021; **Supplemental Table 5**), but was not significant upon further adjustment (HR=1.15, 95% CI=0.45-2.92; P=0.766; **Supplemental Table 5**). Furthermore, levels of the abundant estrogen precursor E_1-S were associated with a higher risk of recurrence (HR=2.67, 95% CI=1.02-6.99; P=0.045; **Fig.3a**). Of note, circulating levels of E_1-S and E_3 were not significantly correlated (not shown).

One month after surgery, nearly all hormone levels were considerably reduced compared to preoperative levels (**Fig.3d; Table 4**). Hence, postoperative E_1-S and E_3 levels were not associated with recurrence in the fully adjusted model (**Fig.3a; Supplemental Table 4**). In contrast, postoperative serum levels of the anticancer metabolite 4MeO-E_2 were significantly increased compared to preoperative levels, with a mean variation of 35% and a median elevation of 6.3 pg/mL (paired data of 187 EC cases). Moreover, EC cases with higher postoperative levels of 4MeO-E_2 were less likely to experience recurrence upon adjustment for prognostic factors in multivariate analysis (HR=0.34, 95% CI=0.14-0.86; P=0.022; **Fig.3a**). Lastly, postoperative levels of the androgen inactive metabolite 3□-diol-17G were linked to an improved OS (HR=0.26, 95% CI=0.07-0.89; P=0.031), whereas preoperative levels were not (**Supplemental Table 5**).

3.3. EC cases have higher levels of circulating steroid hormones compared to healthy women

In a last series of analyses, preoperative levels of steroids in EC cases were compared to those of 110 healthy postmenopausal women (**Supplemental Tables 1-2**) [15]. After adjustment for parity, use of oral contraceptives (OC), use of hormone replacement therapy (HRT), as well as age and BMI, levels of endogenous steroids were significantly associated with increased odds of EC, for both histological types, with ORs ranging from 2.19 to 17.07 (**Fig.4**). In turns, SHBG had a protective effect for Type II (OR=0.18, 95% CI=0.04-0.80; *P*=0.024) but did not reach significance for Type I (OR=0.50, 95% CI=0.24-1.05; *P*=0.067). Obese women (BMI>30 kg/m^2) had increased odds of EC (OR=2.45, 95% CI=1.33-4.48; *P*=0.004) and particularly for Type I adenocarcinomas (OR=2.99, 95% CI=1.60-5.57; *P*<0.001) but not for Type II (OR=0.88, 95% CI=0.36-2.18; *P*=0.783) (**Fig.2c**).

4. Discussion

In this study, we profiled by MS a total of 27 steroid derivatives including adrenal precursors, androgens, parent estrogens and catechol estrogens in circulation of postmenopausal women newly diagnosed with EC undergoing hysterectomy for curative intent. Despite the exploratory nature of our study, to the best of our knowledge, this report provides one of the most comprehensive analysis of circulating steroid hormones by MS in the context of EC, and is the first to report steroid levels prior and after surgery in relation to clinicopathological characteristics, recurrence and survival.

None of the steroids measured were associated with known prognostic factors, except E_3, for which higher levels (>30.5 pg/mL) were linked to non-myoinvasive tumors, lower risk of recurrence and improved OS. This contrasts with higher levels of the most abundant estrogen precursor E_1-S (>0.31 ng/mL), which were associated with an increased risk of relapse, in line with the role of E_1-S as a predominant source of E_2 for endometrial tumor cells, and the proliferative effect of estrogens. Similar to the parent estrogens E_1 and E_2, levels of catechol estrogens varied according to BMI, except for 4MeO-E_2. In fact, this anticancer metabolite was the only steroid increased in circulation of EC cases after surgery with postoperative 4MeO-E_2 levels significantly associated with a lower risk of recurrence. Our observations require further investigations but imply that circulating levels of specific E_2 metabolites, namely E_1-S, E_3 and 4MeO-E_2, may represent independent prognostic markers of cancer recurrence after curative therapy.

Other groups reported similar levels of E_2 derivatives in circulation of endometrial, ovarian and breast cancer cases, as well as for healthy postmenopausal women [14,20-23]. In our study, preoperative levels of E_1-S and E_3 were inversely associated with recurrence, in line with their opposing biological roles and the stimulatory action of E_2 on EC cells. High levels of the most abundant circulating estrogen E_1-S were associated with poor outcome. An increased exposure to this estrogen precursor may favour E_2 synthesis and enhance stimulatory effect on tumor cells. In contrast, cases with higher levels of the E_2 metabolite, E_3, were less likely to experience recurrence. The protective role of E_3 is reinforced by its inverse relationship with myometrium invasion whereas higher E_3 level persisted as an independent marker after adjusting for well-known prognostic factors. E_3 displays modest and mixed antagonist and agonist estrogenic activities in addition to immunological effects [24-26]. Recent studies support that EC cancer, and particularly the most aggressive forms of the disease, are sufficiently immunogenic to be candidate for immunomodulation

[27]. It is thus possible that fluctuations of E_3 in this particular microenvironment might affect angiogenic profile and/or antitumor immunity.

In the analysis of E_2 derivatives in serums collected one month after surgery, we observed that postoperative levels of 4MeO-E_2 predicted risk of relapse independently of prognostic factors. In contrast to quantities of all other steroids, including levels of E_1-S and E_3 that considerably declined after surgery, those of 4MeO-E_2 increased, and EC cases with higher levels were less likely to experience recurrence. This observation could be explained by the fact that an increased methylation activity would reduce the genotoxic effects of 4-hydroxylation pathway catechols such as 4OH-E_2 through a decrease of their levels [11]. In line, less extensive methylation is associated with a higher risk of postmenopausal breast cancer whereas enhanced 2-hydroxylation is associated with a lower risk [28,29]. Furthermore, concentrations of 4MeO-E_2 were not influenced by obesity by opposition to other estrogens, suggesting that its synthesis would not predominantly originate from adipose tissue.

Compared to healthy postmenopausal women, EC cases of both histological types presented significantly higher levels of circulating steroid hormones, with concentrations similar to those reported in previous studies [21,30-33]. The increased exposure to adrenal precursors, androgens and estrogens is thus consistent with an enhanced production of steroids directly or indirectly driven by the tumor, regardless of the histological type. The role of estrogens is well delineated in EC, and most particularly in endometrioid Type I carcinomas recognized as hormonally driven [34]. One month after hysterectomy, circulating steroid levels were considerably reduced, almost reaching those of healthy postmenopausal women, supporting that a significant portion of the steroidogenic activity is driven by the presence of the primary tumor. Besides, local estrogen synthesis in EC tumors has been established to occur predominantly through conversion of E_1-S to E_2 compared to androgen aromatization by the aromatase (CYP19), which expression is barely detectable in EC tumors [7]. Adipose tissue is a primary site of aromatization after menopause, consistent with a greater concentration of potent estrogens and several of their metabolites in obese women, whom had higher odds of Type I endometrioid adenocarcinomas, in line with previous studies [35-39]. In turns, reduced SHBG levels in cancer cases may also contribute to the increased bioavailability of potent steroids [40]. EC cases diagnosed with non-endometrioid type II lesions also presented with significantly higher levels of adrenal precursors and androgens but not estrogens, suggesting an influence of the tumor on the adrenal secretion and on peripheral conversion of adrenal precursors to androgens with no subsequent impact on aromatization. This is in agreement with recent studies sustaining that androgens may play an etiological role in Type II EC, independent of their conversion to estrogens [41-43]. Furthermore, certain risk factors such as cigarette smoking and alcohol intake might influence cancer risk by altering adrenal precursors and androgen levels [44].

Our study has several strengths including long follow-up period and detailed clinicopathological parameters, and to the best of our knowledge, is the only prospective study of estrogen metabolism in the context of EC outcome. We further used fully validated sensitive and specific bioanalytical methods based on mass spectrometry to yield reliable results and portrait a vast array of steroids including precursors, potent androgens and estrogens, and their biologically active and inactive metabolites. Our study excluded cases that have taken HRT prior to surgery to avoid potential confounding effects on hormonal assays. The analytical assay for catechol estrogens was based on a method published by Xu *et al.* [18] that reported a LLOQ for each estrogen metabolite in serum of

8 pg/mL (~29 pmol/L) using 500 uL of serum for extraction. Here, we used 250 uL with a LLOQ of 5 pg/mL (~18 pmol/L). In our study, only levels of catechol estrogens quantitatively determined with suitable precision and accuracy were reported (i.e. above LLOQ). Likewise, our statistical analyses were limited to metabolites detected in most EC cases in order to avoid biases caused by potentially unreliable steroid concentrations measured above detection limit but below LLOQ, potentially corresponding to semi-quantitative or qualitative data [45]. Finally, we are not aware of other studies reporting changes in circulating steroids after curative surgery for EC cases. Limitations of our study need to be considered and include a limited number of relapse events (10%), which prevented us to apply multiple testing adjustments. Also, because of a small number of events, cancer-specific survival could not be assessed and we were unable to determine the association of hormone levels with outcomes by histologic subtypes that may vary. Furthermore, assessment of hormone levels was performed after disease onset and compared to a limited number of healthy postmenopausal women. A single hormone measurement at two different time points was performed with samples from EC cases collected the morning of the surgery and one month after. In addition, BMI has not been assessed at follow-up visit one month after surgery, preventing us from correcting for this potential confounding factor.

In conclusion, despite the exploratory nature of our study, it may help establish a non-invasive stratification of patients as high-risk and low-risk categories using preoperative and postoperative measures of circulating steroids, which could be repeated during follow-up. In addition, a better understanding of estrogen metabolism may provide insights into the mechanisms underlying EC progression. Additional larger studies are warranted to elucidate the relationships between estrogen levels, recurrence and survival of EC cases undergoing hysterectomy for curative intent.

Conflicts of interest

There is no conflict of interest that could be perceived as prejudicing the impartiality of the research reported.

Funding sources

The Cancer Research Society, the Canadian Institutes of Health Research (MOP-68964) and The Canada Research Chair Program supported this work. Y.A.-D. received a studentship from Fonds de la Recherche du Québec – Santé (FRQS). C.G. holds a Canada Research Chair in Pharmacogenomics.

Author contributions

Study design and supervision: CG

Patient's recruitment: JG, MP, PA

Sample preparation and analytics: PC, VT, LV, CG

Statistical analysis and data analysis: YAD, DS, CG

Writing of the manuscript: YAD, CG

All authors revised and accepted the manuscript.

Acknowledgments

We would like to acknowledge and thank all study participants and the efforts of research staff that made this study possible. We also thank Michèle Rouleau for helpful discussion and revision of the manuscript.

Abbreviations: DHEA: dehydroepiandrosterone; DHEA-S: DHEA-sulfate; 5-Diol: androstenediol; 4-Dione: androstenedione; DHT: dihydrotestosterone; ADT: androsterone; ADT-G: ADT-glucuronide; 3□-diol-3G: androstane-3□, 17□-diol 3-glucuronide; 3□-diol-17G: androstane-3□, 17□-diol 17-glucuronide; E_1: estrone; E_1-S: estrone-sulfate; E_2: estradiol; E3: estriol; 2OH-E_1: 2-hydroxyestrone; 2OH-E_2: 2-hydroxyestradiol; 4OH-E_1: 4-hydroxyestrone; 4OH-E_2: 4-hydroxyestradiol; 2MeO-E_1: 2-methoxyestrone; 2MeO-E_2: 2-methoxyestradiol; 4MeO-E_1: 4-methoxyestrone; 4MeO-E_2: 4-methoxyestradiol; 16OH-E1: 16α-hydroxyestrone; BMI: body mass index; LVSI: lymph-vascular space invasion; ANCOVA: analysis of covariance; 95% CI: 95% confidence interval; CYP: Cytochrome P450; SRD5A: Steroid 5α-reductase; 17□-HSD: 17□-hydroxysteroid dehydrogenase; 3□-HSD: 3□-hydroxysteroid dehydrogenase; SULT: Sulfotransferase; CYP19: aromatase; OC: oral contraceptives; HRT: hormone replacement therapy; LC: liquid chromatography; GC: gas chromatography; MS: mass spectrometry; OR: odds ratio.

5. References

1. Westin SN, Broaddus RR. Personalized therapy in endometrial cancer: challenges and opportunities. *Cancer Biol Ther* 2012;13:1-13.

2. Buhtoiarova TN, Brenner CA, Singh M. Endometrial Carcinoma: Role of Current and Emerging Biomarkers in Resolving Persistent Clinical Dilemmas. *Am J Clin Pathol* 2016;145:8-21.

3. Setiawan VW, Yang HP, Pike MC, McCann SE, Yu H, Xiang YB, Wolk A, Wentzensen N, Weiss NS, Webb PM, van den Brandt PA, van de Vijver K, Thompson PJ, Australian National Endometrial Cancer Study G, Strom BL, Spurdle AB, Soslow RA, Shu XO, Schairer C, Sacerdote C, Rohan TE, Robien K, Risch HA, Ricceri F, Rebbeck TR, Rastogi R, Prescott J, Polidoro S, Park Y, Olson SH, Moysich KB, Miller AB, McCullough ML, Matsuno RK, Magliocco AM, Lurie G, Lu L, Lissowska J, Liang X, Lacey JV, Jr., Kolonel LN, Henderson BE, Hankinson SE, Hakansson N, Goodman MT, Gaudet MM, Garcia-Closas M, Friedenreich CM, Freudenheim JL, Doherty J, De Vivo I, Courneya KS, Cook LS, Chen C, Cerhan JR, Cai H, Brinton LA, Bernstein L, Anderson KE, Anton-Culver H, Schouten LJ, Horn-Ross PL. Type I and II endometrial cancers: have they different risk factors? *J Clin Oncol* 2013;31:2607-2618.

4. Busch EL, Crous-Bou M, Prescott J, Chen MM, Downing MJ, Rosner BA, Mutter GL, De Vivo I. Endometrial Cancer Risk Factors, Hormone Receptors, and Mortality Prediction. *Cancer Epidemiol Biomarkers Prev* 2017;26:727-735.

5. Grodin JM, Siiteri PK, MacDonald PC. Source of estrogen production in postmenopausal women. *J Clin Endocrinol Metab* 1973;36:207-214.

6. Africander D, Storbeck KH. Steroid metabolism in breast cancer: Where are we and what are we missing? *Mol Cell Endocrinol* 2017.

7. Lepine J, Audet-Walsh E, Gregoire J, Tetu B, Plante M, Menard V, Ayotte P, Brisson J, Caron P, Villeneuve L, Belanger A, Guillemette C. Circulating estrogens in endometrial cancer cases and their relationship with tissular expression of key estrogen biosynthesis and metabolic pathways. *J Clin Endocrinol Metab* 2010;95:2689-2698.

8. Jeon YT, Park SY, Kim YB, Kim JW, Park NH, Kang SB, Lee HP, Song YS. Aromatase expression was not detected by immunohistochemistry in endometrial cancer. *Ann N Y Acad Sci* 2007;1095:70-75.

9. Hevir N, Sinkovec J, Rizner TL. Disturbed expression of phase I and phase II estrogen-metabolizing enzymes in endometrial cancer: lower levels of CYP1B1 and increased expression of S-COMT. *Mol Cell Endocrinol* 2011;331:158-167.

10. Sinreih M, Knific T, Anko M, Hevir N, Vouk K, Jerin A, Frkovic Grazio S, Rizner TL. The Significance of the Sulfatase Pathway for Local Estrogen Formation in Endometrial Cancer. *Front Pharmacol* 2017;8:368.

11. Cavalieri EL, Rogan EG. Depurinating estrogen-DNA adducts, generators of cancer initiation: their minimization leads to cancer prevention. *Clin Transl Med* 2016;5:12.

12. Kato S, Sadarangani A, Lange S, Villalon M, Branes J, Brosens JJ, Owen GI, Cuello M. The oestrogen metabolite 2-methoxyoestradiol alone or in combination with tumour necrosis factor-related apoptosis-inducing ligand mediates apoptosis in cancerous but not healthy cells of the human endometrium. *Endocr Relat Cancer* 2007;14:351-368.

13. Gong QF, Liu EH, Xin R, Huang X, Gao N. 2ME and 2OHE2 exhibit growth inhibitory effects and cell cycle arrest at G2/M in RL95-2 human endometrial cancer cells through activation of p53 and Chk1. *Mol Cell Biochem* 2011;352:221-230.

14. Brinton LA, Trabert B, Anderson GL, Falk RT, Felix AS, Fuhrman BJ, Gass ML, Kuller LH, Pfeiffer RM, Rohan TE, Strickler HD, Xu X, Wentzensen N. Serum Estrogens

and Estrogen Metabolites and Endometrial Cancer Risk among Postmenopausal Women. *Cancer Epidemiol Biomarkers Prev* 2016;25:1081-1089.
15. Sandanger TM, Sinotte M, Dumas P, Marchand M, Sandau CD, Pereg D, Berube S, Brisson J, Ayotte P. Plasma concentrations of selected organobromine compounds and polychlorinated biphenyls in postmenopausal women of Quebec, Canada. *Environ Health Perspect* 2007;115:1429-1434.
16. Audet-Walsh E, Lepine J, Gregoire J, Plante M, Caron P, Tetu B, Ayotte P, Brisson J, Villeneuve L, Belanger A, Guillemette C. Profiling of endogenous estrogens, their precursors, and metabolites in endometrial cancer patients: association with risk and relationship to clinical characteristics. *J Clin Endocrinol Metab* 2011;96:E330-339.
17. Caron P, Turcotte V, Guillemette C. A chromatography/tandem mass spectrometry method for the simultaneous profiling of ten endogenous steroids, including progesterone, adrenal precursors, androgens and estrogens, using low serum volume. *Steroids* 2015;104:16-24.
18. Xu X, Roman JM, Issaq HJ, Keefer LK, Veenstra TD, Ziegler RG. Quantitative measurement of endogenous estrogens and estrogen metabolites in human serum by liquid chromatography-tandem mass spectrometry. *Anal Chem* 2007;79:7813-7821.
19. Mang C, Birkenmaier A, Cathomas G, Humburg J. Endometrioid endometrial adenocarcinoma: an increase of G3 cancers? *Arch Gynecol Obstet* 2017;295:1435-1440.
20. Oh H, Coburn SB, Matthews CE, Falk RT, LeBlanc ES, Wactawski-Wende J, Sampson J, Pfeiffer RM, Brinton LA, Wentzensen N, Anderson GL, Manson JE, Chen C, Zaslavsky O, Xu X, Trabert B. Anthropometric measures and serum estrogen metabolism in postmenopausal women: the Women's Health Initiative Observational Study. *Breast Cancer Res* 2017;19:28.
21. Dallal CM, Lacey JV, Jr., Pfeiffer RM, Bauer DC, Falk RT, Buist DS, Cauley JA, Hue TF, LaCroix AZ, Tice JA, Veenstra TD, Xu X, Brinton LA, Group BaFR. Estrogen Metabolism and Risk of Postmenopausal Endometrial and Ovarian Cancer: the B approximately FIT Cohort. *Horm Cancer* 2016;7:49-64.
22. Falk RT, Brinton LA, Dorgan JF, Fuhrman BJ, Veenstra TD, Xu X, Gierach GL. Relationship of serum estrogens and estrogen metabolites to postmenopausal breast cancer risk: a nested case-control study. *Breast Cancer Res* 2013;15:R34.
23. Falk RT, Xu X, Keefer L, Veenstra TD, Ziegler RG. A liquid chromatography-mass spectrometry method for the simultaneous measurement of 15 urinary estrogens and estrogen metabolites: assay reproducibility and interindividual variability. *Cancer Epidemiol Biomarkers Prev* 2008;17:3411-3418.
24. Girgert R, Emons G, Grundker C. Inhibition of GPR30 by estriol prevents growth stimulation of triple-negative breast cancer cells by 17beta-estradiol. *BMC Cancer* 2014;14:935.
25. Lappano R, Rosano C, De Marco P, De Francesco EM, Pezzi V, Maggiolini M. Estriol acts as a GPR30 antagonist in estrogen receptor-negative breast cancer cells. *Mol Cell Endocrinol* 2010;320:162-170.
26. Melamed M, Castano E, Notides AC, Sasson S. Molecular and kinetic basis for the mixed agonist/antagonist activity of estriol. *Mol Endocrinol* 1997;11:1868-1878.
27. Gargiulo P, Della Pepa C, Berardi S, Califano D, Scala S, Buonaguro L, Ciliberto G, Brauchli P, Pignata S. Tumor genotype and immune microenvironment in POLE-ultramutated and MSI-hypermutated Endometrial Cancers: New candidates for checkpoint blockade immunotherapy? *Cancer Treat Rev* 2016;48:61-68.
28. Ziegler RG, Fuhrman BJ, Moore SC, Matthews CE. Epidemiologic studies of estrogen metabolism and breast cancer. *Steroids* 2015;99:67-75.

29. Zahid M, Saeed M, Lu F, Gaikwad N, Rogan E, Cavalieri E. Inhibition of catechol-O-methyltransferase increases estrogen-DNA adduct formation. *Free Radic Biol Med* 2007;43:1534-1540.
30. Fortner RT, Husing A, Kuhn T, Konar M, Overvad K, Tjonneland A, Hansen L, Boutron-Ruault MC, Severi G, Fournier A, Boeing H, Trichopoulou A, Benetou V, Orfanos P, Masala G, Agnoli C, Mattiello A, Tumino R, Sacerdote C, Bueno-de-Mesquita HB, Peeters PH, Weiderpass E, Gram IT, Gavrilyuk O, Quiros JR, Maria Huerta J, Ardanaz E, Larranaga N, Lujan-Barroso L, Sanchez-Cantalejo E, Butt ST, Borgquist S, Idahl A, Lundin E, Khaw KT, Allen NE, Rinaldi S, Dossus L, Gunter M, Merritt MA, Tzoulaki I, Riboli E, Kaaks R. Endometrial cancer risk prediction including serum-based biomarkers: results from the EPIC cohort. *Int J Cancer* 2017;140:1317-1323.
31. Potischman N, Hoover RN, Brinton LA, Siiteri P, Dorgan JF, Swanson CA, Berman ML, Mortel R, Twiggs LB, Barrett RJ, Wilbanks GD, Persky V, Lurain JR. Case-control study of endogenous steroid hormones and endometrial cancer. *J Natl Cancer Inst* 1996;88:1127-1135.
32. Zeleniuch-Jacquotte A, Akhmedkhanov A, Kato I, Koenig KL, Shore RE, Kim MY, Levitz M, Mittal KR, Raju U, Banerjee S, Toniolo P. Postmenopausal endogenous oestrogens and risk of endometrial cancer: results of a prospective study. *Br J Cancer* 2001;84:975-981.
33. Lukanova A, Lundin E, Micheli A, Arslan A, Ferrari P, Rinaldi S, Krogh V, Lenner P, Shore RE, Biessy C, Muti P, Riboli E, Koenig KL, Levitz M, Stattin P, Berrino F, Hallmans G, Kaaks R, Toniolo P, Zeleniuch-Jacquotte A. Circulating levels of sex steroid hormones and risk of endometrial cancer in postmenopausal women. *Int J Cancer* 2004;108:425-432.
34. Chuffa LG, Lupi-Junior LA, Costa AB, Amorim JP, Seiva FR. The role of sex hormones and steroid receptors on female reproductive cancers. *Steroids* 2017;118:93-108.
35. Dallal CM, Brinton LA, Bauer DC, Buist DS, Cauley JA, Hue TF, Lacroix A, Tice JA, Chia VM, Falk R, Pfeiffer R, Pollak M, Veenstra TD, Xu X, Lacey JV, Jr., Group BFR. Obesity-related hormones and endometrial cancer among postmenopausal women: a nested case-control study within the B~FIT cohort. *Endocr Relat Cancer* 2013;20:151-160.
36. Wake DJ, Strand M, Rask E, Westerbacka J, Livingstone DE, Soderberg S, Andrew R, Yki-Jarvinen H, Olsson T, Walker BR. Intra-adipose sex steroid metabolism and body fat distribution in idiopathic human obesity. *Clin Endocrinol (Oxf)* 2007;66:440-446.
37. Austin H, Austin JM, Jr., Partridge EE, Hatch KD, Shingleton HM. Endometrial cancer, obesity, and body fat distribution. *Cancer Res* 1991;51:568-572.
38. Ackerman GE, Smith ME, Mendelson CR, MacDonald PC, Simpson ER. Aromatization of androstenedione by human adipose tissue stromal cells in monolayer culture. *J Clin Endocrinol Metab* 1981;53:412-417.
39. Cleland WH, Mendelson CR, Simpson ER. Aromatase activity of membrane fractions of human adipose tissue stromal cells and adipocytes. *Endocrinology* 1983;113:2155-2160.
40. Hammond GL. Plasma steroid-binding proteins: primary gatekeepers of steroid hormone action. *J Endocrinol* 2016;230:R13-25.
41. Tangen IL, Onyango TB, Kopperud R, Berg A, Halle MK, Oyan AM, Werner HM, Trovik J, Kalland KH, Salvesen HB, Krakstad C. Androgen receptor as potential therapeutic target in metastatic endometrial cancer. *Oncotarget* 2016;7:49289-49298.
42. Kamal AM, Bulmer JN, DeCruze SB, Stringfellow HF, Martin-Hirsch P, Hapangama DK. Androgen receptors are acquired by healthy postmenopausal endometrial epithelium

and their subsequent loss in endometrial cancer is associated with poor survival. *Br J Cancer* 2016;114:688-696.
43. Matysiak ZE, Ochedalski T, Piastowska-Ciesielska AW. The evaluation of involvement of angiotensin II, its receptors, and androgen receptor in endometrial cancer. *Gynecol Endocrinol* 2015;31:1-6.
44. Danforth KN, Eliassen AH, Tworoger SS, Missmer SA, Barbieri RL, Rosner BA, Colditz GA, Hankinson SE. The association of plasma androgen levels with breast, ovarian and endometrial cancer risk factors among postmenopausal women. *Int J Cancer* 2010;126:199-207.
45. Tiwari G, Tiwari R. Bioanalytical method validation: An updated review. *Pharmaceutical Methods* 2010;1:25-38.

Figure 1. Schematic representation of steroid biotransformation pathways from adrenal precursors to estrogen metabolites. CYP: Cytochrome P450, SRD5A: Steroid 5α-reductase, 17β-HSD: 17β-hydroxysteroid dehydrogenase, 3α-HSD: 3α-hydroxysteroid dehydrogenase, SULT: Sulfotransferase, CYP19: aromatase; UGT: uridine diphospho-glucuronosyltransferase; G: glucuronide; S: sulfate, E: parent estrogens E_1 and E_2. E_3 may also be produced through 16-hydroxylation of E_2.

Figure 2. Estrogen levels in relation to BMI categories in postmenopausal women with endometrial cancer. Median concentrations of parent estrogens **(a)** and catechol estrogens **(b)** are presented by BMI categories for EC cases. For statistics, data were log-transformed and adjusted for age. Detection rates for all tested catechol estrogens in EC cases are available in **Table 3**. **(c)** Odds of endometrial cancer for BMI categories and histological types. Odds ratios (ORs) were calculated using multinomial logistic regression with adjustment for age. 95% CI: 95% confidence interval. * P<0.05, ** P<0.01, *** P<0.001.

Figure 3. The risk of recurrence of EC cases is associated with preoperative and postoperative steroid levels **(a)**. Hazard ratios (HR) were calculated using Cox regression for all available follow-up and comparing hormone categories separated upon median, with adjustment for age, BMI, histological type and myometrial invasion and SHBG levels. Overall survival (OS) within five years after surgery for preoperative **(b)** and postoperative **(c)** circulating E_3 levels. Similar results were obtained when analyses were performed with all available follow-ups. **(d)** Mean variation in levels of circulating steroids after surgery depicted by comparing the difference in serum levels of each woman, collected on the morning of surgery (preoperative) and one month after surgery (postoperative). * P<0.05, ** P<0.01, *** P<0.001. Analyses of recurrence for all hormones are presented in **Supplemental Table 4** and those for OS in **Supplemental Table 5**.

Figure 4. Higher circulating steroid levels are associated with endometrial cancer in postmenopausal women. Odds ratios (OR) were calculated using logistic regression comparing hormone tertiles (Q1 (reference) and Q3) or according to median (5-Diol, 3α-Diol-3G, 3α-Diol-17G), adjusted for age, BMI, parity, use of oral contraceptives and use of hormone replacement therapy. **Supplemental Table 2** displays steroid levels.

Table 1. Clinicopathological features of endometrial cancer cases treated by radical hysterectomy.

Features	Endometrial cancer cases (n = 246)	
	Mean ± SD	
Age (yr)	65.1 ± 8.9	
Weight (kg)	75.0 ± 19.0	
Height (cm)	158.4 ± 6.4	
Follow-up (months)	65.5 ± 36.7	
5-year survival (%)	90.2	
5-year recurrence rate (%)	9.8	
	n	(%)
Body mass index (BMI)[1]		
Normal Weight	70	(28)
Overweight	66	(27)
Obese	108	(44)
Missing	2	(1)
Histological Type[2]		
Type I	202	(82)
Type II	44	(18)
Grade		
1	90	(37)
2	94	(38)
3	61	(25)
Missing	1	(0)
Stage		
1	197	(80)
2	12	(5)
3	28	(11)
4	9	(4)
Myometrial invasion		
< 50 %	187	(76)
≥ 50 %	59	(24)
Lymph-vascular space invasion		
Absence	183	(74)
Presence	58	(24)
Undetermined	5	(2)
Presence of metastatic nodes		
No	220	(89)
Yes	26	(11)
Relapse after surgery[3]		
No	220	(89)
Yes	26	(11)

[1]Categories of BMI according to WHO Guidelines: normal weight: BMI<25 kg/m^2, overweight: BMI between 25 and 30 kg/m^2, and obese: BMI≥30 kg/m^2

[2]Type I only comprises endometrioid carcinomas. Included in Type II are papillary serous carcinoma, mixed carcinoma, clear cells carcinoma, undifferentiated carcinoma, and malignant mixed Müllerian tumor.

[3]Clinicopathological features of endometrial cancer cases in relation to recurrence post-surgery are presented in Table 2.

Table 2. Clinicopathological features of endometrial cancer cases in relation to recurrence after surgery for curative intent and overall survival (all-cause mortality).

	Recurrence after surgery					Overall survival				
	No recurrence		Recurrence			Alive		Deceased		
Characteristics	N=220	(%)	N=26	(%)	Log-rank *P*	N=204	(%)	N=42	(%)	Log-rank *P*
BMI										
<25	60	(27)	10	(38)	0.752	57	(28)	13	(31)	0.932
25 to 30	59	(27)	7	(27)		54	(26)	12	(29)	
>30	99	(45)	9	(35)		91	(45)	17	(40)	
Missing	2	(1)	0	(0)		2	(1)	0	(0)	
Histological type										
Type I	189	(86)	13	(50)	**<0.001**	176	(86)	26	(62)	**<0.001**
Type II	31	(14)	13	(50)		28	(14)	16	(38)	
Grade										
1	87	(40)	3	(12)	**0.015**	81	(40)	9	(21)	**0.016**
2	83	(38)	11	(42)		80	(39)	14	(33)	
3	49	(22)	12	(46)		42	(21)	19	(45)	
Missing	1	(0)	0	(0)		1	(0)	0	(0)	
FIGO stage										
1	184	(84)	13	(50)	**<0.001**	177	(87)	20	(48)	**<0.001**
2	12	(5)	0	(0)		10	(7)	2	(5)	
3	19	(9)	9	(35)		14	(5)	14	(33)	
4	5	(2)	4	(15)		3	(2)	6	(14)	
Invasion of myometrium										
< 50 %	174	(79)	13	(50)	**<0.001**	165	(81)	22	(52)	**<0.001**
≥ 50 %	46	(21)	13	(50)		39	(19)	20	(48)	
Lymph-vascular space invasion (LVSI)										
Absence	170	(77)	13	(50)	**<0.001**	162	(79)	21	(50)	**0.001**
Presence	46	(21)	12	(46)		38	(19)	20	(48)	
Undetermined	4	(2)	1	(4)		4	(2)	1	(2)	
Metastatic nodes										
No	203	(92)	17	(65)	**<0.001**	191	(94)	29	(69)	**<0.001**
Yes	17	(8)	9	(35)		13	(6)	13	(31)	
Poor prognosis[1]										
Low	167	(76)	12	(46)	**0.001**	158	(77)	21	(50)	**0.001**
High	53	(24)	14	(54)		46	(23)	21	(50)	
Overall survival[2]										
Alive	198	(90)	6	(23)	**<0.001**					
Deceased	22	(10)	20	(77)						

[1]Risk of poor prognosis is categorized as low-risk corresponding to type I (TI) with low-grade G1 and G2 whereas TI-G3 and TII are considered as high risk. [2] *P*-value is derived from a chi-square test. Significant differences are indicated in bold.

Table 3. MS-based measures of 14 catechol estrogens in preoperative and postoperative serums of endometrial cancer cases.

	Percent of detection (%) (LLOQ = 5 pg/ml)	
	Pre-hysterectomy (n=233)	Post-hysterectomy (n=198)
Catechols 2OH		
2OH-E_1	78.1	79.3
2OH-E_2	3.0	1.5
Catechols 4OH		
4OH-E_1	3.0	1.5
4OH-E_2	0.4	0.5
Catechols 16OH		
E_3	90.6	88.4
16OH-E_1	48.1	32.3
16-epi-E_3	24.1	13.6
16-keto-E_2	22.7	16.7
17-epi-E_3	5.2	4.6
Catechols MeO		
2MeO-E_1	61.8	53.0
2MeO-E_2	11.2	21.2
3MeO-E_1	7.7	7.6
4MeO-E_1	0.9	0.0
4MeO-E_2	85.8	93.9

Detection is defined as levels of estrogens above the lower limit of quantification of 5 pg/mL (LLOQ). Catechol estrogens above LLOQ in the majority of cases (shaded grey) were the focus of subsequent analyses.

Table 4. Comparison of median (10th and 90th percentile) paired pre- and post-operative serum levels of 187 endometrial cancer cases, and those of healthy postmenopausal women.

Hormones	Paired serum samples from EC cases (n=187)			Serum levels of healthy women (n = 110)	Fold change[1] (Post-operative *vs.* Healthy)
	Pre-operative	Post-operative	Median variation[2] (Post vs Pre)		
Adrenal Precursors					
DHEA-S (mg/mL)	0.64 (0.24-1.42)	0.61 (0.24-1.42)	**-0.05**[a]	0.60 (0.23-1.27)	**1.00**[b]
DHEA (ng/mL)	2.62 (0.98-7.38)	1.84 (0.82-4.97)	**-0.68**[a]	1.91 (0.85-4.24)	**0.97**[b]
5-diol (pg/mL)	336.5 (139.4-700.7)	276.4 (50.0-529.0)	**-94.0**[a]	230.0 (100.0-495.0)	**1.20**[c]
4-dione (ng/mL)	0.63 (0.36-1.36)	0.46 (0.26-0.92)	**-0.20**[a]	0.44 (0.24-0.80)	1.05
Androgens					
Testosterone (ng/mL)	0.24 (0.13-0.54)	0.13 (0.05-0.28)	**-0.11**[a]	0.14 (0.06-0.24)	0.96
DHT (pg/mL)	37.30 (17.78-80.15)	26.18 (5.00-61.63)	**-10.60**[a]	30.00 (10.00-70.00)	0.87
ADT (pg/mL)	132.3 (62.6-347.4)	97.3 (25.0-240.3)	**-34.4**[a]	n/a	---
ADT-G (ng/mL)	20.45 (6.78-44.45)	18.54 (4.98-42.59)	**-1.30**[a]	14.16 (5.45-28.17)	**1.31**[c]
3α-diol-3G (ng/mL)	0.80 (0.27-1.77)	0.70 (0.13-1.78)	**-0.02**[c]	0.57 (0.25-1.18)	**1.23**[b]
3α-diol-17G (ng/mL)	0.58 (0.13-1.65)	0.50 (0.13-1.42)	**-0.14**[a]	0.25 (0.25-1.41)	2.00
Estrogens					
E_1-S (ng/mL)	0.31 (0.04-0.99)	0.20 (0.04-0.59)	**-0.10**[a]	0.17 (0.04-0.49)	1.21
E_1 (pg/mL)	31.56 (12.84-77.11)	20.56 (5.00-49.32)	**-9.05**[a]	18.36 (10.17-35.07)	1.12
E_2 (pg/mL)	6.46 (2.25-19.90)	3.96 (1.00-11.56)	**-2.35**[a]	3.35 (1.00-9.49)	1.18
Catechol estrogens					
E_3 (pg/mL)	30.4 (5.0-114.0)	31.1 (2.5-143.6)	0.00	n/a	n/a
2OH-E_1 (pg/mL)	23.1 (2.5-77.1)	29.6 (2.5-73.1)	0.00	n/a	n/a
2MeO-E_1 (pg/mL)	7.6 (2.5-22.8)	5.7 (2.5-16.0)	**0.00**[a]	n/a	n/a
4MeO-E_2 (pg/mL)	13.6 (2.5-51.5)	21.7 (6.9-82.6)	**6.30**[a]	n/a	n/a
SHBG (nmol/L)	64.2 (30.5-123.1)	65.2 (29.6-113.9)	**-1.60**[c]	83.0 (25.9-135.1)	0.79

[1]For statistical analysis, data were log-transformed and adjusted for age and BMI. Untransformed values are shown.

[2]Variation in hormone levels between pre- and post- operative levels were established using Wilcoxon signed rank test for paired data.

n/a: not available. ADT and catechol estrogens could not be measured in healthy postmenopausal women. Significant differences are indicated in bold.

[a] $P < 0.001$; [b] $P < 0.01$; [c] $P < 0.05$.

Figures

Figure 1

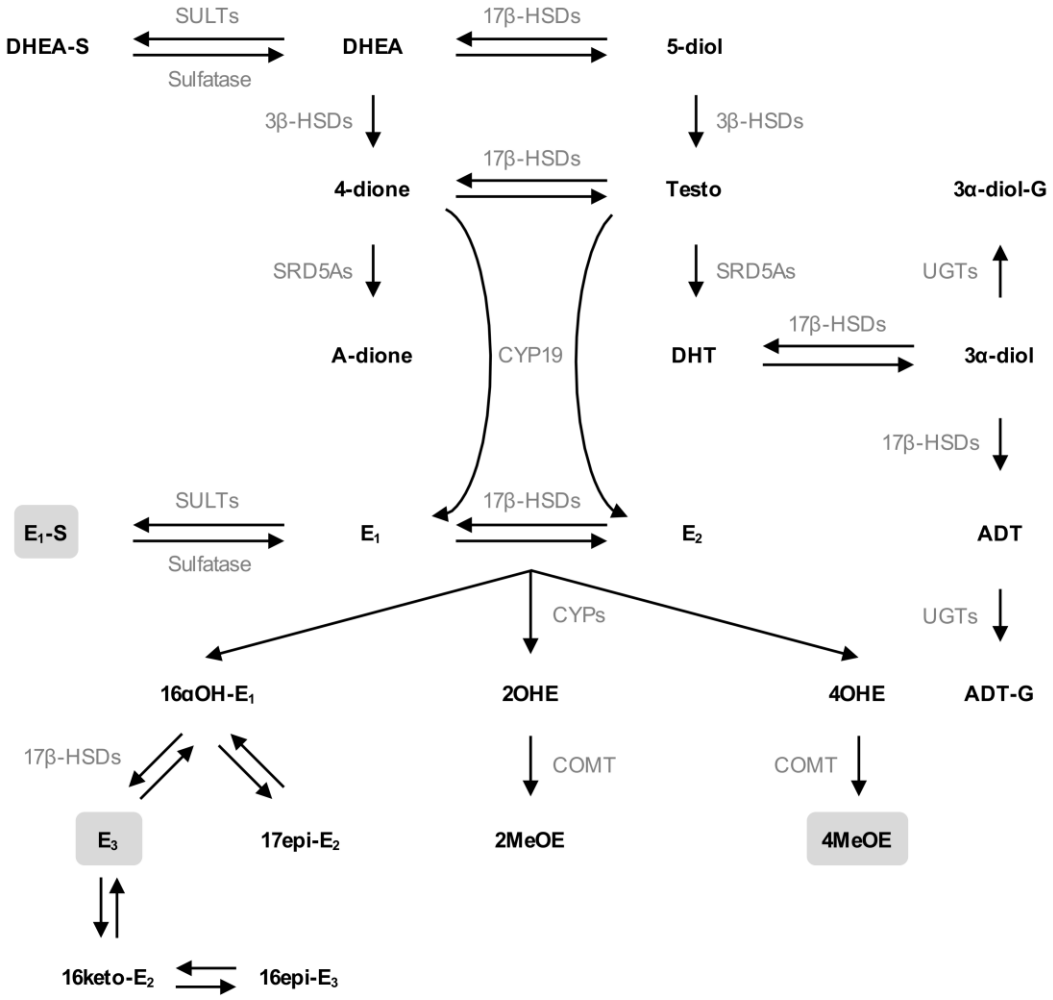

Figure 2

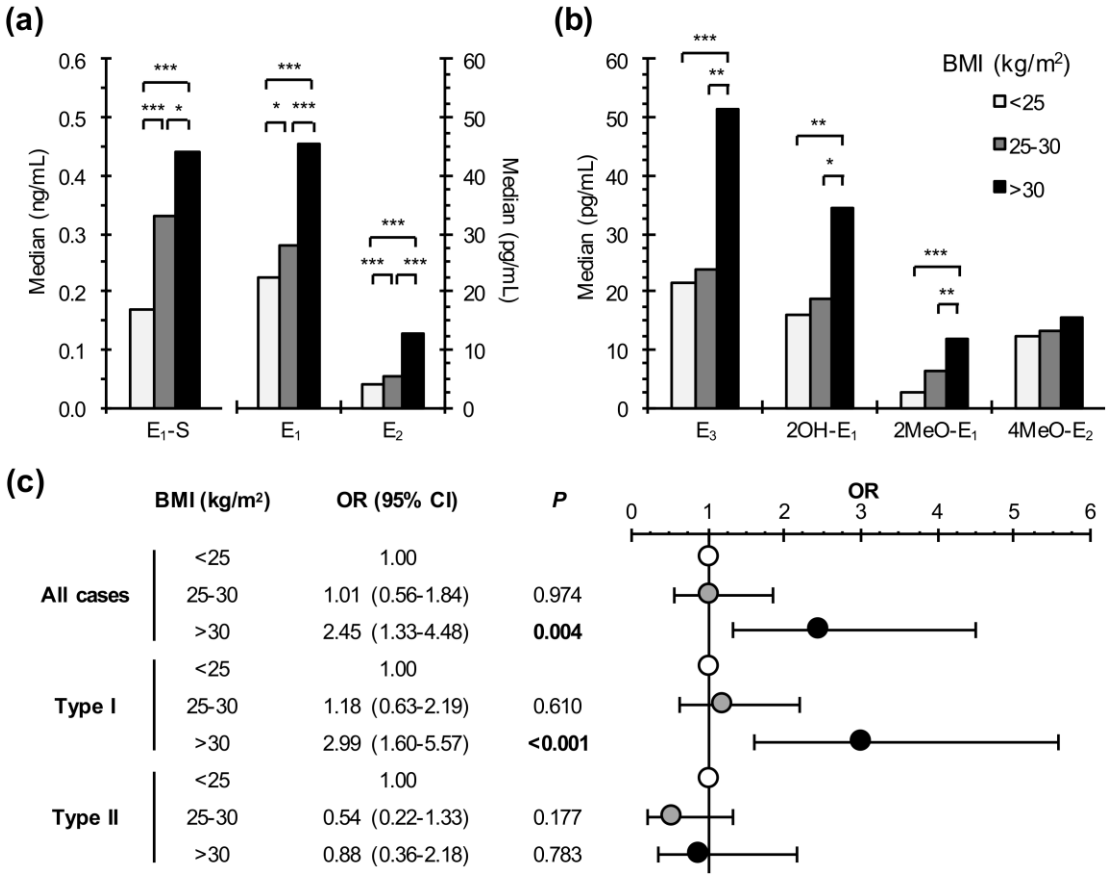
(a)
Median (ng/mL)
Median (pg/mL)
E1-S
E1
E2
(b)
BMI (kg/m2)
<25
25-30
>30
Median (pg/mL)
E3
2OH-E1
2MeO-E1
4MeO-E2
(c)
BMI (kg/m2)
OR (95% CI)
P
OR
All cases
<25 1.00
25-30 1.01 (0.56-1.84) 0.974
>30 2.45 (1.33-4.48) 0.004
Type I
<25 1.00
25-30 1.18 (0.63-2.19) 0.610
>30 2.99 (1.60-5.57) <0.001
Type II
<25 1.00
25-30 0.54 (0.22-1.33) 0.177
>30 0.88 (0.36-2.18) 0.783

Figure 3

(a) Risk of recurrence

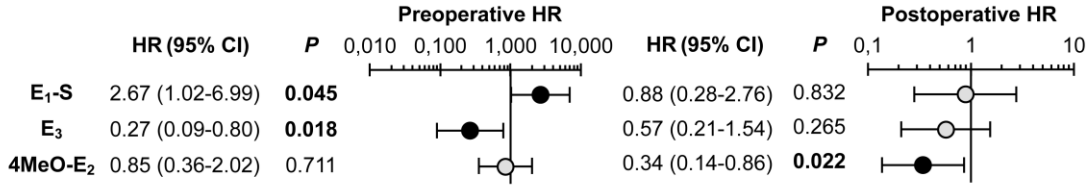

(b) Preoperative

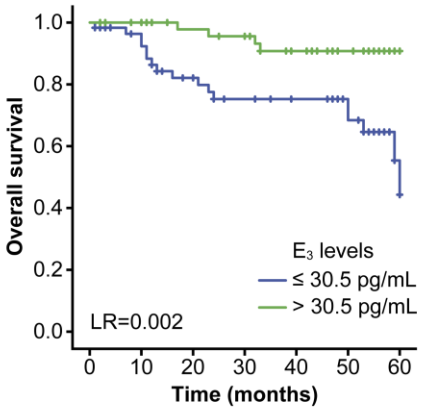

(c) Postoperative

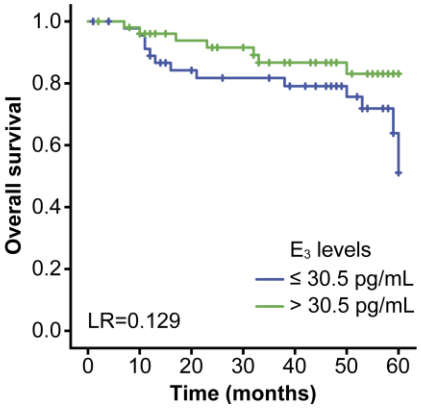

(d) Post/preoperative levels

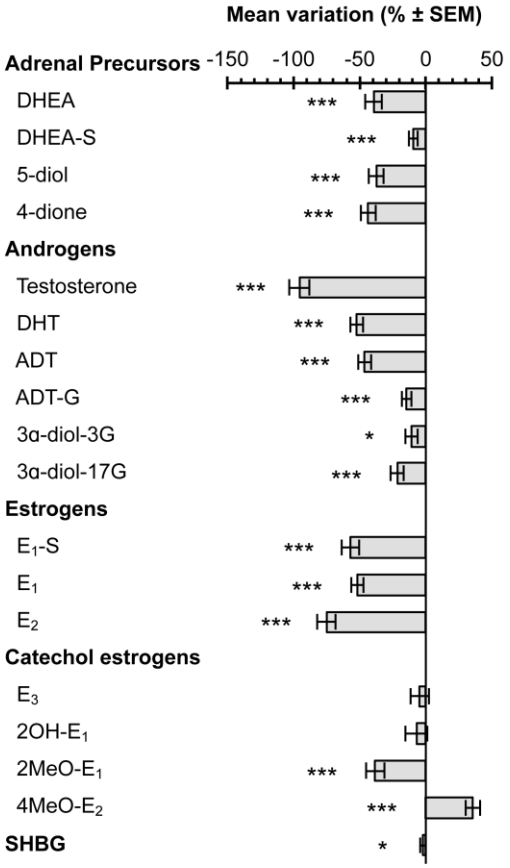

Figure 4

Hormones	Group	OR_{adj} (95% CI)	*P*
Adrenal Precursors			
DHEA	All Cases	4.13 (1.98-8.65)	**<0.001**
	Type I	4.43 (2.03-9.69)	**<0.001**
	Type II	3.17 (0.90-11.12)	*0.072*
DHEA-S	All Cases	1.76 (0.87-3.56)	0.116
	Type I	2.19 (1.03-4.62)	**0.040**
	Type II	0.86 (0.25-2.99)	0.808
5-Diol	All Cases	3.37 (1.81-6.28)	**<0.001**
	Type I	3.07 (1.60-5.88)	**<0.001**
	Type II	5.77 (1.78-18.63)	**0.003**
4-Dione	All Cases	7.37 (3.38-16.07)	**<0.001**
	Type I	9.08 (3.90-21.12)	**<0.001**
	Type II	6.82 (1.73-26.84)	**0.006**
Androgens			
Testosterone	All Cases	11.29 (4.93-25.85)	**<0.001**
	Type I	17.07 (6.52-44.72)	**<0.001**
	Type II	5.22 (1.50-18.12)	**0.009**
DHT	All Cases	6.91 (3.14-15.21)	**<0.001**
	Type I	9.21 (3.85-22.03)	**<0.001**
	Type II	4.47 (1.19-16.77)	**0.026**
ADT-G	All Cases	4.63 (2.16-9.93)	**<0.001**
	Type I	5.75 (2.52-13.10)	**<0.001**
	Type II	3.61 (1.02-12.82)	**0.047**
3α-Diol-3G	All Cases	2.43 (1.35-4.37)	**0.003**
	Type I	2.63 (1.42-4.88)	**0.002**
	Type II	2.28 (0.82-6.34)	0.113
3α-Diol-17G	All Cases	6.91 (3.48-13.71)	**<0.001**
	Type I	5.84 (2.90-11.75)	**<0.001**
	Type II	14.95 (3.47-64.30)	**<0.001**
Estrogens			
E_1-S	All Cases	1.76 (0.86-3.58)	0.119
	Type I	1.84 (0.87-3.88)	0.110
	Type II	2.00 (0.59-6.72)	0.264
E_1	All Cases	3.75 (1.77-7.98)	**<0.001**
	Type I	4.31 (1.95-9.55)	**0.000**
	Type II	4.30 (1.17-15.78)	**0.028**
E_2	All Cases	4.34 (1.87-10.07)	**<0.001**
	Type I	4.95 (2.02-12.17)	**<0.001**
	Type II	3.90 (1.00-15.15)	**0.049**
SHBG	All Cases	0.45 (0.22-0.94)	**0.032**
	Type I	0.50 (0.24-1.05)	*0.067*
	Type II	0.18 (0.04-0.80)	**0.024**

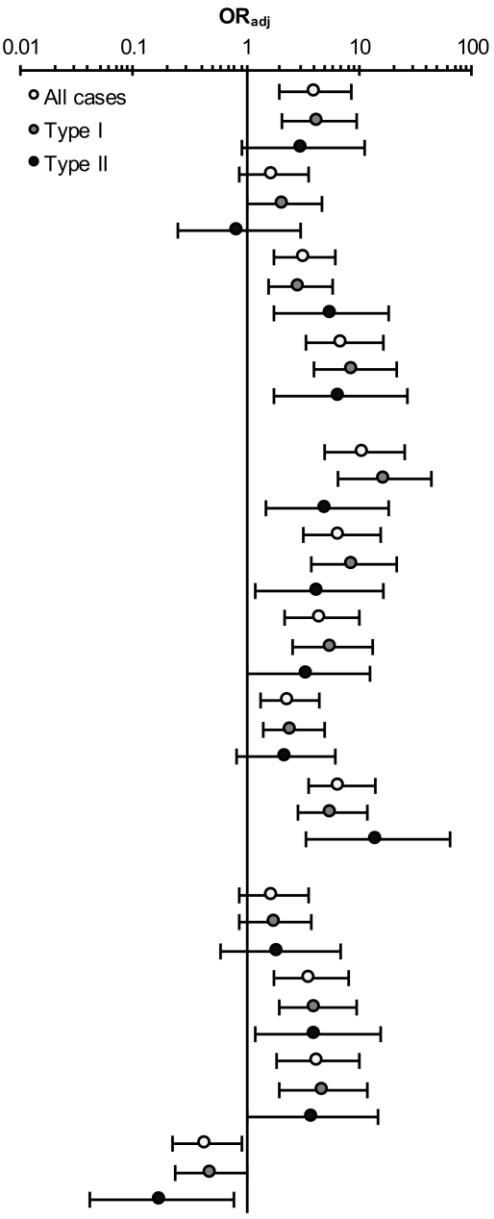

Supplemental Tables

Supplemental Table 1. Characteristics of endometrial cancer cases and healthy women.

	Postmenopausal women			
	Endometrial cancer (n = 246)		**Healthy** (n = 110)	
	Mean ± SD		Mean ± SD	
Age (year)	65.1 ± 8.9		58.3 ± 5.6**	
Weight (kg)	75.0 ± 19.0		68.8 ± 14.0*	
Height (cm)	158.4 ± 6.4		159.6 ± 5.2	
BMI (kg/m^2)	29.9 ± 7.3		27.0 ± 5.4**	
	n	(%)	n	(%)
Full term pregnancy				
Never	68	(28)	27	(25)
Ever	167	(68)	83	(75)
Missing	11	(5)	0	(0)
OC use				
No	145	(59)	19	(17)
Yes	91	(37)	91	(83)
Missing	10	(4)	0	(0)
HRT				
Never	157	(64)	40	(36)
Ever	80	(33)	70	(64)
Missing	9	(4)	0	(0)

OC: Oral Contraceptive, HRT: Hormone Replacement Therapy. **P< 0.001; *P=0.002

Supplemental Table 2. Median hormone levels (10th and 90th percentile) for healthy postmenopausal women and Type I and Type II EC cases.

Hormones	Healthy women (n = 110)	Type I EC cases (n = 202)	Fold change (TI vs Healthy)	Type II EC cases (n = 43)	Fold change (TII vs Healthy)
Adrenal Precursors					
DHEA-S (µg/mL)	0.60 (0.23-1.27)	0.63 (0.24-1.39)	1.04[b]	0.56 (0.28-1.17)	0.93
DHEA (ng/mL)	1.91 (0.85-4.24)	2.58 (1.02-7.13)	1.35[c]	2.28 (1.24-5.37)	1.20[b]
5-diol (pg/mL)	230.0 (100.0-495.0)	345.1 (144.6-734.9)	1.50[c]	322.6 (134.7-652.4)	1.40[c]
4-dione (ng/mL)	0.44 (0.24-0.80)	0.64 (0.34-1.28)	1.45[c]	0.55 (0.37-1.31)	1.25[c]
Androgens					
Testosterone (ng/mL)	0.14 (0.06-0.24)	0.24 (0.13-0.55)	1.78[c]	0.24 (0.11-0.38)	1.78[c]
DHT (pg/mL)	30.00 (10.00-70.00)	38.32 (17.90-82.18)	1.28[c]	33.19 (17.28-66.19)	1.11
ADT (pg/mL)[2]	n/a	132.3 (62.5-324.4)	n/a	99.4 (65.3-310.5)	n/a
ADT-G (ng/mL)	14.16 (5.45-28.17)	19.60 (7.36-47.90)	1.38[c]	20.50 (5.97-35.40)	1.45[a]
3α-diol-3G (ng/mL)	0.57 (0.25-1.18)	0.71 (0.27-1.68)	1.26[b]	0.83 (0.13-1.79)	1.46
3α-diol-17G (ng/mL)	0.25 (0.25-1.41)	0.60 (0.13-1.65)	2.38	0.45 (0.13-1.13)	1.81
Estrogens					
E_1-S (ng/mL)	0.17 (0.04-0.49)	0.34 (0.08-1.06)	2.03[c]	0.25 (0.04-0.51)	1.51
E_1 (pg/mL)	18.36 (10.17-35.07)	33.97 (15.02-72.78)	1.85[c]	25.89 (14.50-50.34)	1.41
E_2 (pg/mL)	3.35 (1.00-9.49)	7.16 (2.62-19.91)	2.14[c]	4.67 (1.00-9.88)	1.39
Catechol estrogens					
E_3 (pg/mL)	n/a	33.3 (5.7-114.0)	n/a	20.6 (2.5-129.1)	n/a
2OH-E_1 (pg/mL)	n/a	24.5 (2.5-78.3)	n/a	19.4 (2.5-80.6)	n/a
2MeO-E_1 (pg/mL)	n/a	8.1 (2.5-2.0)	n/a	5.9 (2.5-25.5)	n/a
4MeO-E_2 (pg/mL)	n/a	14.0 (2.5-51.7)	n/a	8.4 (2.5-53.2)	n/a
SHBG (nmol/L)	83.0 (25.9-135.1)	63.8 (31.1-123.1)	0.77	74.7 (30.8-155.0)	0.90

Fold change is calculated upon median of each group.

For statistical analysis, data were log-transformed and adjusted for age and BMI. Untransformed values are showed. No significant differences in hormone levels between histological types were detected and thus, fold changes are not shown. n/a: not available. [a] $P < 0.001$; [b] $P < 0.01$; [c] $P < 0.05$.

Supplemental Table 3. Median hormone levels (10th and 90th percentile) for endometrial cancer cases by BMI categories.

	Endometrial cancer cases			Fold Change		
Hormones	**Normal Weight BMI = 25 kg/m²** (n=66)	**Overweight BMI = 25-30 kg/m²** (n=62)	**Obese BMI > 30 kg/m²** (n=103)	Overweight vs Normal	Obese vs Normal	Obese vs Overweight
Adrenal Precursors						
DHEA-S (μg/mL)	0.74 (0.20-1.41)	0.60 (0.26-1.40)	0.61 (0.27-1.27)	0.81	0.82	1.02
DHEA (ng/mL)	2.65 (1.05-6.77)	2.37 (1.02-5.85)	2.45 (1.12-6.81)	0.89	0.92	1.03
5-diol (pg/mL)	347.0 (118.2-677.2)	328.5 (152.0-754.7)	325.8 (139.3-641.8)	0.95	0.94	0.99
4-dione (ng/mL)	0.57 (0.35-1.37)	0.65 (0.34-1.49)	0.63 (0.39-1.27)	1.14	1.11	0.97
Androgens						
Testosterone (ng/mL)	0.22 (0.10-0.51)	0.25 (0.15-0.59)	0.23 (0.13-0.48)	1.14	1.05	0.92
DHT (pg/mL)	43.98 (18.43-92.92)	38.22 (16.04-71.97)	32.88 (17.90-65.92)	0.87	0.75	0.86
ADT (pg/mL)	121.5 (63.8-348.5)	116.7 (68.4-310.5)	128.9 (57.2-268.9)	0.96	1.06	1.10
ADT-G (ng/mL)	19.55 (7.02-53.44)	18.50 (4.70-42.10)	20.60 (7.90-44.50)	0.95	1.05	1.11
3α-diol-3G (ng/mL)	0.67 (0.13-1.57)	0.56 (0.13-1.48)	0.91 (0.32-2.01)	0.84	1.36[c]	1.63[c]
3α-diol-17G (ng/mL)	0.46 (0.13-1.13)	0.46 (0.13-1.61)	0.71 (0.32-1.65)	1.00	1.54[a]	1.54[c]
Estrogens						
E_1-S (ng/mL)	0.17 (0.04-0.51)	0.33 (0.08-0.92)	0.44 (0.17-1.31)	1.94[a]	2.59[a]	1.33[c]
E_1 (pg/mL)	22.37 (5.00-41.02)	27.80 (14.50-56.43)	45.25 (20.46-83.36)	1.24[c]	2.02[a]	1.63[a]
E_2 (pg/mL)	3.94 (1.00-7.62)	5.56 (3.29-12.22)	12.79 (4.65-22.93)	1.41[a]	3.25[a]	2.30[a]
Catechol estrogens						
E_3 (pg/mL)	21.5 (2.5-84.5)	24.0 (5.2-75.9)	52.2 (10.1-131.0)	1.12	2.43[a]	2.18[b]
2OH-E_1 (pg/mL)	16.2 (2.5-51.9)	18.7 (2.5-72.8)	34.2 (2.5-93.9)	1.15	2.11[b]	1.83[c]
2MeO-E_1 (pg/mL)	2.5 (2.5-12.1)	6.5 (2.5-21.5)	11.9 (2.5-25.5)	2.60	4.76[a]	1.83[b]
4MeO-E_2 (pg/mL)	12.1 (2.5-45.1)	13.2 (5.9-51.9)	15.6 (2.5-52.3)	1.09	1.29	1.18
SHBG (nmol/L)	92.7 (45.0-155.0)	69.5 (37.0-132.1)	46.9 (28.3-105.2)	0.75	0.51[a]	0.68[b]

Fold change is calculated upon median of each group.

For statistical analysis, data were log-transformed and adjusted for age. Untransformed values are displayed. BMI: Body mass index. [a] $P < 0.001$; [b] $P < 0.01$; [c] $P < 0.05$.

Supplemental Table 4. Risk of EC recurrence estimated in relation to steroid levels.

	Preoperative serum levels					Postoperative serum levels				
Hormones	**LR *P***	**HR_{adj}**	***P***	**HR_{Fadj}**	***P***	**LR *P***	**HR_{adj}**	***P***	**HR_{Fadj}**	***P***
Adrenal precursors										
DHEA-S	0.838	1.00 (0.44-2.28)	0.997	1.01 (0.45-2.30)	0.976	0.706	1.19 (0.46-3.05)	0.720	1.29 (0.51-3.28)	0.594
DHEA	0.527	1.54 (0.66-3.59)	0.321	1.42 (0.60-3.33)	0.425	0.502	0.72 (0.27-1.96)	0.526	0.82 (0.30-2.25)	0.700
5-diol	0.830	1.17 (0.51-2.67)	0.715	1.07 (0.46-2.54)	0.869	0.544	1.05 (0.39-2.80)	0.920	1.06 (0.38-2.94)	0.915
4-dione	0.888	1.10 (0.49-2.49)	0.821	1.22 (0.53-2.77)	0.639	0.117	0.46 (0.13-1.61)	0.223	0.53 (0.15-1.83)	0.316
Androgens										
Testosterone	0.492	0.54 (0.23-1.30)	0.169	0.41 (0.16-1.05)	*0.063*	0.383	0.82 (0.18-3.69)	0.796	0.83 (0.18-3.74)	0.805
DHT	0.637	0.87 (0.38-1.99)	0.733	0.72 (0.31-1.71)	0.458	0.143	0.68 (0.18-2.60)	0.573	0.68 (0.18-2.60)	0.572
ADT	0.537	1.22 (0.74-2.02)	0.427	1.27 (0.77-2.09)	0.355	0.297	1.03 (0.61-1.73)	0.918	1.00 (0.59-1.71)	0.992
ADT-G	0.932	1.00 (0.43-2.30)	0.996	1.08 (0.46-2.49)	0.863	0.482	0.98 (0.37-2.55)	0.959	1.04 (0.40-2.67)	0.938
3α-diol-3G	0.816	1.14 (0.51-2.56)	0.756	1.08 (0.47-2.46)	0.861	*0.055*	0.46 (0.17-1.26)	0.129	0.50 (0.18-1.38)	0.184
3α-diol-17G	0.822	1.58 (0.67-3.75)	0.295	1.59 (0.68-3.74)	0.284	0.775	1.99 (0.68-5.80)	0.206	2.09 (0.73-60)	0.169
Estrogens										
E_1-S	0.260	2.37 (0.97-5.78)	*0.058*	2.67 (1.02-6.99)	**0.045**	0.286	1.00 (0.33-3.05)	0.994	0.88 (0.28-2.76)	0.832
E_1	0.163	0.91 (0.37-2.27)	0.847	0.81 (0.32-2.09)	0.669	0.856	1.44 (0.48-4.35)	0.517	1.24 (0.40-3.88)	0.708
E_2	0.308	1.29 (0.46-3.64)	0.635	1.26 (0.45-3.52)	0.654	0.241	0.98 (0.30-3.25)	0.974	0.81 (0.24-2.76)	0.735
Catechol estrogens										
E_3	**0.001**	0.29 (0.10-0.86)	**0.026**	0.27 (0.09-0.80)	**0.018**	**0.044**	0.63 (0.23-1.69)	0.357	0.57 (0.21-1.54)	0.265
2OH-E_1	0.798	1.05 (0.45-2.44)	0.912	0.98 (0.41-2.36)	0.971	0.625	1.69 (0.66-4.28)	0.272	1.62 (0.64-4.13)	0.312
2MeO-E_1	0.873	1.33 (0.57-3.13)	0.512	1.19 (0.49-2.87)	0.704	**0.040**	0.47 (0.13-1.67)	0.243	0.43 (0.12-1.55)	0.195
4MeO-E_2	0.490	0.78 (0.33-1.84)	0.574	0.85 (0.36-2.02)	0.711	**0.008**	0.32 (0.13-0.80)	**0.015**	0.34 (0.14-0.86)	**0.022**
SHBG	*0.086*	1.56 (0.64-3.83)	0.330	---		0.276	1.50 (0.55-4.08)	0.423	---	

LR *P*: Log-rank *P* from Kaplan-Meier analysis for all available diagnostic; HR_{adj}: Hazard ratio and 95% confidence interval (95% CI), calculated with Cox regression for all available follow-up and adjusted for age, BMI, histological type and myometrial invasion. HR_{Fadj}: Cox regression was calculated as above, and was further adjusted for SHBG levels. Results that are significant in either adjusted models are shaded in grey. When hazard ratio and 95% CI were calculated with a 5-year follow-up after surgery, results were similar.

Supplemental Table 5. Overall survival (OS) of EC cases in relation to steroid levels.

	Preoperative serum levels					Postoperative serum levels				
Hormones	**LR *P***	**HR_{adj}**	***P***	**HR_{Fadj}**	***P***	**LR *P***	**HR_{adj}**	***P***	**HR_{Fadj}**	***P***
Adrenal precursors										
DHEA-S	0.793	1.64 (0.73-3.68)	0.233	1.77 (0.79-3.94)	0.165	0.773	1.07 (0.42-2.75)	0.886	1.08 (0.41-2.82)	0.876
DHEA	0.400	0.84 (0.37-1.93)	0.688	0.77 (0.34-1.74)	0.530	0.272	0.56 (0.18-1.76)	0.323	0.61 (0.19-1.98)	0.408
5-diol	0.898	0.76 (0.36-1.59)	0.463	0.72 (0.33-1.58)	0.407	0.298	0.76 (0.27-2.10)	0.595	0.69 (0.24-2.00)	0.497
4-dione	0.578	0.89 (0.41-1.95)	0.772	0.77 (0.36-1.66)	0.508	0.735	1.14 (0.36-3.62)	0.821	1.06 (0.32-3.54)	0.929
Androgens										
Testosterone	0.394	0.72 (0.35-1.52)	0.393	0.72 (0.34-1.52)	0.388	0.642	0.65 (0.17-2.46)	0.523	0.47 (0.11-1.93)	0.293
DHT	0.759	0.97 (0.44-2.14)	0.946	0.95 (0.43-2.07)	0.893	0.118	0.54 (0.15-1.92)	0.339	0.43 (0.11-1.61)	0.209
ADT	0.532	1.47 (0.69-3.11)	0.316	1.08 (0.68-1.72)	0.746	0.695	0.72 (0.39-1.30)	0.273	0.73 (0.40-1.34)	0.311
ADT-G	0.744	1.30 (0.59-2.86)	0.513	1.36 (0.62-2.99)	0.447	0.302	0.66 (0.23-1.86)	0.429	0.71 (0.25-1.99)	0.511
3α-diol-3G	0.325	1.53 (0.73-3.19)	0.259	1.56 (0.75-3.24)	0.231	0.019	0.39 (0.14-1.11)	*0.079*	0.37 (0.13-1.06)	*0.065*
3α-diol-17G	0.583	1.03 (0.43-2.45)	0.949	1.09 (0.46-2.56)	0.845	0.147	0.25 (0.08-0.84)	**0.025**	0.26 (0.07-0.89)	**0.031**
Estrogens										
E_1-S	0.516	1.04 (0.45-2.38)	0.929	1.01 (0.43-2.36)	0.980	0.601	1.33 (0.48-3.66)	0.587	1.39 (0.51-3.78)	0.514
E_1	*0.098*	1.34 (0.56-3.24)	0.512	1.27 (0.53-3.03)	0.586	0.621	1.15 (0.38-3.49)	0.803	1.02 (0.33-3.21)	0.968
E_2	0.345	1.55 (0.59-4.05)	0.371	1.49 (0.57-3.91)	0.414	0.637	1.91 (0.53-6.91)	0.321	1.60 (0.43-5.93)	0.483
Catechol estrogens										
E_3	**0.021**	1.12 (0.43-2.91)	0.821	1.15 (0.45-2.92)	0.766	0.402	0.92 (0.36-2.34)	0.865	0.74 (0.27-2.03)	0.561
2OH-E_1	0.500	1.80 (0.82-3.96)	0.144	1.82 (0.84-3.93)	0.130	0.416	0.83 (0.32-2.17)	0.711	0.98 (0.36-2.66)	0.971
2MeO-E_1	0.303	1.52 (0.67-3.45)	0.321	1.53 (0.66-3.57)	0.326	0.445	0.65 (0.23-1.87)	0.428	0.51 (0.18-1.46)	0.207
4MeO-E_2	0.334	1.15 (0.51-2.57)	0.737	1.30 (0.58-2.92)	0.530	0.028	0.76 (0.28-2.10)	0.599	0.84 (0.30-2.33)	0.738
SHBG	0.331	0.85 (0.51-1.42)	0.540	---		0.144	1.05 (0.37-2.96)	0.932	---	

All-cause mortality. LR *P*: Log-rank *P* from Kaplan-Meier analysis for all available follow-up; HR_{adj}: Hazard ratio and 95% confidence interval (95% CI), calculated with Cox regression for all available follow-up and adjusted for age, BMI, low/high risk categories, metastases, lymph-vascular space invasion (LVSI) and recurrence; Low/High risk: TI-G1/G2 are categorized as low risk, while TI-G3 and TII are high risk. HR_{Fadj}: Cox regression was calculated as above, and was further adjusted for SHBG levels. Results that are significant in either adjusted models are shaded in grey. When hazard ratio and 95% CI were calculated with a 5-year follow-up after surgery, results were similar.

Annexe 2 : « Identification of metabolomic biomarkers for endometrial cancer and its recurrence after surgery in postmenopausal women ».

Résumé

Le cancer de l'endomètre (CE) est le cancer gynécologique le plus fréquent dans les pays développés. La plupart des CE surviennent après la ménopause et sont diagnostiqués comme étant des carcinomes endométrioïdes (type I), ayant un pronostic favorable. En revanche, les carcinomes non-endométrioïdes (type II), telles que les tumeurs séreuses, ont un mauvais pronostic. Notre but visait à identifier de nouveaux biomarqueurs sanguins associés avec les sous-types de CE et la récidive après chirurgie chez les femmes postménopausées. Par une approche métabolomique non-dirigée, nous avons examiné le sérum préopératoire de femmes en santé (n=18) et de femmes ayant récidivé (R) ou non (NR) et présentant un CE endométrioïde de type I (n=24) ou un CE séreux de type II (n=12). Les cas R et NR étaient similaires quant à leurs caractéristiques pathologiques, leur indice de masse corporelle et leur âge. Nous avons analysé un total de 1592 métabolites, incluant 14 classes de lipides différentes. Les cas de CE montrent une différence dans les niveaux de 137 métabolites lorsque comparés aux contrôles. Une combinaison des niveaux de spermine et d'isovalérate résulte en une aire sous la courbe ROC corrigée pour l'âge ($AUC_{ajustée}$) de 0.914 ($P < 0.001$) pour la détection du CE. La combinaison du 2-oléoylglycérol et du TAG42:2-FA12:0 permet quant à elle de distinguer les cas R des cas NR avec une $AUC_{ajustée}$ de 0.901 ($P < 0.001$). Les cas R de type I sont caractérisés par des niveaux faibles d'acides biliaires et des niveaux élevés du peptide phosphorylé du fibrinogène clivé, tandis que les cas R de type II montrent des niveaux élevés de céramides. Cette étude pilote constitue une première étude détaillée du métabolome du CE et identifie plusieurs biomarqueurs putatifs pouvant servir à définir des groupes cliniques basés sur le risque de progression.

Identification of metabolomic biomarkers for endometrial cancer and its recurrence after surgery in postmenopausal women

Yannick Audet-Delage[1], Lyne Villeneuve[1], Jean Grégoire[2], Marie Plante[2] and Chantal Guillemette[1,3]*

[1]Centre Hospitalier Universitaire (CHU) de Québec Research Center and Faculty of Pharmacy, Laval University, Québec, Canada.

[2]Gynecologic Oncology Service, CHU de Québec, and Department of Obstetrics, Gynecology, and Reproduction, Faculty of Medicine, Laval University, Québec, Canada.

[3]Canada Research Chair in Pharmacogenomics

*Correspondence: CHU de Québec Research Center, R4701.5, 2705 Blvd. Laurier, Québec, QC, Canada, G1V 4G2. Tel: 1-418-654-2296 Email: chantal.guillemette@crchudequebec.ulaval.ca

Running title: Metabolomic biomarkers of endometrial cancer

Word count: 4347

Number of tables: 4

Number of figures: 3

Abstract

Endometrial cancer (EC) is the most frequent gynecological cancer in developed countries. Most EC occurs after menopause and is diagnosed as endometrioid (type I) carcinomas, which exhibit a favorable prognosis. In contrast, non-endometrioid (type II) carcinomas such as serous tumors have a poor prognosis. Our goal was to identify novel blood-based markers associated with EC subtypes and recurrence after surgery in postmenopausal women. Using mass spectrometry–based untargeted metabolomics, we examined preoperative serum metabolites among control women (n = 18) and those with non-recurrent (NR) and recurrent (R) cases of type I endometrioid (n = 24) and type II serous (n = 12) carcinomas. R and NR cases were similar with respect to pathological characteristics, body mass index and age. A total of 1592 compounds were analyzed including 14 different lipid classes. When we compared EC cases with controls, 137 metabolites were significantly different. A combination of spermine and isovalerate resulted in an age-adjusted area under the receiver-operating characteristic curve (AUC_{adj}) of 0.914 ($P < 0.001$) for EC detection. The combination of 2-oleoylglycerol and TAG42:2-FA12:0 allowed the distinction of R cases from NR cases with an AUC_{adj} of 0.901 ($P < 0.001$). Type I R cases were also characterized by much lower levels of bile acids and elevated concentrations of phosphorylated fibrinogen cleavage peptide, whereas type II R cases displayed higher levels of ceramides. The findings from our pilot study provide a detailed metabolomics study of EC and identify putative serum biomarkers for defining clinically relevant risk groups.

Keywords: Metabolomics, Endometrial cancer, Blood-based biomarkers, Recurrence, Mass spectrometry.

1. Introduction

Endometrial cancer (EC) is the sole gynecological neoplasm with a rising incidence and mortality and is currently the most common gynecological cancer in the United States, Canada and other developed countries (Westin and Broaddus, 2012). Occurring predominantly in postmenopausal women, EC is initially treated by surgery including total hysterectomy, bilateral salpingo-oophorectomy and lymph node evaluation. Despite successful surgery, 10–15% of tumors recur within 5 years with poor treatment outcomes and low survival rates (Buhtoiarova et al., 2016).

Predictive and prognostic factors of EC include histological subtype with high-risk features such as high tumor grade, stage and deep myometrial invasion (Sorbe, 2012). Endometrioid type I carcinomas and especially those of low grade exhibit a favorable prognosis and may be cured by primary surgery (Han et al., 2017). Type II carcinomas include non-endometrioid histologies better represented by the prototypical serous carcinoma and account for ~10% of EC. Type II neoplasms represent higher-grade tumors with a more aggressive clinical course, for which recurrence is more frequent and treatment remains a challenge (Mang et al., 2017). Candidate diagnostic biomarkers such as CA125 and HE4 have been identified; however, their low sensitivity and/or specificity limit their use in the clinic (Rizner, 2016; Knific et al., 2017). ECs are strongly associated with cumulative estrogen exposure, obesity and other characteristics of metabolic syndrome (Audet-Walsh et al., 2011; Dallal et al., 2013; Brinton et al., 2016; Dallal et al., 2016; Busch et al., 2017). This does not apply only to type I carcinomas, as type II tumors can also be associated with hormonal, reproductive and metabolic factors (Audet-Walsh et al., 2011). Based on the recognition of the biologic and prognostic differences between pathogenetic types of EC and given the poor prognosis for recurrent disease, it is critical to develop novel biomarkers.

Metabolomics is defined as the comprehensive analysis of metabolites in a biological specimen and includes a more focused form of metabolomics that surveys lipids (referred to as lipidomics). This approach is becoming a very powerful tool for biomarker discovery and has proven itself useful in the study of many metabolic diseases including cancer. For instance, discoveries related to oncometabolites have highlighted the possibility of unsuspected cellular pathways whose components could serve as diagnostic or prognostic biomarkers or may be therapeutically targeted for disease treatment (Wishart, 2016). Still, very few studies have used metabolomics in the context of EC (**Table 1**). In contrast, more than 30 global and targeted mass spectrometry (MS)-based metabolomics studies have been conducted for ovarian cancer and have identified dysregulated metabolic pathways that underlie several histological types of carcinoma (Turkoglu et al., 2016). These discoveries have led to the identification of potential new therapeutic targets and biomarkers that might improve diagnosis and prognostication (Yin et al., 2016; Zhang et al., 2016; Bachmayr-Heyda et al., 2017; Xie et al., 2017).

In the present study, our goal was to identify non-invasive biomarkers of EC cancer and recurrence in postmenopausal women using global metabolomics and lipidomics profiling. We examined preoperative serum metabolites in control women as well as those from women with endometrial cancer of both histological types; these individuals were from a prospective study of women who underwent hysterectomy and were recruited from a single center. We used validated metabolomics platforms capable of identifying and quantifying multiple biochemical species simultaneously across all major metabolite classes as well as complex lipids including phospholipid, sphingolipid and neutral lipid classes. In the first series of analyses, we identified putative EC biomarkers by comparing EC cases to control

women. Then, we compared type I and type II EC cases to find biomarkers associated with histological type. In the third set of analyses, we compared matched recurrent (R) and non-recurrent (NR) cases of both histological type I and type II to detect recurrence biomarkers of EC. Finally, to identify putative biomarkers that would be specific to either type I or type II carcinomas, we compared matched R and NR cases of individual histological type.

2. Materials and Methods

2.1. Study population

All participants provided written informed consent for their participation in the study and for the use of their specimens. The current study was evaluated and approved by the local Ethical Research Committee of the Centre Hospitalier Universitaire (CHU) de Québec - Université Laval (2012-993) and was conducted in accordance with the Declaration of Helsinki. The recruitment and specimen collection have been described (Audet-Walsh et al., 2011). Briefly, participants were all recruited at the Hôtel-Dieu de Québec Hospital (Québec City, Canada), between 2002 and 2014. All women were of postmenopausal status and underwent surgery (hysterectomy and bilateral salpingo-oophorectomy), either for EC treatment or for non-malignant conditions (n = 9 for benign pelvic mass, n = 3 for prophylactic treatment, n = 3 for pre-cancerous cervical lesion, n = 2 for fibroma, n = 1 for uterine prolapse). Fasting blood samples were collected on the morning of surgery and were rapidly processed and stored at –80°C until analysis. To be eligible, women must not have developed prior malignancies nor taken hormone replacement therapy during the 3 weeks preceding specimen collection. EC recurrence was ascertained by computerized tomography scan and further confirmed by histopathology when required. Nurses collected information regarding demographic and anthropometric data through standardized questionnaires. A pathologist assessed the histopathological characteristics of the hysterectomy specimens for women with EC. Systematic compilation and review of medical records were performed by one of the treating gynecologic oncologists (J.G.), for both cases and controls.

R EC cases consisted of endometrioid (n = 12) or serous carcinoma (n = 6). To reduce potential confounding factors, NR EC cases were matched to R cases according to i) histological type, ii) grade, iii) a body mass index (BMI) within an interval of 5 $kg \cdot m^{-2}$ and iv) age. In addition, v) myometrial invasion was also considered for the matching of R and NR type I cases. We achieved a perfect match for the first two criteria for both histological types, as well as myometrial invasion for type I carcinomas. The median difference in BMI was 2.0 $kg \cdot m^{-2}$. For two pairs of matched cases, the differences in BMI were of 7.2 and 11.2 $kg \cdot m^{-2}$ (**Supplemental Table 1**). The median difference in age was 7 years. Control women were not matched to EC cases.

2.2. Metabolomics

Blood sample aliquots were analyzed for metabolites and lipids with the metabolomics platform at Metabolon Inc. (Durham, NC, USA). Global profiling was conducted as described (Shajahan-Haq et al., 2017). Briefly, samples were prepared using the automated MicroLab STAR system (Hamilton Company, Reno, NV). A recovery standard was added prior to the first step in the extraction process for quality control purposes. Metabolites were extracted by vigorous agitation after precipitation of proteins with methanol. Samples were then split to enable analysis by different methods, utilizing a Waters ACQUITY ultra-performance liquid chromatography (UPLC) system coupled to a Thermo Scientific Q-Exactive high-

resolution accurate-mass spectrometer equipped with a heated electrospray ionization (HESI-II) source and an Orbitrap mass analyzer. Raw data extraction, peak identification and quality control processing were carried out using the Metabolon proprietary hardware and software. Compound identification was done through comparison with a library of chromatographic and MS data from authenticated standards.

Complex lipid profiling was conducted according to a modified version of a previously described protocol (Lofgren et al., 2012). Briefly, lipids were extracted from blood samples by a heptane/ethyl acetate mixture after addition of a butanol/methanol solution. Phase separation was induced by addition of aqueous acetic acid and centrifugation. MS analysis was conducted on a Shimadzu LC with nano PEEK tubing coupled to a Sciex SelexIon-5500 QTRAP. The scan was performed in multiple reaction monitoring (MRM) mode. Peaks were quantified using the area-under-the-curve (AUC) method, and data were normalized for inter-day signal differences. The analytical variability was $\leq$10% for both global profiling and lipidomics.

2.3. Statistical analyses

The similarity between groups (EC cases *vs.* controls, R *vs.* NR cases) was assessed by Student's two-sample *t*-test for continuous variables, with correction for variance unequality when required (Welch's two-sample *t*-test). Chi-square tests were used for categorical data or Fisher's exact test when appropriate. Metabolomics data were log-transformed prior to statistical comparisons, and fold changes were calculated based on the geometric mean. The Welch's two-sample *t*-test was conducted for all comparisons, as it offers a slightly better statistical precision than paired sample analysis, which could have been used for the comparison of R to NR cases (Pearce, 2016). Pathway enrichment analyses were performed with Metabolon online tools and using their proprietary database. The enrichment score was calculated by dividing the ratio of statistically significant metabolites within a pathway by the overall proportion of statistically significant metabolites.

Predicted probabilities, calculated with logistic regression, were used to build univariate and multivariate receiver operating characteristic (ROC) curves for EC and recurrence detection. Univariate regression models were made for each of the top four altered metabolites, and multivariate models were adjusted for age. BMI did not significantly contribute to the models ($P > 0.80$). Multivariate models were then optimized to give the best AUC with a maximum of four metabolites. The size of our group allowed the detection ($\alpha = 0.05$, $1 - \beta = 0.80$) of an AUC > 0.700 for EC detection, and an AUC > 0.730 for recurrence (Obuchowski, 2005). Finally, because of the exploratory nature of the study, as well as the number of metabolites tested (n = 1592), statistical adjustment for multiple tests was not performed.

3. Results

3.1. Markers of EC (comparison of all EC cases relative to controls)

We examined pre-operative serum metabolites from control women (n = 18) and from women with NR (n = 18) or R (n = 18) cases of either type I (n = 12 R and n = 12 NR) or type II (n = 6 R and n = 6 NR) carcinomas. To reduce biases that may be caused by menstrual cycling, all of the women were postmenopausal, and none of them had used hormone replacement therapy in the 3 weeks preceding specimen collection. All individuals were selected from a larger cohort recruited at a single center (Audet-Walsh et al., 2011), and pairing of NR cases with R cases was based on pathological (histological type, grade

and myometrial invasion) and clinical (BMI and age) characteristics (**Table 2, Supplemental Table 1**). A total of 1592 compounds of known identity across all major metabolite classes and 14 different lipid classes were assessed by UPLC–tandem MS using global profiling and lipidomics.

When comparing EC cases to control women, 137 metabolites were significantly altered (115 up and 22 down, $P < 0.05$; **Supplemental Figure 1**). Pathway enrichment analysis identified lipid- and glycolysis-related pathways as the most affected in EC cases (**Fig. 1A**). Conjugated forms of lipids, such as acylcholines, monoacylglycerols and acylcarnitines, were generally higher in EC cases as compared with control women, whereas free fatty acids were detected at lower concentrations, supporting a remodeling of fatty acid metabolism in EC (**Fig. 1B**). Of note, the C5 acylcarnitine 2-methylbutyrylcarnitine was also elevated in EC cases (fold change [FC] = 1.27, $P = 0.023$). Five of the top ten most altered features in EC cases were peptides and amino acids (**Table 3**), with spermine (FC = 7.66, $P = 0.0004$) and isovalerate (FC = –2.56, $P = 0.015$) as the most changed metabolites in cancer cases.

To further assess our ability to distinguish EC cases from controls based on these metabolites, we constructed receiver-operating characteristic (ROC) curves based on univariate and multivariate logistic regression models. The combination of spermine and isovalerate resulted in an area under the ROC curve (AUC) of 0.875 (95% confidence interval [CI] = 0.784–0.966), and an age-adjusted AUC (AUC_{adj}) of 0.914 (95% CI = 0.833–0.994), very similar to a more complete model that included spermine, isovalerate, glycylvaline and gamma-glutamyl-2-aminobutyrate and resulted in an AUC_{adj} of 0.921 (95% CI = 0.843–1.000) (**Fig. 1C**). These results support the capacity of these metabolites to discriminate EC cases from controls.

3.2. Markers associated with histological types (comparison of type I and type II EC cases)

A total of 98 metabolites significantly distinguished type I from type II ECs (n = 30 higher in type I, n = 68 lower in type I, $P < 0.05$). The most different metabolites between histotypes were bradykinin, with higher levels in type I (FC = 2.70, $P = 0.003$), and heme, which was 4.52-fold higher in type II ECs ($P = 0.030$) (**Table 3**). Levels of saturated long chain acylcarnitines were higher in type II, with C20, C24 and C26 acylcarnitines displaying FCs of 1.32 ($P = 0.021$), 1.33 ($P = 0.027$) and 1.38 ($P = 0.005$), respectively.

Levels of choline were higher (FC = 1.27, $P = 0.010$) in type II ECs, along with sarcosine (FC = 1.42, $P = 0.023$), which are both metabolites of the tetrahydrofolate-serine/glycine pathway. Glycine levels tended to be elevated in type II ECs as well (FC = 1.23, $P = 0.075$). Levels of sulfated androgenic steroids differed significantly between the two histotypes, with type I EC having higher levels than type II for 10 out of the 18 androgenic compounds assessed by the method.

3.3. Markers of EC recurrence (comparison of R and NR cases of both histological types)

R cases were characterized by an altered lipid metabolism relative to NR cases. Among the 104 metabolites modulated, 80 represented lipid metabolism (68/75 up and 12/29 down; $P < 0.05$). Pathway enrichment analysis (**Fig. 2A**) identified many classes of lipids affected in

R cases, such as monoacylglycerols, for which 16:1, 18:1, 20:5 and 22:6 species of both alpha and beta isomers were significantly elevated (**Fig. 2B, Table 4**).

In addition to modifications in lipid levels, other classes of compounds displayed significant alterations in R cases when compared with NR cases. For example, the pathway of glycine, serine and threonine metabolism was affected, as both serine and threonine levels were lower in R cases, whereas the glycine precursor *N*-acetylglycine was elevated (**Fig. 2C**). Even though higher levels of *N*-acetylglycine were observed, glycine was not affected, suggesting a rerouting of glycine metabolism intermediates in R cases.

Some metabolites had a similar association with recurrence in both type I and type II EC patients. This was the case of the monoacylglycerol 1-oleoylglycerol (18:1), the only metabolite observed among the top modulated metabolites for both histological types (**Table 4**), which displayed a FC of 3.77 (P = 0.045) and 2.29 (P = 0.018) for type I and type II, respectively. A similar observation was noted for other lipid metabolites, namely the acylcarnitine docosahexaenoyl carnitine (C22:6) (FC = 1.51 and 1.46 for type I and type II, respectively; $P < 0.05$) and the monohydroxylated fatty acids 2-hydroxypalmitate (2-OH-C16:0, FC = 1.47 and 1.57 for type I and type II; $P < 0.05$) and 2-hydroxystearate (2-OH-C18:0, FC = 1.30 and 1.56 for type I and type II; $P < 0.05$), suggesting a remodelling of lipid metabolism among R cases of both histological types when compared with NR cases. In addition, these four metabolites were not significantly different when comparing EC cases and control women (data not shown), suggesting their relevance as biomarkers of recurrence, independently of the histological type.

ROC curves identified 2-oleoylglycerol and TAG42:2-FA12:0 as the most effective metabolites to discriminate R cases from NR cases, with an AUC = 0.877 (95% CI = 0.730–0.990) and an AUC_{adj} = 0.901 (95% CI = 0.796–1.000). These results are similar to the model including more metabolites, namely 1-oleoylglycerol, 2-oleoylglycerol, TAG40:0-FA12:0 and TAG42:2-FA12:0, which displayed an AUC_{adj} = 0.904 (95% CI = 0.807–1.000; **Fig. 2D**), confirming the ability of these metabolites to predict recurrence.

3.4. Markers associated with recurrence according to histological types (comparison of R and NR cases according to histological type)

Several metabolites were specifically associated with recurrence in type I endometrioid or type II serous cases. For instance, modifications in bile acid metabolism were mainly observed in type I R cases, which had lower levels of primary and secondary bile acid metabolites such as taurodeoxycholate (FC = –7.14, P = 0.009), glycodeoxycholate (FC = –4.55, P = 0.009) and taurocholate (FC = –3.85, P = 0.038; **Fig. 3A, Table 4**). Type I recurrent cases were also characterized by an enrichment in circulating levels of phosphorylated fibrinogen cleavage peptide ADpSGEGDFXAEGGGVR (FC = 1.68, P = 0.014; **Fig. 3B, Table 4**); an association not found for type II R cases (P = 0.477).

In contrast, multiple classes of sphingolipids were significantly enriched in type II R cases, including ceramides, their precursors dihydroceramides and their glycosylated derivatives lactosylceramides. Though the variations were modest with FCs between 1.29 and 1.60 for significant metabolites, numerous metabolites of this pathway were similarly altered, underscoring the potential significance of these variations (**Fig. 3C**). None of the ceramides were significantly different in type I R cases, suggesting that alterations in these pathways could be specific to type II R cases.

4. Discussion

In this study, we profiled 1592 compounds in 54 postmenopausal women. To the best of our knowledge, this is the first study reporting metabolites associated with type I and type II EC carcinomas and their recurrence following initial surgical treatment. Our findings represent an important pilot study in the identification of putative serum biomarkers useful for detecting EC and predicting recurrence following initial surgery, to ultimately improve patient survival based on better stratification and informed treatment decisions.

We found that the levels of free fatty acids linoleic acid (C18:2) and myristic acid (C14:0) were lower in EC cases as compared with control women, consistent with previous reports comparing EC cases and controls (Gaudet et al., 2012; Troisi et al., 2018). Gaudet et al. (2012) also observed modifications in intermediates from the branched chain amino acid pathway, such as isovalerylcarnitine*/*2-methylbutyrylcarnitine (undistinguishable by the MS method), which were also altered in our set of EC cases compared with controls. Other comparisons between the two studies could not be extended, as their panel of metabolites was targeted to 69 compounds. In our dataset, additional metabolites related to amino acids were affected in EC cases, such as polyamines, which are involved in cancer progression, including endocrine-related neoplasms like breast cancer (Soda, 2011). Accordingly, the most elevated metabolite between EC cases and controls was spermine, a biomarker of EC possibly originating from EC cells. This is conceivable as polyamine synthesis and degradation are actively regulated in the endometrium, notably during the menstrual cycle and pregnancy (Green et al., 1998; Pistilli et al., 2012; Tajima et al., 2012).

Lipids were also considerably affected in EC cases when compared with controls, with lower serum concentrations of free fatty acids but higher levels of conjugated fatty acids such as acylcholines, acylcarnitines and monoacylglycerols. This is consistent with a report from Bahado-Singh et al. (2017). They observed higher acylcholine levels in EC patients. However, very little is known about these lipids (no entries were found in either the Human Metabolome Database (HMDB) or Kyoto Encyclopedia of Genes and Genomes (KEGG) database; accessed on December 15, 2017), although some acylcholines, including palmitoylcholine, stearoylcholine and oleoylcholine, enhance estradiol penetration through tissues (Loftsson et al., 1989). This could be important in the context of a hormone-sensitive cancer, potentially favoring the estrogenic activity of estradiol in the tumor. In addition, acylcarnitines have been linked to EC, as well as to breast cancer, where they are enriched in hypoxic tissues (Gaudet et al., 2012; Chughtai et al., 2013). Acylcarnitines are synthesized by cells to fuel mitochondrial fatty acid oxidation. However, the mechanisms by which they are found in circulation remains unclear, although their levels should reflect cellular activity and concentration (Pochini et al., 2004; Schooneman et al., 2013). It is thus possible that circulating levels of acylcarnitines could reflect the hypoxic status of tumor cells.

We also observed an accumulation of monoacylglycerols to the detriment of free fatty acids. Monoacylglycerols are mainly derived from enzymatic hydrolysis of triacylglycerols and diacylglycerols and can be further metabolized to free fatty acids through the action of monoacylglycerol lipase (MAGL), an enzyme previously identified to be down-regulated in EC (Guida et al., 2010). Accordingly, a lower MAGL activity could explain, at least in part, the observed accumulation of monoacylglycerols in sera of EC cases as compared with controls. Of note, the monoacylglycerol 1-oleoylglycerol (18:1) was strongly elevated in R cases of both tumor types and could represent a marker of EC recurrence. This is consistent with a role for MAGL in various aspects of tumorigenesis (Qin and Ruan, 2014).

Modifications in lipid levels could also be related to bradykinin, a putative biomarker of type I EC that is known to activate phospholipase D in EC (Ahmed et al., 1995). As an inflammatory mediator, bradykinin triggers kinin-activated pathways. These have been associated with EC and breast cancer progression, supporting the role of bradykinin in tumors originating from steroid sensitive tissues (Ehrenfeld et al., 2011; Orchel et al., 2012). Sulfated androgens were also higher in type I EC cases, consistent with the reported implication of sulfated steroids in this histotype (Naitoh et al., 1989; Lepine et al.; Audet-Walsh et al., 2011; Audet-Delage et al., 2017; Sinreih et al., 2017). Furthermore, our data identified heme as a putative biomarker of type II EC and highlighted modifications in pathways closely related to heme synthesis, namely the tetrahydrofolate-serine/glycine pathway (di Salvo et al., 2013). Heme consumption might participate in endometrial carcinogenesis, being associated with a moderate increase in EC risk (Genkinger et al., 2012). Targeting this pathway is currently being tested for the treatment of ovarian cancer and other solid tumors using a new drug, 4-(N-(S-penicillaminylacetyl)amino) phenylarsonous acid (PENAO), acting through the induction of heme degradation by heme oxygenase-1 (Decollogne et al., 2015; Tran et al., 2016).

Putative biomarkers of EC recurrence were also identified. Compared with patients with non-recurrent type I carcinomas, those who experienced recurrence after surgery presented alterations in bile acid levels. Bile acids contribute to cholesterol homeostasis, a precursor of the steroids that drive the development and progression of this histological type of EC (Brinton et al., 2016). Recently, we showed that higher levels of circulating steroids are linked to an increased risk of recurrence (Audet-Delage et al., 2017). Numerous enzymatic pathways are involved in the conversion of both bile acids and steroids, including reduction by aldo-keto reductases (Rizner and Penning, 2014), conjugation by uridine diphospho-glucuronosyltransferases (Guillemette et al., 2014), sulfotransferases (Kurogi et al., 2013) and sulfatase (Jiang et al., 2017). The reduced levels of bile acids may reflect an altered activity of some of these metabolic pathways in R type I cases, consistent with previous findings (Lepine et al., 2010; Audet-Walsh et al., 2011). Bile acids might also act synergistically with steroids by stimulating EC cell growth, as they enhance myometrium sensitivity to hormones such as oxytocin (Germain et al., 2003). Finally, bile acids might initiate signaling events, as some of them display inflammatory functions (Li et al., 2017; Zhuang et al., 2017). In accordance with modifications in the inflammatory status of R type I cases, inflammatory response markers such as the phosphorylated cleavage peptide of fibrinogen were elevated in these patients. This is reinforced by studies that have linked the overexpression of procoagulants with gynecologic malignancies including EC, and further associated this overexpression with more aggressive tumor types (Ghezzi et al., 2010; Seebacher et al., 2010; Suh et al., 2012; Uccella et al., 2016; Zhou et al., 2017). Although fibrinogen may confer a potential advantage to cancer cells in terms of aggressiveness and dissemination, the underlying mechanisms remain unclear.

For the type II ECs analyzed here, all of which were serous carcinomas, our observations revealed enhanced concentrations of numerous ceramides in preoperative sera of R cases compared with NR cases. Others have linked alterations of sphingolipids and ceramides in EC with the differentiation status of the tumors, but they did not include type II carcinomas (Nozawa et al., 1989; Knapp et al., 2010; Mojakgomo et al., 2015; Tajima et al., 2017). Tanaka et al. (2015) showed that serous ovarian cancers exhibit elevated levels of glycosylated ceramides, consistent with high expression of galactosyltransferase in tumors. As ovarian serous cancers share similarities with type II serous EC, this raises the possibility that alterations in ceramide metabolism may be common to both tissues (Merritt and Cramer, 2010; Cramer, 2012). These bioactive lipids participate in tumor progression and the

metastasis process (Knapp et al., 2017) and therefore may represent promising biomarkers for non-invasive detection of recurrent type II EC. However, their metabolism in endometrial malignant tumors has been poorly characterized and our investigation is the first to present complex data on ceramide metabolism in the context of EC. Additional studies are thus warranted.

We identified putative cancer-specific and recurrence biomarkers using an unbiased metabolomics approach for type I and type II EC in postmenopausal women. Although exploratory, our study has several strengths including the analysis of postmenopausal cases and controls, as well as R and NR cases of two of the most common histological EC subtypes, in addition to the quantification of an extensive panel of metabolites through a validated metabolomics platform. This approach is powerful for screening a large and diverse set of metabolites but is limited in terms of absolute quantification. Additional limitations to our study include a restricted number of prospective EC cases, whereas the study design likely reduced variations through sample matching. Even though enrolled women must have not taken HRT during the 3 weeks prior to blood draw, it is not known if this period is sufficient to fully restore circulating metabolite levels potentially affected by HRT. Nonetheless, HRT use was similar between groups, which likely reduced the potential bias it might have introduced. The putative biomarkers identified in this pilot study will require validation in larger cohorts using quantitative methods. Their specificity to EC must also be confirmed, notably in comparison to other gynecological malignancies (ovarian cancer, mixed Müllerian cancer) and benign conditions (hyperplasia, endometriosis, etc.), which will facilitate their translation to the clinic. Finally, mechanistic studies are needed to help gain insights into the underlying biological processes driving the observed changes in metabolites in EC cases and those experiencing recurrence after surgery for curative intent.

5. Abbreviations

EC, endometrial cancer; R, recurrent; NR, non-recurrent; MS, mass spectrometry; UPLC-MS/MS, ultra-performance liquid chromatography–tandem mass spectrometry; ROC, receiver-operating characteristics; AUC, area under the curve; MAGL, monoacylglycerol lipase; PENAO, 4-(N-(S-penicillaminylacetyl)amino) phenylarsonous acid.

6. Acknowledgments

We would like to thank all the study participants and those involved in the recruitment, as well as Dr. Michèle Rouleau for helpful discussions and David Simonyan of the Clinical and Evaluative Research Platform of the CHU de Québec Research Center for statistical support. The Cancer Research Society (CRS) and Canadian Institutes of Health Research (FRN-68964 to CG) supported this work. YAD received a studentship from Fonds de Recherche du Québec – Santé (FRQS). CG holds a Tier I Canada Research Chair in Pharmacogenomics.

7. Author contributions

CG designed and supervised the research. JG and MP were involved in patient recruitment. JG established the clinical database. LV prepared biospecimens. YAD performed statistical analysis. CG and YAD took part in the analysis and interpretation of the data and wrote the manuscript. All authors critically reviewed and approved the final version of the manuscript.

The authors declare that there are no actual or potential conflicts of interest that could inappropriately influence, or be perceived to influence, this work.

8. References

Ahmed, A., Ferriani, R.A., and Smith, S.K. (1995). Activation of human endometrial phospholipase D by bradykinin. *Cell Signal* 7**,** 599-609.

Audet-Delage, Y., Gregoire, J., Caron, P., Turcotte, V., Plante, M., Ayotte, P., Simonyan, D., Villeneuve, L., and Guillemette, C. (2017). Estradiol metabolites as biomarkers of endometrial cancer prognosis after surgery. *J Steroid Biochem Mol Biol*.

Audet-Walsh, E., Lepine, J., Gregoire, J., Plante, M., Caron, P., Tetu, B., Ayotte, P., Brisson, J., Villeneuve, L., Belanger, A., and Guillemette, C. (2011). Profiling of endogenous estrogens, their precursors, and metabolites in endometrial cancer patients: association with risk and relationship to clinical characteristics. *J Clin Endocrinol Metab* 96**,** E330-339.

Bachmayr-Heyda, A., Aust, S., Auer, K., Meier, S.M., Schmetterer, K.G., Dekan, S., Gerner, C., and Pils, D. (2017). Integrative Systemic and Local Metabolomics with Impact on Survival in High-Grade Serous Ovarian Cancer. *Clin Cancer Res* 23**,** 2081-2092.

Bahado-Singh, R.O., Lugade, A., Field, J., Al-Wahab, Z., Han, B., Mandal, R., Bjorndahl, T.C., Turkoglu, O., Graham, S.F., Wishart, D., and Odunsi, K. (2017). Metabolomic prediction of endometrial cancer. *Metabolomics* 14**,** 6.

Brinton, L.A., Trabert, B., Anderson, G.L., Falk, R.T., Felix, A.S., Fuhrman, B.J., Gass, M.L., Kuller, L.H., Pfeiffer, R.M., Rohan, T.E., Strickler, H.D., Xu, X., and Wentzensen, N. (2016). Serum Estrogens and Estrogen Metabolites and Endometrial Cancer Risk among Postmenopausal Women. *Cancer Epidemiol Biomarkers Prev* 25**,** 1081-1089.

Buhtoiarova, T.N., Brenner, C.A., and Singh, M. (2016). Endometrial Carcinoma: Role of Current and Emerging Biomarkers in Resolving Persistent Clinical Dilemmas. *Am J Clin Pathol* 145**,** 8-21.

Busch, E.L., Crous-Bou, M., Prescott, J., Chen, M.M., Downing, M.J., Rosner, B.A., Mutter, G.L., and De Vivo, I. (2017). Endometrial Cancer Risk Factors, Hormone Receptors, and Mortality Prediction. *Cancer Epidemiol Biomarkers Prev* 26**,** 727-735.

Chughtai, K., Jiang, L., Greenwood, T.R., Glunde, K., and Heeren, R.M. (2013). Mass spectrometry images acylcarnitines, phosphatidylcholines, and sphingomyelin in MDA-MB-231 breast tumor models. *J Lipid Res* 54**,** 333-344.

Cramer, D.W. (2012). The epidemiology of endometrial and ovarian cancer. *Hematol Oncol Clin North Am* 26**,** 1-12.

Dallal, C.M., Brinton, L.A., Bauer, D.C., Buist, D.S., Cauley, J.A., Hue, T.F., Lacroix, A., Tice, J.A., Chia, V.M., Falk, R., Pfeiffer, R., Pollak, M., Veenstra, T.D., Xu, X., Lacey, J.V., Jr., and Group, B.F.R. (2013). Obesity-related hormones and endometrial cancer among postmenopausal women: a nested case-control study within the B~FIT cohort. *Endocr Relat Cancer* 20**,** 151-160.

Dallal, C.M., Lacey, J.V., Jr., Pfeiffer, R.M., Bauer, D.C., Falk, R.T., Buist, D.S., Cauley, J.A., Hue, T.F., Lacroix, A.Z., Tice, J.A., Veenstra, T.D., Xu, X., Brinton, L.A., and Group, B.a.F.R. (2016). Estrogen Metabolism and Risk of Postmenopausal Endometrial and Ovarian Cancer: the B approximately FIT Cohort. *Horm Cancer* 7**,** 49-64.

Decollogne, S., Joshi, S., Chung, S.A., Luk, P.P., Yeo, R.X., Nixdorf, S., Fedier, A., Heinzelmann-Schwarz, V., Hogg, P.J., and Dilda, P.J. (2015). Alterations in the mitochondrial responses to PENAO as a mechanism of resistance in ovarian cancer cells. *Gynecol Oncol* 138**,** 363-371.

Di Salvo, M.L., Contestabile, R., Paiardini, A., and Maras, B. (2013). Glycine consumption and mitochondrial serine hydroxymethyltransferase in cancer cells: the heme connection. *Med Hypotheses* 80**,** 633-636.

Ehrenfeld, P., Conejeros, I., Pavicic, M.F., Matus, C.E., Gonzalez, C.B., Quest, A.F., Bhoola, K.D., Poblete, M.T., Burgos, R.A., and Figueroa, C.D. (2011). Activation of kinin B1

receptor increases the release of metalloproteases-2 and -9 from both estrogen-sensitive and -insensitive breast cancer cells. *Cancer Lett* 301**,** 106-118.

Gaudet, M.M., Falk, R.T., Stevens, R.D., Gunter, M.J., Bain, J.R., Pfeiffer, R.M., Potischman, N., Lissowska, J., Peplonska, B., Brinton, L.A., Garcia-Closas, M., Newgard, C.B., and Sherman, M.E. (2012). Analysis of serum metabolic profiles in women with endometrial cancer and controls in a population-based case-control study. *J Clin Endocrinol Metab* 97**,** 3216-3223.

Genkinger, J.M., Friberg, E., Goldbohm, R.A., and Wolk, A. (2012). Long-term dietary heme iron and red meat intake in relation to endometrial cancer risk. *Am J Clin Nutr* 96**,** 848-854.

Germain, A.M., Kato, S., Carvajal, J.A., Valenzuela, G.J., Valdes, G.L., and Glasinovic, J.C. (2003). Bile acids increase response and expression of human myometrial oxytocin receptor. *Am J Obstet Gynecol* 189**,** 577-582.

Ghezzi, F., Cromi, A., Siesto, G., Giudici, S., Serati, M., Formenti, G., and Franchi, M. (2010). Prognostic significance of preoperative plasma fibrinogen in endometrial cancer. *Gynecol Oncol* 119**,** 309-313.

Green, M.L., Chung, T.E., Reed, K.L., Modric, T., Badinga, L., Yang, J., Simmen, F.A., and Simmen, R.C.M. (1998). Paracrine Inducers of Uterine Endometrial Spermidine/Spermine N1-Acetyltransferase Gene Expression during Early Pregnancy in the Pig1. *Biology of Reproduction* 59**,** 1251-1258.

Guida, M., Ligresti, A., De Filippis, D., D'amico, A., Petrosino, S., Cipriano, M., Bifulco, G., Simonetti, S., Orlando, P., Insabato, L., Nappi, C., Di Spiezio Sardo, A., Di Marzo, V., and Iuvone, T. (2010). The levels of the endocannabinoid receptor CB2 and its ligand 2-arachidonoylglycerol are elevated in endometrial carcinoma. *Endocrinology* 151**,** 921-928.

Guillemette, C., Levesque, E., and Rouleau, M. (2014). Pharmacogenomics of human uridine diphospho-glucuronosyltransferases and clinical implications. *Clin Pharmacol Ther* 96**,** 324-339.

Han, K.H., Kim, H.S., Lee, M., Chung, H.H., and Song, Y.S. (2017). Prognostic factors for tumor recurrence in endometrioid endometrial cancer stages IA and IB. *Medicine (Baltimore)* 96**,** e6976.

Jiang, M., Xu, M., Ren, S., Selcer, K.W., and Xie, W. (2017). Transgenic Overexpression of Steroid Sulfatase Alleviates Cholestasis. *Liver Res* 1**,** 63-69.

Knapp, P., Baranowski, M., Knapp, M., Zabielski, P., Blachnio-Zabielska, A.U., and Gorski, J. (2010). Altered sphingolipid metabolism in human endometrial cancer. *Prostaglandins Other Lipid Mediat* 92**,** 62-66.

Knapp, P., Bodnar, L., Blachnio-Zabielska, A., Swiderska, M., and Chabowski, A. (2017). Plasma and ovarian tissue sphingolipids profiling in patients with advanced ovarian cancer. *Gynecol Oncol* 147**,** 139-144.

Knific, T., Osredkar, J., Smrkolj, S., Tonin, I., Vouk, K., Blejec, A., Frkovic Grazio, S., and Rizner, T.L. (2017). Novel algorithm including CA-125, HE4 and body mass index in the diagnosis of endometrial cancer. *Gynecol Oncol* 147**,** 126-132.

Kurogi, K., Liu, T.A., Sakakibara, Y., Suiko, M., and Liu, M.C. (2013). The use of zebrafish as a model system for investigating the role of the SULTs in the metabolism of endogenous compounds and xenobiotics. *Drug Metab Rev* 45**,** 431-440.

Lepine, J., Audet-Walsh, E., Gregoire, J., Tetu, B., Plante, M., Menard, V., Ayotte, P., Brisson, J., Caron, P., Villeneuve, L., Belanger, A., and Guillemette, C. (2010). Circulating estrogens in endometrial cancer cases and their relationship with tissular expression of key estrogen biosynthesis and metabolic pathways. *J Clin Endocrinol Metab* 95**,** 2689-2698.

Li, M., Cai, S.Y., and Boyer, J.L. (2017). Mechanisms of bile acid mediated inflammation in the liver. *Mol Aspects Med* 56**,** 45-53.
Lofgren, L., Stahlman, M., Forsberg, G.B., Saarinen, S., Nilsson, R., and Hansson, G.I. (2012). The BUME method: a novel automated chloroform-free 96-well total lipid extraction method for blood plasma. *J Lipid Res* 53**,** 1690-1700.
Loftsson, T., Somogyi, G., and Bodor, N. (1989). Effect of choline esters and oleic acid on the penetration of acyclovir, estradiol, hydrocortisone, nitroglycerin, retinoic acid and trifluorothymidine across hairless mouse skin in vitro. *Acta Pharm Nord* 1**,** 279-286.
Mang, C., Birkenmaier, A., Cathomas, G., and Humburg, J. (2017). Endometrioid endometrial adenocarcinoma: an increase of G3 cancers? *Arch Gynecol Obstet* 295**,** 1435-1440.
Merritt, M.A., and Cramer, D.W. (2010). Molecular pathogenesis of endometrial and ovarian cancer. *Cancer Biomark* 9**,** 287-305.
Mojakgomo, R., Mbita, Z., and Dlamini, Z. (2015). Linking the ceramide synthases (CerSs) 4 and 5 with apoptosis, endometrial and colon cancers. *Exp Mol Pathol* 98**,** 585-592.
Naitoh, K., Honjo, H., Yamamoto, T., Urabe, M., Ogino, Y., Yasumura, T., and Nambara, T. (1989). Estrone sulfate and sulfatase activity in human breast cancer and endometrial cancer. *J Steroid Biochem* 33**,** 1049-1054.
Nozawa, S., Narisawa, S., Kojima, K., Sakayori, M., Iizuka, R., Mochizuki, H., Yamauchi, T., Iwamori, M., and Nagai, Y. (1989). Human monoclonal antibody (HMST-1) against lacto-series type 1 chain and expression of the chain in uterine endometrial cancers. *Cancer Res* 49**,** 6401-6406.
Obuchowski, N.A. (2005). ROC analysis. *AJR Am J Roentgenol* 184**,** 364-372.
Orchel, J., Witek, L., Kimsa, M., Strzalka-Mrozik, B., Kimsa, M., Olejek, A., and Mazurek, U. (2012). Expression patterns of kinin-dependent genes in endometrial cancer. *Int J Gynecol Cancer* 22**,** 937-944.
Pearce, N. (2016). Analysis of matched case-control studies. *BMJ* 352**,** i969.
Pistilli, M.J., Petrik, J.J., Holloway, A.C., and Crankshaw, D.J. (2012). Immunohistochemical and functional studies on calcium-sensing receptors in rat uterine smooth muscle. *Clin Exp Pharmacol Physiol* 39**,** 37-42.
Pochini, L., Oppedisano, F., and Indiveri, C. (2004). Reconstitution into liposomes and functional characterization of the carnitine transporter from renal cell plasma membrane. *Biochim Biophys Acta* 1661**,** 78-86.
Qin, H., and Ruan, Z.H. (2014). The role of monoacylglycerol lipase (MAGL) in the cancer progress. *Cell Biochem Biophys* 70**,** 33-36.
Rizner, T.L. (2016). Discovery of biomarkers for endometrial cancer: current status and prospects. *Expert Rev Mol Diagn* 16**,** 1315-1336.
Rizner, T.L., and Penning, T.M. (2014). Role of aldo-keto reductase family 1 (AKR1) enzymes in human steroid metabolism. *Steroids* 79**,** 49-63.
Schooneman, M.G., Vaz, F.M., Houten, S.M., and Soeters, M.R. (2013). Acylcarnitines: reflecting or inflicting insulin resistance? *Diabetes* 62**,** 1-8.
Seebacher, V., Polterauer, S., Grimm, C., Husslein, H., Leipold, H., Hefler-Frischmuth, K., Tempfer, C., Reinthaller, A., and Hefler, L. (2010). The prognostic value of plasma fibrinogen levels in patients with endometrial cancer: a multi-centre trial. *Br J Cancer* 102**,** 952-956.
Shajahan-Haq, A.N., Boca, S.M., Jin, L., Bhuvaneshwar, K., Gusev, Y., Cheema, A.K., Demas, D.D., Raghavan, K.S., Michalek, R., Madhavan, S., and Clarke, R. (2017). EGR1 regulates cellular metabolism and survival in endocrine resistant breast cancer. *Oncotarget* 8**,** 96865-96884.
Shao, X., Wang, K., Liu, X., Gu, C., Zhang, P., Xie, J., Liu, W., Sun, L., Chen, T., and Li, Y. (2016). Screening and verifying endometrial carcinoma diagnostic biomarkers based on

a urine metabolomic profiling study using UPLC-Q-TOF/MS. *Clin Chim Acta* 463**,** 200-206.
Sinreih, M., Knific, T., Anko, M., Hevir, N., Vouk, K., Jerin, A., Frkovic Grazio, S., and Rizner, T.L. (2017). The Significance of the Sulfatase Pathway for Local Estrogen Formation in Endometrial Cancer. *Front Pharmacol* 8**,** 368.
Soda, K. (2011). The mechanisms by which polyamines accelerate tumor spread. *J Exp Clin Cancer Res* 30**,** 95.
Sorbe, B. (2012). Predictive and prognostic factors in definition of risk groups in endometrial carcinoma. *ISRN Obstet Gynecol* 2012**,** 325790.
Suh, D.H., Kim, H.S., Chung, H.H., Kim, J.W., Park, N.H., Song, Y.S., and Kang, S.B. (2012). Pre-operative systemic inflammatory response markers in predicting lymph node metastasis in endometrioid endometrial adenocarcinoma. *Eur J Obstet Gynecol Reprod Biol* 162**,** 206-210.
Tajima, M., Harada, T., Ishikawa, T., Iwahara, Y., and Kubota, T. (2012). Augmentation of arginase expression in the human endometrial epithelium in the secretory phase. *J Med Dent Sci* 59**,** 75-82.
Tajima, T., Miyazawa, M., Hayashi, M., Asai, S., Ikeda, M., Shida, M., Hirasawa, T., Iwamori, M., and Mikami, M. (2017). Enhanced expression of hydroxylated ceramide in well-differentiated endometrial adenocarcinoma. *Oncol Lett* 13**,** 45-50.
Tanaka, K., Mikami, M., Aoki, D., Kiguchi, K., Ishiwata, I., and Iwamori, M. (2015). Expression of sulfatide and sulfated lactosylceramide among histological types of human ovarian carcinomas. *Hum Cell* 28**,** 37-43.
Tran, B., Hamilton, A.L., Horvath, L., Lam, M., Savas, P.S., Grimison, P.S., Whittle, J.R., Kuo, J.C.-Y., Signal, N., Edmonds, D., Hogg, P.J., Rischin, D., and Desai, J. (2016). First-in-man trial of 4-(N-(S-penicillaminylacetyl)amino) phenylarsonous acid (PENAO) as a continuous intravenous infusion (CIVI), in patients (pt) with advanced solid tumours. *J Clin Oncol* 34**,** e14025-e14025.
Troisi, J., Sarno, L., Landolfi, A., Scala, G., Martinelli, P., Venturella, R., Di Cello, A., Zullo, F., and Guida, M. (2018). Metabolomic Signature of Endometrial Cancer. *J Proteome Res* 17**,** 804-812.
Trousil, S., Lee, P., Pinato, D.J., Ellis, J.K., Dina, R., Aboagye, E.O., Keun, H.C., and Sharma, R. (2014). Alterations of choline phospholipid metabolism in endometrial cancer are caused by choline kinase alpha overexpression and a hyperactivated deacylation pathway. *Cancer Res* 74**,** 6867-6877.
Turkoglu, O., Zeb, A., Graham, S., Szyperski, T., Szender, J.B., Odunsi, K., and Bahado-Singh, R. (2016). Metabolomics of biomarker discovery in ovarian cancer: a systematic review of the current literature. *Metabolomics* 12.
Uccella, S., Cromi, A., Vigetti, D., Cimetti, L., Deleonibus, S., Casarin, J., Passi, A., Riva, C., and Ghezzi, F. (2016). Endometrial cancer cells can express fibrinogen: Immunohistochemistry and RT-PCR analysis. *J Obstet Gynaecol* 36**,** 353-358.
Westin, S.N., and Broaddus, R.R. (2012). Personalized therapy in endometrial cancer: challenges and opportunities. *Cancer Biol Ther* 13**,** 1-13.
Wishart, D.S. (2016). Emerging applications of metabolomics in drug discovery and precision medicine. *Nat Rev Drug Discov* 15**,** 473-484.
Xie, H., Hou, Y., Cheng, J., Openkova, M.S., Xia, B., Wang, W., Li, A., Yang, K., Li, J., Xu, H., Yang, C., Ma, L., Li, Z., Fan, X., Li, K., and Lou, G. (2017). Metabolic profiling and novel plasma biomarkers for predicting survival in epithelial ovarian cancer. *Oncotarget* 8**,** 32134-32146.
Yin, R., Yang, T., Su, H., Ying, L., Liu, L., and Sun, C. (2016). Saturated fatty acids as possible important metabolites for epithelial ovarian cancer based on the free and

esterified fatty acid profiles determined by GC-MS analysis. *Cancer Biomark* 17**,** 259-269.
Zhang, Y., Liu, Y., Li, L., Wei, J., Xiong, S., and Zhao, Z. (2016). High resolution mass spectrometry coupled with multivariate data analysis revealing plasma lipidomic alteration in ovarian cancer in Asian women. *Talanta* 150**,** 88-96.
Zhou, X., Wang, H., and Wang, X. (2017). Preoperative CA125 and fibrinogen in patients with endometrial cancer: a risk model for predicting lymphovascular space invasion. *J Gynecol Oncol* 28**,** e11.
Zhuang, S., Li, Q., Cai, L., Wang, C., and Lei, X. (2017). Chemoproteomic Profiling of Bile Acid Interacting Proteins. *ACS Cent Sci* 3**,** 501-509.

9. Tables

Table 1. Summary of previous metabolomics studies of EC.

Reference	Specimens	Platform (nb of metabolites)[a]	Up-regulated metabolites	Down-regulated metabolites
Trousil et al. (2014)	Tissue from n = 10 controls n = 8 EC cases	H^1 NMR (68)	Valine, Leucine, Alanine, Proline, Tyrosine, Phosphatidylcholine	Glutathione, Scyllo-inositol, Myo-inositol, Inosine/adenosine
Shao et al. (2016)	Urine from n = 25 controls n = 25 EC cases n = 10 EH cases	UPLC-QToF[b]	*N*-Acetylserine, Urocanic acid, Isobutyrylglycine	Porphobilinogen, Acetylcysteine
Gaudet et al. (2012)	Serum from n = 250 controls n = 250 EC cases	GC-MS (43)	None	C5-acylcarnitines, octenoylcarnitine, decatrienoylcarnitine, linoleic acid, stearic acid
Bahado-Singh *et al*. (2017)	Serum from n = 60 controls n = 56 EC cases	LC-MS/MS (181) H^1 NMR (32)[c]	2-Hydroxybutyrate, 3-Hydroxybutyric acid, Acetone, C10, C14:1, C14:2, C16, C18:1, C18:2, C2, C5-DC (C6-OH), C6 (C4:1-DC), C7-DC, C8, Glutamate, SM C18:0	Asparagine, C3, Histidine, Hydroxyproline, Kynurenine, L-Methionine, lysoPC a C17:0, lysoPC a C18:0, lysoPC a C18:1, lysoPC a C18:2, Methionine, Several PC aa and PC ae[d]
Troisi et al. (2018)	Serum from n = 130 controls n = 118 EC cases n = 30 OCa cases n = 10 BED cases	GC-MS (259)	Lactic acid, homocysteine, 3-hydroxybutyric acid	Progesterone, linoleic acid, stearic acid, myristic acid, threonine, valine

EC, endometrial cancer; EH, endometrial hyperplasia; BED, benign endometrial disease; OCa, Ovarian cancer; GC-MS, gas chromatography–mass spectrometry; H^1 NMR, proton nuclear magnetic resonance; UPLC-QToF, ultra-performance liquid chromatography–quadrupole time-of-flight mass spectrometry; LC-MS/MS, liquid chromatography–tandem MS; PC, phosphatidylcholines; PCaa, diacyl-phosphatidylcholines; PCae, acyl-alkyl-phosphatidylcholines.

[a] The number of metabolites examined is shown in parentheses.

[b] The authors did not report the number of metabolites detected.

[c] Metabolites detected by H^1 NMR were also detected by LC-MS/MS.

[d] PC aa and PC ae were PC aa C36:0, PC aa C36:1, PC aa C36:3, PC aa C36:5, PC aa C36:6, PC aa C38:0, PC aa C38:5, PC aa C40:2, PC aa C42:2, PC aa C42:6, PC ae C34:0, PC ae C34:2, PC ae C34:3, PC ae C36:1, PC ae C36:2, PC ae C36:3, PC ae C38:0, PC ae C38:1, PC ae C38:2, PC ae C38:5, PC ae C38:6, PC ae C40:1, PC ae C40:6, PC ae C42:1, PC ae C42:2, PC ae C42:3.

Table 2. Demographics of control postmenopausal women and those who were newly diagnosed with EC.

		EC cases (n = 36)	
Characteristic	**Controls (n = 18)**	**Non-recurrent (n = 18)**	**Recurrent (n = 18)**
Continuous variable data:	Mean ± SD	Mean ± SD	Mean ± SD
Age (years)	58.9 ± 10.4[a]	66.3 ± 8.3	67.5 ± 9.4
Height (cm)	159.2 ± 5.3	157.9 ± 5.4	156.5 ± 6.7
Weight (kg)	70.1 ± 20.1	70.7 ± 16.9	68.3 ± 14.1
BMI	27.5 ± 7.2	28.4 ± 7.0	28.0 ± 6.4
Mean follow-up (months)	NA	56.3 ± 26.5	65.4 ± 48.7
Categorical data:	n (%)	n (%)	n (%)
Full-term pregnancy			
No	4 (22)	7 (39)	8 (44)
Yes	14 (78)	10 (56)	9 (50)
Missing	0 (0)	1 (6)	1 (6)
OC use			
No	8 (44)	10 (56)	12 (67)
Yes	10 (56)	7 (39)	5 (28)
Missing	0 (0)	1 (6)	1 (6)
Smoking			
Never	12 (67)	11 (61)	13 (72)
Current	4 (22)	4 (22)	3 (17)
Ex-smoker	2 (11)	3 (17)	2 (11)
HRT			
No	14 (78)	10 (56)	11 (61)
Yes	4 (22)	7 (39)	6 (33)
Missing	0 (0)	1 (6)	1 (6)

[a] Control women were slightly younger than EC cases ($P < 0.05$). No other significant differences were noted between cases and controls. No statistical differences were noted between R and NR cases. Student's *t*-test was used for continuous variable data, with adjustment for variance inequality when required (Welch's two-sample *t*-test). Categorical data were assessed using the chi-square test (χ^2) or Fisher's exact test, when applicable. HRT, hormone replacement therapy; OC, oral contraceptive; BMI, body mass index; NA, not applicable.

Table 3. Top 10 modulated preoperative serum metabolites in EC cases.

Subpathway	Biochemical name	Fold change	*P*-value
Biomarkers of EC			
EC cases (n = 36) *vs.* control postmenopausal women (n = 18)			
Leucine, Isoleucine and Valine Metabolism	isovalerate	–2.56	0.0154
Gamma-Glutamyl Amino Acid	gamma-glutamyl-2-aminobutyrate	–1.72	0.0170
Fatty Acid, Dicarboxylate	adipate	–1.64	0.0456
Nicotinate and Nicotinamide Metabolism	1-methylnicotinamide	–1.47	0.0118
Histidine Metabolism	trans-urocanate	–1.45	0.0125
Methionine, Cysteine, SAM and Taurine Metabolism	cystathionine	2.73	0.0011
Secondary Bile Acid Metabolism	isoursodeoxycholate	3.40	0.0146
Glycogen Metabolism	maltose	3.41	0.0005
Dipeptide	glycylvaline	3.92	0.0075
Polyamine Metabolism	spermine	7.66	0.0004
Biomarkers of EC histological types			
Type II EC cases (n = 12) *vs.* type I EC cases (n = 24)			
Polypeptide	bradykinin, des-arg(9)	-2.70	0.003
Androgenic Steroids	androsteroid monosulfate C19H28O6S	-2.33	0.030
Xanthine Metabolism	1,3,7-trimethylurate	-2.33	0.047
Androgenic Steroids	5-alpha-androstan-3beta,17beta-diol disulfate	-2.17	0.025
Androgenic Steroids	androstenediol (3alpha, 17alpha) monosulfate	-2.08	0.017
TAG Ester	TAG42:1-FA12:0	2.92	0.049
TAG Ester	TAG46:3-FA18:3	3.05	0.030
TAG Ester	TAG44:2-FA12:0	3.26	0.038
TAG Ester	TAG44:2-FA18:2	3.38	0.041
Hemoglobin and Porphyrin Metabolism	heme	4.52	0.030

Table 4. Top 10 modulated preoperative serum metabolites in recurrent EC cases.

Subpathway	Biochemical name	Fold change	*P*-value
Biomarkers of recurrence after initial surgery			
R cases (n = 18) *vs.* NR cases (n = 18) for type I and type II carcinomas			
Ester	TAG40:0-FA12:0	–7.14	0.0427
Ester	TAG42:2-FA12:0	–5.00	0.0460
Primary Bile Acid Metabolism	chenodeoxycholate	–2.86	0.0263
Glycogen Metabolism	maltose	–2.78	0.0028
Secondary Bile Acid Metabolism	glycoursodeoxycholate	–2.00	0.0343
Fatty Acid Metabolism (Acyl Glycine)	hexanoylglycine	2.04	0.0454
Monoacylglycerol	1-palmitoleoylglycerol (16:1)	2.73	0.0484
Monoacylglycerol	2-palmitoleoylglycerol (16:1)	2.86	0.0283
Monoacylglycerol	2-oleoylglycerol (18:1)	2.95	0.0076
Monoacylglycerol	1-oleoylglycerol (18:1)	3.37	0.0046
Biomarkers of recurrence after initial surgery by histological type			
R cases (n=12) *vs.* NR cases (n=12) for type I endometrioid carcinomas			
Secondary Bile Acid Metabolism	taurodeoxycholate	–7.14	0.0093
Secondary Bile Acid Metabolism	glycodeoxycholate	–4.55	0.0088
Primary Bile Acid Metabolism	taurocholate	–3.85	0.0383
Glycogen Metabolism	maltose	–3.45	0.0065
Primary Bile Acid Metabolism	glycocholate	–3.23	0.0263
Free Fatty Acids	FFA(22:5)	1.66	0.0006
Fibrinogen Cleavage Peptide	ADpSGEGDFXAEGGGVR	1.68	0.0135
Oxidative Phosphorylation	phosphate	1.76	0.0250
Ester	TAG58:10-FA20:5	1.88	0.0032
Monoacylglycerol	1-oleoylglycerol (18:1)	3.77	0.0450
R cases (n = 6) *vs.* NR cases (n = 6) for type II serous carcinomas			
Fatty Acid Metabolism (Acyl Carnitine)	3-hydroxybutyrylcarnitine	–2.17	0.0494
Pentose Metabolism	ribitol	–1.56	0.0192
Purine Metabolism, (Hypo)Xanthine/Inosine Containing	allantoin	–1.45	0.0481
Histidine Metabolism	histidine	–1.45	0.0028
Glutathione Metabolism	2-aminobutyrate	–1.39	0.0132
Fatty Acid Metabolism (Acyl Choline)	docosahexaenoylcholine	2.18	0.0413
Monoacylglycerol	1-docosahexaenoylglycerol (22:6)	2.28	0.0036
Monoacylglycerol	1-oleoylglycerol (18:1)	2.29	0.0175
Phospholipid Metabolism	glycerophosphoinositol	2.38	0.0022
Monoacylglycerol	2-docosahexaenoylglycerol (22:6)	2.55	0.0067

10. Figure legends

Figure 1. Comparison of EC cases and controls reveals that lipid metabolism is perturbed in EC cases. (**A)** Pathway enrichment analysis is based on enrichment scores. Pathways containing at least three metabolites and having an enrichment score > 3 are displayed. (**B)** Free fatty acid levels are lower in EC cases, whereas conjugated forms of fatty acids are elevated. Fold changes are displayed in radar graphs. Significantly enriched and depleted metabolites are marked in red and blue circles, respectively. (**C**) ROC curves of the most accurate regression models for detecting EC. $^{\dagger}P < 0.10$, $^{*}P < 0.05$, $^{**}P < 0.01$.

Figure 2. Monoacylglycerols and amino acids are remodelled in R EC cases when compared to NR cases. (**A**) Most-enriched pathways in R cases as compared with NR cases. Pathways containing at least three metabolites and having an enrichment score > 3 are displayed. (**B**) Several species of monoacylglycerol are elevated in R cases. (**C**) The metabolism of glycine, serine and threonine is perturbed in R cases in comparison to NR cases. Normalized levels of detected metabolites are displayed in dot plots, and means are represented by grey diamonds (♦). (**D**) ROC curves of the most-accurate regression models to detect recurrence. $^{*}P < 0.05$, $^{**}P < 0.01$.

Figure 3. Metabolic alterations of R EC differ between the histological subtypes. (**A**) R cases of type I histology are associated with reduced bile acid levels. Metabolites in bold were significantly altered ($P < 0.05$), whereas a trend ($P < 0.10$) was detected for underscored metabolites. Bile acids can be conjugated with glucose (G-), taurine (T-), glucuronic acid (-GA) or sulfate (-S). CA, cholic acid; DCA, deoxycholic acid; UDCA, ursodeoxycholic acid; IUDCA, isoursodeoxycholic acid; CDCA, chenodeoxycholic acid; LCA, lithocholic acid. (**B**) Normalized levels of the phosphorylated fibrinogen cleavage peptide ADpSGEGDFXAEGGGVR were higher in type I R cases. (**C**) Ceramide levels were significantly altered in type II R cases. Fold change is shown, and significant metabolites ($P < 0.05$) are identified by a black background, whereas a trend ($P < 0.10$) in metabolite differences is shown by grey shading. Cer, ceramide; -FA, fatty acid group; DEGS, dihydroceramide desaturase; CEGT, ceramide glucosyltransferase; GALT, galactosyltransferase; Gal, galactose; Glu, glucose.

Figure 1

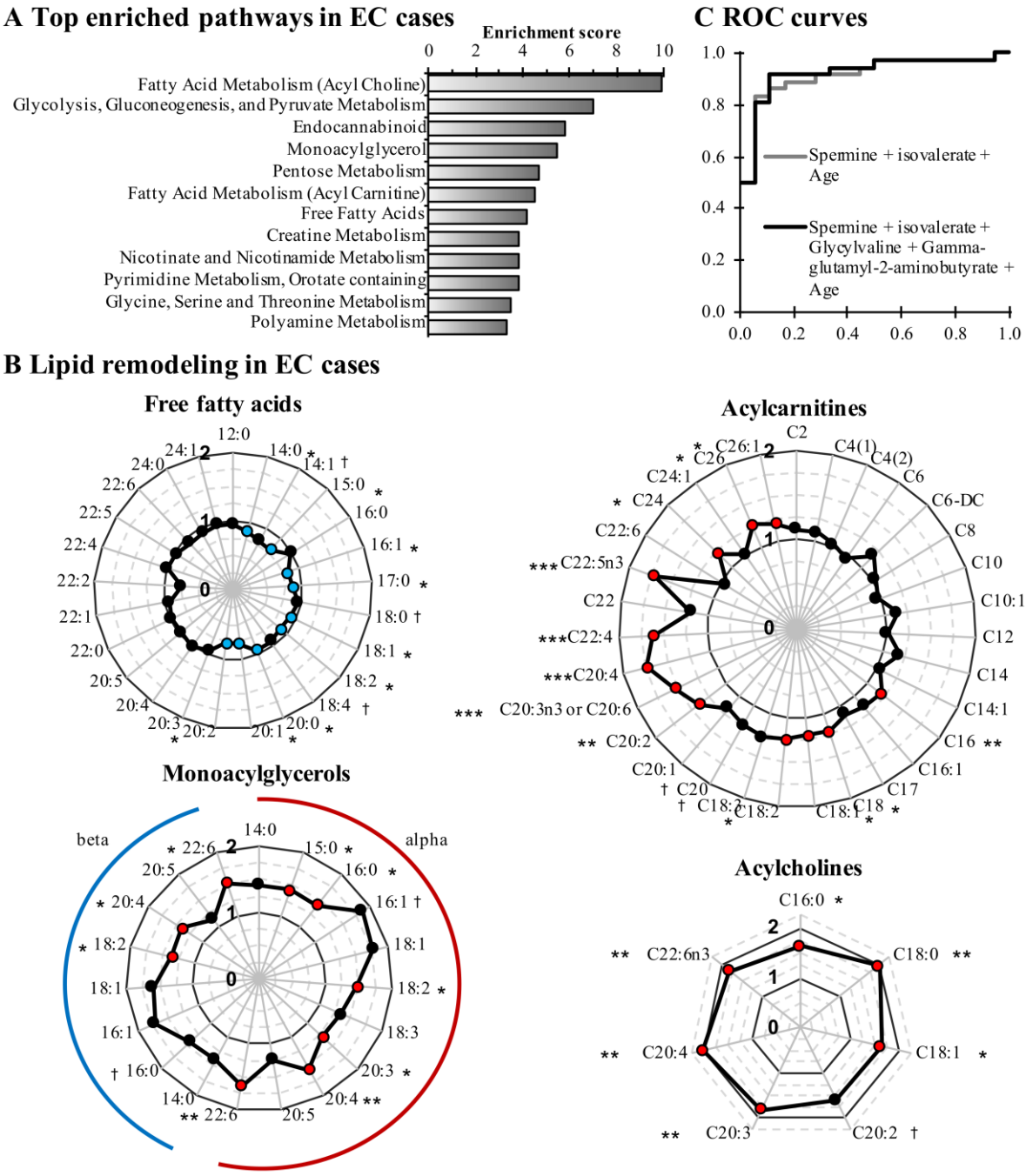
A Top enriched pathways in EC cases
Enrichment score
0 2 4 6 8 10
Fatty Acid Metabolism (Acyl Choline)
Glycolysis, Gluconeogenesis, and Pyruvate Metabolism
Endocannabinoid
Monoacylglycerol
Pentose Metabolism
Fatty Acid Metabolism (Acyl Carnitine)
Free Fatty Acids
Creatine Metabolism
Nicotinate and Nicotinamide Metabolism
Pyrimidine Metabolism, Orotate containing
Glycine, Serine and Threonine Metabolism
Polyamine Metabolism
C ROC curves
1.0
0.8
0.6
0.4
0.2
0.0
0.0 0.2 0.4 0.6 0.8 1.0
Spermine + isovalerate + Age
Spermine + isovalerate + Glycylvaline + Gamma-glutamyl-2-aminobutyrate + Age
B Lipid remodeling in EC cases
Free fatty acids
12:0
14:0 *
14:1 †
15:0 *
16:0
16:1 *
17:0 *
18:0 †
18:1 *
18:2 *
18:4 †
20:0 *
20:1
20:2
20:3 *
20:4
20:5
22:0
22:1
22:2
22:4
22:5
22:6
24:0
24:1
Acylcarnitines
C2
C4(1)
C4(2)
C6
C6-DC
C8
C10
C10:1
C12
C14
C14:1
C16 **
C16:1
C17
C18
C18:1 *
C18:2 *
C20 † C18:3 *
C20:1 †
C20:2 **
C20:3n3 or C20:6 ***
C20:4 ***
C22:4 ***
C22 ***
C22:5n3 ***
C22:6 *
C24 *
C24:1 *
C26 *
C26:1 *
Monoacylglycerols
beta
alpha
14:0
15:0 *
16:0 *
16:1 †
18:1
18:2 *
18:3
20:3 *
20:4 **
20:5
22:6 **
14:0
16:0 †
16:1
18:1
18:2 *
20:4 *
20:5
22:6 *
Acylcholines
C16:0 *
C18:0 **
C18:1 *
C20:2 †
C20:3 **
C20:4 **
C22:6n3 **

Figure 2

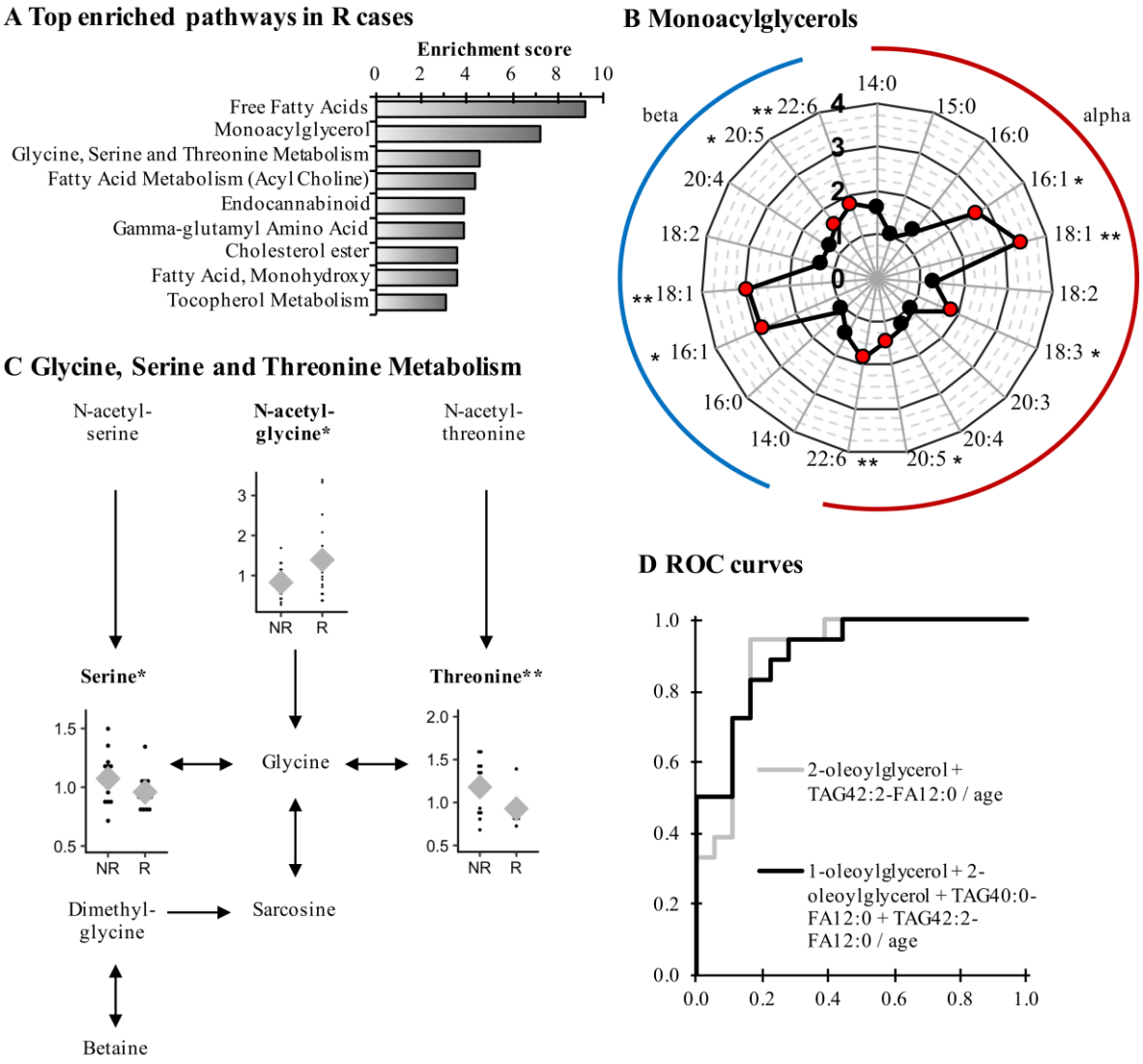
A Top enriched pathways in R cases
Enrichment score
0 2 4 6 8 10
Free Fatty Acids
Monoacylglycerol
Glycine, Serine and Threonine Metabolism
Fatty Acid Metabolism (Acyl Choline)
Endocannabinoid
Gamma-glutamyl Amino Acid
Cholesterol ester
Fatty Acid, Monohydroxy
Tocopherol Metabolism
B Monoacylglycerols
beta
alpha
14:0
15:0
16:0
16:1 *
18:1 **
18:2
18:3 *
20:3
20:4
20:5 *
22:6 **
14:0
16:0
16:1 *
18:1 **
18:2
20:4
20:5 *
22:6 **
C Glycine, Serine and Threonine Metabolism
N-acetyl-serine
N-acetyl-glycine*
N-acetyl-threonine
Serine*
Threonine**
Glycine
NR R
Dimethyl-glycine
Sarcosine
Betaine
D ROC curves
2-oleoylglycerol + TAG42:2-FA12:0 / age
1-oleoylglycerol + 2-oleoylglycerol + TAG40:0-FA12:0 + TAG42:2-FA12:0 / age

Figure 3

A Bile acid metabolism in Type I R cases

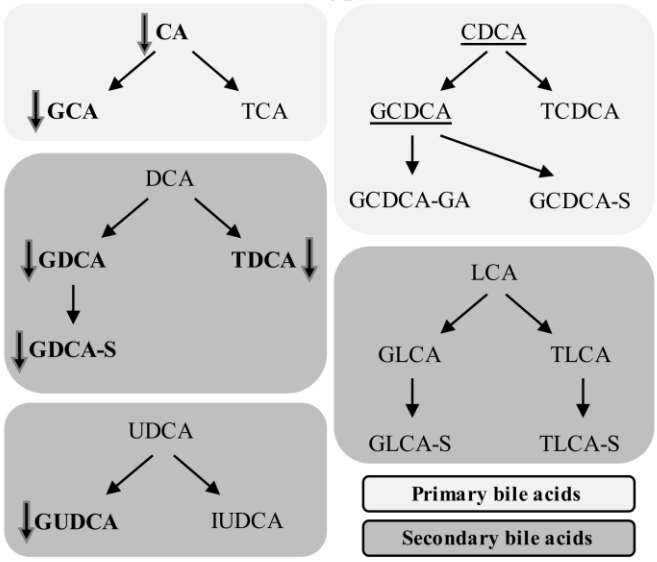

B Phosphorylated fibrinogen peptide in Type I R cases

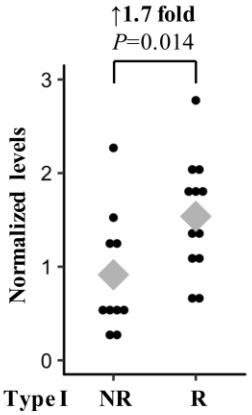

C Ceramides in Type II R cases

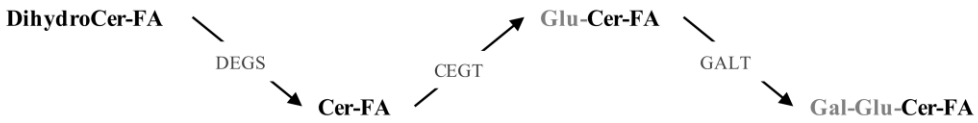

-FA	Dihydroceramide	Ceramide	Hexosylceramide	Lactosylceramide
14:0	1.02	1.11	1.15	1.25
16:0	1.18	1.34	1.27	1.21
18:0	1.35	1.60	1.12	1.24
18:1	1.26	1.60	1.45	1.16
20:0	1.18	1.55	1.33	1.32
20:1	1.10	1.45	1.24	1.29
22:0	1.23	1.32	1.20	1.22
22:1	1.17	1.40	1.31	1.24
24:0	1.13	1.19	1.18	1.17
24:1	1.18	1.28	1.12	1.18
26:0	1.13	1.26	1.43	1.11
26:1	1.17	1.19	1.09	1.29
Total	1.17	1.25	1.20	1.21